

**DEVELOPMENT OF CHIRAL
CONDUCTING POLYMERS FOR
ASYMMETRIC ELECTROSYNTHESIS**

A thesis submitted in fulfilment of the requirements for
the award of the degree

DOCTOR OF PHILOSOPHY

from the

UNIVERSITY OF WOLLONGONG

by

YINGPIT PORNPOTTKUL, M.Sc.(Biochemistry)

**INTELLIGENT POLYMER RESEARCH INSTITUTE
DEPARTMENT OF CHEMISTRY**

July 2005

CERTIFICATION

I, Yingpit Pornputtkul, declare that this thesis, submitted in fulfilment of the requirements for the award of Doctor of Philosophy, in the Department of Chemistry, University of Wollongong, is wholly my own work unless otherwise referenced or acknowledged. The document has not been submitted for qualifications at any other academic institution.

Yingpit Pornputtkul

July 2005

ACKNOWLEDGEMENTS

I wish to express my gratitude to my supervisors Professor Gordon Wallace and Professor Leon Kane-Maguire for their enthusiastic supervision, encouragement, support and friendship for the past three years.

I appreciated the assistance and friendship of the staff and students at IPRI. In particular I wish to thank Associate Professor Chee Too (for supplying experimental accessories and general help), Dr. Peter Innis (for training in Raman spectroscopy and general help), Dr. Syed Ashraf (for preparation of ionic liquids), and Dr. Violeta Misoska (for performing the SEM and AFM).

I also appreciated the help of Dr. John Korth from the Department of Chemistry (for running mass spectra), Dr. Wilford (for NMR measurements), Dr Chris Lukey from the Steel Institute (for training on DSC), Dr. Kosta Konstantinov from the Institute for Superconducting and Electronic Materials (for performing the TGA measurements of polyanilines) and Dr. Jenny Pringle at Monash University (for performing the DSC measurement of a chiral ionic liquid).

Finally, I gratefully acknowledge the Ministry of Science and Technology, Thailand, for a scholarship and the Department of Industrial Chemistry, King Mongkut's Institute of Technology North Bangkok Thailand for the leave to carry out this research study.

TABLE OF CONTENTS

CERTIFICATION	I
ACKNOWLEDGMENTS	II
TABLE OF CONTENTS	III
LIST OF ABBREVIATIONS	XII
ABSTRACT	XV
Chapter 1 - Introduction	1
1.1 Introduction	1
1.1.1 General Properties of Conducting Polymers	1
1.1.2 Synthesis of Conducting Polymers	2
1.1.3 Doping and De-doping in Conducting Polymers	2
1.2 Polyaniline	4
1.2.1 Synthesis of polyaniline	4
1.2.1.1 Electrochemical Polymerization	5
1.2.1.2 Chemical Polymerization	13
1.2.2 pH and Redox Switching Properties of Polyaniline	14
1.2.3 Spectroscopic Properties of Polyaniline	17
1.2.3.1 UV-visible Spectra of Polyaniline	17
1.2.3.2 Raman Spectra of Polyaniline	19
1.2.4 Electrochemical Behaviours and Stability of Polyanilines	20
1.3 Self-doped Polyaniline	24
1.4 Chiral Conducting Polymers	25
1.4.1 Chirality	25
1.4.2 Chiral Conducting Polymers	27
1.4.2.1 Chiral Polypyrroles	28
1.4.2.2 Chiral Polythiophenes	29
1.4.2.3 Chiral Polyanilines	31
1.5 Potential Applications of Chiral Conducting Polymers	34
1.5.1 Chiral Separations	35
1.5.2 Chiral Sensor/analysis	36

1.5.3 Asymmetric Electrosynthesis	37
1.6 Ionic Liquids	39
1.6.1 General Overviews	39
1.6.2 General Properties of Ionic Liquids	40
1.6.3 Potential Applications of Ionic Liquids	43
1.7 Aims of This Project	44
1.8 References	45
Chapter 2 - General Experimental	51
2.1 Introduction	51
2.2 Materials	51
2.2.1 Monomers and Polymers	51
2.2.2 Reagents	51
2.2.3 Solvents	52
2.2.4 Ionic Liquids	52
2.2.5 Electrodes	53
2.3 Techniques used for Preparation of Polyanilines	55
2.3.1 Electrochemical Polymerization	55
2.3.2 Chemical Polymerization	57
2.3.3 De-doping/Re-doping of Polyanilines	57
2.4 Polymer Characterization Techniques	58
2.4.1 UV-Visible-Near Infrared Spectroscopy	58
2.4.2 Circular Dichroism Spectroscopy (CD)	58
2.4.3 UV-visible and Circular Dichroism Spectroelectrochemistry	60
2.4.4 Raman Spectroscopy	60
2.4.5 Scanning Electron Microscopy (SEM) and Atomic Force Microscopy (AFM)	61
2.4.6 Cyclic Voltammetry (CV)	62
2.4.7 Thermogravimetric Analysis (TGA)	63
2.4.8 Differential Scanning Calorimetry (DSC)	64
2.4.9 Electrical Conductivity	65
2.4.10 Polarimetry	66
2.5 References	66

Chapter 3 - A Novel Route to Optically Active Polyaniline via Thermal Treatment	67
3.1 Introduction	67
3.2 Experimental	68
3.2.1 Sample Preparations	68
3.2.2 Spectroscopic Studies	70
3.2.3 Thermal Treatment	70
3.2.4 Thermal Analysis	70
3.3 Results and Discussions	71
3.3.1 Heat Treatment of Electrochemically Derived Emeraldine Base Doped with (+)-HCSA or (-)-HCSA	71
3.3.2 Heat Treatment of Chemically Derived Emeraldine Base Doped with (+)-HCSA	75
3.3.3 Thermal Analysis of Polyanilines	77
3.4 Conclusions	86
3.5 References	87
Chapter 4 - Asymmetric Proliferation with Optically Active Polyanilines	88
4.1 Introduction	88
4.2 Experimental	89
4.2.1 Chemicals	89
4.2.2 Preparation of Optically Active Polyaniline via Chiral Emeraldine Salt Inducer	89
4.2.3 Chiral Amplification	90
4.2.4 UV-visible and CD Spectral Measurements	90
4.2.5 De-doping/Re-doping of a Polyaniline Film	90
4.2.6 Electrochemical Studies	90
4.3 Results and Discussion	91
4.3.1 Chiroptical Properties of Electrodeposited PAn.HA Films	91
4.3.2 Synthesis of Optically Active Polyanilines Using a Thin	93

PAn.(+)-HCSA Film as Chiral Inducer	
4.3.3 Synthesis of Optically Active Polyanilines Using a Thin PAn.(+)-HCSA Film as Chiral Inducer	97
PAn.(-)-HCSA Film as Chiral Inducer	
4.3.4 The Origin of the Macromolecular Asymmetric Induction	100
4.3.5 Optimum Thickness of the Initial PAn.(+)-HCSA Films	103
4.3.6 Influence of Deposition Charge Passed on the Chiroptical Properties of the PAn.HA Films Macromolecular Asymmetric Proliferation	103
4.3.7 Chiroptical Stability of Optically Active PAn.(+)-HCSA/HCl Block Co-polymers During pH and Redox Switching	106
4.3.7.1 pH Switching	106
4.3.7.2 Redox Switching	108
4.3.8 The Role of the (+)-CSA- Dopant Anions of Thin PAn.(+)-HCSA Films in Inducing Chirality into Subsequent Deposited Emeraldine Salts	110
4.3.9 Electrochemical Study	112
4.3.9.1 Cyclic Voltammetry	112
4.3.9.2 Chronoamperometry during Growth	114
4.3.10 Attempted Asymmetric Electrochemical Synthesis of Optically Active Polypyrrole Induced by Chiral PAn.(+)-HCSA	117
4.4 Conclusions	119
4.5 References	120
Chapter 5 - pH and Redox Switching Properties of PMAS	122
5.1 Introduction	122
5.2 Experimental	125
5.2.1 Materials	125
5.2.2 Behaviours of PMAS in Basic Aqueous Solutions	125
5.2.3 Chemical Oxidation and Reduction of Aqueous PMAS	126
5.2.4 Solvatochromism - Effect of Solvents on the Conformation of PMAS	126
5.3 Results and Discussion	126
5.3.1 Behaviours of PMAS in Basic Aqueous Solutions	126
5.3.1.1 PMAS in Aqueous NH ₄ OH	127
5.3.1.2 Aqueous PMAS with Sterically Crowded Amines	130
5.3.2 Redox Switching of Aqueous PMAS	135

5.3.2.1 Oxidation of PMAS with Ammonium Persulfate	135
5.3.2.2 Reduction of Aqueous PMAS with Hydrazine	136
5.3.2.3 Thermochromism of the Reduced PMAS Species	140
5.3.2.4 Solvatochromism of the Reduced PMAS Species	142
5.3.2.5 Reduction of “Compact Coil” PMAS Emeraldine Salt with Hydrazine	145
5.3.2.6 Reduction of Aqueous Emeraldine Base	148
5.4 Conclusions	148
5.5 References	150
Chapter 6 - Preparation and Characterization a Chiral Complex of Fully Sulfonated Polyaniline with Poly-L-Lysine	151
6.1 Introduction	151
6.2 Experimental	152
6.2.1 Materials	152
6.2.2 PMAS-PLL Complex Formation	153
6.2.3 UV-visible and CD spectra of PMAS-PLL Films and Solutions	154
6.2.4 Chemical Treatments	154
6.2.5 Electroactivity of PMAS-PLL Films	154
6.2.6 <i>In-situ</i> UV-visible Spectroelectrochemical Studies of PMAS- PLL Films	155
6.2.7 Conductivity of PMAS-PLL Films	155
6.3 Results and Discussion	155
6.3.1 UV-Visible and CD Spectra of PMAS-PLL Complexes	155
6.3.2 Electroactivity of PMAS-PLL Films	159
6.3.3 Acid-Base Treatment of PMAS-PLL Films	164
6.3.4 Chemical Reduction / Oxidation of PMAS-PLL Films	167
6.3.5 <i>In situ</i> Spectroelectrochemical Studies of PMAS-PLL Films	171
6.3.6 Electrical Conductivity of PMAS-PLL Complex	173
6.4 Conclusions	173
6.5 References	175

Chapter 7 - Influence of Electropolymerization Temperature on the Chiroptical Properties of (+)-Camphorsulfonic Acid-Doped Polyaniline	177
7.1 Introduction	177
7.2 Experimental	180
7.2.1 Preparation of PAn.(+)-HCSA Films	180
7.2.2 UV-Visible and CD Spectra of PAn.(+)-HCSA Films	180
7.2.3 Post-Polymerization Heat Treatment of PAn.(+)-HCSA Films	181
7.2.4 De-doping/Re-doping of a PAn.(+)-HCSA Film	181
7.2.5 Chemical Reduction and Oxidation of a PAn.(+)-HCSA Film	181
7.2.6 PAn.(+)-HCSA Film Morphology	181
7.3 Results and Discussion	182
7.3.1 Influence of Temperature during Electropolymerization	182
7.3.2 Influence of Polymerization Temperature on the Morphology of PAn.(+)-HCSA Films	188
7.3.3 Effect of Heat Treatment after Polymerization	189
7.3.4 Explanation for the Temperature Dependent Chiral Discrimination during Electropolymerization	193
7.3.5 Influence of Polymerization Temperature on the Chemical Reactivity of PAn.(+)-HCSA Salts	194
7.4 Conclusions	200
7.5 References	201
Chapter 8 - Electrochemical Preparation of Chiral Polyaniline in Ionic Liquids	203
8.1 Introduction	203
8.2 Experimental	206
8.2.1 Electrochemical Synthesis of Polyanilines in Ionic Liquids	206
8.2.2 Spectroscopic Characterization	207
8.2.3 Electrochemical Characterization	207
8.2.4 Surface Studies	208
8.3 Results and Discussion	208
8.3.1 Cyclic Voltammetry during Potentiodynamically Synthesis of	208

Polyaniline in Aqueous Solution and in Ionic Liquids	
8.3.1.1 Electropolymerization in Aqueous Solution	208
8.3.1.2 Electropolymerization in Achiral Ionic Liquids	209
8.3.1.3 Electropolymerization in a Chiral Ionic Liquids	214
8.3.2 Potentiostatic Preparation of Polyaniline in Ionic Liquids	216
8.3.2.1 Spectroscopic Characterization of Potentiostatically Prepared Polyaniline	216
8.3.2.2 Raman Studies	223
8.3.3 Surface Studies	226
8.3.3.1 Morphology	226
8.3.3.2 Atomic Force Microscopy	228
8.4 Conclusions	229
8.5 References	230

Chapter 9 - Electrochemical Behaviour and Chiroptical Properties

of Chiral Polyaniline Film in Ionic Liquids	232
9.1 Introduction	232
9.2 Experimental	234
9.2.1 Materials	234
9.2.1 Physical Properties of the Novel MBEA-TFSI Ionic Liquids	234
9.2.2 Electrochemical Preparation of PAn.(+)-HCSA Films	236
9.2.3 Cyclic Voltammetry	236
9.2.4 <i>In situ</i> UV-visible and CD Spectroelectrochemical Studies	237
9.2.5 Raman Spectra	237
9.3 Results and Discussion	237
9.3.1 Properties of the Novel Chiral Ionic Liquid, MBEA-TFSI	237
9.3.1.1 Density	238
9.3.1.2 Viscosity	238
9.3.1.3 Conductivity	238
9.3.1.4 Differential Scanning Calorimeter (DSC)	240
9.3.1.5 Thermal Stability	241
9.3.1.6 Specific Rotations	242
9.3.1.7 Chiroptical Properties	242

9.3.1.8 Electrochemical Window	243
9.3.1.9 Miscibility and Solubility	244
9.3.1.10 Redox Couple of Ferrocene in Neat (\pm)-MBEA-TFSI	245
9.3.2 Cyclic Voltammetry of PAn.(+)-HCSA Films in Acidic and Neutral Aqueous Electrolytes and Ionic Liquids	245
9.3.2.1 CVs of PAn.(+)-HCSA Films in Acidic and Neutral Aqueous Electrolytes	246
9.3.2.2 CVs of PAn.(+)-HCSA Film in Ionic Liquids	252
9.3.3 <i>In situ</i> Spectroelectrochemical Studies of PAn.(+)-HCSA Films in Various Electrolytes	262
9.3.3.1 <i>In situ</i> UV-visible and CD Spectroelectrochemical Studies of PAn.(+)-HCSA Films in Aqueous Electrolytes	263
9.3.3.2 <i>In situ</i> UV-visible and CD Spectroelectrochemical Studies of PAn.(+)-HCSA Films in Ionic Liquids	271
9.3.4 Raman Spectroscopy	285
9.3.4.1 Raman Spectrum of PAn.(+)-HCSA Films after Holding at High Positive Potentials in Ionic Liquids	285
9.3.4.2 Raman Spectrum of PAn.(+)-HCSA Films after Holding at High Negative Potentials in Ionic Liquids	287
9.3.5 Explanations for Electrochemical Unstability and Racemization of Chiral PAn.(+)-HCSA Films in Ionic Liquids	288
9.4 Conclusions	299
9.5 References	300
Chapter 10 - Electroorganic Reactions in Ionic Liquids	302
10.1 Introduction	302
10.2 Experimental	304
10.2.1 Materials	304
10.2.2 Preparation of Chiral PAn.(+)-HCSA Modified Electrodes	305
10.2.3 Electrochemical Behaviour of Prochiral Organic Substrates in Ionic Liquids	305
10.2.4 Electrolyses	305
10.2.5 Analysis Techniques	306
10.3 Results and Discussion	306

10.3.1 Electrochemical Reduction of Acetophenone in EMI-TFSI	307
10.3.2 Electrochemical Studies of Acetylpyridine in Ionic Liquids	310
10.3.2.1 Electrochemical Reduction of 2-Acetylpyridine in EMI-TFSI	311
10.3.2.2 Electrochemical Reduction of 4-Acetylpyridine in (-)-MBEA-TFSI	314
10.3.2.3 Electrochemical Reduction of 4-Acetylpyridine in (±)-MBEA-TFSI	316
10.3.3 Electrochemical Oxidation of Organosulfides in Ionic Liquids	319
10.3.3.1 Electrochemical Oxidation of MNPS in EMI-TFSI	320
10.3.3.2 Electrochemical Studies of MNPS and MPTS in BMI-BF ₄	321
10.4 Conclusions	326
10.5 References	328

ABBREVIATIONS

μ	micro
$\Delta\epsilon$	difference in molar extinction coefficients
λ	wavelength
$^{\circ}\text{C}$	degree Celsius
$[\alpha]$	specific rotation
A	ampere
A^{-}	anion
AE	auxiliary electrodes
Ag/AgCl	silver/silver chloride reference electrode
BMI-BF ₄	1-butyl-3-methylimidazolium tetrafluoroborate
BMI-PF ₆	1-butyl-3-methylimidazolium hexafluorophosphate
C	coulomb
CD	circular dichroism
cm	centimetre
cm^{-1}	wave number
CS	chemical synthesis
CV	cyclic voltammetry
DSC	differential scanning calorimetry
E	potential
EB	emeraldine base
ECS	electrochemical synthesis
EMI-TFSI	1-ethyl-3-methylimidazolium bis(trifluoromethanesulfonyl)imide
ES	emeraldine salt
g	gram
GC	glassy carbon
HA	protonic acid
HCSA	10-camphorsulfonic acid
hr	hour
I	current

IL	ionic liquid
ITO	indium-tin oxide
LB	leucoemeraldine base
LS	leucoemeraldine salt
M	molar
mA	milliampere
MBEA-TFSI	methylbenzylethylamine bis(trifluoromethanesulfonyl)imide
mdeg	millidegree
min	minute
mm	millimetre
mM	millimolar
m.p.	melting point
MNPS	methyl 4-nitrophenyl sulfide
MPTS	methyl- <i>p</i> -tolyl sulfide
mV	millivolt
nm	nanometre
NMP	1-methyl-2-pyrrolidinone
P ₁₃ -TFSI	1-methyl-1-propylpyrrolidinium bis(trifluoromethanesulfonyl)imide
PAn	polyaniline
PB	pernigraniline base
PLL	poly-L-lysine
PMAS	poly(2-methoxyaniline-5-sulfonic acid)
PPy	polypyrrole
PS	pernigraniline salt
Pt	platinum
PVDF	Poly(vinylidene)difluoride
Q	charge
RE	reference electrode
Rs	resistivity
RVC	reticulated vitreous carbon

S/cm	siemens per centimetre
sec	second
SPAN	sulfonated polyaniline
T _g	glass transition temperature
T _m	melting temperature
TGA	thermogravimetric analysis
UV-vis	ultraviolet-visible
V	volt
WE	working electrode

Abstract

This thesis describes novel synthetic routes and characterization of chiral conducting polymers based on aniline and substituted anilines that have potential applications in the areas of asymmetric electrosynthesis and chiral separations. Ionic liquids and novel chiral ionic liquids are used as novel electrolytes for the polymer synthesis and for improvement of the electrochemical stability of chiral polyaniline doped with (+)-10-camphorsulfonic acid. Electroorganic syntheses using bare or chiral polyaniline modified electrodes in ionic liquids or chiral ionic liquid electrolytes are explored. Following an Introduction and a General Experimental Chapter, the new studies are described in Chapters 3 to 10.

Chapter 3 reports a novel route to prepare optically active emeraldine salts via thermal treatment. Emeraldine base films were prepared by alkaline de-doping of PAn.HCl emeraldine salt films electrochemically deposited or chemically prepared. Chemically prepared emeraldine base films were cast onto glass slides from NMP solution. Re-doping these films with aqueous (+)-10-camphorsulfonic acid (1.0 M (+)-HCSA) gave optically inactive PAn.(+)-HCSA films. Significantly, after heat treatment at 170°C, optically active polyaniline were generated, as evidenced by their circular dichroism spectra. This is believed to be due to the polyaniline chains preferentially adopting a one-handed helix under the influence of the chiral dopant CSA⁻ anion during heating of the films at temperatures above the glass transition temperature (T_g) of polyaniline.

An unprecedented route to optically active polyanilines from achiral reagents using a chiral emeraldine salt inducer is described in Chapter 4. This macromolecular asymmetric proliferation is performed via electrochemical polymerization of aniline in

racemic (e.g. (\pm) -HCSA) or achiral (e.g. HCl and *p*-TSA) acid solutions using a thin film of chiral PAn.(+)-HCSA or PAn.-)-HCSA pre-electrodeposited on the working electrode as a chiral inducer. The thin film of PAn.(+)-HCSA or PAn.-)-HCSA was deposited on ITO-coated glass electrodes using 25 mC/cm^2 electrodeposition charge, giving a thickness of *ca.* 100 nm. Remarkably, strongly optically active PAn.HA films of the same hand as the chiral inducer were produced during the second stage electrodepositions (another 100 mC/cm^2) using (\pm) -HCSA or achiral acids. A possible mechanism for this chiral induction is discussed. Experiments using deposition charges of between 50 and 300 mC/cm^2 in the second electrodeposition showed that induction by the thin PAn.(+)-HCSA film occurred undiminished for final films as thick as 700 nm. This novel asymmetric synthesis method presents potential applications such as using thin chiral polyaniline films as inducers for the electrochemical asymmetric synthesis of other chiral conducting polymers.

The fully sulfonated polyaniline poly(2-methoxyaniline-5-sulfonic acid) (PMAS) was found in Chapter 5 to be remarkably resistant to alkaline de-doping, even in 3 M NaOH or conc. NH_4OH . Instead of de-doping to the corresponding emeraldine base, UV-visible spectral studies showed that a change of conformation for the polyaniline chains from an “extended coil” to a “compact coil” arrangement occurred. However, when the sterically crowded amines tetrabutylammonium hydroxide (Bu_4NOH) and diisopropylamine were added to aqueous PMAS, de-doping of the “compact coil” emeraldine salt to emeraldine base was observed ($\text{pH} \geq 11.5$), as evidenced by the appearance of a characteristic absorption band at *ca.* 630 nm. The resistance to de-doping in NaOH and NH_4OH may therefore be associated with the electrostatic binding of the relatively small Na^+ and NH_4^+ ions to sulfonate (SO_3^-) groups on the PMAS chains, which is sterically hindered for the larger ammonium ions.

The redox switching properties of PMAS were also investigated in Chapter 5. The oxidation behaviour of PMAS was similar to that previously observed for unsubstituted polyaniline. However, an unexpected sharp peak at 408 nm was observed for the reduced leucoemeraldine base (LB) form of PMAS generated by treatment with aqueous hydrazine, together with the usual 330 nm peak of LB assigned as a π - π^* transition. Thermochromism and solvatochromism of the reduced PMAS species was observed involving reversible interconversion between the 408 nm and 330 nm species. These phenomena may involve a rearrangement of the PMAS leucoemeraldine base chains between two conformations.

A novel chiral composite is prepared in Chapter 6 by mixing aqueous solutions of PMAS and poly-L-lysine (PLL) and casting as films. The highest degree of chiral induction in the PMAS-PLL films was observed using a PMAS/PLL molar ratio of 1. The electrical conductivity of the PMAS-PLL (1:1) films was *ca.* 4×10^{-3} S/cm, an order of magnitude less than PMAS itself. The chiral PLL in the complex is believed to induce optical activity into the main chain of the PMAS moiety, as evidenced by its CD spectrum in visible region. The observed optical activity of the PMAS-PLL films may arise from the PMAS chains adopting a one-handed helical structure due to electrostatic interactions between free sulfonic acid groups on the PMAS with ammonium side chain groups on the PLL. The PMAS-PLL composite films remained optically active during treatment with 1.0 M NH_4OH and when reduced with hydrazine or oxidized with ammonium persulfate.

The temperature employed in the electrochemical polymerization of aniline is found in Chapter 7 to have a critical effect upon the chiroptical properties of PAn.(+)-HCSA films deposited on ITO-coated glass from aqueous 0.2 M aniline/1.0 M (+)-HCSA.

Films grown at elevated temperatures (35-65°C) have inverted CD spectra compared to analogous films grown at lower temperatures (0-25°C). These observations are explained in terms of a temperature-induced interconversion between two diastereomeric emeraldine salt products during the doping of the growing polyaniline chains with the chiral (+)-CSA⁻ anion. The critical effect of polymerization temperature found in this study highlights the importance of employing a controlled temperature during electrochemical synthesis of optically active polyanilines.

The influence of solvents on the chiroptical properties of PAn.(+)-HCSA emeraldine salt films prepared in ionic liquids are explored in Chapter 8. Polymerizations at high temperature (50-55°C) are required for dissolution of the (+)-HCSA (0.5 M) in all ionic liquids studied, except for (-)-MBEA-TFSI in which solvent HCSA is highly soluble at room temperature. Electroactive polyaniline can be prepared from the electrochemical polymerization of aniline in the presence of (+)-HCSA in the ionic liquids BMI-BF₄, BMI-PF₆, EMI-TFSI, P₁₃-TFSI and chiral (-)-MBEA-TFSI. Raman spectra of the films generally showed characteristics of emeraldine salts, and were very similar to those previously reported for PAn.HCSA synthesized via conventional methods. However, the polymer grown from EMI-TFSI showed different features indicating the presence of unusual chemical structures. These are probably generated by *ortho*-coupling and cross-linking during electropolymerization. The optical activity of the PAn.(+)-HCSA films grown from EMI-TFSI, BMI-BF₄ and P₁₃-TFSI were relatively low, and much less than previously observed for analogous films electrodeposited from aqueous solution, while the emeraldine salt grown from BMI-PF₆ was optically inactive. This probably arises from competition between chiral (+)-CSA⁻ and the achiral anions of the ionic liquids (BF₄⁻, TFSI⁻, PF₆⁻) as the dopant incorporated into the polymer during polymerization. An attempt to prepare a chiral emeraldine salt from electrochemical polymerization of

aniline with racemic (\pm)-HCSA using the novel chiral ionic liquid (-)-MBEA-TFSI as electrolyte was unsuccessful. Anodic degradation during polymerization at high positive potential (+1.3 V) apparently generated low molecular weight polyaniline oligomers whose length may be too short to maintain a helical structure, as the green product dissolved/dispersed in the polymerization solution.

The electrochemical and chiroptical properties of chiral PAn.(+)-HCSA emeraldine salts prepared in aqueous (+)-camphorsulfonic acid and investigated in ionic liquids are explored in Chapter 9. The nature of the ionic liquids employed and the applied potential have a marked effect on the stability of the chiral polyaniline films. Reversible loss of the electroactivity of the PAn.(+)-HCSA films occurred when the polyaniline films were potential cycled in the ionic liquids EMI-TFSI, BMI-PF₆ and BMI-BF₄. Electrochemical degradation of the polyaniline films occurred in EMI-TFSI and MBEA-TFSI electrolytes when they were polarized at high positive potentials ($> +1.1$ V). However, significantly, in BMI-PF₆ and BMI-BF₄ electrolytes the optical activity and electrochemical stability of the polyaniline films were retained at potentials as extreme as + 2.0 V. However, cross-linking involving a phenazine-type structure occurred when the PAn.(+)-HCSA films were exposed to high positive potentials in BMI-PF₆, as evidenced by their Raman spectra. Racemization of the PAn.(+)-HCSA films occurred when electrochemical reduction was carried out in all of the ionic liquids examined except (+)-, (-)-, or (\pm)-MBEA-TFSI. In the later ionic liquid electrolyte, strong CD signals were observed for the leucoemeraldine base film formed. Incorporation of the cation from the ionic liquids during the reduction (rather than expulsion of the (+)-CSA⁻ anion) and resultant swelling of the polyaniline films may be the reason for the racemization observed in the other ionic liquids.

These are important observations, since they open the possibility of using such PAn.(+)-HCSA films as chiral electrodes in electrochemical asymmetric syntheses in appropriate ionic liquids. BMI-PF₆ and BMI-BF₄ appear to have potential as electrolytes in electrochemical asymmetric oxidations (e.g. the oxidation of prochiral sulfides to chiral sulfoxides) at high positive potentials, while MBEA-TFSI would appear useful for electrochemical asymmetric reductions (e.g. the reduction of prochiral ketones to chiral alcohols) at very negative potentials.

Electroreduction of carbonyl compounds such as acetophenone and acetylpyridine to alcohols and electrooxidation of organosulfides such as methyl 4-nitrophenyl sulfide and methyl-*p*-tolyl sulfide to the corresponding sulfoxides in ionic liquids are explored in Chapter 10. The expected alcohol products were obtained from potentiostatic reduction of acetophenone and 2-acetylpyridine in EMI-TFSI on glassy carbon electrodes at -1.9 and -1.8 V, respectively. Reduction of 4-acetylpyridine in (-)-MBEA-TFSI on a glassy carbon electrode at -1.6 V yielded 4-pyridylethanol. However, the optical rotation of the product could not be measured due to interference from the chiral ionic liquid which could not be completely separated from the product. 4-Acetylpyridine was not reduced in (±)-MBEA-TFSI on a PAn.(+)-HCSA modified ITO-Pt-coated electrode to the corresponding alcohol, the corresponding achiral pinacol being instead formed.

Oxidation of methyl 4-nitrophenyl sulfide in EMI-TFSI and methyl-*p*-tolyl sulfide in BMI-BF₄ on glassy carbon electrodes was shown to yield the corresponding sulfoxides products. However, the asymmetric electrosyntheses of these sulfoxides in ionic liquids by using a chiral polyaniline modified electrode was not successful due to oxidative degradation of the polyaniline.

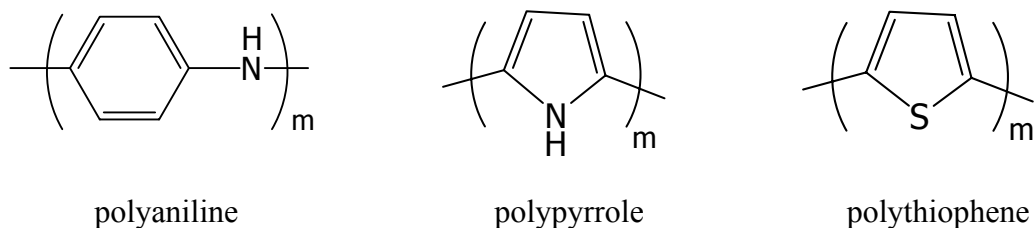
Chapter 1

Introduction

1.1 Conducting Polymers

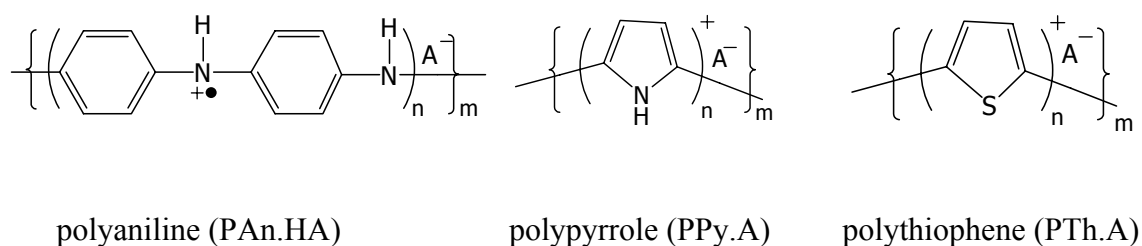
1.1.1 Introduction

A common feature of conducting polymers is conjugation of π -electrons extending over the length of the polymer backbone. The chemical structures of some common conducting polymers: polyaniline (PAn), polypyrrole (PPy) and polythiophene (PTh), are shown in Scheme 1.1 in their non-conducting (undoped) forms. It is seen that all have alternative single and double carbon-carbon bonds along their polymer chains.



Scheme 1.1

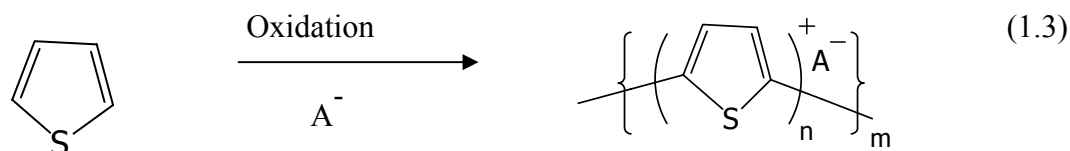
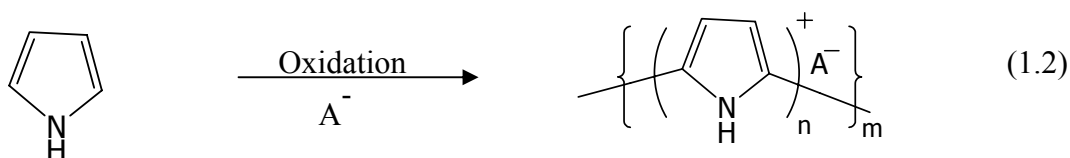
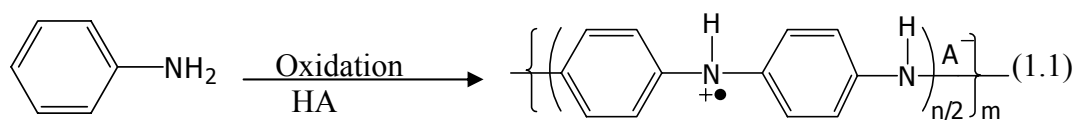
In their conducting forms, obtained by oxidation of the undoped forms, the polymers have positive charges located along their chains, as illustrated in Scheme 1.2.



Scheme 1.2

1.1.2 Synthesis of Conducting Polymers

Conducting polymers are commonly prepared through chemical or electrochemical oxidative polymerization of the appropriate monomers. An important step is the incorporation of a counteranion (dopant) into the polymer chains during polymerization to neutralize the electrical charge, a process called “doping”. The overall reactions for the synthesis of polyaniline, polypyrrole and polythiophene are shown in Equations (1.1), (1.2) and (1.3), respectively (A^- = dopant/counteranion).



1.1.3 Doping and De-doping in Conducting Polymers

A common characteristic of all organic conducting polymers is that the conductivity is dependent on the oxidation state of the polymer. A redox process, oxidation or reduction, causes a change in the electronic structure that allows it to conduct electricity. This process is called “doping”. “p-type doping” refers to a doping process that involves polymer oxidation and results in the formation of charge carriers that are holes, while “n-type doping” refers to a reductive doping process that results in the formation of charge carriers that are electrons. In turn, the term “de-doping” is used for processes that transform polymers from their conducting state to their insulating state. Oxidation (p-type) doping of conducting polymers results in the polymer backbone

being converted from a neutral polymeric chain to a polymeric cation. Subsequently, the overall charge neutrality of the polymer chain is preserved by incorporation of “dopant” counter anions (or cations in the case of reductive doping) into the polymer matrix. Thus, de-doping (reduction) of oxidized polymers generally results in the expulsion of these dopant counterions or ingress of cations.

Doping/de-doping is a reversible process which can be performed a number of times without significant change in the structure or properties of conducting polymers, leading to switching properties and colour changes in the polymer. The switching processes can be induced either chemically or electrochemically. In the latter case the polymer itself acts as the electrode in an electrochemical cell. In the electrochemical process, the level of oxidation or reduction of the polymer is controlled by the applied potential, and the ion movement involved in charge compensation is usually the anion (or cation for n-type doping) of the supporting electrolyte present in the electrochemical cell. However, in the case of large anionic dopants such as polyelectrolytes, cation movement may predominate in redox processes. For example, these alternative p-doping/de-doping processes for polypyrrole are presented in Figure 1.1.

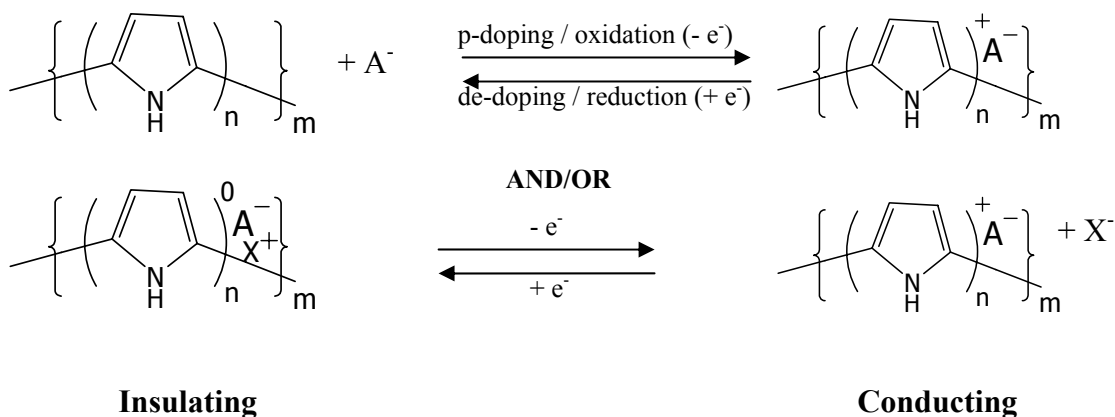
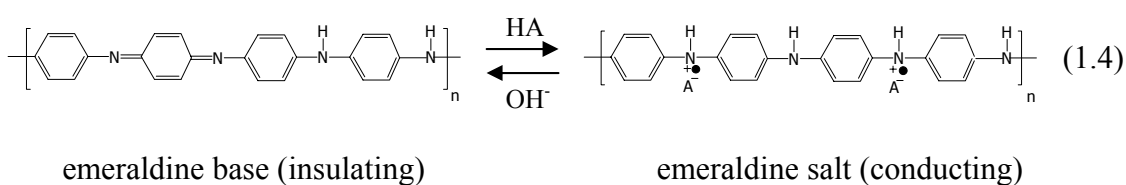


Figure 1.1 Electrochemical switching process for polypyrrole.¹

Doping Mechanism in Polyaniline

Polyaniline has a unique doping process among conducting polymers in that its conducting doped form can be obtained not only by oxidative p-type doping of leucoemeraldine base (LB), but also by protonic acid doping of emeraldine base (EB) (Equation 1.4). Moreover, p-type doping of polyaniline results in the formation of salts bearing nitrogen radical cations, while doping of other conducting polymers (e.g. polypyrrole and polythiophene) results in the formation of carbonium ions along the polymer chains.



1.2 Polyaniline

Polyaniline (PAN) has received much attention because of its electronic, thermoelectric and optical properties, as well as its good environmental stability and ease of synthesis. Polyaniline is also unique among organic conducting polymers in that its electrical properties are controlled by both its oxidation state and degree of protonation. Consequently, polyaniline is widely used for various applications such as rechargeable batteries,^{2,3} chemical transistors,⁴ supercapacitors,⁵⁻⁷ electrochromic displays,⁸⁻¹⁰ actuators,¹¹⁻¹³ sensors,¹⁴⁻¹⁷ and anti-corrosion coatings.^{18, 19}

1.2.1 Synthesis of Polyaniline

Polyanilines are commonly synthesized by chemical or electrochemical oxidation of aniline in acidic aqueous solution. However, other polymerization techniques have now been developed such as enzymatic,²⁰⁻²³ plasma,²⁴ ultrasonic irradiation,²⁵ photochemically initiated^{26, 27} and polymerization using electron acceptors.²⁸

The properties of polyanilines, such as morphology,²⁹⁻³¹ crystallinity,^{25,31} conductivity,³¹⁻³³ molecular weight,^{31,34} electrochemical behaviour,^{35,36} and processibility³⁷ strongly depend upon the method and conditions of preparation.

1.2.1.1 Electrochemical Polymerization

Electrochemical synthesis of polyaniline has some advantages including greater control over the oxidation potential and the fact that the products do not need to be exhaustively purified from excess monomer, oxidant and acid due to the deposition of polymer on the working electrode. The properties of the electrochemically deposited films are greatly influenced by the polymerization conditions employed^{38,39} such as monomer concentration,⁴⁰ counterion or supporting electrolyte,^{40,41} solvent, pH of the electrolyte,⁴² synthesis temperature,³⁰ deposition time, electrochemical technique (e.g. potentiostatic, potentiodynamic or galvanostatic),^{40,43} and working electrode substrate.^{40,}

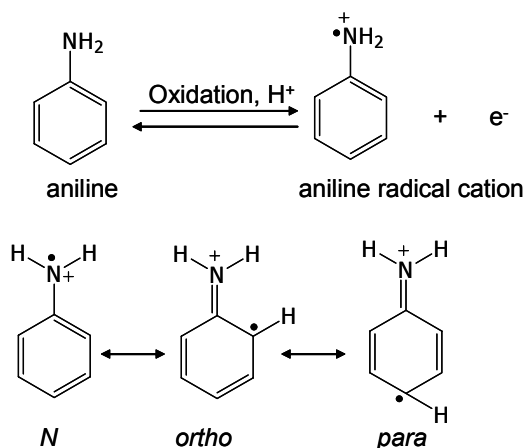
44

Mechanism of Electropolymerization. — The generally accepted mechanism of electrochemical oxidation is described as an electrochemical-chemical-electrochemical (ECE) process,⁴⁵⁻⁴⁷ as shown in Scheme 1.3. The polymerization is initiated by an electrochemical (E) process, and is propagated by the repetition of a chemical (C) process followed by an electrochemical (E) process. Oxidation of aniline (step 1) to form its radical cation on the electrode surface is independent of the pH of the synthesis medium, and is the rate-determining step of the process. There are three different resonance forms of the oxidized aniline radical. The forms with the radical on the *N*- and on the *para*-position of the aromatic ring are the most likely to react in a coupling reaction (step 2) to give a dimer, by elimination of two protons - so called “head-to-tail” or “*para*-coupling”. This dimer then undergoes re-aromatization to the neutral state, giving the *p*-aminodiphenylamine (PADPA) intermediate.

Although coupling between *ortho*-aniline radical cations is less likely to be involved due to electrostatic repulsion between the adjacent charged amine groups, *ortho*-coupling may proceed to a limited extent. This results in the formation of undesirable products.^{42,48} In propagation of the chain (step 3), the radical cation of the dimer/oligomer is oxidized at the potential required to oxidize the aniline and then couples with a *para*-aniline radical cation to increase the polymer chain length. The conducting emeraldine salt (PAn.HA) deposited on the working electrode is obtained from the simultaneous doping of the polymer by protonation (step 4) during chain propagation. As the intermediate species and polymers are in the cationic form, neutralization of charge is achieved by incorporation of counter anions (A^-) from the electrolyte. Autocatalytic polymerization of aniline has been observed.^{49,50}

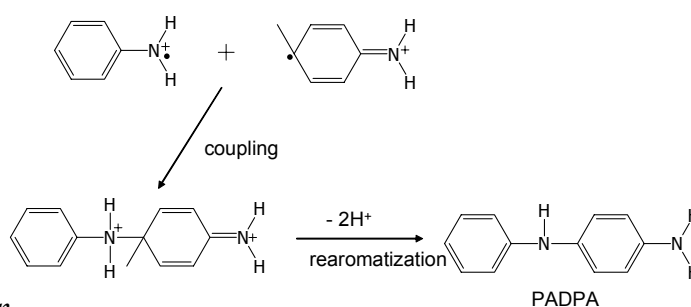
Polymerization in Aqueous Solution.— The electrochemical polymerization of aniline is usually carried out in acidic aqueous solution to maximize aniline monomer solubility, and electroactive and conductive polyaniline emeraldine salt films only form when the pH is less than 3.^{33,42,48} Unusual chemical bonds, *N-N* bonds characteristic of “head-to-head” coupling are observed for polyaniline electrodeposited at $pH > 3$.⁴² The unusual bonds interrupt the conjugation length of the polymer backbone⁴² leading to low conductivity of the polymer product. Acid (HA) solutions generally used include inorganic acids such as HCl, HF, H₂SO₄, HNO₃ and HClO₄, as well as large organic sulfonic acids such as camphorsulfonic acid (HCSA), *p*-toluenesulfonic acid (*p*-TSA) and dodecylbenzenesulfonic acid (DBSA) which also provide a sufficiently low pH. The conjugate base from these acids is the dopant anion (A^-) incorporated into the polymer chains during polymerization.

Step 1. Oxidation of monomer

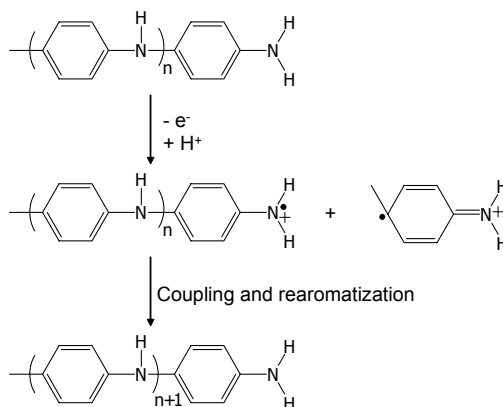


Resonance forms of aniline radical cation

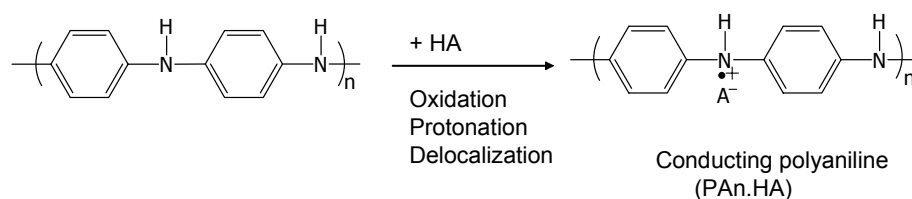
Step 2. Radical coupling and re-aromatization



Step 3. Chain propagation



Step 4. Oxidation and doping of the polymer



Scheme 1.3 Mechanism for the electrochemical polymerization of aniline in aqueous acid (HA) forming polyaniline emeraldine salt (PAn.HA).¹

The dopant anion incorporated affects the rate of deposition,⁵¹ the morphology,⁵¹ conductivity,^{13,51} and electrochemical behaviour^{35,52,53} of the polyaniline film. For example, sulfate anion promotes higher polymerization rates than do chloride or perchlorate ions. The conductivity of polyaniline emeraldine salt (PAn.HA) films electrodeposited from aqueous inorganic acids decreases in the order $\text{HClO}_4 > \text{HCl} > \text{HBF}_4 > \text{H}_2\text{SO}_4$.¹³ Moreover, films deposited slowly are denser and less porous than rapidly deposited films.

Polymerization in Non-Aqueous Solutions.— Electrochemical polymerization in non-aqueous electrolytes has also been investigated. The main objective has been to avoid degradation and undesirable side reactions during polymerization in aqueous electrolytes. In addition, there is no need to remove water from the deposited films before using in non-aqueous systems such as batteries. Several types of non-aqueous solvents have been used for preparation of electroactive polyaniline films. Miras *et al.*⁵⁴ have reported the electropolymerization of aniline in a protophobic solvent with a large donor number such as acetonitrile containing LiClO_4 as supporting electrolyte, without adding any acid. The formation of electroactive and conductive polyaniline can occur in such a solvent because the proton from oxidation of aniline is retained around the reaction layers and can protonate the polymer chain during growth. In contrast, electroinactive films were obtained from protophilic solvents such as propylene carbonate, DMSO and THF.

However, with the organic solvents acetonitrile,^{5,55} propylene carbonate^{55,56} and ethylene carbonate,⁵⁵ polymerization of aniline using the very strong organic acid trifluoroacetic acid (CF_3COOH) resulted in electroactive and conductive polyaniline and also enhanced the polymerization efficiency. However, polymerization of aniline in

1,2-dimethoxyethane (DME) containing LiClO_4 and CF_3COOH yielded an electrically inactive material.⁵⁵ Osaka *et al.*⁵⁶ reported that the mole ratio of CF_3COOH to aniline influences the electroactivity and morphology of the resultant polyaniline films. With $[\text{CF}_3\text{COOH}] / [\text{aniline}]$ less than one, electroactive films were obtained. Increasing the acidity of the polymerization solution improved the electroactivity and charge-discharge performance of the polymer. Osaka *et al.*⁵⁵ also found that the dielectric constant of the solvent plays an important role in the deposition of electroactive polyaniline, because protons dissociated from CF_3COOH in high dielectric constant solvents are necessary to generate protonated aniline radicals in the initial step of polymerization.

Another approach is the use of an organic solvent such as acetonitrile^{35,57} and propylene carbonate (PC)⁵⁷ containing anilinium tetrafluoroborate (ATFB) as supporting electrolyte and precursor for polyaniline. SEM photographs of the polyaniline films prepared in the various electrolytes were different.^{35,57} The Walden products (W , product of the viscosity and conductivity) of the polymerization solutions indicated that the degree of dissociation of ATFB in MeCN is smaller than in PC, which influences the charge-discharge properties of the polyaniline.⁵⁷

Pekmez and Yildiz⁵⁸ have prepared polyaniline by electropolymerization of aniline in the presence of anhydrous cuprous ions in acetonitrile containing tetrabutylammonium perchlorate as supporting electrolyte. During electropolymerization by potential cycling, *in situ* electrooxidation of Cu^+ ions to Cu^{2+} ions during the positive scans and *in situ* electroreduction of molecular H_2 to H^+ ions take place concurrently. Aniline can also be oxidized by electrogenerated Cu^{2+} ions, producing a much higher concentration of aniline cation radicals which enhances the polymerization efficiency. Without H^+ ions generated during polymerization, non-conductive polyaniline was formed.

Electrochemical preparation of polyaniline in ionic liquids was first investigated by Tang and Osteryoung in 1991.⁵⁹ A mixture of aluminum chloride with 1-methyl-3-ethyl-imidazolium chloride in different molar ratios was used as solvent and electrolyte for electropolymerization of aniline. Electroactive polyaniline was produced in all conditions. The oxidation potential of aniline in acidic melt was lower than in neutral and basic melts. By-reactions probably generating cross-linking and multiple substitution of the benzene ring occurred, resulting in a “middle peak” being observed in the cyclic voltammograms of the polymer films.

The electrochemical stability of polyaniline grown in 1-Butyl-3-methylimidazolium tetrafluoroborate (BMI-BF₄) containing 0.5 M aniline and 2.0 M CF₃COOH was greatly improved.⁶⁰ No significant degradation of the polymer was observed after potential cycling for up to 10⁶ cycles in BMI-BF₄.

In summary, there are two important factors in order to obtain conductive and electroactive polyaniline from electropolymerization in non-aqueous systems: sufficient concentration of protons and good ionic conductivity of the electrolyte. Polyanilines grown from non-aqueous media have the same molecular structures as those deposited from aqueous acid, with mainly “head-to-tail” or *para*-coupling of aniline monomers.^{55, 57, 61} This suggests that the mechanism of electrochemical polymerization of aniline in aqueous and organic solvents is the same.

Reagent Concentrations.— The influence of monomer and acid concentrations on the properties of polyaniline electrodeposited from aqueous media has been reported. Defective poly(2-methoxyaniline), having cross-linking with phenazine rings, was observed when the polymerization was carried out with low monomer concentration.⁶²

Product yield, morphology and electrochemical properties of the polyaniline produced by electrochemical synthesis from aqueous 0.5 M aniline in the presence of 0.5 - 2.0 M HClO₄ showed large differences with increasing acid concentration.⁶³ The surface morphology of electrodeposited polyaniline was granular when 0.5 M HClO₄ was employed, but fibrous for 2.0 M HClO₄.

Electrochemical Modes and Potentials.— The three electrochemical methods that have been employed for the polymerization of aniline are potentiostatic (constant potential), potentiodynamic (potential scanning) and galvanostatic (constant current).^{43,64} However, potentiostatic or potentiodynamic techniques are usually used because the overoxidation potential for polyaniline is very close to that required for monomer oxidation. Using the constant potential mode sometimes produces a powdery film which poorly adheres to the working electrode,⁶⁵ while using potential cycling generally produces a more homogeneous⁴⁹ film which adheres strongly to the electrode surface.^{65, 66}

Cyclic voltammetry of aniline in acidic solution initially shows an oxidation peak for the monomer at *ca.* 0.8 V (*vs* Ag/AgCl).⁶⁷ On subsequent cycles, two redox couples relating to redox switching between different oxidation states in deposited polyaniline appear at *ca.* -0.1 and 0.7 V.³⁸ The peak potential of the second redox reaction depends on the type of acid used as electrolyte⁶⁸ and the solution pH, with the oxidation potential of polyaniline shifting more positive with decreasing pH.^{40,69,70} If the polymerization of aniline is performed at a higher potential than the second voltammetric peak, defects and degradation of the polymer backbone are observed. A cross-linking reaction involving *ortho*-coupling of the nitrenium aniline cation (C₆H₅NH₂²⁺) with the nitrenium of the polyaniline chain (-C₆H₄N⁺ -) generated at high potential causes a two-dimensional polymer containing phenazine rings (Figure 1.2)⁶⁸. Cross-linking between

linear polymer chains (Figure 1.3), has also been proposed.⁷⁰ These unusual polymer structures result in low conductivity and insolubility.⁷⁰

Figure 1.2

Figure 1.2

Another undesirable reaction occurring at high potentials is oxidative degradation of the polymer due to nucleophilic attack at bipolaronic (dicationic) sites by water and electrolytes. This process causes a decrease in polymerization yield and the formation of soluble degraded products such as benzoquinone and hydroquinone.^{33,71-73} Faster degradation is observed at higher potentials⁷⁴ and higher acid concentrations.⁵³ Thus, electrochemical deposition of polyaniline is usually carried out using an applied potential as low as possible.

Substrates.— A variety of working electrodes have been employed, including platinum, glassy carbon, reticulated vitreous carbon (RVC), stainless steel, and indium-tin oxide (ITO)-coated glass.³⁹ The conductivity of the electrode has been reported to affect the electropolymerization process.⁴⁴ The efficiency of electrodeposition of polyaniline on platinum is higher than on ITO-coated glass electrode, as indicated by a higher amount of coloured oligomers dispersing into the aqueous medium during electropolymerization in the latter case.⁷⁵ The role of the electrode substrate on the stability of electrodeposited polyaniline and on charge transfer between the substrate and polyaniline has also been investigated.^{53, 76}

1.2.1.2 Chemical Polymerization

Polyaniline can be synthesized by oxidation of aniline using various chemical oxidants in acid solution. Chemical polymerization has the advantage of being a simple process capable of producing bulk quantities of polyaniline on a batch basis.

The major parameters affecting the course of the polymerization and the properties of the final product are: (1) nature of the solvent, (2) nature of the acid, (3) nature of the oxidant, and (4) the temperature. Although optimal conductivities are obtained when ammonium persulfate ((NH₄)₂S₂O₈) is used as oxidant,⁷⁷ other chemical oxidants such as ceric sulfate (Ce(SO₄)₂),³⁸ potassium dichromate (K₂Cr₂O₇),⁷⁸ potassium iodate (KIO₃),⁷⁹ hydrogen peroxide (H₂O₂),⁷⁹ and iron (III) chloride (FeCl₃)⁸⁰ have also been employed. For battery applications, Fe(ClO₄)₃ and Cu(BF₄)₂ are preferably used as oxidizing agents because the polyanilines produced contain ClO₄⁻ or BF₄⁻ anions, which are usually used in lithium batteries. Polyaniline chemically synthesized with Cu(BF₄)₂ is fibrous, while a granular shape is usually observed in polyaniline prepared using (NH₄)₂S₂O₈.⁸¹

Protonic acids used in aqueous polymerizations have been varied from strong inorganic acids, e.g. hydrochloric acid, hydrobromic acid, perchloric acid, sulfuric acid, and nitric acid, to large-anion organic acids such as camphorsulfonic acid (HCSA), dodecylbenzenesulfonic acid (DBSA) and *p*-toluenesulfonic acid (*p*-TSA).

Chemical synthesis of polyaniline has generally been carried out in aqueous solution at low temperature since this leads to polyanilines with high molecular weight^{82, 83} and less defect sites such as undesirable branching due to *ortho*-coupling.^{79, 84} At extremely low temperature (-30° and -40°C), high molecular weights of up to 400,000^{82, 83} have been

obtained. However, the reaction time required is more than 2 days and the polydispersity is relatively high ($PD > 2.5$). Consequently, the most widely used temperature for chemical polymerization of aniline monomers has been 0° - 5° C.

Mechanism of Chemical Polymerization

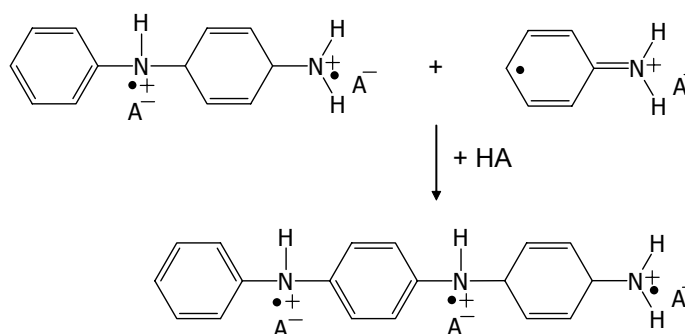
The reaction mechanism^{39, 85-87} now generally accepted for the synthesis of polyaniline with ammonium persulfate as the oxidizing agent is shown in Scheme 1.4. The first step involves formation of the radical cation of aniline. Subsequently, re-aromatization of the cation *p*-aminodiphenylamine (PADPA) occurs. This is then oxidized to a diradical dication. Although ‘head-to-tail’ (e.g. *N*-*para*) coupling is predominant, some coupling in the *ortho*-position also occurs, leading to defects in conjugation in the resultant polymer.^{88, 89} Chain propagation occurs in the third step - the diradical dication couples with the monomeric radical cation of aniline forming a trimer, and the chain propagates further via coupling of polymer fragment-radicals with the aniline radical cation. The resultant polymer is a pernigraniline salt. In the last step, when all oxidant is consumed, the remaining aniline reduces the pernigraniline to form the final product, the green emeraldine salt. Prolonged reaction times lead to degradation of the polymer,⁸⁵ especially with an excess of oxidant, as the pernigraniline form undergoes hydrolysis at the imine double bond more readily than the emeraldine form.

1.2.2 pH and Redox Switching Properties of Polyaniline

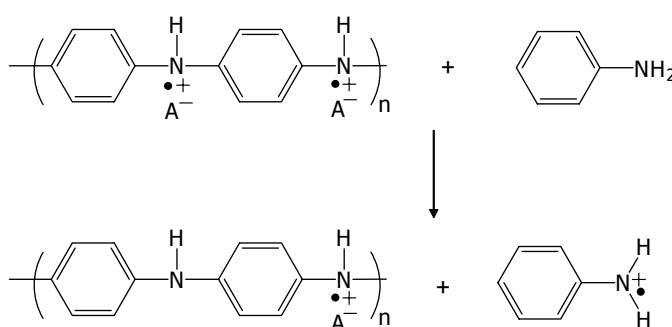
Polyaniline exists in a variety of forms that differ in the degree of oxidation of the polymer backbone and the degree of protonation of the imine nitrogen atoms. The oxidation state in the unprotonated (base, B) form and protonated (salt, S) form can vary from fully oxidized (pernigraniline: PB, PS), a repeat unit containing one benzenoid

ring and one quinoid ring, to the half-oxidized form (emeraldine: EB, ES), to that of the fully reduced form (leucoemeraldine: LB, LS) where the repeat unit contains two benzenoid rings (see Scheme 1.5).

Chain Propagation



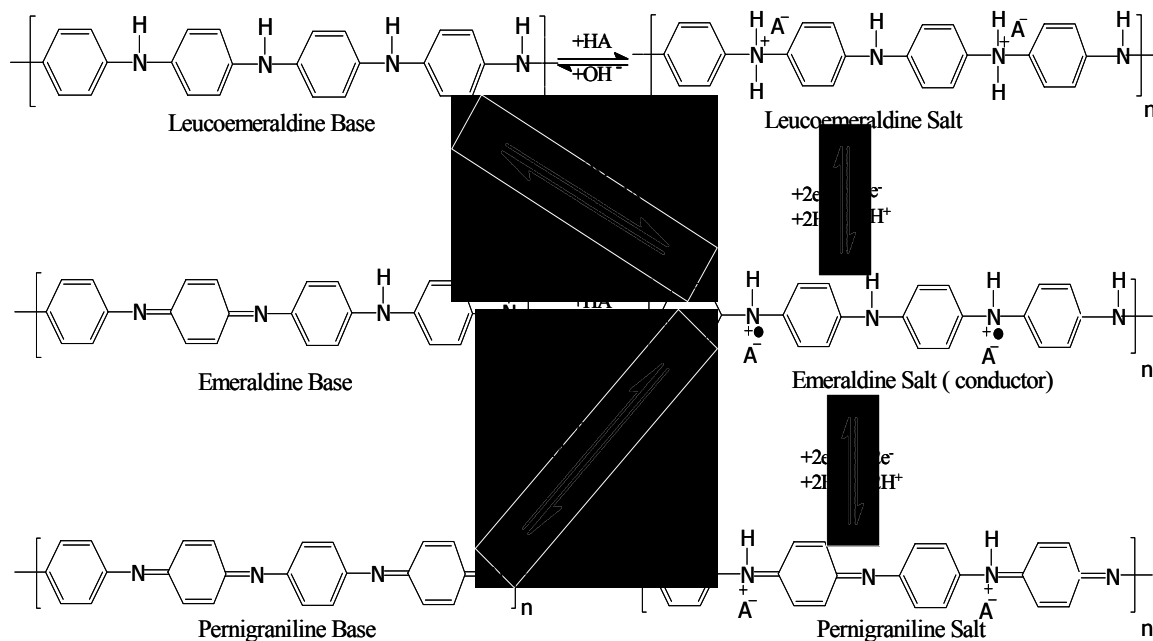
Reduction of Pernigraniline Salt to Emeraldine Salt



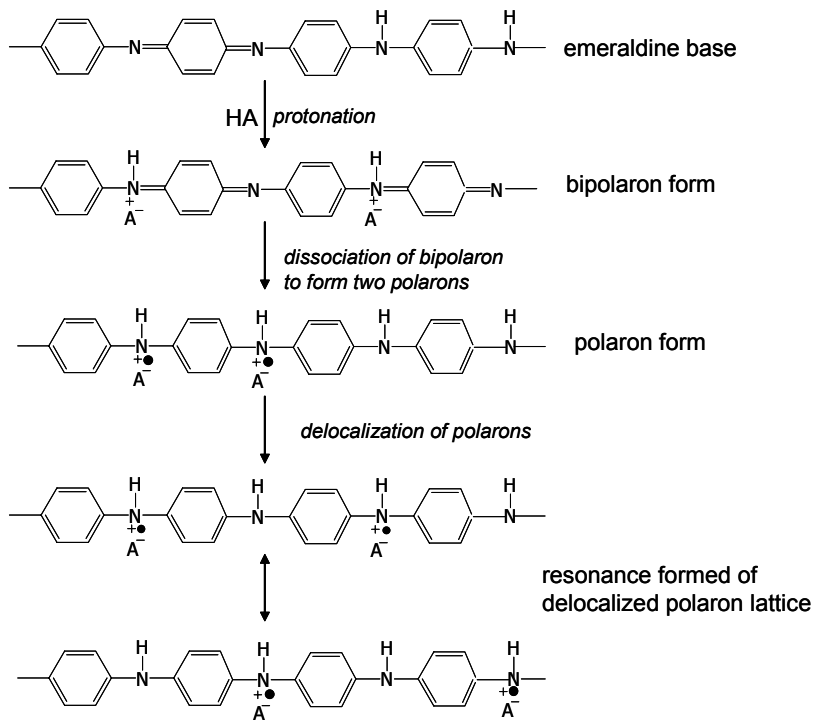
Scheme 1.4 Mechanism of chemical polymerization of aniline in aqueous acid (HA) forming polyaniline emeraldine salt (PAn.HA).¹

The three oxidation states of polyaniline can be interconverted by redox processes, achieved either chemically or electrochemically. Only the emeraldine salt form is conductive. The polymer can also be switched between the conducting emeraldine salt and the insulating emeraldine base forms by the addition of acids or bases, processes that are called doping and de-doping, as seen in Scheme 1.5.¹ It has been reported that de-doping can occur in neutral or low acidity solution (pH 3-6).⁹⁰ Protonation with acid (HA) of the imine nitrogens of emeraldine base (EB) gives a bipolaron which

dissociates into two polarons that then delocalize into a polysemiquinone radical cation, as shown in Scheme 1.6.



Scheme 1.5 Redox and pH switching of polyaniline.¹



Scheme 1.6

The colour and physical and chemical properties of polyaniline can thus be controlled by the application of a potential or by changing the pH. Importantly, the conductor-insulator switching of polyaniline is a function of the pH and applied potential.^{33, 73, 91} Characteristic colour and UV-visible spectral changes are also observed when the various redox reactions occur for polyaniline between -0.2 and 1.0 V.^{69, 74, 92}

Leucoemeraldine salt (LS) is reported to be formed by protonation of leucoemeraldine base (LB) only in extremely strong acid solution (e.g. $\text{pH} \leq -0.2$ in HCl),^{93, 94} while emeraldine and pernigraniline salt are generated by protonation of emeraldine and pernigraniline base, respectively, in acidic media ($\text{pH} \text{ ca. } 0-1$).^{85, 94}

1.2.3 Spectroscopic Properties of Polyaniline

1.2.3.1 UV-visible Spectra of Polyaniline

The UV-visible spectra of green emeraldine salts (ES), typically exhibit three absorption bands at *ca.* 350, 430, and 810 nm, assigned to a $\pi-\pi^*$ band, a π -polaron and a polaron- π^* band transition, respectively.^{85, 94, 95} Protonated emeraldine salt converts to the blue emeraldine base in neutral or basic medium and even at $\text{pH } 3-6$.⁹⁰ A colour change from green to blue accompanies this process. The emeraldine base (EB) exhibits two strong bands in UV-visible spectrum at *ca.* 340 and 620 nm.⁸⁵ These are assigned to a $\pi-\pi^*$ band and an exciton band transition, respectively.^{94, 96} The $\pi-\pi^*$ band is associated with the polymer benzenoid rings while the intermolecular charge transfer exciton is associated with the quinoid rings.⁹⁷

Colourless leucoemeraldine base (LB), generated via chemical or electrochemical reduction of emeraldine salt or base, shows only one absorption band in its UV-visible

spectrum at *ca.* 320 nm, assigned to a π - π^* transition.⁹⁴ Leucoemeraldine salt also exhibits a π - π^* band, at lower wavelength to leucoemeraldine base.⁹⁴

Violet pernigraniline base (PB) exhibits two strong absorption bands at 340 and 540 nm,⁸⁵ assigned to a π - π^* band and a Peierls gap transition,^{94,98} respectively. Blue protonated pernigraniline salts (PS) shows two strong absorption bands at *ca.* 350 and 690 nm⁸⁵ and is a different shade of blue compared to emeraldine base (EB). The colours, UV-visible absorption peaks and corresponding electronic transitions of the various polyaniline forms are summarized in Table 1.1.

Table 1.1 Colours, UV-visible absorption peaks and corresponding electronic transitions of polyaniline forms.

Polyaniline	Colouration	λ_{\max} (nm)	Electronic transition
Emeraldine salt	green	350, 430 and 810	π - π^* , π -polaron and polaron- π^*
Emeraldine base	blue	340 and 620	π - π^* and exciton
Leucoemeraldine salt	colourless	298	π - π^*
Leucoemeraldine base	pale yellow-green	320	π - π^*
Pernigraniline salt	blue	350 and 690	π - π^* and Peierls gap transition
Pernigraniline base	violet	340 and 540	π - π^* and Peierls gap transition

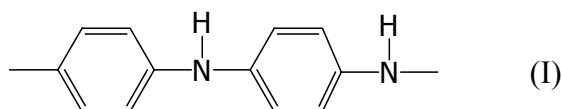
The absorption spectrum of polyaniline also depends on the conformation adopted by the polymer chains and on the conjugation length. For example, λ_{\max} for the longest wavelength absorption band of emeraldine salt is red shifted for polymers with longer conjugation length and/or replaced by a broad, strong free-carrier tail in the near-

infrared region. The λ_{\max} is red shifted to 1500 – 2500 nm when the polyaniline chain changes conformation from a “compact coil” to an “extended coil” conformation.^{95, 99} The conformation of polyanilines, and therefore the position of their UV-visible bands, has recently been shown to depend on the solvent (solvatochromism)¹⁰⁰ and the temperature (thermochromism).^{100, 101}

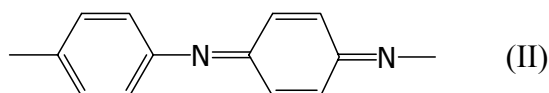
1.2.3.2 Raman Spectra of Polyaniline

There are four main electronic structures found in polyaniline chains depending on the oxidation and protonation state, as follows:

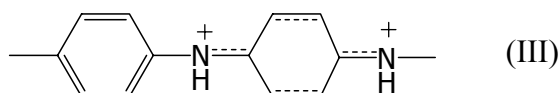
(i) unprotonated reduced segment of *para*-substituted benzenoid rings joined together by amine nitrogens,



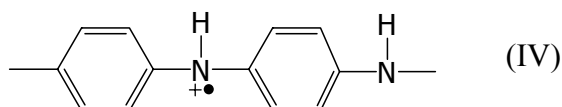
(ii) unprotonated oxidized segment consisting of benzenoid and quinoid rings joined together by imine nitrogens,



(iii) protonated oxidized segment (bipolaron form),



(iv) protonated oxidized segment (polaron form/ semiquinone radical cation).



Segment (I) is found in leucoemeraldine base (fully reduced) and part of emeraldine base (half-oxidized), while segment (II) occurs in emeraldine base (half-oxidized) and pernigraniline base (fully oxidized). The segments (III) and (IV) appear in only the emeraldine salt form.

Raman bands characteristic of polyaniline occur in the 1000-1700 cm^{-1} spectral range. For segment (I) there are three major Raman bands, associated with C-C stretching (*ca.* 1600-1620 cm^{-1}), C-H bending (*ca.* 1160-1180 cm^{-1}), and C-N stretching (*ca.* 1230-1255 cm^{-1}) of benzenoid rings.¹⁰²⁻¹⁰⁵ Bands characteristic of the bipolaron and semiquinone radical segments (III) and (IV) appear in the 1300-1350 cm^{-1} region at *ca.* 1317 and 1338 cm^{-1} .¹⁰⁶ The other forms of polyaniline do not give bands in this region.^{102, 104, 105, 107} Raman bands in the 1450-1580 cm^{-1} region are related to the oxidized, quinoid ring of segment (II). A band located at *ca.* 1580 cm^{-1} is ascribed to C=C stretching while the band at *ca.* 1470-1490 cm^{-1} originates from C=N stretching.¹⁰³⁻¹⁰⁷ A Raman band at *ca.* 1515-1520 cm^{-1} is associated with N-H bending deformations of polyaniline.¹⁰⁴ An unusual bond N=N stretch, arising from head-to-head coupling, is observed at *ca.* 1404 cm^{-1} .¹⁰⁸ Assignments of Raman bands of polyaniline are summarized in Table 1.2.

Table 1.2 Frequencies (cm^{-1}) and assignments of Raman bands of polyaniline.

Frequencies (cm^{-1})	Assignments
1160-1180	C-H bending
1230-1255	C-N stretching
1317-1338	C-N ⁺ stretching
1470-1490	C=N stretching
1515-1520	N-H bending
1580	C=C stretching
1600-1620	C-C stretching

1.2.4 Electrochemical Behaviour and Stability of Polyanilines

Redox processes in most conducting polymers are controlled by electronic and ionic charge transport. Cyclic voltammetry has been used to investigate the electronic and electrochemical properties of conducting polymers.

A typical cyclic voltammogram of polyaniline in aqueous acid is shown in Figure 1.4. The voltammogram exhibits two well-resolved peaks at $E_{1/2}$ ca. 0.2 and 0.7 V corresponding to two quasi-reversible redox processes. The first redox process corresponds to the conversion of amine units (leucoemeraldine base) to semiquinone radical cations (emeraldine salt), while the second redox process is attributed to the conversion of the emeraldine state into the pernigraniline fully oxidized form (complete quinoidal structure) (see Scheme 1.5). Only the emeraldine salt form is conductive. Results from *in situ* conductivity measurements on polyaniline films in aqueous sulfuric acid indicate that the polymer has a minimum in resistance between 0.3 and 0.5 V.³⁹

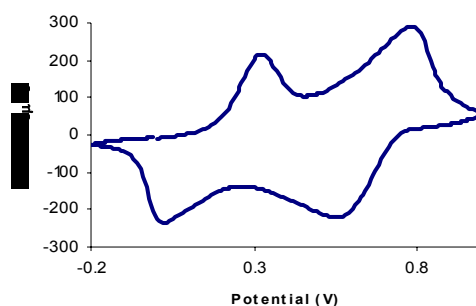


Figure 1.4 Cyclic voltammogram of a PAn.(+)-HCSA film on a glassy carbon disk (surface area = 0.07 cm²) electrode in supporting electrolyte 1.0 M HCSA. Scan rate: 50 mV/s.

For strong acid, the shape of cyclic voltammograms for polyaniline is independent of the nature of the aqueous acid electrolyte.¹⁰⁹ However, the redox peak potentials strongly depend on the film thickness, scan rate, and pH of the medium. The peak potentials move to more positive potential as the pH is decreased, due to partial or complete protonation of the amine nitrogens in the polymer under more acidic conditions.^{69, 91, 110} In the pH range -0.2 to -2.12 (1-6 M HCl), the $E_{1/2}$ of the first redox process moves to higher values at a rate of ca. 0.58 mV per pH unit as the pH is

decreased.^{76, 93} Voltammograms obtained for polyaniline films in electrolytes with $\text{pH} > 3$ exhibit ill-defined redox peaks due to merging of the two peaks with a simultaneous decrease in the current response,^{33, 110, 111} due to partial deprotonation of the amine nitrogens in the polymer chains. This loss in electroactivity at high pH is reversible.³⁹

In situ electrogravimetric studies show that the mass of the polymer increases and decreases during oxidation (charging) and reduction (discharging), respectively, at the first redox couple in aqueous media.^{39, 73, 109, 112} The mass changes depend strongly on the molecular weight of the anion present but there is no effect from the cation in the solution.⁷³ This indicates that anions in the medium are incorporated into the polymer films to compensate the positive electric charges generated during oxidation from leucoemeraldine base to emeraldine salt and then expelled during subsequent reduction. When the anion has a high charge to radius ratio, e.g. Cl^- , the anion involved in the insertion/expulsion process is solvated by the solvent.⁷³

Oxidative degradation of polyaniline has been observed in both potentiodynamic^{38, 74, 113} and potentiostatic experiments.⁷⁴ Cyclic voltammograms of polyaniline generally exhibit a small third redox couple at *ca.* 0.5 V vs. Ag/AgCl, called the “middle peak” by many researchers. When the anodic potential exceeds the second redox potential, the growth of the middle peak and simultaneously decrease of the initial two redox couples of the polyaniline are observed. There have been many interpretations for the origin of the middle peak. However, most researchers assign it to redox reactions of degraded products, either quinone or hydroquinone, generated from overoxidation of polyaniline and hydrolysis at imine sites,^{33, 71-73} or to cross-linked polymer containing phenazine rings generated by electropolymerization of aniline at high anodic potentials and/or by overoxidation of the polyaniline.^{68, 70, 71}

The mass decrease observed during the second oxidation process at *ca.* 0.7 V has been attributed to degradation of the hydrolytically unstable pernigraniline salt, the hydrolysis products being water soluble.⁷³ Due to the pH dependence of the second redox process, the electrochemical stability of polyaniline depends on not only the applied potential but also the pH. It has been reported that polyaniline is easier to oxidize and degrade at higher pH.^{33,69,73} The rate of degradation is potential dependent.⁷⁴

The electrochemical behaviour and stability of polyaniline also depends on the solvents and electrolyte employed. However, the number of reports in non-aqueous systems is much less than in aqueous electrolytes.

Desilvestro *et al.*¹¹² and Okabayashi *et al.*¹¹⁴ reported that perchlorate ions solvated by 2-3 molecules of propylene carbonate (PC) are inserted into the polymer during oxidation of polyaniline films in LiClO₄/PC solution. Garcia *et al.*¹¹⁵ reported that the release of water molecules simultaneously occurs together with anion exchange in LiClO₄/acetonitrile media, due to trace water in the polymer grown from aqueous solution.

Vanela and Torrsi¹¹⁶ have found that both the cation and anion of the supporting electrolyte and the solvent participate in the polyaniline redox mechanism. Swelling was more pronounced in higher dielectric constant solvents, which also allowed more cation movement together with the solvent. However, the major species participating in charge compensation process were the anion and the solvent.

Lu and Mattes¹³ have recently reported that the solubility of the dopant anion in non-aqueous electrolytes is a paramount factor affecting the electroactivity and actuation of polyaniline, because the insertion and expulsion of the anion in the charge compensation process are more facile.

Kabumoto and Shinozaki⁷⁴ reported that the degradation of polyaniline commences at about 0.7 V in the organic solvents DME and PC. The voltammograms in these non-aqueous electrolytes exhibit broadening and then gradual disappearance of the redox peaks due to decomposition of the polymer. A faster degradation rate was observed at higher applied potentials. The rate of degradation also depended on the organic solvent employed. Polymer chain scission was suggested to explain the degradation, because no major change in chemical structure of the polymer was detected by UV-visible and infrared spectra. Even trace water trapped within the polymer film resulted in hydrolysis of fully oxidized polyaniline in PC medium.¹¹²

In summary, the most important factors for the electrochemical behaviour and stability of polyaniline are the anion incorporated during polymerization and the solvent/electrolyte system used. The properties of the polyaniline can be controlled by the application of a potential and/or by changing the pH.

1.3 Self-doped Polyaniline

Polyanilines are generally insoluble in aqueous and most common organic solvents. To improve solubility and processability in organic solvents, large organic anions such as dodecylbenzenesulfonate or camphorsulfonate are used as dopants. To improve solubility and processability from aqueous media, sulfonation of the polyaniline chains is an option.

Partial sulfonation of polyaniline with sulfonic acid results in a material **1** (SPAN), that is able to self-dope the polyaniline backbone. SPANs in which 50 or 75% of the aniline rings are substituted with sulfonic acid groups are obtained by reaction of pre-formed emeraldine base or leucoemeraldine base, respectively, with fuming sulfonic acid.¹¹⁷⁻¹¹⁹

1 (SPAN)**2 (PMAS)**

A fully sulfonated polyaniline can be obtained via either chemical¹²⁰ or electrochemical^{121, 122} polymerization of the 2-methoxyaniline-5-sulfonic acid (MAS) monomer to produce poly(2-methoxyaniline-5-sulfonic acid **2** (PMAS)). In the PMAS dimer repeat unit, one sulfonic acid group is involved in self-doping while the other is free and can interact with a proton or other cationic species to form electrostatically bound complexes. However, these self-doped polyanilines generally have only moderate electrical conductivity presumably due to twisting of the polyaniline chains by the bulky substituents.^{118, 123, 124}

In contrast, unlike parent polyaniline, the conductivity of the self-doped sulfonated polyanilines does not depend on pH in the 1 to 14 range. This suggests that alkaline dedoping to their emeraldine base form is hindered.¹²⁵ Applications of sulfonated polyanilines have been focused to date on photovoltaic devices,^{126,127} sensors,¹²⁸ and rechargeable batteries.¹²⁹

1.4 Chiral Conducting Polymers

1.4.1 Chirality

A chiral molecule is one that is not superimposable on its mirror image (enantiomer). Enantiomers have identical chemical and physical properties in non-chiral environment. For example, they have identical melting points, boiling points, solubility and electronic absorption spectra. However, enantiomers interact with plane-polarized light in opposite ways. The enantiomer causing a clockwise rotation of the plane polarized light is called the dextrorotatory (+)- or *d*-isomer, while that causing an anti-clockwise rotation is

termed the laevorotatory (-)- or *l*- isomer. This phenomenon is called optical activity. A chiral compound composed of equimolar amounts of two enantiomers is called a racemate and is optically inactive.

Circular dichroism (CD) is the most sensitive and powerful method for the measurement of the optical activity of chiral molecules. The difference ($\Delta\epsilon$) in the molar extinction coefficients for left and right circularly polarized light passing through a sample of the compound is measured in this technique.

$$\Delta\epsilon = \epsilon_L - \epsilon_R$$

Individual enantiomers often exhibit different properties in chiral environments such as biological systems, which contain many chiral compounds such as proteins, carbohydrates and nucleic acids. This means that the biological activity of an enantiomer may differ markedly from that of its mirror image. One form can have a desirable therapeutic effect while the other may be useless or even toxic. Due to this, the use of enantiomerically pure compounds in pharmaceuticals and agricultural chemicals has grown greatly in importance in recent years. There is a growing concern against marketing of racemates.

Stereoselectivity in biological activity may be related to the interaction between an enantiomer and a chiral biological receptor. Senses of taste and smell are highly sensitive to stereochemical differences in the molecules that stimulate them. For example, *R*-carvone has the odor of spearmint but *S*-carvone smells like caraway. Similarly, the *L*-enantiomers of many amino acids such as leucine, phenylalanine, tyrosine and tryptophan taste bitter, while the corresponding *D*-enantiomers are sweet. For chiral agrochemical compounds, it has been noted that only one form may be active. For example, with the fluazifop butyl herbicide, only the (*R*)-form has the desired effect.

Thalidomide which was used in the early 1960s to treat morning sickness during pregnancy is perhaps the best known case used in arguments against the marketing of racemic pharmaceutical products. Only one enantiomer of thalidomide is effective against morning sickness, while the other is teratogenic.¹³⁰

1.4.2 Chiral Conducting Polymers

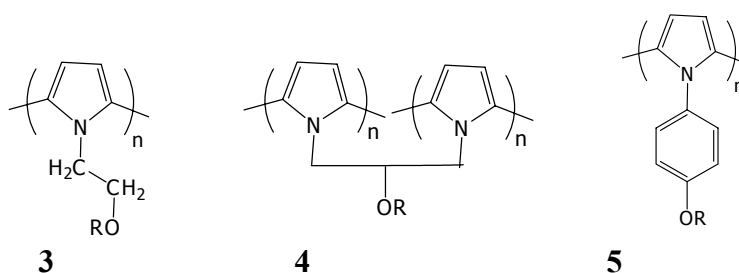
Following the first reports of chiral polypyrroles in 1985 by Baughman *et al.*,¹³¹ there has been considerable interest in optically active conducting polymers due to their potential applications in areas such as asymmetric synthesis, chiral separations and chiral sensors.

The two types of chirality mostly found in chiral conducting polymers are central chirality and helical chirality. Central chirality typically arises when a carbon atom in a molecule has four different groups attached to it in a tetrahedral arrangement. Polymers such as polyanilines whose backbones can have a helical structure can adopt either a left- or right-handed twist giving rise to helical chirality. A helix with a right-handed screw sense is symbolized by P (plus) and a left-handed helix by M (minus).¹³²

Optically active conducting polymers have been prepared via polymerization of (i) monomers bearing chiral substituents, (ii) achiral monomers in the presence of a chiral dopant anion, or (iii) achiral monomers in the presence of a chiral template/ substrate. The induction of chirality in pre-formed achiral conducting polymers such as emeraldine base may also occur via acid-base or electrostatic interactions with chiral acids.

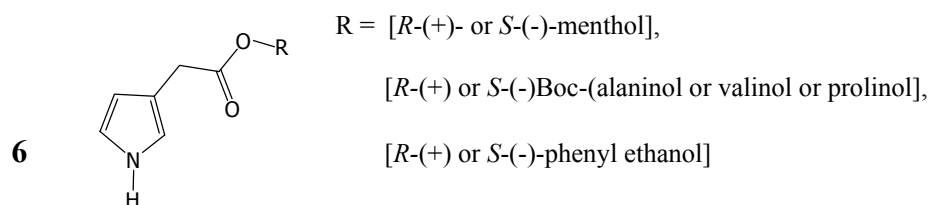
1.4.2.1 Chiral Polypyrroles

Most chiral polypyrroles have been synthesized via polymerization of monomers bearing chiral substituents at the 3-position on the pyrrole ring or containing chiral *N*-substituents. Salmon and Saloma¹³³ described the synthesis of stable optically active pyrrole monomers (**3-5**). Baughman *et al.*¹³¹ similarly prepared various pyrrole monomers bearing chiral substituents on the nitrogen atom. However, electrochemical polymerization resulted in polymers with low electrical conductivity compared to unsubstituted polypyrrole.

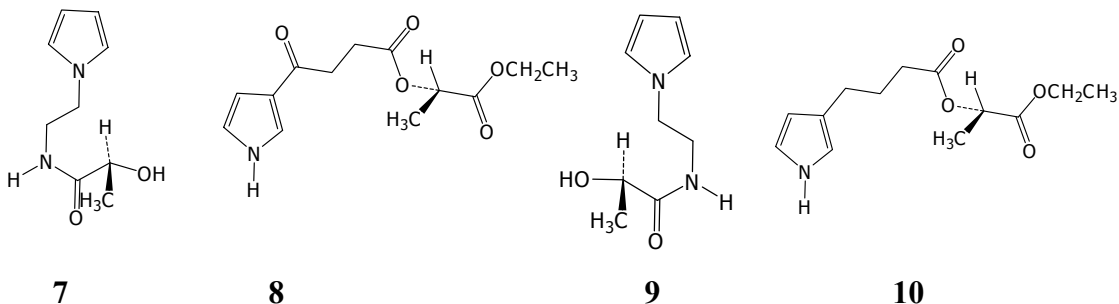


R = (+)- camphor-10-sulfonyl group

Costello *et al.*¹³⁴ recently prepared a series of chiral polypyrroles via polymerization of 3-substituted pyrrole monomers (**6**) possessing chiral ester substituents. Polymerization was carried out in aqueous/acetonitrile solution using ferric ions as oxidizing agent. Chiral discrimination properties were found for chiral vapor phase sensors fabricated from these polymer materials.



Recently, Pleus *et al.*¹³⁵⁻¹³⁷ have synthesized a series of *N*- and 3-substituted pyrrole monomers (**7-10**), which were polymerized electrochemically. Although the optical activity of the polymer films was not investigated, enantioselectivity of the polymers synthesized from **7** and **8** was reported.

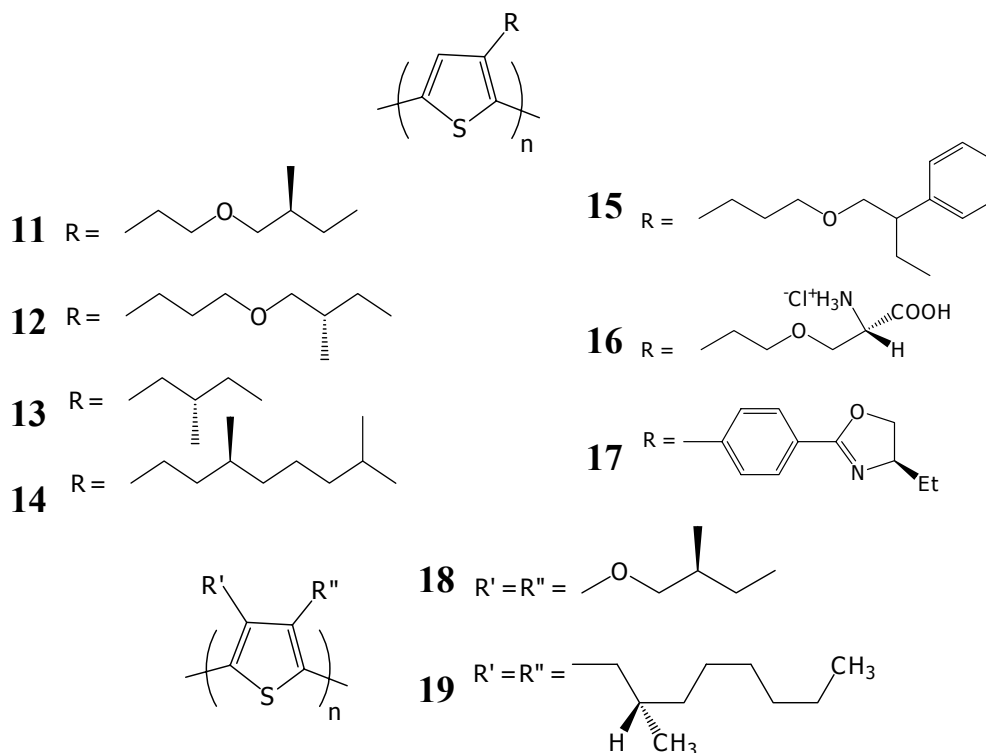


1.4.2.2 Chiral Polythiophenes

The preparations of chiral polythiophenes have generally involved the polymerization of thiophene monomers containing chiral substituents covalently bound at the 3-position (**11-17**) or di-substituted at the 3- and 4-positions (**18-19**). The strong optical activity of the polymers measured by circular dichroism spectroscopy was attributed in early reports (**15** and **16**¹³⁸⁻¹⁴⁰) to the adoption of a one-handed helical conformation by the polymer chains under the influence of the chiral side chain. However, an elegant series of papers by Meijer *et al.*¹⁴¹⁻¹⁴⁶ suggest that chiral induction is associated with the aggregation of the polymer chains to give supramolecular helical structures. This hypothesis is supported by the fact that optical activity is only observed when the polymer is in a “poor” solvent or when cast as a film. The only exception appears to be polymer **18**, which in “good” solvents such as chloroform, THF and iso-octane exhibits bisignate Cotton effect in the near-UV region.

These chiral poly(alkylthiophenes) also exhibit thermochromism (**11**¹⁴⁴, **12**¹⁴⁴, **18**¹⁴¹) and solvatochromism (**11**¹⁴⁴, **12**¹⁴⁴, **14**¹⁴⁷, **16**¹⁴⁸, **17**^{139, 149}, **18**¹⁴¹). Thus, upon heating or adding of a “good solvent”, a marked blue-shift is observed for the π - π^* absorption band. Improved regularity in of poly(3-alkylthiophene)s results in enhanced electrical conductivity and optical properties due to a longer conjugation length.^{150, 151} A comparison of the chiroptical properties of regioregular and regioirregular (**11** and **14**)

revealed that the regioregularity in the side-chain substitution pattern is very important to obtain high optical activity. This is probably due to a high degree of interaction order in the regioregular form.¹⁴⁷

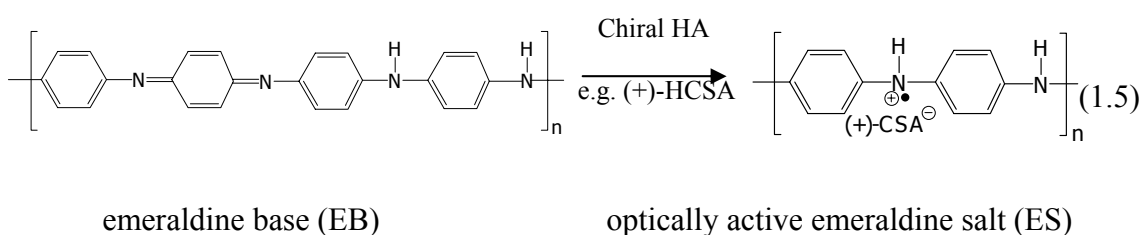


Polymer **16** containing amino acid functionalized side chains exhibits pH-dependent absorption, emission, and circular dichroism spectra in aqueous solution.^{140, 152, 153} The protonation and deprotonation of the zwitterionic group in the amino acid side chain is believed to be responsible for the conformational changes and aggregation /separation of the polymer chains.

The chiral aggregated polymer **17** exhibits a CD signal in the π - π^* region in the presence of a “poor” solvent (acetonitrile), or with added metal salt in a “good” solvent (chloroform). The chirality of the supramolecular aggregates in a “poor” solvent (chloroform/acetonitrile mixture) can be switched “on” and “off” through a doping and undoping process by adding copper (II) trifluoromethane sulfonate and triethylenetetramine, respectively.^{148, 149}

1.4.2.3 Chiral Polyanilines

Chiral polyanilines were initially prepared either by electrochemical polymerization of aniline in the presence of aqueous (+)- or (-)-10-camphorsulfonic acid (HCSA)^{64, 154} or the doping of pre-formed emeraldine base with one hand of a chiral acid (**20-25**) in organic solvents.¹⁵⁵⁻¹⁵⁸ Chirality in the polymer backbone was confirmed by the presence of circular dichroism bands in the visible region, whereas the chiral CSA⁻ dopant does not exhibit circular dichroism bands in this region. Doping via Equation 1.5 of pre-formed emeraldine base (EB) with the structurally diverse group of chiral sulfonic, phosphoric and carboxylic acids shown in Figure 1.5 gave optically active PAn.HA emeraldine salts with similar CD spectra. This suggested that hydrogen bonding between the acid and the polyaniline chains is not important in the polymer adopting its chiral structure.¹⁵⁸



Doping of the chiral dopant anions into the polymer structure during either electropolymerization in water or during doping of EB in organic solvents has been suggested to cause the polyaniline chains to adopt a one-handed helical conformation.^{64, 154-156} Alternatively, the optical activity observed in the emeraldine salt products may arise from the formation of chiral supramolecular aggregates in which the polyaniline chains are nearly planar.¹⁵⁷ Supporting the latter suggestion is the observation that no optical activity in the visible region was observed for PAn.(+)-HCSA produced by doping EB with (+)-HCSA in a “good” solvent such as *m*-cresol.²⁸

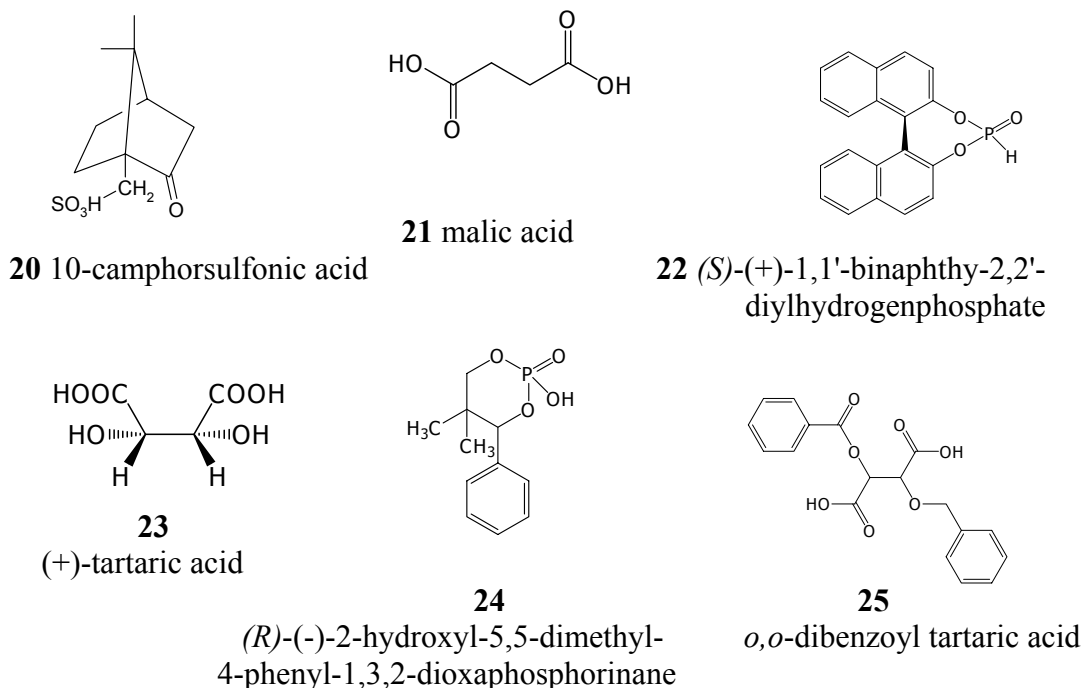


Figure 1.5 Structures of some chiral dopants used to produce optically active polyanilines.

PAn.(+)-HCSA and PAn.(-)-HCSA films produce mirror imaged circular dichroism spectra.¹⁵⁵ Interestingly, electrochemically and chemically prepared PAn.(+)-HCSA films show markedly different features in their UV-visible and circular dichroism spectra. This is attributed to different conformations for their polyaniline chains, namely “extended coil” and “compact coil”.¹⁰¹

Alternative routes to optically active polyaniline doped with one-hand of camphorsulfonic acid have been reported using *in situ* chemical polymerization¹⁵⁹ or the strong electron acceptor 2,3-dichloro-5,6-dicyanobenzoquinone (DDQ) in an organic solvent.²⁸ The CD spectra of the PAn.(+)-HCSA films prepared in both cases are quite different from those previously reported for PAn.(+)-HCSA films prepared by electrodeposition in water.^{64,154} These observations again indicate that the conformations of PAn.(+)-HCSA emeraldine salts depend on the synthetic route.

Chiral polyaniline colloids^{160, 161} and nanocomposites¹⁶²⁻¹⁶⁴ have also been synthesized. Routes include chemical,^{162, 163} electrochemical^{160, 161} and enzymatic¹⁶⁴ polymerization of aniline in the presence of chiral HCSA as dopant and with poly(acrylic acid) (PAA) as a template,^{162,164} or polystyrene sulfonate (PSS) as a steric stabilizer.^{160,161} Interestingly, a positive CD band at 420 nm is observed for chiral PAn.HCSA enzymatically synthesized whether the chiral dopant is either (+)-HCSA or (-)-HCSA.¹⁶⁴ This suggests that the hand of the polymer product is determined by the enzyme rather than the hand of the dopant anion present.

Chiral poly(2-methoxyaniline).HCSA emeraldine salts (POMA.(+)-HCSA and POMA.(-)-HCSA) can also be prepared by either the electropolymerization of 2-methoxyaniline in the presence of one enantiomer of HCSA or via doping pre-formed emeraldine base of POMA with one hand of HCSA. The bisignate CD bands of POMA.(+)-HCSA and POMA.(-)-HCSA films exhibit mirror imaged CD spectra in the visible region, suggesting the adoption of opposite helical hands for the POMA chains in the two polymers.^{165, 166}

The alternative use of chiral ammonium cations for chiral induction has been recently successfully used to prepare optically active poly(2-methoxyaniline-5-sulfonic acid) (PMAS). Chiral induction is believed to involve acid-base interaction between free acidic SO₃H groups on the polymer chain and the chiral amines and amino alcohols shown in Figure 1.6.^{121, 167}

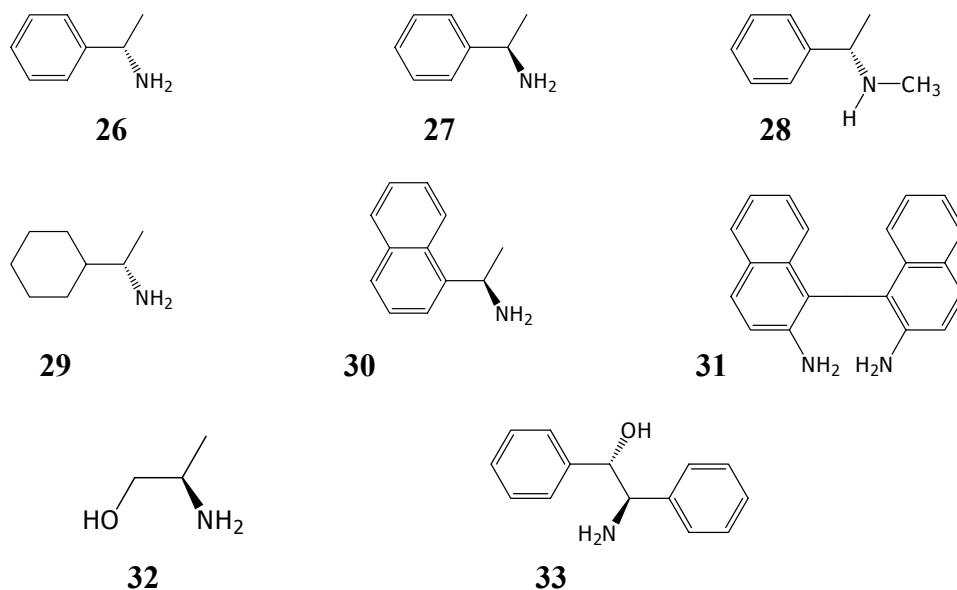


Figure 1.6 Structures of chiral amines and amino alcohols used to prepare optically active PMAS.

1.5 Potential Applications of Chiral Conducting Polymers

As discussed earlier in Section 1.4.1, the chirality of pharmaceutical and agricultural products is a very important issue. A recent analysis has revealed that the active ingredients in nine of the top ten drugs marketed worldwide are chiral. However, only six of these are currently sold as single enantiomers while the others are marketed as racemates.¹⁶⁸ Demand for optically pure compounds continues to rise, primarily for use in pharmaceutical industries but also in three other sectors: food chemicals, agricultural chemicals and specialty chemicals. A survey by Frost& Sullivan estimates that global sales of single-enantiomer compounds are expected to reach \$15 billion by the end of 2009, growing annually by about 11%.

This increasing demand for optically pure compounds has increased pressure on the chemical and pharmaceutical industries to develop new or more efficient processes for the production of such compounds in only the one desired enantiomeric form. Two general approaches have been employed to obtain such single-enantiomer drugs: (a)

chiral separation, and (b) asymmetric synthesis. The optical activity and potential stereoselectivity of chiral conducting polymers might have useful applications in this area, including their use as enantioselective chromatographic phases or enantioselective membranes for chiral separations, and as chiral modified electrodes for asymmetric electrosynthesis or for enantioselective electrochemical detection (chiral sensors).

For electrochemical asymmetric synthesis, chiral conducting polymers might be used as optically active polymer-coated electrodes which could induce the formation of asymmetric centers during redox reactions of prochiral organic substrates. For chiral separations, chiral conducting polymers are very promising because they could be used as chiral stationary phases for gas and/or liquid chromatography and for membrane-based separations. For chiral discrimination in sensors, the utilization of chiral conducting polymer modified electrodes for stereoselective analyses also has an interesting prospect.

1.5.1 Chiral Separations

Achiral polypyrrole has been developed for use in chromatographic stationary phases.^{169, 170} Recently, Nagaoka *et al.*¹⁷¹⁻¹⁷³ prepared molecularly imprinted polypyrrole by overoxidation of polypyrrole doped with L-lactate¹⁷² and L-glutamate.^{171,173} These chiral dopant anions were removed during electrochemical overoxidation and a complementary cavity for the anion created. The resultant imprinted polypyrroles exhibited high enantioselectivity for the L-acids over the D-enantiomers. A column packed with carbon fibers modified with the imprinted polypyrroles was used for the enantioselective uptake of the particular acid anion.

Separation of enantiomeric amino acids using chiral conducting polymer membranes has also been reported by Ogata.¹⁷⁴ The enantioselective membranes were prepared by electrodeposition of polypyrrole in the presence of the chiral dopants poly(L-glutamic acid) or dextran sulfate onto a platinum-coated poly(vinyl difluoride) membrane. The chiral separation of racemic tryptophan was demonstrated.

Kaner *et al.*¹⁷⁵⁻¹⁷⁷ have recently reported enantiomeric discrimination of amino acids by chiral polyaniline films. The emeraldine base form of polyaniline doped with (*S*)-(+)- or (*R*)-(-)-10-camphrosulfonic acid was used to separate racemates of DL-amino acids. The interactions of the chiral polyaniline films with amino acids suggested that the chiral recognition ability of dedoped polyaniline is size and shape dependent. These properties may be useful in the use of chiral polyaniline as a chiral stationary phase for chromatography.

1.5.2 Chiral Sensors/Analysis

Recently, Costello *et al.*¹³⁴ prepared chiral vapour phase sensors based on chiral polypyrroles. Chiral 3-substituted pyrrole monomers were synthesized and subsequently polymerized via chemical oxidation. The chiral polypyrroles were fabricated into chiral sensors using a three-step process: (1) coating of the chiral monomer onto poly(vinylidene)difluoride (PVDF) membrane, (2) polymerization of the monomer within the membrane structure using an excess of aqueous ferric chloride oxidant, and (3) mounting the membrane between silver contacts to obtain the sensor. Chiral discrimination and quantitative sensor properties of the sensors were investigated using enantiomers of butanol, limonene and carvone. The chiral polymer sensors were found to show differential changes in electrical resistance and mass when exposed to different enantiomers in the vapour phase. The results suggested that the chiral side group on the

pyrrole repeat units plays the main role in the selective adsorption characteristics of the polymers.

1.5.3 Asymmetric Electrosynthesis

In principle, asymmetric synthesis is the most economically effective and environmentally conservative method for producing optically pure compounds, because the entire precursor is converted to the desired enantiomer. Basically, the chiral polymer environment may force the substrate/reactant into a specific geometric order, which is reflected by the extent of the asymmetric induction.¹³⁶ To date almost all asymmetric syntheses have been achieved by either chemical or enzymatic routes. However, interest has recently grown in an alternative electrochemical approach to asymmetric synthesis in which a prochiral substrate is electrochemically oxidized or reduced in a chiral environment to produce enantiomerically enriched or pure chiral products.

If successful, this electrochemical route to asymmetric synthesis would have advantages over more conventional chemical^{178,179} and enzymatic methods.¹⁸⁰⁻¹⁸² For example, synthetic steps such as the attachment and removal of chiral auxiliaries would not be required, and operation may be possible in a wider range of solvents than with enzyme-based systems.

Several different routes to achieve asymmetric induction in electrochemical reactions have been reported, including the use of chiral solvents,¹⁸³ chiral supporting electrolytes or chiral additives,^{184, 185} chiral redox mediators,¹⁸⁶ and chiral modified electrodes.¹⁸⁷⁻¹⁹³ However, electrochemical reactions occur at the surface of electrodes. Therefore, using electrodes as the chiral auxiliary would seem to be an excellent approach to asymmetric synthesis, because extremely small amounts of chiral inducers (which are permanently

bound at an electrode surface) would be required. Chiral layers can be attached to electrode surfaces through strong adsorption or by design and synthesis of covalent linkages to the molecular layer.

The use of optically active alkaloids adsorbed at the electrode surface for asymmetric reduction of 4-methylcoumarin and related coumarins has been reported¹⁹⁴. Chiral electrodes have also been prepared by modification of graphite^{188, 190}, DSA (tantalum and iridium oxides) and SnO₂¹⁸⁹ surfaces by the covalently linked optically active amino acid (*S*)-(-)-phenylalanine methyl ester. These chiral modified electrodes were used to perform asymmetric reduction of 4-acetylpyridine^{188,190} and asymmetric oxidation of *p*-tolyl methyl sulfide^{188, 189} and nitrobenzyl methyl sulfide.¹⁸⁹ Optically active alcohols and sulfoxides, respectively, were produced with chemical and electrical yields > 90% and enantiomeric excesses of *ca.* 2-2.5%.

Nonaka *et al.*¹⁹¹⁻¹⁹³ were the first to prepare chiral polymer-coated electrodes for asymmetric electrosynthesis. Poly-L-valine was initially coated on graphite electrodes by dip-coating and the chiral modified electrode used for the asymmetric reduction of citraconic acid and 4-methylcoumarin.¹⁹¹ The highest optical yields of the products methylsuccinic acid and 3,4-dihydro-4-methylcoumarin were 25 and 43% *ee*, respectively. In an attempt to improve the optical yield, poly-L-valine was alternatively (i) coated onto bare platinum electrodes or polypyrrole films that had been electrodeposited on Pt, or (ii) covalently immobilized on the platinum surface. Electrochemical asymmetric oxidation of phenylcyclohexyl sulfide gave optically active phenylcyclohexyl sulfoxide product with optical yields of 28, 40, and 54% *ee*, respectively, for these three types of chiral electrodes.^{192, 193}

In recent work, Pleus *et al.*¹⁸⁷ reported the synthesis of chiral polypyrroles by anodic polymerization of chiral pyrrole monomers containing *N*- and 3-substituted chiral moieties. These were used to prepare chiral polypyrrole modified platinum electrodes for the asymmetric electroreduction of acetophenone and 4-methylbenzophenone in DMF/LiBr in the presence of phenol as proton donor. The nature of the electrolyte used for electrodeposition of the polymers influenced the optical purity of the chiral alcohol products produced. In the best case, reduction of 4-methylbenzophenone gave a chemical yield of 80 % and an optical yield of 17% *ee*.

1.6 Ionic Liquids

1.6.1 General Overview

Ionic liquids (ILs) are salts that are generally liquids at temperatures below 100°C. Synonyms of ionic liquid are low/ambient/room temperature molten salt, ionic fluid, liquid organic salt, fused salt, and neoteric solvent.^{195, 196} The first ambient temperature ionic liquid (ethylammonium nitrate, [EtNH₃][NO₃], with melting point 12°C) was discovered in 1914.¹⁹⁷ Interest developed rapidly after the discovery of an ionic liquid made from mixtures of *N*-ethylpyridinium bromide and aluminium chloride.¹⁹⁸ Many kinds of ionic liquids involving the tetrachloroaluminate salt have since been synthesized.^{195, 199}

However, the chloroaluminate salt ionic liquids are moisture-sensitive. In the presence of water, aluminium tetrachloride hydrolyses to form hydrochloric acid. This undesirable property has limited their applications. Therefore, air and water stable ionic liquids such as organic salts of nitrate, hexafluorophosphate, tetrafluoroborate, and bis(trifluoromethanesulfonyl)imide (TFSI) anions have been subsequently prepared. They are usually formed by reacting quaternary ammonium salts with acids like HBF₄

and HPF_6 . The development of ionic liquids that are air and moisture stable has provided a wide range of applications for these ionic liquids. Common cations and anions employed in ionic liquids are shown in Figure 1.7.

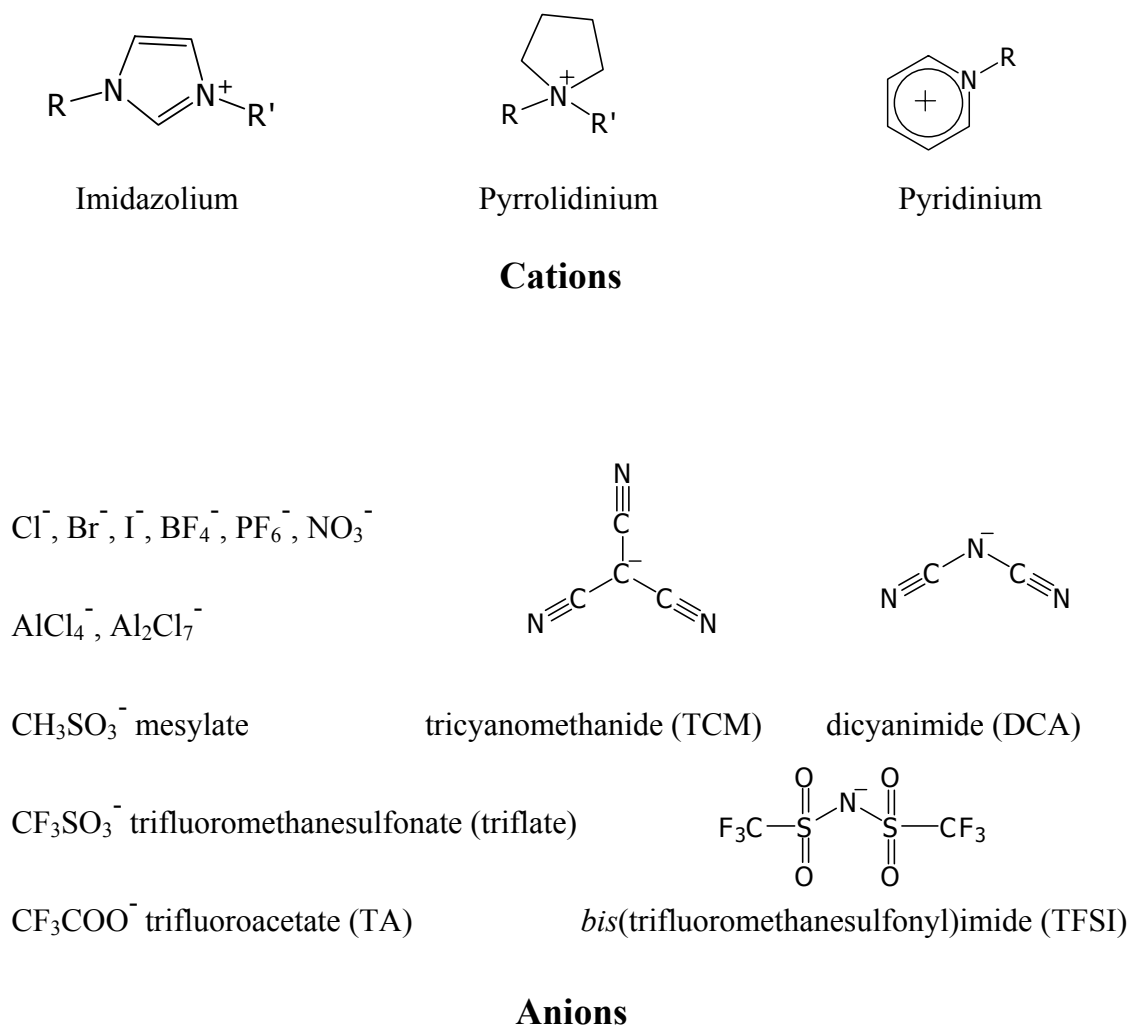


Figure 1.7 Chemical structures of some cations and anions of ionic liquids.

1.6.2 General Properties of Ionic Liquids

The special properties of ionic liquids that have generated great interest in their use as solvents are: high thermal stability, lack of significant vapor pressure, absence of flammability, good conductivity and large electrochemical potential window.

Ionic liquids generally consist of a cation with a low degree of symmetry to reduce the lattice energy of the crystalline form of the salt, thus lowering the melting temperature¹⁹⁷. Longer alkyl chains of some organic cations facilitate the decrease in melting point of the ionic liquid. The melting point, therefore, is usually governed by the cationic part, while the anionic component influences the chemical and other physical properties. Most of the anions that form room temperature ionic liquids are weakly basic species having a protected negative charge. Anions such as imides (e.g. bis(perfluoroethanesulfonyl)imide, $(\text{SO}_2\text{CF}_2\text{CF}_3)_2\text{N}^-$) and methanides (e.g. tris(trifluoromethanesulfonyl)methanide, $(\text{SO}_2\text{CF}_3)_3\text{C}^-$) produce ionic liquids with low melting points and low viscosities.²⁰⁰

The chemical structure of the cation and anion has a particularly strong influence on the viscosity and hydrophobicity of ionic liquids. The most common anions producing hydrophilic ionic liquids include acetate (CH_3COO^-), trifluoroacetate (CF_3COO^-), thiocyanate (SCN^-), dicyanimide ($\text{N}(\text{CN})_2^-$), mesylate (CH_3SO_3^-), and tosylate ($\text{CH}_3\text{PhSO}_3^-$). Hexafluorophosphate (PF_6^-), bis(trifluoromethanesulfonyl) imide ($(\text{SO}_2\text{CF}_3)_2\text{N}^-$), bis(pentafluoroethanesulfonyl)imide, $(\text{SO}_2\text{CF}_2\text{F}_3)_2\text{N}^-$, and tris(trifluoromethanesulfonyl)-methanide, $((\text{SO}_2\text{CF}_3)_3\text{C}^-)$ produce hydrophilic ionic liquids with most cations based on tetraalkylammonium, 1,3-dialkyl-imidazolium, *N*-alkylpyridinium, and *N,N*-dialkylpyrrolidinium units. The PF_6^- anion typically is much less hydrophilic than BF_4^- . However, the BF_4^- anion requires cations having *N*-butyl or *N*-hexyl substituents in order to produce hydrophobic ionic liquids. Generally, the hydrophobicity of an ionic liquid affects the nature and solubility of solutes, including water.

Most ionic liquids show high chemical stability, although some exhibit Lewis acid/base properties. For example, the dicyanamide and acetate anions of ionic liquids show Lewis base character. Substituted imidazolium cations that form ionic liquids with Brønsted-acid character have also been reported.²⁰¹

Recently, chiral ionic liquids containing either chiral cations or chiral anions have been reported, as shown in Figure 1.8. Chiral recognition ability of the chiral ionic liquid thiazolinium salt **42** ($R = n\text{-C}_4\text{H}_9$)²⁰² by diastereomeric formation with racemic Mosher's acid was demonstrated.

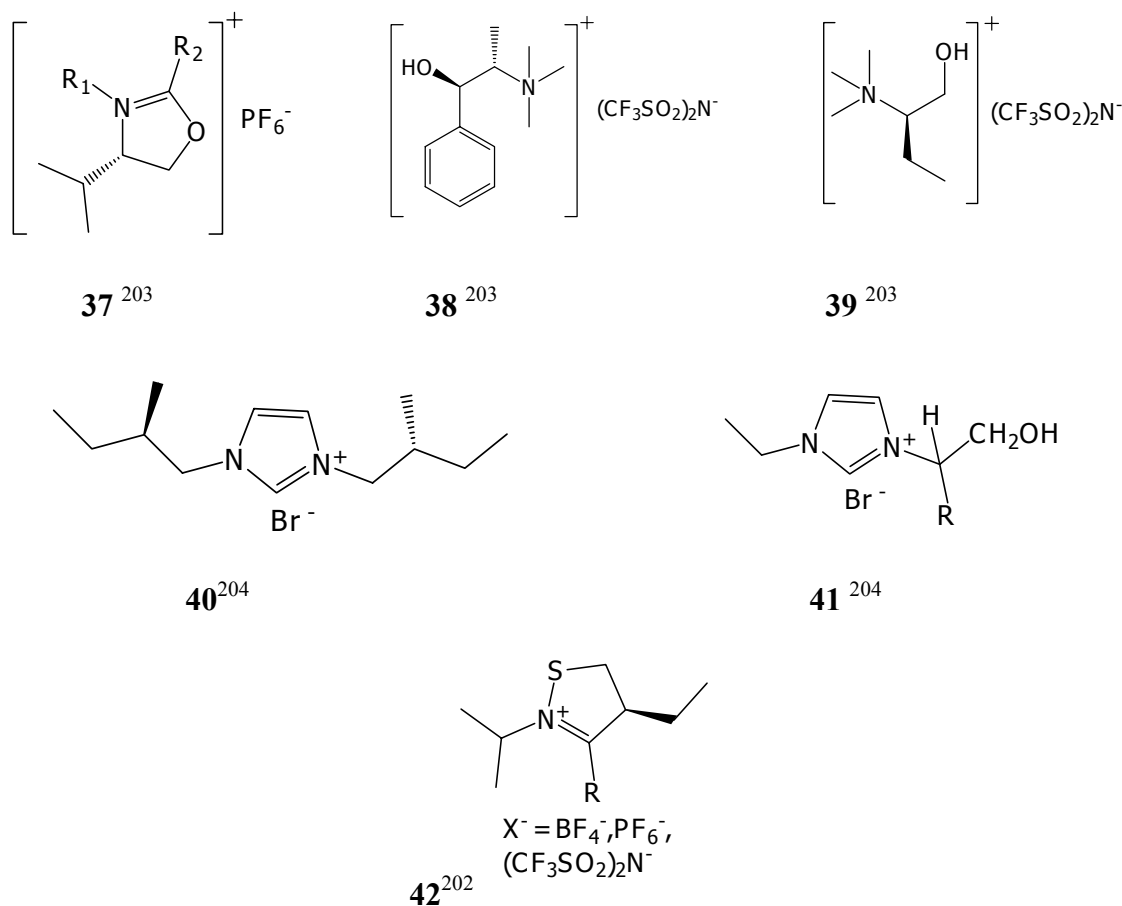


Figure 1.8 Chemical structures of some chiral ionic liquids.

1.6.3 Potential Applications of Ionic Liquids

The exceptional properties of ionic liquids make them interesting for many applications, as summarized below:

(1) Ionic liquids are non-volatile, inflammable, and good solvents for a wide range of organic and inorganic compounds, and are re-useable/recycleable; hence they may be ideal for use as extraction solvents.²⁰⁵

(2) The wide range of chemical reactions and catalytic reactions that have been undertaken in ionic liquids is quite remarkable. They are therefore promising as novel media for synthesis²⁰⁶⁻²¹⁰ and catalysis^{206, 211-215} to replace volatile organic solvents traditionally used in industry. Brønsted acid-ionic liquids can be used as both the solvent and the catalyst for acid-promoted organic reactions.¹⁹⁶

(3) Ionic liquids have good conductivity, a wide electrochemical potential window and are non-volatile. Thus, there is much recent interest in using them as electrolytes for battery applications,²¹⁶ electrodeposition of metals and semiconductors,²¹⁷⁻²²³ in actuator devices,^{60, 224-226} and for the electrochemical synthesis of organic compounds including conducting polymers.^{59, 227-229}

(4) Chiral ionic liquids have shown diastereoselective interactions with dissolved racemic compounds,²⁰³ including their potential applications in chiral separation and asymmetric synthesis to obtain optically pure compounds.

(5) The task-specific design of ionic liquids to have a desired property also has exciting potential applications. For example, addition of a functionality to dissolve saccharides made them useful as media to form bilayer membranes and self-assembling structures when suitable glycolipids were dissolved.²³⁰

1.7 Aims of This Project

This thesis explores as its ultimate goal the development of chiral conducting polymers for applications in electrochemical asymmetric synthesis. One of the most promising chiral conducting polymers for this purpose is chiral polyaniline doped with (+)- or (-)-camphorsulfonic acid, because it is easy to synthesize and produce as chiral modified electrodes and because it exhibits high optical activity arising from main chain chirality.

Ionic liquids would appear to have exciting potential as novel solvents/electrolytes for such electrochemical syntheses because of their properties of wide electrochemical window, high conductivity and negligible vapor pressure. Therefore, the ultimate goal of the thesis was to explore electrochemical asymmetric synthesis using chiral polyaniline modified electrodes with achiral ionic liquid electrolytes, or alternatively using achiral electrodes and chiral ionic liquid electrolytes. These studies are described in the final Chapter of the thesis.

The earlier Chapters explore more fundamental aspects of chiral polyaniline chemistry in order to support the proposed electrochemical syntheses. Chapters 3-6 focus on the development of new synthesis routes to chiral polyanilines. Chapter 3 explores whether the thermal treatment of optically inactive PAn.HCSA emeraldine salts (obtained by doping emeraldine base films with (+)- or (-)-camphorsulfonic acid) could convert them to optically active films. If successful this would provide a very simple method to produce optically active polyaniline in bulk quantities. A second novel approach, examined in Chapter 4, explores the electrochemical synthesis of optically active polyaniline films using racemic or achiral acids as dopant, by employing a chiral polyaniline thin film for chiral induction. Chapter 5 elucidates the pH and redox switching, thermochromism and solvatochromism of the fully sulfonated polyaniline

poly(2-methoxyaniline-5-sulfonic acid) (PMAS), while Chapter 6 examines its conversion into optically active PMAS via the electrostatic interaction of sulfonic acid groups on the PMAS chains with amino groups of poly-L-lysine.

Chapter 7 and 8 are focused on the influence of various factors on the chiroptical properties of polyanilines. Chapter 7 explores the influence of electrochemical polymerization temperature, revealing a remarkable dependence of the polymer optical activity on the temperature employed. The influence of solvents on the chiroptical properties of polyaniline emeraldine salts doped with (+)-camphorsulfonic acid prepared in ionic liquids are explored in Chapter 8.

The electrochemical and chiroptical properties of chiral polyanilines prepared in aqueous (+)-camphorsulfonic acid and investigated in ionic liquids are explored in Chapter 9. Preliminary studies of potential asymmetric induction during the electrochemical oxidations and reductions of prochiral organic substrates in ionic liquids with both bare and chiral polyaniline modified electrodes are described in Chapter 10.

1.8 References

1. G.G. Wallace, G.M. Spinks, A.L.P. Kane-Maguire, and P.R. Teasdale, *Conductive Electroactive Polymers*. 2 nd ed. (2003) USA: CRC Press.
2. H. Karami, M.F. Mousavi, and M. Shamsipur, *J. Power Sources*. **117** (2003): 255.
3. M.S. Rahmanifar, M.F. Mousavi, M. Shamsipur, and M. Ghaemi, *J. Power Sources*. **132** (2004): 296.
4. C. Shuchi and M.S. Wrighton, *J. Am. Chem. Soc.* **109** (1987): 6627.
5. F. Fusalba, P. Goueree, D. Villers, and D. Belanger, *J. Electrochem. Soc.* **148** (2001): A1.
6. K.S. Ryu, K.M. Kim, N.-G. Park, Y.J. Park, and S.H. Chang, *Journal of Power Sources*. **103** (2002): 305.
7. K.S. Ryu, K.M. Kim, Y.J. Park, N.-G. Park, M.G. Kang, and S.H. Chang, *Solid State Ionics*, (2002): 861.
8. E.A.R. Duek, M.A. De Paoli, and M. Mastragostino, *Adv. Mater.* **5** (1993): 650.
9. J.R. Heflin, J.A. Janik, D. Marciu, M. Miller, H.G. Wang, H.W., and R.M. Davis, *Polymer Preprints*. **43** (2002): 510.
10. M.K. Ram, N.S. Sundaresan, and B.D. Malhotra, *J. Mater. Sci. Let.* **13** (1994): 1490.
11. J. Gao, J.-M. Sansinena, and H.-L. Wang, *Synth. Met.* **135-136** (2003): 809.
12. H.-L. Wang, J. Gao, J.-M. Sansinena, and P.A. McCarthy, *Chem. Mater.* **14** (2002): 2546.

13. W. Lu and B.R. Mattes, *J. Electrochem. Soc.* **150** (2003): E416.
14. V. Shabnam, R.B. Kaner, and B.H. Weiller, *Chem. Mater.* **17** (2005): 1256.
15. Y. Andreu, S. de Marcos, J.R. Castillo, and J. Galban, *Talanta*. **65** (2005): 1045.
16. J.-B. Yu, K.-M. Lee, H.-G. Byun, and J.-S. Huh, *Chemical Sensors*. **20** (2004): 684.
17. J. Huang, V. Shabnam, B.H. Weiller, and R.B. Kaner, *Chemistry A European Journal*. **10** (2004): 1314.
18. R.J. Holness, G. Williams, D.A. Worsley, and H.N. McMurray, *J. Electrochem. Soc.* **152** (2005): B73.
19. J.L. Lu, N.J. Liu, X.H. Wang, J. Li, X.B. Jing, and F.S. Wang, *Synth. Met.* **135-136** (2003): 237.
20. W. Liu, J. Kumar, S. Tripathy, K.J. Senecal, and L. Samuelson, *J. Am. Chem. Soc.* **121** (1999): 71.
21. Z. Jin, Y. Su, and Y. Duan, *Synth. Met.* **122** (2001): 237.
22. R. Cruz-Silva, J. Romero-Garcia, and J. Angulo-Sanchez, *European Polymer Journal*. **41** (2005): 1129.
23. S. Takamuku, Y. Takeoka, and M. Rikukawa, *Synth. Met.* **135-136** (2003): 331.
24. X.Y. Gong, L.M. Dai, W.H. Mau, and H.J. Griesser, *J. Polym. Sci.* **36** (1998): 633.
25. H. Liu, X.B. Hu, J.Y. Wang, and R.I. Boughton, *Macromolecules*. **35** (2002): 9414.
26. K. Teshima, S. Uemura, N. Kobayashi, and R. Hirohashi, *Macromolecules*. **31** (1998): 6783.
27. Y. Kim, S. Fukai, and N. Kobayashi, *Synth. Met.* **119** (2001): 337.
28. S.-J. Su and N. Kuramoto, *Macromolecules*. **34** (2001): 7249.
29. M.-C. Bernard, A.H.-L. Goff, and W. Zeng, *Synth. Met.* **85** (1997): 1347.
30. S. Patil, J.R. Mahajan, M.A. More, P.P. Patil, S.W. Gosavi, and S.A. Gangal, *Polym. Inter.* **46** (1998): 99.
31. J. Stejskal, A. Riede, D. Hlavata, J. Prokes, M. Helmstedt, and P. Holler, *Synth. Met.* **96** (1998): 55.
32. S. Mu and J. Kan, *Synth. Met.* **92** (1998): 149.
33. W.W. Focke, G.E. Wnek, and Y. Wei, *J. Phys. Chem.* **91** (1987): 5813.
34. S. Davied, Y.F. Nicolau, F. Melis, and A. Revillon, *Synth. Met.* **69** (1995): 125.
35. E. Naudin, P. Gouerec, and D. Belanger, *J. Electroanal. Chem.* **459** (1998): 1.
36. J. Widera, B. Patys, J. Bukwska, and K. Jackowska, *Synth. Met.* **94** (1998): 265.
37. S.M. Yang and J.T. Chen, *Synth. Met.* **69** (1995): 153.
38. A.A. Syed and M.K. Dinesan, *Talanta*. **38** (1991): 815.
39. E.M. Genies, A. Boyle, M. Lapkowski, and C. Tsintavis, *Synth. Met.* **36** (1990): 139.
40. D. Bejan and A. Duca, *CROATICA CHEMICA ACTA*. **71** (1998): 745.
41. D.D. Borole, U.R. Kapadi, P.P. Kumbhar, and D.G. Hundiwale, *Materials Letters*. **56** (2002): 685.
42. H. Okamoto and T. Kotaka, *Polymer*. **39** (1998): 4349.
43. S.K. Mondal, K.R. Prasad, and N. Munichandraiah, *Synth. Met.* **148** (2005): 275.
44. S.F. Patil and A.G. Bedekar, *Materials Letters*. **14** (1992): 307.
45. D.M. Mohilner, R.N. Adams, and W.J. Argersinger, *J. Am. Chem. Soc.* **84** (1962): 3618.
46. G. Zotti, S. Cattarin, and N. Comisso, *J. Electroanal. Chem.* **177** (1984): 387.
47. F. Lux, *Polymer*. **35** (1994): 2915.
48. T. Ohsaka, Y. Ohnuki, N. Oyama, G. Katagiri, and K. Kamisako, *J. Electroanal. Chem.* **161** (1984): 399.
49. A. Thyssen, A. Hochfeld, R.M. Kessel, A., and J.W. Schultze, *Synth. Met.* **29** (1989): 357.
50. H. Okamoto, M. Okamoto, and T. Kotaka, *Polymer*. **39** (1998): 4359.
51. L.J. Duic, Z. N Mandic, and F. Kovacicek, *J. Polym. Sci., Part A*. **32** (1994): 105.
52. A.Q. Zhang, C.Q. Cui, and Y.J. Lee, *Synth. Met.* **72** (1995): 217.
53. A.M. Fenelon and C.B. Breslin, *Synth. Met.* **144** (2004): 125.
54. M.C. Miras, C. Barbero, R. Kotz, and O. Haas, *J. Electrochem. Soc.* **138** (1991): 335.
55. T. Osaka, T. Nakajima, K. Shiota, and T. Momma, *J. Electrochem. Soc.* **138** (1991): 2853.
56. T. Osaka, T. Nakajima, K. Naoi, and B.B. Owens, *J. Electrochem. Soc.* **137** (1990): 2139.
57. E. Naudin, H. Anh, L. Breau, and D. Belanger.
58. N. Pekmez and A. Yildiz, *J. Electroanal. Chem.* **386** (1995): 121.
59. J. Tang and R.A. Osteryoung, *Synth. Met.*, (1991).
60. W. Lu, A.G. Fadev, B. Qi, and B.R. Mattes, *Synth. Met.* **135-136** (2003): 139.
61. A.A. Pud, *Synth. Met.* **66** (1994): 1.
62. F.A. Viva, E.M. Andrade, F.V. Molina, and M.I. Florit, *J. Electroanal. Chem.* **471** (1999): 180.
63. B. Scrosali, *Applications of Electroactive Polymers*. (1993): Kluwer Academic Publishers Group.

-
64. M.R. Majidi, L.A.P. Kane-Maguire, and G.G. Wallace, *Aust. J. Chem.* **51** (1998): 23.
 65. A.F. Diaz and J.A. Logan, *J. Electroanal. Chem.* **111** (1980): 111.
 66. E.M. Genies and C. Tsintavis, *J. Electroanal. Chem.* **195** (1985): 109.
 67. B. Wang, J. Tang, and F. Wang, *Synth. Met.* **13** (1986): 329.
 68. M. Lapkowski, *Synth. Met.* **35** (1990): 169.
 69. C.D. Batich, H.A. Laitineen, and H.C. Zhou, *J. Electrochem. Soc.* **137** (1990): 883.
 70. A. Kitani, M. Kaya, J. Yano, K. Yoshikawa, and K. Sasaki, *Synth. Met.* **18** (1987): 341.
 71. Y.-B. Shim, M.-S. Won, and S.-M. Park, *J. Electrochem. Soc.* **137** (1990): 538.
 72. R.L. Hand and R.F. Nelson, *J. Electrochem. Soc.* **125** (1978): 1059.
 73. D. Orata and D.A. Buttry, *J. Am. Chem. Soc.* **109** (1987): 3574.
 74. A. Kabumoto, K. Shinozaki, K. Watanabe, and N. Nishikawa, *Synth. Met.* **26** (1988): 349.
 75. R. Mazeikiene and A. Malinauskas, *Synth. Met.* **123** (2001): 349.
 76. E.S. Matveeva, C.F. Gimenez, and M.J.G. Tejera, *Synth. Met.* **123** (2001): 117.
 77. N. Commiso, S. Daolio, G. Mengoli, S. Zecchin, and G. Zotti, *J. Electroanal. Chem.* **97** (1988): 255.
 78. A. Pron, F. Genoud, C. Menardo, and M. Nechstein, *Synth. Met.* **24** (1988): 193.
 79. P.N. Adams, D.C. Apperley, and A.P. Monkman, *Polymer.* **34** (1993): 328.
 80. A. Yasuda and T. Shimidzu, *Synth. Met.* **61** (1993): 239.
 81. *Applications of Conducting Polymers.*
 82. L.H.C. Mattoso, A.G. MacDiarmid, and A. Epstein, *Synth. Met.* **68** (1994): 1.
 83. J. Stejskal, A. Riede, D. Hlavata, J. Prokes, M. Helmstedt, and P. Holler, *Synth. Met.* **96** (1998): 55.
 84. A.G. Kenwright, W.J. Feas, P.N. Adams, A.J. Malton, and A.P. Monkman, *Polymer.* **33** (1992): 4292.
 85. J. Stejskal, P. Kratochvil, and A.D. Jenkins, *Collect. Czech. Chem. Commun.* **60** (1995): 1747.
 86. F.L. Klavetter and Y. Cao, *Synth. Met.* **55-57** (1993): 989.
 87. D.E. Stilwell and S.-M. Park, *J. Electrochem. Soc.* **135** (1998): 2254.
 88. L.T. Yu, M.S. Borrdon, M. Jozefovizc, G. Belogrey, R. Buvet, and F.H. Cristofini, *J. Polym. Sci.* **10** (1987): 2931.
 89. M. Doriomedoff, F.H. Cristofini, R. De Surville, M. Jozefovizc, L.T. Yu, and R. Buvet, *J. Chem. Phys.* **68** (1971): 1055.
 90. J. Stejskal and P. Kratochvil, *Synth. Met.* **61** (1993): 225.
 91. Y. Wei, W.W. Focke, G.E. Wnek, A. Ray, and A.G. MacDiarmid, *J. Phys. Chem.* **93** (1989): 495.
 92. A. Watanabe, K. Mori, M. Mikuni, and Y. Nakamura, *Macromolecules.* **22** (1989): 3323.
 93. W.S. Huang, B.D. Humphrey, and A.G. MacDiarmid, *J. Chem. Soc., Faraday Trans. 1.* **82** (1986): 2385.
 94. W.S. Huang and A.G. MacDiarmid, *Polymer.* **34** (1993): 1833.
 95. Y. Xia, J.M. Wiesinger, and A.G. MacDiarmid, *Chem. Mater.* **7** (1995): 443.
 96. V. Egan, R. Bernstein, L. Hohmann, T. Tran, and R.B. Kaner, *Chem. Commun.*, (2001): 801.
 97. R.P. McCall, J.M. Ginder, J.M. Leng, H.J. Ye, S.K. Manohar, J.G. Masters, G.E. Asturias, and A.G. MacDiarmid, *Phys. Rev.* **41** (1990): 5202.
 98. J.E. Albuquerque, L.H.C. Mattoso, D.T. Balogh, R.M. Faria, J.G. Masters, and A.G. MacDiarmid, *Synth. Met.* **113** (2000): 19.
 99. A.G. MacDiarmid and A.J. Epstein, *Synth. Met.* **69** (1995): 85.
 100. S. Ghosh, *Chemical Physics Letters.* **226** (1994): 344.
 101. I.D. Norris, L.A.P. Kane-Maguire, and G.G. Wallace, *Macromolecules.* **31** (1998).
 102. M. Lapkowski, K. Berrada, S. Quillard, G. Louarn, S. Lefrant, and A. Pron, *Macromolecules.* **28** (1995): 1233.
 103. M. Boyer, S. Quillard, G. Louarn, S. Lefrant, E. Rebourt, and A.M. Monkman, *Synth. Met.* **84** (1997): 787.
 104. G. Louarn, M. Lapkowski, S. Quillard, A. Pron, J.P. Buisson, and S. Lefrant, *J. Phys. Chem.* **100** (1996): 6998.
 105. E. Cintra and S.I.C. Torresi, *J. Electroanal. Chem.* **2002** (2002): 33.
 106. J.E.P. Silva, D.L.A. Faria, S.I.C. Torresi, and M.L.A. Temperini, *Macromolecules.* **33** (2000): 3077.
 107. J.E.P. Silva, S.I.C. Torresi, D.L.A. Faria, and M.L.A. Temperini, *Synth. Met.* **101** (1999): 834.
 108. I. Harada and Y. Furukawa, *Vib. Spectra. Struct.* **19** (1991): 439.
 109. R.M. Torresi and S.I. Torresi, *Synth. Met.* **61** (1993): 291.

110. L.V. Lukachova, E.A. Shkerin, E.A. Puganova, E.E. Karyakina, and A.A. Karyakin, *J. Electroanal. Chem.* **544** (2003): 59.
111. R. Sivakumar and R. Saraswathi, *Synth. Met.* **138** (2003): 381.
112. J. Desilvestra, W. Scheifele, and O. Haas, *J. Electrochem. Soc.* **139** (1992): 2727.
113. S.-A. Chen and G.-W. Hwang, *Macromolecules.* **29** (1996): 3950.
114. K. Okabayashi, F. Goto, K. Abe, and T. Yoshida, *Synth. Met.* **18** (1987): 365.
115. B. Garcia, F. Fusalba, and D. Belanger, *Can. J. Chem.* **75** (1997): 1536.
116. H. Varela and R.M. Torresi, *J. Electrochem. Soc.* **147** (2000): 665.
117. J. Yue and A. Epstein, *J. Am. Chem. Soc.* **112** (1990): 2800.
118. X.-L. Wei, Y.Z. Wang, S.M. Long, C. Bobeczko, and A. Epstein, *J. Am. Chem. Soc.* **118** (1996): 2545.
119. X.L. Wei, M. Fahlman, and A.J. Epstein, *Macromolecules.* **32** (1999): 3114.
120. S. Shimizu, T. Saitoh, M. Uzawa, M. Yuasa, K. Yano, T. Maruyama, and K. Watanabe, *Synth. Met.* **85** (1997): 1337.
121. E.V. Strounina, L.A.P. Kane-Maguire, and G.G. Wallace, *Synth. Met.* **106** (1999): 129.
122. R. Guo, J.N. Barisci, P.C. Innis, C.O. Too, G.G. Wallace, and D. Zhou, *Synth. Met.* **114** (2000): 267.
123. J. Yue, Z.H. Wang, K.R. Cromack, A. Epstein, and A.G. MacDiarmid, *J. Am. Chem. Soc.* **113** (1991): 2665.
124. A. Malinauskas, *J. Power Sources.* **126** (2003): 214.
125. X.-L. Wei, Y.Z. Wang, S.M. Long, C. Bobeczko, and A.J. Epstein, *J. Am. Chem. Soc.* **118** (1996): 2545.
126. K.Y.K. Man, H.L. Wong, W.K. Chan, C.Y. Kwong, and A.B. Djuris, *Chem. Mater.* **16** (2004): 365.
127. T. Cao, L. Wei, S. Yang, M. Zhang, C. Huang, and W. Cao, *Langmuir.* **18** (2002): 750.
128. T. Tatsuma, T. Ogawa, R. Sato, and N. Oyama, *J. Electroanal. Chem.* **501** (2001): 180.
129. C. Barbero, M.C. Miras, R. Kotz, and O. Hass. in *Proceedings-Electrochemical Society: Lithium Batteries.* 1994.
130. R. Bishop, I. Hermansson, B. Jaderlund, G. Lindgren, and C. Pernow, *Amer. Lab.* **18** (1986): 138.
131. R.L. Elsenbaumer, H. Eckhardt, Z. Iqbal, J. Toth, and R.H. Baughman, *Mol. Cryst. Liq. Cryst.* **118** (1985): 111.
132. R.S. Cahn, C. Ingold, and V. Prelog, *Angew. Chem., Int. Ed. Engl.* **5** (1966): 385.
133. M. Salmon and M. Saloma, *Electrochimica Acta.* **34** (1989): 117.
134. B.P.J. de Lacy Costello, M.N. Ratcliffe, and P.S. Sivanand, *Synth. Met.* **139** (2003): 43.
135. S. Pleus and M. Schwientek, *Synthetic Communications.* **27** (1997): 2917.
136. S. Pleus and B. Schulte, *Journal of Solid State Electrochem.* **2001** (2001): 522.
137. S. Pleus and M. Schwientek, *Synth. Met.* **95** (1998): 233.
138. M. Anderson, P.O. Ekeblad, T. Hjerberg, and O. Wennerstrom, *Polymer.* **32** (1991): 546.
139. H. Goto, Y. Okamoto, and E. Yashima, *Macromolecules.* **35** (2002): 4590.
140. K. Peter, R. Nilsson, J.D.M. Olsson, P. Konradsson, and O. Inganas, *Macromolecules.* **37** (2004): 6316.
141. B.M.W. Langeveld-Voss, E. Peeters, R.A.J. Janssen, and E.W. Meijer, *Synth. Met.* **84** (1997): 611.
142. B.M.W. Langeveld-Voss, R.A.J. Janssen, and E.W. Meijer, *J. Mol. Struct.* **521** (2000): 285.
143. M.M. Bouman and E.W. Meijer, *Adv. Mater.* **7** (1995): 385.
144. B.M.W. Langeveld-Voss, M.P.T. Christiaans, R.A.J. Janssen, and E.W. Meijer, *Macromolecules.* **31** (1998): 6702.
145. B.M.W. Langeveld-Voss, R.J.M. Waterval, R.A.J. Janssen, and E.W. Meijer, *Macromolecules.* **32** (1999): 227.
146. B.M.W. Langeveld-Voss, D. Beljonne, Z. Shugi, R.A.J. Janssen, S.C.J. Meskers, E.W. Meijer, and J.-L. Bredas, *Adv. Mater.* **10** (1998): 1343.
147. G. Bidan, S. Guillerez, and V. Sorokin, *Adv. Mater.* **8** (1996): 157.
148. E. Yashima, H. Goto, and Y. Okamoto, *Macromolecules.* **32** (1999): 7942.
149. H. Goto and E. Yashima, *J. Am. Chem. Soc.* **124** (2002): 7943.
150. R.D. McCullough, R.D. Lowe, M. Jayaraman, and D.L. Anderson, *J. Org. Chem.* **58** (1993): 904.
151. T.-A. Chen, X. Wu, and R.D. Rieke, *J. Am. Chem. Soc.* **117** (1995): 233.
152. K. Peter, R. Nilsson, J. Rydberg, L. Baltzer, and O. Inganas, *PNAS.* **100** (2003): 10170.
153. R. Nilsson, M.R. Anderson, and O. Inganas, *Synth. Met.* **2003** (2003): 291.

154. M.R. Majidi, L.A.P. Kane-Maguire, and G.G. Wallace, *Polymer*. **35** (1994): 3113.
155. M.R. Majidi, L.A.P. Kane-Maguire, and G.G. Wallace, *Polymer*. **36** (1995): 3597.
156. M.R. Majidi, L.A.P. Kane-Maguire, and G.G. Wallace, *Polymer*. **37** (1996): 359.
157. E.E. Havinga, M.M. Bouman, E.W. Meijer, A. Pomp, and M.M.J. Simenon, *Synth. Met.* **66** (1994): 93.
158. M. Bodner and M.P. Espe, *Synth. Met.* **135-136** (2003): 403.
159. L.A.P. Kane-Maguire, A.G. MacDiarmid, I.D. Norris, G.G. Wallace, and W. Zheng, *Synth. Met.* **106** (1999): 171.
160. P.C. Innis, I.D. Norris, L.A.P. Kane-Maguire, and G.G. Wallace, *Macromolecules*. **1998** (1998): 6521.
161. V. Aboutanos, L.A.P. Kane-Maguire, and G.G. Wallace, *Synth. Met.* **114** (2000): 313.
162. W. Li, P.A. McCarthy, D. Liu, J. Huang, S.-C. Yang, and H.-L. Wang, *Macromolecules*. **35** (2002): 9975.
163. P.A. McCarthy, J. Huang, S.-C. Yang, and H.-L. Wang, *Langmuir*. **18** (2002): 259.
164. M. Thiagarajan, L.A. Samuelson, J. Kumar, and A.L. Cholli, *J. Am. Chem. Soc.* **125** (2003): 11502.
165. S.A. Ashraf, L.A.P. Kane-Maguire, M.R. Majidi, S.G. Pyne, and G.G. Wallace, *Polymer*. **38** (1997): 2627.
166. I.D. Norris, L.A.P. Kane-Maguire, and G.G. Wallace, *Macromolecules*. **53** (2000): 89.
167. E.V. Strounina, *Synthesis and Characterisation of Chiral Substituted Polyanilines*, in *Chemistry Department*. 2001, University of Wollongong.
168. A.M. Rouhi, *C&EN*, (2004): 47.
169. R.S. Deinhammer, M.D. Porter, and K. Shimazu, *J. Electroanal. Chem.* **387** (1995): 33.
170. H. Ge and G.G. Wallace, *J. Liq. Chromatogr.* **588** (1991): 25.
171. B. Deore, Z. Chen, and T. Nagaoka, *Anal. Chem.* **72** (2000): 39893994.
172. Z. Chen, Y. Takei, B. Deore, and T. Nagaoka, *Analyst*. **125** (2000): 2249.
173. B. Deore, H. Yakabe, H. Shiigi, and T. Nagaoka, *Analyst*. **127** (2002): 935.
174. N. Ogata, *Macromol. Symp.* **118** (1997): 693.
175. R.B. Kaner, *Synth. Met.* **125** (2002): 65.
176. H. Guo, C.M. Knobler, and R.B. Kaner, *Synth. Met.* **101** (1999): 44.
177. H. Guo, V. Egan, C.M. Knobler, and R.B. Kaner, *Polymer Preprints*. **40** (1999).
178. G. Li, D. Patel, and V.J. Hruby, *J. Chem. Soc., Perkin Transactions 1: Organic and Bio-Oganic Chemistry*, (1994): 3057.
179. J.L. Vicario, D. Badia, L. Carrillo, E. Reyes, and J. Etxebarria, *Current Organic Chemistry*. **9** (2005): 219.
180. D. Basavaiah and P. Krishna, *Pure and Applied Chemistry*. **64** (1992): 1067.
181. P. Hechtberger, G. Wirnsberger, M. Mischitz, M. Martin, N. Klempier, and K. Faber, *Tetrahedron: Asymmetry*. **4** (1993): 1161.
182. T. Matsuda, T. Harada, K. Nakamura, and T. Ikariya, *Tetrahedron: Asymmetry*. **16** (2005): 909.
183. D. Seebach and H.A. Oei, *Angew. Chem.* **87** (1975): 629.
184. J. Kopilov, E. Kariv, and L.L. Miller, *J. Am. Chem. Soc.*, (1977): 3450.
185. W.J.M. Tilborg and C.J. Smit, *Journal of the Royal Netherlands Chemical Society*. **97/3** (1978): 89.
186. A.R. Amundsen and E.N. Balko, *J. Appl. Electrochem.* **22** (1992): 810.
187. M. Schwientek, S. Pleus, and C.H. Hamann, *J. Electroanal. Chem.* **461** (1999): 94.
188. B.E. Firth, L.L. Miller, J. Lennox, and R.W. Murray, *J. Am. Chem. Soc.*, (1976): 8271.
189. B.E. Firth and L.L. Miller, *J. Am. Chem. Soc.*, (1976): 8272.
190. B.F. Watkins, J.R. Behling, E. Kariv, and L.L. Miller, *J. Am. Chem. Soc.*, (1975): 3549.
191. S. Abe, T. Nonaka, and T. Fuchigami, *J. Am. Chem. Soc.*, **105** (1983): 3630.
192. T. Komori and T. Nonaka, *J. Am. Chem. Soc.* **105** (1983): 5690.
193. T. Komori and T. Nonaka, *J. Am. Chem. Soc.* **106** (1984): 2656.
194. R.N. Gourley, J. Grimshaw, and P.G. Millar, *J. Chem. Soc.*, (1970): 2318.
195. J.S. Wilkes, *Green Chemistry*. **4** (2002): 73.
196. S.A. Forsyth, J.M. Pringle, and D.R. MacFarlane, *Aust. J. Chem.* **57** (2004): 113.
197. M.J. Earle and K.R. Seddon, *Pure Appl. Chem.* **72** (2000): 1391.
198. F.H. Hurley and T.P. Wier, *J. Electrochem. Soc.* **98** (1951): 203.
199. V. Braun, *Ber. Dtsch. Chem. Ges. B.* **60** (1927): 2557.
200. H. Matsumoto, H. Kageyama, and Y. Miyazaki, *Chem. Commun.*, (2002): 1726.
201. A.C. Cole, J.L. Jensen, I. Ntai, K.L.T. Tran, K.J. Weaver, D.C. Forbes, and J.H. Davis, *J. Am. Chem. Soc.* **124** (2002): 5962.

-
202. J. Levillain, G. Dobant, I. Abrunhosa, M. Gulea, and A. Gaumont, *Chem. Commun.*, (2003): 2914.
203. P. Wasserscheid, A. Bosmann, and C. Bolm, *Chem. Commun.*, (2002): 200.
204. W. Bao, Z. Wang, and Y. Li, *J. Org. Chem.* **68** (2003): 591.
205. J.G. Huddeleston, H.D. Willauer, R.P. Swatloski, A.E. Visser, and R.D. Rogers, *Chem. Commun.*, (1998): 1765.
206. T. Welton, *Chem. Rev.* **99** (1999): 2071.
207. T. Biedron and P. Kubisa, *J. Polym. Sci., Part A.* **40** (2002): 2799.
208. P. Lucas, N.E. Mehdi, H.A. Ho, D. Belanger, and L. Breau, *Synthesis*, (2000): 1253.
209. D. Behar, C. Gonzalez, and P. Neta, *J. Phys. Chem. A.* **105** (2001): 7607.
210. M.J. Earle, P.B. McCormac, and K.R. Seddon, *Green Chemistry*, (1999): 23.
211. A. Nelson, *Angew. Chem. Int. Ed.* **38** (1999): 1583.
212. J.S. Wilkes, *J. Molecular Catalysis A : Chemical.* **214** (2004): 11.
213. C.R. Oh, D.J. Choo, W.H. Shim, D.H. Lee, E.J. Roh, S. Lee, and C.E. Song, *Chem. Commun.*, (2003): 1100.
214. S. Lee, Y.J. Zhang, J.Y. Piao, H. Yoon, C.E. Song, J.H. Choi, and J. Hong, *Chem. Commun.*, (2003): 2624.
215. C.E. Song and E.J. Roh, *Chem. Commun.*, (2000): 837.
216. D.R. MacFarlane and M. Forsyth, *Adv. Mater.* **13** (2001): 957.
217. F. Endres, *Chemphyschem.* **3** (2002): 144.
218. F. Endres and A. Schweizer, *Phys. Chem. Chem. Phys.* **2** (2000): 5455.
219. K. Matiasovsky, Z. Lubyova, and V. Danek, *Electrodepos. Surface Treat.* **1** (1972/73): 43.
220. C.A. Zell, F. Endres, and W. Freyland, *Phys. Chem. Chem. Phys.* **1** (1999): 697.
221. K. Murase, K. Nitta, T. Hirato, and Y. Awakura, *J. Appl. Electrochem.* **31** (2001): 1089.
222. C. Hussey, L.A. King, and R.A. Carpio, *J. Electrochem. Soc.: Solid-State Science and Technology*, (1979): 1029.
223. B.J. Tierney, W.R. Pitner, J.A. Mitchell, C.L. Hussey, and G.R. Stafford, *J. Electrochem. Soc.* **145** (1998): 3110.
224. W. Lu, A.G. Fadev, B. Qi, E. Smela, B.R. Mattes, J. Ding, G.M. Spinks, J. Mazurkiewicz, D. Zhou, G.G. Wallace, D.R. MacFarlane, S.A. Forsyth, and M. Forsyth, *Science.* **297** (2002): 983.
225. D. Zhou, G.M. Spinks, G.G. Wallace, C. Tiyapiboonchiya, D.R. MacFarlane, M. Forsyth, and J. Sun, *Electrochimica. Acta.* **48** (2003): 2355.
226. J. Ding, D. Zhou, G.M. Spinks, G.G. Wallace, S.A. Forsyth, M. Forsyth, and D.R. MacFarlane, *Chem. Mater.* **15** (2003): 2392.
227. J.M. Pringle, J. Efthimiadis, P.C. Howlett, J. Efthimiadis, D.R. MacFarlane, A.B. Chaplin, S.B. Hall, D.L. Officer, G.G. Wallace, and M. Forsyth, *Polymer.* **45** (2004): 1447.
228. E. Naudin, H.A. Ho, S. Branchaud, L. Breau, and D. Belanger, *J. Phys. Chem. B.* **106** (2002): 10585.
229. P.G. Pickup and R.A. Osteryoung, *J. Am. Chem. Soc.* **106** (1984): 2294.
230. N. Kimizuka and T. Nakashima, *Langmuir.* **17** (2001): 6759.

Chapter 2

General Experimental

2.1 Introduction

General details of the materials and experimental procedures employed in this thesis are described in this Chapter. Included are brief explanations of the theoretical and practical aspects of each technique. Specific details of particular procedures will be given in the Experimental section of the relevant Chapters.

2.2 Materials

2.2.1 Monomers and Polymers

Aniline and pyrrole were purchased from Aldrich and Merck, respectively. Both were purified by distillation and stored under nitrogen at -18°C in a freezer prior to use. Poly(2-methoxyaniline-5-sulfonic acid) (PMAS) ($M_w = 18067$, $M_n = 5700$ and polydispersity = 3.16), synthesized at 5°C and purified by a cross flow dialysis¹, was kindly provided by Fatemeh Masdarolomoor in our laboratories. Poly-L-lysine hydrochloride (PLL) (MW 30,000-70,000 Da) was purchased from Sigma-Aldrich and used as received.

2.2.2 Reagents

(1*S*)-(+)-and (1*R*)-(-)-10-camphorsulfonic acid (HCSA) were purchased in the highest grade available from Aldrich and used as supplied. Ajax Chemicals supplied all aqueous acids and aqueous ammonia. The sources of other chemicals and reagents used in this thesis, such as ammonium persulfate oxidizing agent, hydrazine hydrate reducing agent,

acids and bases, prochiral sulfides and alcohols, are detailed in the Chapters where they are employed.

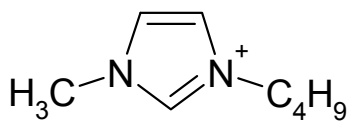
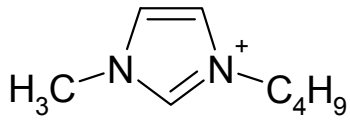
2.2.3 Solvents

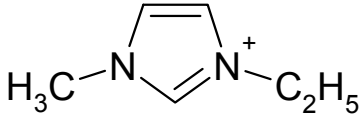
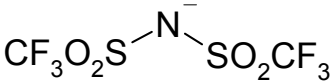
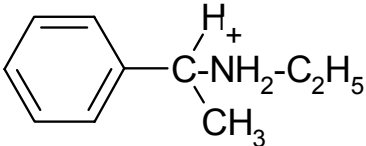
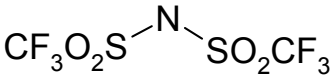
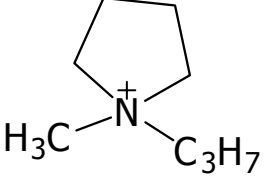
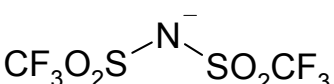
Acetonitrile, chloroform, methanol, diethylether, ethylacetate and hexane were supplied by Ajax Chemicals. NMP was purchased from Aldrich. All solvents were used as received.

2.2.4 Ionic Liquids

The ionic liquids, 1-butyl-3-methylimidazolium hexafluorophosphate (BMI-PF₆),² 1-ethyl-3-methylimidazolium bis(trifluoromethanesulfonyl)imide (EMI-TFSI),² 1-methyl-1-propylpyrrolidinium bis(trifluoromethanesulfonyl)imide (P₁₃-TFSI)³ and the chiral (+)- or (-)- and (±)- α -methylbenzylethylamine bis(trifluoromethanesulfonyl)imide (MBEA-TFSI) were synthesized in-house following previously described methods⁴. 1-Butyl-3-methylimidazolium tetrafluoroborate (BMI-BF₄) was purchased from Solvent Innovation. All ionic liquids were deoxygenated by purging with nitrogen gas for at least 30 min prior to use. The structures of the ionic liquids are shown in Table 2.1.

Table 2.1 Structures of the ionic liquids used in this thesis.

Ionic liquids	Cation	Anion
BMI-BF ₄		BF ₄ ⁻
BMI-PF ₆		PF ₆ ⁻

EMI-TFSI		
(+)-, (-)-, or (±)- MBEA-TFSI	 (+)- (-)- or (±)-	
P13-TFSI		

2.2.5 Electrodes

Various electrodes were used as working, auxiliary and reference electrodes. Working electrodes included: platinum (Pt) disc (surface area 0.014 cm²) purchased from Bioanalytical Systems Inc. (BAS), Pt plate (5 cm x 5 cm) obtained from Goodfellow Ltd., glassy carbon (GC) disc (surface area 0.07 cm²), GC plate (2 cm x 4 cm) purchased from BAS, and indium-tin-oxide (ITO)-coated glass (resistivity 8-12 Ω) obtained from Delta Technologies Ltd.

The platinum and glassy carbon electrodes were polished with alpha alumina (LECO®, 0.3 μm) slurries, thoroughly washed with Milli-Q water and scrubbed with Kim-wipe paper before using.

ITO-coated glass was sputter coated with platinum using a magnetron sputter coater SC100MS (Dynavac Engineering, AU), to assist the adherence of uniform polyaniline films on the surface. The ITO-coated glasses were cut (1 cm x 3 cm) and placed in the

chamber of the sputter coater, with the conductive side to be coated facing a platinum target. Plasma of platinum ions was generated under a pressure of 2×10^{-6} bar of argon by applying a current of 30 mA. The sputter-coating was usually allowed to proceed for 5 seconds.

To investigate the effect of the Pt coating on ITO-coated glass, UV-visible transmittance, electrical conductivity and AFM of the ITO-coated glasses were measured before and after sputter-coating with platinum for 0, 5, 10 and 15 sec. The surface morphology and roughness were shown by AFM not to vary significantly among these samples. The surface conductivity of the samples increased with sputter-coating time; whereas the % transmittance of the ITO-Pt-coated glasses decreased as shown in Figure 2.1. However, for 5 sec sputter-coating, the % transmittance is only slightly less (between 350 and 550 nm) than that of untreated ITO-coated glass.

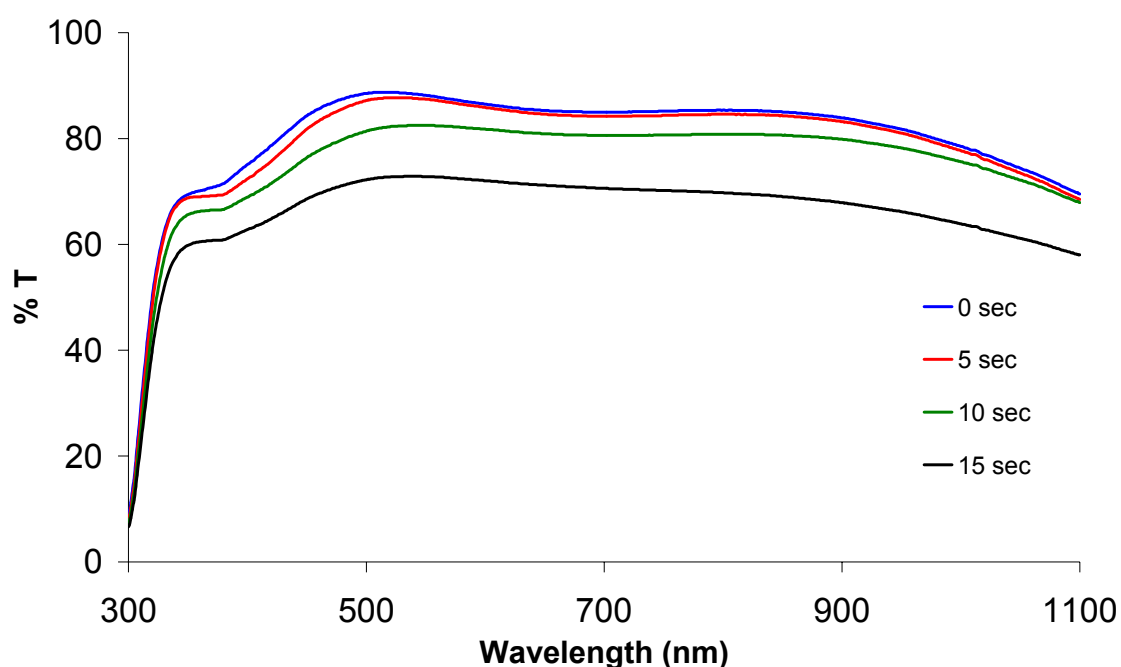


Figure 2.1 UV-visible transmittance of ITO-coated glass before and after sputter-coating with platinum by applying a current of 30 mA for various periods of time (0, 5, 10, and 15 sec).

Auxiliary electrodes used included reticulated vitreous carbon (RVC) (surface area $65 \text{ cm}^2/\text{cm}^3$) obtained from ERG Materials and Aerospace Corporation, Oakland, CA, USA, as well as platinum and stainless steel mesh.

Ag/AgCl (3M NaCl (aq)) or Ag/Ag^+ ($0.1 \text{ M TBAP in CH}_3\text{CN}$) reference electrodes were used for experiments in aqueous solution and organic solvents, respectively; while for the experiments in ionic liquids, Ag/AgCl (EMI-TFSI) or silver wire were used as reference electrode or quasi-electrode, respectively.

2.3 Techniques used for Preparation of Polyanilines

2.3.1 Electrochemical Polymerization

Electrochemical polymerization of aniline was normally carried out using a three-electrode electrochemical cell such as that shown in Figure 2.2.

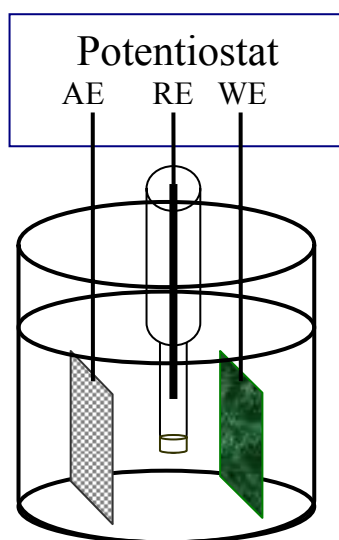


Figure 2.2 A three-electrode electrochemical cell.

The material and size of the working electrode (WE) on which the polyaniline film was formed depended on the further use planned. For example, ITO-coated glass was used for subsequent characterization of the polyaniline by UV-visible or circular dichroism

spectroscopy. A Pt-disc or GC-disc electrode was normally used for electrochemical characterization of the polymer during or after growth. A large size Pt or GC plate was used for the preparation of large amounts of polyaniline.

Auxiliary electrodes (AE) were usually made of platinum, stainless steel mesh, or RVC, because they have a large surface area so that they do not limit the passage of current. A Ag/AgCl electrode in conjunction with a 3.0 M NaCl salt bridge was used as reference electrode (RE) in aqueous solution; while for synthesis in ionic liquids, Ag/AgCl with a EMI-TFSI salt bridge was usually employed.

The aqueous solutions used for electrodeposition of optically active PAn.(+)-HCSA emeraldine salt typically contained 0.2 M aniline monomer and 1.0 M (1*S*)-(+)-10-camphorsulfonic acid⁵ chiral dopant, and were purged with nitrogen gas. Unless otherwise stated, the polymerizations were performed at room temperature (18-25°C).

Both potentiostatic and potentiodynamic polymerization were used. In the potentiostatic method, the PAn.(+)-HCSA emeraldine salt films were formed by applying a constant potential of +0.8 V when using a GC working electrode and +0.9 V when employing an ITO-Pt-coated glass electrode, due to the different resistivity of the two electrodes. By controlling the total charge passed during polymerization it is possible to control the film thickness or the amount of polymer formed/deposited. The constant potential was applied to the working electrode using a BAS CV-27, which also recorded the charge passed.

To produce polyaniline films suitable for spectroscopic characterization, a deposition charge of 120 mC/cm² was usually used for deposition onto ITO coated glass, while a charge of 50-70 mC/cm² was generally used for electrodeposition onto GC electrodes to

give films for electrochemical characterization. The thin polyaniline films were washed with methanol to remove monomer, oligomers and excess dopant acid trapped on the films before further use.

Potentiodynamic polymerization of aniline in the presence of acid dopant was achieved by applying a potential sweep between -0.2 V and 1.0 V, -0.2 V and 1.1 V, or -0.2 V and 1.2 V at a specified scan rate (e.g. 50 mV/s) to the working electrode for 10-20 cycles, using a BAS CV-27 and a Mac Lab/ 2e (AD Instruments) with E.Chem software. The polymer films were usually washed with methanol to remove oligomer, excess monomer and unincorporated HCSA.

2.3.2 Chemical Polymerization

The polyaniline hydrochloride (PAn.HCl) emeraldine salt was synthesized by the oxidative polymerization of 1.0 mL of aniline in 100 mL of 1.0 M HCl, using 2.5 g of ammonium persulfate ((NH₄)₂S₂O₈) (APS) oxidant dissolved in 25 mL of 1.0 M HCl. The APS solution was added drop-wise using a burette. The reaction mixture was magnetically stirred in an ice bath to control the reaction temperature between 0-2°C. After two hrs, the PAn.HCl precipitate was collected by vacuum filtration and then washed with 100 mL of 1.0 M HCl and methanol until the filtrate was colourless.

2.3.3 De-doping/Re-doping of Polyanilines

De-doping

Powders or films of the emeraldine salts (ES) (e.g. PAn.HCl or PAn.(+)-HCSA) were converted to their emeraldine base (EB) form by stirring the powder or soaking the film in 50-100 mL of 1.0 M ammonium hydroxide for 30-60 min. The green colour of ES immediately turned to the blue of EB.

Re-doping

Powders or films of the EB were re-doped to the ES form (e.g. PAn.HCl or PAn.(+)-HCSA) by stirring the EB powder or soaking the EB film in 50-100 mL of 1.0 M HCl or 1.0 M (+)-HCSA for 30-60 min. The blue colour of EB returned to the green of ES.

2.4 Polymer Characterization Techniques

2.4.1 Ultraviolet-Visible-Near Infrared Spectroscopy

UV-visible-NIR spectroscopy is a very useful technique for probing the molecular and conformational structures of conducting polymers. Absorption of light in the UV-visible region causes electronic transitions between the valence and conduction bands. The particular absorption bands observed are indicative of the nature of the polymers, including the charge carriers and the polymer chain conformations. The absorption spectra of conducting polymers are also a function of their oxidation states. Absorption in near-infrared (NIR) region provides further information on the molecular conformations of conducting polymers.

Routine absorption spectra of thin polymer films electrodeposited on ITO-coated glass or evaporatively cast onto ordinary glass were measured using a Shimadzu UV-1601 spectrophotometer (300-1100 nm) or a Shimadzu MultiSpec-1501 with Hyper UV 1.50 software. A Cary 500 spectrophotometer (Variant) was used to record spectra over the extended region 300 to 2500 nm. The absorption spectra (250 to 1100 nm) of solutions were measured in 1 cm path length quartz cells.

2.4.2 Circular Dichroism (CD) Spectroscopy

Circular dichroism (CD) spectroscopy is one of the most powerful techniques for studying the optical activity and conformation of chiral molecules, particularly for

optically active macromolecules such as proteins and chiral synthetic polymers. This technique involves measuring the difference in molar absorption coefficient/ molar absorptivity ($\Delta\varepsilon$) of left- and right-handed circularly polarized light by a chiral molecule, as shown in Equation (2.1).

$$\Delta\varepsilon = \varepsilon_L - \varepsilon_R \quad (2.1)$$

When $\Delta\varepsilon$ is positive, the CD band is called a positive circular dichroism Cotton effect. In contrast, if $\Delta\varepsilon$ is negative, the CD band is called a negative circular dichroism Cotton effect. When two (or more) chromophores of the same type are present nearby in the same molecule, bisignate or split CD bands may be observed because the energy level of the excited state is split. The bisignate CD bands are opposite in sign.

The CD bands of an optically active compound appear at the same wavelengths as the absorption bands in its UV-visible spectrum. For example, an aqueous solution of (+)-10-camphorsulfonic acid exhibits absorption maxima at 190 nm and 286 nm, while its corresponding CD spectrum shows a negative CD band at 192.5 nm and a positive band at 290.5 nm.⁶

The CD spectra of thin polyaniline films or dilute polymer solutions/dispersions were measured using a Jobin Yvon Dichrograph 6. Visible region (300-800 nm) was usually used when the polymer films were deposited/cast onto ITO-coated glass/glass, while CD spectra in UV-visible region could be recorded for aqueous solutions/dispersions using a 1 cm path length quartz cell. The CD spectrometer was calibrated using a 1 g/L aqueous solution of (+)-10-camphorsulfonic acid.

2.4.3 UV-visible and Circular Dichroism Spectroelectrochemistry

Spectroelectrochemistry combines the techniques of electrochemistry and spectroscopy. In a specially desired electrochemical cell, absorption spectra or circular dichroism spectra of polymer films deposited/coated on transparent ITO-coated glass can be monitored *in situ* as the films are oxidized or reduced by the application of a fixed potential. The electrochemical cell used for *in situ* UV-visible/CD spectroelectrochemistry in this thesis is shown in Figure 2.3.

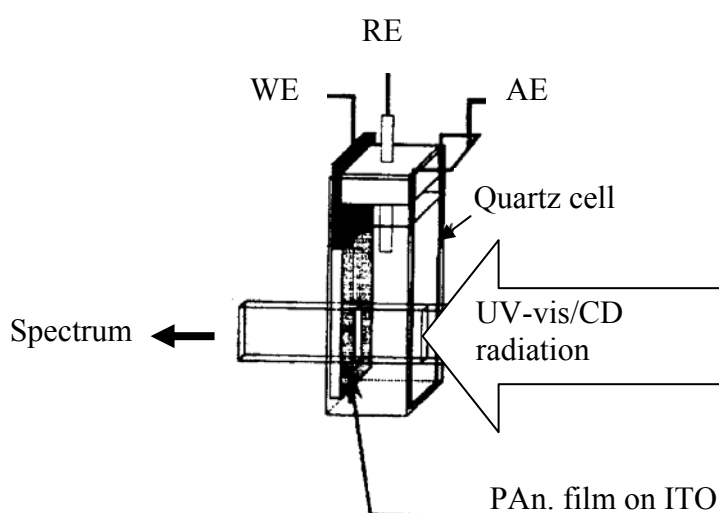


Figure 2.3 A three-electrode electrochemical cell for *in situ* UV-vis/CD spectroelectrochemical measurements.

2.4.4 Raman Spectroscopy

Raman spectroscopy typically provides qualitative information on the chemical structure of samples. The Raman spectrum is obtained by irradiating the sample with laser light of a certain frequency (or excitation radiation) and analysis of the scattered radiation caused by the Stokes shift. The difference in frequency of the incident and scattered radiation corresponds to the vibrational frequencies of the sample.

For polymer characterization, the simplest application of Raman spectroscopy is to look for the presence of specific vibrations of particular chemical groups that can be used to identify/confirm the kind of polymer. Moreover, absorption of the incident radiation by water and many other electrolytes is minimal. It is possible, therefore, to obtain the Raman spectrum for a sample while it is in solution or immersed in an electrolyte.

Raman spectra of polymer films or powders were measured using a Jobin Yvon Horiba Raman spectrometer connected to a CCD detector. The laser beam (He-Ne laser), with 632.8 nm exciting radiation, was focused on the sample by a x 100 lens. The laser was calibrated with SnO₂. Baseline correction and smooth were incorporated in the spectra using LabSpec software.

2.4.5 Scanning Electron Microscopy (SEM) and Atomic Force

Microscopy (AFM)

SEM and AFM are generally used for investigating the surface morphology and micro/nanostructure of conducting polymers as grown. They can also be used to observe the morphology changes in a polymer after reaction with other chemicals or following thermal treatment.

The SEM images of polyaniline films electrodeposited onto ITO-Pt-coated glass were assessed with a Leica Cambridge 440 scanning electron microscope located in the Materials Engineering Department at the University of Wollongong. Prior to measurements, the polymer films were washed with methanol and coated with a very thin layer of gold to improve resolution.

Atomic force micrographs of polyaniline films electrodeposited on ITO-Pt-coated glass were obtained using the Atomic Force Microscope located in the Materials Engineering

Department at the University of Wollongong. The two- and three-dimensional images of $50\ \mu\text{m}^2$ sections of the films were obtained using the contact mode. A commercially available gold tip was used.

2.4.6 Cyclic Voltammetry (CV)

Cyclic voltammetry (CV) is one of the most common electrochemical techniques. It provides useful information on the electrochemical behaviour of compounds including conducting polymers, as well as on the mechanisms of polymer growth. In a general sense, CV involves scanning the potential between a potential more negative than the reduction potential to a potential higher than the oxidation potential of the compound under investigation, and plotting the current response at the working electrode as a function of the applied potential. The resulting current-potential plot is called the cyclic voltammogram. Cyclic voltammetry provides a rapid method for determination the potentials at which redox reactions take place.

In this thesis, cyclic voltammetry was used to study the redox properties of the conducting polymers after growth and during potentiodynamic polymerization, as well as to determine the redox potentials of monomers and prochiral substrates. In addition, it was used to determine the potential at which irreversible over-oxidation/degradation of the polymers occurs and to establish the useful potential windows of ionic liquids. A typical cyclic voltammogram for a reversible process is shown in Figure 2.4. The electrochemical cell and instrumentation used in these experiments are previously described in section 2.3.1.

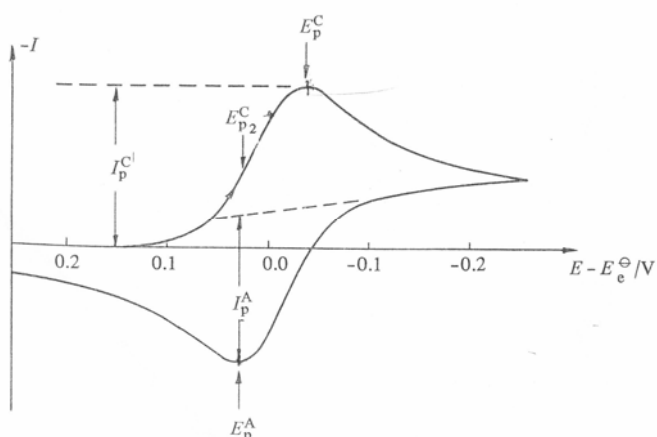


Figure 2.4 A typical cyclic voltammogram for a reversible process.

2.4.7 Thermogravimetric Analysis (TGA)

Thermogravimetric analysis (TGA) is extensively used for determining the weight changes of a sample upon heat treatment. This change results from physical or chemical transformations of the sample. The TGA profile is normally a plot of the weight change as a function of temperature or time. For the thermal analysis of polyaniline, TGA is widely used to determine the amount of solvent/water incorporated in the polymer, the onset temperature for the loss or decomposition of dopant acid, and the decomposition of the polymer backbone.

Thermogravimetric analyses of the polymer powders, accurately weighed (*ca.* 8-10 mg) in alumina crucibles were conducted using a Setaram DTA/TGA 92B instrument located in the Institute for Superconducting and Electronic Materials (University of Wollongong). The temperature range between 50° and 700°C was used, with a heating rate of 10°C/min, under a nitrogen flow of 15 mL/min. The TGA of an ionic liquid sample was conducted using a STA 1500 (Rheometric Scientific) located at Monash University, in air or a nitrogen flow (20 mL/min) between 25°C and 450°C at a heating rate of 10°C/min. Accurately weighed samples (*ca.* 20-25 mg) were analyzed.

2.4.8 Differential Scanning Calorimetry (DSC)

Differential scanning calorimetry (DSC) is used to determine the amount of heat that is involved as a sample undergoes an exothermic or endothermic transition when the sample is heated at a controlled heating rate. It provides information on the thermal properties of the samples as they undergo physical and chemical transformations during thermal treatment. This technique is usually complementary to thermogravimetric analysis of the samples. From DSC results, information on physical changes (evaporation of solvents/moisture content, the glass transition temperature, melting temperature) and chemical changes (cross-linking, degradation/decomposition) can be obtained.

DSC profiles of polyaniline were obtained using a DSC Q100 (TA Instruments). Accurately weighed powder samples were placed in a sealed medium-pressure DSC aluminium pan. The analysis conditions were programmed by equilibrating samples at 105°C for 10 min to eliminate trace water and then cooling down to 40°C at a cooling rate of 20°C/min. The first scan was automatically started by heating at a temperature ramp of 10°C/min from 40°C to 200-350°C. The temperature was cooled down to 40°C at a cooling rate of 20°C/min before starting the second scan using the same conditions as the first run. All measurements were carried out under a nitrogen atmosphere at a flow rate of 50 mL/min.

DSC curves of ionic liquids were obtained using a DSC Q100 (TA Instruments) in a nitrogen flow (50 mL/min) between -80° and 200°C at a heating rate of 10°C/min for the first scan, and then cooling down to -80°C at a rate of 10° C/min before conducting the second scan under the same condition. Accurately weighed samples were loaded into aluminium pans and sealed with medium pressure in an atmosphere of nitrogen.

Glass transition temperature (T_g), crystallization point (T_c) and melting point (T_m) were obtained from the DSC profile.

2.4.9 Electrical Conductivity

The electrical conductivity of conducting polymers is generally measured using a four-point probe. This involves using four tip electrodes about 1 mm apart in a straight line, as shown in Figure 2.5.

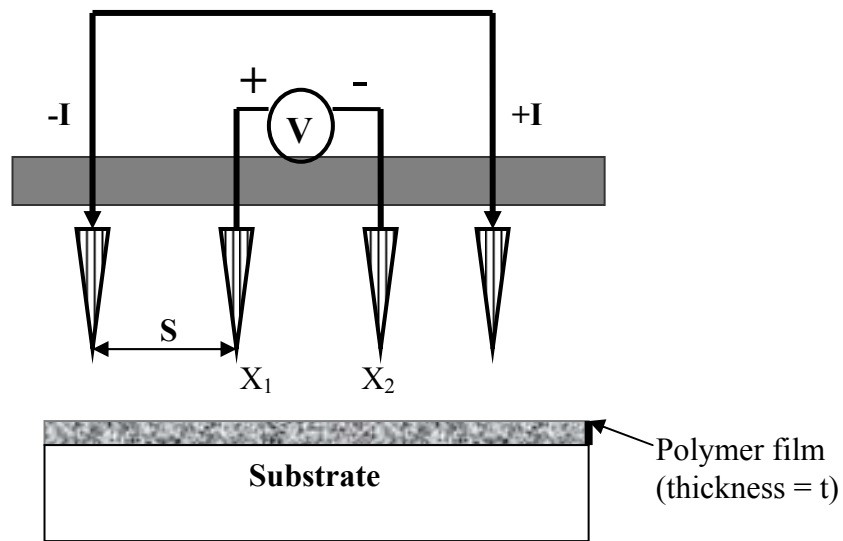


Figure 2.5 Four-point probe configuration.

The probe head can be raised and lowered from a stage. A constant current is applied through the two outermost probes and a voltage measurement is made across the two inner probes that are at distances X_1 and X_2 . For a film of thickness $t \ll s$ (t = film thickness, s = distance between the inner and outer probes), the sheet resistance (ρ) for thin wafers and films is defined as follows:

$$\rho = \pi t / \ln 2 (V/I)$$

$$R_s = \rho / t = 4.532 (V/I)$$

where V is the voltage expressed in volts and I is current expressed in amperes. The conductivity of the sample can then be calculated from the reciprocal of resistivity.

The conductivity of a polymer film of the complex between PMAS and PLL cast onto a glass slide was measured using a Jandel four-point probe head Model RM2 (Jandel Engineering Ltd.). Thickness of the films was measured with a Mutiutoyo Digital micrometer (0.001 mm).

2.4.10 Polarimetry

In polarimetry, the specific rotation $[\alpha]$ of a substance is defined by Equation (2.2).

$$[\alpha] = \alpha / l \cdot c \quad (2.2)$$

where α is the rotation of the plane of polarization expressed in degrees; l is the length of the cell expressed in decimeters; and c is the concentration of the substance expressed in g/cm^3 of solution. The specific rotation of the substance also depends on the solvent employed, the temperature, and the wavelength of the polarized light. Therefore, specific rotations are usually reported in the form $[\alpha]_{\lambda}^T$, with the concentration and the solvent used given alongside. Generally, a wavelength of 589 nm (sodium D-line) is used.

Optical rotations of samples in this thesis were measured with a Jasco DIP-370 Digital polarimeter in analytical reagent grade solvents, using a 10 cm path length cell.

2.5 References

1. F. Masdarolomoor, P.C. Innis, S.A. Ashraf, and G.G. Wallace. *Purification and Characterization of Poly(2-methoxy aniline-5-sulfonic acid)* in *The International Conference on the Science and Technology of Synthetic Metals*. 2004. Wollongong, Australia.
2. J. Sun, M. Forsyth, and D.R. MacFarlane, *J. Phys. Chem. B.* **102** (1998): 8858.
3. D.R. MacFarlane, P. Meakin, J. Sun, N. Amini, and M. Forsyth, *J. Phys. Chem. B.* **103** (1999).
4. S.A. Ashraf, Y. Pornputtkul, A.L.P. Kane-Maguire, and G.G. Wallace, (*to be submitted*).
5. V. Aboutanos, L.A.P. Kane-Maguire, and G.G. Wallace, *Synth. Met.* **114** (2000): 313.
6. D.F. Gerald, *Circular Dichroism and The Conformational Analysis of Biomolecules*. (1996) New York and London: Plenum Press.

Chapter 3

A Novel Route to Optically Active Polyaniline via Thermal Treatment

3.1 Introduction

Optically active polyanilines (PAn.HA) have generally been prepared via the incorporation of chiral dopant anions (A^-) either (i) during electrochemical polymerization of aqueous aniline in the presence of a chiral dopant acid HA,^{1,2} or (ii) by acid doping of emeraldine base with the chiral acid in an organic solvent such as 1-methyl-2-pyrrolidinone (NMP).³⁻⁵ To prepare large amounts of chiral polyaniline for applications such as chromatographic materials for chiral separations,^{6,7} preparation by route (ii) using chemically synthesized polyaniline seems to be advantageous because of its ready scale-up. However, using toxic and expensive organic solvents such as NMP is undesirable for commercial scale production.

A solid-state route to optically active polyaniline, avoiding the use of such solvents, would therefore be of considerable value. However, in the chemical and electrochemical preparation of optically active polyanilines to date, induction of chirality into the polyaniline chains (via the adoption of a one-handed helical structure¹⁻⁴) is believed to occur in “solution” prior to deposition of the polymer. Steric crowding in the solid state apparently prevents the rearrangement of the polyaniline chains into a preferred one-handed helical arrangement.

Thus, acid doping of solid emeraldine base with the aqueous chiral dopant (+)-HCSA generated a PAn.(+)-HCSA emeraldine salt that was optically inactive in the visible region.⁸ However, the motion of polyaniline chains in the solid state has recently been demonstrated at elevated temperatures above the polymer glass transition temperature, T_g ,⁹ where heating electrochemically deposited PAn.(+)-HCSA films at $\geq 140^\circ\text{C}$ caused a change from an “extended coil” to a “compact coil” conformation.

The latter thermochromic behaviour of emeraldine salts in the solid state prompted the exploration in this Chapter of the possibility that optically active polyaniline could be generated by heating optically inactive PAn.(+)-HCSA or PAn.(-)-HCSA films (prepared from emeraldine base). It was hypothesized that one-handed helices may be preferentially adopted by the polyaniline chains arising from movement of the polyaniline chains at high temperature in the presence of the chiral CSA^- dopant. If successful, this would provide a new route to optically active polyanilines avoiding the use of solvents that may be useful for the preparation of large amounts of chiral polyanilines for various applications. Thermal properties, thermogravimetric analysis (TGA) and differential scanning calorimetry (DSC) of the polyaniline materials produced by this thermal route are also examined.

3.2 Experimental

3.2.1 Sample Preparations

(i) Electrochemically Synthesized Films for Thermal Treatment

PAn.HCl films were electrodeposited at room temperature ($18^\circ\text{-}20^\circ\text{C}$) on ITO-coated glass electrodes (without Pt-sputter coating) at 0.9 V, from aqueous 0.2 M aniline/1.0 M HCl, while passing 120 mC/cm^2 of charge. The films were de-doped by treatment with aqueous 1.0 M NH_4OH for 30 min to give emeraldine base (EB) films. Optically

inactive PAn.(+)-HCSA or PAn.(-)-HCSA films were then obtained by re-doping the EB films with aqueous 1.0 M (+)- or (-)-HCSA for 30 min.

(ii) Chemically Synthesized Films for Thermal Treatment

A solution/dispersion of 2% (w/v) emeraldine base (chemically synthesized) in NMP solvent was stirred for 3 hrs at room temperature. 80 μ L samples of this solution were cast onto 2 cm² ordinary glass slides. Drying at 60°C for 6 hours gave emeraldine base (EB) films. Optically inactive PAn.(+)-HCSA films were subsequently obtained by doping these films in aqueous 1.0 M of (+)-HCSA for 12 hrs at room temperature.

(iii) Sample Preparation for Thermal Analyses

There were five powder samples prepared for TGA and DSC thermal studies: optically inactive EB-CS (1), optically inactive PAn.(+)-HCSA-CS (2), optically inactive PAn.HCl-ECS (3), optically inactive PAn.(+)-HCSA-ECS (4), and optically active PAn.(+)-HCSA-ECS (5). (CS = chemically synthesized, ECS = electrochemically synthesized).

The emeraldine base sample EB-CS (1) was prepared by alkaline de-doping of chemically synthesized PAn.HCl with 1.0 M NH₄OH (see Chapter 2 for details). The emeraldine salt sample (2) was prepared by re-doping sample (1) with aqueous 1.0 M (+)-HCSA (see Chapter 2 for details). Sample (3) was prepared by the electrodeposition of PAn.HCl onto a Pt sheet (5 x 5 cm) at 0.9 V, in 200 mL of aqueous 0.2 M aniline/1.0 M HCl. Ag/AgCl_(3M NaCl) and RVC were used as reference and auxiliary electrodes, respectively. The PAn.HCl was scraped from the working electrode and washed three times with 100 mL of aqueous 0.1 M HCl, then collected and sucked dry by vacuum filtration. The powder was dried and stored in a vacuum dessicator. Sample (4) was

prepared by alkaline de-doping of sample (3) with aqueous 1.0 M NH₄OH and re-doping with aqueous 1.0 M (+)-HCSA. Sample (5) was prepared using the same procedure as sample (3), but aqueous 0.2 M aniline/1.0 M (+)-HCSA was used for electrodeposition and 0.1 M (+)-HCSA for washing the deposited polymer film.

3.2.2 Spectroscopic Studies

UV-visible and CD spectra of the films were recorded at room temperature as described in Chapter 2.

3.2.3 Thermal Treatment

After their UV-visible and circular dichroism spectra were measured, the above films were treated at 120° - 170°C for fixed periods in a hot air oven (Binder model E28).

3.2.4 Thermal Analysis

(i) Thermogravimetric Analysis (TGA)

TGAs were conducted using Setaram DTA/TGA 92B in a nitrogen flow (15 mL/min) between 50°C and 700°C at a heating rate of 10°C/min. Accurately weighed samples (*ca.* 10 mg) in alumina crucibles were analyzed.

(ii) Differential Scanning Calorimetry (DSC)

DSC profiles were obtained using a DSC Q100 (TA Instruments). Accurate weights of powder samples were placed into a sealed medium-pressure DSC aluminium pan. The analyses were generally programmed to include equilibrating the samples at 105°C for 10 min to eliminate trace water and then cooling down to 40°C at a cooling rate of 20° C/min. The first scan was carried out with a temperature ramp of 10°C/min from 40°C to 200°-350°C. The temperature was decreased to 40°C at a cooling rate of 20°C/min before starting the second scan using the same condition as the first run. All

measurements were carried out under a nitrogen atmosphere at a flow rate of 50 mL/min.

3.3 Results and Discussion

3.3.1 Heat Treatment of Electrochemically Derived Emeraldine Base Doped with (+)-HCSA or (-)-HCSA

An optically inactive emeraldine base film (initially electrodeposited as PAn.HCl onto ITO-coated glass) was re-doped by treatment with aqueous (+)-HCSA. Its UV-visible spectrum exhibited absorption bands at *ca.* 320 and 440 nm attributed to a π - π^* transition and a polaron band, a broad peak at *ca.* 900 nm attributed to a second polaron band, and a free carrier tail in the near-infrared (Figure 3.1, trace 1). This is characteristic of the partially “extended coil” conformation generally found for electrochemically deposited emeraldine salts.⁹ The corresponding CD spectrum (Figure 3.2, trace 1) confirmed that this film was optically inactive. That is, there was no chiral induction when the emeraldine base film was doped with (+)-HCSA in the solid state at room temperature.

The UV-visible spectrum of this PAn.(+)-HCSA film altered after heat treatment at 170°C for 40 min (Figure 3.1, trace 2). Only a single broad peak was exhibited into the 300-430 nm region, presumably arising from overlapping π - π^* and polaron bands. A strong shoulder was now observed at 800 nm attributable to a second polaron band, and there remained significant near-infrared absorption.

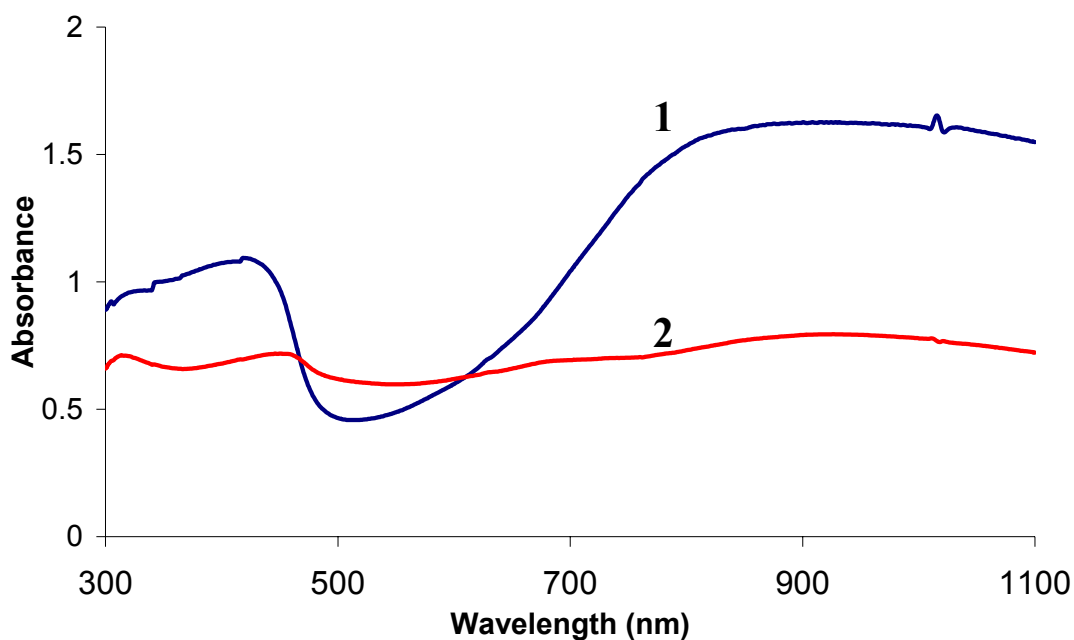


Figure 3.1 Effect of heat treatment on the UV-visible spectrum of an optically inactive PAN.(+)-HCSA film (initially electrochemically prepared as PAN.HCl): (1) initial film, (2) after heating at 170°C for 40 min.

Figure 3.2 presents the CD spectra for the PAN.(+)-HCSA film before and after heat treatment at 120°, 140°, and 170°C. The spectral changes reveal that the emeraldine salt film changed from an optically inactive to an optically active material during thermal treatment. Weak, ill-defined CD spectra were recorded after heating in the temperature range 120-140°C (e.g. after heating at 120°C for 10 min, in Figure 3.2). However, after treatment at 170°C, two distinct CD bands of negative and positive sign appeared at *ca.* 400 and 460 nm, respectively (Figure 3.2). These bands may be assigned as bisignate, exciton-coupled bands associated with the polaron absorption band at *ca.* 425 nm. This CD spectrum is a characteristic of the “compact coil” conformation of chiral PAN.(+)-HCSA, which has been previously obtained via doping EB with (+)-HCSA in an organic solvent.⁹

These chiroptical results indicate that the PAn.(+)-HCSA films not only became optically active upon heating at 170°C, but the polyaniline also underwent a conformational change from an initial largely “extended coil” conformation to a partly “compact coil” conformation. A similar conformational change for electrochemically deposited emeraldine salts from “extended coil” to “compact coil” conformation at temperatures above 140°C has been reported previously.⁹

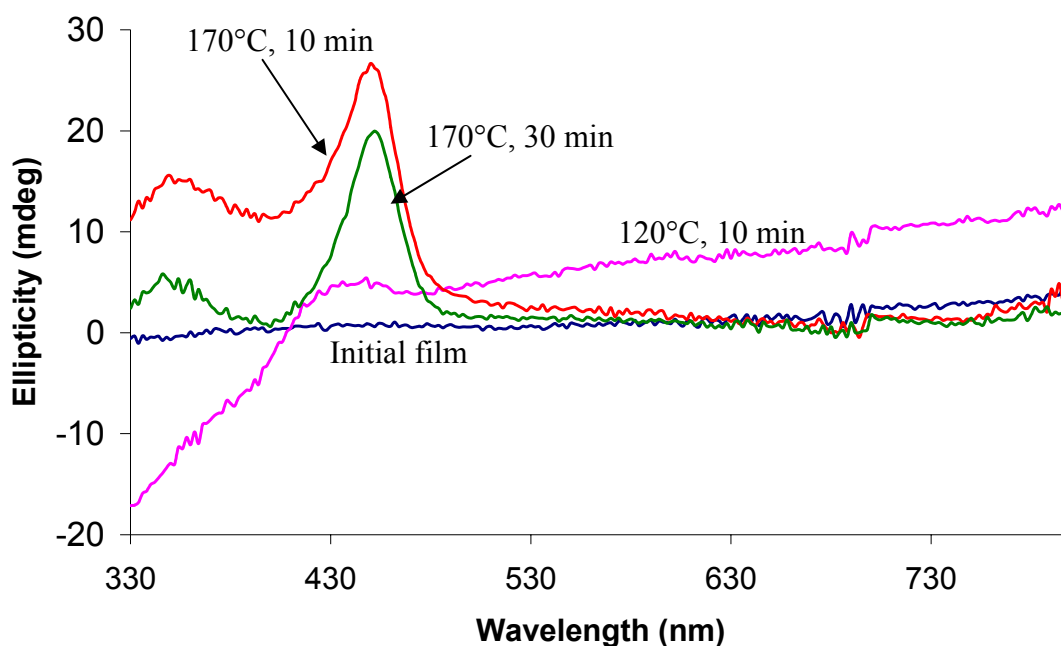


Figure 3.2 Effect of heat treatment at various temperatures on the CD spectrum of an initially optically inactive PAn.(+)-HCSA film. All CD spectra recorded after cooling to room temperature.

Related experiments were also carried out in which an emeraldine base film (obtained by alkaline de-doping of electrochemically deposited PAn.HCl) was doped with the enantiomeric (-)-HCSA to give a PAn.(-)-HCSA film. Its UV-visible spectra before and after heating at 170°C are shown in Figure 3.3a, revealing relatively small changes. However, as found above for the corresponding PAn.(+)-HCSA film, heating at 170°C for 10-20 min again caused the development of visible region optical activity, as evidenced by the CD spectra in Figure 3.3b. Bisignate CD bands were observed at *ca.*

400 and 460 nm which were the mirror image of those seen above for the thermally produced PAn.(+)-HCSA film (Figure 3.2). These results indicate that, at elevated temperatures, the chiral CSA⁻ dopant anions in these initially optically inactive emeraldine salt films induce chirality into the polyaniline chains, possibly by the partial adoption of a preferred one-handed helical arrangement. The molecular movement required for this is presumably permitted by the greater mobility possible at temperatures above the polyaniline glass temperature (*ca.* 140° -150°C).^{10, 11}

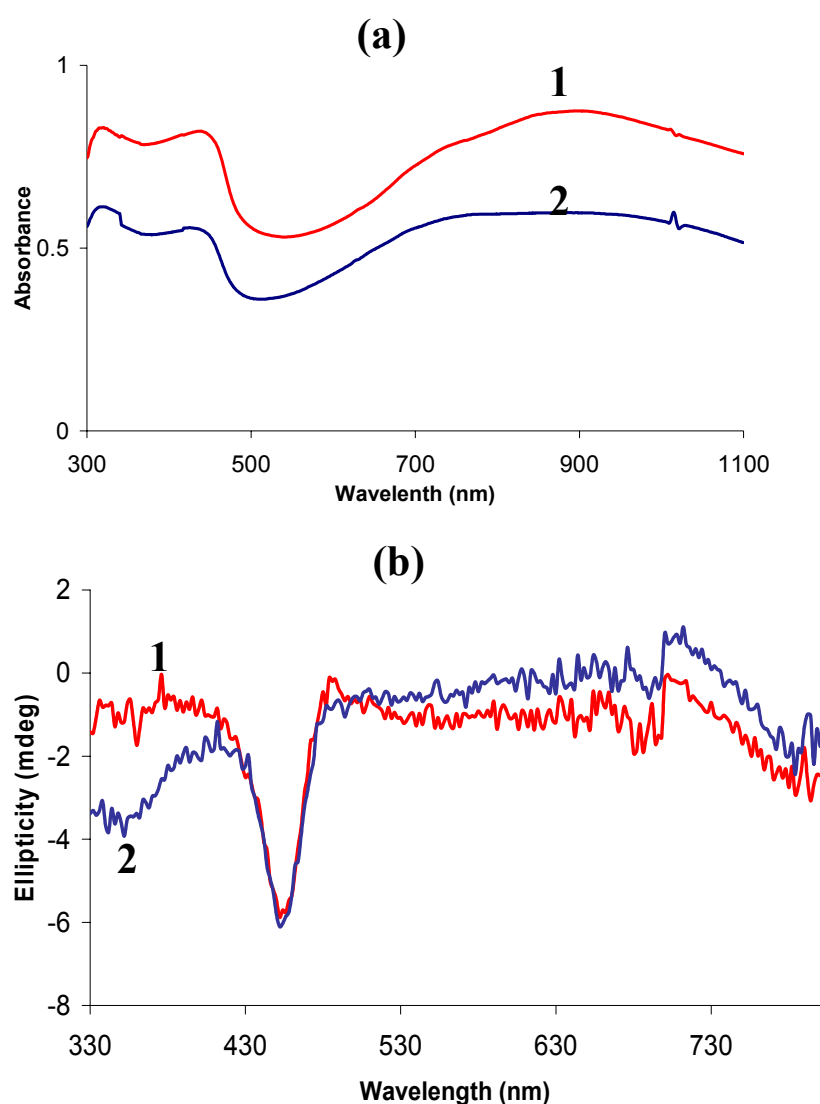


Figure 3.3 Effect of heat treatment at 170°C on the UV-visible (a) and CD spectra (b) of an initially optically inactive PAn.(-)-HCSA film (all spectra recorded after cooling to room temp): (1) after heating at 170°C for 10 min, (2) after heating at 170°C for 20 min.

3.3.2 Heat Treatment of Chemically Derived Emeraldine Base Doped with (+)-HCSA

Related heat treatment studies were carried out on optically inactive PAn.(+)-HCSA films whose precursor was chemically (rather than electrochemically) derived emeraldine base. PAn.HCl was prepared via the chemical oxidation of aniline with ammonium persulphate in aqueous HCl, and then de-doped with NH₄OH to give the emeraldine base (EB) starting material. A film of this EB was evaporatively cast from NMP solution, and then doped with aqueous (+)-HCSA to give a PAn.(+)-HCSA film.

The UV-visible spectrum for this PAn.(+)-HCSA film after heating at 170°C for 10 min (Figure 3.4a, trace 1) exhibited a broad polaron band centered at *ca.* 850 nm, as well as two lower wavelength bands at 350 nm and 420 nm assignable as a π - π^* transition and a second polaron band, respectively. This spectrum is similar to that observed before heat treatment, with no significant change observed after heating at 170°C for 20 min (Figure 3.4a, trace 2).

As expected, the initial PAn.(+)-HCSA film was found to be optically inactive. However, a weak CD spectrum was observed after heating at 170°C for 10 min (Figure 3.4b-trace 1) confirming the generation of optical activity in the polymer. After a further 10 min heating at 170°C, the CD spectrum became better defined (Figure 3.4b-trace 2), and showed two bands at 400 and 460 nm with negative and positive signs, respectively. These bands may be assigned as the bisignate, exciton-coupled CD band associated with the 420 nm absorption band.

In summary, heating electrochemically or chemically derived optically inactive PAn.(+)-HCSA films at 170°C causes the generation of visible region optical activity in the polyaniline materials. However, only relatively weak optical activity (with CD

bands of up to 27 mdeg) is generated. Thus, although revealing an interesting new method for producing optically active polyanilines, this thermal method at present appears unsuitable for the preparation of highly optically active materials.

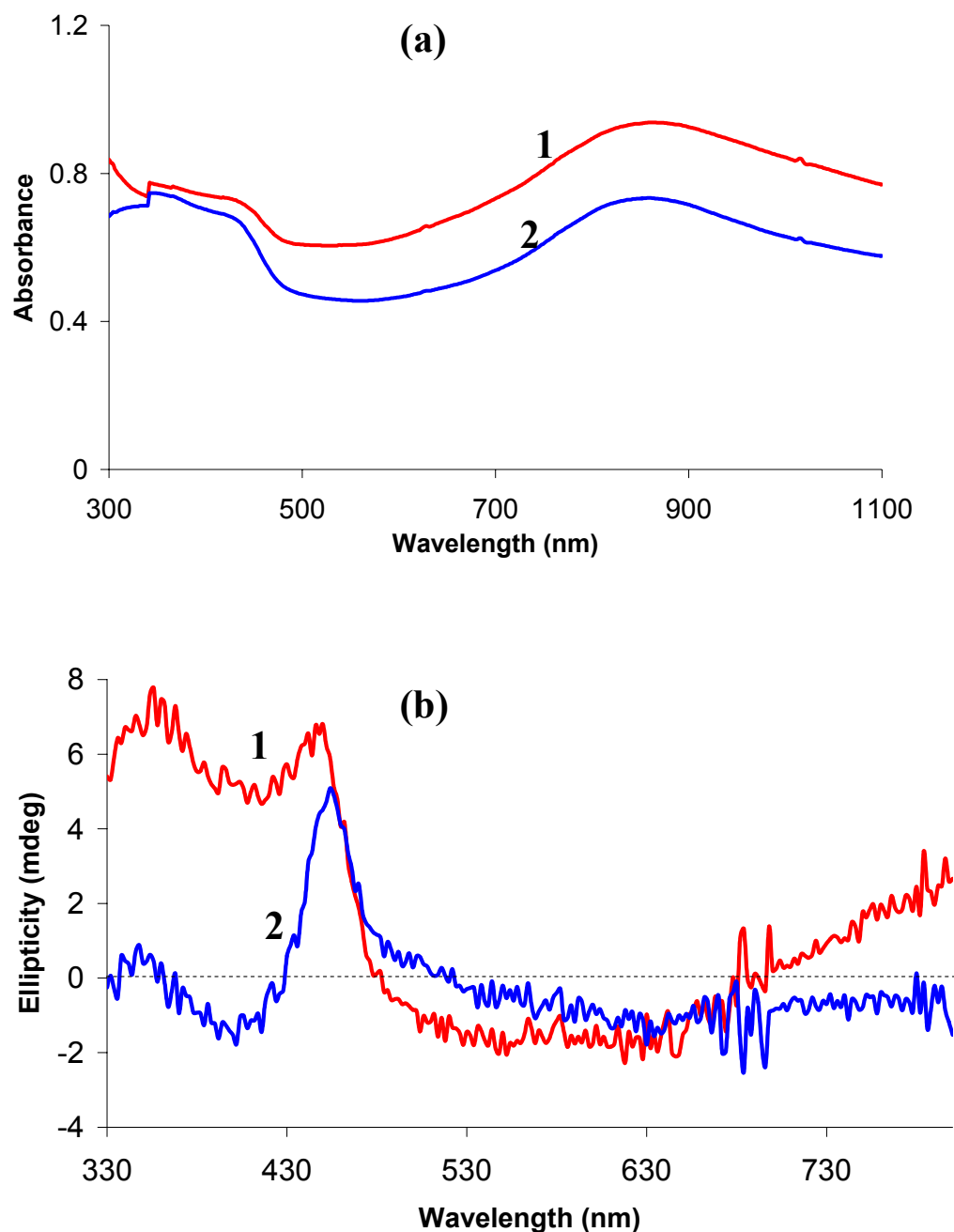


Figure 3.4 Effect of heat treatment on the UV-visible (a) and CD spectra (b) of a chemically prepared PAn.(+)-HCSA film made by doping EB film with aqueous (+)-HCSA: (1) after heating at 170°C for 10 min, (2) after heating at 170°C for 20 min.

3.3.3 Thermal Analysis of Polyanilines

In order to throw further light on the nature of this novel thermal route to optically active polyaniline emeraldine salts, detailed thermogravimetric analysis (TGA) and differential scanning calorimetry (DSC) studies were carried out on the polymers during heat treatment.

(i) TGA Study

The TGA thermograms of chemically derived EB (sample 1) under a nitrogen atmosphere are given in Figure 3.5. Two major stages of weight loss were observed for the EB-CS powder. The first, small weight loss at 100°-150°C results from moisture evaporation. The second large weight loss of *ca.* 22% was observed in the range 475°-600°C, indicating some structural decomposition of the polymer backbone. No further weight loss occurred up to 700°C, indicating that EB powder is relatively thermal stable under a nitrogen atmosphere. This TGA result is in good agreement with a previous report on EB powder by Ding *et al.*¹² Their results also showed that EB powder is much more stable under nitrogen than in air, as less than 20% weight loss was observed at 600°C in nitrogen compared to nearly 100% weight loss in air.

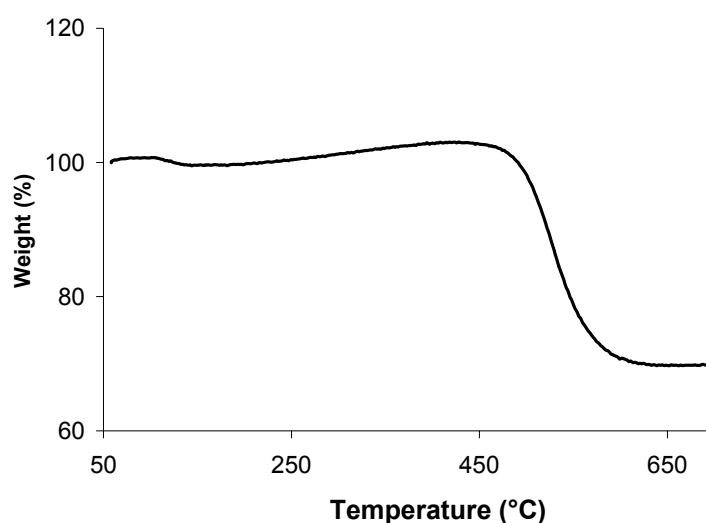


Figure 3.5 TGA thermogram of sample 1 (EB-CS) under N₂ (15 mL/min). Sample size: 9.4 mg.

Figures 3.6 and 3.7 show the TGA curves for optically inactive PAn.(+)-HCSA powders prepared by chemical (sample 2) and electrochemical (sample 4) synthesis. The results are similar in general, with both samples exhibiting typical three-step weight-loss behaviour. The shape of the TGA curve for the PAn.(+)-HCSA emeraldine salts can be explained as follows: The first small weight loss around 100°C is due to the evaporation of trace water. The major weight loss (*ca.* 30%) observed in the second step between 250° and 350°C is attributed to removal of (+)-HCSA dopant from the PAn.(+)-HCSA, assisted by its melting (198°C) and subsequent decomposition at temperatures above 230°C.¹⁰ The third weight loss stage, starting at *ca.* 370° - 400°C, is assigned to structural decomposition of the polymer.

These TGA results indicate that no polymer or dopant loss/decomposition occurred during the heat treatment of the PAn.(+)-HCSA emeraldine salt films described in Section 3.3.1 and 3.3.2 above, since heating was only to 170°C.

The general shape of the TGA thermograms described for the emeraldine salts in the present study is similar to those reported previously for chemically synthesized PAn.HCl,^{13,14} PAn.H₃PO₄,¹⁵ chemically derived PAn(±)-HCSA obtained from *m*-cresol,¹⁰ and electrochemically prepared racemic PAn.(±)-HCSA¹⁶ and chiral PAn.(+)-HCSA.⁹ The most significant differences among these are the temperature at which the acid dopants are removed/decomposed and the amount of weight loss in the second step. The third weight loss stage above 300°C is generally attributed to degradation of the polymer backbone that can lead to the production of acetylene and ammonia gases.¹⁷

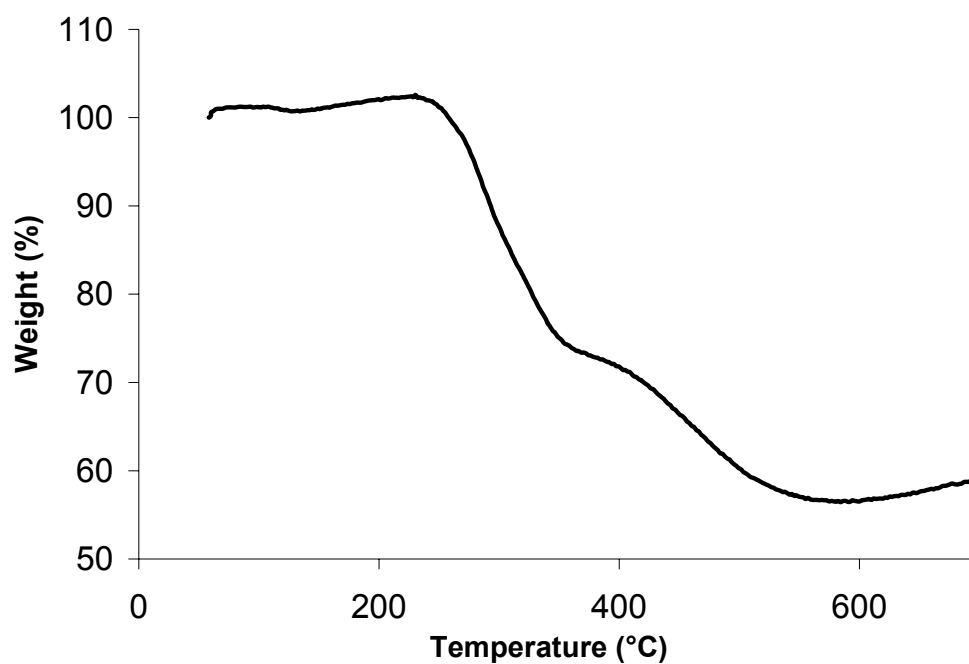


Figure 3.6 Thermogravimetric profile of sample 2 (optically inactive PAn.(+)-HCSA-CS) under N₂ (15 mL/min). Sample size: 9.5 mg.

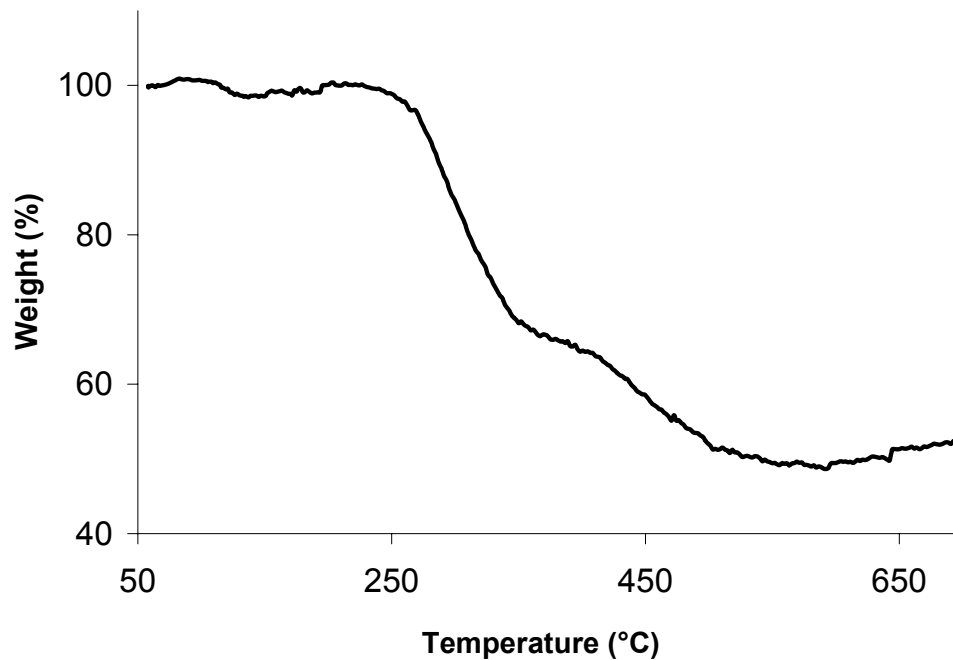


Figure 3.7 Thermogravimetric profile of sample 4 (optically inactive PAn.(+)-HCSA-ECS) under N₂ (15 mL/min). Sample size: 9.8 mg.

(ii) DSC Study

The DSC thermograms of chemically prepared optically inactive PAn.(+)-HCSA (sample **2**) under a nitrogen atmosphere are shown in Figures 3.8 and 3.9, which were measured without and with the pre-heat program (at 105°C for 10 min), respectively. In Figure 3.8 only one broad endothermic peak at 50°-150°C was observed between 40°C and 200°C in the first run. This endotherm is most likely due to evaporation of water present in the polymer powder, which was consistent with the TGA result (Figure 3.6). Therefore, no endotherm was observed in the second run. The glass transition (T_g) temperature reported for polyaniline at 140°-150°C^{10, 11} was not observed as it may have been masked by the large, broad peak attributed to water evaporation. A similar DSC profile recorded in air (50°-250°C) was reported by Palaniappan and Narayana¹⁵ for chemically prepared PAn.H₃PO₄ emeraldine salt. They also reported that no glass transition (T_g) and melting (T_m) temperatures were observed for the polyaniline salts PAn.H₃PO₄, PAn.H₂SO₄, PAn.HCl, PAn.HCOOH, and PAn.*p*-TSA under the conditions employed.

Interestingly, the DSC thermogram of PAn.(+)-HCSA sample **2**, measured after pre-heating at 105°C for 10 min to eliminate water trapped in the sample, exhibited a broad endothermic peak between 110°-170°C in the first run (Figure 3.9). This endothermic peak presumably corresponds to the glass transition¹⁸ and/or the conformational changes⁹ identified from the chiroptical studies in the present work (see Section 3.3.2), and/or morphological changes within the polymer matrix,^{14,19} as no weight loss was observed in this temperature range in the TGA results (Figure 3.6). Evaporation of water or decomposition of the (+)-HCSA dopant are unlikely because the sample was equilibrated at 105°C to eliminate water.

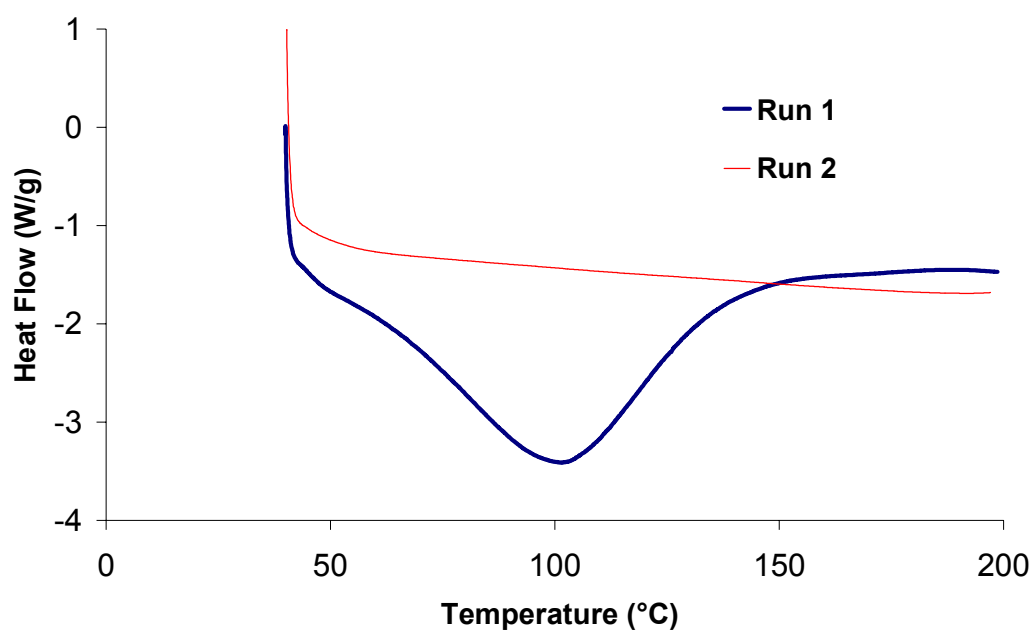


Figure 3.8 DSC thermogram of sample 2 (optically inactive PAn.(+)-HCSA-CS) under N₂ (15 mL/min). Sample size: 4.9 mg.

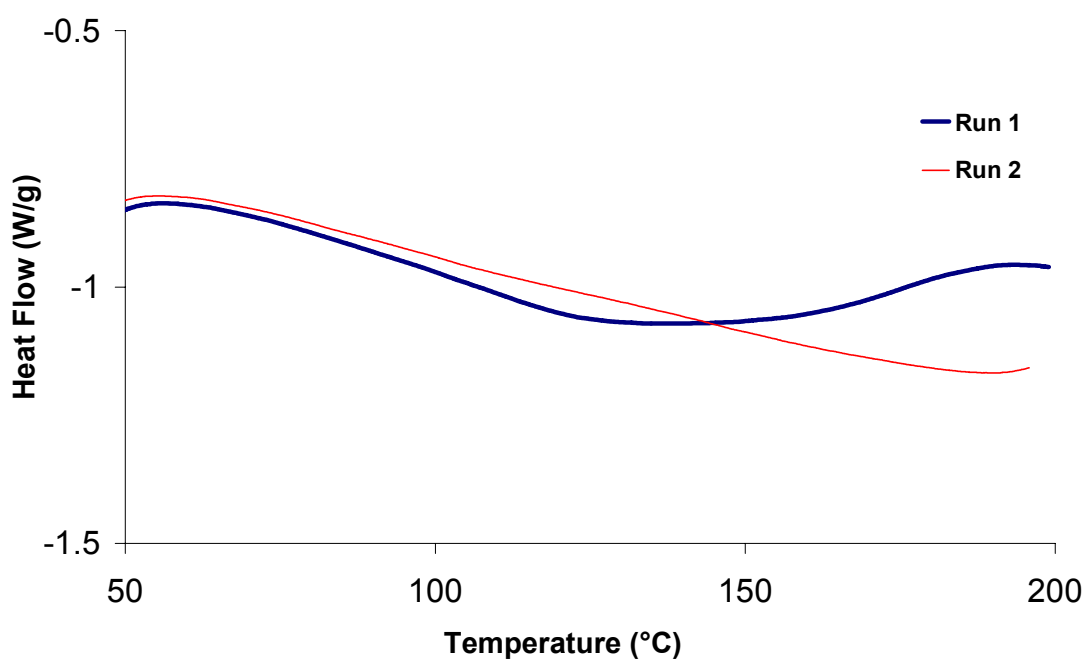


Figure 3.9 DSC thermogram (40°-200°C) of sample 2 (optically inactive PAn.(+)-HCSA-CS) under N₂ (15 mL/min), with pre-heat program (at 105°C for 10 min). Sample size: 5.0 mg.

Similar results were also observed in the DSC measurements of the electrochemically prepared optically inactive PAn.(+)-HCSA (sample 4), as shown in Figures 3.10 and 3.11. The DSC thermogram obtained without pre-heating at 105°C is presented in Figure 3.10. In the first run, an endothermic peak observed at 50°-150°C correlates with the loss of water in the first step of the TGA curve. When the sample was pre-equilibrated at 105°C for 10 min before the DSC measurement, an endotherm between *ca.* 110° and 170°C was observed in the first run (Figure 3.11). Again, it is probably associated with the glass transition and/or the conformational changes and/or morphological changes discussed above.

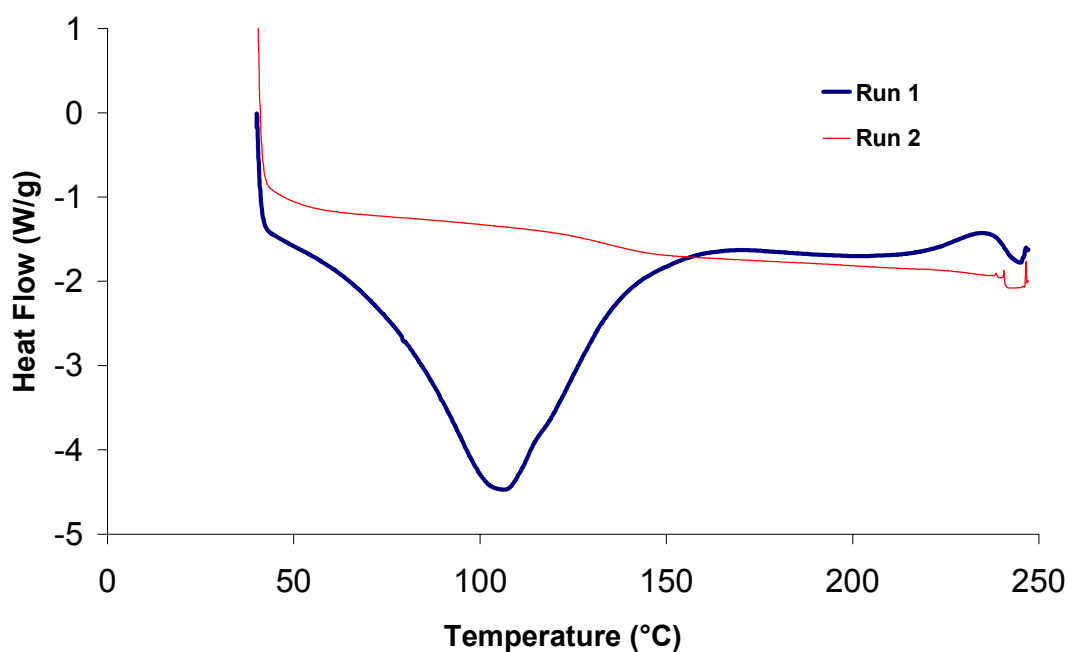


Figure 3.10 DSC thermogram (40°-250°C) of sample 4 (optically inactive PAn.(+)-HCSA-ECS) under N₂ (15 mL/min). Sample size: 5.6 mg.

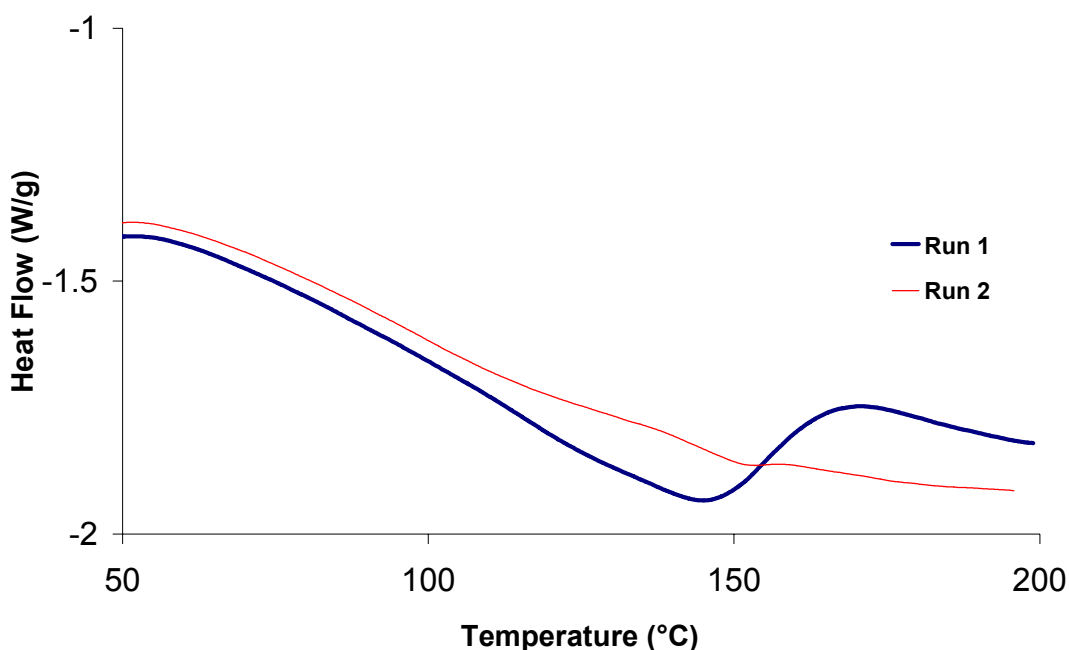


Figure 3.11 DSC thermogram (40°-200°C) of sample 4 (optically inactive PAn.(+)-HCSA-ECS) under N₂ (15 mL/min), with pre-heat program (at 105°C for 10 min). Sample size: 6.5 mg.

To confirm the loss of HCSA dopant at elevated temperature, DSC measurements of PAn.(+)-HCSA (sample 4) and emeraldine base (sample 1) were performed in the range 40°-350°C after pre-heat at 105°C for 10 min. The large endothermic peak at 250°-350°C observed in Figure 3.12 may be related to the decomposition/loss of the (+)-HCSA dopant incorporated on the polyaniline chains, which agrees well with the TGA result.

A large exothermic peak at 180°- 350°C was observed in the DSC thermogram of the EB powder (Figure 3.13). The chemical process associated with this exothermic peak may be related to cross-linking reactions.^{16,18,19} The exothermic peak observed previously in this temperature range for chemically prepared EB powder¹² and PAn.HCl¹⁸ under nitrogen atmosphere has been attributed to such chemical cross-linking. An

endothermic peak at 110°-160°C, attributable to the glass transition of the polyaniline, was also observed (Figure 3.13).

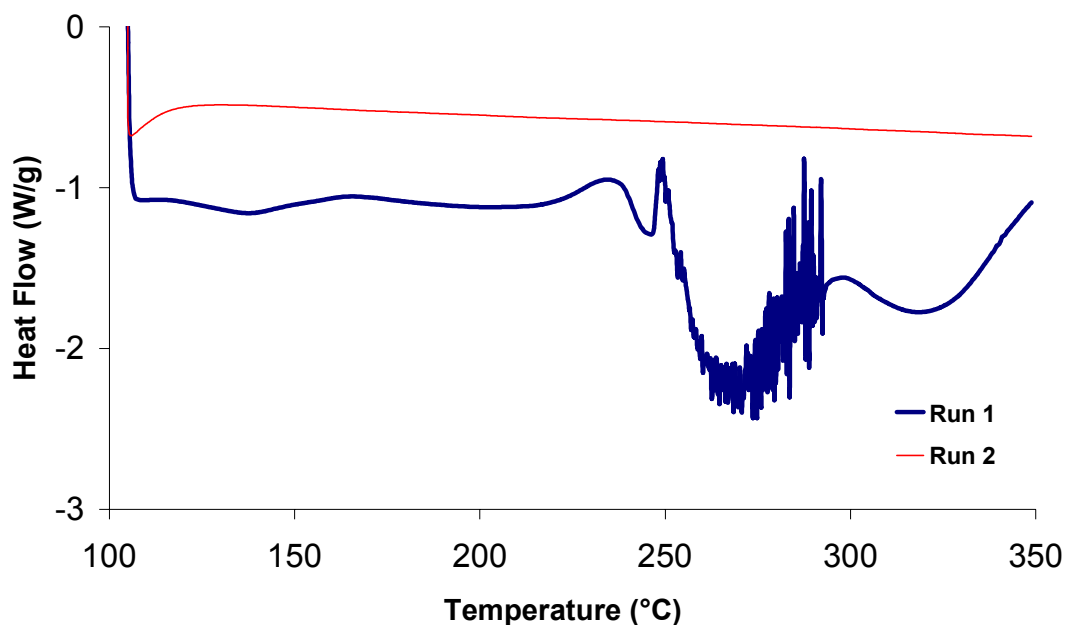


Figure 3.12 DSC thermogram (40°-350°C) of sample 4 (optically inactive PAn.(+)-HCSA-ECS) under N₂ (15 mL/min), with pre-heat program (at 105°C for 10 min). Sample size: 6.5 mg.

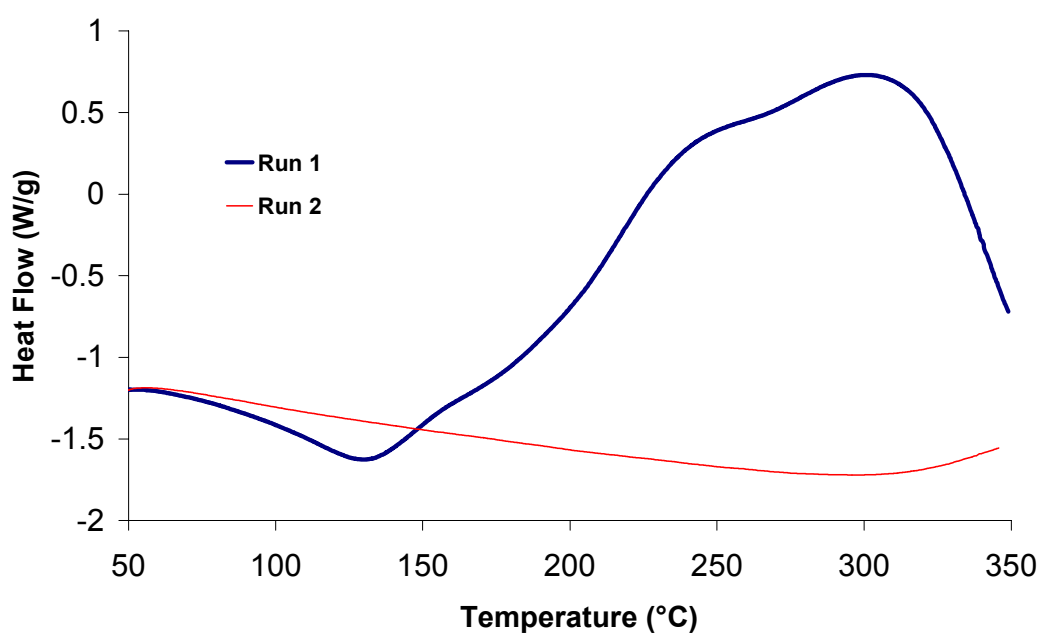


Figure 3.13 DSC thermogram (40°-350°C) of sample 1 (EB-CS) under N₂ (15 mL/min), with pre-heat program (at 105°C for 10 min). Sample size: 6.6 mg.

To verify the origin of the endothermic peak at *ca.* 110°-180°C, the DSC of electrochemically deposited PAn.HCl (sample **3**) and optically active PAn.(+)-HCSA (sample **5**) were studied with pre-heat condition. These showed similar DSC thermogram features, with a broad endothermic peak being observed at 110°-170°C for the achiral PAn.HCl and for the optically active chiral Pan.(+)-HCSA emeraldine salts (Figures 3.14 and 3.15, respectively). The results suggest that this broad endothermic peak is due to the overlapping of many processes such as the glass transition^{10, 11} and/or the conformational change⁹ as observed in thermal treatment of the polyaniline films (see section 3.3.2) and morphological changes.^{12, 14, 19}

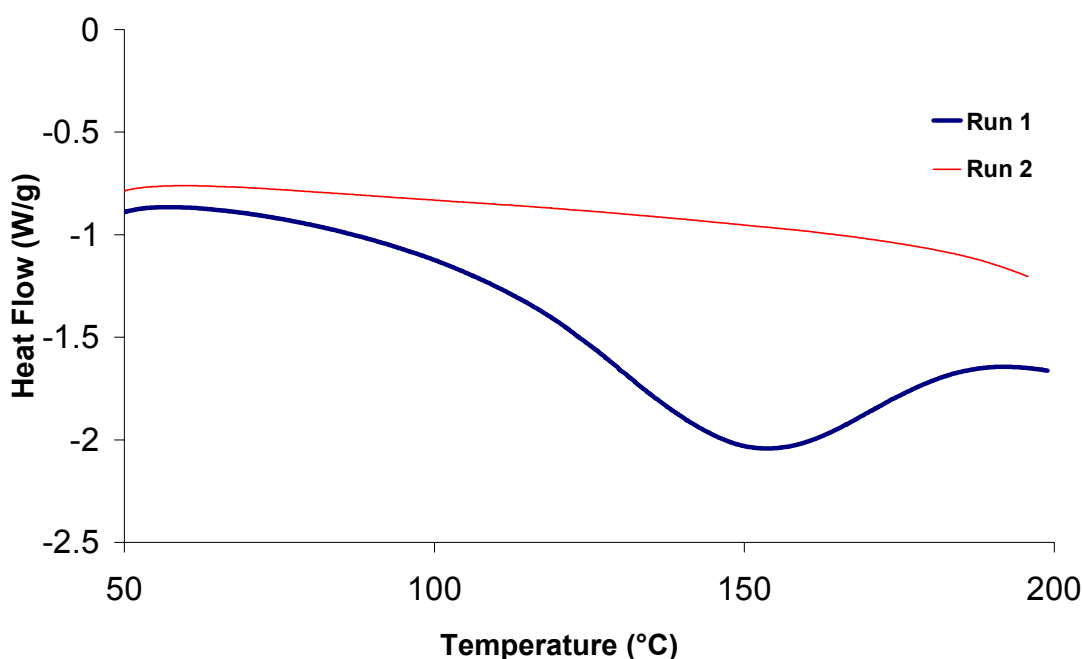


Figure 3.14 DSC thermogram (40°-200°C) of sample **3** (PAn.HCl-ECS) under N₂ (15 mL/min), with pre-heat program (at 105°C for 10 min). Sample size: 4.4 mg.

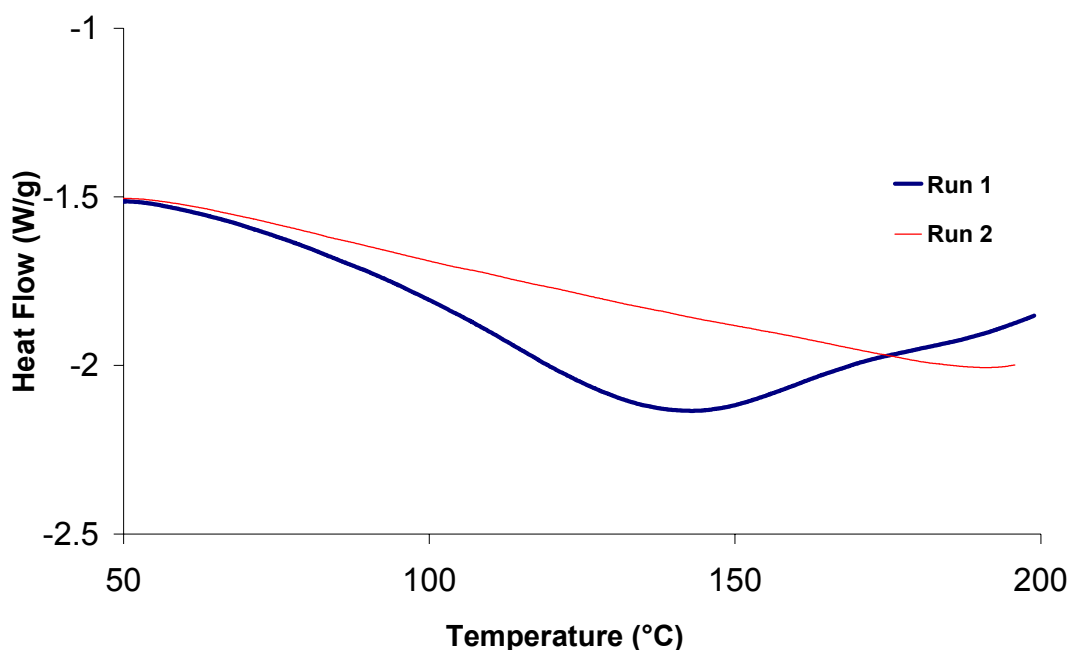


Figure 3.15 DSC thermogram (40°-200°C) of sample 5 (optically active PAn.(+)-HCSA-ECS) under N₂ (15 mL/min), with pre-heat program (at 105°C for 10 min). Sample size: 6.9 mg.

3.4 Conclusions

A new solid state, thermal route to optically active PAn.(+)-HCSA emeraldine salts has been developed, commencing with optically inactive emeraldine base, avoiding the use of organic solvents. Whereas the doping of solid emeraldine base films with chiral dopant acids such as aqueous (+)-HCSA generates optically inactive PAn.(+)-HCSA salts, subsequent heating of these emeraldine salt films at 170°C (above the glass transition temperature; 140°-150°C) generates optically active materials. This is believed to be due to the polyaniline chains preferentially adopting a one-handed helix under the influence of the chiral dopant CSA⁻ anion. Employing (+)-or (-)-HCSA as the dopant acid, mirror imaged circular dichroism spectra are generated after heating the PAn.(+)-HCSA and PAn.(-)-HCSA films.

Optically active polyaniline films generated via this novel method using EB film precursors synthesized via chemical and electrochemical polymerization exhibit similar chiroptical properties, suggesting that they have the same conformation/configuration.

Thermal analysis (TGA and DSC) reveals that heating the PAn.(+)-HCSA films above 200°C results in decomposition/loss of the dopant CSA⁻ anion, followed by decomposition of the polymer backbone at 370° - 400°C. Conformational changes and/or morphological changes and/or chemical cross-linking probably occur upon heat treatment, as indicated in the DSC thermograms.

These results provide a new route for the preparation of low cost, chiral polyanilines because they can be produced in large scale without using toxic organic solvents. However, the optical activity of the materials is presently quite low, and would have to be improved if the method was to be used in applications such as chiral stationary phases for chiral chromatography.

3.5 References

1. M.R. Majidi, L.A.P. Kane-Maguire, and G.G. Wallace, *Polymer*. **35** (1994): 3113.
2. M.R. Majidi, L.A.P. Kane-Maguire, and G.G. Wallace, *Aust. J. Chem.* **51** (1998): 23.
3. M.R. Majidi, L.A.P. Kane-Maguire, and G.G. Wallace, *Polymer*. **37** (1996): 359.
4. M.R. Majidi, L.A.P. Kane-Maguire, and G.G. Wallace, *Polymer*. **36** (1995): 3597.
5. E.E. Havinga, M.M. Bouman, E.W. Meijer, A. Pomp, and M.M.J. Simenon, *Synth. Met.* **66** (1994): 93.
6. H. Guo, V. Egan, C.M. Knobler, and R.B. Kaner, *Polymer Preprints*. **40** (1999).
7. H. Guo, C.M. Knobler, and R.B. Kaner, *Synth. Met.* **101** (1999): 44.
8. L.A.P. Kane-Maguire (unpublished result).
9. I.D. Norris, L.A.P. Kane-Maguire, and G.G. Wallace, *Macromolecules*. **31** (1998).
10. L. Abell, S.J. Pomfret, P.N. Adams, and A.P. Monkman, *Synth. Met.* **84** (1997): 127.
11. L. Abell, S.J. Pomfret, E.R. Holland, P.N. Adams, and A.P. Monkman, *ANTEC*. **54** (1996): 1417.
12. J.L. Lu, N.J. Liu, X.H. Wang, J. Li, X.B. Jing, and F.S. Wang, *Synth. Met.* **135-136** (2003): 237.
13. V.M. Mzenda, S.A. Goodman, F.D. Auret, and L.C. Prinsloo, *Synth. Met.* **127** (2002): 279.
14. H.S.O. Chan, S.C. Ng, W.S. Sim, K.L. Tan, and B.T.G. Tan, *Macromolecules*. **25** (1992): 6029.
15. S. Palaniappan and B.H. Narayana, *J. Polym. Sci., Part A*. **32** (1994): 2431.
16. J.E.P. Silva, D.L.A. Faria, S.I.C. Torresi, and M.L.A. Temperini, *Macromolecules*. **33** (2000): 3077.
17. Y. Wei and K.F. Hsueh, *J. Polym. Sci.: Part A - Polymer Sci.* **27** (1989): 4351.
18. M. Baibarac, I. Baltog, S. Lefrant, J.Y. Mevellec, and O. Chauvet, *Chem. Mater.* **15** (2003): 4149.
19. F. Fusalba and D. Belanger, *J. Phys. Chem. B*. **103** (1999): 9044.

Chapter 4

Asymmetric Proliferation with Optically Active Polyanilines

4.1 Introduction

In all the reported routes to optically active polyanilines, summarized in Chapter 1 (Section 1.4.2.3), a chiral dopant anion is incorporated into the polyaniline chains during growth. The chiral dopant is believed to induce optical activity in the polymer chains through electrostatic and/or hydrogen bonding interactions, leading to a preferred one-handed helical structure for the polyaniline backbone.¹⁻⁴

In this Chapter, an alternative approach to optically active polyanilines is explored. It is based on the hypothesis that an initial thin film of an optically active conducting polymer deposited on an electrode may cause asymmetric induction during the subsequent polymerization of aniline in the presence of racemic or achiral acids. Thin films of electrodeposited PAn.(+)-HCSA and PAn.(-)-HCSA are examined as the potential chiral inducer. This novel route, which will be called macromolecular asymmetric proliferation, is found to be remarkably effective using either (\pm)-HCSA, HCl or *p*-toluenesulfonic acid (*p*-TSA) as the acid dopants during the second stage of electrodeposition, yielding highly optically active emeraldine salts. The potential use of chiral polyaniline thin films as chiral inducers for the preparation of other optically active conducting polymers such as polypyrrole is also briefly studied.

4.2 Experimental

4.2.1 Chemicals

Chemical reagents were obtained as described in Chapter 2. All aqueous solutions were prepared with Milli-Q water.

4.2.2 Preparation of Optically Active Polyanilines via a Chiral Emeraldine Salt Inducer

All electrochemical polymerizations were carried out in a three-electrode cell. ITO-Pt-coated glass described in Chapter 2 was used as working electrode. Ag/AgCl (3 M NaCl) and Pt mesh were employed as reference and auxiliary electrodes, respectively. A constant potential was applied to the working electrode by means of a BAS CV-27 potentiostat and the charge passed during polymer growth also measured. Two steps of electrodeposition are required in this method:

Step 1: Electrodeposition of Chiral PAn.(+)-HCSA or PAn.(-)-HCSA Thin Film

PAn.(+)-HCSA (or PAn.(-)-HCSA) thin films were potentiostatically deposited at room temperature (18° - 20°C) from aqueous 0.2 M aniline/1.0 M (+)-HCSA (or 1.0 M (-)-HCSA), using an applied potential of 0.9 V and passing 25 mC/cm² of charge. The thin films of PAn.(+)-HCSA or PAn.(-)-HCSA were washed well with methanol to remove excess aniline monomer and unincorporated (+)- or (-)-HCSA by dipping ten times into a large amount of methanol for 15 sec. Their UV-visible and CD spectra were measured before using the chiral films as the working electrode in the second electrodeposition step.

Step 2: Further Electrodeposition of PA.HA Emeraldine Salts with Achiral or Racemic Dopants

Polyaniline emeraldine salt (PAn.HA) or polypyrrole (PPy.A) films were then potentiostatically deposited on the thin films of PAn.(+)-HCSA or PAn.(-)-HCSA

obtained from step 1, using an applied potential of 0.9 V with 100 mC/cm² of charge passed and aqueous 0.2 M aniline/1.0 M HA {HA = HCl, *p*-TSA, (±)-HCSA or (-)-HCSA} as the polymerization medium. Similar deposition of polypyrroles was carried out on thin optically active PAn.(+)-HCSA substrates from aqueous 0.2 M pyrrole/1.0 M (±)-HCSA at room temperature (*ca.* 18° - 20°C).

4.2.3 Chiral Amplification

Polyaniline emeraldine salt films were potentiostatically electrodeposited on ITO-Pt-coated glass at 0.9 V (deposition charge = 120 mC/cm²) from aqueous 0.2 M aniline/1.0 M HA {HA = 2%(+)-HCSA/98% (±)-HCSA, 5% (+)-HCSA/95% (±)-HCSA, 2% (+)-HCSA/98% HCl, or 5% (+)-HCSA/95% HCl} at room temperature (*ca.* 18° - 20°C).

4.2.4 UV-visible and CD Spectral Measurements

UV-visible and CD spectra were recorded as described in Chapter 2. Films were washed with methanol before the measurements unless otherwise stated.

4.2.5 De-doping/Re-doping of a Polyaniline Film

A co-polymer emeraldine salt film, prepared by deposition of an initial thin film (25 mC/cm² passed) of PAn.(-)-HCSA and further depositing PAn.HCl (another 100 mC/cm² passed), was de-doped in 1.0 M NH₄OH for 30 min to give an emeraldine base film, and then re-doped to PAn.HCl emeraldine salt by treatment with 1.0 M HCl for 30 min. UV-visible and CD spectra were recorded before and after the base/acid treatments.

4.2.6 Electrochemical Studies

4.2.6.1 Cyclic Voltammetry

Polymer Synthesis: Preparation of polyaniline films was based on a procedure described in Section 4.2.2. A glassy carbon disc (surface area: 0.07 cm^2) or ITO-Pt coated glass was used as working electrode. The polymerization solution was an aqueous solution containing 0.2 M aniline and 1.0 M acid HA {HA = (+)-HCSA, (\pm)-HCSA, or HCl}.

Cyclic Voltammograms: Cyclic voltammetric measurements were performed as described in Chapter 2. The current was measured at potentials swept between -0.2 and 1.1 V or -0.3 and 0.9 V, using a scan rate of 50 mV/s. The electrolyte (aqueous 1.0 M HCl or 1.0 M H_2SO_4) was de-oxygenated by gentle bubbling with N_2 prior to measurements.

4.2.6.2 Chronoamperometry and Chronocoulometry

Chronoamperograms and chronocoulomograms were recorded during the potentiostatic deposition of polyaniline emeraldine salts onto the glassy carbon electrode (surface area = 0.07 cm^2) or ITO-Pt-coated glass (surface area *ca.* 1.0 cm^2) at +0.9 V, using an eDAQ potentiostat with Chart software (version 5.1.2). The polymerizations were carried out in a three-electrode cell, using Ag/AgCl (3 M NaCl) and Pt mesh as reference and auxiliary electrodes, respectively.

4.3 Results and Discussion

4.3.1 Chiroptical Properties of Electrodeposited PAn.HA Films

Polyaniline films were deposited using the conditions described in the Experimental Section. Typical UV-visible and circular dichroism spectra of racemic PAn.(\pm)-HCSA and optically active PAn.(+)-HCSA films obtained by passing 125 mC/cm^2 charge during conventional potentiostatic polymerization of aniline in the presence of (\pm)-HCSA and (+)-HCSA, respectively, are shown in Figure 4.1. Similar UV-visible spectra

were obtained for both emeraldine salt films, with a broad absorption peak in the 350-450 nm region, assigned as overlapping benzenoid π - π^* and polaron bands, as well as a strong free-carrier tail in the near-infrared (Figure 4.1a). These spectra are consistent with a largely “extended coil” conformation for the polyaniline chains.⁵⁻⁷

As expected, the PAn.(\pm)-HCSA film exhibited no optical activity (curve 2-Figure 4.1b). However, the PAn.(+)-HCSA film was strongly optically active, exhibiting CD bands at *ca.* 350, 440 and 730 nm (curve 1-Figure 4.1b). Similar results have been reported previously by Kane-Maquire *et al.*^{1,3}

Polyaniline films prepared by electropolymerization of aniline in the presence of an achiral acid (e.g. HCl) exhibited similar UV-visible and CD spectra to those recorded for PAn.(\pm)-HCSA. Therefore, it can be concluded that optically active polyaniline emeraldine salt (PAn.HA) films can usually only be obtained by conventional electropolymerization in the presence of an optically active acid dopant.

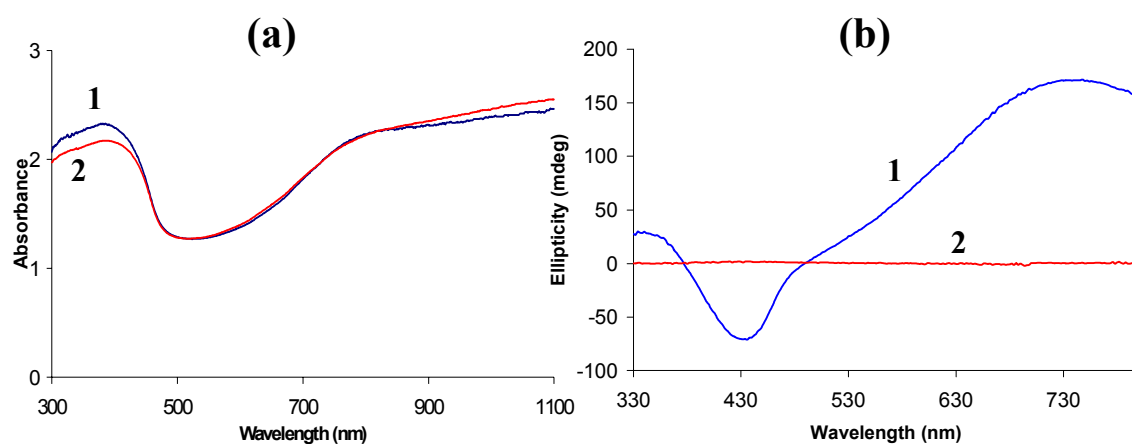
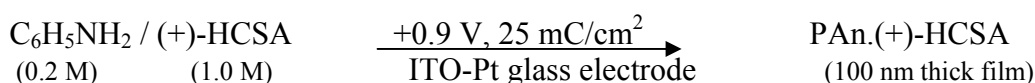


Figure 4.1 (a) UV-visible and (b) CD spectra of: (1) a PAn.(+)-HCSA film, and (2) a PAn.(\pm)-HCSA film, electrodeposited on ITO-Pt-coated glass at 0.9 V (deposition charge = 125 mC/cm²) at room temperature.

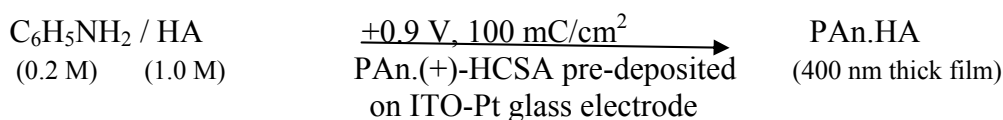
4.3.2 Synthesis of Optically Active Polyanilines Using a Thin PAn.(+)-HCSA Film as Chiral Inducer

The novel asymmetric polymerization method explored in this study involved two electrodeposition steps (Scheme 4.1). In the first step, a thin film of chiral PAn.(+)-HCSA emeraldine salt was prepared by electropolymerization of aniline in the presence of the chiral acid (+)-HCSA. The thickness of the film deposited on the ITO-coated glass working electrode was controlled by the deposition charge (25 mC/cm²). The thin PAn.(+)-HCSA film was thoroughly washed with methanol to remove excess aniline, oligomers, and unincorporated (+)-HCSA before using this as a chiral inducer in a further polymerization step. In this second stage, electrodeposition of PAn.HA emeraldine salts onto the thin chiral polyaniline film was carried out in an aqueous solution containing aniline and the racemic acid (±)-HCSA or an achiral acid such as HCl and *p*-TSA.

Step 1.



Step 2.



Scheme 4.1

(i) Using (±)-HCSA in the Second Polymerization Step

The UV-visible spectra measured for the thin initial PAn.(+)-HCSA film and for the film after further deposition of PAn.(±)-HCSA film on top, show that the absorbance intensity of the final product was much higher than that of the initiator film (Figure 4.2

a). This is consistent with the amount of charge passed during each electrodeposition step. Remarkably, the intensity of the CD spectrum also increased by a similar factor (Figure 4.2 b). That is, strongly optically active polyaniline was deposited in the second polymerization step, even though the polymerization was performed in a racemic acid solution. This indicated that the initial thin PAn.(+)-HCSA film acts to induce chirality into the final polyaniline product. In contrast, as mentioned earlier, optically inactive PAn.(±)-HCSA is obtained when this emeraldine salt is deposited on a bare ITO-Pt-coated glass electrode.

The thickness of emeraldine salt films can be estimated* from their optical absorption at 400 nm. On this basis, the film thickness of the initial thin PAn.(+)-HCSA film and of the final film after depositing PAn.(±)-HCSA on top were estimated to be *ca.* 100 and 400 nm, respectively.

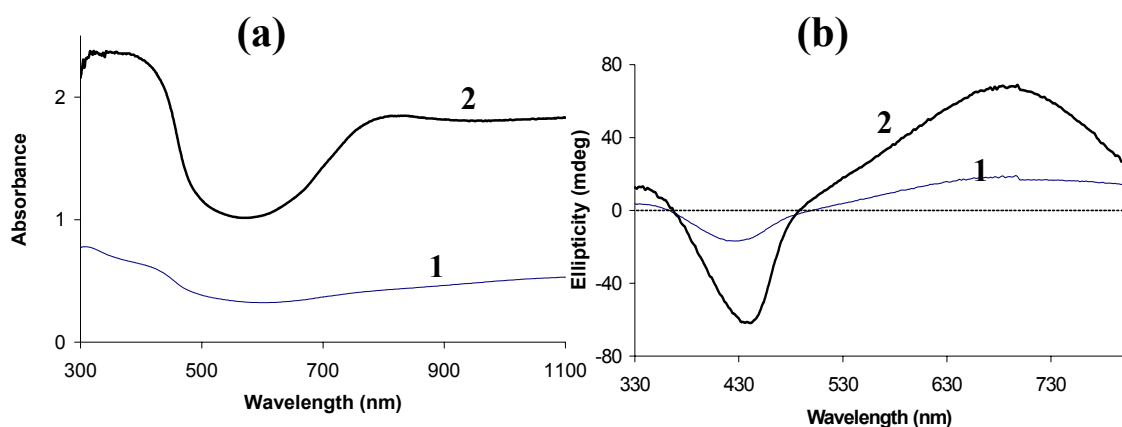


Figure 4.2 (a) UV-visible and (b) CD spectra of: (1) a PAn.(+)-HCSA film electrodeposited on ITO-Pt-coated glass at 0.9 V (deposition charge = 25 mC/cm²), and (2) after depositing a further PAn.(±)-HCSA film (another 100 mC/cm² charge passed).

* *Footnote*: The absorbance of PAn.HA salt film was found in a study by Stejskal *et al*^{8,9} to be related to the film thickness, given by the equation: Film thickness (in nm) = 185 x Abs_(400 nm).

(ii) Using Achiral Acids in the Second Polymerization Step

In subsequent studies the achiral acids HCl and *p*-TSA were employed as the acid dopant in the second electrodeposition step. Significantly, when PAn.HCl and PAn.*p*-TSA were electrodeposited on top of the thin PAn.(+)-HCSA film, the intensity of the UV-visible absorption and CD signals of the final films (Figure 4.3 and 4.4) again increased by similar amounts.

The CD spectra obtained had the same sign and general characteristics as those observed for the PAn.(±)-HCSA film described in Figure 4.2b above. This confirms that optical activity (presumably originating from a helical chain structure) can be induced into polyanilines during electrochemical polymerization of aniline when employing optically inactive dopant anions, via the use of a chiral polyaniline-modified working electrode.

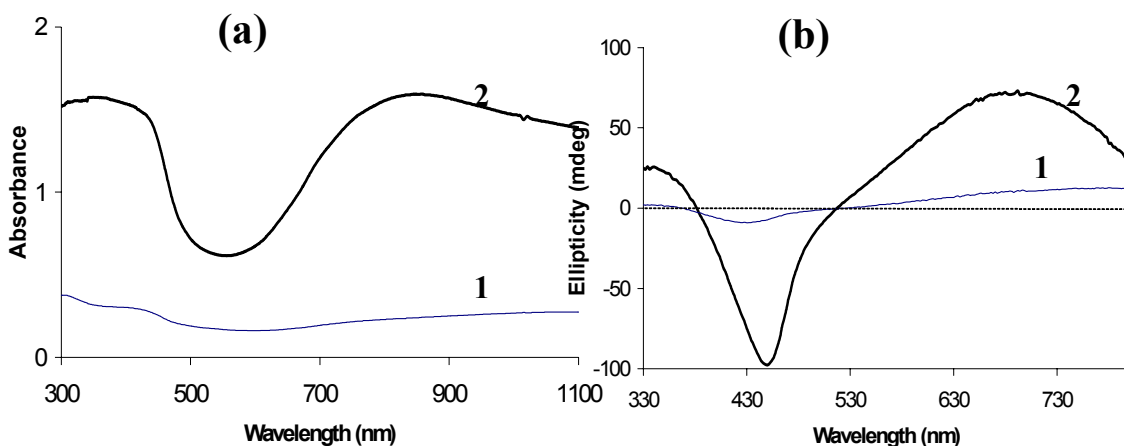


Figure 4.3 (a) UV-vis and (b) CD spectra of: (1) a PAn.(+)-HCSA film electrodeposited on ITO-Pt-coated glass at 0.9 V (deposition charge = 25 mC/cm²), and (2) after depositing a further PAn.HCl film (another 100 mC/cm² passed).

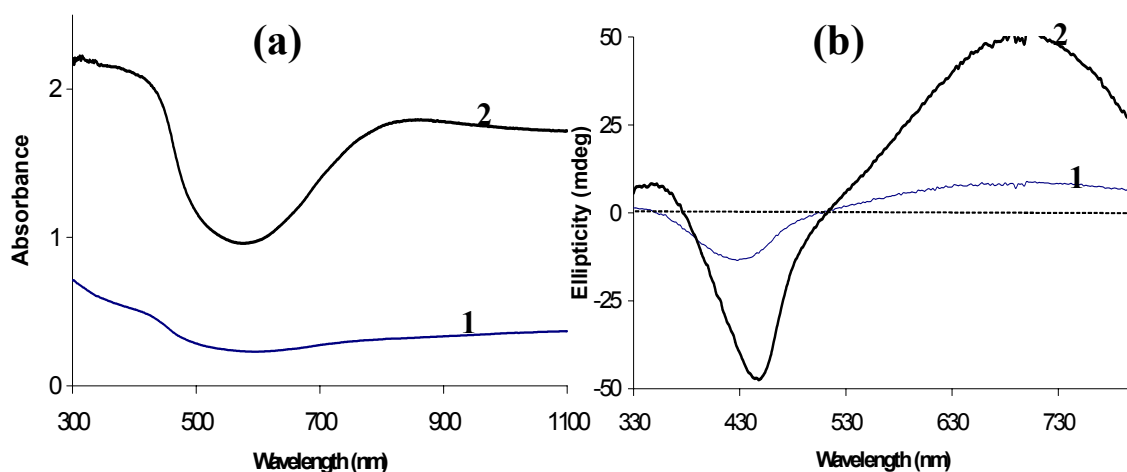


Figure 4.4 (a) UV-visible and (b) CD spectra of: (1) a PAn.(+)-HCSA film electrodeposited on ITO-Pt-coated glass at 0.9 V (deposition charge = 25 mC/cm²), and (2) after depositing a further PAn.*p*-TSA film (another 100 mC/cm² charge passed).

(iii) Using (-)-HCSA in the Second Polymerization Step

The most striking result occurred when the enantiomeric (-)-HCSA was employed as the dopant acid in the second electropolymerization step in Scheme 4.1. The PAn.(-)-HCSA film obtained after passing 100 mC/cm² exhibited chiroptical properties (Figure 4.5) the same as those observed above when (±)-HCSA, HCl or *p*-TSA acids were employed.

Kane-Maguire *et.al.*¹ have reported that the CD spectra of emeraldine salt films electrodeposited onto ITO-coated glass in the presence of 1.0 M (+)-HCSA and 1.0 M (-)-HCSA were mirror imaged. In contrast, the result in Figure 4.5 indicates that PAn.HCSA emeraldine salts electrodeposited on an initial thin PAn.(+)-HCSA film exhibit the same CD spectra in the visible region regardless of whether the HCSA employed in the second stage deposition is the (+)- or (-)- enantiomer. This indicates that the chiroptical property of the initial thin PAn.(+)-HCSA film plays a dominant role in preferentially forming polyanilines with the same helical conformation as itself.

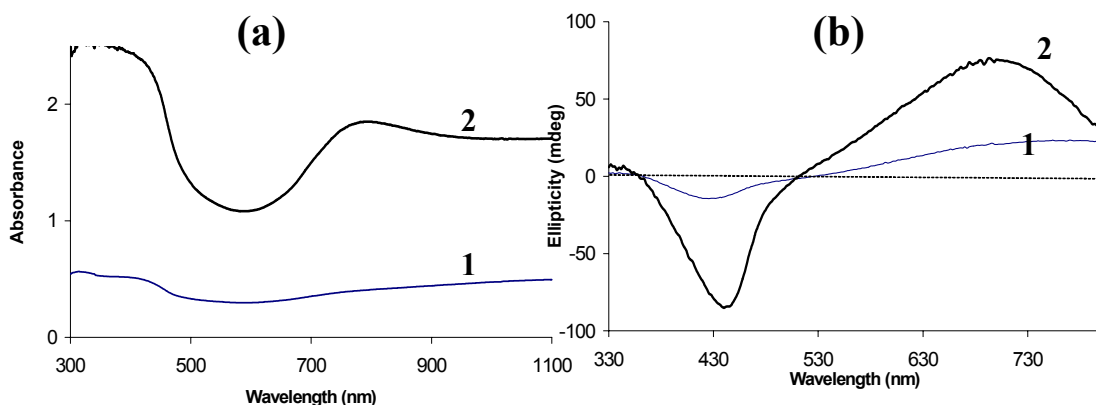


Figure 4.5 (a) UV-visible and (b) CD spectra of: (1) a PAn.(+)-HCSA film electrodeposited on ITO-Pt-coated glass at 0.9 V (deposition charge = 25 mC/cm²), and (2) after depositing a further PAn.(-)-HCSA film (another 100 mC/cm² charge passed).

4.3.3 Synthesis of Optically Active Polyanilines Using a Thin PAn.(-)-HCSA Film as Chiral Inducer

This hypothesis was further tested by carrying out similar polymerizations in which a thin PAn.(-)-HCSA film was used as the working electrode for the second stage deposition. Thin films of PAn.(-)-HCSA were prepared as previously described in section 4.3.2 (electrodeposition charge = 25 mC/cm²), but 1.0 M (-)-HCSA was used rather than 1.0 M (+)-HCSA. The thin films were washed with methanol and then PAn.(±)-HCSA or PAn.HCl films deposited on top (step 2) using an applied potential of 0.9 V and 100 mC/cm² charge passed, employing aqueous 0.2 M aniline/1.0 M HA (HA = (±)-HCSA or HCl) as the polymerization solution.

(i) Using (±)-HCSA in the Second Polymerization Step

The UV-visible spectra measured for the initial thin PAn.(-)-HCSA film and for the film after further deposition of PAn.(±)-HCSA film on top, showed that the absorbance of the final product was markedly increased compared to that of the initial film (Figure 4.6a). This is consistent with the amount of charge passed for each electropolymerization step. The initial thin PAn.(-)-HCSA film exhibited mirror imaged

CD signals at the same wavelengths (*ca.* 350, 440 and 730 nm) as those observed for the thin PAn.(+)-HCSA films in Section 4.3.2.

Significantly, the ellipticity of the CD bands of the final product also increased by a similar factor (Figure 4.6b). This result showed that optically active polyaniline was synthesized in the second polymerization step, although it was carried out in a racemic acid solution. This indicated that the initial thin PAn.(-)-HCSA film again induces its own chirality into the final polyaniline product. The mirror imaged nature of the chiral polyaniline final products prepared by using the initial thin PAn.(-)-HCSA and PAn.(+)-HCSA films (from Figure 4.2) are seen in Figure 4.7.

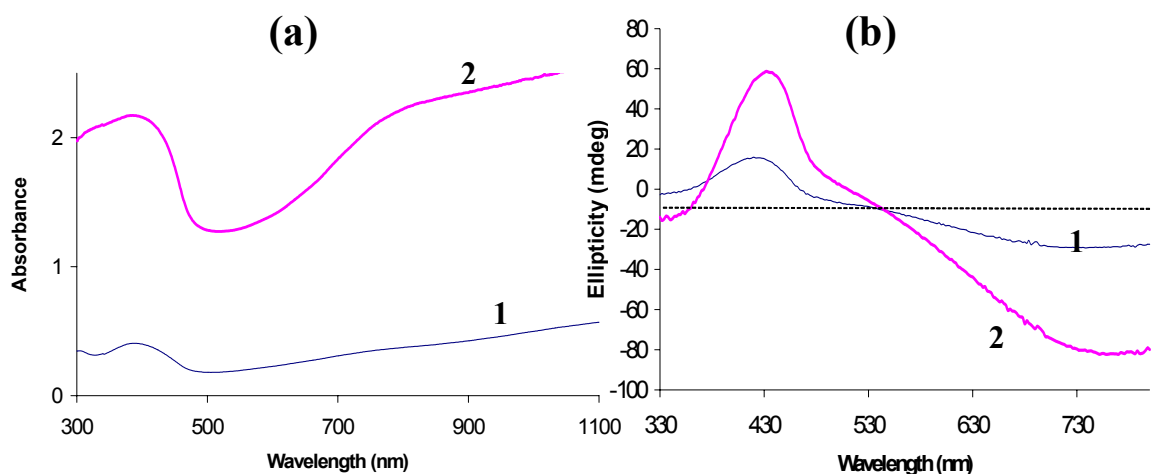


Figure 4.6 (a) UV-visible and (b) CD spectra of: (1) a PAn.(-)-HCSA film electrodeposited on ITO-Pt-coated glass at 0.9 V (deposition charge = 25 mC/cm²), and (2) after depositing a further PAn.(±)-HCSA film (another 100 mC/cm² charge passed).

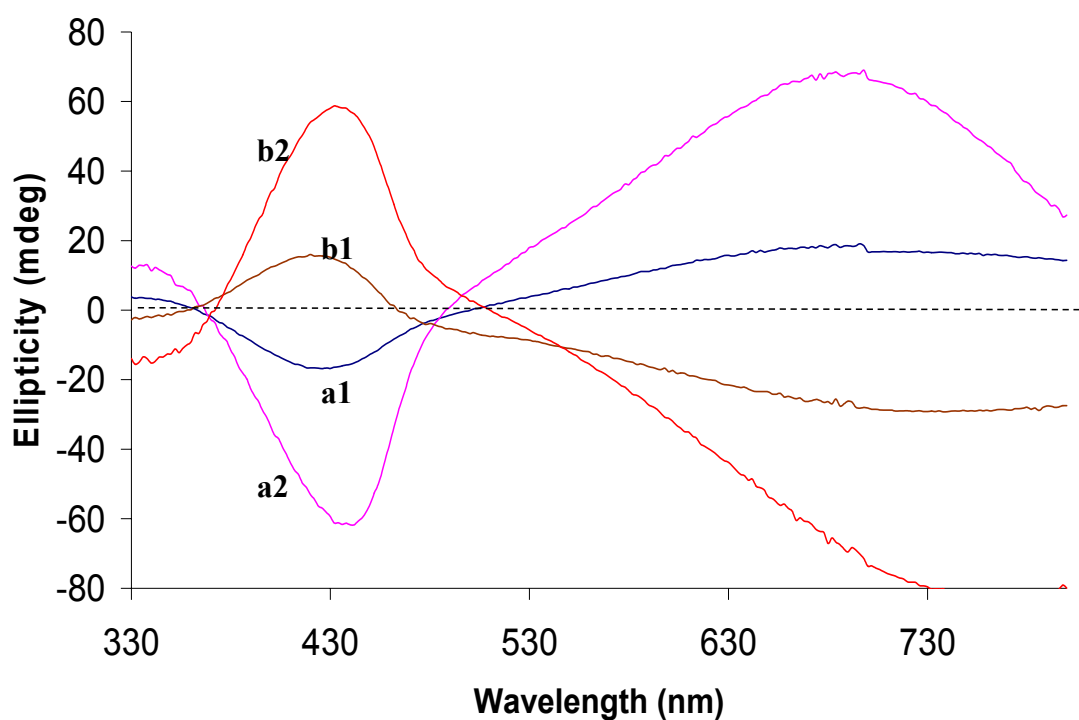


Figure 4.7 CD spectra of initial thin films (25 mC/cm^2 passed) of PAn.(+)-HCSA (a1) and PAn.(-)-HCSA (b1), and after depositing further PAn.(±)-HCSA films (another 100 mC/cm^2 passed) on top of each film, respectively.

(ii) Using HCl in the Second Polymerization Step

Very similar results were obtained when a PAn.HCl was electrodeposited upon an initial thin PAn.(-)-HCSA film. The visible region absorbance of the final product was much higher than that of the initial thin film (Figure 4.8a). Significantly, the ellipticity of the CD bands of the final product also increased by a similar factor (Figure 4.8b). This confirms that optical activity can be induced into polyaniline chains during electropolymerization of aniline when using achiral dopant anions such as Cl^- , via the use of a chiral polyaniline initiator. The CD spectrum for the final film in Figure 4.8b is again the mirror image of that previously grown on a thin PAn.(+)-HCSA film (Figure 4.3b).

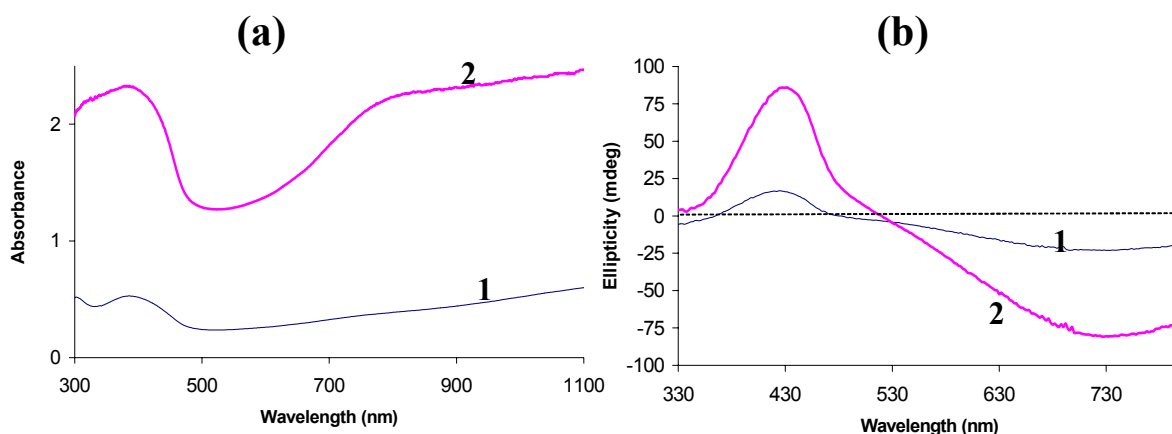


Figure 4.8 (a) UV-visible and (b) CD spectra of: (1) a PAn.(-)-HCSA film electrodeposited on ITO-Pt-coated glass at 0.9 V (deposition charge = 25 mC/cm²), and (2) after depositing a further PAn.HCl film (another 100 mC/cm² charge passed).

4.3.4 The Origin of the Macromolecular Asymmetric Induction

Several possible mechanisms have been considered to explain the origin of the remarkable macromolecular asymmetric induction found in the above studies. One possibility is that the thin initial PAn.(+)-HCSA film may act as a chiral inducer, promoting a one-screw sense helical arrangement (the same as the chiral inducer itself) on the growing polymer chains during polymerization in the presence of racemic or achiral acid dopants. In this regard, our results may be usefully compared to the report by Maeda *et al.*¹⁰ of the asymmetric polymerization of achiral alkylisocyanate monomers to give optically active polyalkylisocyanates (-[OCNR]_n-) using optically active anionic metal complexes as catalysts. The presence of the chiral initiator on a chain terminus was believed to induce a single-screw sense on the growing poly(alkylisocyanate) chains. Recently, Samuelson *et al.*¹¹ have observed related asymmetric induction in the horseradish peroxidase catalysed synthesis of PAn.(+)-HCSA/PAA, PAn.(-)-HCSA/PAA and PAn.(± HCSA)/PAA nanocomposites {PAA = poly(acrylic acid)}; where the polyaniline chains adopted the same helical hand,

irrespective of the hand of the HCSA employed. This result contrasts with electrochemical^{1, 3, 12} and chemical¹³⁻¹⁸ polymerization of aniline where the use of opposite hands of the HCSA acid dopant gives rise to PAn.HCSA salts with opposite helical hands. The horseradish peroxidase enzyme must therefore play a critical role, as yet undefined, in inducing a constant hand on the polyaniline chains.

Another possibility that has been considered is that the (+)-CSA⁻ anion in the thin initial PAn.(+)-HCSA films could reversibly exchange on the polyaniline surface during further polymerization in the presence of racemic HCSA or achiral dopants, and that the asymmetric proliferation exhibited may then arise from cooperative effects of the “majority-rules” and “sergeant-and-soldiers” type recently observed in poly(alkylisocyanate)s^{19, 20} and poly(alkylthiophene)s.²¹ The latter mechanism appears highly unlikely on two counts: (i) the maximum possible concentration of (+)-CSA⁻ in the second-stage polymerization medium is extremely low ($\leq 10^{-4}$ M) compared to the racemic CSA⁻ or achiral anion (1.0 M); (ii) no significant chiral amplification was observed in the electrochemical synthesis of PAn.HCSA salts, as shown by chiral amplification studies that we separately carried out.

As shown in Figures 4.9 and 4.10, the observed optical activity of emeraldine salt films grown in the presence of 5% (+)-HCSA/95% (±)-HCSA (Figure 4.9-curve b) and 5% (+)-HCSA/95% HCl (Figure 4.10-curve b) were *ca.* 5/100 the intensity of an analogous film grown in 100% (+)-HCSA. No chiral amplification was observed for electropolymerizations using as the dopant acid mixtures of HCl and (+)-HCSA with only 2-5% of the chiral acid.

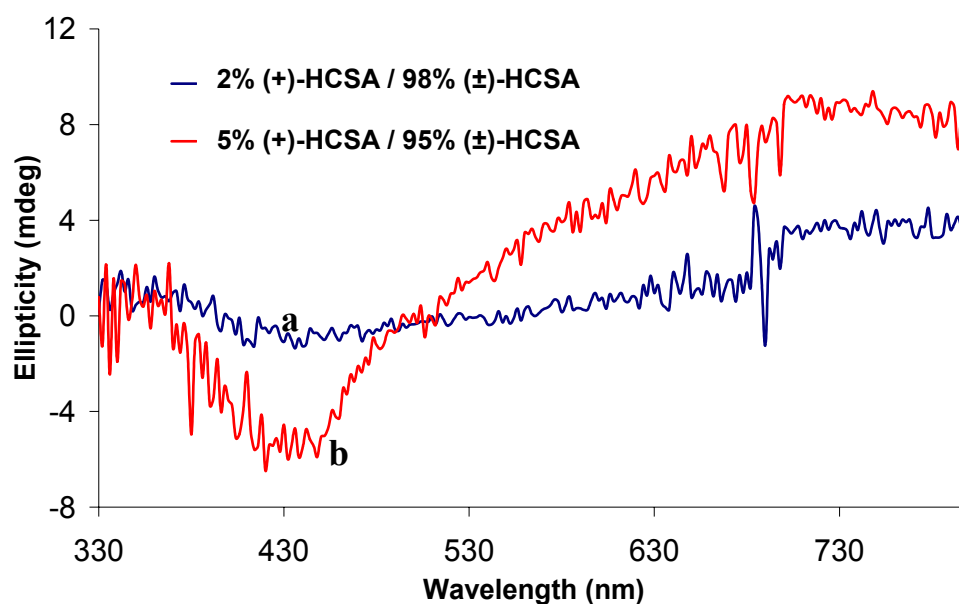


Figure 4.9 CD spectra of emeraldine salt films electrodeposited on ITO-Pt-coated glass at 0.9 V (deposition charge = 120 mC/cm^2) from: (a) 0.2 M aniline/1.0 M HCSA (2% (+)-HCSA, 98% (±)-HCSA); and (b) 0.2 M aniline/1.0 M HCSA (5% (+)-HCSA, 95% (±)-HCSA).

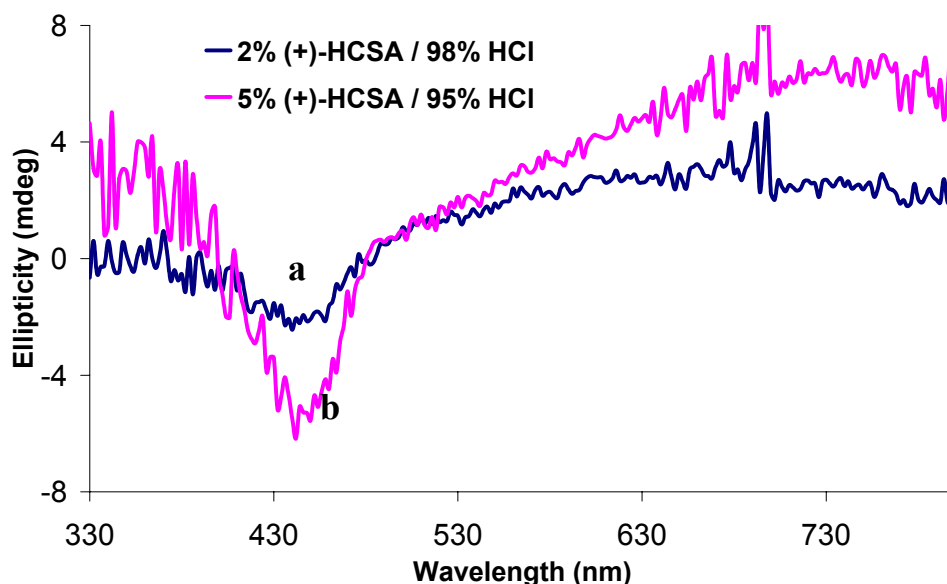


Figure 4.10 CD spectra of emeraldine salt films electrodeposited on ITO-Pt-coated glass at 0.9 V (deposition charge = 120 mC/cm^2) from: (a) 0.2 M aniline/1.0 M HA (2% (+)-HCSA, 98% HCl); and (b) 0.2 M aniline/1.0 M HA (5% (+)-HCSA, 95% HCl).

4.3.5 Optimum Thickness of the Initial PAn.(+)-HCSA Film

The optically active polyaniline films produced in the above asymmetric syntheses may be considered as block co-polymers in which an initial short length of polyaniline is composed of PAn.(+)-HCSA, while the second longer block is the chiral PAn.HA species.

It was of interest to determine the minimum thickness of the initial PAn.(+)-HCSA film that could be used as the chiral electrode for subsequent asymmetric polymerizations (step 2 in Scheme 4.1). For this purpose, thin films of PAn.(+)-HCSA were electrodeposited while passing only 5 and 10 mC/cm² of charge (step 1 in Scheme 4.1). Unfortunately, these very thin PAn.(+)-HCSA films came off the ITO-Pt-coated glass electrode during removal from the polymerization solution and methanol washing. Their use as substrates for further electrodeposition was therefore not possible. Initial PAn.(+)-HCSA films of *ca.* 100 nm thickness (25 mC/cm² of charge passed) were therefore used in all subsequent studies.

4.3.6 Influence of Deposition Charge Passed on the Chiroptical Properties of PAn.HA Films Formed Via Macromolecular Asymmetric Proliferation

In all of the above studies the charge passed during the second polymerization step in Scheme 4.1 was 100 mC/cm². Figures 4.11 and 4.12 show the effect of employing a range of deposition charges between 50 and 300 mC/cm² during the stage 2 deposition of PAn.HCl from aqueous 1.0 M HCl.

As expected, increasing the charge passed caused thicker PAn.HCl films to be deposited onto the thin initial PAn.(+)-HCSA substrates, as evidenced by the increase in intensity

of the UV-visible spectra of the final products (Figure 4.11). The PAn.HCl film grown by passing 300 mC/cm^2 of charge in step 2 onto the PAn.(+)-HCSA substrate (25 mC/cm^2 charge) gave a UV-visible spectrum (curve 7) only slightly less intense than that shown in curve 8 for a PAn.(+)-HCSA film electrodeposited directly onto ITO-Pt-coated glass from 1.0 M (+)-HCSA . The thickness of the former film is estimated to be *ca.* 700 nm using the method described by Stejskal *et al.*^{8,9} However, their equation may be inapplicable for such thick films. Films deposited using greater than 300 mC/cm^2 charge passed in step 2 could not be examined quantitatively by UV-visible or CD spectroscopy due to their very strong absorbance.

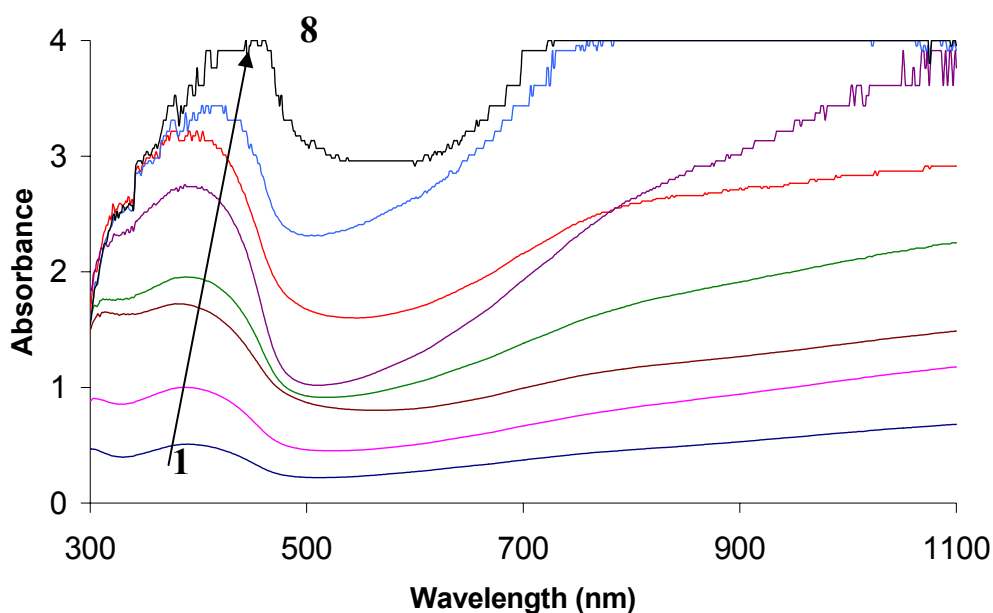


Figure 4.11 UV-visible spectra of emeraldine salt films prepared by deposition of an initial thin film (25 mC/cm^2 passed) of PAn.(+)-HCSA (curve 1), then further depositing PAn.HCl ($50, 70, 100, 150, 200$ and 300 mC/cm^2 passed) (curves 2-7). For comparison, curve 8 is for a PAn.(+)-HCSA film deposited directly onto ITO-Pt-coated glass from 1.0 M (+)-HCSA while passing 325 mC/cm^2 of charge.

The optical activity of the above films also increased markedly with increasing charge passed in the second deposition step, as shown by the CD spectra in Figure 4.12.

Significantly, the ellipticity of the 440 nm CD band of the deposited emeraldine salts increased linearly with the charged passed (Figure 4.13). Chiral induction by the thin initial PAn.(+)-HCSA film therefore extends undiminished for the deposition of PAn.HCl of at least 700 nm thickness. Significantly, the ellipticity of emeraldine salt film grown by passing 300 mC/cm² charge during the second deposition from 1.0 M HCl is seen to be very similar quantitatively to that of a PAn.(+)-HCSA film grown directly onto ITO-Pt-coated glass from 1.0 M (+)-HCSA, despite the fact that > 90% of the dopant acid used in the former case is achiral HCl.

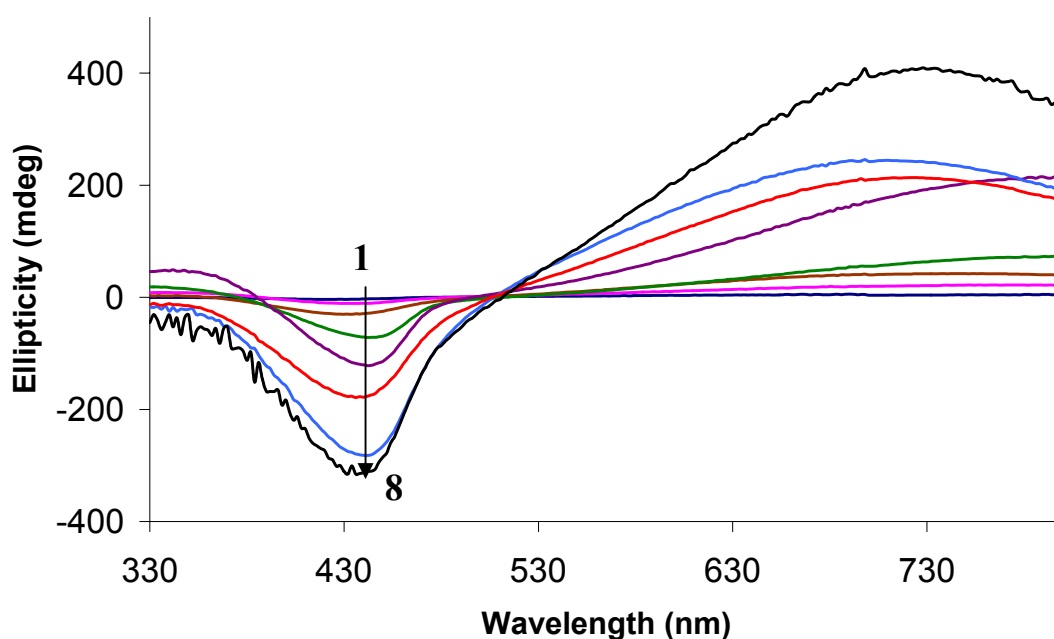


Figure 4.12 CD spectra of emeraldine salt films prepared by deposition of an initial thin film (25 mC/cm² passed) of PAn.(+)-HCSA (curve 1), then further depositing PAn.HCl (50, 70, 100, 150, 200 and 300 mC/cm² passed) (curves 2-7). For comparison, curve 8 is for a PAn.(+)-HCSA film deposited directly onto ITO-Pt-coated glass from 1.0 M (+)-HCSA while passing 325 mC/cm² of charge.

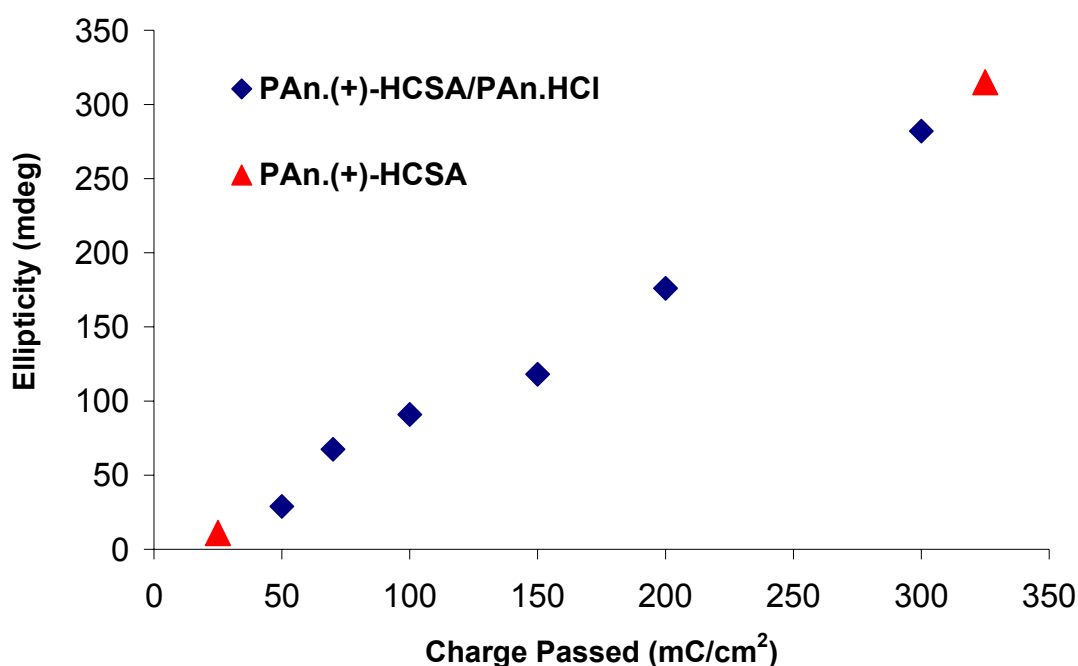


Figure 4.13 Dependence of the optical activity of emeraldine salt films on the deposition charge employed. Each point is the average of duplicate measurements.

4.3.7 Chiroptical Stability of Optically Active PAn.(+)-HCSA/HCl Block Co-polymers During pH and Redox Switching

The effect of pH and redox switching on the chiroptical properties of the optically active block co-polymers produced via the above macromolecular asymmetric proliferation was then investigated. All experiments were performed on emeraldine salt films prepared by deposition of an initial thin film (25 mC/cm² passed) of PAn.(+)-HCSA and then further depositing PAn.HCl (another 100 mC/cm² passed).

4.3.7.1 pH Switching

Treatment of the co-polymer emeraldine salt film with 1.0 M NH₄OH led to rapid dedoping to generate a blue emeraldine base (EB) film. As seen in Figure 4.14a (curve 2), this EB film exhibited characteristic absorption bands at *ca.* 350 and 630 nm. The emeraldine base was optically active, as shown by its CD spectrum in Figure 4.14b

(curve 2). This exhibited two sets of bisignate CD bands at *ca.* 330 and 390 associated with the 350 nm absorption band, and at 500 and 760 nm associated with the 630 nm absorption peak.

Re-doping the EB film with 1.0 M HCl regenerated the emeraldine salt form, as shown by the characteristic UV-visible spectrum in Figure 4.14a (curve 3, λ_{max} *ca.* 390 and 800 nm). The corresponding CD spectrum of the polyaniline re-doped film, showed CD bands at *ca.* 340, 435 and 685 nm (Figure 4.14b – curve 3), similar to those of the film prior to alkaline de-doping. The intensity of the various UV-visible spectra and the ellipticity of the CD bands in Figure 4.14 cannot be quantitatively compared because part of the film came off during the base/acid treatments. However, the CD spectra confirm that the optical activity of the polyaniline is at least largely retained during the de-doping/re-doping cycle. The retention of optical activity presumably arises from constraints in the solid state preventing rearrangement of the polyaniline chains.

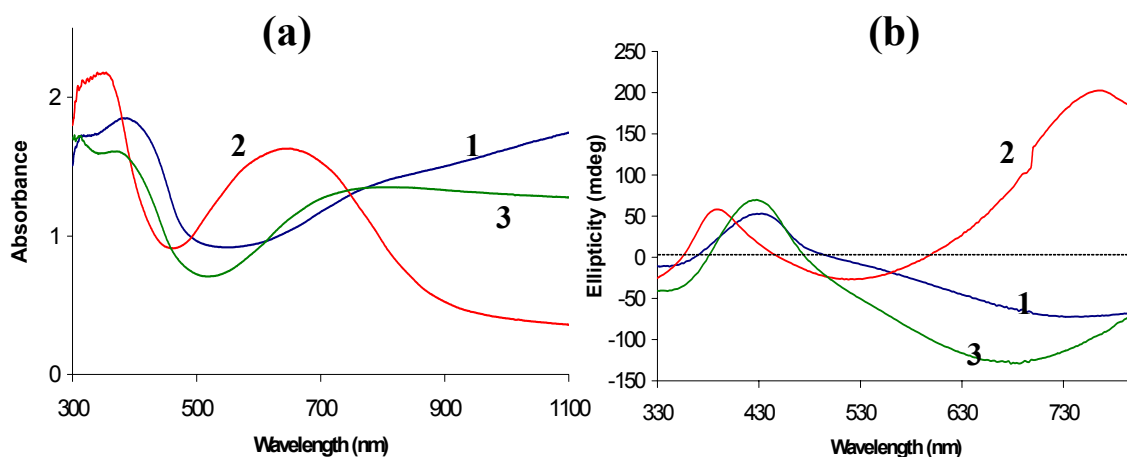
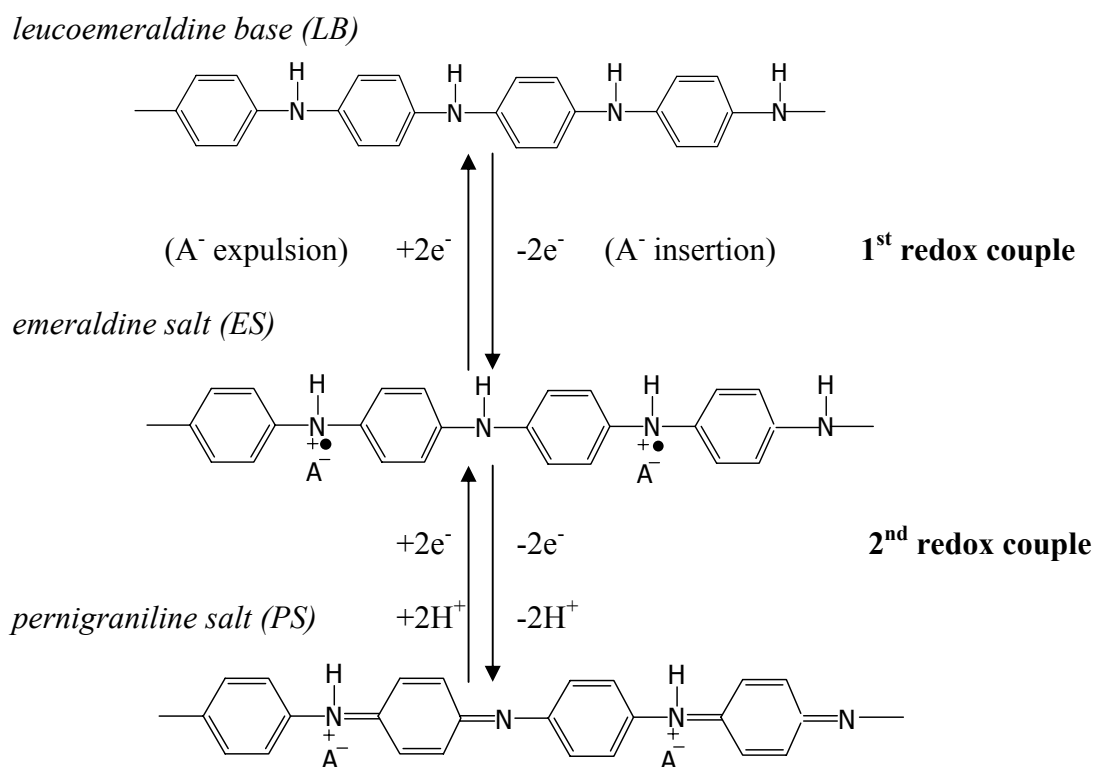


Figure 4.14 UV-vis spectra (a) and CD spectra (b) of an optically active PAN.(+)-HCSA/HCl film : (1) as prepared, (2) after de-doping in 1.0 M NH_4OH for 30 min, and (3) after then re-doping in 1.0 M HCl for 30 min.

4.3.7.2 Redox Switching

As described in Chapter 1 (see Figure 1.4), two main redox couples are usually observed in cyclic voltammograms of polyaniline in aqueous acid. The first redox pair is associated with interconversion between the fully reduced (leucoemeraldine) and semiquinone (emeraldine) forms of polyaniline, while the second redox couple is attributed to interconversion between the emeraldine and fully oxidized (pernigraniline) forms of polyaniline.²²⁻²⁴ It has been reported²⁵⁻²⁷ that anions from the electrolyte are incorporated into the polyaniline films to compensate the positive charges generated during oxidation from leucoemeraldine base to emeraldine salt and then expelled during subsequent reduction, as shown in Scheme 4.2 below.



Scheme 4.2

Therefore, repeated potential scanning in 1.0 M H₂SO₄ of a PAn.HCl film electrodeposited onto a thin PAn.(+)-HCSA film should cause the Cl⁻ and CSA⁻ ions incorporated in the block co-polymer to be replaced by HSO₄⁻ ions.

To avoid oxidative degradation of polyaniline, the potential scanning was performed from -0.3 V to a maximum positive potential of 0.9 V. Thus, the more anodic of the two expected oxidations was not fully observed in the cyclic voltammogram shown in Figure 4.15a. Upon repeated potential cycling the two initial redox peaks gradually decreased in current intensity and a new redox peak or “middle peak” appeared with $E_{1/2}$ *ca.* 0.55 V. This “middle peak” in the CVs of polyanilines is believed to be the redox couple of benzoquinone/hydroquinone, the main product of polyaniline oxidative degradation in aqueous acid at high positive potentials.^{27, 28}

The decrease in the intensity of the UV-visible (Figure 4.15b) and CD spectral bands (Figure 4.15c) of the polyaniline film after the potential cycling may be caused by dissolution of degradation products from the polyaniline film into aqueous solution. However, the decrease in ellipticity of the 440 nm CD band was similar to that observed for the corresponding absorption bands. This suggests that the optical activity of the remaining polyaniline was preserved when the initial (+)-CSA⁻ and Cl⁻ dopant anions were replaced by achiral HSO₄⁻ anions during the repeated potential scanning.

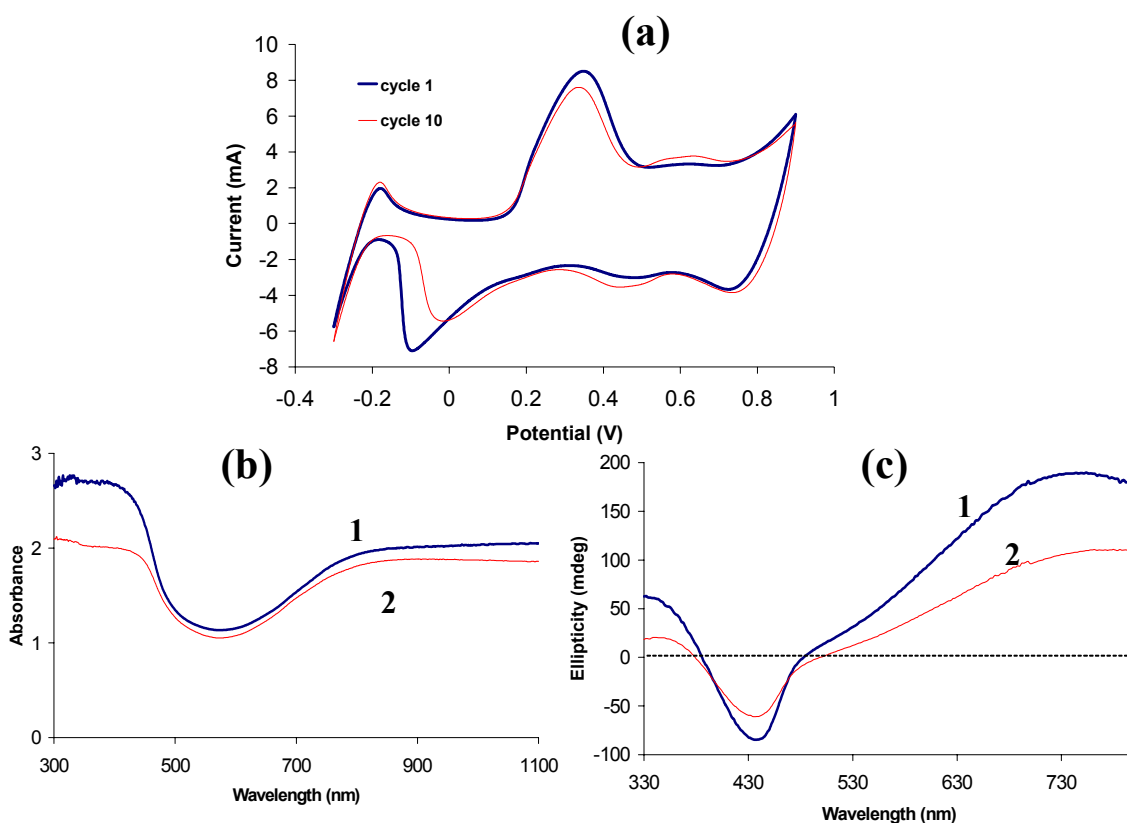
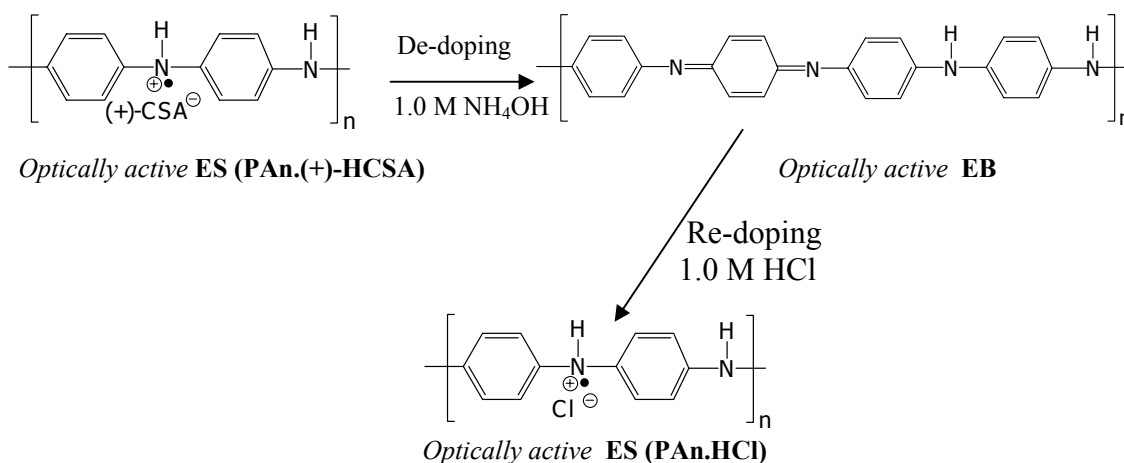


Figure 4.15 (a) CVs of a PAN.(+)-HCSA/PAN.HCl co-polymer film in 1.0 M H₂SO₄, scan rate 50 mV/s; (b) UV-vis spectra and (c) CD spectra measured before (1) and after (2) the cyclic voltammetry.

4.3.8 Role of the (+)-CSA⁻ Dopant Anion of Thin PAN.(+)-HCSA Films in Inducing Chirality into Subsequently Deposited Emeraldine Salts

The origin of the chiral induction in the above asymmetric syntheses of optically active emeraldine salts is uncertain. Induction may be associated with the one-handed helicity of the polyaniline chains in the initial thin PAN.(+)-HCSA film. Alternatively, chiral induction in the subsequently deposited PAN.HA films may be exerted by the CSA⁻ dopant in the thin film. Previous work on chiral PAN.(+)-HCSA films²⁹ indicated that the optical activity of polyanilines in the solid state was not lost after the chiral (+)-CSA⁻ dopant was removed by alkaline de-doping and replaced by achiral Cl⁻ ions via re-doping with HCl, as shown in Scheme 4.3.



Scheme 4.3

In order to explore the possible influence of the (+)-CSA⁻ dopant anion of the initial thin PAn.(+)-HCSA film in the induction of optical activity in PAn.HA emeraldine salts electrodeposited on this substrate, an analogous polymerization study was therefore carried out where the (+)-CSA⁻ dopant anion in the thin film was replaced by Cl⁻ via Scheme 4.3. However, this de-doping/re-doping cycle caused the polymer film to crack and come off the ITO-Pt-coated glass electrode.

An alternative anion exchange procedure was therefore carried out by performing cyclic voltammetry on the initial PAn.(+)-HCSA film in 1.0 M HCl solution. To avoid degradation of the polyaniline at high potential, cycling from -0.2 V to only +0.65 V was employed (scan rate 50 mV/s, 200 cycles). Stable cyclic voltammograms were recorded, indicating no polymer degradation. This was also confirmed by UV-visible and circular dichroism spectra recorded before and after the potential scanning, which showed only relatively small changes (Figure 4.16).

This thin optically active PAn.HCl film was then tested as a potential chiral inducer for the subsequent electrodeposition of a thick PAn.HCl film by potentiostatic

polymerization at 0.9 V of aqueous 0.2 M aniline/1.0 M HCl (100 mC/cm² charge passed). Unfortunately, only poor quality films could be obtained preventing reliable assessment of the chiroptical properties of the final emeraldine salt product. The potential role of the (+)-CSA⁻ dopant in initial PAn.(+)-HCSA in the chiral induction observed during macromolecular asymmetric proliferation therefore remains uncertain at present.

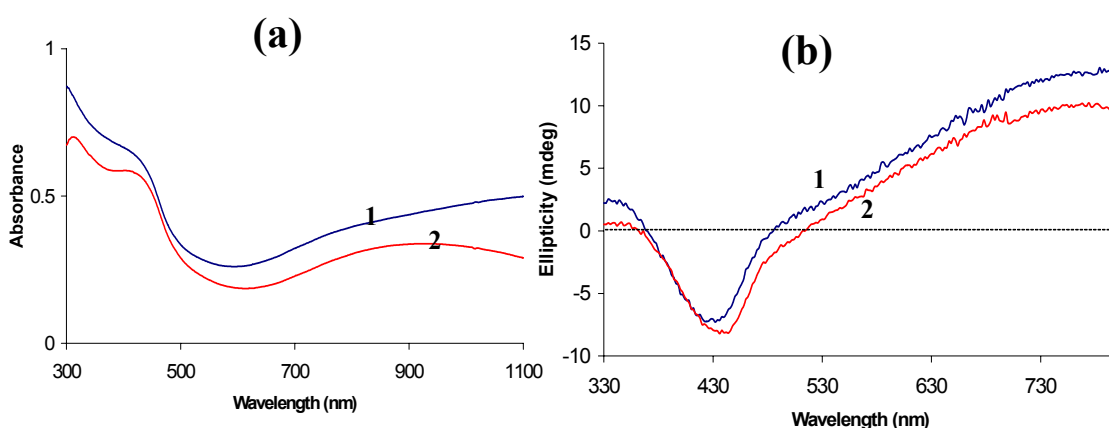


Figure 4.16 (a) UV-visible and (b) CD spectra of: (1) a PAn.(+)-HCSA film electrodeposited on ITO-Pt-coated glass at 0.9 V (deposition charge = 25 mC/cm²), and (2) after potential scanning in 1.0 M HCl between -0.2 and +0.65 V (scan rate 50 mV/s, 200 cycles).

4.3.9 Electrochemical Study

Further understanding of the process of chiral induction in aniline polymerizations using thin PAn.(+)-HCSA films as chiral working electrodes has come from electrochemical characterisation of the films during and after growth of the polymers.

4.3.9.1 Cyclic Voltammetry

(i) PAn.(+)-HCSA and PAn.HCl Films

Previous studies on the electrochemical preparation of polyanilines have indicated that the type of acid dopant employed during growth is one of the main factors leading to

different electrochemical properties for the polyaniline products.³⁰⁻³² This has been confirmed in the present study for PAn.(+)-HCSA and PAn.HCl films electrodeposited onto glassy carbon electrodes at 0.9 V (125 mC/cm² charge passed) from aqueous 0.2 M aniline containing 1.0 M (+)-HCSA and 1.0 M HCl, respectively. Cyclic voltammograms for the two modified electrodes recorded in 1.0 M HCl (Figure 4.17) reveal that the redox couples for PAn.HCl appear at potentials more positive than those observed for PAn.(+)-HCSA.

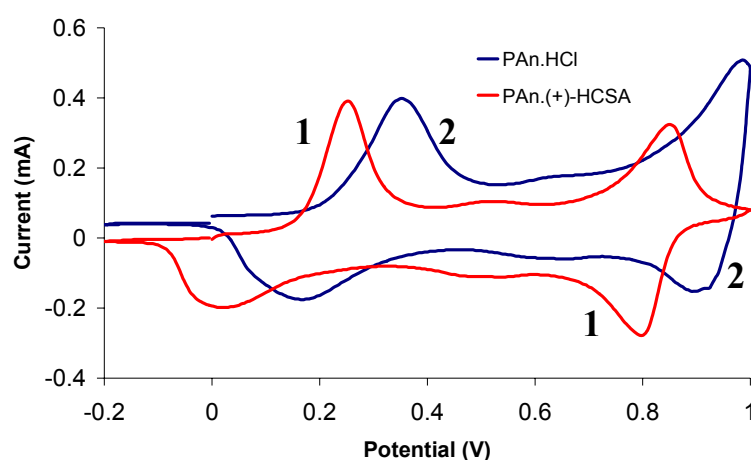


Figure 4.17 Cyclic voltammograms for (1) PAn.(+)-HCSA and (2) PAn.HCl films deposited on GC-disc (0.07 cm²) in 1.0 M HCl (scan rate = 50 mV/s). The polymer films were prepared by electrodeposition at 0.9 V (125 mC/cm² of charge passed) in 0.2 M aniline containing 1.0 M (+)-HCSA and 1.0 M HCl, respectively.

(ii) *PAn.HCl Film Deposited Upon a Thin PAn.(+)-HCSA Film*

Figure 4.18 illustrates the cyclic voltammograms measured in 1.0 M HCl (glassy carbon electrode) for a thin PAn.(+)-HCSA film grown for 25 mC/cm², and after further deposition of PAn.HCl for 100 mC/cm² (1st and 5th cycles shown). Interestingly, double redox peaks appeared in the low and high potential regions of the cyclic voltammogram recorded after depositing the PAn.HCl layer. This may arise from the different electrochemical behaviour of the two polymers, PAn.(+)-HCSA and PAn.HCl, in the final block co-polymer.

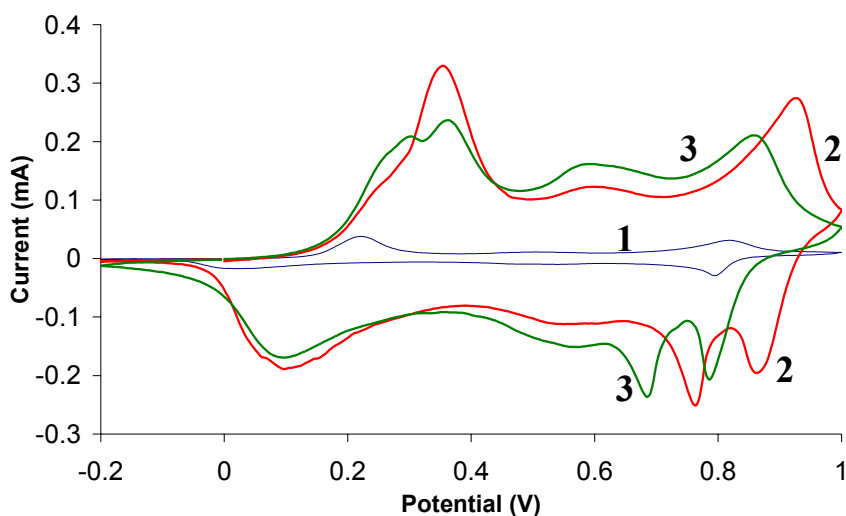


Figure 4.18 Cyclic voltammograms measured in 1.0 M HCl (scan rate of 50 mV/s) for: (1) a thin PAn.(+)-HCSA film on glassy carbon electrode (0.07 cm^2); (2) and (3), the 1st and 5th cycles after further deposition of PAn.HCl on top.

4.3.9.2 Chronoamperometry during Growth

Typical chronoamperograms obtained during potentiostatic deposition of PAn.(+)-HCSA and PAn.HCl onto ITO-Pt-coated glass electrodes (constant potential of + 0.9 V, 125 mC/cm^2 charge passed) are shown in Figure 4.19. These indicate that for both polyanilines the polymer growth occurs in two stages. The first stage corresponds to a decrease in current, which can be explained by the creation of nuclei on the surface of bare electrode under diffusion control. The increase in current with time during the second stage is associated with the rapid deposition of the polymer on the polyaniline-covered electrode, similar to the autoacceleratic growth of polyaniline that has been observed previously.³³

Interestingly, the polymerization rates seem to be anion dependent. Polymerization in 1.0 M (+)-HCSA was faster than in 1.0 M HCl. For 125 mC/cm^2 of charge passed, the electrodeposition time for PAn.(+)-HCSA was usually less than 60 sec (Figure 4.19a), while the time for depositing PAn.HCl was *ca.* 90 sec (Figure 4.19b).

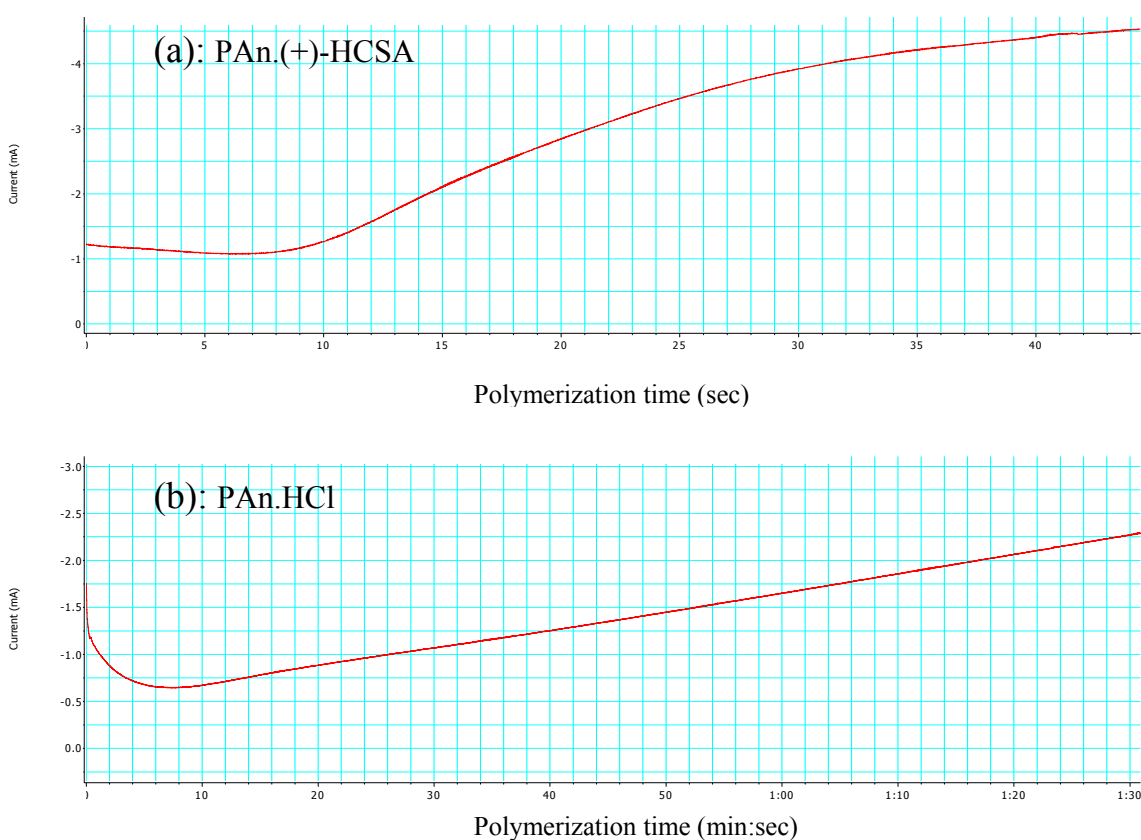


Figure 4.19 Chronoamperograms obtained during deposition of: (a) PAn.(+)-HCSA, and (b) PAn.HCl onto ITO-Pt-coated glass (*ca.* 1 cm²), using + 0.9 V and 125 mC/cm² charge passed.

Duić *et al.*³⁴ have reported the influence of anions on the electrochemical polymerization of polyaniline. They found that the polymerization rate varied in the order $\text{HSO}_4^- > \text{NO}_3^- > \text{Cl}^- > \text{ClO}_4^-$. Differences in the specific adsorption of the anions on the electrode surface were proposed to explain the results.

The influence of the anions present in the polymerization solution on the rate of electrodeposition of polyaniline was also observed in the 1st and 2nd steps of the asymmetric preparation of chiral polyanilines via the novel method in Scheme 4.1 presented here. The deposition time of PAn.HCl during the 2nd step (100 mC/cm²

charge passed) was 85 sec (Figure 4.20b). This indicates that Cl^- might be incorporated into the polyaniline chain during polymerization rather than $(+)\text{-CSA}^-$, where the deposition time was 40 sec for 100 mC/cm^2 charge passed. This suggests that the $(+)\text{-CSA}^-$ bound in the initial thin PAn.(+)-HCSA film is not involved in the electrodeposition of PAn.HCl .

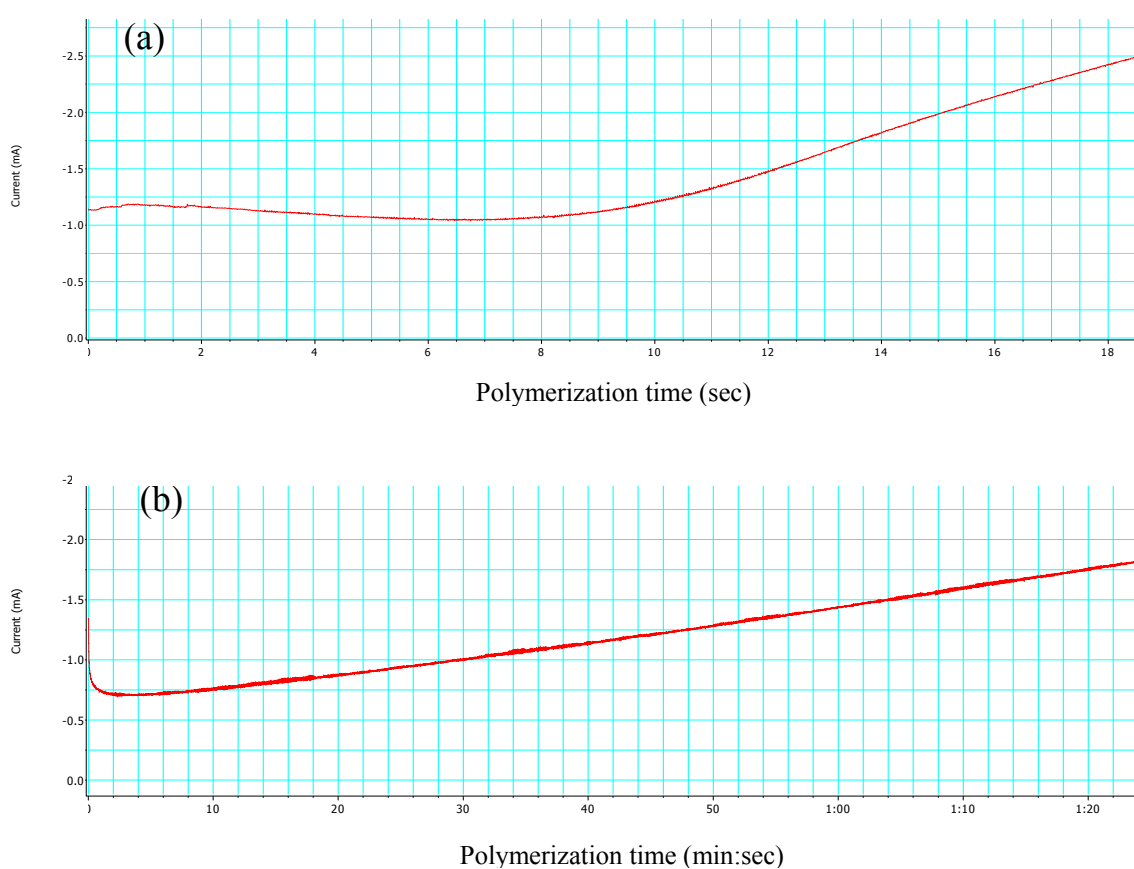


Figure 4.20 Chronoamperograms obtained during deposition of: (a) PAn.(+)-HCSA onto ITO-Pt-coated glass (*ca.* 1 cm^2), and (b) PAn.HCl on top of (a) for 100 mC/cm^2 , at $+0.9\text{V}$.

4.3.10 Attempted Asymmetric Electrochemical Synthesis of Optically Active Polypyrrole Induced by Chiral PAn.(+)-HCSA

It was of interest to determine whether thin PAn.(+)-HCSA films could be similarly used as chiral inducers for the asymmetric synthesis of other optically active conducting polymers. A preliminary study was therefore undertaken to explore the asymmetric synthesis of chiral polypyrrole (PPy).

A thin film of PAn.(+)-HCSA was prepared as previously described (electrodeposition charge = 25 mC/cm²), washed with methanol and its chiroptical properties measured. PPy.(±)-CSA was then potentiostatically deposited on top of this chiral polyaniline electrode using an applied potential of 0.9 V and 100 mC/cm² charge passed, employing aqueous 0.2 M pyrrole (monomer)/1.0 M racemic (±)-HCSA as the polymerization solution.

The UV-visible and CD spectra of the thin, initial PAn.(+)-HCSA film are shown in Figures 4.21 (curve 1) and 4.21(curve 2), respectively. After electrodepositing a PPy.(±)-CSA film onto this chiral electrode, the UV-visible spectrum became much more intense (Figure 4.21 - curve 2), with a strong peak at 470 nm and an intense free carrier tail into the near-infrared. These bands may be attributed to the presence of bipolarons, and are indicative of the deposition of a conducting polypyrrole. The spectrum was not significantly modified by washing the film with methanol (Figure 4.21 - curve 3).

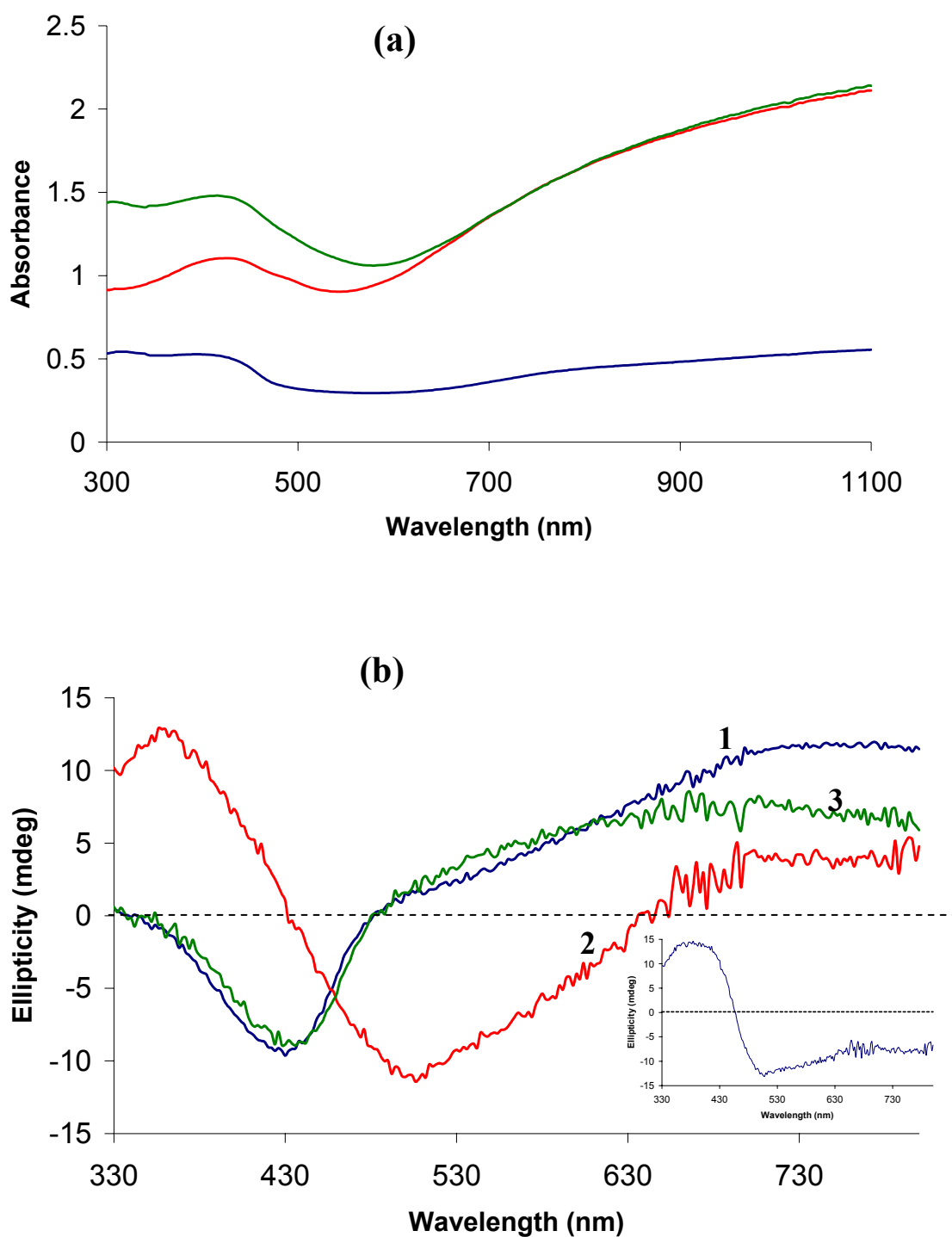


Figure 4.21 (a) UV-visible and (b) CD spectra of: (1) a PAn.(+)-HCSA film electrodeposited on ITO-Pt-coated glass at 0.9 V (deposition charge = 25 mC/cm^2); (2) after depositing a PPy.(±)-CSA film on top of (1) for 100 mC/cm^2 passed, as grown, and (3) after washing with MeOH. Inset: curve 2 after subtracting the spectrum of the PAn.(+)-HCSA under-layer (*i.e.* subtracting curve 1).

Interestingly, before washing with methanol, the CD spectrum of the final composite PAn.(+)-HCSA/ PPy.(±)-CSA film after subtracting that of the thin PAn under-layer, exhibited a pair of bisignate CD bands at *ca.* 370 and 500 nm, which could be associated with the absorption band of the thicker PPy.(±)-CSA over-layer at 470 nm. This suggests the formation of a weakly optically active polypyrrole via induction by the PAn initiator. However, after methanol washing, while not much change in the UV-visible spectrum was observed, the CD spectrum reverted to that recorded for the initial thin chiral PAn.(+)-HCSA film. Further studies will therefore be required to establish whether the asymmetric synthesis of polypyrroles can be achieved using a thin chiral PAn.(+)-HCSA film for chiral induction.

4.4 Conclusions

It is possible to induce optical activity into PAn.HA emeraldine salt chains via electrochemical polymerization of aniline in aqueous racemic or achiral acids (HA) at ITO-Pt-coated glass electrodes coated with a thin film of either PAn.(+)-HCSA or PAn.(-)-HCSA. Strongly optically active polyaniline with the same chiroptical properties as the chiral inducer employed are produced, with PAn.HA films grown on PAn.(+)-HCSA and PAn.(-)-HCSA electrodes having mirror imaged CD spectra. Remarkably, optical activity of the same hand as the chiral inducer (PAn.(+)-HCSA) is also produced when the enantiomeric (-)-HCSA is used as the dopant acid in the second polymerization step.

The preparation of the initial chiral PAn.HCSA electrode requires a minimum of 25 mC/cm² electrodeposition charge, giving a thickness of *ca.* 100 nm for the film. Optically active polyanilines doped with racemic or achiral acids, with film thicknesses

of *ca.* 400 nm are deposited onto this thin film after a further 100 mC/cm² of charge is passed. The ellipticity of the deposited emeraldine salt films increases linearly as the deposition charge is increased from 50-300 mC/cm², indicating that chiral induction by the thin initial polyaniline layer extends undiminished for films of at least 700 nm in thickness.

The optical activity of emeraldine salt films produced by this novel method is retained upon de-doping to emeraldine base and then re-doping to emeraldine salt, or upon redox switching to leucoemeraldine or pernigraniline during potential cycling between -0.3 and +0.9 V in aqueous acid different from the acid used in the polymer growth.

Electrochemical cyclic voltammetric studies both during and after the deposition steps have thrown some light on the mechanism of this macromolecular asymmetric induction. However, the detailed mechanism remains uncertain at the moment. This novel asymmetric synthesis method presents potential applications such as using thin chiral polyaniline films as inducers for the asymmetric synthesis of other conducting polymers.

4.5 References

1. Majidi, M.R., L.A.P. Kane-Maguire, and G.G. Wallace. *Polymer*, 1994. **35**: p. 3113-3116.
2. Majidi, M.R., L.A.P. Kane-Maguire, and G.G. Wallace. *Polymer*, 1996. **37**: p. 359-362.
3. Majidi, M.R., L.A.P. Kane-Maguire, and G.G. Wallace. *Aust. J. Chem.*, 1998. **51**: p. 23-30.
4. Majidi, M.R., L.A.P. Kane-Maguire, and G.G. Wallace. *Polymer*, 1995. **36**: p. 3597-3599.
5. Xia, Y., J.M. Wiesinger, and A.G. MacDiarmid. *Chem. Mater.*, 1995. **7**: p. 443-445.
6. Norris, I.D., L.A.P. Kane-Maguire, and G.G. Wallace. *Macromolecules*, 1998. **31**.
7. MacDiarmid, A.G. and A.J. Epstein. *Synth. Met.*, 1995. **69**: p. 85-92.
8. Sapurina, I., A. Riede, and J. Stejskal. *Synth. Met.*, 2001. **123**: p. 503-507.
9. Stejskal, J., et al. *Synth. Met.*, 1999. **105**: p. 195-202.
10. Maeda, K., et al. *Polym. J.*, 1995. **30**: p. 100.
11. Thiyagararjan, M., et al. *J. Am. Chem. Soc.*, 2003. **125**: p. 11502-11503.
12. Innis, P.C., et al. *Macromolecules*, 1998. **1998**: p. 6521-6528.
13. Kane-Maguire, L.A.P., et al. *Synth. Met.*, 1999. **106**: p. 171-176.
14. Yuan, G.-L. and N. Kuramoto. *Macromolecules*, 2002. **35**: p. 9773-9779.
15. Li, W., et al. *Macromolecules*, 2002. **35**: p. 9975-9982.
16. McCarthy, P.A., et al. *Langmuir*, 2002. **18**: p. 259-263.
17. Yang, Y. and M. Wan. *J. Mater. Chem.*, 2002. **12**: p. 897-901.
18. Li, W., et al. *Langmuir*, 2003. **19**: p. 4639-4644.
19. Jha, S.K., et al. *J. Am. Chem. Soc.*, 1999. **121**: p. 1665-1673.

-
20. Green, M.M., et al. *Angew. Chem. Int. Ed.*, 1999. **38**: p. 3138-3154.
 21. Langeveld-Voss, B.M.W., et al. *Macromolecules*, 1999. **32**: p. 227-230.
 22. Garcia, B., F. Fusalba, and D. Belanger. *Can. J. Chem.*, 1997. **75**: p. 1536-1541.
 23. Syed, A.A. and M.K. Dinesan. *Talanta*, 1991. **38**: p. 815-837.
 24. Genies, E.M., et al. *Synth. Met.*, 1990. **36**: p. 139-182.
 25. Torresi, R.M. and S.I. Torresi. *Synth. Met.*, 1993. **61**: p. 291-296.
 26. Desilvestra, J., W. Scheifele, and O. Haas. *J. Electrochem. Soc.*, 1992. **139**: p. 2727-2736.
 27. Orata, D. and D.A. Buttry. *J. Am. Chem. Soc.*, 1987. **109**: p. 3574-3581.
 28. Shim, Y.-B., M.-S. Won, and S.-M. Park. *J. Electrochem. Soc.*, 1990. **137**: p. 538-544.
 29. Kane-Maguire, L.A.P., I.D. Norris, and G.G. Wallace. *Synth. Met.*, 1999. **101**: p. 817-818.
 30. Palys, B., et al. *Synth. Met.*, 2000. **108**: p. 111-119.
 31. Zhang, A.Q., C.Q. Cui, and Y.J. Lee. *Synth. Met.*, 1995. **72**: p. 217-223.
 32. Fenelon, A.M. and C.B. Breslin. *Synth. Met.*, 2004. **144**: p. 125-131.
 33. Okamoto, H., M. Okamoto, and T. Kotaka. *Polymer*, 1998. **39**: p. 4359-4367.
 34. Duic, L.J., Z. N Mandic, and F. Kovacicek. *J. Polym. Sci., Part A*, 1994. **32**: p. 105-111.

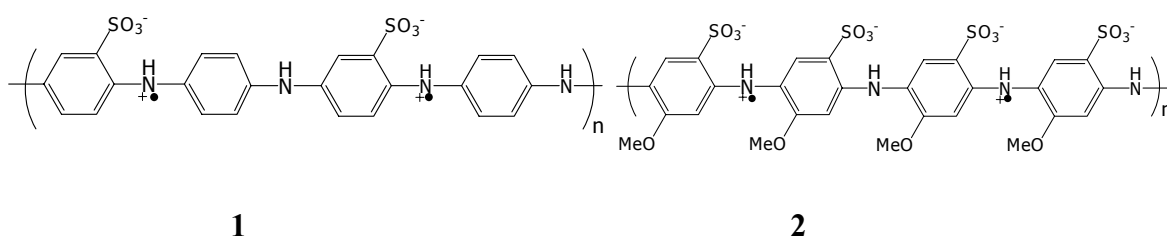
Chapter 5

pH and Redox Switching Properties of PMAS

5.1 Introduction

As discussed in greater detail in Chapter 1, polyaniline differs from other conducting polymers in that it has three readily accessible oxidation states: leucoemeraldine, emeraldine and pernigraniline. It can also be switched from an insulating to a conducting material without changing the number of π -electrons by protonic doping of the emeraldine base form to the emeraldine salt form.¹ However, there are some disadvantages with polyaniline due to its insolubility in water and common organic solvents and its instability at melting temperature. These limitations make it difficult to process for applications.

In order to enhance its solubility in organic solvents, alkyl- and alkoxy- ring-substituted polyanilines have been synthesized.²⁻⁶ However, their conductivity is quite low compared to the parent polyaniline. The most successful approach to date towards water soluble polyanilines is via sulfonation of the benzenoid rings in polyaniline chains with sulfonic acid to obtain the sulfonated polyaniline SPAN, **1**. It has been reported that 50% or 75% of the aniline rings were substituted with sulfonic acid groups via this reaction using emeraldine base or leucoemeraldine base as starting material.⁷⁻⁹ SPAN has an intrinsic acid, sulfonic acid, which is able to dope the polyaniline backbone via so called “self-doping”. The water soluble SPAN is in the conductive self-doped emeraldine salt form, and has a moderate electrical conductivity of *ca.* 0.1 S/cm. The electronic spectra and redox properties of SPAN are similar to unsubstituted polyaniline emeraldine salts.⁹⁻¹¹



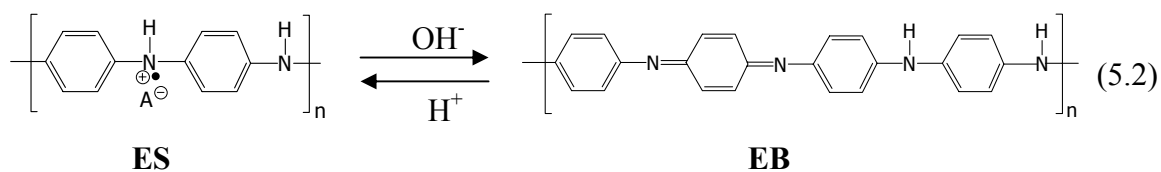
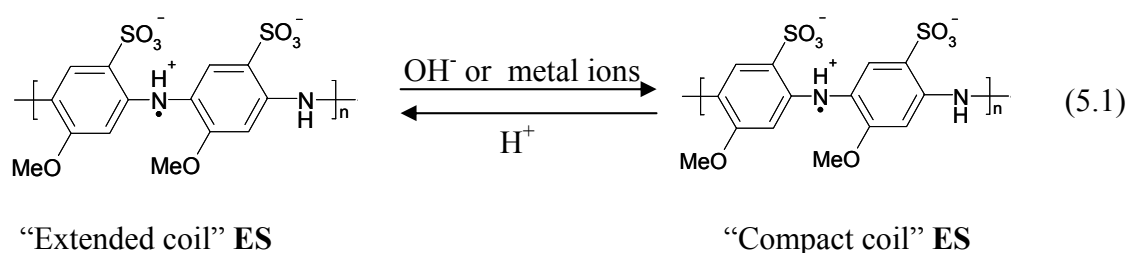
1 sulfonated polyaniline (SPAN)

2 poly(2-methoxyaniline-5-sulfonic acid) (PMAS)

Highly water soluble, self-doped poly(2-methoxyaniline-5-sulfonic acid) (PMAS, **2**), is the first reported fully sulfonated polyaniline. It has been synthesized by both chemical¹² and electrochemical^{13, 14} polymerization of 2-methoxyaniline-5-sulfonic acid (MAS) monomer. In its dimer repeating unit, one sulfonate group is involved in self-doping with an adjacent radical cation ($+•\text{NH}$), while the other sulfonate group is available for electrostatic interaction. This latter “free” sulfonate can be bound to a proton or to cations such as Na^+ or NH_4^+ . As synthesized, PMAS has a moderate electrical conductivity (*ca.* 0.1-0.4 S/cm).

Unlike SPAN, the spectrochemistry of aqueous PMAS is remarkably different to that of parent polyaniline. The UV-visible spectrum of aqueous PMAS emeraldine salt (ES) exhibits a broad band at 320-390 nm attributed to π - π^* transitions, and a strong sharp peak at 473 nm assigned as a low wavelength polaron band.^{15,16} Strong absorption is also observed in the near-infrared region at wavelengths greater than 1000 nm, attributed to a delocalized polaron band. These spectroscopic features have led to the conclusion¹⁵ that aqueous PMAS exists in an “extended coil” conformation. The localized polaron band at *ca.* 700-800 nm observed for emeraldine salts of polyaniline and other substituted polyanilines in their “compact coil” conformation is not seen. However, a strong absorption band at around 750 nm is observed when NaOH or alkali metal ions are added to aqueous PMAS solution.¹⁵ This was interpreted as a metal ion

initiated transformation of the PMAS chains from an initial “extended coil” conformation to a “compact coil” arrangement (Equation 5.1). This behaviour of PMAS emeraldine salt in alkaline solution is remarkable, as unsubstituted polyaniline emeraldine salts (and SPAN) are in contrast de-doped to give emeraldine base (EB) (Equation 5.2).



Furthermore, the optical properties of the reduced leucoemeraldine base form of PMAS were recently reported¹⁷ to differ from that of the leucoemeraldine form of parent polyaniline. Reduction of PMAS with hydrazine gives a polymer with a band at *ca.* 330-340 nm (similar to that of unsubstituted polyaniline), assigned as a π - π^* transition. However, a further strong sharp peak is also seen at *ca.* 408 nm, which is not observed in the reduction of parent polyaniline. The origin of the latter peak has remained unclear.¹⁷

In this Chapter, the pH and redox switching properties of PMAS are further explored. Treatment with a range of bases is investigated in order to further elucidate the unusual base-promoted conformational change in Equation 5.1 above, and to explore whether

alkaline de-doping of PMAS emeraldine salt can be achieved under certain conditions. The unusual reduction of PMAS is also systematically investigated under a wide range of conditions. Of particular interest is the origin and nature of the 408 nm peak observed in the hydrazine reduction of PMAS. The effect of temperature and solvent on the behaviour of the species with λ_{max} at 408 nm is also studied, revealing fascinating thermochromic and solvatochromic behaviour. Finally, the oxidation of aqueous PMAS to pernigraniline is examined.

5.2 Experimental

5.2.1 Materials

PMAS (synthesized at 5°C and purified using a cross flow dialysis) was kindly provided by Fatemeh Masdarolomoor (IPRI). GPC analysis of this PMAS showed: $M_w = 18067$, $M_n = 5700$ and polydispersity = 3.2. Ammonium persulfate, sodium hydroxide, hydrazine monohydrate, sodium chloride, tetrabutylammonium hydroxide {40% (w/v) Bu_4NOH }, *N*-methylpyrrolidinone (NMP), and di-isopropylamine were purchased from Aldrich. Ammonium hydroxide (28% NH_3) and methanol were purchased from Ajax.

5.2.2 Behaviour of PMAS in Basic Aqueous Solutions

Accurate amounts of aqueous NH_4OH , NaOH , Bu_4NOH or di-isopropylamine (DIPA) were successively added by micropipette to 0.03 mM or 0.06 mM PMAS aqueous solutions. UV-visible spectra (250-1100 nm) were measured after each addition using a Shimadzu UV-1601 spectrophotometer.

5.2.3 Chemical Oxidation and Reduction of Aqueous PMAS

PMAS in aqueous solution (A_{475} ca. 0.5) was oxidized with ammonium persulfate (0.1 M) at room temperature, and absorption spectral changes with times were monitored.

Reductions of PMAS with hydrazine were commonly carried out in water, with the pH determined by the concentration of hydrazine employed ($[N_2H_4] = 0.01-0.4$ M). In other cases, phosphate buffer (pH 7) was added to the reduction medium, or the bases NaOH, NH_4OH , or Bu_4NOH added. UV-visible spectra were recorded immediately after mixing and monitored until no further spectral change occurred. The pH of the solutions was measured using pH paper. The influence of temperature, both during and after reduction, on the spectral and conformational properties of the reduced PMAS was examined by carrying out the reductions in a thermostatted bath.

5.2.4 Solvatochromism - Effect of Solvents on the Conformation of Reduced PMAS

Reduction of PMAS with hydrazine was carried out in aqueous solution and then various amounts of organic solvents (MeOH, NMP or acetone) added. The UV-visible spectra of these mixtures were monitored with time. To enable comparisons, the concentration of PMAS was maintained constant in all experiments.

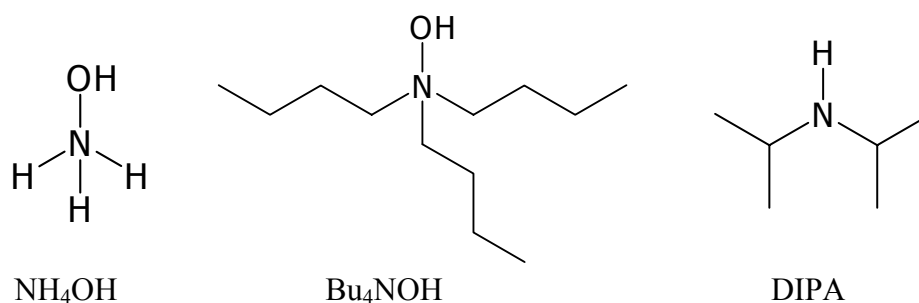
5.3 Results and Discussion

5.3.1 Behaviours of PMAS in Basic Aqueous Solutions

Strounina *et al.*¹⁵ have recently observed two stages of spectral change during the titration of aqueous PMAS emeraldine salt with NaOH. The spectral changes during the first stage from pH 3.7-8.0 were attributed to deprotonation of “free” sulfonic acid groups on the PMAS chains. The spectral changes during the second stage (pH 9-14) were believed to arise from a conformational change from “an extended coil” to a “compact coil” structure initiated by binding of Na^+ ions to “free” sulfonate groups on the PMAS chains. Evidence for this latter conclusion was the appearance of a strong peak at 750 nm, similar to the high wavelength polaron band typically observed for the

“compact coil” conformation of polyaniline emeraldine salts. The fact that aqueous PMAS, unlike parent polyaniline and partially sulfonated SPAN polymers, did not deprotonate to the corresponding emeraldine base in 1.0 M NaOH (pH 14) is remarkable. It has significant implications since, by remaining as an emeraldine salt (of altered conformation), it remains an electrical conductor even under highly alkaline conditions.

To further elucidate this fascinating behaviour of PMAS in alkaline solution, the influence of the nature of the base on the spectral/ conformational changes of PMAS in aqueous solution has been explored. Ammonium hydroxide, tetrabutylammonium hydroxide (Bu_4NOH) and di-isopropylamine (DIPA) were used in this study.



5.3.1.1 PMAS in Aqueous NH_4OH

The absorption spectra of aqueous PMAS (0.03 mM) in the presence of various concentrations of NH_4OH (0.05 mM – 0.1 M) are shown in Figure 5.1. As with the earlier titration of PMAS with NaOH,¹⁵ two distinct stages were seen in the spectral changes with increasing pH (increasing $[\text{NH}_4\text{OH}]$).

First Stage

The first stage was observed in the pH range 5.8-7.7 (Figure 5.1). The initial aqueous PMAS (0.03 mM, pH 5.8) exhibited a broad band between 320 and 360 nm attributed to π - π^* transitions of the benzenoid rings; and a strong, sharp peak at 475 nm assigned as a

polaron band, characteristic of the emeraldine salt form of PMAS. Upon increasing the pH of the solution from 5.8 to 7.7, the following spectral changes were observed:

- (i) a marked increase in the intensity of the initial π - π^* bands, a small red shift and the development of a separate peak at 340 nm and a shoulder at 375 nm;
- (ii) a marked decrease in the intensity of the initial polaron band at 475 nm;
- (iii) the growth of a weak band in the 600 – 800 nm region;
- (iv) a decrease of the NIR absorption.

Three isosbestic points at 420, 510 and 920 nm were observed during this first stage, confirming a clean process. The spectral changes were similar to those observed by Strounina *et al.*¹⁵ for the first stage of the titration of PMAS emeraldine salt with NaOH (pH 3.7 to 8.0). They may arise from deprotonation of “free” sulfonic acid groups on the PMAS chains with subsequent changes in chain conformation.

Second Stage

When the pH was raised above 8.0 (to 10.5), further marked changes occurred in the UV-visible spectrum of the PMAS (Figure 5.2), again mirroring those observed by Strounina for related titrations with NaOH. A further increase in absorbance occurred at lower wavelengths with the appearance of distinct bands at 340 and 377 nm, while the 475 nm polaron band almost completely disappeared. A strong peak appeared at 830 nm. This spectrum is consistent with an emeraldine salt in a “compact coil” conformation.¹⁸
¹⁹ The new peak at 830 nm and the shoulder peak at *ca.* 377 nm can be assigned to a localized polaron absorption band and a second polaron band, respectively; while the band at *ca.* 340 nm is attributed to a π - π^* transition. Three isosbestic points were seen at 410, 515, and 1030 nm, indicating a clean process. Therefore, as in the related titration of PMAS with NaOH, these spectral changes for Stage 2 with NH₄OH may be interpreted as involving a change in conformation of the PMAS chains from “extended

coil” to “compact coil”, initiated by binding of NH_4^+ ions to “free” sulfonate groups on the PMAS chains.

Interestingly, de-doping of PMAS (the third stage, see Section 5.3.1.2 below) was not observed even in concentrated aqueous NH_4OH (28% NH_3 , *ca.* 14.5 M, pH 13) or 3.0 M NaOH (pH 14) (Figure 5.3).

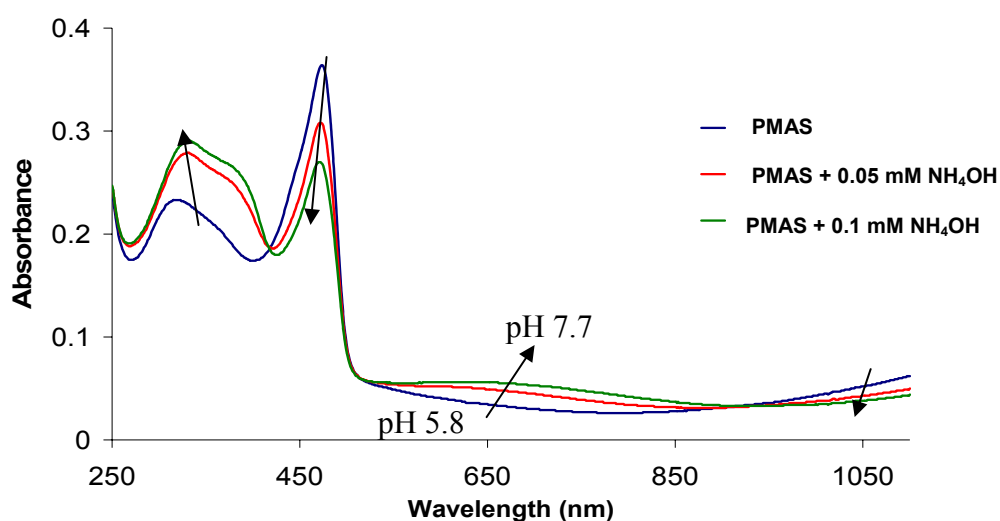


Figure 5.1 UV-visible spectral changes when NH_4OH (0.05 mM or 0.1 mM) was added to 0.03 mM aqueous PMAS (final pH 5.8 - 7.7).

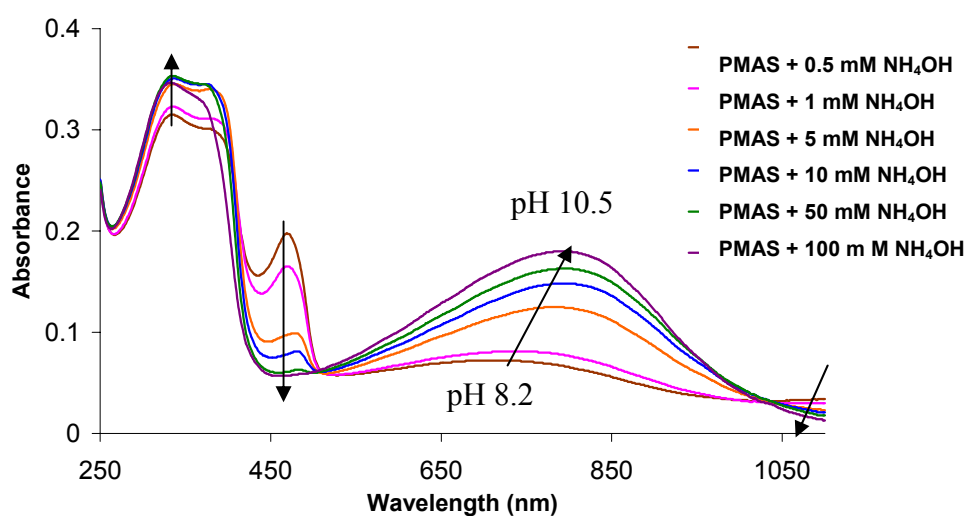


Figure 5.2 UV-visible spectral changes when 0.5 mM – 100 mM NH_4OH were added to 0.03 mM aqueous PMAS (final pH 8.2 – 10.5).

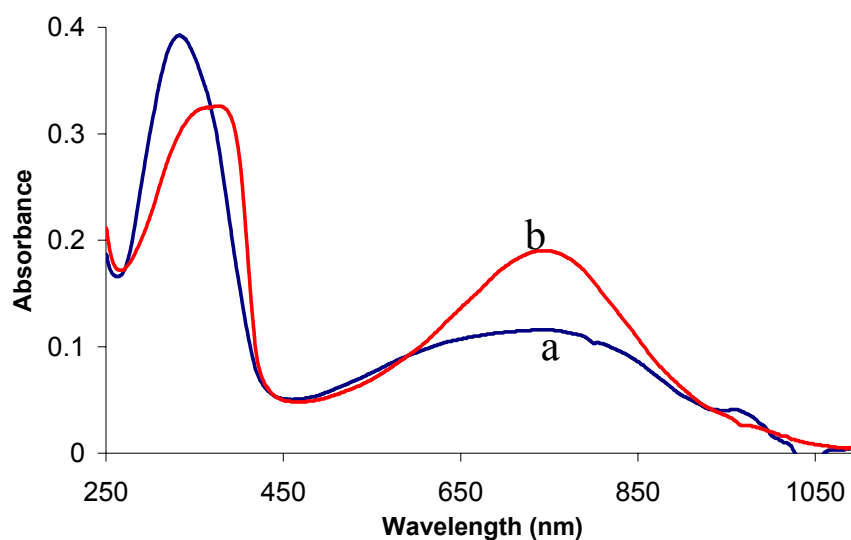


Figure 5.3 UV-vis spectra of aqueous PMAS in: (a) conc. NH_4OH (final pH 13), and (b) 3.0 M NaOH (final pH 14).

5.3.1.2 Aqueous PMAS with Sterically Crowded Amines

The hypothesis that the above conformational change of PMAS emeraldine salt from “extended coil” to “compact coil” in NaOH ¹⁵ and NH_4OH is associated with electrostatic binding of the relatively small Na^+ and NH_4^+ ions, was tested by carrying out similar titrations of aqueous PMAS with sterically crowded amines. The amines chosen for this study were tetrabutylammonium hydroxide ($\text{Bu}_4\text{N}^+\text{OH}^-$) and diisopropylamine (Pr_2^iNH) (DIPA). The latter amine generates hydroxide ions in aqueous solution as shown in Equation 5.3, generating the sterically crowded ammonium ion $\text{Pr}_2^i\text{NH}_2^+$.



(i) PMAS in Aqueous Bu_4NOH

The UV-visible spectra of aqueous PMAS before and after mixing with various amounts of Bu_4NOH are shown in Figures 5.4 - 5.6. These reveal three stages, depending on the pH.

First Stage

As the concentration of Bu₄NOH was increased from zero to 0.1 mM (pH 5.8 to 8.0) the characteristic polaron band of the initial PMAS at 475 nm decreased in intensity (Figure 5.4). The initial π - π^* band of the PMAS benzenoid rings at 340 nm simultaneously grew in intensity. At the same time, a shoulder peak appeared at 390 nm and a broad strong band at *ca.* 800 nm. The presence of three isosbestic points at 415, 500, and 950 nm indicated a clean process. These spectral changes with increasing pH are similar to those observed for the first stage of the titrations of PMAS emeraldine salt with NaOH (pH 3.7 to 8.0)¹⁵ or NH₄OH (pH 5.8 – 7.7, see Figure 5.1). They may arise from deprotonation of “free” SO₃H groups on the PMAS chains causing partial conformational changes.

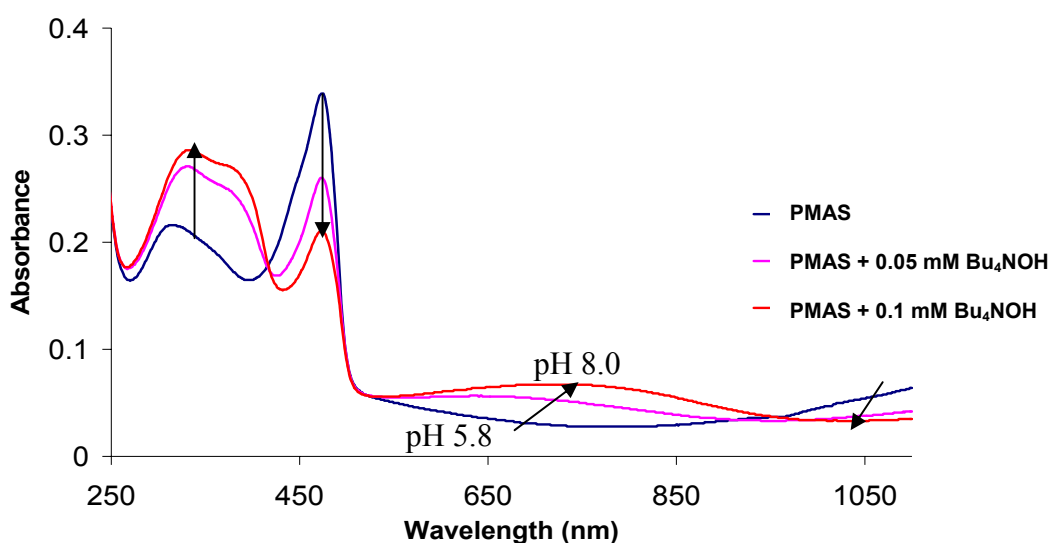


Figure 5.4 UV-vis spectral changes when Bu₄NOH (0.05 mM or 0.1 mM) was added to 0.03 mM aqueous PMAS (final pH 5.8 - 8.0).

Second Stage

When the pH was subsequently raised above 8.0 (to 10.1 and 10.6), further marked changes occurred in the UV-visible spectrum of the PMAS (Figure 5.5). The absorbance increased at lower wavelengths with the appearance of distinct bands at 340 and 377 nm,

while the 475 nm polaron band almost disappeared. A strong peak instead now appeared at 830 nm. This spectrum is consistent an emeraldine salt in a “compact coil” conformation. The new peak at 830 nm and the shoulder peak at *ca.* 377 nm can be assigned to polaron bands, while the band at *ca.* 340 nm is attributed to a π - π^* transition. Therefore, as in the related titration of PMAS with NaOH or NH_4OH , these spectral changes during Stage 2 in Bu_4NOH may be attributed to a change in conformation of the PMAS chains from “extended coil” to “compact coil”.

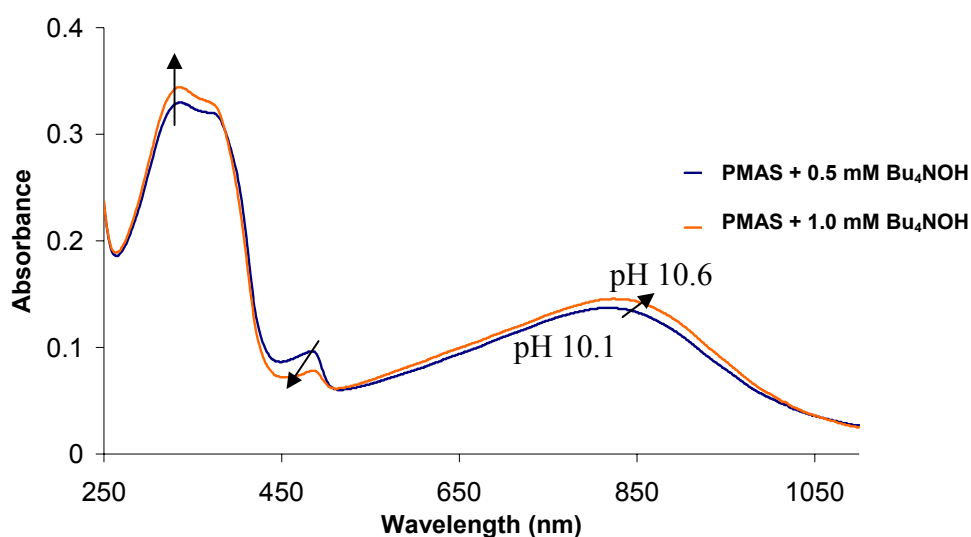


Figure 5.5 UV-vis spectral changes when 0.5 mM and 1.0 mM Bu_4NOH were added to 0.03 mM aqueous PMAS (final pH 10.1 -10.6).

Third Stage

Significantly, a third stage of spectral changes was observed using higher Bu_4NOH concentrations (final pH in the range 11.5 to 13.1), as shown in Figure 5.6. With increasing pH, the π - π^* band at 340 nm became more intense, while the shoulder peak at 377 nm and the peak at 830 nm gradually decreased and had disappeared by pH 12.8-13.1. At the same time, a distinct new absorption band appeared at 630 nm. This latter peak is at a similar wavelength to the characteristic “exciton” band found for the emeraldine base forms of unsubstituted polyaniline and SPAN from 580-640 nm.⁹⁻¹¹

Therefore, the spectral changes observed in this high pH range with Bu₄NOH strongly suggest de-doping of the PMAS emeraldine salt to its emeraldine base form.

This de-doping of aqueous PMAS emeraldine salt at high pH in aqueous Bu₄NOH contrasts with the behaviour observed by Strounina¹⁵ (and in this work, see Figure 5.3) in NaOH solutions of similar pH, where the emeraldine salt instead underwent a conformational change. This different behaviour in Bu₄NOH may arise from the steric bulk of the Bu₄N⁺ cation hindering its electrostatic binding to “free” sulfonate groups on PMAS emeraldine salt chains, proposed above as the cause of the alternative conformational change. However, it remains uncertain why the “compact coil” form of PMAS emeraldine salt thus formed in NaOH and NH₄OH is resistant to de-doping.

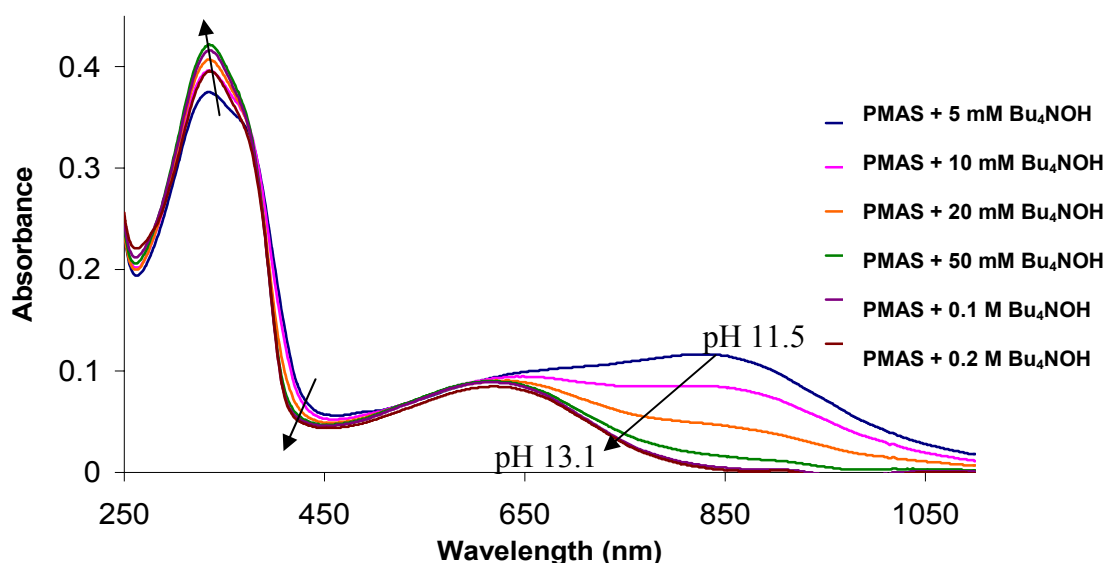


Figure 5.6 UV-vis spectral changes when 5 mM – 0.2 M Bu₄NOH (pH 11.5 - 13.1) were added to 0.03 mM aqueous PMAS.

(ii) PMAS in Aqueous DIPA

When 10 μ L of DIPA was added to 10 mL solution of aqueous PMAS (0.06 mM), giving [DIPA] = 0.007 mM, the initial PMAS spectrum with its characteristic peak at

477 nm completely vanished. Three new peaks appeared at 340, 390 and 760 nm. This new UV-visible spectrum is similar to that found above in the second stage of the alkaline treatments of PMAS with NH_4OH and NaOH , and may be attributed to the generation of the “compact coil” conformation of PMAS emeraldine salt.

Subsequent addition of further aliquots of DIPA (up to 510 μL , where $[\text{DIPA}] = 0.8$ mM) progressively caused a small blue shift and an increase in intensity for the peak at 340 nm, together with the disappearance of the shoulder peak at 390 nm. Most significantly, the absorption band at 760 nm showed a blue shift to 630 nm when $[\text{DIPA}] = 0.8$ mM. An isosbestic point at 375 nm was observed, as shown in Figure 5.7. As found with Bu_4NOH treatment above, these spectral changes in relatively high concentrations of DIPA strongly indicate de-doping of the PMAS emeraldine salt to its emeraldine base form.

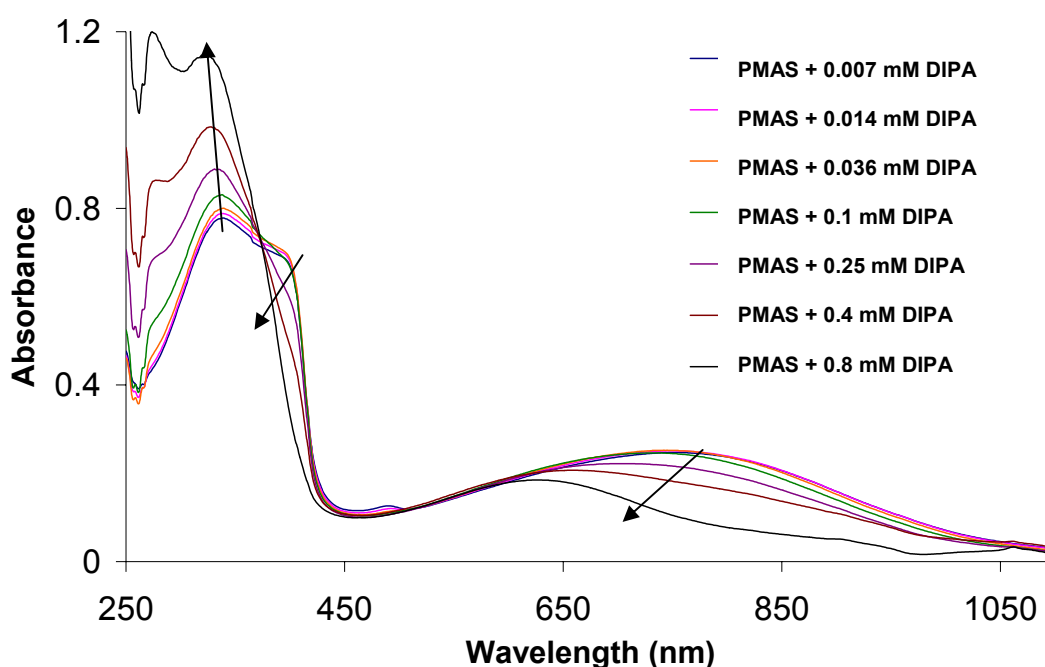


Figure 5.7 UV-vis spectral changes when 0.007 – 0.8 mM DIPA were added to 0.06 mM aqueous PMAS.

5.3.2 Redox Switching of Aqueous PMAS

Strounina¹⁷ has studied the redox switching properties of aqueous PMAS by monitoring absorption spectral changes during chemical oxidation/ reduction processes. However, PMAS employed in this earlier study is now known to have contained both the polymer (M_w 15500, M_n 10100, polydispersity 1.5) as well as an ill-defined oligomer of *ca.* 2000 molecular weight. A new method for the purification of PMAS using a cross flow dialysis has been recently developed by Fatemeh *et al.*²⁰. This provides PMAS (M_w = 18067, M_n = 5700, polydispersity = 3.2) without oligomer. Different chemical, physical and electrochemical properties between polymers and oligomers of conducting polymers have been reported.²¹ Therefore, in this Chapter, the redox switching properties of purified PMAS (without oligomer) have now been investigated.

5.3.2.1 Oxidation of PMAS with Ammonium Persulfate

The UV-visible spectrum was recorded immediately after adding $(NH_4)_2S_2O_8$ (0.1 M) to aqueous PMAS (*ca.* 0.04 mM) at room temperature and then monitored with time, giving the spectral changes shown in Figure 5.8.

The two initial polaron bands of PMAS emeraldine salt at 475 nm and in the near-infrared region gradually decreased as oxidation proceeded, while two new peaks grew at 330 and 550 nm. These latter peaks are characteristic of the fully oxidized pernigraniline base form of polyaniline. Three isosbestic points were observed at 380, 500 and 685 nm throughout the 30 min reaction, indicating a clean conversion from emeraldine salt to the pernigraniline base form of PMAS.

In an attempt to obtain the spectrum of the pernigraniline salt form of PMAS, two drops of conc. HCl were added to the solution of pernigraniline base. However, due to the

very fast decomposition of the PMAS pernigraniline salt, the spectrum of this polymer could not be recorded. These results were very similar to those previously observed by Strounina¹⁷ for a PMAS/oligomer mixture, and mirror the oxidation behaviour of parent unsubstituted polyaniline.

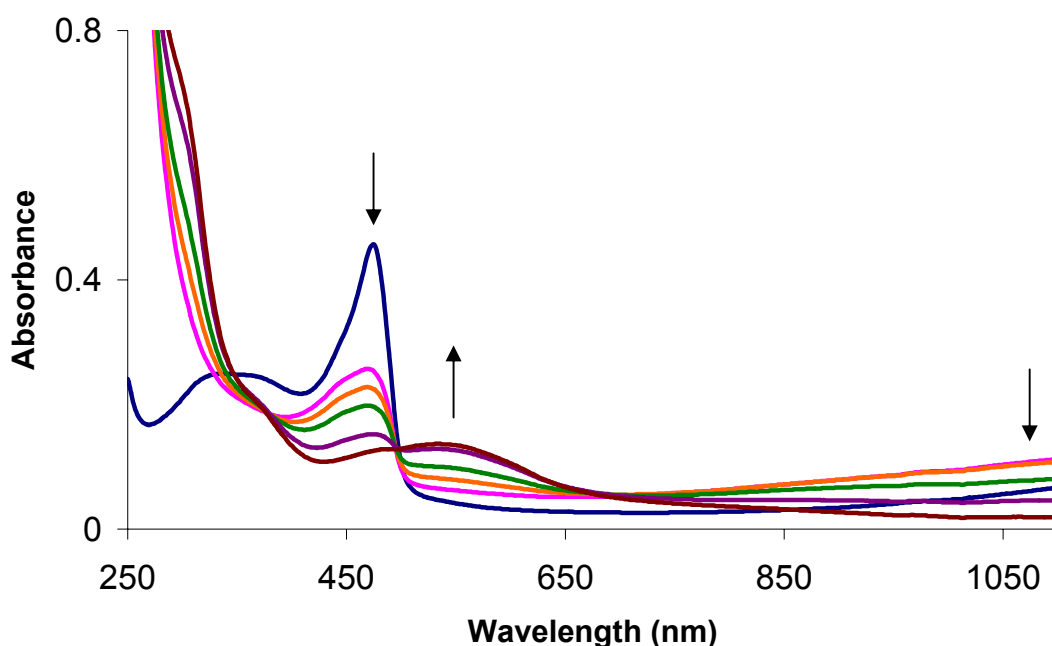


Figure 5.8 UV-visible spectral changes for aqueous PMAS during oxidation with 0.1 M $(\text{NH}_4)_2\text{S}_2\text{O}_8$, pH 4.5-5. The spectra were recorded at 1, 3, 5, 15, and 30 min.

5.3.2.2 Reduction of Aqueous PMAS with Hydrazine

In the previous study by Strounina¹⁷ of the reduction of aqueous PMAS with hydrazine, it was very interesting that an unexpected sharp peak at 408 nm was observed, together the normal 330 nm peak (assigned as a π - π^* transition) found for the reduced leucoemeraldine base form of polyanilines. The origin of the peak at 408 nm was unclear. The nature of this reduced PMAS species with λ_{max} at 408 nm has therefore been further explored, using a variety of experimental conditions (various $[\text{N}_2\text{H}_4]$, pH, temperature, solvent), as described below.

(i) Reduction in Aqueous Hydrazine (pH 10)

Treatment of aqueous pure PMAS with 0.4 M hydrazine (pH 10) at room temperature caused the rapid (< 1 min) disappearance of the characteristic peak of the initial emeraldine salt at 475 nm (as well as its NIR absorption), and the appearance of an intense sharp peak at 408 nm (with a shoulder at *ca.* 365 nm) - see Figure 5.9. This behaviour is very similar to that previously observed by Strounina for a PMAS/oligomer sample treated in a similar fashion. Other studies in our laboratory have shown the oligomer present in Strounina's PMAS sample to be redox inactive.²²

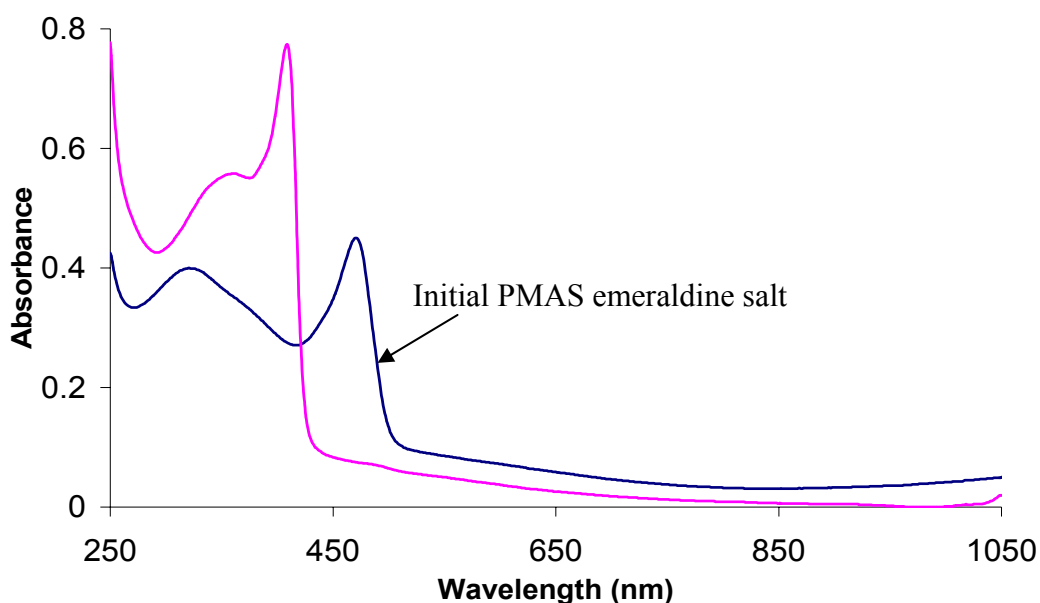


Figure 5.9 UV-visible spectral change after 1 min when aqueous PMAS is reduced with hydrazine ($[N_2H_4] = 0.4$ M, pH 9.5).

The dominant species from the hydrazine reduction of PMAS emeraldine salt therefore has λ_{max} 408 nm. The spectrum of this reduced mixture did not change over 15 min at room temperature. It is clearly different to the leucoemeraldine base product produced in all previously reported reductions of polyaniline and substituted polyanilines, which have a single characteristic peak at *ca.* 330 nm.

Further studies, outlined in (ii)-(iii) below, were therefore carried out in order to investigate the nature of this unprecedented λ_{\max} 408 nm species.

(ii) Reduction in 0.2 M Phosphate Buffer (pH 7.0)

(a) [Hydrazine] = 0.01 M

The UV-visible spectrum of aqueous PMAS in 0.2 M phosphate buffer (pH 7.0) was recorded before and after addition of 0.01 M hydrazine at room temperature. As shown in Figure 5.10, the initial PMAS emeraldine salt peak at 475 nm gradually decreased in intensity over 60 min, while an intense sharp peak grew at 408 nm (accompanied by a shoulder at *ca.* 360 nm).

Thus, the same dominant reduced PMAS species with $\lambda_{\max} = 408$ nm was obtained in pH 7.0 buffer as was found above in hydrazine at pH 10. However, the reduction was much slower at the low hydrazine concentration ($[\text{N}_2\text{H}_4] = 0.01$ M), and the reaction was not complete after 60 min. Three isosbestic points were observed at 305, 423, and 496 nm throughout the reduction (Figure 5.10), confirming a clean redox process.

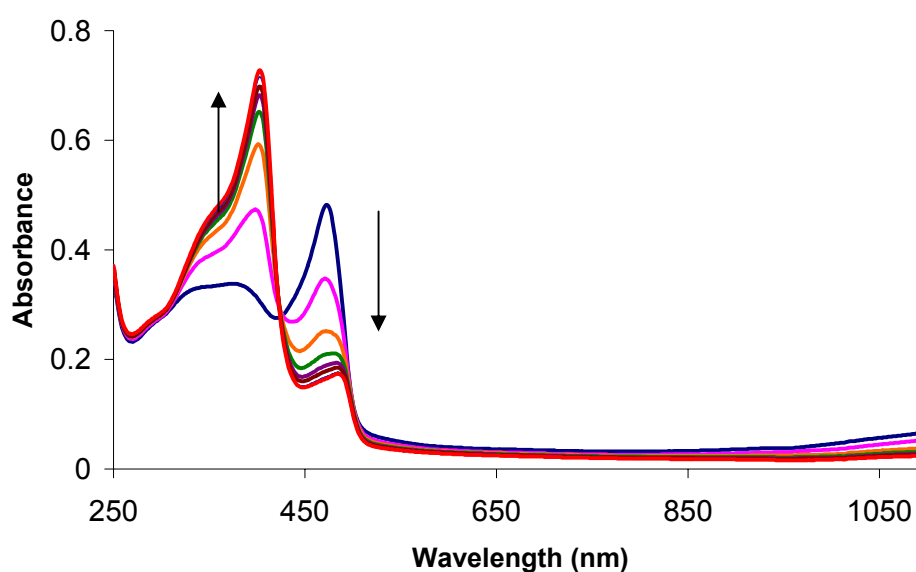


Figure 5.10 UV-visible spectral changes for aqueous PMAS in 0.2 M phosphate buffer (pH 7.0) during reduction with 0.01 M N_2H_4 .

(b) $[\text{Hydrazine}] = 0.10 \text{ M}$

An analogous reduction of aqueous PMAS emeraldine salt at pH 7.0 using 0.10 M hydrazine reduction was much faster. Within 1 min the initial PMAS peak at 475 nm had disappeared and a strong sharp peak appeared at 408 nm (with a shoulder at *ca.* 355 nm), as shown in Figure 5.11a. The rate of reduction of PMAS is therefore strongly dependent on the concentration of hydrazine employed.

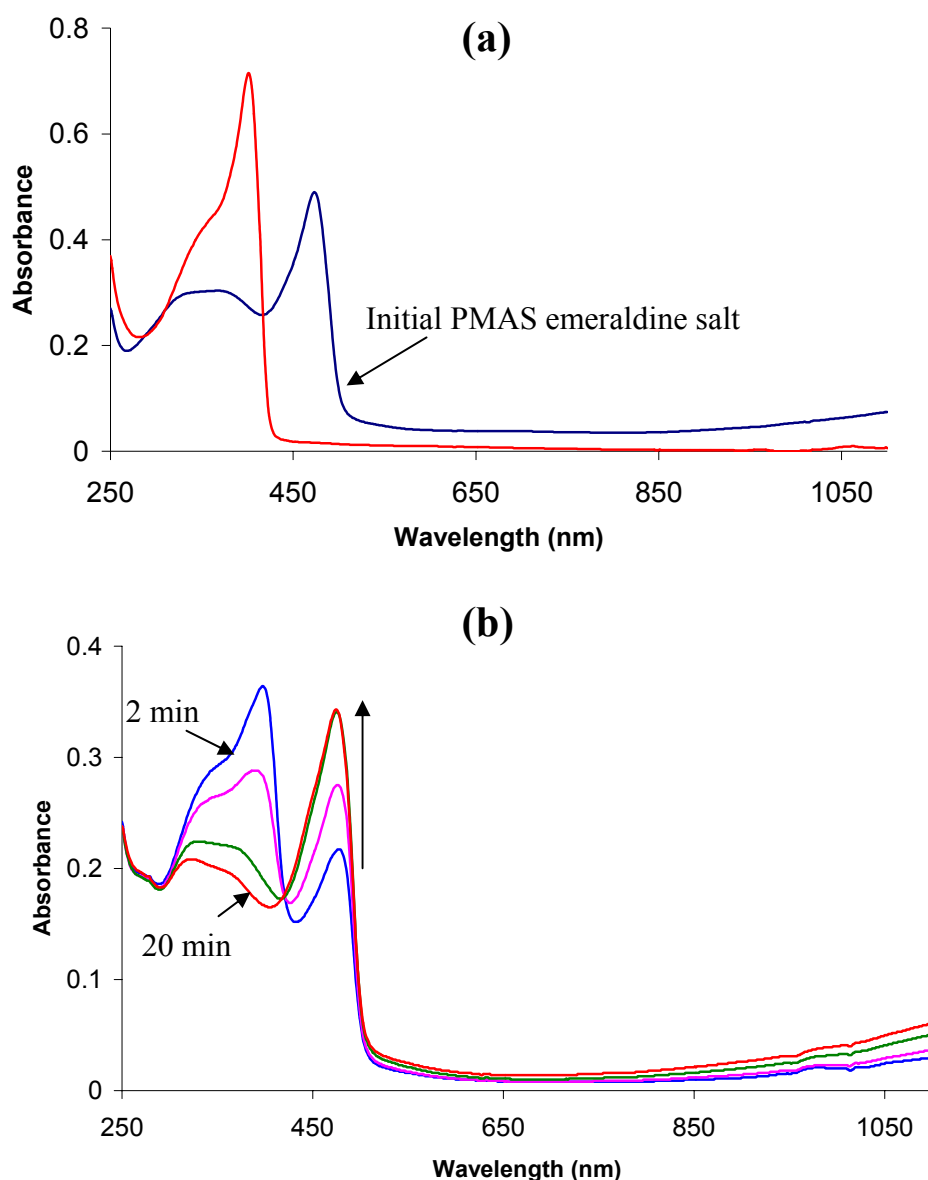


Figure 5.11 UV-visible spectral changes for aqueous PMAS in 0.2 M phosphate buffer (pH 7.0) when: (a) reduced with 0.1 M N₂H₄; (b) after subsequent addition of conc. HCl to pH 1-2.

(iii) Re-oxidation

When the pH of this reduced PMAS solution was raised to 1-2 by the dropwise addition of conc. HCl, re-oxidation of the polymer occurred over 20 min, as shown by the disappearance of the 408 nm peak and the reappearance of the peak at 475 nm characteristic of PMAS emeraldine salt (Figure 5.11b). The same isosbestic points were observed in this re-oxidation process as were seen in Figure 5.8 for the prior reduction of PMAS. The re-oxidation is presumably caused by dissolved oxygen in the solution. Acid is necessary for this re-oxidation, as it converts hydrazine to its acid salt which is no longer a reducing agent.

5.3.2.3 Thermochromism of the Reduced PMAS Species

The reduced PMAS species with $\lambda_{\max} = 408$ nm was stable for hours at room temperature, with no significant change in its UV-visible spectrum observed. However, when heated at 40°C, its spectrum changed markedly as shown in Figure 5.12. Within 1 min, the intensity of the 408 nm peak decreased markedly and the shoulder peak at ca. 330 nm underwent a small blue shift. The 408 nm peak continued to decrease in intensity with further heating at 40°C until stabilizing after 30 min. The dominant peak in the spectrum now appeared at ca. 335 nm. This latter peak is characteristic of the leucoemeraldine base species generally obtained from the reduction of polyanilines. Elevated temperatures thus convert the λ_{\max} 408 nm species to the previously known leucoemeraldine base form of PMAS. This conversion is incomplete at 40°C. A sharp isosbestic point was observed at 355 nm indicating a clean process. The changes were slowly reversed by cooling to 0°C, confirming a temperature dependent equilibrium.

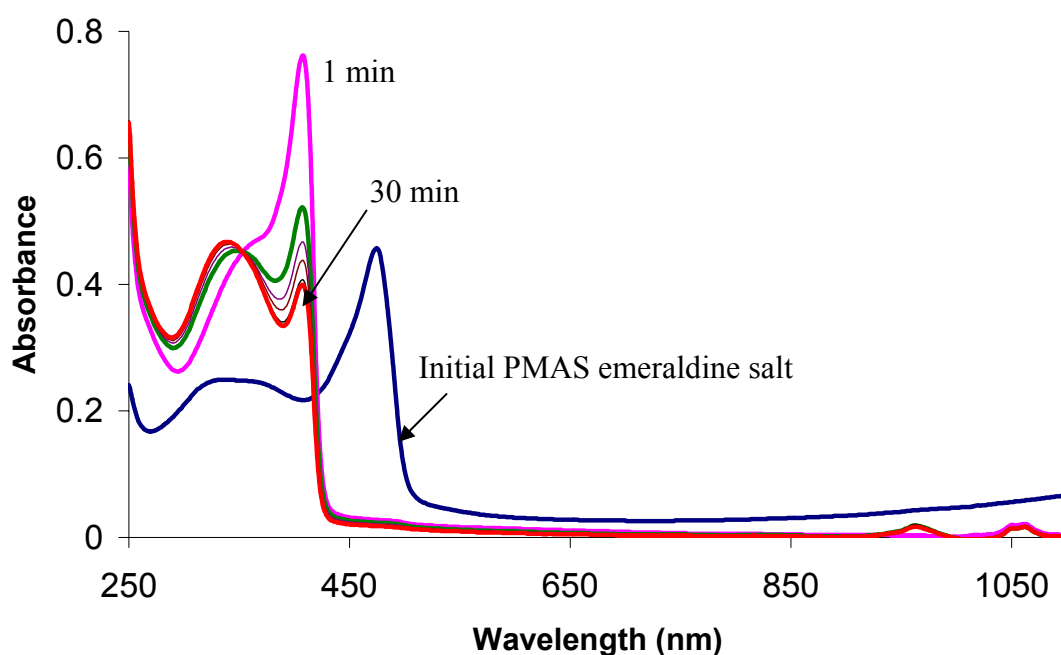


Figure 5.12 UV-vis spectra of initial and reduced aqueous PMAS with 0.4 M N_2H_4 (pH 10) at room temperature and after being held at 40°C for 1, 5, 10, 20 and 30 min.

The thermal interconversion proceeded almost to completion when PMAS was reduced at 50°C, as shown by the almost complete disappearance of the 408 nm peak after 3 hrs (Figure 5.13). This confirms the strong influence of temperature on the position of the equilibrium between the two reduced PMAS species.

As far as we are aware, this reversible thermochromic behaviour of aqueous PMAS is the first such example for a reduced polyaniline species, although reversible thermochromic behaviour has been reported for poly(alkylthiophene)s.²³⁻²⁶ In the latter polythiophene systems, the polymer chains are believed to rearrange upon heating from an original highly ordered form to a less ordered arrangement.

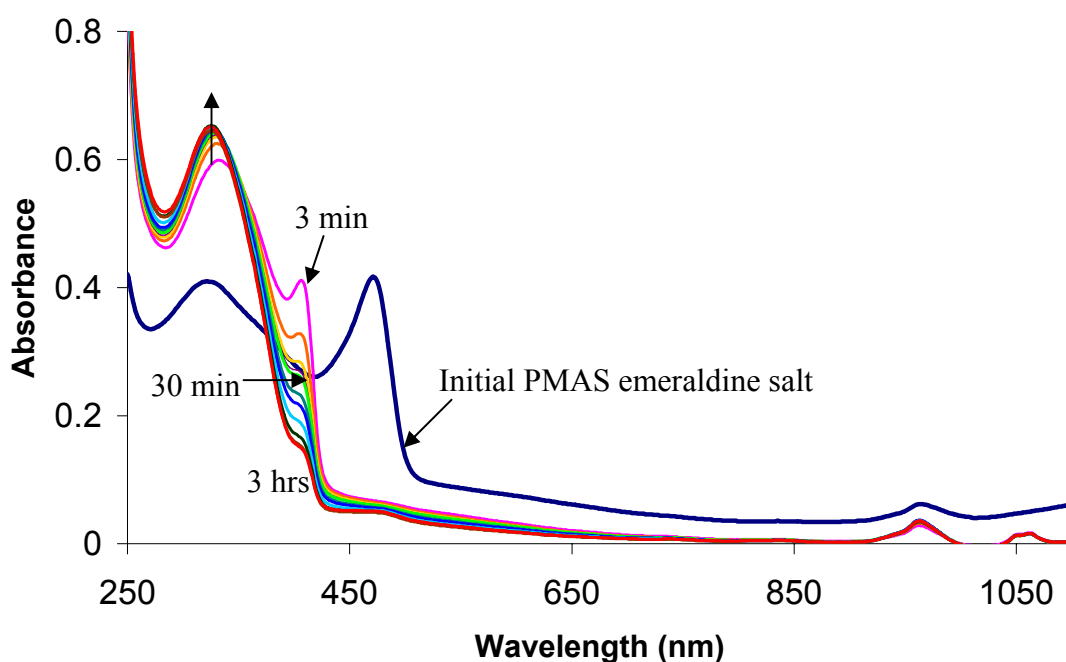


Figure 5.13 UV-visible spectra of initial aqueous PMAS and after reduction with 0.4 M N_2H_4 (pH 10) at 50°C.

It seems likely that the thermochromism seen above for the reduced form of PMAS similarly involves a rearrangement of the PMAS polymer chains, possibly between two conformers (without change in oxidation state). In order to further explore this possibility, the effect of solvent on the UV-visible spectrum of reduced PMAS was then explored.

5.3.2.4 Solvatochromism of the Reduced PMAS Species

The UV-visible spectrum of the reduced PMAS species was found to be very sensitive to changes in solvent. Figures 5.14, 5.15 and 5.16 show the effects of adding the solvents methanol, NMP and acetone, respectively, to an aqueous solution of PMAS that had been reduced in 0.1 M hydrazine at room temperature.

In each case, addition of the organic solvent caused similar spectroscopic changes to those observed in Section 5.3.2.3 by increasing the temperature. The λ_{\max} 408 nm peak

found in aqueous solution was shifted progressively to 335 nm as increasing amounts of the organic solvent were added. Complete conversion to the λ_{\max} 335 nm reduced species was achieved by the addition of 50% methanol (Figure 5.14), with a clean isosbestic point observed at 365 nm for solutions containing between 5% and 50% methanol. Only 10% of added NMP was required to achieve the same interconversion (Figure 5.15), while with acetone complete conversion to the λ_{\max} 335 nm species occurred with 20% added organic component (Figure 5.16a).

This solvatochromism exhibited by reduced aqueous PMAS in the presence of added organic solvents is not due to a redox process, since methanol, NMP and acetone do not cause redox switching in polyanilines. They are consistent with a conformational change in the PMAS polymer chains. Similar solvatochromism has been reported for poly(alkylthiophenes).^{23, 24, 26}

It was noted that reduced PMAS in water/acetone solutions slowly re-oxidized to emeraldine salt during standing at ambient condition, as evidenced by the appearance of the characteristic peak of emeraldine salt at 475 nm. Complete conversion to the λ_{\max} 475 nm species was observed in 1 hr (Figure 5.16b). In contrast, no significant spectral changes were observed for the reduced PMAS species in water/MeOH and water/NMP solutions after standing in air for 3 hrs. The aerial re-oxidation in water/acetone may be attributed to the conversion of the hydrazine to the corresponding hydrazone by reaction with acetone, as supported by the decrease in pH to 6.

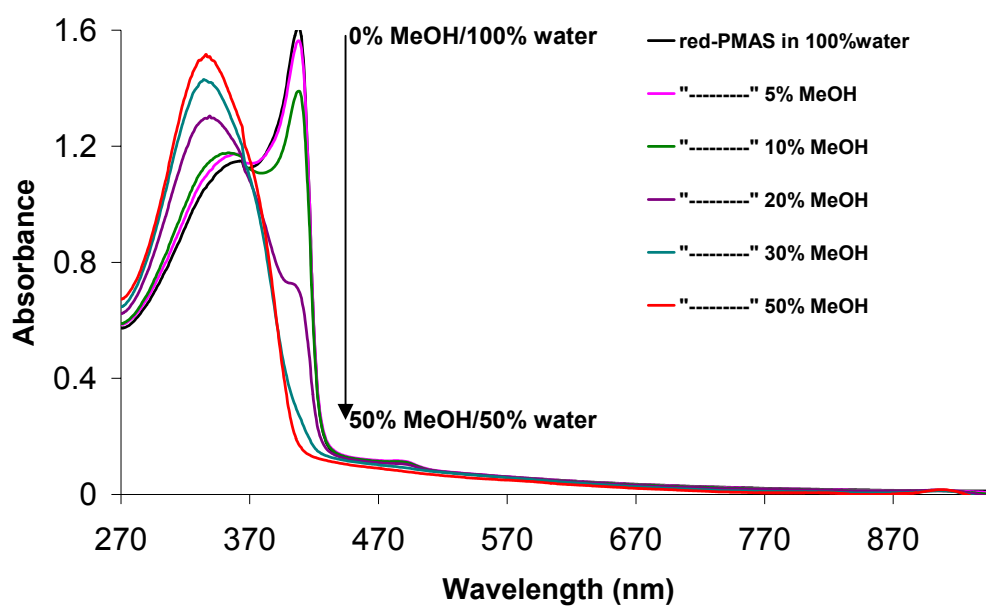


Figure 5.14 UV-visible spectra of aqueous PMAS upon reduction with 0.1 M hydrazine at room temperature, and after the subsequent addition of methanol (pH 9.5-10).

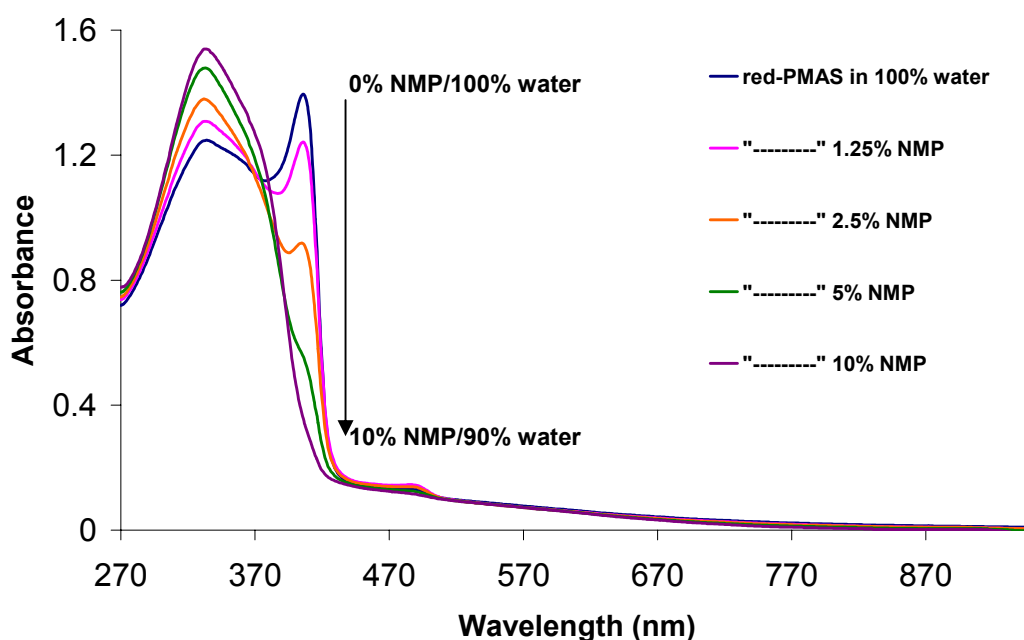


Figure 5.15 UV-visible spectra of aqueous PMAS upon reduction with 0.1 M hydrazine at room temperature, and after the subsequent addition of NMP (pH 9.5-10).

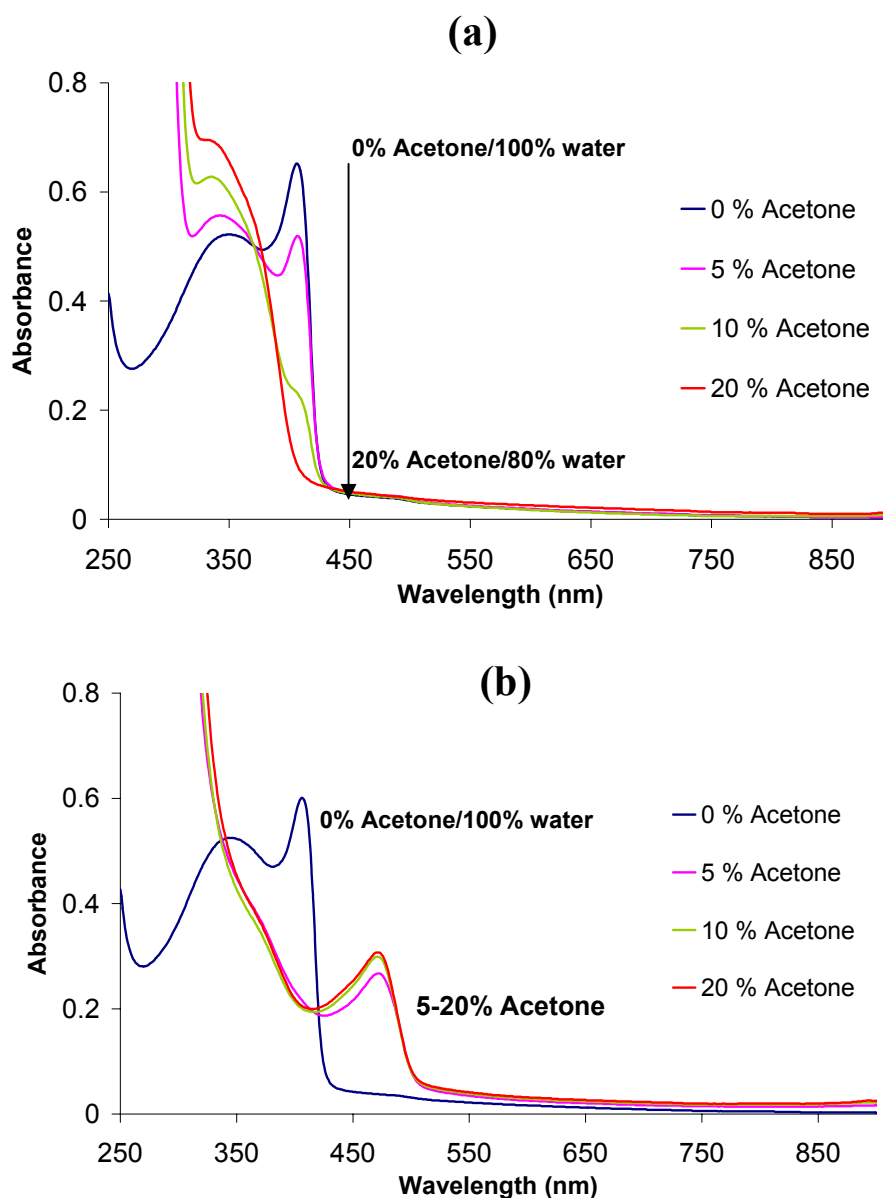


Figure 5.16 UV-visible spectra of aqueous PMAS reduced with 0.1 M hydrazine at room temperature and mixed with acetone: (a) measured immediately after mixing (pH 9.5-10), (b) after standing for 1 hr (pH changed to 6).

5.3.2.5 Reduction of “Compact Coil” PMAS Emeraldine Salt with Hydrazine

To further investigate the influence of polymer chain conformation on the reduction of PMAS, the initial emeraldine salt was converted from its usual “extended coil” conformation to a “compact coil” arrangement by treatment with aqueous 0.1 M NaOH prior to reduction. As previously reported in Section 5.3.1, this “compact coil”

conformation of PMAS emeraldine salt exhibited λ_{max} at 390 and 750 nm (Figure 5.17). Upon reduction with 0.4 M hydrazine at 20°C, the intensity of the initial band at 750 nm decreased and disappeared in ≤ 45 min, while the initial peak at 390 nm shifted to 408 nm.

The reduction product is thus the same as that obtained above (Section 5.3.2.2) when “extended coil” PMAS emeraldine salt was similarly reduced. Clean isosbestic points were observed at 320, 424 and 1050 nm throughout the reduction. However, the reduction is surprisingly slow compared to the analogous reduction of “extended coil” PMAS, which is complete in less than 1 min in 0.4 M hydrazine. The reason for the difference in rate is uncertain, but may be associated with the high pH for the reduction in 0.1 M NaOH.

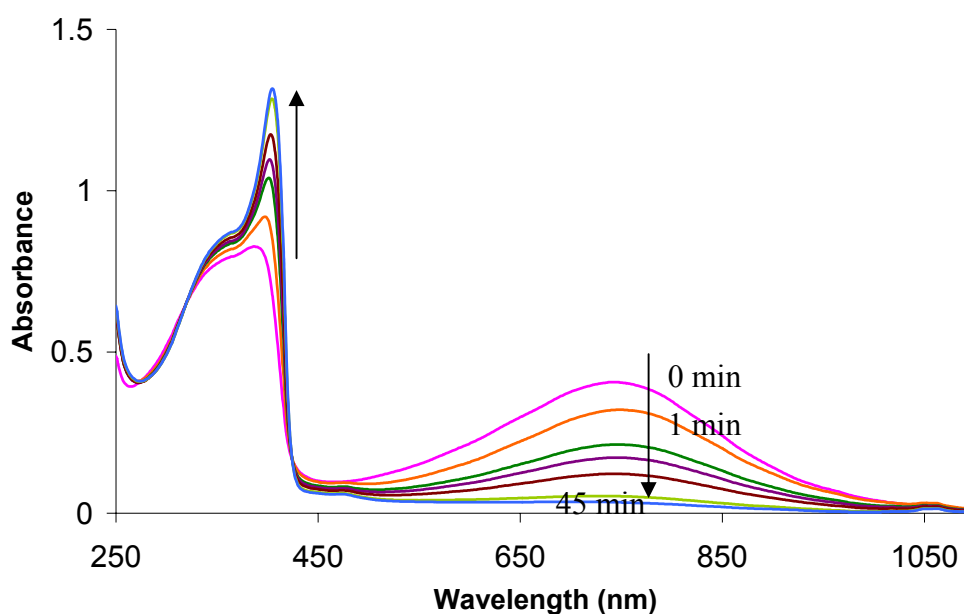


Figure 5.17 UV-vis spectral changes for reduction of “compact coil” aqueous 0.06 mM PMAS (in 0.1 M NaOH) with 0.4 M N_2H_4 at 20°C.

The strong, sharp peak at 408 nm for the reduced PMAS again rapidly decreased when the solution was heated to 45°C (Figure 5.18a), giving a mixture in which the species

with λ_{max} 340 nm dominated. These spectral changes were rapidly reversed when the solution was subsequently cooled to room temperature (Figure 5.18b), again confirming marked thermochromism for reduced PMAS.

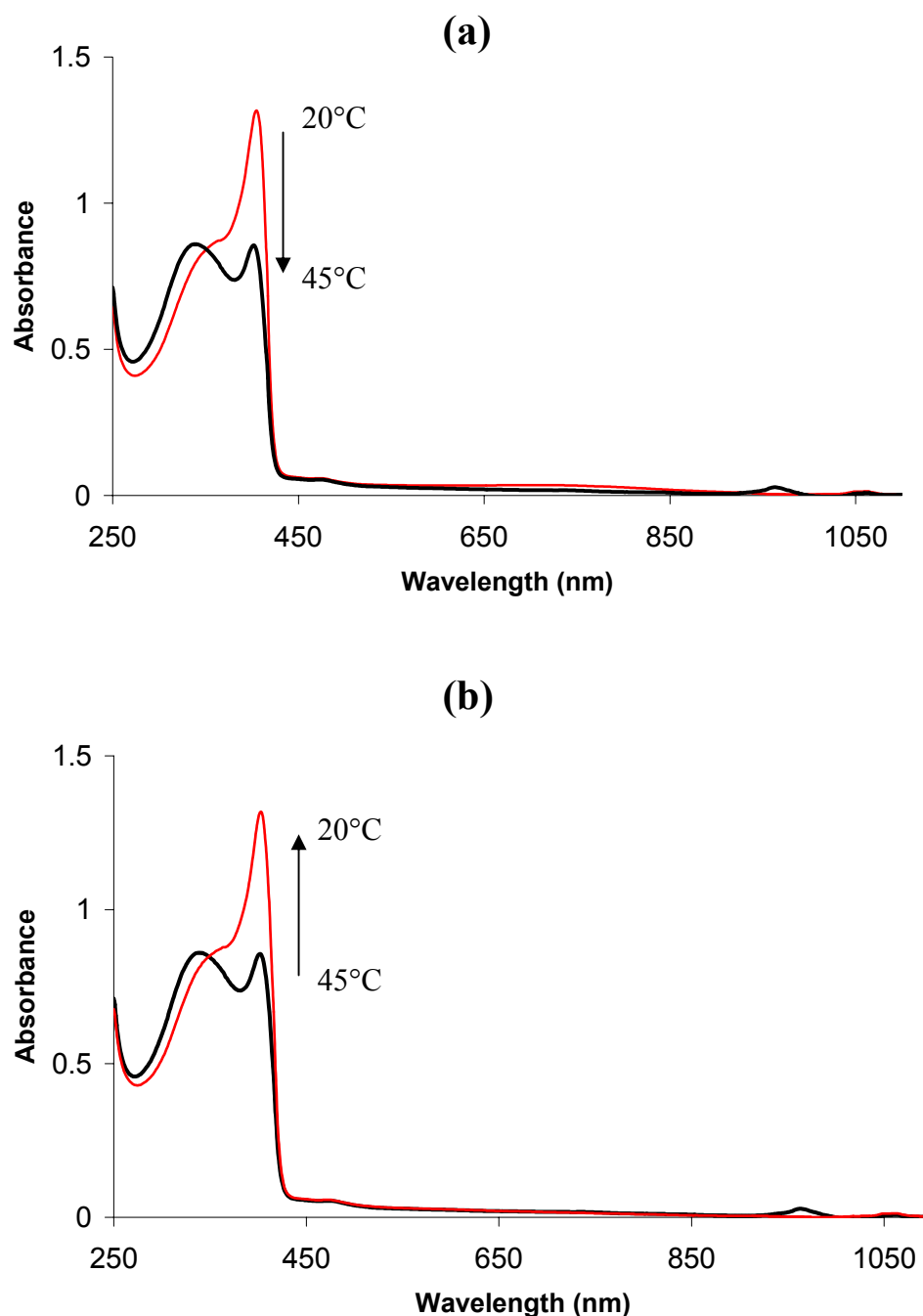


Figure 5.18 UV-visible spectra of (a) aqueous 0.06 mM PMAS reduced in 0.1 M NaOH with 0.4 M N_2H_4 at 20°C for 45 min and then kept at 45°C; (b) after subsequent cooling to room temperature.

5.3.2.6 Reduction of Aqueous Emeraldine Base

In contrast to the reduction of PMAS emeraldine salt in NaOH, the sharp product peak at 408 nm was not observed when the emeraldine base form of PMAS (produced from 0.03 mM PMAS in 0.1 M Bu₄NOH) was reduced with 0.4 M hydrazine at room temperature (Figure 5.19). The characteristic exciton band of the emeraldine base at 620 nm gradually decreased upon reduction, disappearing completely after 90 min, while a band grew at *ca.* 340 nm assigned to a π - π^* transition band of leucoemeraldine base. Clean isosbestic points were observed at 260, 322, 410 and 890 nm.

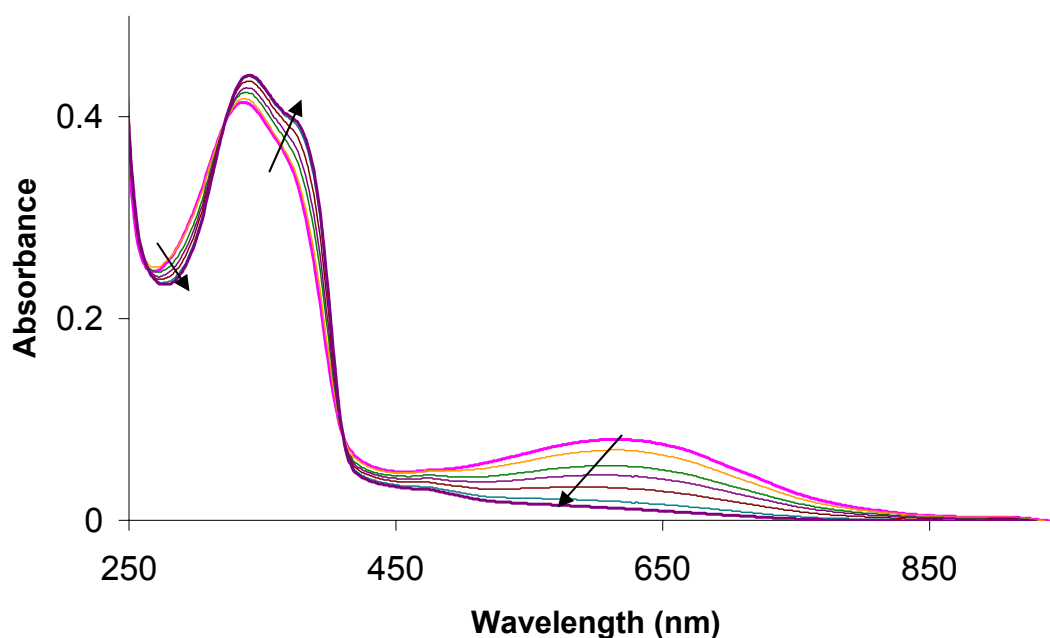


Figure 5.19 UV-visible spectra during the reduction of 0.03 mM PMAS in aqueous 0.1 M Bu₄NOH with 0.4 M N₂H₄ at room temperature.

5.4 Conclusions

Unlike parent polyaniline, PMAS is remarkably resistant to de-doping with aqueous NaOH and NH₄OH, even in 3.0 M NaOH (pH 14) or conc. NH₄OH (28% NH₃). During the titration of aqueous PMAS with NH₄OH, two stages of UV-visible spectral changes are observed. The first stage (pH 5.8-7.7) is attributed to a conformational change

associated with deprotonation of “free” SO₃H groups on the PMAS chains. The second stage (pH 8-10.5) is believed to involve rearrangement of the polymer from an “extended coil” to a “compact coil” conformation.

However, titration of aqueous PMAS with the sterically crowded amines Bu₄NOH and di-isopropylamine shows a third stage in the spectral changes at high pH (11.5-13). This stage is attributed to de-doping of the “compact coil” PMAS emeraldine salt to the emeraldine base form, supported by the appearance of the characteristic “exciton” band for the emeraldine base at 630 nm. The resistance of PMAS emeraldine salt to de-doping in NaOH and NH₄OH may therefore be associated with electrostatic binding of the relatively small Na⁺ and NH₄⁺ ions to free sulfonate groups on the PMAS chains, which is sterically hindered in the case of the bulky Bu₄N⁺ and Pr₂NH₂⁺ ions.

The redox switching properties of purified PMAS (without oligomer) are found to be very similar to those previously observed for a PMAS/oligomer mixture. UV-visible spectral changes during oxidation with S₂O₈²⁻ are very similar in both cases, and also similar to that previously reported for unsubstituted polyaniline. The pernigraniline base form of PMAS is generated at pH 4.5-5. Very fast decomposition occurs for the corresponding PMAS pernigraniline salt generated at pH 1-2.

In contrast to other polyanilines, the room temperature reduction of PMAS (both pure and as a PMAS/oligomer mixture) gives a dominant 408 nm species together with the usual 330 nm peak found for the reduced leucoemeraldine base form of parent polyaniline. Aerial re-oxidation of the reduced PMAS occurs in acidic solution.

Although the chemistry of the species with λ_{max} 408 nm is still not clear, thermochromism and solvatochromism of this reduced PMAS species are observed. The

intensity of the peak at 408 nm rapidly decreases and the shoulder peak at 330 nm undergoes a small blue shift when the reduced PMAS is heated at 40°-50°C. Elevated temperatures thus convert the species with λ_{max} 408 nm to the normal leucoemeraldine base form of PMAS. This process is reversible. Addition of organic solvents such as methanol and acetone causes similar spectroscopic changes to those observed by increasing the temperature. These phenomena maybe involve a rearrangement of the PMAS chains, possibly between two conformations.

5.5 References

1. G.G. Wallace, G.M. Spinks, A.L.P. Kane-Maguire, and P.R. Teasdale, *Conductive Electroactive Polymers*. 2 nd ed. (2003) USA: CRC Press.
2. Y. Wei, W.W. Focke, G.E. Wnek, A. Ray, and A.G. MacDiarmid, *J. Phys. Chem.* **93** (1989): 495.
3. F.A. Viva, E.M. Andrade, F.V. Molina, and M.I. Florit, *J. Electroanal. Chem.* **471** (1999): 180.
4. L.H.C. Mattoso and L.O.S. Bulhoes, *Synth. Met.* **52** (1992): 171.
5. W.A. Gazotti, R. Faez, and M.A. Paoli, *J. Electroanal. Chem.* **415** (1996): 107.
6. J. Widera, B. Patys, J. Bukwska, and K. Jackowska, *Synth. Met.* **94** (1998): 265.
7. X.L. Wei, M. Fahlman, and A.J. Epstein, *Macromolecules.* **32** (1999): 3114.
8. J. Yue and A. Epstein, *J. Am. Chem. Soc.* **112** (1990): 2800.
9. X.-L. Wei, Y.Z. Wang, S.M. Long, C. Bobeczko, and A. Epstein, *J. Am. Chem. Soc.* **118** (1996): 2545.
10. S.-A. Chen and G.-W. Hwang, *Macromolecules.* **29** (1996): 3950.
11. J. Yue, Z.H. Wang, K.R. Cromack, A. Epstein, and A.G. MacDiarmid, *J. Am. Chem. Soc.* **113** (1991): 2665.
12. S. Shimizu, T. Saitoh, M. Uzawa, M. Yuasa, K. Yano, T. Maruyama, and K. Watanabe, *Synth. Met.* **85** (1997): 1337.
13. E.V. Strounina, L.A.P. Kane-Maguire, and G.G. Wallace, *Synth. Met.* **106** (1999): 129.
14. R. Guo, J.N. Barisci, P.C. Innis, C.O. Too, G.G. Wallace, and D. Zhou, *Synth. Met.* **114** (2000): 267.
15. E.V. Strounina, R. Shepherd, L.A.P. Kane-Maguire, and G.G. Wallace, *Synth. Met.* **135-136** (2003): 289.
16. T. Yamamoto, A. Ushiro, I. Yamaguchi, and S. Sasaki, *Macromolecules.* **36** (2003): 7075.
17. E.V. Strounina, PhD thesis, *Synthesis and Characterisation of Chiral Substituted Polyanilines*, Chemistry Department. 2001, Univeristy of Wollongong.
18. A.G. MacDiarmid and A.J. Epstein, *Synth. Met.* **69** (1995): 85.
19. Y. Xia, J.M. Wiesinger, and A.G. MacDiarmid, *Chem. Mater.* **7** (1995): 443.
20. F. Masdarolomoor, P.C. Innis, S.A. Ashraf, and G.G. Walace. *Purification and Characterization of Poly(2-methoxy aniline-5-sulfonic acid)*, ICSM 2004. Wollongong, Australia.
21. Z.T. Oliveira and M.C. Santos, *Chem. Phys.* **260** (2000): 95.
22. A.L.P. Kane-Maguire, F. Masdarolomoor, and P.C. Innis.(unpublished results)
23. B.M.W. Langeveld-Voss, E. Peters, R.A.J. Janssen, and E.W. Meijer, *Synth. Met.* **84** (1997): 611.
24. B.M.W. Langeveld-Voss, R.A.J. Janssen, and E.W. Meijer, *J. Mol. Struc.* **521** (2000): 285.
25. B.M.W. Langeveld-Voss, M.P.T. Christiaans, R.A.J. Janssen, and E.W. Meijer, *Macromolecules.* **31** (1998): 6702.
26. B.M.W. Langeveld-Voss, R.J.M. Waterval, R.A.J. Janssen, and E.W. Meijer, *Macromolecules.* **32** (1999): 227.

Chapter 6

Preparation and Characterization a Chiral Complex of Fully Sulfonated Polyaniline with Poly-L-Lysine

6.1 Introduction

Poly-L-lysine (PLL) is a chiral synthetic polypeptide. Because of the amine group on the aliphatic side chain of the lysine residues, protonation of poly-L-lysine generates a poly-cationic electrolyte. It can therefore interact with anionic species (e.g. dodecylsulfate) to form water-insoluble polyelectrolyte surfactant complexes¹ via electrostatic interaction. It has been reported that poly-L-lysine adopts a helical or beta-sheet conformation in solution and the solid state depending on the conditions.^{1, 2} Synthetic polypeptides such as poly-L-valine, poly-L-leucine and poly-L-lysine have been used for a wide variety of applications, for instance, as chiral modified electrodes for asymmetric electrosynthesis³⁻⁶ and as biosensors.⁷

Poly(2-methoxyaniline-5-sulfonic acid) (PMAS) is a fully sulfonated, water soluble and self-doped polyaniline. Since it contains anionic SO_3^- groups along its polymer chains, the anionic polyelectrolyte property of the polymer has attracted attention. Optically active poly(2-methoxyaniline-5-sulfonic acid) emeraldine salts (PMAS) have been recently synthesized by the electrochemical polymerization of 2-methoxyaniline-5-sulfonic acid (MAS) in the presence of one handed chiral amines such as (+)- or (-)-1-phenylethylamine (PhEA).⁸ Chiral induction in pre-formed PMAS through acid-base interaction with chiral amines (RNH_2) has also been reported by Strounina.⁹ For some applications, cross-linking with poly(4-vinylpyridine) (PVP) was also carried out to

prepare water-insoluble immobilized films. However, this significantly reduced the optical activity of the immobilized chiral PMAS(PVP⁺) films, presumably due to partial racemization during the replacement of the chiral RNH₃⁺ cations by protonated PVP.

A water-insoluble complex of PMAS with a cationic poly(4-vinylpyridine) (PVP) has been prepared and characterized by Tallman and Wallace.¹⁰ A conductive and electroactive PMAS/PVP polymer complex was obtained.

The work presented in the present chapter was carried out to determine whether similar electrostatic interactions between pre-formed PMAS and the chiral cationic polyelectrolyte poly-L-lysine (PLL) would induce optical activity in the PMAS chains. If successful, this would provide a facile route to the self-doped, optically active, conductive and electroactive polyaniline, PMAS-PLL.

The optical activity of PMAS-PLL films prepared using various ratios of PMAS and PLL starting materials was investigated. The electroactivity and redox switching properties of the PMAS-PLL complexes formed were also studied, using cyclic voltammetry and *in situ* spectroelectrochemistry. In addition, the chiral stability of the PMAS-PLL films during acid-base and oxidation-reduction treatments was also explored.

6.2 Experimental

6.2.1 Materials

Pure poly(2-methoxyaniline-5-sulfonic acid) PMAS, was kindly provided by Fatemeh Masdarolomoor (IPRI).¹¹ Poly-L-lysine hydrochloride (MW 30,000-70,000) was purchased from Sigma-Aldrich. Ordinary glass slides and ITO-coated glass slides were

cleaned with washing detergent, isopropanol and then treated under UV light for 15 min prior to use in order to generate a hydrophilic surface. All solutions were prepared in Milli-Q water.

6.2.2 PMAS-PLL Complex Formation

An aqueous solution of 0.25 % (w/v) (6 mM PMAS assuming a dimer repeat unit) was prepared by dissolving 0.0625 g of PMAS in 25 mL water and filtering through a 0.45 μm filter. This was then mixed with an aqueous solution of the protonated form (hydrochloride) of 0.03 M PLL (as monomer, prepared by dissolving of 0.0055 g of PLL in 1 mL water and stirring for 15 min). In an electrostatically stoichiometric complex between PMAS and PLL, one PMAS dimer repeat unit should be reacted with one monomer unit of PLL. Thus, a 1:1 molar ratio of PMAS : PLL is *ca.* 2.5 : 1 by weight. However, various mole ratios of PMAS and PLL were examined, as summarized in Table 6.1 below.

Table 6.1 Mole ratios used for mixing PLL and PMAS.

Mole Ratio of PMAS (as dimer) / PLL (as monomer)	Mixing of 0.006M PMAS (μL) + 0.03M PLL (μL)	
1	1000	200
2	1000	100
4	2000	100

The mixed solutions were magnetically stirred at room temperature for 10 min.

To prepare PMAS-PLL films, 80 μL of the above solutions were drop cast onto 2 cm^2 glass slides or ITO-coated glass. Dried films of PMAS-PLL were obtained after standing at room temperature for 3 hrs.

6.2.3 UV-visible and CD Spectra of PMAS-PLL Films and Solutions

PMAS-PLL solutions diluted 40-fold were prepared by mixing 50 μL of PMAS-PLL solution with 1950 μL of water. UV-visible spectra of these dilute solutions were measured between 190 and 1100 nm using a Shimadzu UV-1601 spectrophotometer. CD spectra were recorded with a Jobin-Yvon Dichrograph 6 in the range of 300-800 nm. PMAS-PLL films on glass slides had their UV-visible and CD spectra similarly recorded in the ranges 300-1100 and 330-800 nm, respectively.

6.2.4 Chemical Treatments

Acid-base Treatment

An evaporatively cast PMAS-PLL film was de-doped by immersing in 1.0 M NaOH or 1.0 M NH_4OH for 30 min and subsequently re-doped by soaking in 1.0 M HCl for 30 min. UV-visible and CD spectra were recorded before and after these base/acid treatments.

Reduction / Oxidation

Reduction: A PMAS-PLL cast film was reduced via 30 min reaction with aqueous 0.2 M N_2H_4 (pH 10.2). After removal and drying its UV-visible and CD spectrum were recorded.

Oxidation: A PMAS-PLL cast film was oxidized in a 1 cm quartz cell containing 0.2 M $(\text{NH}_4)_2\text{S}_2\text{O}_8$ (pH 3.3), and its UV-visible spectrum monitored with time. The UV-visible and CD spectra of the film were also recorded in air after the film was removed from the oxidizing solution.

6.2.5 Electroactivity of PMAS-PLL Films

Cyclic voltammetry of PMAS-PLL films on ITO-coated glass electrodes was carried out in aqueous 0.1 M HCl or 0.3 M NaNO_3 with a scan rate of 50 mV/s. Pt mesh and $\text{Ag}/\text{AgCl}_{(3\text{M NaCl})}$ were used as auxiliary and reference electrodes, respectively. The

cyclic voltammogram of 0.3 mM PMAS in aqueous 0.1 M HCl was performed for comparison.

6.2.6 *In-situ* UV-visible Spectroelectrochemical Studies of PMAS-PLL Films

Spectroelectrochemical experiments were performed in a 1 cm path length quartz cell containing aqueous 0.1 M HCl. A PMAS-PLL film cast on ITO-coated glass was used as the working electrode in an electrochemical cell with three electrodes, as shown in Figure 2.3, Chapter 2. After polarization at a particular potential for 1 min, UV-visible spectra were recorded using a MultiSpec-1501 spectrophotometer.

6.2.7 Conductivity of PMAS-PLL Films

The electrical conductivities of PMAS-PLL (1:1) films cast on ordinary glass slides were measured using a Jandel four-point probe head Model RM2 (see Chapter 2). Thickness of the films was measured with a Mutiutoyo Digital micrometer (0.001 mm).

6.3 Results and Discussion

6.3.1 UV-Visible and CD Spectra of PMAS-PLL Complexes

PMAS-PLL complexes were prepared by mixing PMAS with PLL in aqueous solution at room temperature using PMAS (dimer) / PLL (monomer) mole ratios of 1, 2 and 4. The UV-visible spectra of these PMAS-PLL complexes (Figure 6.1a) were similar to that of PMAS itself in aqueous solution (see Chapter 5). The UV-visible spectra were recorded within 15 min of mixing, since a yellow-brown precipitate of the PMAS-PLL complex was observed after standing for 30 min. A broad absorption band around 320-390 nm assigned to π - π^* transitions, and a strong sharp peak at *ca.* 475 nm assigned to a polaron transition, were observed for all PMAS-PLL complexes. This indicates that the PMAS moiety in the complexes is in the conducting emeraldine salt form. The absence

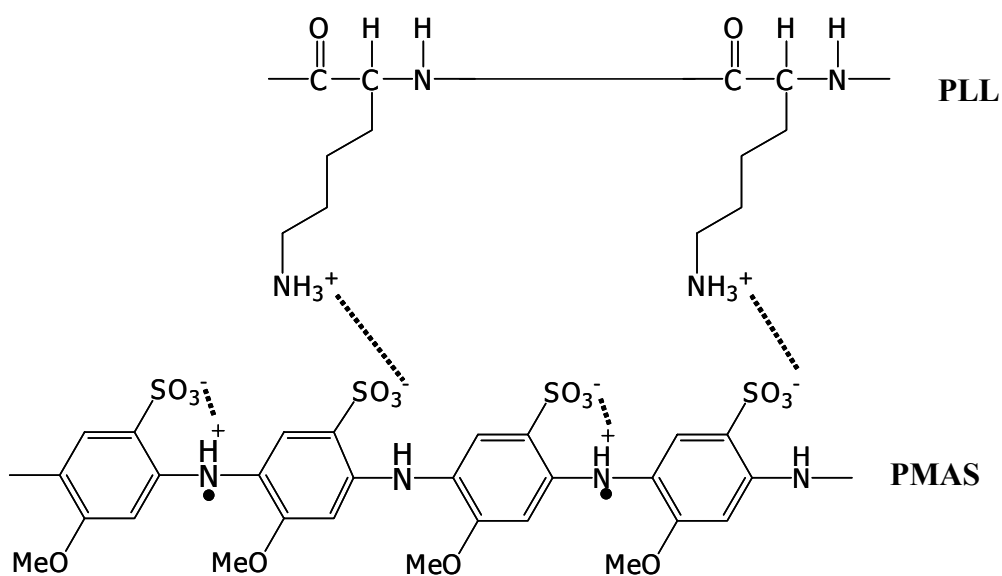
of a polaron band at 800-900 nm, and the presence of a free carrier tail in the near-infrared indicate that the PMAS chains are in an “extended coil” conformation.

Significantly, the corresponding CD spectra (Figure 6.1b) of the PMAS-PLL complexes in aqueous solution showed that the complexes were weakly optically active. In particular, a sharp CD band was observed for all complexes at *ca.* 485 nm, associated with the corresponding absorption band at 475 nm. This is believed to arise from chiral induction in the PMAS polymer chains caused by electrostatic binding with the one-handed helical chains of poly-L-lysine.

The intensity of the CD signals for these PMAS-PLL complexes depended on the PMAS/PLL ratio used in their preparation. The chiral anisotropy factors ($g = \Delta\varepsilon / \varepsilon$) of the complexes calculated for the polaron chromophore at 475 nm in Figures 6.1a and 6.1b are presented in Table 6.2. These indicate that the highest degree of chiral induction is observed when the PMAS/PLL ratio is 1. This is not surprising since the stoichiometric complex is proposed to be formed by electrostatic binding of the ammonium ion on each unit of PLL to free ionized sulfonate groups on each dimer repeat unit of PMAS, as depicted in Scheme 6.1.

Table 6.2 Chiral anisotropy factors ($g = \Delta\varepsilon / \varepsilon$) for PMAS-PLL complexes in aqueous solutions and as films cast onto glass slides.

PMAS/PLL ratio	$\Delta\varepsilon/\varepsilon$ (%)	
	Solution	Film
1:1	0.011	0.011
2:1	0.009	0.010
4:1	0.004	0.006



Scheme 6.1

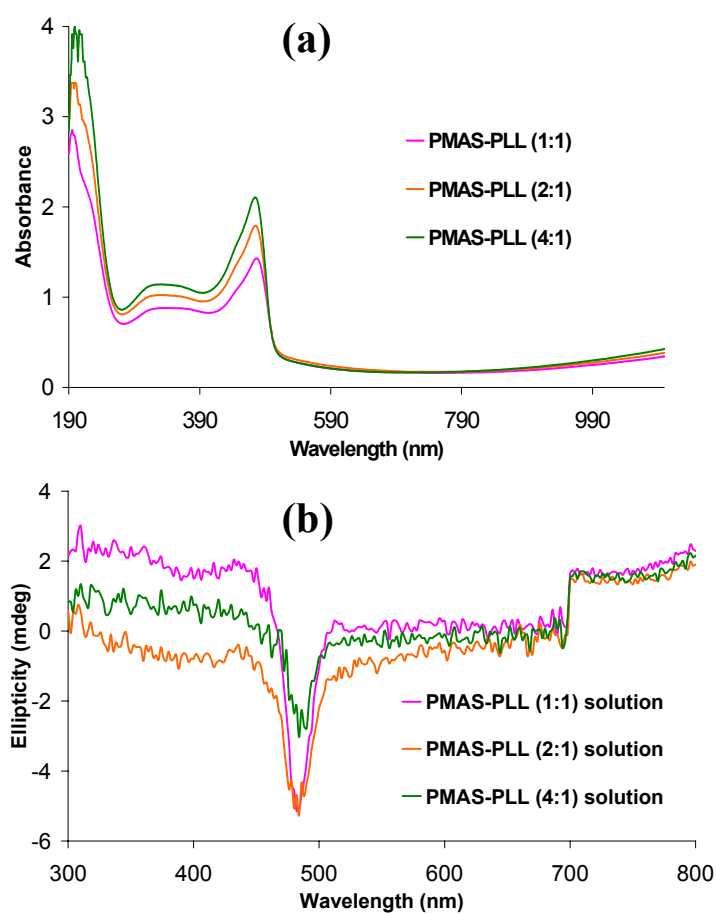


Figure 6.1 (a) UV-visible and (b) CD spectra of PMAS-PLL complexes in water.

Significantly, the CD spectra of the PMAS-PLL complexes were dramatically affected by filtration. For example, the CD signals for the PMAS-PLL (2:1) complex completely disappeared when the solution/dispersion was filtered through a 0.45 μm filter (Figure 6.2b), while its UV-visible spectrum (Figure 6.2a) much less affected. This suggests that aggregates larger than 0.45 μm in size are responsible for the generation of optical activity in these complexes. A similar observation has been recently found by Strounina⁹ for the optically active PMAS.(+)-PhEA polymer (PhEA = 1-phenylethylamine).

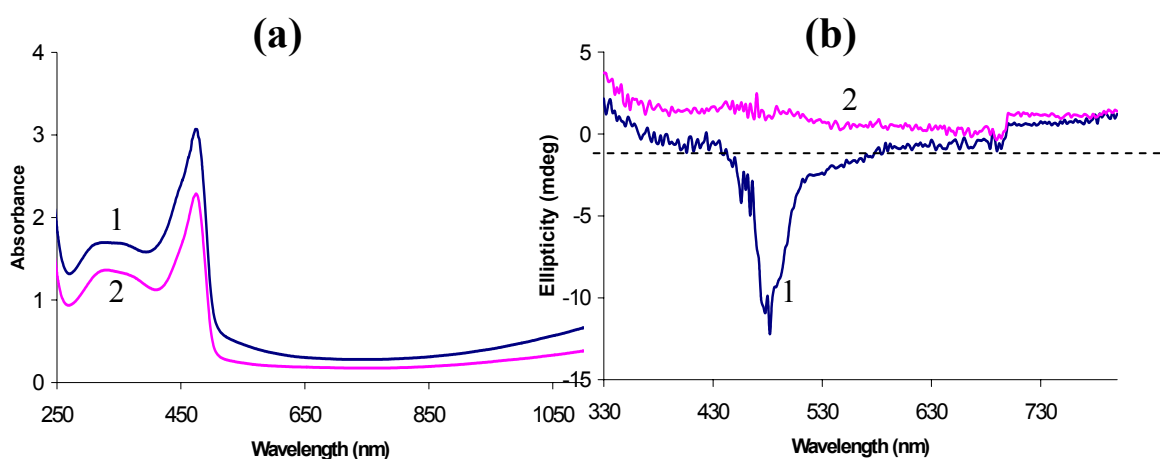


Figure 6.2 (a) UV-vis and (b) CD spectra of a PMAS-PLL (2:1) solution before (1) and after (2) filtering through a 0.45 μm filter.

PMAS-PLL films cast from the above solutions onto glass slides exhibited similar UV-visible (Figure 6.3a) and CD (Figure 6.3b) spectra to those obtained in the solution/dispersion, indicating that evaporation of water to deposit the films did not significantly affect their optical activity. The highest anisotropy factor was again observed (Table 6.2) when the PMAS/PLL ratio was 1.

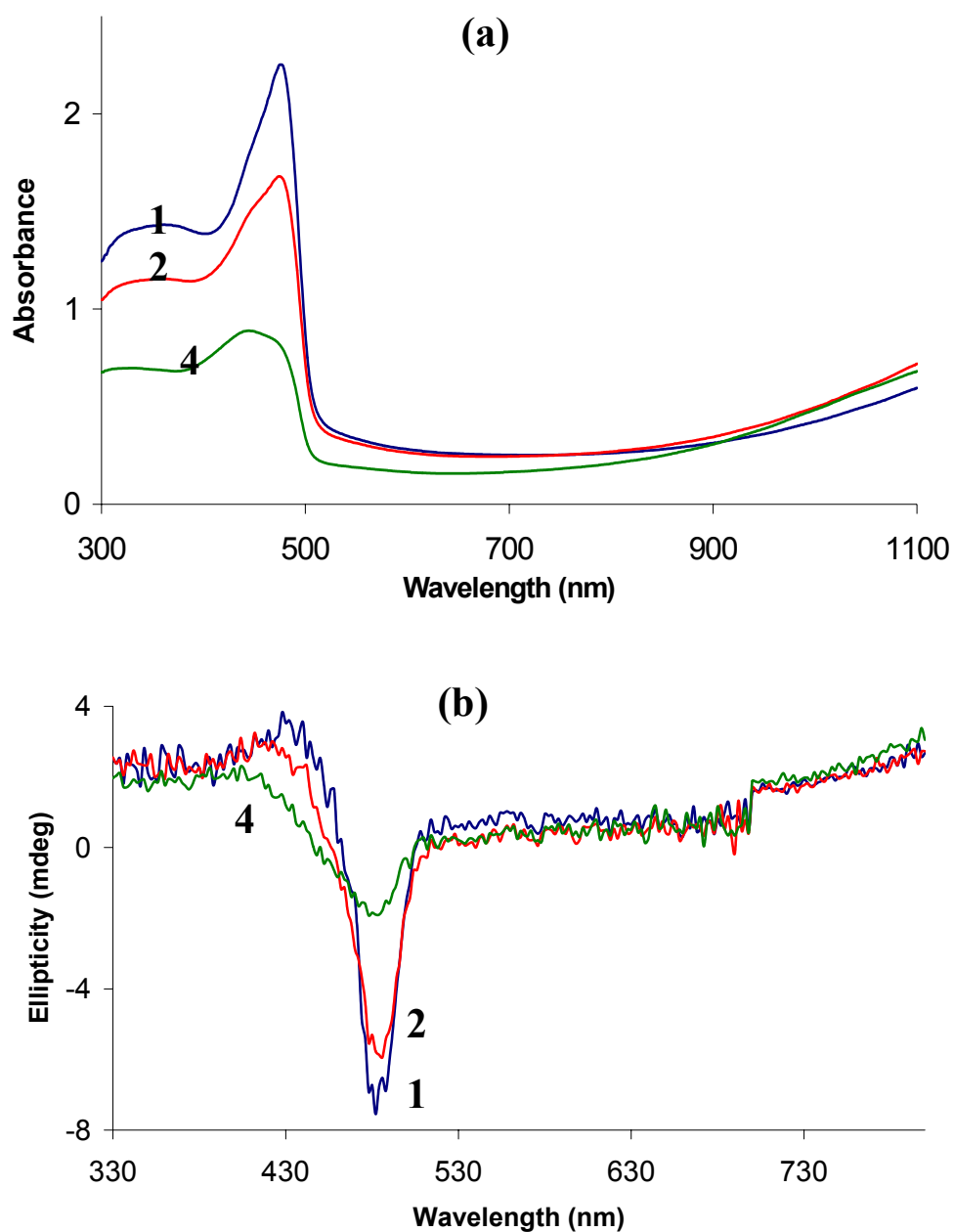


Figure 6.3 (a) UV-visible and (b) CD spectra of PMAS-PLL complex films cast onto glass slides. The mole ratios of PMAS/PLL were 1, 2, and 4, as indicated on the curves.

6.3.2 Electroactivity of PMAS-PLL Films

The electroactivity of the PMAS-PLL complex films evaporatively cast from aqueous solution onto ITO-coated glass electrodes was investigated by cyclic voltammetry. The medium used was either aqueous 0.1 M HCl or 0.3 M NaNO₃.

Cyclic Voltammetry in Aqueous HCl

Figures 6.4a-c show the first five scans of the cyclic voltammograms for the PMAS-PLL complex films with PMAS/PLL ratios of 1, 2 and 4, respectively, carried out in 0.1 M HCl. Two well-defined oxidation waves were observed at +0.27 and +0.83 V when the PMAS/PLL ratio was 1 (Figure 6.4a). In the reverse cathodic sweep, the corresponding reduction processes appeared at peak potentials of +0.45 and -0.04 V. These CV features are similar to those observed for parent polyaniline,¹²⁻¹⁵ sulfonated polyaniline (SPAN)^{16, 17} and poly(2-methoxyaniline).^{13, 18-20} The first redox pair (at $E_{1/2}$ *ca.* 0.11 V) corresponds to the interconversion between leucoemeraldine and emeraldine, while the second redox pair (at $E_{1/2}$ *ca.* 0.64 V) are attributed to the emeraldine ↔ pernigraniline transformation.

The films with PMAS/PLL ratios of 2 and 4 (Figures 6.4b and 6.4c) showed broadly similar but less well defined CVs. Unlike Figure 6.4a, significant changes in their CVs were also observed in subsequent scans. In addition, especially for the PMAS/PLL (4:1) film, an additional oxidation wave grew at *ca.* 0.52 V with a corresponding peak in the reverse cathodic sweep. These new features may be due to dissolution of excess PMAS, which had not bound to PLL, into the aqueous medium upon potential cycling.

In order to explain the three redox peaks observed in Figures 6.4b and especially 6.4c, the CV for PMAS itself dissolved in 0.1 M HCl was recorded at a bare ITO-coated glass electrode. Three anodic peaks were observed at 0.14, 0.50 and 0.70 V, and three corresponding cathodic peaks at 0.055, 0.42 and 0.62 V. It should be noted that the similar presence of a third redox couple between the two main redox peaks of polyaniline,^{21, 22} sulfonated polyaniline (SPAN)¹⁶ and poly(2-methoxyaniline)^{23, 24} has been reported. Interpretations proposed for this “middle peak” include cross-linking

between the polymer chains,^{18, 22, 25, 26} unusual bonding or branching,^{27, 28} or oxidative degradation products.^{14,21} However, in the present case these interpretations seem unlikely because the same batch of PMAS was used for all experiments, yet only two redox pairs were observed for the stoichiometric (1:1) PMAS-PLL film.

A number of CV peaks have also been recently observed by Tallman and Wallace¹⁰ for aqueous PMAS in 0.1 M KCl at a Pt electrode. They attributed each of these peaks to a one electron transfer. Our CV in Figure 6.5 for PMAS itself may confirm that the three redox pairs observed for PMAS-PLL complexes with PMAS/PLL ratios of 2 and 4 (Figure 6.4b and 6.4c) originate from unbound PMAS trapped in the films. The absence of the middle peak for the 1:1 PMAS/PLL film may be due to stabilization by the PLL of the PMAS complex to redox cycling.

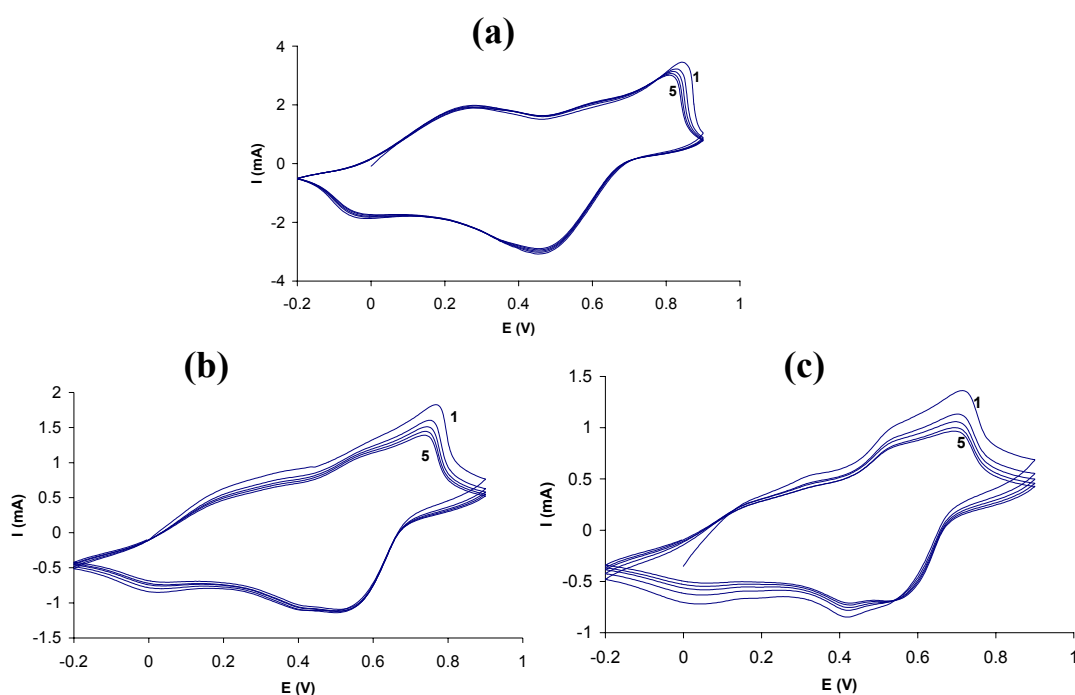


Figure 6.4 Cyclic voltammograms of (a) PMAS-PLL (1:1), (b) PMAS-PLL (2:1), and (c) PMAS-PLL (4:1) films carried out in aqueous 0.1M HCl. Scan rate = 50 mV/s.

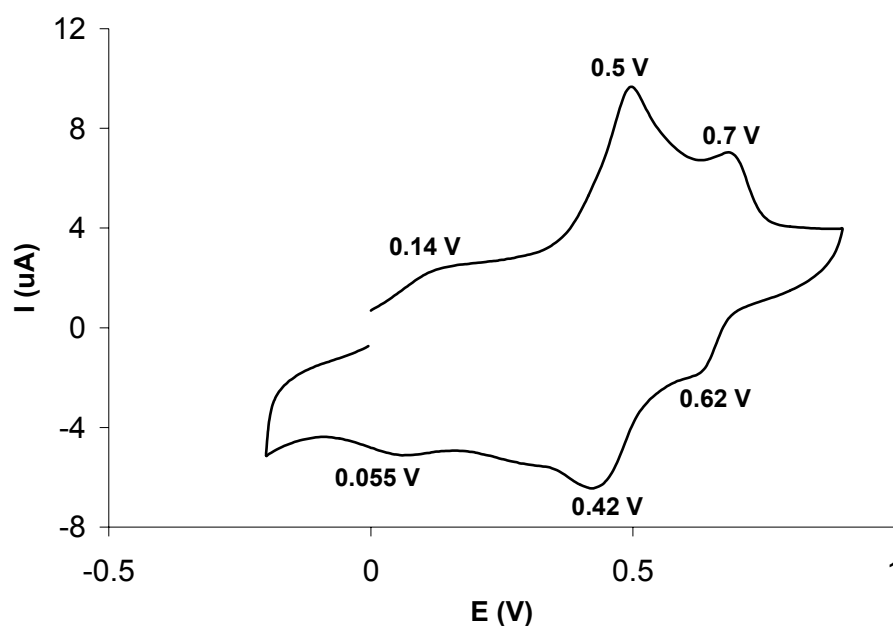


Figure 6.5 Cyclic voltammogram of 0.3 mM PMAS in aqueous 0.1 M HCl at an ITO-coated glass electrode. Scan rate = 50 mV/s.

Cyclic Voltammetry in Aqueous NaNO_3

Since the highest chiral anisotropy factor ($g = \Delta\varepsilon/\varepsilon$) and electrochemical stability were observed for the PMAS-PLL complexes when the PMAS/PLL ratio was 1, this ratio was used in all subsequent experiments.

The cyclic voltammogram of a PMAS-PLL film was recorded in 0.1 M HCl. After washing with water, this film was then potential cycled in aqueous 0.3 M NaNO_3 . Figure 6.6 shows the CV of the film in the latter neutral aqueous electrolyte. Even on the first sweep the oxidation peaks are different to those in 0.1 M HCl (see Figure 6.4a). Upon potential scanning, the first broad redox couple appeared at a constant potential ($E_{1/2}$ ca. 0.1 V), while the second redox couple gradually decreased in intensity and shifted to lower potential. After ca. 30 cycles, only one redox couple was observed. However, the two main redox pairs were recovered without significant change when this film was placed back in aqueous 0.1 M HCl (Figure 6.7).

These results show that the PMAS-PLL complex is electroactive in both acidic and neutral electrolytes. The first redox pair was observed at the same potential ($E_{1/2}$ ca. 0.1 V) in both media and was seen (Figure 6.6) to be reversible in both acidic and neutral media. This indicates that there is no proton transfer process involved. In contrast, the marked changes in the second redox couple for the PMAS-PLL complex observed at $E_{1/2}$ ca. 0.65 V in neutral NaNO_3 indicate that protons participate in this redox process. This electrochemical behaviour for the PMAS-PLL (1:1) complex is similar to that observed for unsubstituted polyaniline emeraldine salts¹²⁻¹⁴ and sulfonated SPAN.¹⁶ pH-dependent cyclic voltammograms have also been recently reported by Tatsuma *et al.*⁷ for a PMAS-PLL film.

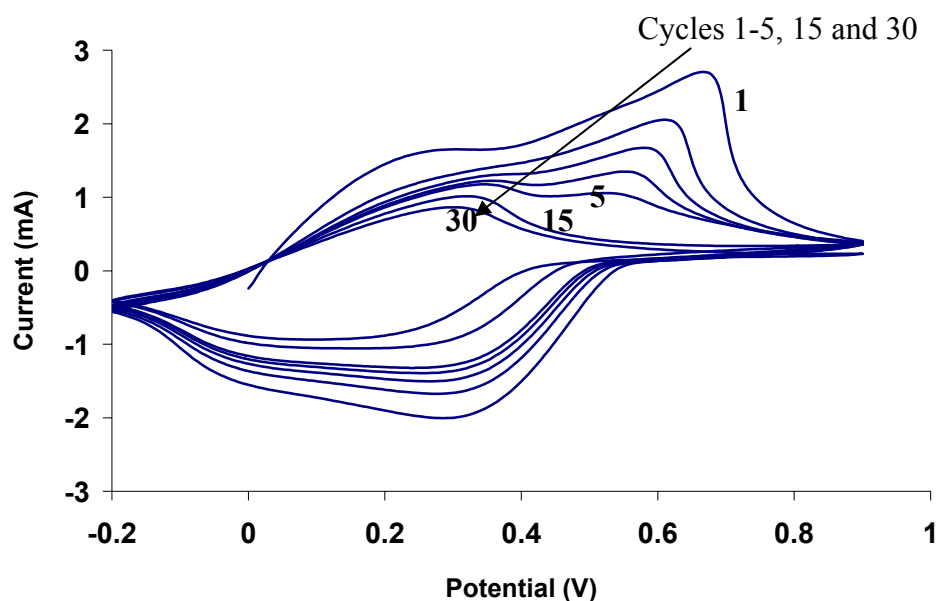


Figure 6.6 Cyclic voltammogram of a PMAS-PLL (1:1) film on an ITO-coated glass electrode in aqueous 0.3 M NaNO_3 . Scan rate = 50 mV/s.

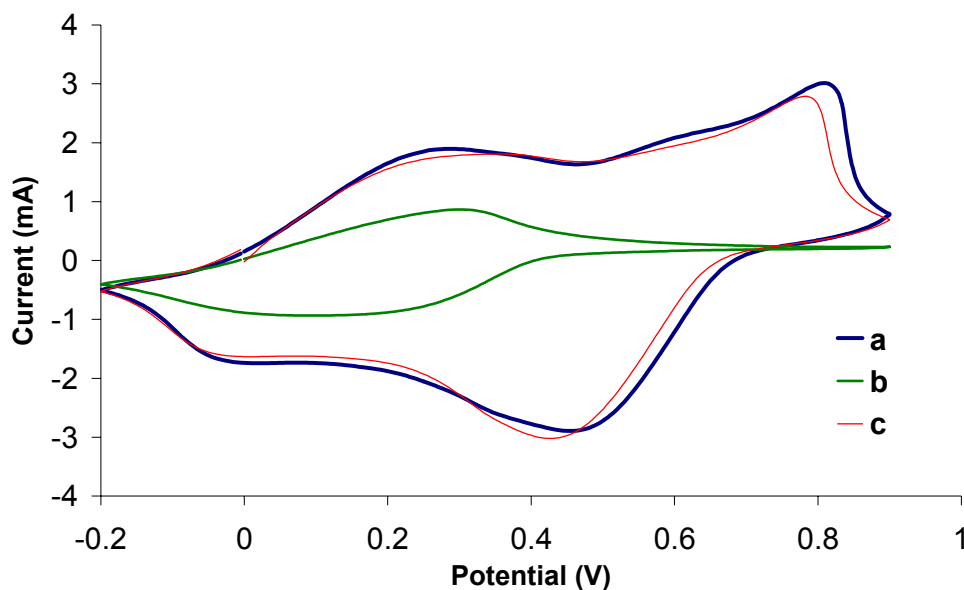
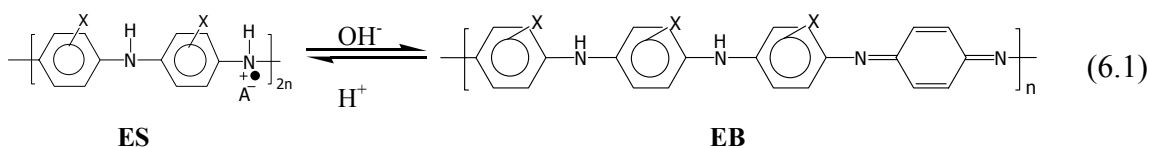


Figure 6.7 Cyclic voltammograms of a PMAS-PLL (1:1) film: (a) in 0.1 M HCl; (b) after subsequent cycling in 0.3 M NaNO₃ for 30 cycles; then (c) after replacing the film in 0.1 M HCl.

6.3.3 Acid-Base Treatment of PMAS-PLL Films

Alkaline treatment of emeraldine salts (ES) of polyaniline and substituted polyanilines typically causes de-doping of the polyaniline chains to give the corresponding emeraldine base (EB) form (Equation 6.1).



Significantly, similar alkaline treatment of a PMAS-PLL (1:1) film caused quite different behaviour. When the PMAS-PLL film was soaked in 1.0 M NH₄OH, the film changed colour immediately from yellow-brown to blue. However, the UV-visible spectrum of the blue film (Figure 6.8a) was not that expected for emeraldine base (i.e. two peaks at *ca.* 330 and 600 nm). Instead, absorption bands were observed at 365 (sh),

408 and 720 nm. This spectrum is that anticipated for a polyaniline emeraldine salt in the “compact coil” conformation. This indicates that alkaline treatment of PMAS-PLL films causes the PMAS moiety to change from an initial “extended coil” conformation to a “compact coil” arrangement of its chains. Similar behaviour has recently been noted by Strounina²⁹ and myself (see Section 5.3.1 in Chapter 5) for aqueous PMAS solutions.

The corresponding CD spectrum of the PMAS-PLL film in 1.0 M NH₄OH (Figure 6.8b) confirmed that this “compact coil” complex is optically active. Interestingly, only one strong, bisignate CD signal centred at *ca.* 410 nm was observed. This is associated with the absorption band at 408 nm. However, no CD signal associated with the absorption band at 720 nm was observed. The blue PMAS-PLL film returned to its initial colour and UV-visible spectrum after subsequent treatment with 1.0 M HCl (Figure 6.8a), confirming rearrangement of the PMAS chains back to an “extended coil” conformation. Interestingly, the recovered CD spectrum after this sequential NH₄OH and HCl treatment (Figure 6.8b) was more intense than that of the initial PMAS-PLL film. This suggests more effective binding of the PLL chiral inducer to the PMAS chains after such treatment.

When a PMAS-PLL film was dipped into aqueous 1.0 M NaOH, the colour again changed to blue, but the film then quickly dissolved in the solution. The blue solution showed absorption bands at 385 and 750 nm (Figure 6.9a), again confirming a change in conformation for the PMAS moiety from “extended coil” to “compact coil”. Dissolution in aqueous NaOH caused the CD signals for the PMAS to disappear (Figure 6.9b). These effects are believed to arise from cation exchange, *i.e.* replacement of ammonium ion groups of the PLL by Na⁺ ions at the electrostatic binding site of the complex. This would release free PMAS into the aqueous solution. Related films of chiral PMAS.(+)-

PhEA salts have also been recently reported⁸ to completely lose their optical activity when dissolved in water.

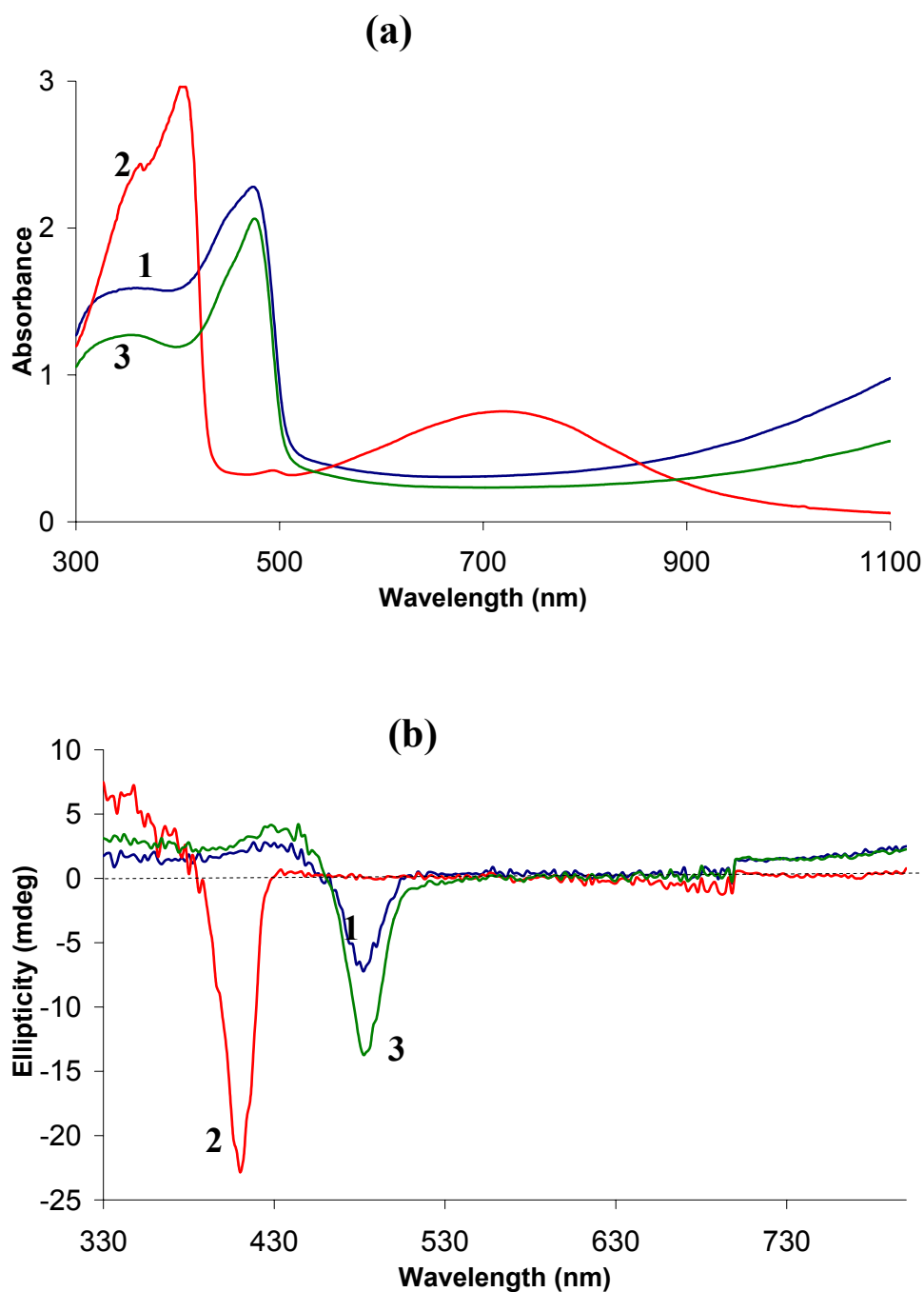


Figure 6.8 UV-visible (a) and CD spectra (b) of a PMAS-PLL (1:1) film: (1) initial film, (2) after treatment with 1.0 M NH_4OH , and (3) after treatment with 1.0 M HCl .

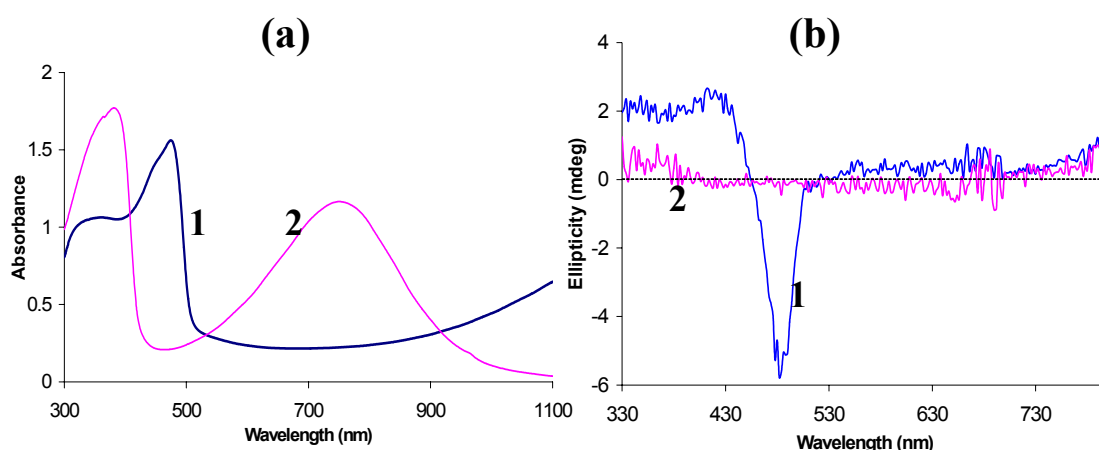


Figure 6.9 UV-visible spectra (a) and CD spectra (b) of a PMAS-PLL (1:1) film: in (1) air, and (2) after dissolution in 1.0 M NaOH.

6.3.4 Chemical Reduction / Oxidation of PMAS-PLL Films

6.3.4.1 Reduction of PMAS-PLL Film with Hydrazine

When a PMAS-PLL film was dipped into aqueous 0.2 M hydrazine (pH 10.2), it quickly changed colour from yellow-brown to colourless. Figure 6.10a shows the UV-visible spectra of the initial (curve 1) and reduced (curve 2) films. The reduced film exhibited a shoulder band at 364 nm and a sharp peak at 410 nm, consistent with formation of the reduced leucoemeraldine form of PMAS in the complex. The absorption spectrum of this reduced PMAS-PLL film is very similar to that previously observed for aqueous PMAS itself when similarly treated with hydrazine (see Chapter 5).

The CD spectrum of the reduced film (Figure 6.10b) exhibited a bisignate CD signal centred at *ca.* 400 nm, corresponding to the absorption band at 410 nm. This suggests that the PMAS chains retain optical activity after reduction.

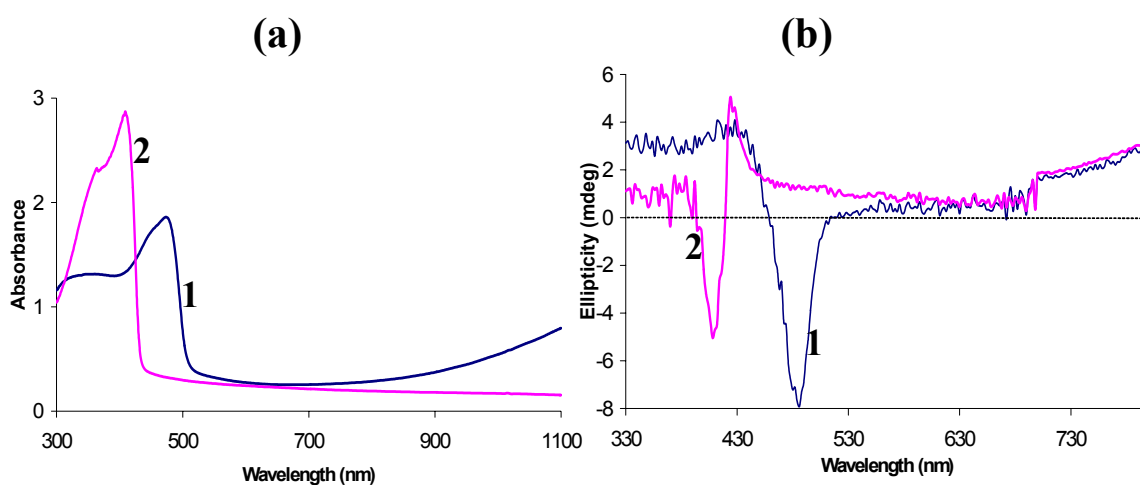


Figure 6.10 UV-visible (a) and CD (b) spectra of a PMAS-PLL film before (1) and after (2) treatment with 0.2 M N_2H_4 (pH 10.2). Spectra measured in air.

6.3.4.2 Oxidation of PMAS-PLL Film with Ammonium Persulfate

After immersion of a PMAS-PLL film in aqueous 0.2 M ammonium persulfate (pH 3.3), its UV-visible spectrum was recorded *in situ* every 1.5 min (Figure 6.11). A new absorption peak appeared over 10 min at 540 nm, together with the disappearance of the original polaron band of the PMAS moiety at 475 nm. The initial near-infrared absorption also disappeared within 10.5 min. These spectral changes indicate the formation of the oxidized pernigraniline base form of PMAS, with a characteristic band at 540 nm, as previously observed for oxidation of pure PMAS in aqueous solution (see Chapter 5). Sharp isosbestic points were observed at 385, 493 and 650 nm, indicating a clean transformation from emeraldine to the pernigraniline form of PMAS in the complex.

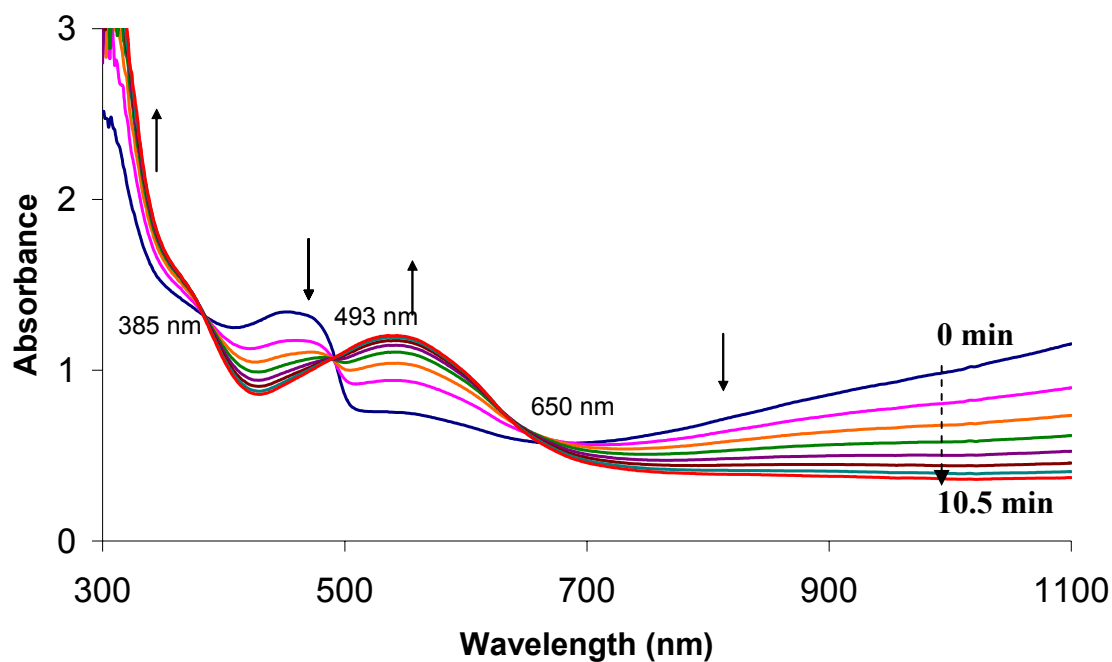


Figure 6.11 UV-visible spectral changes for a PMAS-PLL film recorded *in situ* during oxidation in 0.2 M $(\text{NH}_4)_2\text{S}_2\text{O}_8$ (pH 3.3). The spectrum was recorded every 1.5 min.

The UV-visible and CD spectra of the PMAS-PLL film before and after treatment with ammonium persulfate for 10 min are presented in Figures 6.12a and 6.12b, respectively. The bisignate CD signal centered at *ca.* 540 nm (peaks at 484 and 615 nm) for the oxidized film is associated with the absorption band at 540 nm. The strong CD band at *ca.* 350 nm is related to a shoulder absorption band in this region. This is the first time that the CD spectrum of chiral PMAS pernigraniline base has been described.

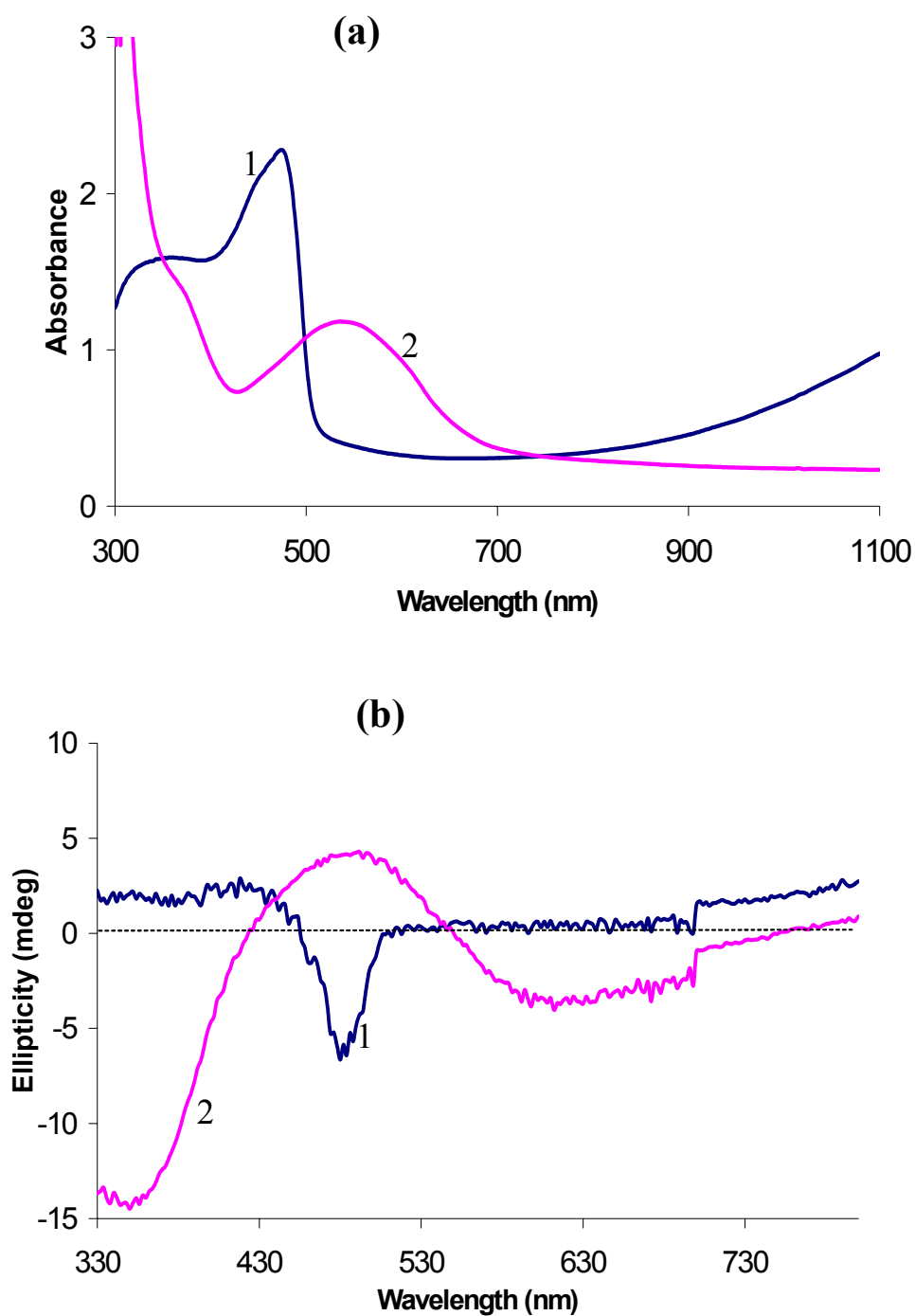


Figure 6.12 UV-visible spectrum (a) and CD spectrum (b) of a PMAS-PLL (1:1) film before (1) and after (2) treatment with 0.2 M $(\text{NH}_4)_2\text{S}_2\text{O}_8$ (pH 3.3). Spectra measured in air.

6.3.5 *In situ* Spectroelectrochemical Studies of PMAS-PLL Film

In order to further study the redox switching properties of the PMAS-PLL complex, an *in situ* spectroelectrochemical technique was used. UV-visible spectra of the film were measured after polarization at different potentials for 1 min in 0.1 M HCl as supporting electrolyte.

Figure 6.13a shows spectra recorded as the potential was increased stepwise from -0.2 V to +1.0 V. A UV-visible spectrum characteristic of the reduced leucoemeraldine base form of PMAS (λ_{max} *ca.* 370-410 nm) was observed when the potential was initially hold at -0.2 V (Figure 6.13a). The spectral change from leucoemeraldine base to emeraldine salt commenced when a potential $> +0.2$ V was applied. At +0.8 and 1.0 V, the spectrum of the fully oxidized pernigraniline form of PMAS was largely observed. These results agree with the results of cyclic voltammetry studies described in section 6.3.2, which showed two successive oxidation peaks at 0.2 V and 0.8 V, respectively.

When the applied potential was subsequently stepped down from +1.0 V to -0.2 V, the UV-visible spectral changes were reversed (Figure 6.14b). It should be mentioned that oxidation degradation of the polyaniline film in acidic aqueous electrolyte was observed when it was hold at potentials above the second redox potential ($> +0.8$ V) (see Section 9.3.2.1 in Chapter 9).

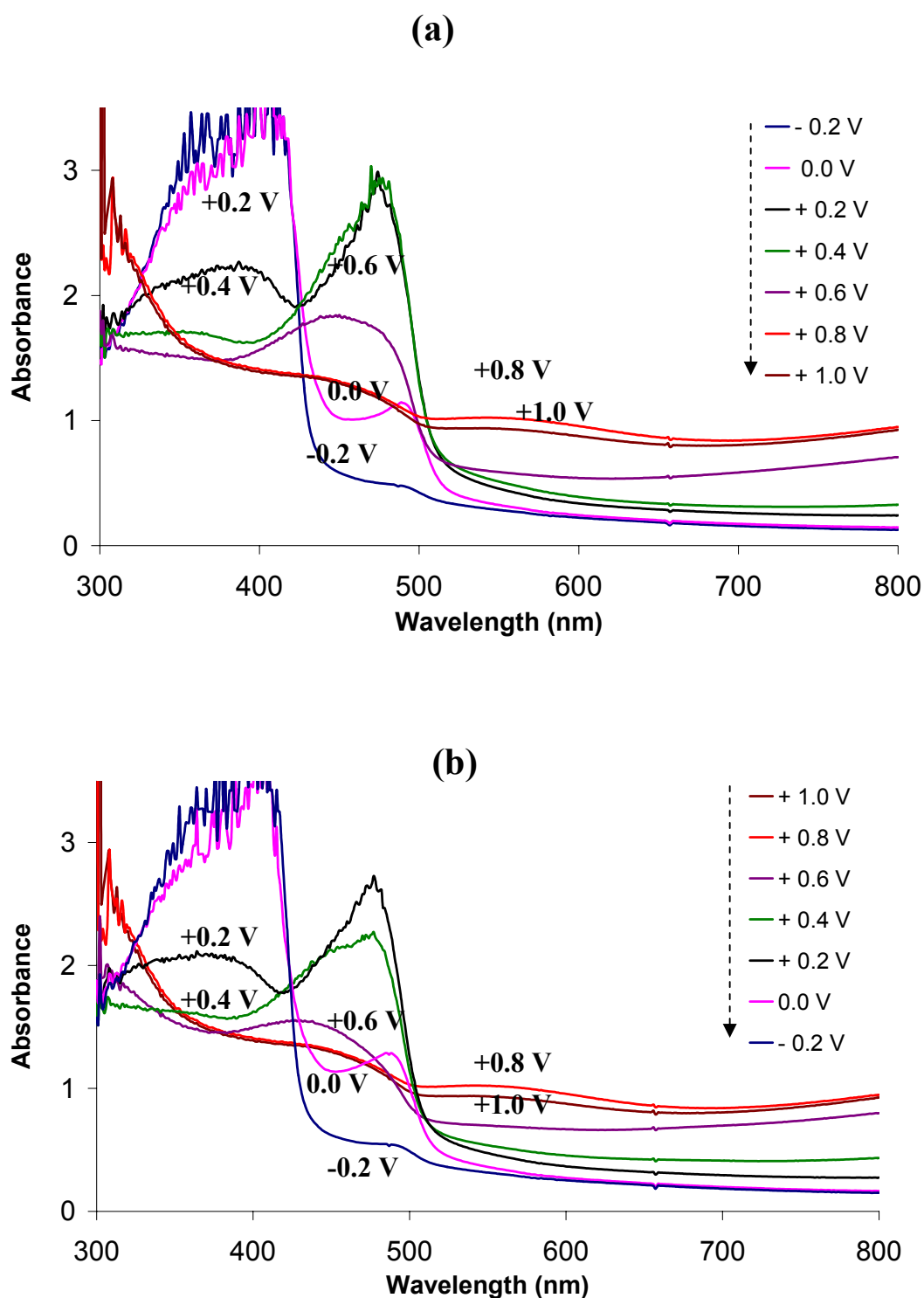


Figure 6.13 *In situ* UV-visible spectra of a PMAS-PLL (1:1) film in 0.1 M HCl, recorded after holding at various potentials for 1 min: (a) between -0.2 V and +1.0 V, and then (b) between +1.0 and -0.2 V.

6.3.6 Electrical Conductivity of PMAS-PLL Complex

An aqueous solution of the PMAS-PLL (1:1) complex was cast onto glass slides and evaporation allowed to take place at ambient temperature. The resultant films were kept under vacuum in a desiccator containing activated silica gel for 24 hrs. The thickness of the dried films was measured by micrometer to be 0.01-0.02 mm. The electrical conductivity of the PMAS-PLL films, determined via four-point probe measurements, was 4×10^{-3} S/cm (average for 3 films). This conductivity for the complex is lower than that found for uncomplexed PMAS, which was *ca.* 0.01-0.04 S/cm,^{30, 31} However, it is quite high when compared with the conductivity found recently for complexes of PMAS with poly(4-vinylpyridine) (10^{-5} - 10^{-6} S/cm).¹⁰

6.4 Conclusions

Optically active PMAS-PLL complex films can be readily formed by mixing an aqueous solution of PMAS with an aqueous solution of poly(L-lysine). Free sulfonate groups not participating in self-doping at the radical cation N sites of PMAS are believed to bind electrostatically to ammonium groups on the PLL. The strong electrostatic interaction causes the formation of a water insoluble complex. The optical activity induced in the PMAS moiety may arise from the PMAS chains following the one-handed helical structure of the PLL via the formation of the above electrostatic bonds.

The UV-visible spectrum of the PMAS-PLL film confirms that the PMAS moiety in the complex is in the emeraldine salt form and possesses an “extended coil” conformation. The PMAS-PLL film exhibits a moderate conductivity of 4×10^{-3} S/cm, albeit a little lower than that of free PMAS polymer.

The PMAS moiety in the PMAS-PLL complex is resistant to alkaline de-doping. Rather than de-doping to its emeraldine base, treatment of a PMAS-PLL film with 1.0 M NH_4OH causes UV-visible spectral changes consistent with a transformation of the PMAS from an “extended coil” to a “compact coil” conformation. Subsequent treatment with 1.0 M HCl changes the PMAS back to an “extended coil” conformation. CD spectral studies show that both the “extended coil” and “compact coil” conformations formed for the PMAS moiety are optically active.

Treatment of a PMAS-PLL film with aqueous 0.2 M hydrazine (pH 10.2) causes reduction of the PMAS moiety to its leucoemeraldine base form, as evidenced by its UV-visible spectrum. Bisignate CD bands at 408 and 424 nm associated with the absorption band at 410 nm confirm that the PMAS moiety remains optically active during its reduction.

Like uncomplexed PMAS, PMAS-PLL films are oxidized by aqueous 0.2 M ammonium persulfate (pH 3.3) to give the corresponding pernigraniline base form, exhibiting a characteristic absorption band at 540 nm. A clean oxidation is confirmed by the observation of three sharp isosbestic points during the oxidation. Bisignate CD bands centered at 540 nm confirm that the fully oxidized PMAS in the complex is optically active. This is the first time that the CD spectrum of the pernigraniline base form of PMAS has been described.

The electrical conductivity of the PMAS-PLL films is 4×10^{-3} S/cm, which is lower than that found for uncomplexed PMAS. However, it is quite high when compared with the conductivity for other complexes of PMAS.

Cyclic voltammograms of PMAS-PLL films demonstrate that the PMAS moiety is electroactive in both acidic and neutral electrolytes. Two redox couples, attributed to the transformation of the PMAS from leucoemeraldine to emeraldine and subsequently to its pernigraniline form, are observed when cyclic voltammetry is performed in 0.1 M HCl; while only the redox couple at lower potential is seen in CV's recorded in 0.3 M NaNO₃. However, the second redox couple at the high potential can be restored in acid solution. These results suggest that proton transfer is involved in this second redox couple. This redox switching of PMAS-PLL complexes is also confirmed by *in-situ* spectroelectrochemical studies, with the presence of isosbestic points for UV-visible spectra recorded at different temperatures confirming clean redox processes.

The successful synthesis of chiral PMAS.PLL complexes, suggests that a similar approach may lead to the preparation of chiral PMAS via complex formation with natural chiral cationic polyelectrolytes such as chitosan.

6.5 References

1. W.J. Macknight, E.A. Ponomarenko, and D.A. Tirrell, *Acc. Chem. Res.* **31** (1998): 781.
2. O. Pieroni, A. Fissi, and G. Popova, *Prog. Polym. Sci.* **23** (1998): 81.
3. S. Abe, T. Nonaka, and T. Fuchigami, *Journal of the American Chemical Society.* **105** (1983): 3630.
4. T. Komori and T. Nonaka, *J. Am. Chem. Soc.* **105** (1983): 5690.
5. T. Komori and T. Nonaka, *J. Am. Chem. Soc.* **106** (1984): 2656.
6. P.K. Ghosh and A.J. Bard, *J. Am. Chem. Soc.* **105** (1983): 5691.
7. T. Tatsuma, T. Ogawa, R. Sato, and N. Oyama, *J. Electroanal. Chem.* **501** (2001): 180.
8. E.V. Strounina, L.A.P. Kane-Maguire, and G.G. Wallace, *Synth. Met.* **106** (1999): 129.
9. E.V. Strounina, PhD thesis, *Synthesis and Characterisation of Chiral Substituted Polyanilines*, Chemistry Department. 2001, Univeristy of Wollongong.
10. D.E. Tallman and G.G. Wallace, *Synth. Met.* **90** (1997): 13.
11. F. Masdarolomoor, P.C. Innis, S.A. Ashraf, and G.G. Walace. *Purification and Characterization of Poly(2-methoxy aniline-5-sulfonic acid)*, ICSM 2004. Wollongong, Australia.
12. W.W. Focke, G.E. Wnek, and Y. Wei, *J. Phys. Chem.* **91** (1987): 5813.
13. L.H.C. Mattoso, A.G. MacDiarmid, and A.J. Epstein, *Synth. Met.* **68** (1994).
14. D. Orata and D.A. Buttry, *J. Am. Chem. Soc.* **109** (1987): 3574.
15. A. Kabumoto, K. Shinozaki, K. Watanabe, and N. Nishikawa, *Synth. Met.* **26** (1988): 349.
16. J. Yue, Z.H. Wang, K.R. Cromack, A. Epstein, and A.G. MacDiarmid, *J. Am. Chem. Soc.* **113** (1991): 2665.
17. X.-L. Wei, Y.Z. Wang, S.M. Long, C. Bobeczko, and A. Epstein, *J. Am. Chem. Soc.* **118** (1996): 2545.

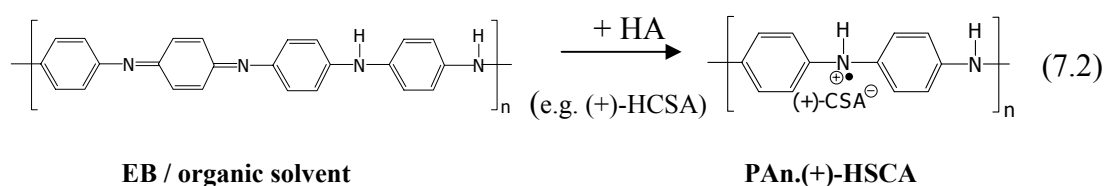
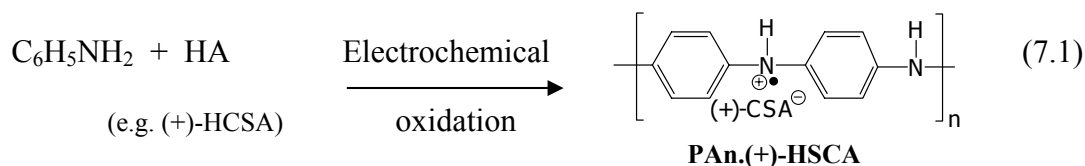
18. J. Widera, B. Patys, J. Bukwska, and K. Jackowska, *Synth. Met.* **94** (1998): 265.
19. P.A. Kilmartin and G.A. Wright, *Synth. Met.* **88** (1997): 153.
20. P.A. Kilmartin and G.A. Wright, *Synth. Met.* **88** (1997): 163.
21. Y.-B. Shim, M.-S. Won, and S.-M. Park, *J. Electrochem. Soc.* **137** (1990): 538.
22. A. Kitani, M. Kaya, J. Yano, K. Yoshikawa, and K. Sasaki, *Synth. Met.* **18** (1987): 341.
23. S. Patil, J.R. Mahajan, M.A. More, P.P. Patil, S.W. Gosavi, and S.A. Gangal, *Polym. Inter.* **46** (1998): 99.
24. F.A. Viva, E.M. Andrade, F.V. Molina, and M.I. Florit, *J. Electroanal. Chem.* **471** (1999): 180.
25. M. Lapkowski, *Synth. Met.* **35** (1990): 169.
26. W.A. Gazotti, R. Faez, and M.A. Paoli, *J. Electroanal. Chem.* **415** (1996): 107.
27. E.M. Genies and C. Tsintavis, *J. Electroanal. Chem.* **195** (1985): 109.
28. E.M. Genies and M. Lapkowski, *J. Electroanal. Chem.* **236** (1987): 189.
29. E.V. Strounina, R. Shepherd, L.A.P. Kane-Maguire, and G.G. Wallace, *Synth. Met.* **135-136** (2003): 289.
30. R. Guo, J.N. Barisci, P.C. Innis, C.O. Too, G.G. Wallace, and D. Zhou, *Synth. Met.* **114** (2000): 267.
31. S. Shimizu, T. Saitoh, M. Uzawa, M. Yuasa, K. Yano, T. Maruyama, and K. Watanabe, *Synth. Met.* **85** (1997): 1337.

Chapter 7

Influence of Electropolymerization Temperature on the Chiroptical Properties of (+)-Camphorsulfonic Acid-Doped Polyaniline

7.1 Introduction

The preparation of optically active polyanilines has been reported via the electropolymerization of aniline in the presence of aqueous chiral acids (HA) such as (+)- or (-)-10-camphorsulfonic acid (HCSA), as presented in Equation (7.1);^{1, 2} or by the acid-doping of emeraldine base (EB) with a wide range of chiral acids in a number of organic solvents, as shown in Equation (7.2).³⁻⁵



It has been suggested^{1, 4} that the optical activity of the electrodeposited polyaniline films arises from the preferential adoption of a one-handed helical screw by the developing polyaniline chains, depending on the hand of the CSA⁻ dopant anion employed. The chiral induction was believed to be initiated by specific electrostatic and hydrogen bonding interactions between radical cation $-\text{N}^{\cdot+}-$ and amine $-\text{NH}-$

sites on the polyaniline chains with SO_3^- and carbonyl groups, respectively, on the enantiomeric CSA^- dopant anions.

It is well known that the properties of polyanilines greatly depend on the method and conditions of their polymerization. Most studies to date have concentrated on the influence of these polymerization conditions on the electrical conductivity,^{1,6} molecular weight,⁷⁻⁹ electrochemical properties^{6,10-11} and morphology^{9,10,11,12} of the resultant polyanilines. On the other hand, information on the relationship between the preparative conditions and the conformation/structure of polyanilines is rare in the literature.

Kane-Maguire *et al.*^{1,2} reported that optically active PAn.(+)-HCSA films prepared by electropolymerization of aniline in the presence of (+)-HCSA possess a partly “extended coil” conformation for their polyaniline chains. This conclusion was based on the absence of a localized polaron absorption band around 800 nm and the presence of an intense free carrier tail in the near-infrared region. These features were identified by MacDiarmid *et al.*^{13,14} as diagnostic of “extended coil” emeraldine salts. PAn.(+)-HCSA films obtained by Kane-Maguire *et al.*^{1,2} under constant potential (0.8-1.1 V vs Ag/AgCl), constant current (0.4-1.0 mA/cm²) and potential cycling (from -0.2 to 0.9/1.0 V) conditions exhibited similar UV-visible and circular dichroism (CD) spectra.

In more recent chiroptical studies, Kane-Maguire *et al.*¹⁵ provided further evidence of the influence of synthesis route on the structures and consequent chiroptical properties of PAn.(+)-HCSA films. They reported the first unequivocal evidence that PAn.(+)-HCSA films prepared chemically and electrochemically possess different

conformations, assigned as “compact coil” and partial “extended coil”, respectively. Due to the high sensitivity of the CD spectra of polymers to the molecular conformation of their chains, significant differences were observed in the CD spectra of chemically and electrochemically prepared PAn.(+)-HCSA films. The visible region CD spectrum of electrodeposited PAn.(+)-HCSA films exhibited one pair of bisignate, exciton-coupled bands, with positive and negative signs at *ca.* 360 and 450 nm, respectively. In contrast, the CD spectra of PAn.(+)-HCSA films prepared chemically as in Equation (7.2) exhibited negative and positive CD bands at *ca.* 405 and 460 nm, respectively. Interestingly, irreversible transformation of the polyaniline chain conformation from “extended coil” to “compact coil” occurred when the electrochemically deposited PAn.(+)-HCSA films were heated at $\geq 140^{\circ}\text{C}$.

Recently, Kaner *et al.*¹⁶ demonstrated that the chirality of polyaniline induced by protonation of the emeraldine base (EB) with optically active (+)-HCSA (Equation 7.2) is critically dependent upon the water content of the EB prior to doping. Doping of wet and dry EB in NMP solvent with (+)-HCSA gave PAn.(+)-HCSA salts exhibiting mirror imaged CD spectrum over the short region 350-550 nm. Later studies by Kane-Maguire *et al.*¹⁷ have similarly shown that the water content in solutions of EB in NMP, DMPU, DMF and DMSO prior to doping with (+)-HCSA has a great effect on the conformation of the PAn.(+)-HCSA. Markedly different (but not mirror imaged) CD spectra were obtained between 320 and 800 nm in the presence of 1-10% (w/v) added water; while with $\geq 25\%$ added water a complete loss of CD signals was observed together with a marked change in the UV-visible spectra. They proposed that the effects of added water arise from hydrogen bonding of the initial EB substrate by water prior to acid doping.

Chiral polyanilines are of considerable interest because of their potential applications such as novel stationary phases for the chromatographic separation of enantiomeric chemicals,¹⁸⁻²⁰ as chiral electrodes for chiral sensors²¹ and electrochemical asymmetric synthesis.²² The factors that influence the conformation and chiroptical properties of such chiral polyanilines need to be understood prior to using them in the above applications. The present Chapter investigates the influence of the electropolymerization temperature on the chiroptical properties of PAn.(+)-HCSA films.

7.2 Experimental

7.2.1 Preparation of PAn.(+)-HCSA Films

Electropolymerizations were carried out in a one-compartment cell with a three electrode configuration using a BAS CV-27 potentiostat. The PAn.(+)-HCSA films were potentiostatically deposited on 1 x 3 cm ITO-coated glass (sputter coated with Pt) working electrodes from aqueous 0.2 M aniline containing 1.0 M (+)-HCSA, using an applied potential of + 0.9 V and passing 120 mC/cm² of charge. The polymerization temperature was maintained ($\pm 0.5^\circ\text{C}$) using a thermostatted water bath. Pt-mesh and Ag/AgCl_(3M NaCl) were employed as auxiliary and reference electrodes, respectively.

7.2.2 UV-Visible and CD Spectra of PAn.(+)-HCSA Films

After electrodeposition, the PAn.(+)-HCSA films were washed with MeOH to remove oligomers, excess monomer and unincorporated (+)-HCSA. Their UV-visible (300-1100 nm), UV-visible-NIR (300-3000 nm), and CD spectra were then recorded as described in Chapter 2.

7.2.3 Post-Polymerization Heat Treatment of PAn.(+)-HCSA Films

A PAn.(+)-HCSA film electrochemically grown at room temperature (*ca.* 20°C) was heated at 45°C in 1.0 M (+)-HSCA for 1½ hours, and its UV-visible and CD spectra recorded again. Another PAn.(+)-HCSA film was heated for successive 30 min periods in an air oven at 70°C and 100°C and its UV-visible and CD spectra recorded after cooling to room temperature.

7.2.4 De-doping/Re-doping of a PAn.(+)-HCSA Film

A PAn.(+)-HCSA emeraldine salt film electrodeposited at 65°C was de-doped in 1.0 M NH₄OH for 1 hr to give an emeraldine base film, and then re-doped to PAn.HCl by treatment with 1.0 M HCl for 1 hr. This de-doping/re-doping cycle was then repeated. UV-visible and CD spectra were recorded before and after each of these base/acid treatments.

7.2.5 Chemical Reduction and Oxidation of a PAn.(+)-HCSA Film

A PAn.(+)-HCSA film electrochemically deposited at 70°C was reduced to leucoemeraldine base (LB) by immersing in aqueous 0.1 M hydrazine for 2 hrs. The UV-visible and CD spectra of the LB film were recorded before its subsequent oxidation to pernigraniline base (PB) by treatment with 0.2 M ammonium persulfate for 3 hrs, and its UV-visible and CD spectra re-measured.

7.2.6 PAn.(+)-HCSA Film Morphology

The surface morphology of the PAn.(+)-HCSA films electrodeposited at temperatures between 0°C and 65°C was assessed with SEM as described in Chapter 2.

7.3 Results and Discussion

Chiral polyaniline can be synthesized by electropolymerization of aniline in the presence of (+)- or (-)-HCSA via galvanostatic, potentiodynamic or potentiostatic methods.² However, the potentiostatic (constant potential) method has been generally used to avoid overoxidation and degradation of the polyaniline films at high potentials.²³⁻²⁷ With potentiostatic polymerization, Kane-Maguire *et al.*² reported that the rate of polymerization and the chirality of the deposited PAn.(+)-HCSA films strongly depend on the potential employed. Very weak CD signals (*ca.* 10 mdeg at 450 nm) and slow electro-polymerization were observed using an applied potential of 0.8 V; while strong CD signals (*ca.* 150 mdeg at 450 nm) and relatively rapid polymerization occurred when using a potential of 1.1 V for 120 mC/cm² of charge passed. Therefore, to avoid overoxidation / degradation of the polyaniline chains and to obtain a suitable absorbance intensity and ellipticity in the UV-visible and CD spectra of the PAn.(+)-HCSA films, electropolymerization at +0.9 V in 0.2 M aniline/1.0 M (+)-HCSA for 120 mC/cm² of charge passed was carried out for all the studies in this Chapter.

7.3.1 Influence of Temperature during Electropolymerization

The majority of polymerization temperature studies on polyaniline to date have focused on the electrical conductivity,⁹ molecular weight,^{7,9} mechanical properties⁸ and morphology²⁸ of the emeraldine salt products. It has been reported that high conductivity and high molecular weight polyanilines are synthesized at low temperature ($\leq 0^{\circ}\text{C}$).^{7,29}

Electrodeposition of PAn.(+)-HCSA films has historically been performed at room temperature (20° - 25°C). The influence of electropolymerization temperature on the chiroptical properties of the emeraldine salt films is explored in this Chapter by carrying out the electrodepositions using temperatures between 0°C and 70°C, and then measuring their UV-visible and CD spectra.

As expected, when the polymerization temperature was raised the rate of electrodeposition of PAn.(+)-HCSA films increased. To achieve 120 mC/cm² of deposition charge on the 3 cm² surface area of the ITO-coated glass working electrode (giving films of suitable thickness for UV visible and CD spectral analysis), polymerization times of *ca.* 5, 2 and 1 minute were used for temperatures of 0°, 25° and 70°C, respectively.

There were only relatively small differences in the UV-visible-NIR spectra of PAn.(+)-HCSA films electrodeposited at temperatures between 0°C and 65°C, as illustrated in Figure 7.1. Each film exhibited a strong absorption band at *ca.* 390 nm, a weak shoulder at *ca.* 800 nm and an intense broad band in the near-infrared region with a maximum absorption at *ca.* 1300 nm. These features are characteristic of an “extended coil” conformation for the polyaniline chains.^{13,14} Increasing the electropolymerization temperature from 0°C to 65°C caused an increase in the relative intensity of the 1300 nm peak compared to the 390 nm band. These changes are consistent with further enhancement of the “extended coil” conformation for the polyaniline chains with increasing temperature.

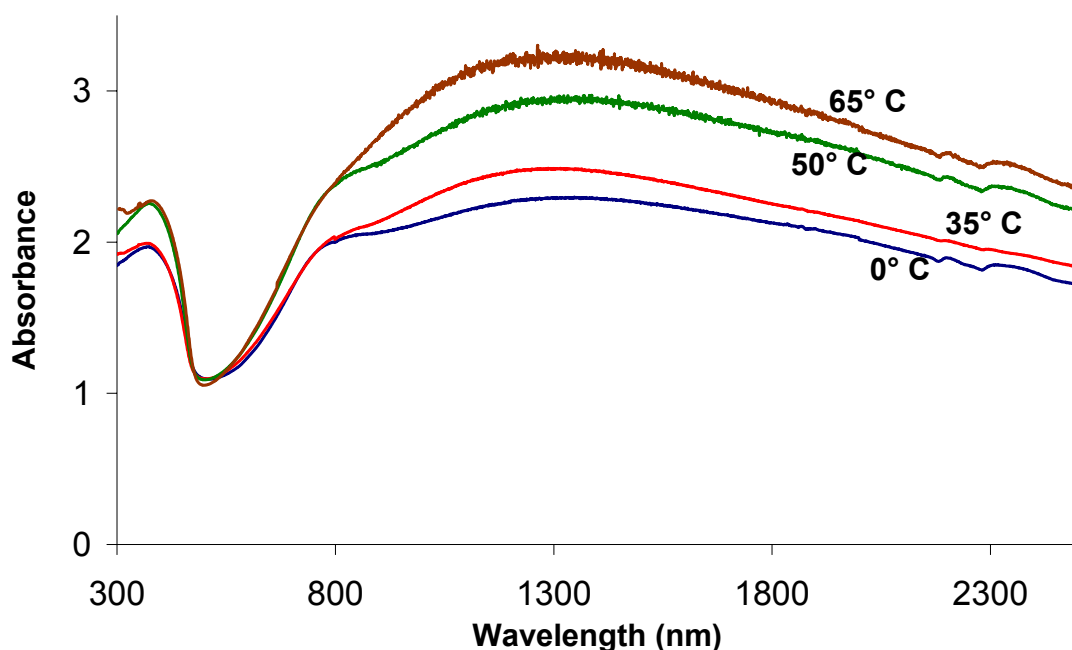


Figure 7.1 UV-visible-NIR spectra of PAN.(+)-HCSA films electrochemically deposited at 0°C, 35°C, 50°C and 65°C onto ITO-Pt-coated glass.

In contrast to their UV-visible spectra, the chiroptical properties of the PAN.(+)-HCSA films strongly depended on the polymerization temperature employed. In Figure 7.2a, the emeraldine salt films grown at 0° and 25°C are seen to exhibit a bisignate CD band (positive and negative signals at *ca.* 350 and 440 nm, respectively) associated with the absorption band at 390 nm, as well as a broad CD band at *ca.* 700 nm. This latter CD band is believed to be the low wavelength component of the expected bisignate CD signal associated with the very broad absorption band centered at *ca.* 1300 nm. These CD spectra were qualitatively similar to that previously reported for PAN.(+)-HCSA electrodeposited at room temperature.^{1, 2} However, the CD bands for the PAN.(+)-HCSA film deposited at 0°C are considerably more intense than those for the film grown at 25°C (Figure 7.2a), indicating higher diastereoselectivity during electrodeposition at the lower temperature. This may be partly attributed to more regular head-to-tail coupling of the polyaniline chains during electropolymerization at 0°C, with

fewer faults such as *ortho*-coupling interfering with the adoption of regular predominantly one-handed helical chains.

Remarkable changes occurred for the CD spectra of the PAn.(+)-HCSA films electrodeposited at higher temperatures. The CD bands for the film grown at 30°C were very weak in intensity (Figure 7.2a and inset), although qualitatively still similar to the films grown at 0°- 25°C. Surprisingly, weak CD signals of inverted sign were observed for the PAn.(+)-HCSA film grown at 40°C (Figure 7.2b). The intensity of these inverted CD signals increased progressively for emeraldine salt films deposited at 50° and 65°C (Figure 7.2b). In addition, an apparently optically inactive polyaniline product was obtained when the polymer was polymerized at 33°C. The results therefore show that the inversion started between 30°C and 35°C.

The mirror imaged nature of the PAn.(+)-HCSA films electrodeposited at 25°C and 65°C are clearly shown in Figure 7.3. These two films are diastereomeric rather than enantiomeric, as they both contain the same (+)-HCSA dopant. The latter dopant only absorbs in the UV region and therefore gives no CD signals in the visible region examined.

It has previously been shown that when PAn.(+)-HCSA and PAn.(-)-HCSA films are electrodeposited at room temperature, mirror imaged CD spectra are observed.¹ It was proposed that the opposite screw sense of helical polyaniline chains was generated by electropolymerization with the enantiomeric (+)- and (-)-HCSA dopant acids.^{1,2} Assuming, as suggested previously,^{1,2} that the visible region optical activity observed for these emeraldine salts arises from the presence of predominantly one-handed helical polyaniline chains, the inversion observed here for the CD spectra of PAn.(+)-

HCSA films grown at different temperatures indicates an inversion of the favoured helical hand of the polyaniline chains.

These remarkable temperature effects on the conformation of electrochemically grown PAN.(+)-HCSA emeraldine salts have important implications for researchers wishing to synthesize optically active polyanilines for use in applications such as chiral separations and electrochemical asymmetric synthesis. The widely different room temperatures experienced in different laboratories around the world would cause such PAN.(+)-HCSA emeraldine salts grown in tropical/sub-tropical laboratories to have the opposite visible region chiroptical properties to those grown in temperate regions (temperature $\leq 25^{\circ}\text{C}$). Should the laboratory temperature be 33°C , the researcher would obtain an optically inactive polyaniline product, as has been confirmed here by carrying out the electropolymerization at this temperature.

These observations represent the first example of temperature-induced helix inversion *during* the electrochemical synthesis of a conducting organic polymer. However, inversion of polymer CD spectra via *post-synthesis* heating or cooling has recently been reported³⁰⁻³² for some chiral polythiophenes, where the optical activity was believed to arise from helical superstructures of aggregated polythiophene chains. Similar temperature-induced helix reversal has also been recently reported for synthetic DNA,³³ poly(L-aspartic acid ester)s,^{34,35} poly(isocyanate)s,^{36,37} polyacetylenes³⁸⁻⁴¹ and polysilanes,^{42,43} where the energy barrier to helix-helix interconversion is relatively low. These temperature-sensitive, chiral polymers have generated considerable recent interest because of their potential applications as molecular switches or for data storage.

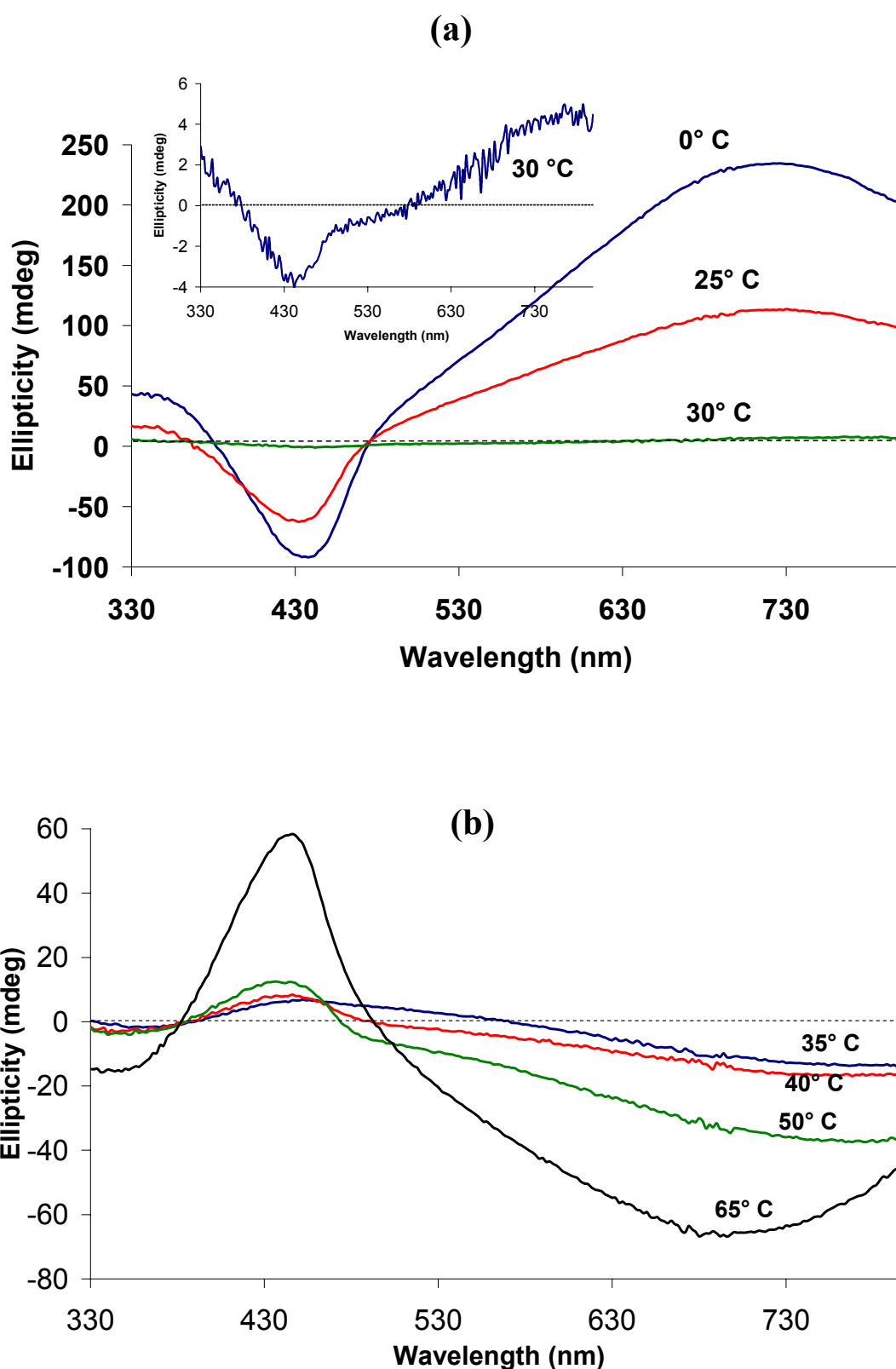


Figure 7.2 CD spectra of PAN.(+)-HCSA films electrochemically deposited onto ITO-Pt-coated glass at: (a) 0°C, 25°C and 30°C; (b) 33°C, 35°C, 40°C, 50°C and 65°C.

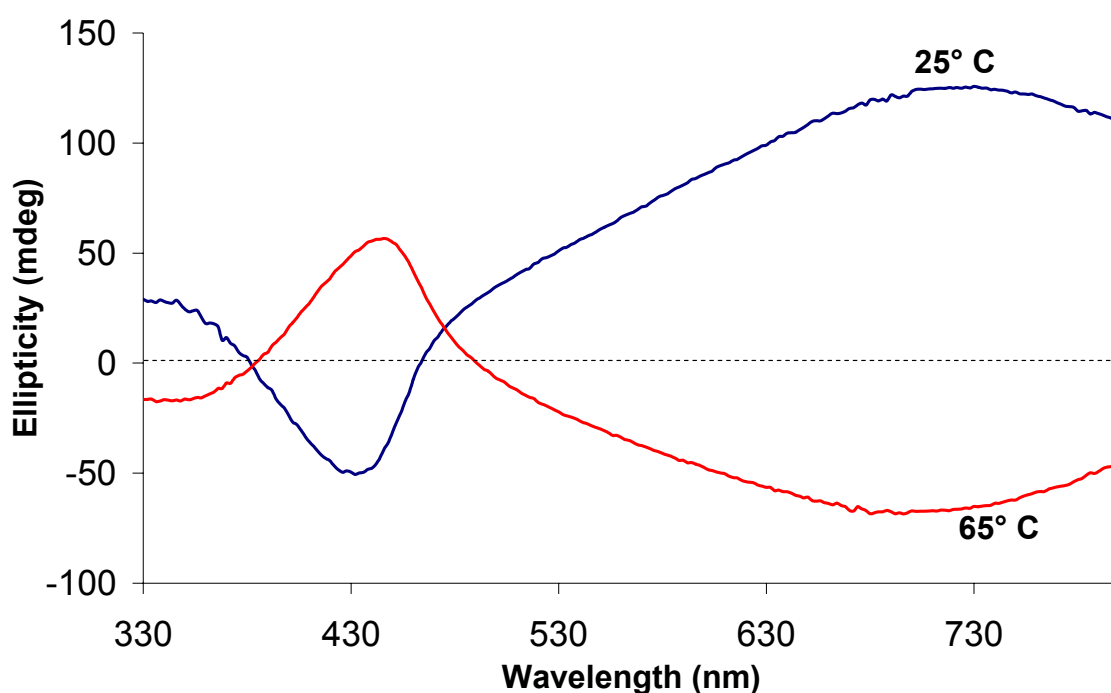


Figure 7.3 Comparison of the CD spectra for PAn.(+)-HCSA films electrochemically synthesised at 25°C and 65°C.

7.3.2 Influence of Polymerization Temperature on the Morphology of PAn. (+)-HCSA Films

The effect of electropolymerization temperature on the morphology of deposited PAn.(+)-HCSA films was examined by scanning electron microscopy (SEM). Scanning electron micrographs of the films grown over the range 0°-65°C (Figure 7.4) revealed similar fibrous morphologies or ‘noodle like’ structure in each case. It may therefore be concluded that the temperature of electropolymerization has no significant effect on the morphology of the deposited polyanilines.

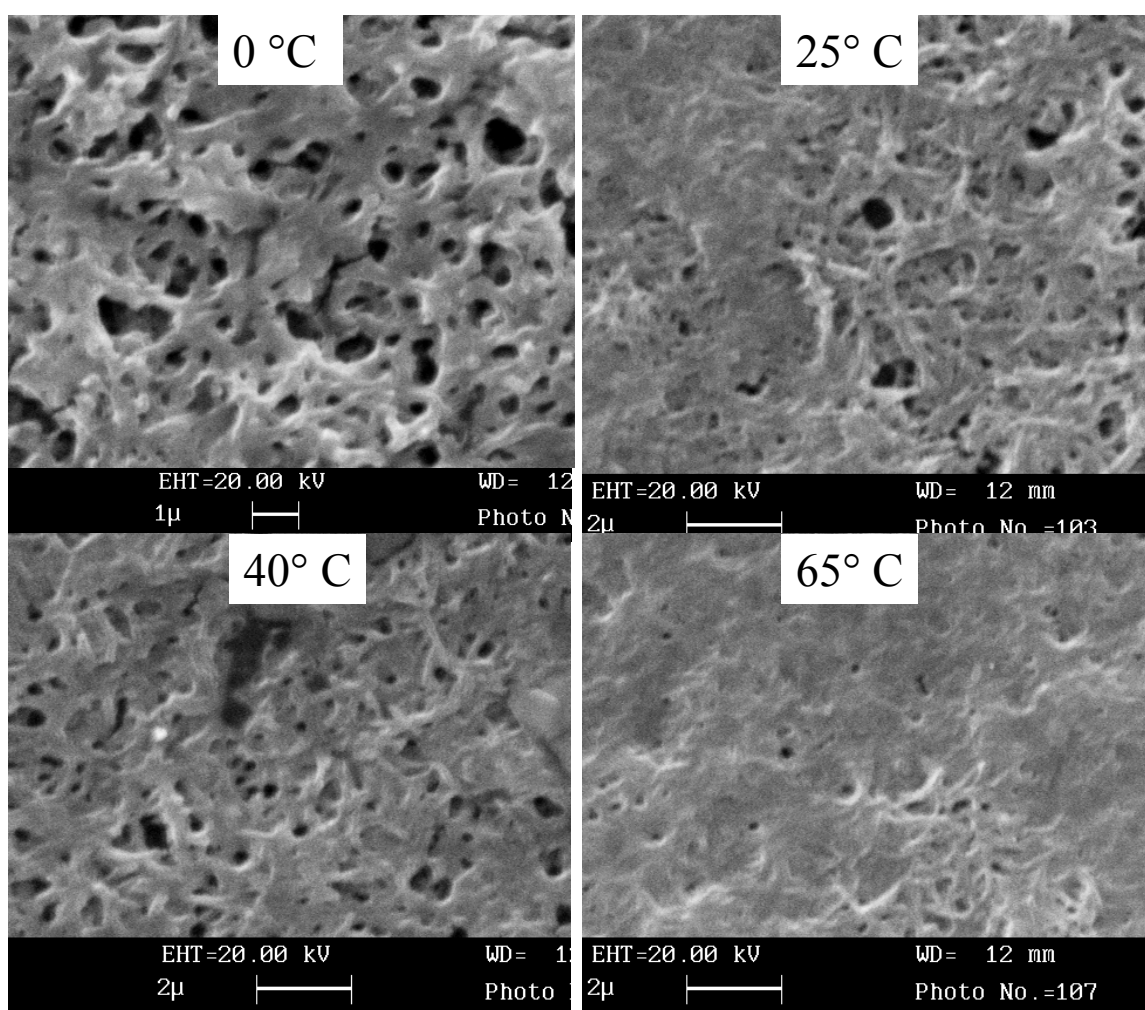


Figure 7.4 SEMs of PAN.(+)-HCSA films electrodeposited at 0°, 25°, 40° and 65°C on ITO-coated glass.

7.3.3 Effect of Heat Treatment after Polymerization

In an attempt to understand the inversion of the CD spectra observed for the PAN.(+)-HCSA films electrochemically deposited above *ca.* 30°C, the effect of post-polymerization heat treatment of PAN.(+)-HCSA films grown at room temperature (20°C–25°C) was investigated. This study should establish whether the preferred hand of the chiral polyaniline product was determined *prior* or *subsequent* to electrodeposition on the working electrode.

(i) Heating a PAn.(+)-HCSA Film in Aqueous 1.0 M (+)-HCSA

No significant change was observed in the UV-visible and CD spectra of a PAn.(+)-HCSA film (grown at 25°C) after heating at 45°C in aqueous 1.0 M (+)-HCSA for 1.5 hrs, as shown in Figure 7.5. Heat treatment at temperatures > 45°C could not be tested due to the film beginning to peel off the ITO-coated glass.

(ii) Heating a PAn.(+)-HCSA Film in an Air Oven

A PAn.(+)-HCSA film electrochemically deposited at 20°C was subsequently heated at 70°C for 30 min in a hot air oven, and its UV-visible and CD spectra recorded after cooling to room temperature. No significant changes in the UV-visible and CD spectra of the film were observed, even after further heating at 100°C for 30 min (Figure 7.6).

The results of these post-polymerization heat treatments in (i) and (ii) above indicate that the conformation/ configuration of chiral polyaniline chains in solid state films cannot be changed by heating at 45°C in aqueous media or at 100°C in air *after* electrodeposition. Therefore, the chiral discrimination in the electropolymerization must occur during the polymer growth prior to or during deposition onto the working electrode.

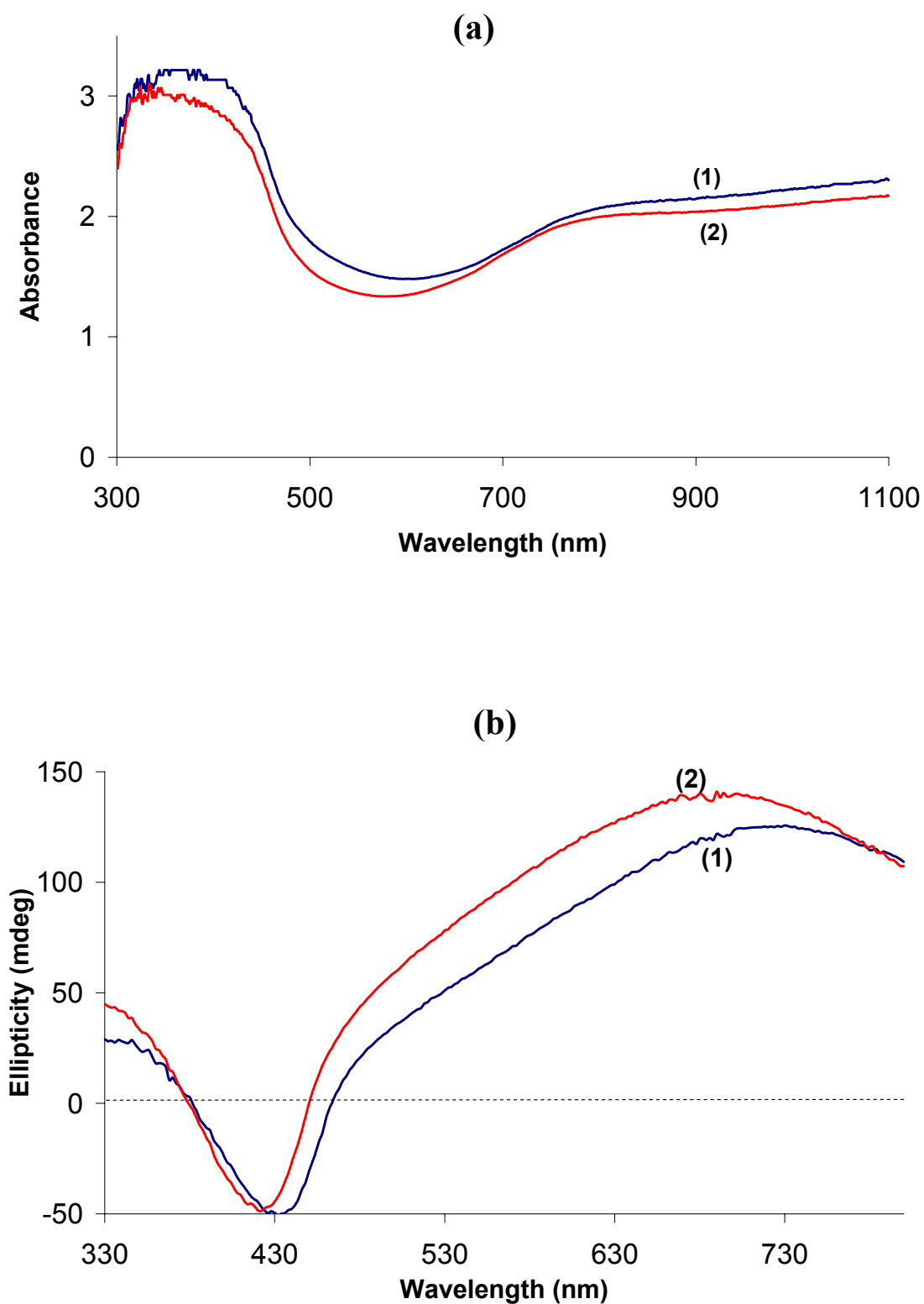


Figure 7.5 UV-visible spectra (a) and CD spectra (b) of a PAn.(+)-HCSA film: (1) as electrochemically deposited at 25°C; and (2) after heating at 45°C in aqueous 1.0 M (+)-HCSA for 1.5 hr.

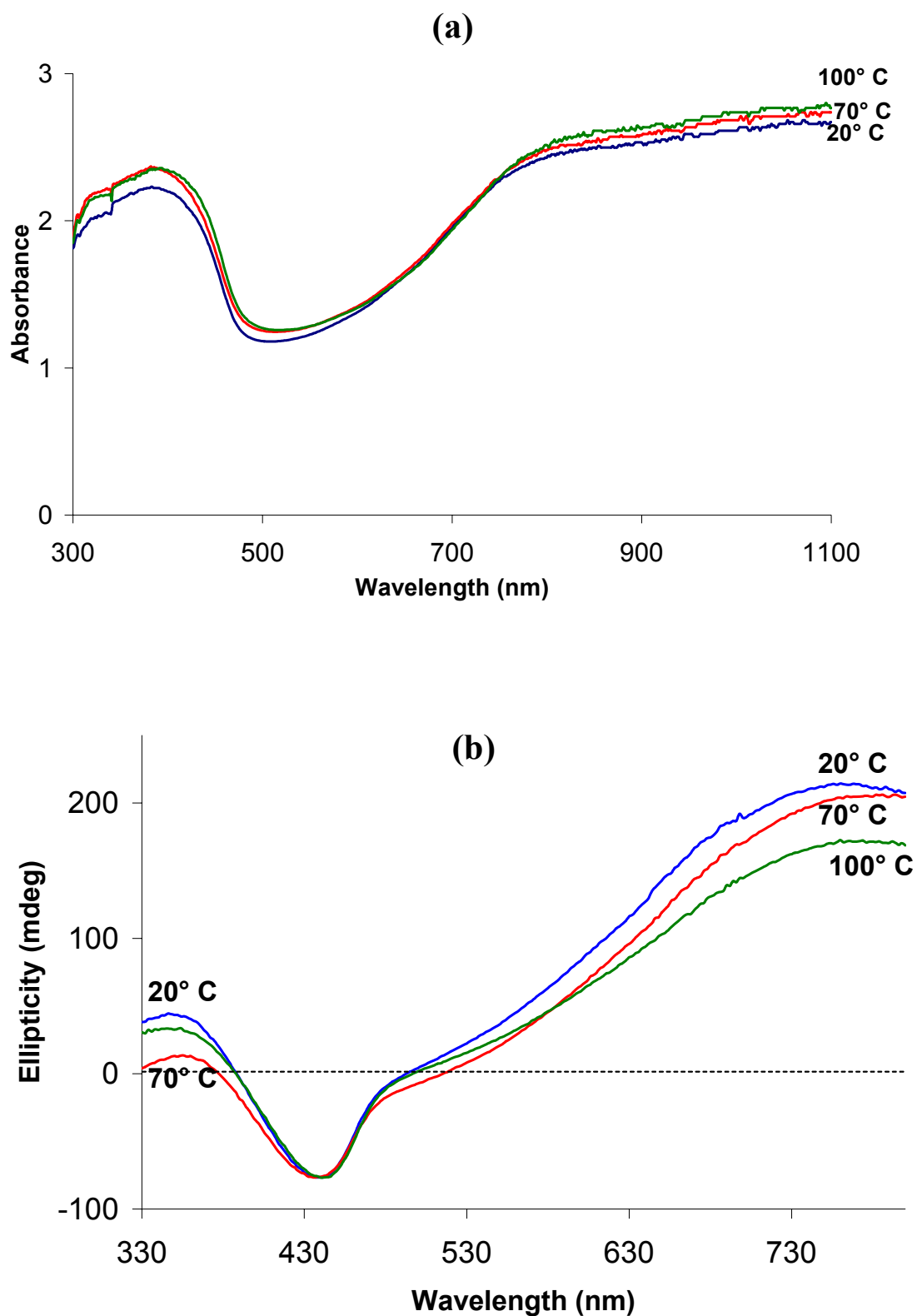
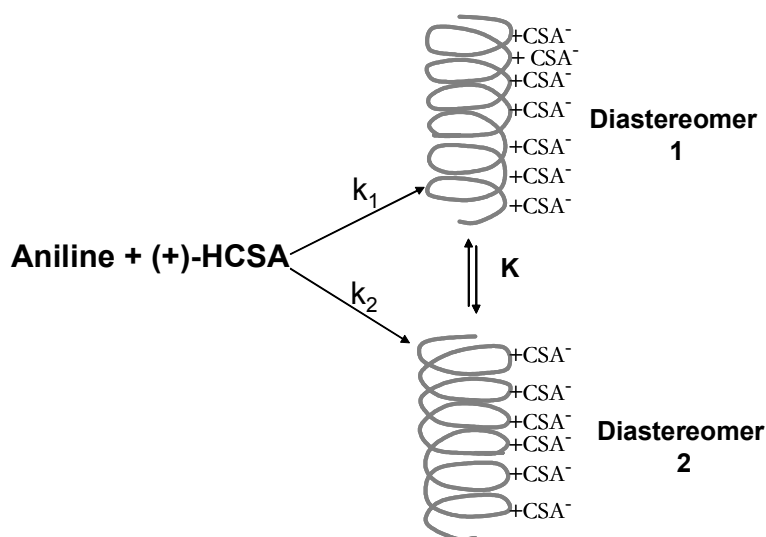


Figure 7.6 UV-visible spectra (a) and CD spectra (b) of a PAn.(+)-HCSA film: (i) as electrochemically deposited at 20°C, (ii) after heating at 70°C for 30 min, and (iii) after further heating at 100°C for 30 min.

7.3.4 Explanation for the Temperature Dependent Chiral Discrimination during Electropolymerization

The inverted CD spectra obtained for chiral PAn.(+)-HCSA films grown at different temperatures may be explained in terms of the formation and interconversion of the two diastereomeric emeraldine salt products **1** and **2** shown in Scheme 7.1. These diastereomers possess inverted helices (M and P, respectively) for their polyaniline chains, while sharing a common *S*-configuration for the dopant (+)-CSA⁻ anions. Their CD spectra in the visible region (330-800 nm) should therefore appear mirror imaged (as observed) due to their enantiomeric helical chains, since the chiral (+)-CSA⁻ dopant anions only exhibit CD bands in the UV region (at 193 and 290 nm).

Kinetic discrimination in the attachment of the (+)-CSA⁻ anions to the growing polyaniline chains would lead to an initial preponderance of one of the diastereomers, depending on the relative magnitudes of the two rate constants k_1 and k_2 in Scheme 7.1. However, a relatively low energy barrier to helix-helix (P-M) interconversion is expected for the flexible chains of unsubstituted polyanilines prior to deposition (*vide infra*), leading to facile interconversion of diastereomers **1** and **2** via equilibrium K. Thus, the observed diastereoselection in aniline electropolymerization is expected to be thermodynamically controlled, with the ratio of diastereomeric products **1** and **2** being determined by the magnitude of equilibrium constant K. A strong temperature dependence for the position of equilibrium K would consequently provide a likely rationale for the remarkable temperature effects observed in the current electrosyntheses of chiral PAn.(+)-HCSA salts.



Scheme 7.1

7.3.5 Influence of Polymerization Temperature on the Chemical Reactivity of PAn. (+)-HCSA Salts

It has been recently shown⁴⁵ that chiral PAn.(+)-HCSA salts prepared at room temperature undergo pH and redox switching cycles with retention of conformation/configuration for their polyaniline chains. Similar pH and redox switching experiments have now been carried out on PAn.(+)-HCSA films electrochemically grown at 65°C or 70°C to determine whether the chemical reactivity of such chiral emeraldine salts is affected by the higher temperatures employed in their electrodeposition.

(i) De-doping/Re-doping of a PAn.(+)-HCSA Film

The alkaline (1.0 M NH₄OH) de-doping of a PAn.(+)-HCSA emeraldine salt film, electrochemically deposited at 65°C (Figure 7.7– trace A), generated an emeraldine base (EB) film (Figure 7.7– trace B) exhibiting characteristic absorption bands at 320

and 620 nm. These bands are associated with a benzenoid π - π^* transition and the molecular exciton arising from a quinoid group, respectively. The CD bands observed at 390, 500 and 760 nm for the EB film (Figure 7.8 – trace B) were opposite in sign to those previously reported for an EB film generated⁴⁴ by de-doping PAn.(+)-HCSA electrochemically grown at room temperature. This was anticipated, as the initial PAn.(+)-HCSA films employed had mirror imaged CD spectra.

Re-doping the EB film with 1.0 M HCl regenerated the emeraldine salt form (as PAn.HCl), as shown by the characteristic UV-visible spectrum in Figure 7.7 – trace C (λ_{max} *ca.* 390, 800 (weak shoulder) and > 1100 nm). The corresponding CD spectrum of the re-doped PAn.HCl film, showing CD bands at *ca.* 340, 445 and 695 nm (Figure 7.8 – trace C), was almost identical to that of the film prior to alkaline de-doping. This confirmed retention of the polyaniline chain conformation/configuration during the de-doping/re-doping cycle shown in Scheme 7.2. Further alkaline (1.0 M NH₄OH) de-doping of the regenerated PAn.HCl film generated an emeraldine base film that exhibited UV-visible and CD spectra (Figure 7.7 and 7.8 – trace D, respectively) effectively identical to the EB produced in the initial alkaline de-doping.

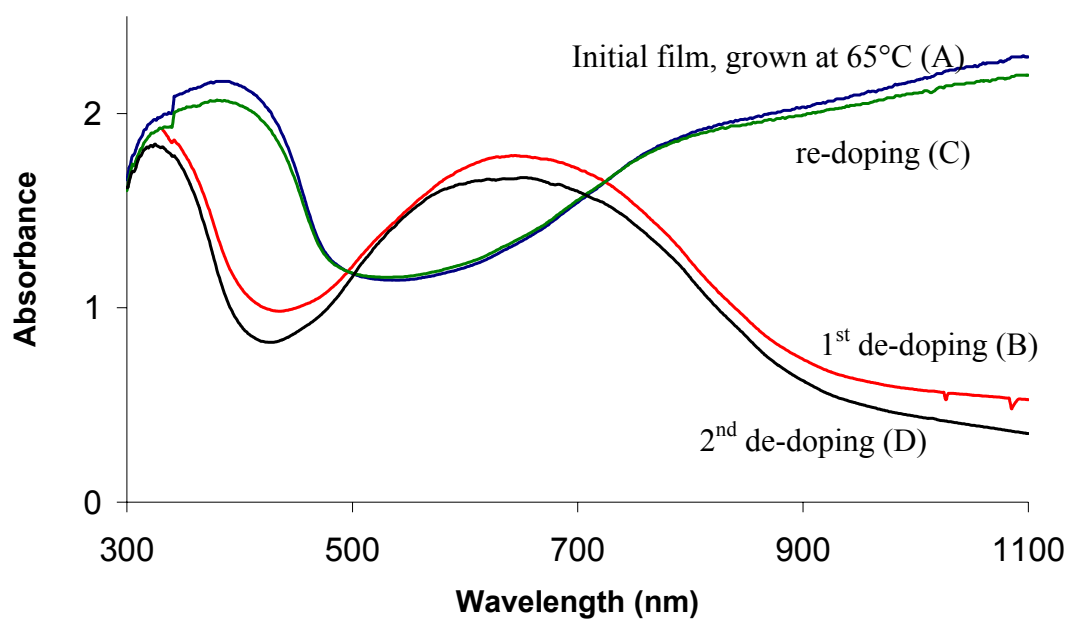


Figure 7.7 UV-visible spectra of: (A) initial PAN.(+)-HCSA film electrochemically deposited at 65°C, (B) after de-doping with 1.0 M NH_4OH , (C) after re-doping with 1.0 M HCl, and (D) after further de-doping with 1.0 M NH_4OH .

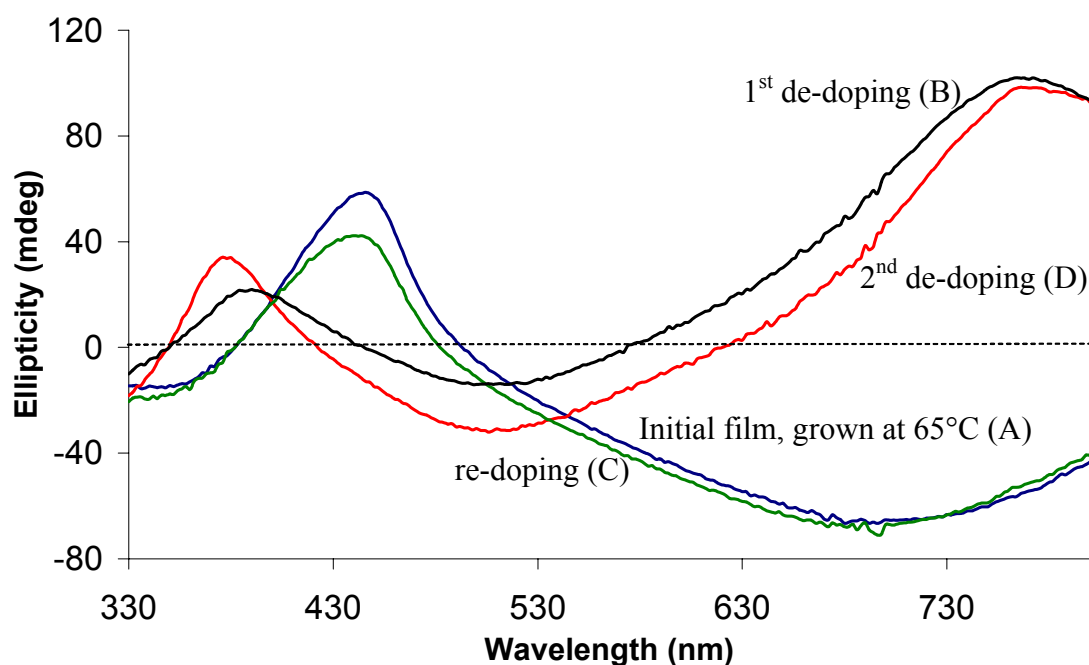
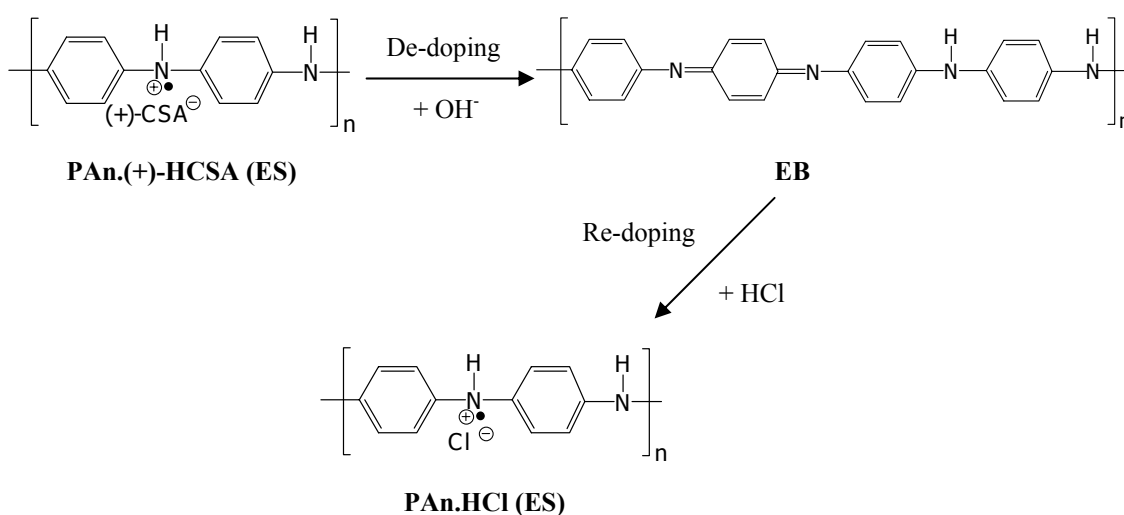


Figure 7.8 CD spectra of: (A) initial PAN.(+)-HCSA film electrochemically deposited at 65°C, (B) after de-doping with 1.0 M NH_4OH , (C) after re-doping with 1.0 M HCl, and (D) after further de-doping with 1.0 M NH_4OH .

The retention of optical activity and polyaniline chain conformation during the repeated release (alkaline de-doping) and re-attachment (acid re-doping) of the dopant anion presumably arises from constraints in the solid state preventing rearrangement of the polymer chains. However, dissolution of an optically active emeraldine base film in an organic solvent such as *N*-methylpyrrolidinone resulted in rapid racemization, as evidenced by the loss of all CD signals (data not shown). This is consistent with the relatively facile helix-helix (P to M) interconversion expected for unsubstituted polyaniline chains in solution, as proposed in the temperature dependence studies above.



Scheme 7.2

(ii) Chemical Reduction and Oxidation of a PAn.(+)-HCSA Film

In order to confirm that no further structural changes in a PAn.(+)-HCSA film occurred after electrodeposition at high temperature, the chiroptical properties of reduced and oxidized polyaniline film grown at 70°C were investigated. Immersion of a PAn.(+)-HCSA film grown at 70°C in aqueous 0.2 M hydrazine generated a leucoemeraldine base (LB) film exhibiting a characteristic π - π^* absorption band at *ca.*

300-350 nm⁴⁵ (Figure 7.9 – trace B), similar to the LB film generated via analogous reduction of a PAn.(+)-HCSA film electrodeposited at room temperature.⁴⁴ However, its CD spectrum (Figure 7.10 – trace B) was the inverse of that previously reported⁴⁴ for LB generated by reduction of a PAn.(+)-HCSA film grown at room temperature.

Treatment of the LB film in Figure 7.9 with aqueous 0.1 M ammonium persulfate generated a UV-visible spectrum characteristic of fully oxidized pernigraniline base (PB), showing a benzenoid π - π^* transition band at 330 nm and a Peierls gap transition^{45, 46} at *ca.* 540 nm (Figure 7.9 – trace C). Again, the signs of the CD signals at 370, 480, and 800 nm (Figure 7.10 – trace C) were opposite to those previously reported for a PB film obtained by oxidizing PAn.(+)-HCSA polymerized at room temperature.

These results demonstrate that the optical activity of polyaniline films grown at high temperature (70°C) is maintained despite the loss of the chiral (+)-HCSA dopant during reduction to leucoemeraldine base and subsequent oxidation to pernigraniline base.

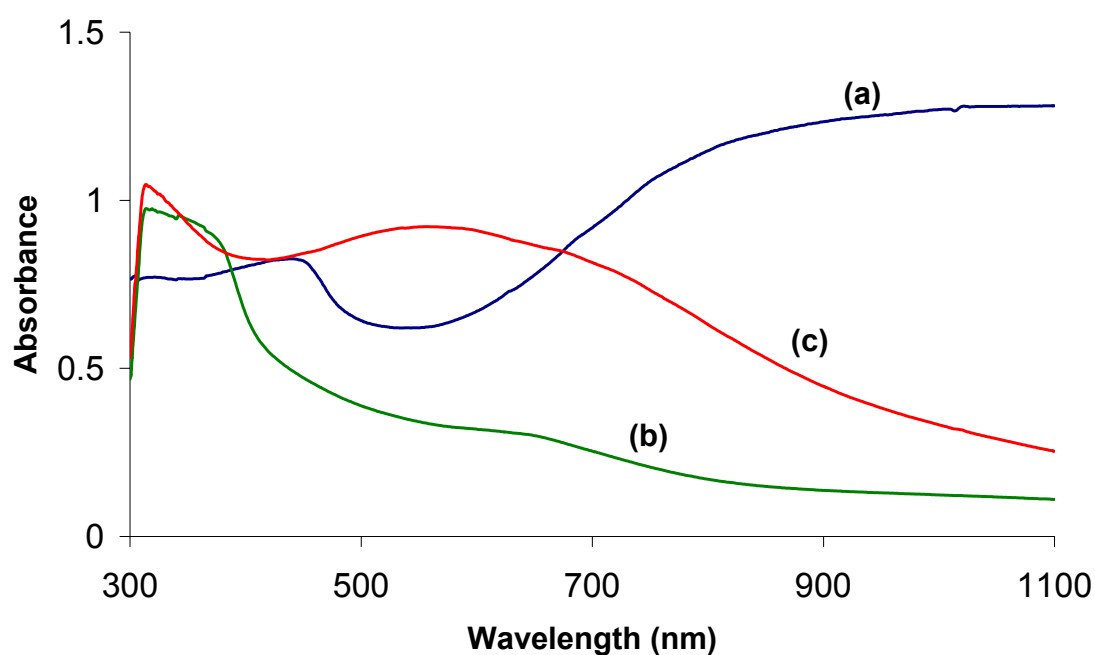


Figure 7.9 UV-visible spectra of a PAN.(+)-HCSA film: (a) as electrodeposited at 70°C, (b) after treatment with 0.2 M N_2H_4 , and (c) after treatment with 0.2 M $(\text{NH}_4)_2\text{S}_2\text{O}_8$.

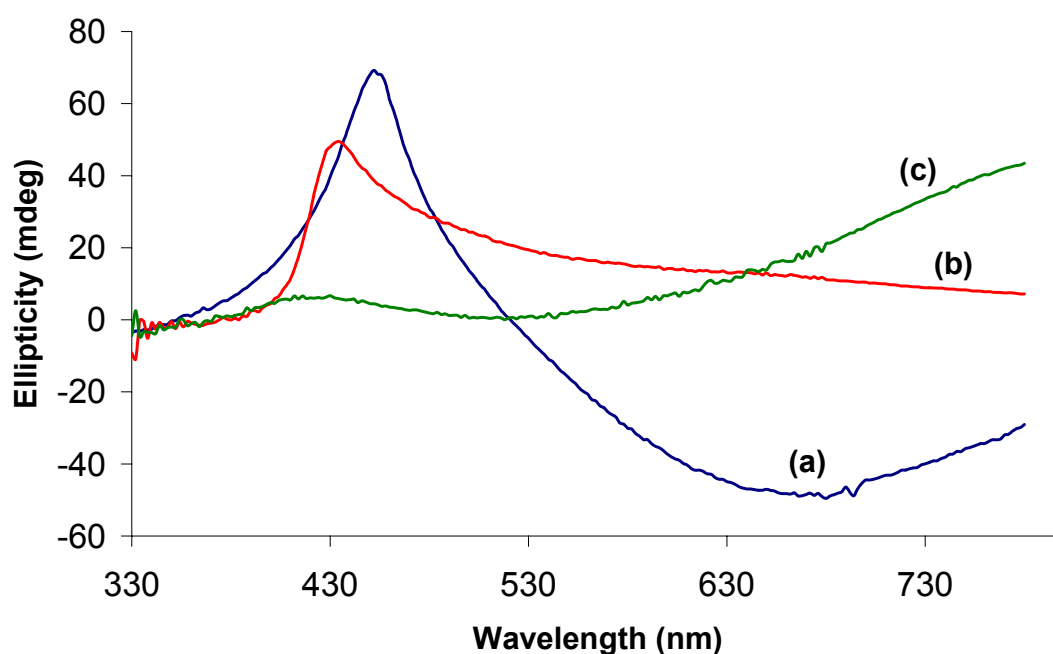


Figure 7.10 CD spectra of a PAN.(+)-HCSA film: (a) as electrodeposited at 70°C, (b) after treatment with 0.2 M N_2H_4 , and (c) after treatment with 0.2 M $(\text{NH}_4)_2\text{S}_2\text{O}_8$ (the same film as shown in Figure 7.9).

7.4 Conclusions

The temperature of electropolymerization is shown to have a critical effect upon the chiroptical properties of PAn.(+)-HCSA emeraldine salt films deposited on ITO-Pt-coated glass. The CD spectra of such films grown at 35°-70°C are the mirror image of those deposited at room temperature or lower. This unprecedented behaviour is rationalized in terms of a temperature-induced interconversion between two diastereomeric emeraldine salt products during the growth of the polyaniline chains doped with the chiral (+)-CSA⁻ anion. This is facilitated by the relatively low energy barrier to helix inversion in unsubstituted polyaniline chains.

This chiral discrimination has been shown to occur either prior or during electrodeposition on the working electrode, since post-deposition heat treatment up to 100°C does not significantly alter the UV-visible or CD spectra of the PAn.(+)-HCSA films. That is, the polyaniline chains are not able to rearrange between enantiomeric helical forms in the solid state.

The temperature of electropolymerization, in contrast, has no significant effect on the morphology of deposited PAn.(+)-HCSA films over the temperature range studied (0°- 65°C).

The optical activity of polyaniline films electrodeposited at high temperature (65°- 70°C) is retained upon redox switching to leucoemeraldine or pernigraniline base, despite the loss of (+)-HCSA dopant during the redox processes. Similar maintenance of optical activity occurs for such polyaniline films upon alkaline de-doping to emeraldine base and subsequent re-doping with HCl. This stability of the polymer conformation/configuration for electrodeposited PAn.(+)-HCSA films is believed to

arise from constraints in the solid state preventing rearrangement of the polymer chains during the chemical treatments.

The marked temperature dependence of the chiroptical properties of electrochemically grown PAn.(+)-HCSA films highlights the importance of employing a fixed temperature during the electrosynthesis of optically active polyanilines.

7.5 References

1. M.R. Majidi, L.A.P. Kane-Maguire, and G.G. Wallace, *Polymer*. **35** (1994): 3113.
2. M.R. Majidi, L.A.P. Kane-Maguire, and G.G. Wallace, *Aust. J. Chem.* **51** (1998): 23.
3. M.R. Majidi, L.A.P. Kane-Maguire, and G.G. Wallace, *Polymer*. **36** (1995): 3597.
4. M.R. Majidi, L.A.P. Kane-Maguire, and G.G. Wallace, *Polymer*. **37** (1996): 359.
5. M. Bodner and M.P. Espe, *Synth. Met.* **135-136** (2003): 403.
6. D.D. Borole, U.R. Kapadi, P.P. Kumbhar, and D.G. Hundiwale, *Materials Letters*. **56** (2002): 685.
7. K. Huang and M. Wan, *Synth. Met.* **135-136** (2003): 173.
8. S.M. Yang and J.T. Chen, *Synth. Met.* **69** (1995): 153.
9. J. Stejskal, A. Riede, D. Hlavata, J. Prokes, M. Helmstedt, and P. Holler, *Synth. Met.* **96** (1998): 55.
10. R. Mazeikiene and A. Malinauskas, *Synth. Met.* **108** (2000): 9.
11. S. Yonezawa, K. Kanamura, and Z. Takehara, *J. Electrochem. Soc.* **140** (1993): 629.
12. J.K. Avlyanov, J.Y. Josefowicz, and A.G. MacDiarmid, *Synth. Met.* **73** (1995): 205.
13. A.G. MacDiarmid and A.J. Epstein, *Synth. Met.* **69** (1995): 85.
14. Y. Xia, J.M. Wiesinger, and A.G. MacDiarmid, *Chem. Mater.* **7** (1995): 443.
15. I.D. Norris, L.A.P. Kane-Maguire, and G.G. Wallace, *Macromolecules*. **31** (1998).
16. V. Egan, R. Bernstein, L. Hohmann, T. Tran, and R.B. Kaner, *Chem. Commun.*, (2001): 801.
17. C. Boonchu, L.A.P. Kane-Maguire, and G.G. Wallace, *Synth. Met.* **135-136** (2003): 241.
18. R.B. Kaner, *Synth. Met.* **125** (2002): 65.
19. H. Guo, C.M. Knobler, and R.B. Kaner, *Synth. Met.* **101** (1999): 44.
20. H. Guo, V. Egan, C.M. Knobler, and R.B. Kaner, *Polymer Preprints*. **40** (1999).
21. B.P.J. de Lacy Costello, M.N. Ratcliffe, and P.S. Sivanand, *Synth. Met.* **139** (2003): 43.
22. L.A.P. Kane-Maguire, M.R. Majidi, and G.G. Wallace, *Polymeric Materials Encyclopedia*. **2** (1996): 1195.
23. Y.-B. Shim, M.-S. Won, and S.-M. Park, *J. Electrochem. Soc.* **137** (1990): 538.
24. R.L. Hand and R.F. Nelson, *J. Electrochem. Soc.* **125** (1978): 1059.
25. W.W. Focke, G.E. Wnek, and Y. Wei, *J. Phys. Chem.* **91** (1987): 5813.
26. D. Orata and D.A. Buttry, *J. Am. Chem. Soc.* **109** (1987): 3574.
27. A. Kabumoto, K. Shinozaki, K. Watanabe, and N. Nishikawa, *Synth. Met.* **26** (1988): 349.
28. S. Patil, J.R. Mahajan, M.A. More, P.P. Patil, S.W. Gosavi, and S.A. Gangal, *Polym. Inter.* **46** (1998): 99.
29. L.H.C. Mattoso, A.G. MacDiarmid, and A.J. Epstein, *Synth. Met.* **68** (1994).
30. M.M. Bouman and E.W. Meijer, *Adv. Mater.* **7** (1995): 385.
31. B.M.W. Langeveld-Voss, E. Peeters, R.A.J. Janssen, and E.W. Meijer, *Synth. Met.* **84** (1997): 611.
32. B.M.W. Langeveld-Voss, M.P.T. Christiaans, R.A.J. Janssen, and E.W. Meijer, *Macromolecules*. **31** (1998): 6702.
33. S. Mahadevan and M. Palaniandavar, *Chem. Commun.*, (1996): 2547.
34. J. Watanabe, S. Okamoto, K. Satoh, K. Sakajiri, H. Furuya, and A. Abe, *Macromolecules*. **29** (1996): 7084.

-
35. K. Sakajiri, K. Satoh, S. Kawaguchi, and J. Watanabe, *J. Mol. Struct.* **476** (1999): 1.
 36. K.S. Cheon, J.V. Selinger, and M.M. Green, *Angew. Chem. Int. Ed.* **39** (2000): 1482.
 37. K. Tang, M.M. Green, K. Cheon, J.V. Selinger, and B.A. Garetz, *J. Am. Chem. Soc.* **125** (2003): 7313.
 38. E. Yashima, J. Maeda, and O. Sato, *J. Am. Chem. Soc.* **123** (2001): 8159.
 39. H. Nakako, R. Nomura, and T. Masuda, *Macromolecules.* **34** (2001): 1496.
 40. J. Tabei, R. Nomura, and T. Masuda, *Macromolecules.* **36** (2003): 573.
 41. J. Tabei, R. Nomura, F. Sanda, and T. Masuda, *Macromolecules.* **37** (2004): 1175.
 42. M. Fujiki, *J. Am. Chem. Soc.* **122** (2000): 3336.
 43. A. Teramoto, K. Terao, Y. Terao, H. Nakashima, T. Sato, and M. Fujiki, *J. Am. Chem. Soc.* **123** (2001): 12303.
 44. L.A.P. Kane-Maguire, I.D. Norris, and G.G. Wallace, *Synt. Met.* **101** (1999): 817.
 45. W.S. Huang and A.G. MacDiarmid, *Polymer.* **34** (1993): 1833.
 46. J.E. Albuquerque, L.H.C. Mattoso, D.T. Balogh, R.M. Faria, J.G. Masters, and A.G. MacDiarmid, *Synth. Met.* **113** (2000): 19.

Chapter 8

Electrochemical Preparation of Chiral Polyaniline in Ionic Liquids

8.1 Introduction

Chiral polyaniline doped with one hand of 10-camphorsulfonic acid (HCSA) can be readily synthesized via the diastereoselective electropolymerization of aniline in an aqueous solution containing (+)- or (-)-HCSA by using potentiodynamic, potentiostatic and galvanostatic techniques.^{1, 2} An acidic aqueous solution is generally used to improve the solubility of aniline monomer in water, and because the electroactive and conductive polyaniline emeraldine salt films are only generated when the pH is less than 3.³⁻⁶ Undesirable N-N bonds characteristic of “head-to-head” coupling have been reported for the polymers electrodeposited at pH > 3.^{3, 7} These unusual bonds interrupt the conjugation length of the polymer backbone,³ leading to low conductivity of the polymer product.

However, a major disadvantage of using aqueous acid media for aniline polymerization is the degradation of the polyaniline product during^{8, 9} and after¹⁰⁻¹² growth. Anodic degradation of polyaniline in acid aqueous solution occurs even at low potentials (0.3 V¹¹-0.5 V¹²) and the degradation rate is faster at higher positive potentials.¹¹ The main products of degradation are *p*-benzoquinone and hydroquinone-type compounds.^{8, 10}

It has been reported that the stability of polyaniline can be extended to higher potential values in non-aqueous media.¹³⁻¹⁵ For some applications when polyaniline is used in non-

aqueous media it is possible to synthesize polyaniline from aqueous acidic solution and then to dry it before use.^{13, 15, 16} However, trace amounts of water trapped in the structure between the polymer chains via hydrogen/covalent bonding¹⁷ are sufficient to induce degradation when polyaniline grown in aqueous solution is used in non-aqueous solutions.¹³

Therefore, to avoid the degradation encountered in aqueous solutions, the electrochemical polymerization of aniline in non-aqueous solvents has been investigated. Most of these studies to date used common organic solvents such as propylene carbonate (PC),^{14, 18, 19} acetonitrile (MeCN),^{14, 18, 20, 21} ethylene carbonate and 1,2-dimethoxyethane (DME)¹⁴ containing supporting electrolyte and aniline monomer with a very strong organic acid (trifluoroacetic acid, CF_3COOH)^{14, 19, 20} or anilinium tetrafluoroborate^{18, 21} as polymerization solutions to prepare electroactive polyaniline.

However, some disadvantages of conventional organic solvents are low solubility of electrolyte salt, flammability and high volatility. Moreover, electro-inactive materials were obtained from electropolymerization of aniline in PC containing LiClO_4 ²² or DME containing LiClO_4 and CF_3COOH .¹⁹ Therefore, ionic liquids (ILs) might provide ideal electrolytes for electrochemical preparation of polyaniline because of their excellent properties such as high ionic conductivity, low volatility, large potential window, unique solvent properties, and thermal and chemical stability.²³⁻²⁸

Recently, several papers have described the preparation of conducting polymers via electrochemical polymerization of the appropriate monomer in ionic liquids, for development of these materials in a variety of applications. Electrochemical synthesis of

polypyrrole have been carried out in AlCl_3/N -1-butylpyridinium chloride,²⁹ 1-ethyl-3-methylimidazolium triflate,³⁰ 1-ethyl-3-methylimidazolium bis(trifluoromethanesulfonyl)imide (EMI-TFSI), 1-butyl-3-methylimidazolium hexafluorophosphate (BMI- PF_6), and *N,N*-butylmethypyrrolidinium bis(trifluoromethanesulfonyl)imide (P_{14} -TFSI).³¹ The morphology and electrochemical properties of the polypyrrole films obtained depended on the nature of the ionic liquid employed.

Electroactive poly(3-(4-fluorophenyl)thiophene) (PFPT) film has been electrochemically synthesized in 1-ethyl-2,3-dimethylimidazolium bis(trifluoromethanesulfonyl)imide (EDMI-TFSI) and 1,3-diethyl-5-methylimidazolium bis(trifluoromethanesulfonyl)imide (DEMI-TFSI). The PFPT grown in the ionic liquids was similar to that synthesized in tetraethylammonium tetrafluoroborate/acetonitrile, but slower ion insertion kinetics and rapid loss of electroactivity of the polymer were observed.³² In contrast, impressive enhancement of electrochemical stability and fast redox switching speeds of poly(3,4-ethylenedioxythiophene) (PEDOT) film grown in 1-butyl-3-methylimidazolium tetrafluoroborate (BMI- BF_4) has been reported.³³

The use of ionic liquids for the preparation of electroactive polyaniline was first reported in 1991 by Tang and Osteryoung.³⁴ However, the ionic liquid used, AlCl_3 -1-ethyl-3-methylimidazolium chloride was environmentally unstable due to the high moisture sensitivity of the anion the ionic liquid. Recently, electrodeposition of polyaniline in 1-butyl-3-methylimidazolium tetrafluoroborate (BMI- BF_4), an environmentally stable ionic liquid, containing 0.5 M aniline and 2.0 M trifluoroacetic acid (CF_3COOH) was investigated by Lu *et al.*³³ The spectacular stability of the polyaniline grown in this ionic liquid was

demonstrated by potential cycling for up to 1 million cycles without a significant decrease in electroactivity in the ionic liquid. However, a high concentration of a strong and harmful acid was used.

In the present study, the utilization of four ionic liquids, 1-butyl-3-methylimidazolium hexafluorophosphate (BMI-PF₆), 1-butyl-3-methylimidazolium tetrafluoroborate (BMI-BF₄), 1-ethyl-3-methylimidazolium bis(trifluoromethanesulfonyl)imide (EMI-TFSI), and *N,N*-methylpropylpyrrolidinium bis(trifluoromethanesulfonyl)imide (P₁₃-TFSI) as solvent and electrolyte for electrochemical polymerization of aniline in the presence of (+)-10-camphorsulfonic acid {(+)-HCSA} has been investigated. One hand of chiral HCSA was used with the aim of depositing chiral polyaniline (PAn.(+)-HCSA), on the working electrode. The resultant chiral electrode should have significant potential for use in the asymmetric electrosynthesis of organic compounds in ionic liquids. Also explored in this Chapter is the possible use of the recently prepared³⁵ chiral ionic liquid (-)-MBEA-TFSI for the preparation of chiral polyaniline from racemic HCSA.

8.2 Experimental

8.2.1 Electrochemical Synthesis of Polyanilines in Ionic Liquids

Polyanilines were electrochemically synthesized by the potentiostatic and potentiodynamic methods. Either room temperature or higher temperatures (50-65°C) were used, depending on the solubility of HCSA in the ionic liquid employed. The polymerizations were carried out at high temperature in solutions of 0.2 M aniline/0.5 M (+)-HCSA in the ionic liquids EMI-TFSI, BMI-PF₆, P₁₃-TFSI or BMI-BF₄; while the synthesis of polyaniline in (-)-MBEA-TFSI containing 0.2 M aniline/0.7 M (±)-HCSA was performed at room

temperature. The polymerization solutions were degassed by purging with N₂ and maintained at a set temperature by heating the electrochemical cell on a thermostatted hot plate and stirring the polymerization solution with a magnetic stirrer.

The electrochemical polymerizations were performed in a one-compartment cell using the three electrode configuration as described in Chapter 2.

8.2.2 Spectroscopic Characterization

UV-visible and CD Spectral Measurements

UV-visible and circular dichroism (CD) spectra of the polymer films or solutions were recorded using procedures described in Chapter 2.

Raman Studies

Raman spectra of the polyaniline films were recorded using procedures described earlier in Chapter 2.

8.2.3 Electrochemical Characterization

After washing the polymer films with methanol to remove excess reactants, oligomers and ionic liquid, the cyclic voltammograms were carried out at room temperature in aqueous 1.0 M (+)-HCSA or 1.0 M HCl employing procedures described earlier in Chapter 2.

8.2.4 Surface Studies

Morphology and surface studies were performed using a Scanning Electron Microscopy and Contact Mode Atomic Force Microscopy (CAFM) using procedures described earlier in Chapter 2.

8.3 Results and Discussion

8.3.1 Cyclic Voltammetry during Potentiodynamic Synthesis of Polyaniline in Aqueous Solution and in Ionic Liquids

8.3.1.1 Electropolymerization in Aqueous Solution

Initially, for comparative purposes, PAn.(+)-HCSA was potentiodynamically grown on a glassy carbon electrode (surface area = 0.07 cm²) at room temperature in aqueous 0.2 M aniline/1.0 M (+)-HCSA by sweeping the potential from -0.2 to +0.9 V. Cyclic voltammograms recorded during the growth of the polymer are shown in Figure 8.1. Oxidation of aniline monomer to the radical cation commences at *ca.* +0.9 V, as observed in the first scan. The significant increase in current response observed in successive cycles indicates that electrochemically active polyaniline was depositing on the working electrode. The CVs showed two main anodic peaks at *ca.* +0.20 and +0.75 V assigned as the oxidation from leucoemeraldine to emeraldine and emeraldine to pernigraniline, respectively. Two main cathodic peaks were also observed: a peak at *ca.* +0.65 V corresponding to reduction of pernigraniline to emeraldine, and a peak at *ca.* 0.0 V corresponding to reduction of emeraldine to leucoemeraldine.

A small peak observed between the two main oxidation peaks has been called the “middle peak” by many researchers. The “middle peak” was more pronounced when the potential range employed was extended to more positive potentials. Three main interpretations have been proposed for this middle peak observed during growth or after growth of polyaniline: (i) cross-linking between polyaniline chains yielding phenazine type structures,³⁶⁻³⁸ (ii) coupling in the *ortho*-position yielding branching polyaniline,^{39, 40} and (iii) degradation

products (benzoquinone/hydroquinone type compounds) of polyaniline generated at high positive potentials.^{8,9}

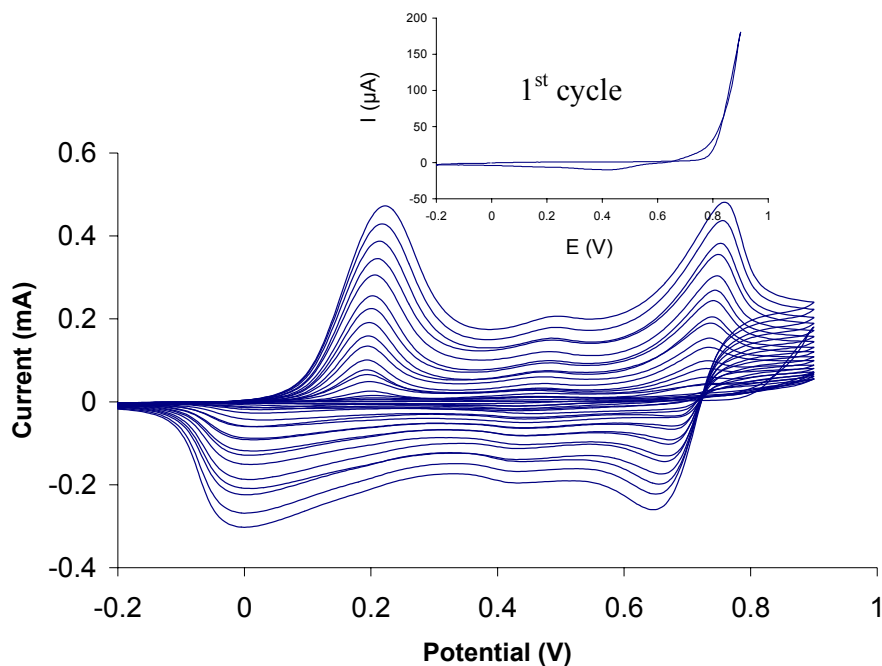


Figure 8.1 Cyclic voltammograms during the potentiodynamic growth of a PAn.(+)-HCSA film on a glassy carbon electrode (surface area = 0.07 cm²) in aqueous 0.2 M aniline/0.5 M (+)-HCSA. Temp 20°C, scan rate 50 mV/s. Potentials vs. Ag/AgCl (3 M NaCl).

8.3.1.2 Electropolymerization in Achiral Ionic Liquids

These studies were initiated by recording cyclic voltammograms during polyaniline growth at a glassy carbon electrode from a solution of 0.2 M aniline/0.5 M (+)-HCSA in the ionic liquid BMI-BF₄. Polymerization at 50-55°C was required due to the very low solubility of HCSA in the ionic liquid at room temperature. Cyclic voltammograms obtained over the potential ranges of - 0.2 to 1.0, - 0.2 to 1.1, and - 0.2 to 1.2 V are presented in Figures 8.2a, 8.2b, and 8.2c, respectively. The initial oxidation of aniline to its radical cation occurs at *ca.* +1.0 V in each case, as shown by the associated anodic current response observed on

the first scans. The current increased with successive scans indicating the formation of an electroactive polymer on the working electrode. When the potential was scanned to more positive values, the anodic and cathodic current responses were seen to increase rapidly. This means more polymers were deposited on the electrode for each scan.

The features of the CVs in Figures 8.2a-c are similar to that previously observed for polyaniline growth from aqueous acid solution. The two main oxidation peaks associated with the oxidation of leucoemeraldine to emeraldine and emeraldine to pernigraniline were observed at *ca.* + 0.45 and + 0.90 V, respectively, in the ionic liquid. During the cathodic sweep, the two main peaks attributed to reduction of pernigraniline to emeraldine and emeraldine to leucoemeraldine were observed at + 0.85 and + 0.30 V, respectively. The “middle peak” at *ca.* 0.70 V for the anodic sweep and at *ca.* 0.65 V for the cathodic sweep was again observed, and was stronger when the potential range employed was extended to higher potentials (Figures 8.2b and 8.2c). The origin of this middle peak will be discussed latter.

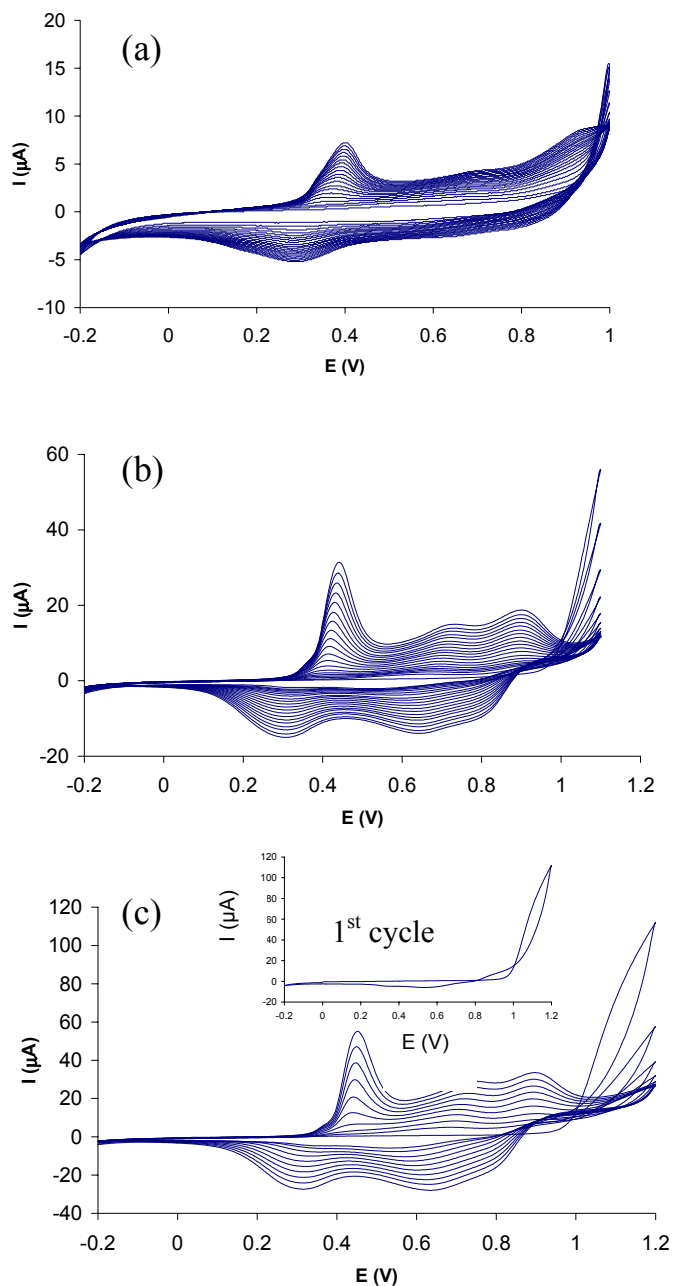


Figure 8.2 Cyclic voltammograms during the potentiodynamic synthesis of PAN.(+)-HCSA films on a GC- electrode (surface area = 0.07 cm^2) in BMI- BF_4 containing 0.2 M aniline/0.5 M (+)-HCSA. Temp 50-55°C, scan rate 50 mV/s. (a) potential range -0.2 to 1.0 V (b) potential range, -0.2 to 1.1 V, (c) potential range, -0.2 to 1.2 V. Potentials vs. $\text{Ag}/\text{AgCl}_{(\text{EMI-TFSI})}$.

Subsequently, three other ionic liquids, namely BMI-PF₆, EMI-TFSI and P₁₃-TFSI, were used as solvent and electrolyte for the growth of polyaniline in the presence of (+)-HCSA. The CVs recorded during potentiodynamic synthesis of polyaniline at 50-55°C from solutions of 0.2 M aniline/0.5 M (+)-HCSA in these ionic liquids are shown in Figures 8.3-8.5. These exhibited similar features to those previously obtained in BMI-BF₄ (Figure 8.2). Two main redox couples corresponding to the conversion of leucoemeraldine to emeraldine and emeraldine to pernigraniline were again observed. However, the peak potentials were slightly shifted, as summarized in Table 8.1. The current responses in Figures 8.3-8.5 confirmed that electroactive polymers were deposited on the working electrode in each case, while the deposition efficiency was seen to increase in the order BMI-BF₄ > BMI-PF₆ > EMI-TFSI > P₁₃-TFSI.

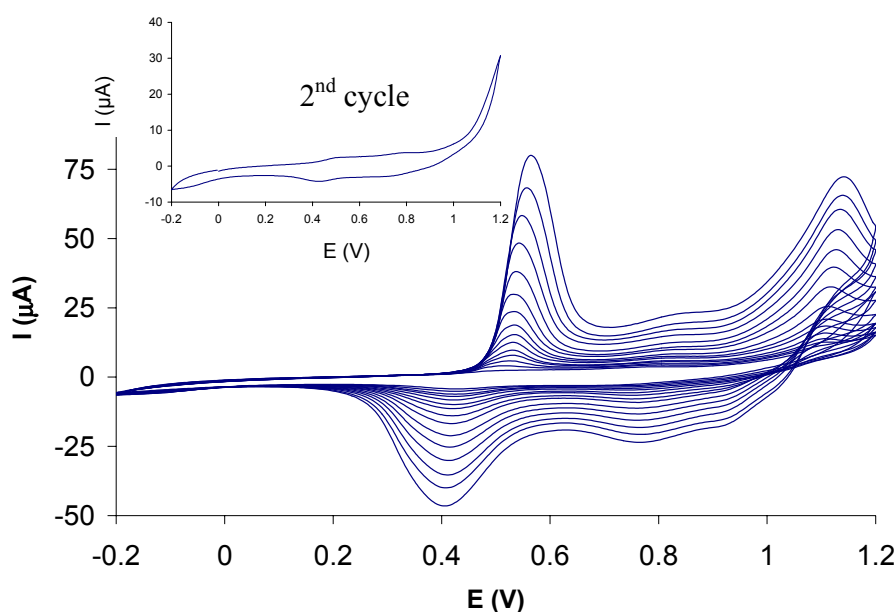


Figure 8.3 Cyclic voltammograms during the potentiodynamic growth of a PAn.(+)-HCSA film on a glassy carbon electrode (surface area = 0.07 cm²) in BMI-PF₆ containing 0.2 M aniline/0.5 M (+)-HCSA. Temp 50-55°C, scan rate 50 mV/s. Potentials vs. Ag/AgCl (EMI-TFSI).

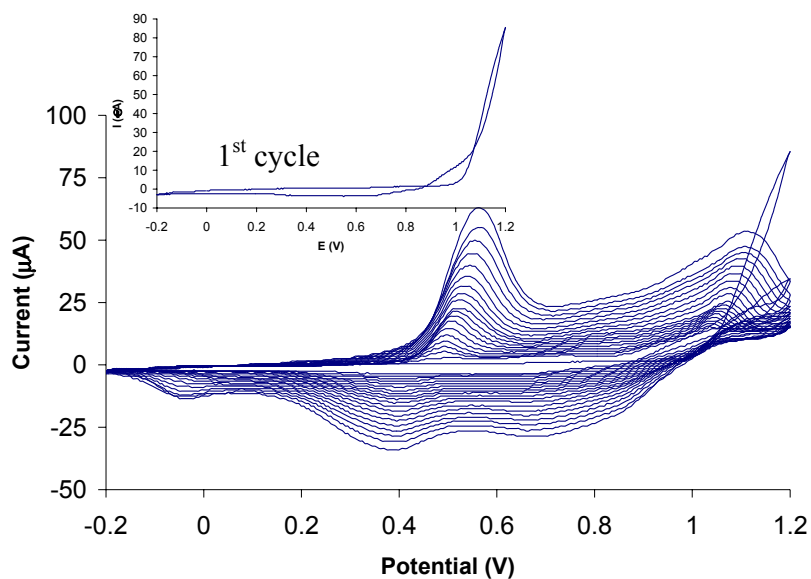


Figure 8.4 Cyclic voltammograms during the potentiodynamic growth of a PAn.(+)-HCSA film on a glassy carbon electrode (surface area = 0.07 cm²) in BMI-PF₆ containing 0.2 M aniline/0.5 M (+)-HCSA at 50-55°C. Scan rate = 50 mV/s.

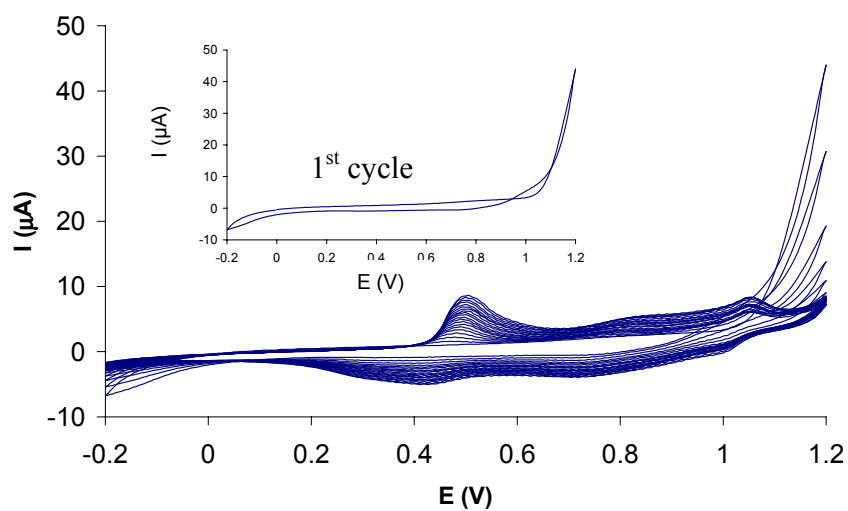


Figure 8.5 Cyclic voltammograms during the potentiodynamic growth of a PAn.(+)-HCSA film on a glassy carbon electrode (surface area = 0.07 cm²) in P₁₃-TFSI containing 0.2 M aniline/0.5 M (+)-HCSA at 50-55°C. Scan rate = 50 mV/s.

8.3.1.3 Electropolymerization in a Chiral Ionic Liquid

The possibility of preparing an optically active polyaniline by using a chiral ionic liquid as the electrolyte was then explored. For this study, the chiral ionic liquid (-)-MBEA-TFSI, recently prepared in our laboratory (see Chapter 9), was employed.

Cyclic voltammograms obtained during polyaniline growth from a solution of 0.2 M aniline/0.7 M (\pm)-HCSA in the ionic liquid (-)-MBEA-TFSI were recorded at room temperature. This low temperature could be used due to the high solubility of HCSA in this chiral ionic liquid. Significantly, no current response due to polymerization was observed when the potential was scanned between - 0.2 and + 1.2 V. When the potential range -0.2 to +1.3 V was used, Figure 8.6 revealed that some electropolymerization occurred, but of low efficiency. The two redox couples characteristic of polyaniline were seen, together with a relatively strong “middle peak”. The prominent middle peak suggests a high rate of polymer degradation. The degradation of a PAn.(+)-HCSA at >1.1 V has been observed in MBEA-TFSI (see Chapter 9). The accumulation of degradation products at the reaction sites probably interrupts the polymer growth.

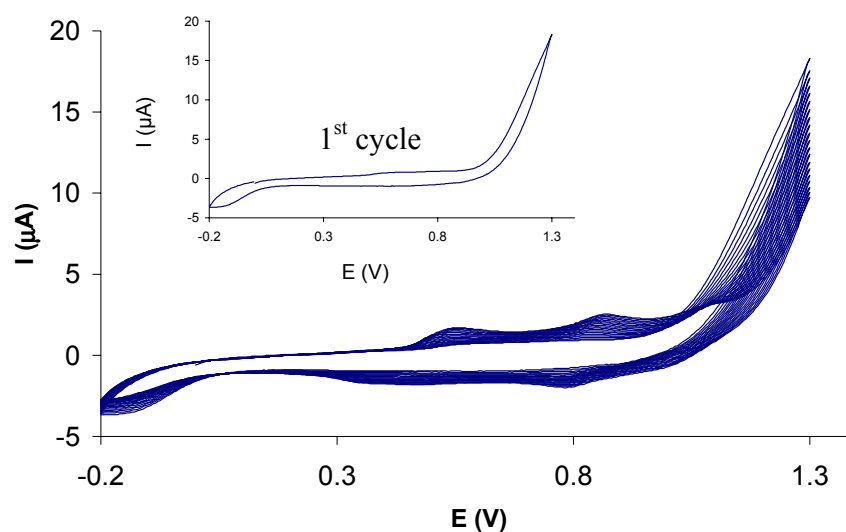


Figure 8.6 Cyclic voltammograms on a glassy carbon electrode (surface area = 0.07 cm²) recorded for 0.2 M aniline/0.7 M (±)-HCSA in (-)-MBEA-TFSI at 20°C; scan rate 50 mV/s, 20 cycles. Potentials vs. Ag/AgCl_(EMI-TFSI).

Table 8.1 Influence of ionic liquids employed on the redox peaks observed in cyclic voltammograms during polyaniline growth. Scan rate = 50 mV/s. [Aniline] = 0.2 M, [(+)-HCSA] = 0.5 M. Temp. 50-55°C.

Ionic Liquid	Anodic Peaks (V)		Cathodic Peaks (V)	
	leucoemeraldine to emeraldine	emeraldine to pernigraniline	pernigraniline to emeraldine	emeraldine to leucoemeraldine
BMI-BF ₄	0.45	0.90	0.85	0.3
BMI-PF ₆	0.55	1.1	0.95	0.4
EMI-TFSI	0.55	1.1	0.85	0.4
P ₁₃ -TFSI	0.50	1.05	1.0	0.45
(-)-MBEA-TFSI*	0.55	1.0	1.0	0.4

* [Aniline] = 0.2 M, [(±)-HCSA] = 0.7 M; at 20°C.

8.3.2 Potentiostatic Preparation of Polyaniline in Ionic Liquids

8.3.2.1 Spectroscopic Characterization of Potentiostatically Prepared Polyaniline

Five different ionic liquids (BMI-BF₄, BMI-PF₆, EMI-TFSI, P₁₃-TFSI and (-)-MBEA-TFSI) were used as solvents and electrolytes for the potentiostatic polymerization of aniline to produce PAn.(+)-HCSA films. In order to study the electronic absorption spectra of the polymer films deposited, ITO-Pt-coated glass was used as the working electrode. Using any of the ionic liquids under investigation, no polymer film was observed to deposit on the ITO-Pt-coated glass electrode when the potential applied was less than +1.2 V. Although the polymerizations in the ionic liquids were carried out at relatively high potentials (+1.2 V) and high temperature (50-55°C), the rate of polymerization was much lower than the reaction rate in acidic aqueous solution at + 0.9 V and 20°C.

PAn.(+)-HCSA Deposited from BMI-BF₄

The UV-visible spectrum of the green film electrodeposited at 50-55°C at 1.2 V from 0.2 M aniline/0.5 M (+)-HCSA in BMI-BF₄ (Figure 8.7a) exhibited absorption bands at *ca.* 350, 450 and 850 nm, characteristic of a polyaniline emeraldine salt. These bands are assigned to π - π^* , polaron- π^* and π -polaron transitions, respectively. The corresponding CD spectrum shown in Figure 8.7b indicated that the PAn.(+)-HCSA electrodeposited in BMI-BF₄ was optically active. The CD band at 425 nm is associated with the absorption band in this region, and the poorly defined CD band at *ca.* 700 nm is associated with the polaron absorption band. The presence of one hand of HCSA in the polymerization mixture is believed to induce a one-handed helical structure on the polymer chains, giving rise to the optical activity. It should be noted that the magnitude of the CD signals observed for

this film is much smaller than generally seen for PAn.(+)-HCSA films obtained from potentiostatic polymerization in aqueous 0.2 M aniline/1.0 M (+)-HCSA. The weak CD signals for the PAn.(+)-HCSA film grown in BMI-BF₄ may arise from competition between chiral (+)-CSA⁻ and achiral BF₄⁻ as the dopant anions incorporated into the polymer during polymerization.

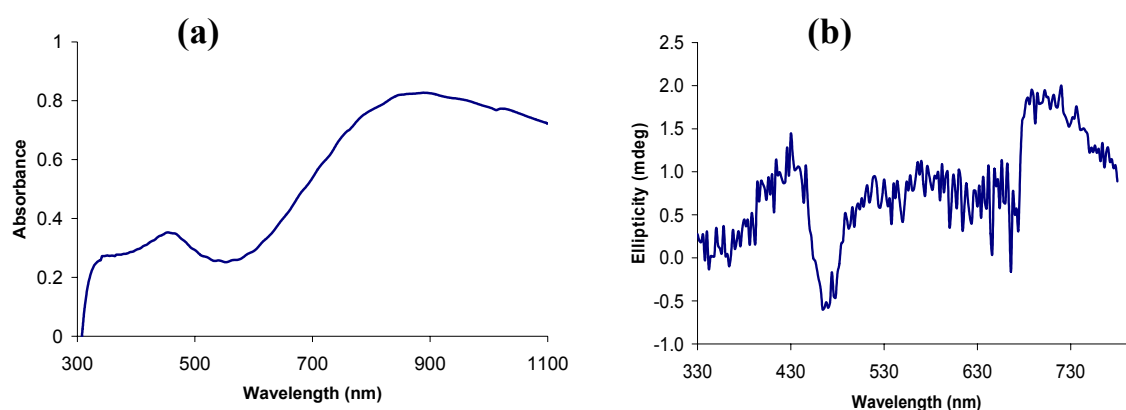


Figure 8.7 (a) UV-vis and (b) CD spectra of a PAn.(+)-HCSA film potentiostatically deposited on ITO-Pt coated glass at 1.2 V from BMI-BF₄ solution containing 0.2 M aniline /0.5 M (+)-HCSA. 120 mC/cm² charge passed, at 50-55°C.

PAn.(+)-HCSA Deposited from BMI-PF₆

The potentiostatic polymerization of aniline (0.2 M) at 1.2 V in BMI-PF₆ at 50-55°C in the presence of 0.5 M (+)-HCSA deposited a green film on the ITO-coated glass electrode. Its UV-visible spectrum (Figure 8.8a) showed bands at *ca.* 350, 450 and 850 nm, assigned as a π - π^* band and low and high wavelength polaron bands, respectively. The spectrum again indicates the formation of an emeraldine salt polyaniline film. The CD spectrum (Figure 8.8b) revealed that the polyaniline film was optically inactive - no CD signals were observed. This may be due to a strong preference for incorporation of achiral PF₆⁻ (from the ionic liquid) into the growing polyaniline chains rather than the chiral (+)-CSA⁻ anion.

The smaller size of the PF_6^- anion may contribute to its easier/faster incorporation as the dopant.

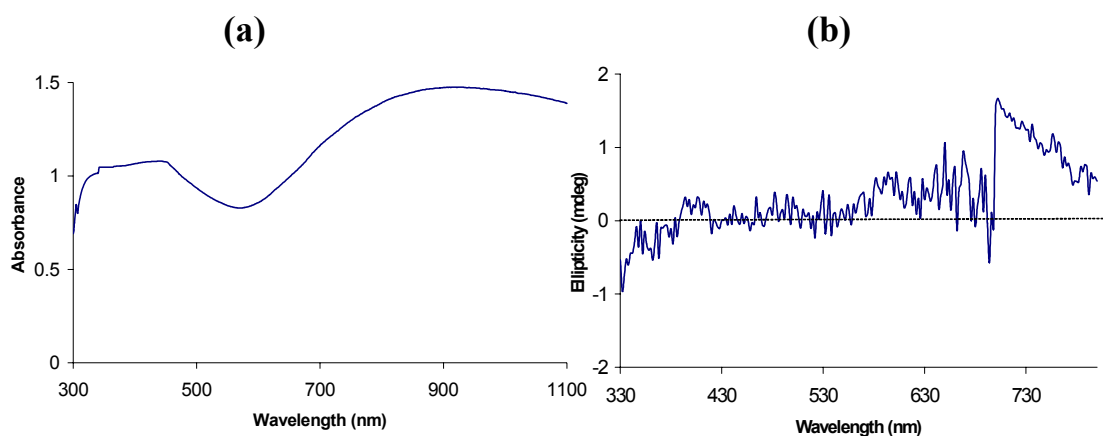


Figure 8.8 UV-visible (a) and CD spectra (b) of a polyaniline emeraldine salt film electrostatically deposited on ITO-Pt-coated glass at 1.2 V from BMI- PF_6 solution containing 0.2 M aniline/0.5 M (+)-HCSA. 120 mC/cm^2 charge passed, at 50-55°C.

PAn.(+)-HCSA Deposited from EMI-TFSI

The UV-visible spectrum (Figure 8.9a) obtained for the green film electrodeposited from 0.2 M aniline/0.5 M (+)-HCSA in EMI-TFSI at 50-55°C again exhibited a UV-vis spectrum typical of a polyaniline emeraldine salt. The corresponding CD spectrum (Figure 8.9b) showed only weak CD bands at *ca.* 440 nm and 720 nm associated with the absorption bands in these regions. This low optical activity is again probably due to competition between chiral (+)- CSA^- and achiral TFSI^- as the dopant anions incorporated into the polymer during polymerization. It should be noted that in this case some polymer dissolved into the solution, probably due to degradation of polyaniline at +1.2 V, as found later in Chapter 9.

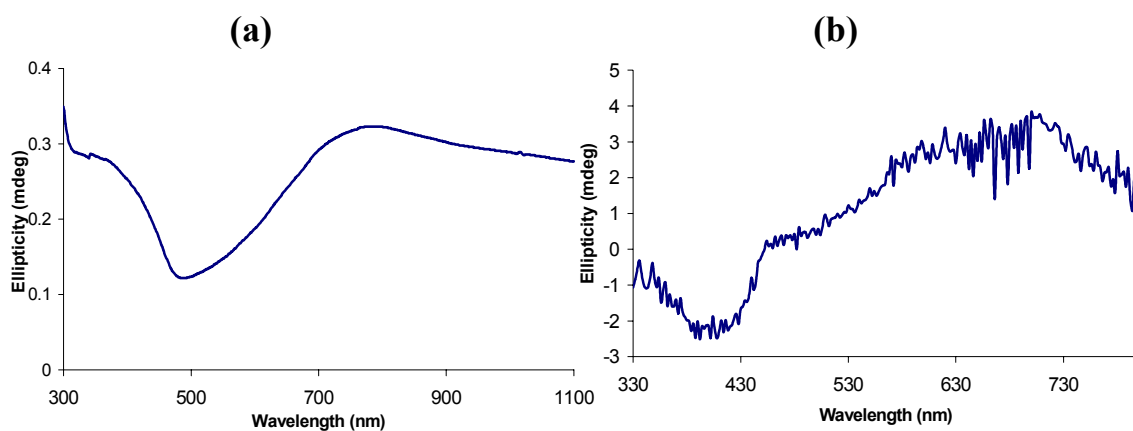


Figure 8.9 UV-visible (a) and CD spectra (b) of an emeraldine salt film electrostatically deposited on ITO-Pt coated glass at 1.2 V from EMI-TFSI solution containing 0.2 M aniline/0.5 M (+)-HCSA. 120 mC/cm² charge passed at 50-55°C.

In an attempt to increase the optical activity of the deposited polyaniline film, the concentration of (+)-HCSA in the polymerization solution was increased from 0.5 M to 1.0 M. Polymerization at higher temperature (65-70°C) was required for dissolution in EMI-TFSI. The UV-visible spectrum of the green emeraldine salt film grown under these condition (Figure 8.10a) exhibited a broad band at *ca.* 350-450 nm attributable to overlapping π - π^* and polaron transitions and a high wavelength polaron band around 750 nm. Interestingly, this polyaniline film has adopted a more “compact coil” conformation than that grown at 50-55°C in 0.5 M (+)-HCSA, as evidenced by the more well-defined polaron band at 750 nm. However, the CD spectrum again showed only weak CD signals, with a negative CD band at *ca.* 440 nm and a positive CD band at *ca.* 700 nm (Figure 8.10b). It was noted that the solution turned green after being used for the electropolymerization of a few polyaniline films, due to some of the polymer dissolving/dispersing into the solution. The absorption spectrum for the solution showed a

shoulder band at *ca.* 400 nm and a distinct band at 800 nm (Figure 8.11), indicating the presence of a “soluble” emeraldine salt oligomer. This suggests that high anodic potentials during polymerization caused significant chain scission (see Section 9.3.5 in Chapter 9).

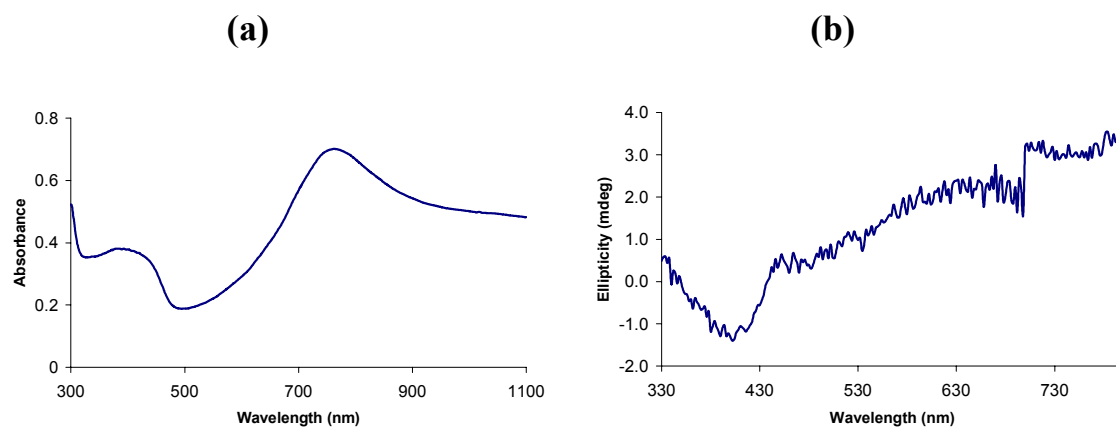


Figure 8.10 (a) UV-visible and (b) circular dichroism spectra of a PAn.(+)-HCSA film potentiostatically deposited on ITO-Pt coated glass at 1.2 V from an EMI-TFSI solution containing 0.2 M aniline/1.0 M (+)-HCSA. 120 mC/cm² charge passed, at 65-70°C.

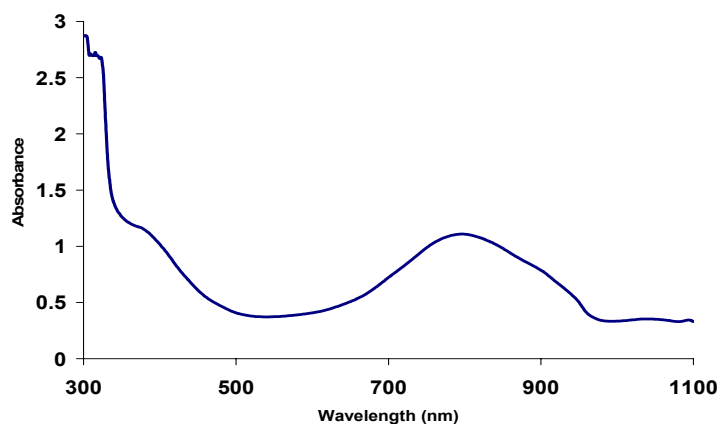


Figure 8.11 UV-visible absorption spectrum of the polymerization solution/dispersion after using for the electrochemical deposition of several polyaniline films at 1.2 V in EMI-TFSI containing 0.2 M aniline/1.0 M (+)-HCSA, at 65-70°C.

PAn.(+)-HCSA Deposited from P₁₃-TFSI

A green emeraldine salt film can also be electrodeposited on an ITO-Pt-coated glass electrode from 0.2 M aniline/0.5 M (+)-HCSA in the ionic liquid P₁₃-TFSI at +1.3 V, 50-55°C. Interestingly, UV-visible and CD spectra characteristic of a “compact coil” conformation were observed for the chiral polyaniline emeraldine salt product (Figure 8.12a). Some of the polymer film dissolved/dispersed into the solution during polymerization, as was observed above with EMI-TFSI as solvent. Non-uniform films deposited on the ITO-Pt-coated glass working electrode and the optical activity of these films was weak (Figure 8.12b).

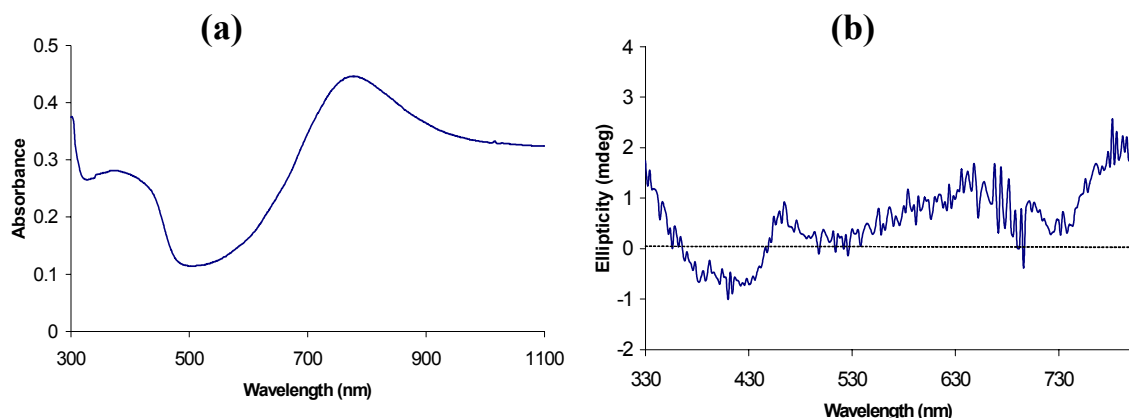


Figure 8.12 UV-visible (a) and CD spectra (b) of a polyaniline film potentiostatically deposited on ITO-Pt coated glass at +1.2 V from P₁₃-TFSI solution containing 0.2 M aniline/0.5 M (+)-HCSA. 120 mC/cm² charge passed, at 50-55°C.

PAn.(+)-HCSA Deposited from Chiral MBEA-TFSI

Electrochemical polymerization of aniline in the chiral ionic liquid (-)-MBEA-TFSI containing 0.2 M aniline/0.7 M racemic (±)-HCSA deposited a green polymer on the ITO-Pt-coated glass working electrode after applying a potential of +1.3 V for several minutes at 20°C. The rate of polymerization was slower than that observed in the other ionic liquids

above. The lower rate of reaction in this chiral ionic liquid may be due to its lower conductivity and/or to the lower polymerization temperature employed.

The green product did not adhere well on the ITO-Pt-coated glass. This may be due to a low molecular weight polymer being produced. The UV-visible spectrum of the polymerization solution/dispersion (Figure 8.13a) was typical of a polyaniline emeraldine salt. The broad bands at 360 and 420 nm are assigned as a π - π^* and polaron- π^* transitions, respectively, while a band at 700-800 nm is attributed to a π -polaron transition. The latter strong and sharp band, without a free carrier tail in near infra-red region, indicates that a “compact coil” polyaniline was produced.

Of particular interest in this experiment was also the possibility that the chiral ionic liquid (-)-MBEA-TFSI solvent employed would induce the formation of a chiral polyaniline product while using racemic HCSA as the potential dopant. However, the CD spectrum of the deposited film (Figure 8.13b) revealed that it was optically inactive. This indicates that asymmetric electrosynthesis of PAn.HCSA cannot be achieved by using the (-)-MBEA-TFSI chiral ionic liquid as both solvent and as chiral inducer. This may be due to only low molecular weight emeraldine salt being formed, as Kane-Maguire *et al.*⁴¹ have reported that the emeraldine salt PAn.(+)-HCSA prepared by doping emeraldine base with (+)-HCSA in NMP was not optically active when low molecular weight emeraldine base/oligomers were used.

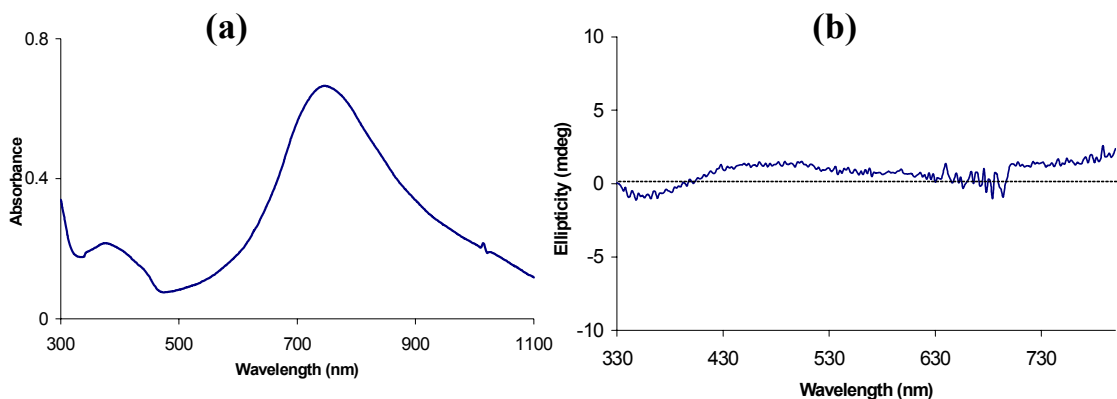


Figure 8.13 (a) UV-visible and (b) CD spectra of an emeraldine salt film potentiostatically synthesized at +1.3 V in (-)-MBEA-TFSI solution containing 0.2 M aniline and 0.7 M (\pm)-HCSA, at 20°C.

8.3.2.2 Raman Studies

In order to further investigate the chemical structure of the above polyaniline films prepared in ionic liquids, Raman spectra were recorded using the excitation line $\lambda_{\text{exc}} = 632.8$ nm. Figure 8.14a shows the Raman spectrum of an emeraldine salt film prepared potentiostatically in aqueous 0.2 M aniline/1.0 M (+)-HCSA (0.9 V, 120 mC/cm², 20°C); while Figures 8.14b-8.14e show the corresponding spectra obtained in various ionic liquids.

The emeraldine salt film prepared in aqueous solution (Figure 8.14a) exhibited peaks in the 1100-1800 cm⁻¹ range at 1170, 1259, 1336, 1511 and 1595 cm⁻¹. This Raman spectrum is in agreement with those previously reported for PAn.HCSA,⁴²⁻⁴⁶ PAn.HCl,⁴⁷⁻⁴⁹ and PAn.HClO₄.⁴⁹ Bands for the dopant anions are hardly visible in this region, as previously reported.⁴⁸

The band at 1170 cm^{-1} assigned to the C-H bending deformation is characteristic for semiquinone structures,^{44, 47, 49} because bands ascribed to C-H bending deformations in quinoid and benzenoid rings appear at 1160 and 1180 cm^{-1} , respectively.⁴⁷ The broad band at $1215\text{-}1255\text{ cm}^{-1}$ corresponds to the C-N stretching mode of the polaron units.^{47, 49} A band characteristic of localized polarons⁴² was observed as a broad signal at *ca.* 1336 cm^{-1} . The 1484 cm^{-1} peak was assigned to quinoid ring C=N stretching,^{42, 43, 47, 50} and that at *ca.* 1511 cm^{-1} to N-H bending deformations,⁴⁷ while the band at 1595 cm^{-1} can be assigned to C-C stretching of benzenoid units.⁴³ Finally, the 1484 cm^{-1} peak was assigned to the quinoid ring C-C stretching vibrationally coupled with C-H bending.⁴⁴

The Raman spectra of the emeraldine salt films prepared in the ionic liquid solvents BMI-BF₄, BMI-PF₆, and P₁₃-TFSI (Figures 8.14b, c, d) are similar to that obtained for the PAn.(+)-HCSA grown in aqueous solution. This suggests that the polyanilines grown in ionic liquids and aqueous acidic solutions have the same chemical structure. In contrast, the Raman spectrum obtained for the film grown in EMI-TFSI (Figure 8.14e) is notably different from those prepared in the other ionic liquids. This indicates a different chemical structure, unlike the usual polyaniline emeraldine salts.

A variety of unusual products have been reported from electrochemical polymerizations of aniline. A polymer containing N-N bonds generated from “head-to-head” coupling has been described when electropolymerization was carried out with low acid concentration.^{3, 7} Cross-linking produced from *ortho*-coupling during polymerization of aniline³⁶⁻³⁸ at high potentials has been proposed. This was believed to lead to heterocyclic nitrogen species with a phenazine-type structure. Defective poly(2-methoxyaniline) having cross-linking

with phenazine rings has also been proposed when electropolymerization of 2-methoxyaniline was performed using a low concentration of monomer. Substitution of the benzene ring and side-reactions, generating cross-linked products, has been suggested for polymerization of aniline in the ionic liquid AlCl_3 -1-ethyl-3-methyl imidazolium chloride.³⁴

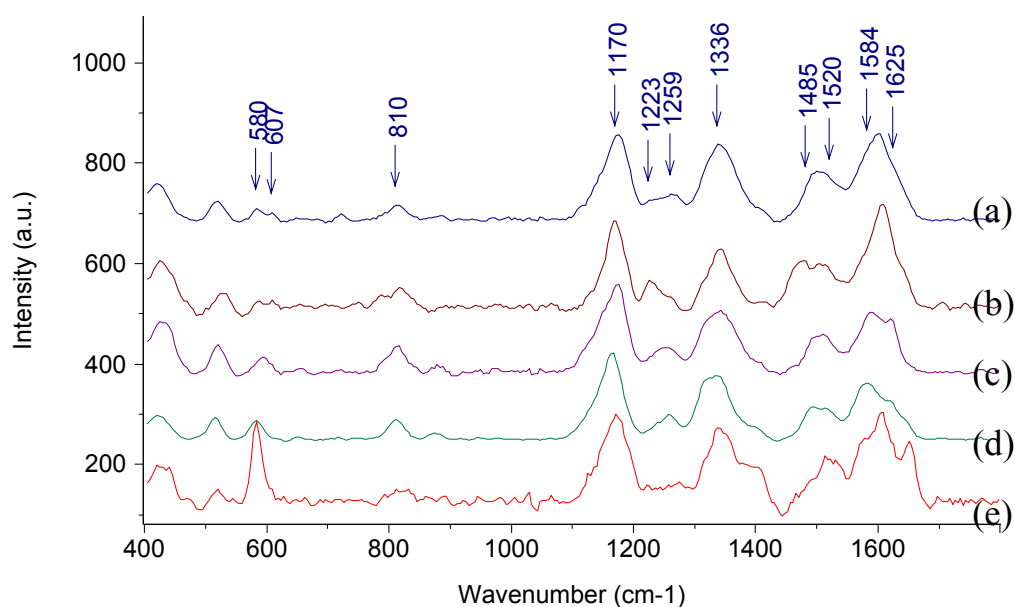


Figure 8.14 Raman spectra recorded (with 632.8 nm excitation) for polyaniline emeraldine salt films electrodeposited on a ITO-Pt-coated glass electrode. Growth conditions:

- (a) at +0.9 V, in aqueous 0.2 M aniline / 1.0 M (+)-HCSA, 20°C
- (b) at +1.2 V, in BMI-BF₄ containing 0.2 M aniline / 0.5 M (+)-HCSA, 50-55°C
- (c) at +1.2 V, in BMI-PF₆ containing 0.2 M aniline / 0.5 M (+)-HCSA, 50-55°C
- (d) at +1.2 V, in P₁₃-TFSI containing 0.2 M aniline / 0.5 M (+)-HCSA, 50-55°C
- (e) at +1.2 V, in EMI-TFSI containing 0.2 M aniline / 0.5 M (+)-HCSA, 50-55°C

8.3.3 Surface Studies

8.3.3.1 Morphology

Surface morphology is useful for investigating the intrinsic characteristics of synthesized polyanilines. It has been reported that the mechanical and electrical properties of polyaniline films are strongly related to their morphology.^{5, 6, 51, 52} Studies indicate that the morphology of electrodeposited polyaniline strongly depends on the kind of solvent, the mode of electropolymerization, and the nature and concentration of dopant acid employed.^{18, 53} The surface morphology of the polyaniline films electrodeposited from ionic liquid media in the present study was therefore examined using scanning electron microscopy (SEM).

The scanning electron micrographs shown in Figure 8.17 were obtained for polyaniline films electrodeposited on ITO-Pt coated glass at 1.2 V and 50-55°C from BMI-BF₄, BMI-PF₆, EMI-TFSI, and P₁₃-TFSI containing 0.2 M aniline/0.5 M (+)-HCSA. These SEMs showed different morphologies for the films grown in the different ionic liquids. Polyaniline films electrodeposited in BMI-BF₄ and EMI-TFSI have a powdery morphology. They are relatively smooth and uniform, while the SEM micrographs of the polyaniline films grown in BMI-PF₆ and P₁₃-TFSI show very rough morphology. Significantly, the morphologies for the polyaniline films prepared in ionic liquids are different to the fibrous morphology previously observed for PAN.(+)-HCSA films grown in aqueous solution at 0-65°C (see Chapter 3).

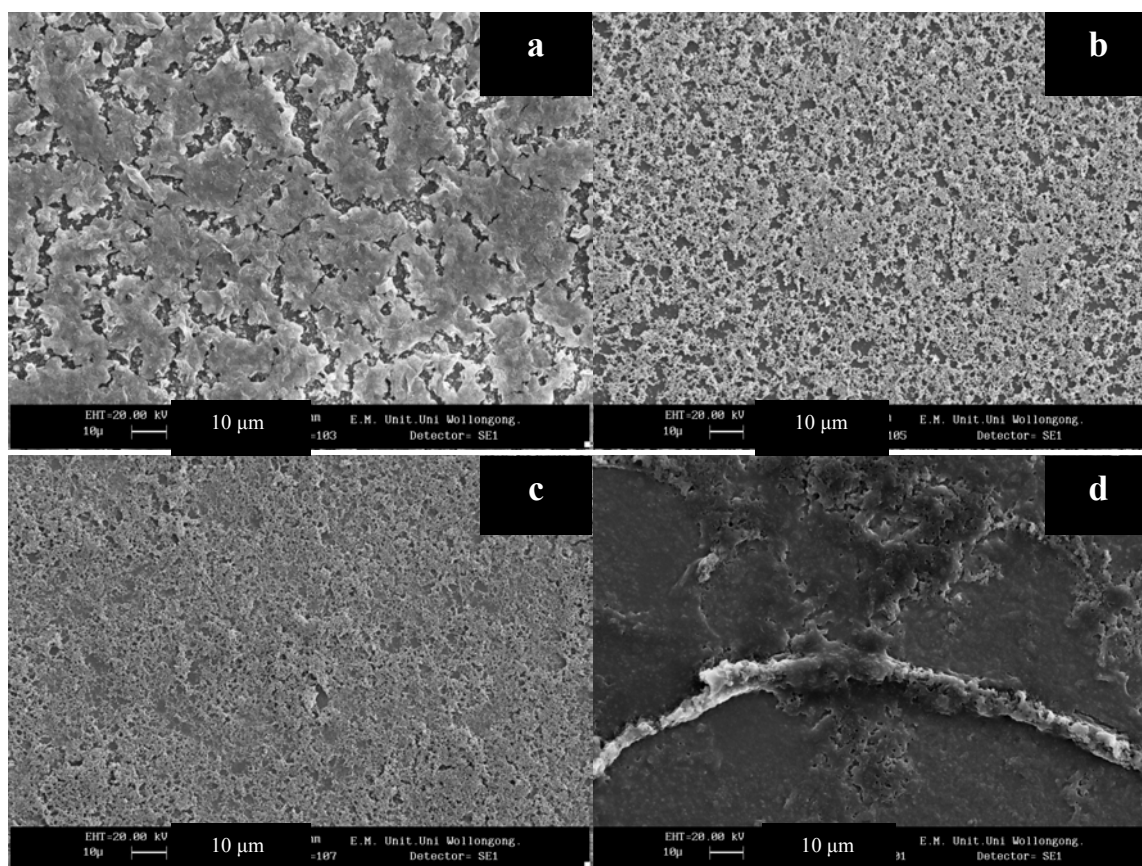


Figure 8.17 SEM of polyaniline emeraldine salt films electrodeposited on ITO-Pt-coated glass in (a) BMI- PF₆, (b) BMI- BF₄, (c) EMI-TFSI, (d) P₁₃-TFSI containing 0.2 M aniline /0.5 M (+)-HCSA at 50-55°C. All films were washed with methanol and coated with Au.

8.3.3.2 Atomic Force Microscopy

Contact mode atomic force microscopy (CAFM) was also used to investigate the surface of polyaniline films electrodeposited on ITO-Pt-coated glass electrodes in ionic liquids. Figures 8.18a-d present the three-dimensional images of 50 μm² sections of the films grown from BMI-PF₆, BMI-BF₄, EMI-TFSI and P₁₃-TFSI, respectively. AFM image for polyaniline film electrodeposited in BMI-BF₄ (Figure 8.18b) shows relatively smooth and uniform morphology more than the polyaniline films grown in others ionic liquids.

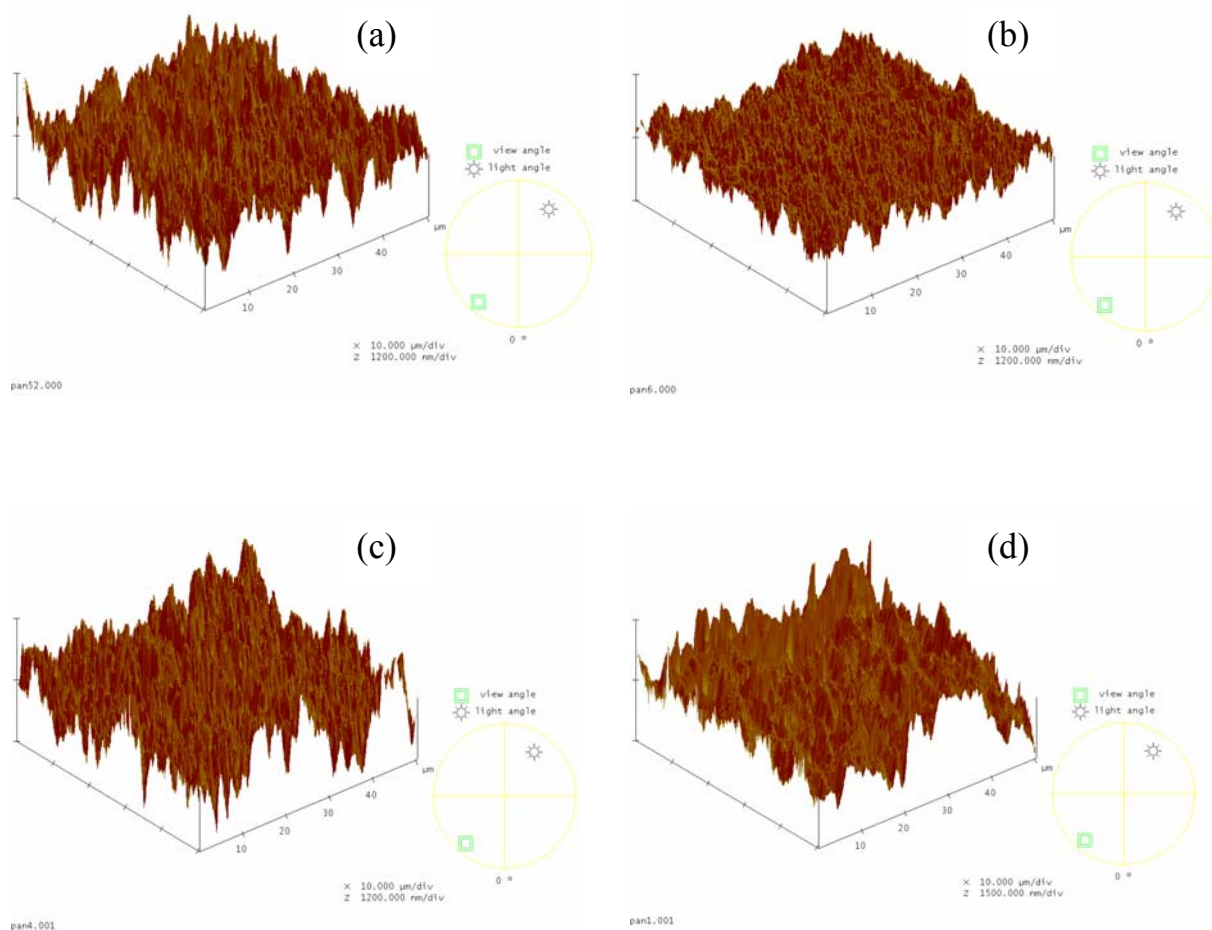


Figure 8.18 Three-dimensional AFM images ($50 \mu\text{m}^2$ sections) for polyaniline emeraldine salt films grown from (a) BMI- PF_6 , (b) BMI- BF_4 , (c) EMI-TFSI and (d) P_{13} -TFSI.

8.4 Conclusions

Electroactive polyaniline films can be prepared via the electrochemical polymerization of aniline in the presence of (+)-HCSA in the ionic liquids BMI- BF_4 , BMI- PF_6 , EMI-TFSI, P_{13} -TFSI and chiral (-)-MBEA-TFSI. The cyclic voltammograms during growth on glassy carbon show two redox couples typical of polyaniline, with the current response increasing

with successive cycles. Polymerization at high temperature (50-55°C) is required for dissolution of the HCSA (0.5 M) dopant acid in all the ionic liquids studied, except for (-)-MBEA-TFSI in which solvent the HCSA is highly soluble at room temperature.

The green polymer films electrodeposited on ITO-coated glass from a range of ionic liquids exhibit UV-visible spectra characteristic of polyaniline emeraldine salts. The presence in each case of a distinct localized polaron band at *ca.* 750-780 nm and decreased near-infrared absorption indicates that these polymers possess a less “extended coil” conformation than that obtained via electrodeposition in aqueous acidic solution – instead they possess a more “compact coil” conformation for their polyaniline chains.

The emeraldine salt films grown from EMI-TFSI, BMI-BF₄ and P₁₃-TFSI ionic liquids containing (+)-HCSA are optically active. This is believed to arise from chiral induction by (+)-CSA⁻ dopant ions incorporated into the polyaniline chains during polymerization. However, the optical activity for the films is low, being much less than previously observed for PAn.(+)-HCSA films electrodeposited from aqueous solution. This probably arises from competition between the chiral (+)-CSA⁻ and the achiral anion of the ionic liquids (e.g. BF₄⁻, TFSI) as the dopant incorporated into the polymer during polymerization.

Polyaniline grown from the ionic liquid BMI-PF₆ in the presence of (+)-HCSA is optically inactive. This suggests that only the small achiral PF₆⁻ anion of this ionic liquid is incorporated as the dopant anion during polymerization.

The Raman spectra of the electrodeposited polymers generally confirm that emeraldine salts are obtained with the normal “*para*-coupling”. However, the Raman spectrum of the polymer grown from EMI-TFSI shows different features indicating the presence of unusual

chemical structures. It is likely that cross-linking containing phenazine-like structures, probably generated by *ortho*-coupling during electropolymerization, is the origin for this.

An attempt to prepare optically active polyaniline via electrochemical polymerization of aniline in the chiral ionic liquid solvent (-)-MBEA-TFSI containing racemic (\pm)-HCSA was unsuccessful. The green product obtained is soluble in the polymerization solution and is possibly a low molecular weight polyaniline whose length may be too short to maintain a fixed helical structure. Anodic degradation may occur during polymerization at +1.3 V causing short chains/fragments in the polymer product.

The surface morphology of polyaniline emeraldine salt films electrodeposited in ionic liquids depends on the nature of ionic liquid employed and is different from that of related films grown in aqueous acid solution.

8.5 References

1. M.R. Majidi, L.A.P. Kane-Maguire, and G.G. Wallace, *Polymer*. **35** (1994): 3113.
2. M.R. Majidi, L.A.P. Kane-Maguire, and G.G. Wallace, *Aust. J. Chem.* **51** (1998): 23.
3. H. Okamoto and T. Kotaka, *Polymer*. **39** (1998): 4349.
4. W.W. Focke, G.E. Wnek, and Y. Wei, *J. Phys. Chem.* **91** (1987): 5813.
5. A.A. Syed and M.K. Dinesan, *Talanta*. **38** (1991): 815.
6. E.M. Genies, A. Boyle, M. Lapkowski, and C. Tsintavis, *Synth. Met.* **36** (1990): 139.
7. T. Ohsaka, Y. Ohnuki, N. Oyama, G. Katagiri, and K. Kamisako, *J. Electroanal. Chem.* **161** (1984): 399.
8. Y.-B. Shim, M.-S. Won, and S.-M. Park, *J. Electrochem. Soc.* **137** (1990): 538.
9. A.Q. Zhang, C.Q. Cui, and Y.J. Lee, *Synth. Met.* **72** (1995): 217.
10. A.M. Fenelon and C.B. Breslin, *Synth. Met.* **144** (2004): 125.
11. R. Mazeikiene and A. Malinauskas, *Synth. Met.* **123** (2001): 349.
12. C.D. Batich, H.A. Laitineen, and H.C. Zhou, *J. Electrochem. Soc.* **137** (1990): 883.
13. J. Desilvestra, W. Scheifele, and O. Haas, *J. Electrochem. Soc.* **139** (1992): 2727.
14. T. Osaka, T. Nakajima, K. Shiota, and T. Momma, *J. Electrochem. Soc.* **138** (1991): 2853.
15. N. Pekmez and A. Yildiz, *J. Electroanal. Chem.* **386** (1995): 121.
16. B. Garcia, F. Fusalba, and D. Belanger, *Can. J. Chem.* **75** (1997): 1536.
17. E.S. Matveeva, R.D. Calleja, and V.P. Parkhutik, *Synth. Met.* **72** (1995): 105.
18. E. Naudin, H. Anh, L. Breau, and D. Belanger.
19. T. Osaka, T. Nakajima, K. Naoi, and B.B. Owens, *J. Electrochem. Soc.* **137** (1990): 2139.
20. F. Fusalba, P. Gouerec, D. Villers, and D. Belanger, *J. Electrochem. Soc.* **148** (2001): A1.
21. E. Naudin, P. Gouerec, and D. Belanger, *J. Electroanal. Chem.* **459** (1998): 1.

-
22. Z. Takehara, K. Kanamura, and S. Yonezawa, *ibid.* **136** (1989): 2767.
 23. T. Welton, *Chem. Rev.* **99** (1999): 2071.
 24. P. Bonhote, A.-P. Dias, N. Papageorgiou, K. Kalyanasundaram, and M. Gratzel, *Inorg. Chem.* **35** (1996): 1168.
 25. J.S. Wilkes, *Green Chemistry.* **4** (2002): 73.
 26. V.R. Kock, L.A. Dominey, and C. Nanjundiah, *J. Electrochem. Soc.* **143** (1996): 798803.
 27. S.A. Forsyth, J.M. Pringle, and D.R. MacFarlane, *Aust. J. Chem.* **57** (2004): 113.
 28. J. Sun, M. Forsyth, and D.R. MacFarlane, *J. Phys. Chem. B.* **102** (1998): 8858.
 29. P.G. Pickup and R.A. Osteryoung, *J. Am. Chem. Soc.* **106** (1984): 2294.
 30. K. Sekiguchi, M. Atobe, and T. Fuchigami, *Electrochem. Commun.* **4** (2002): 881.
 31. J.M. Pringle, J. Efthimiadis, P.C. Howlett, J. Efthimiadis, D.R. MacFarlane, A.B. Chaplin, S.B. Hall, D.L. Officer, G.G. Wallace, and M. Forsyth, *Polymer.* **45** (2004): 1447.
 32. E. Naudin, H.A. Ho, S. Branchaud, L. Breau, and D. Belanger, *J. Phys. Chem. B.* **106** (2002): 10585.
 33. W. Lu, A.G. Fadev, B. Qi, and B.R. Mattes, *Synth. Met.* **135-136** (2003): 139.
 34. J. Tang and R.A. Osteryoung, *Synth. Met.*, (1991).
 35. S.A. Ashraf, Y. Pornputtkul, A.L.P. Kane-Maguire, and G.G. Wallace, (*to be submitted*).
 36. E.M. Genies, M. Lapkowski, and J.F. Penneau, *J. Electroanal. Chem.* **249** (1988): 97.
 37. M. Lapkowski, *Synth. Met.* **35** (1990): 169.
 38. A. Kitani, M. Kaya, J. Yano, K. Yoshikawa, and K. Sasaki, *Synth. Met.* **18** (1987): 341.
 39. E.M. Genies and C. Tsintavis, *J. Electroanal. Chem.* **195** (1985): 109.
 40. E.M. Genies and M. Lapkowski, *J. Electroanal. Chem.* **236** (1987): 189.
 41. A.L.P. Kane-Maguire. *The Synthesis and Applications of Chiral polyanilines.* in "Abstracts, 2nd Workshop on Multifunctional and Smart Polymer Systems". 1997. Wellington, N. Z.
 42. J.E.P. Silva, S.I.C. Torresi, D.L.A. Faria, and M.L.A. Temperini, *Synth. Met.* **101** (1999): 834.
 43. J.E.P. Silva, D.L.A. Faria, S.I.C. Torresi, and M.L.A. Temperini, *Macromolecules.* **33** (2000): 3077.
 44. G.M. Nascimento, J.E.P. Silva, S.I.C. Torresi, and M.L.A. Temperini, *Macromolecules.* **35** (2002): 121.
 45. A.E. Khalki, A. Gruger, and P. Colomban, *Synth. Met.* **139** (2003): 215.
 46. J.E.P. Silva, S.I.C. Torresi, M.L.A. Temperini, D. Goncalves, and O.N. Oliveira, *Synth. Met.* **101** (1999): 691.
 47. G. Louarn, M. Lapkowski, S. Quillard, A. Pron, J.P. Buisson, and S. Lefrant, *J. Phys. Chem.* **100** (1996): 6998.
 48. M. Grzeszczuk and R. Szostak, *Solid State Ionics.* **157** (2003): 257.
 49. M. Tagowska, B. Palys, and K. Jackowska, *Synth. Met.* **142** (2004): 223.
 50. M. Boyer, S. Quillard, G. Louarn, S. Lefrant, E. Rebourt, and A.M. Monkman, *Synth. Met.* **84** (1997): 787.
 51. J. Huang, S. Virji, B.H. Weiller, and R.B. Kaner, *J. Am. Chem. Soc.* **125** (2003): 314.
 52. J. Huang, V. Shabnam, B.H. Weiller, and R.B. Kaner, *Chemistry A European Journal.* **10** (2004): 1314.
 53. B. Scrosali, *Applications of Electroactive Polymers.* (1993): Kluwer Academic Publishers Group.

Chapter 9

Electrochemical Behaviour and Chiroptical Properties of Chiral Polyaniline Film in Ionic Liquids

9.1 Introduction

As outlined in earlier Chapters, chiral polyaniline doped with (+)- or (-)-camphorsulfonic acid¹⁻⁵ has been proposed as a novel material for asymmetric electrosynthesis.⁶ For electrochemical asymmetric synthesis of organic compounds, non-aqueous systems are generally required in order to solubilise the organic reactants and to provide an electrochemical window wherein the polymer and the electrolyte are stable. Room temperature ionic liquids have attracted recent interest as novel solvents and electrolytes for chemical and electrochemical synthesis, catalysis and devices. They have been suggested as ideal media as they simultaneously satisfy the requirements of a large potential window, high ionic conductivity, unique solvent properties and very low volatility.⁷⁻¹² Recently, chiral ionic liquids containing either a chiral cation^{11,13} or a chiral anion¹⁴ have been prepared.

In recent years, the electrochemical behaviour¹⁵⁻²⁰ and optical properties^{19,21,22} of polyaniline films have been extensively studied in aqueous solutions. However, studies of this conducting polymer in non-aqueous media,^{20, 23-25} particularly in ionic liquids,^{26, 27} are extremely rare in the literature. There have been no reports of the electrochemical behaviour and chiroptical properties of chiral polyanilines in ionic liquids. Kane-Maguire *et al.*²⁸ have reported the chiroptical properties of the reduced (leucoemeraldine) and

oxidized (pernigraniline) forms of polyaniline, generated by treatment with a chemical reductant or oxidant, respectively. However, leucoemeraldine base is sensitive to aerial oxidation,²⁹ while pernigraniline undergoes hydrolytic cleavage.³⁰⁻³² Therefore, *in situ* electro-chiroptical studies may provide the best method to establish the chiroptical properties of polyaniline films in various oxidation states generated electrochemically.

Chiral polyaniline-modified electrodes and room temperature ionic liquid electrolytes may provide exciting new systems for electrochemical asymmetric synthesis. In this Chapter we explore the electrochemical behaviour of electrodeposited PAn.(+)-HCSA films using cyclic voltammetry in various ionic liquids, as well as the chiroptical properties of the films by *in situ* electrochemical UV-visible and circular dichroism spectroscopy. The ionic liquids examined are 1-butyl-3-methylimidazolium tetrafluoroborate (BMI-BF₄), 1-butyl-3-methylimidazolium hexafluorophosphate (BMI-PF₆), and 1-ethyl-3-methylimidazolium bis(trifluoromethanesulfonyl)imide (EMI-TFSI). The new chiral ionic liquids (-)- and (+)-(α)-methylbenzylethylamine bis(trifluoromethanesulfonyl)imide (MBEA-TFSI) and the racemic analogue (\pm)-MBEA-TFSI, both recently synthesized in our laboratories by Dr. Syed Ashraf, are also investigated. These novel chiral ionic liquids have exciting potential applications for chemical and electrochemical asymmetric synthesis or chiral chromatographic separations. Therefore, their physical properties such as density, viscosity, conductivity, melting temperature, thermal stability, specific rotation, electrochemical window, spectroscopic properties and solubility in a range of organic solvents are also investigated.

9.2 Experimental

9.2.1 Materials

Aniline (Aldrich) and (1*S*)-(+)-10-camphorsulfonic acid, as well as the ionic liquids BMI-PF₆, BMI-BF₄, EMI-TFSI, and the chiral (+)- or (-) and (±)-MBEA-TFSI were synthesized or purchased as described in Chapter 2. The structures of the ionic liquids are shown in Table 2.1 in Chapter 2. All ionic liquids were deoxygenated by purging with nitrogen gas for at least 30 min prior to use.

9.2.1 Physical Properties of the Novel MBEA-TFSI Ionic Liquid

9.2.1.1 *Density* of the ionic liquids was determined by weighing 1.0 mL (using a 1000 μL micropipette) of the ionic liquid with an analytical balance at room temperature (18°C). An average value from 4 determinations was obtained in each case.

9.2.1.2 *Viscosity measurements* were carried out on a Viscosity Monitoring and Control Electronics ViscoLab-Viscometer 3000 (Cambridge Applied System), calibrated with standard oils in the ranges of 5 to 100 cP and 100 to 2000 cP.

9.2.1.3 *Conductivity measurements* were performed using a conductivity meter Model 20 (Denver Instrument) under thermostatted conditions. The conductivity probe was calibrated with aqueous 0.01 M KCl standard solution, $\sigma = 141.3 \mu\text{S}/\text{cm}$.

Conductivity was also determined using the ac impedance technique. The measurements were carried out in a cell fitted with two glassy carbon electrodes (surface area = 0.07 cm²) at 20°C. Complex impedance spectra between 1 Hz and 10 kHz were obtained with a Solartron SI 1260, 1275, 1287 impedance meter.

9.2.1.4 *Specific rotations* for (-)- and (+)-MBEA-TFSI were measured using a digital polarimeter (JASCO polarimeter-DIP-370) calibrated with aqueous (+)-HCSA (2 g/100 mL) at 24°C. An accurate weight of (+)- or (-)-MBEA-TFSI was dissolved in 5 mL MeOH, and the optical rotation, α , of the solutions measured in a 5 cm path-length cell. The specific rotations $[\alpha]$ were calculated from the Equation 2.2 in Chapter 2.

9.2.1.5 *UV-visible and CD spectra* of (+)-, (-)- and (\pm)-MBEA-TFSI in MeCN (*ca.* 0.05% v/v) and in MeOH (*ca.* 0.15% v/v) were measured in the range of 230-300 nm using a Shimadzu UV-1601 spectrophotometer and a Jobin Yvon Dichrograph 6, respectively.

9.2.1.6 *Thermal analysis and temperature-dependent phase behaviour studies* were conducted by differential scanning calorimetry, using a TA Instruments DSC Q 100 in a nitrogen flow (50 mL/min) between -80° and 200°C. A heating rate of 10°C/min was used for the first scan and then cooling down to -80°C at a rate of 10°C/min before conducting the second scan with the same condition. An accurately weighed sample was loaded into an aluminium pan and compressed under medium pressure. Glass transition temperature (T_g), crystallization point (T_c) and melting point (T_m) were determined.

9.2.1.7 *Thermogravimetric analyses* were conducted using a STA 1500 (Rheometric Scientific) in air or a nitrogen flow (20 mL/min) between 25°C and 450°C at a heating rate of 10° C/min. Accurately weighed samples (*ca.* 20-25 mg) were analyzed.

9.2.1.8 *Electrochemical behaviour* was examined in a one-compartment electrochemical cell with a three electrode configuration. Glassy carbon (GC-disc, 0.07 cm² surface area), platinum mesh and Ag/AgCl_(EMI-TFSI) were used as working, auxiliary and reference electrodes, respectively. Ionic liquids were gently purged with nitrogen gas at least 30 min

prior to use and during electrochemical experiments. A PC-controlled CV-27 potentiostat with Mac Lab and E Chem software was used for cyclic voltammetry studies.

9.2.2 Electrochemical Preparation of PAn.(+)-HCSA Films

Electrochemical polymerizations in aqueous solution were carried out at room temperature (20-25°C) using glassy carbon (0.07 cm² surface area) or platinised ITO-coated glass, platinum mesh and Ag/AgCl_(3M NaCl) as working, auxiliary and reference electrodes, respectively. The polymerization solution was aqueous 1.0 M (+)-HCSA containing 0.2 M aniline, deoxygenated by bubbling with nitrogen gas for 15 min. The PAn.(+)-HCSA films were deposited on the GC-disc working electrode at 0.8 V for 70 mC/cm² charge passed, and on ITO-Pt coated glass at 0.9 V (120 mC/cm²), respectively, using a BAS CV-27 potentiostat. The PAn.(+)-HCSA modified electrodes were washed with methanol to remove oligomers, excess (+)-HCSA and monomer and then vacuum dried at room temperature for at least 3 hrs.

9.2.3 Cyclic Voltammetry

Cyclic voltammetry studies of PAn.(+)-HCSA deposited on glassy carbon (0.07 cm² surface area) were carried out in a one-compartment electrochemical cell with three electrode configuration using platinum mesh and Ag/AgCl_(EMI-TFSI) as the auxiliary and reference electrodes, respectively. The ionic liquid electrolytes were purged with nitrogen gas for at least 30 min prior to use and during the experiments.

9.2.4 *In situ* UV-visible and CD Spectroelectrochemical Studies

Spectroelectrochemical experiments were performed in a 1 cm pathlength quartz cuvette using the three electrode configuration described in Chapter 2 (see Figure 2.3). A PAn.(+)-HCSA film deposited on ITO-Pt coated glass was used as working electrode, installed perpendicularly to the light path. The auxiliary electrode was ITO-coated glass bordered with Pt wire and installed parallel to the working electrode, while the reference electrode used in the ionic liquid electrolytes was Ag/AgCl_(EMI-TFSI). After polarization at a certain potential using a BAS CV-27 potentiostat, UV-visible and CD spectra were recorded with a Shimadzu UV-1601 spectrophotometer and a Jobin Yvon Dichrograph 6, respectively.

9.2.5 Raman Spectra

Raman spectra of the polyaniline films were recorded using procedures described in Chapter 2. All films were thoroughly washed with methanol to remove ionic liquid prior to measuring the Raman spectra.

9.3 Results and Discussion

9.3.1 Properties of the Novel Chiral Ionic Liquid, MBEA-TFSI

The physical properties measured for the new ionic liquid, MBEA-TFSI, are summarized in Table 9.1. Each of these properties is discussed individually below.

Table 9.1 Properties of chiral ionic liquid: (-)-MBEA-TFSI.

Density (18°C)	1.45 g/cm ³	$[\alpha]_D$ (3.3% w/v, MeOH)	- 7.9
Viscosity (25°C)	470 cP	Molecular rotation (M $[\alpha]_D$ /100)	- 34
Melting point ^a	- 42°C	Circular dichroism ($\Delta\epsilon_{l-r}$)	0.18 M ⁻¹ cm ⁻¹
Glass temperature ^a	- 68°C	Electrical conductivity	0.37 mS/cm
Decomposition temp ^b	>270°C	Electrochemical window	4.0 V

^a From DSC

^b From TGA

9.3.1.1 Density

Density is a physical property of ionic liquids that is required for many applications. The density of (-)-MBEA-TFSI was determined as 1.4473 g/cm³ at 18°C. This is quite similar to that of other ionic liquids which are denser than water.³³

9.3.1.2 Viscosity

Dynamic viscosity (η) of (-)-MBEA-TFSI was found to be 470 cP \pm 5% at 25°C. The viscosity as a function of temperature (18° - 80°C) is presented in Figure 9.1. In general, ionic liquids are much more viscous than traditional organic solvents, and vary over a range of <10 to > 1000 cP at room temperature.³⁴ The viscosity of MBEA-TFSI is slightly higher than those reported for ILs based on imidazolium salts (*ca.* 50-300 cP at 20°C).⁸

9.3.1.3 Conductivity

Figure 9.2 shows the conductivity of (-)-MBEA-TFSI, measured by conductivity probe, between 18°C and 80°C. The conductivity of this chiral ionic liquid at 25°C was 0.048 mS/cm. This is similar to the conductivity of the imidazolium-based ionic liquid BMI-PF₆ measured by the same method (0.105 mS/cm at 18°C).

Fuller *et al.*³⁵ have previously reported that the conductivity of BMI-PF₆ at 22° - 23°C measured by ac impedance was 1.8 mS/cm. Therefore, the conductivity of (-)-MBEA-TFSI was also measured here by ac impedance. It was found to be 0.374 mS/cm at 20°C, significantly higher than that obtained from the conductivity probe measurement. However, the conductivity of this chiral ionic liquid is still quite low when compared with highly conductive ionic liquids such as EMI-TFSI (8.8 mS/cm).⁸ The conductivities of ionic liquids are related to other physical parameters such as viscosity, formula weight, density, and the radii of constituent ions.⁸ In general, the lower the viscosity, formula weight and ion size of an ionic liquid, the higher is its conductivity.

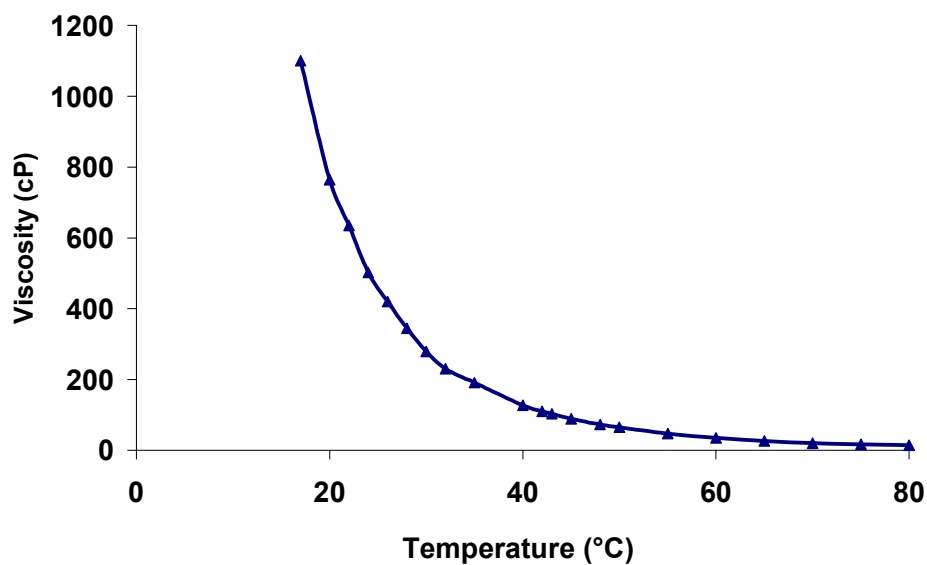


Figure 9.1 Viscosity (η) of (-)-MBEA-TFSI as a function of temperature (estimated error: $\pm 5\%$).

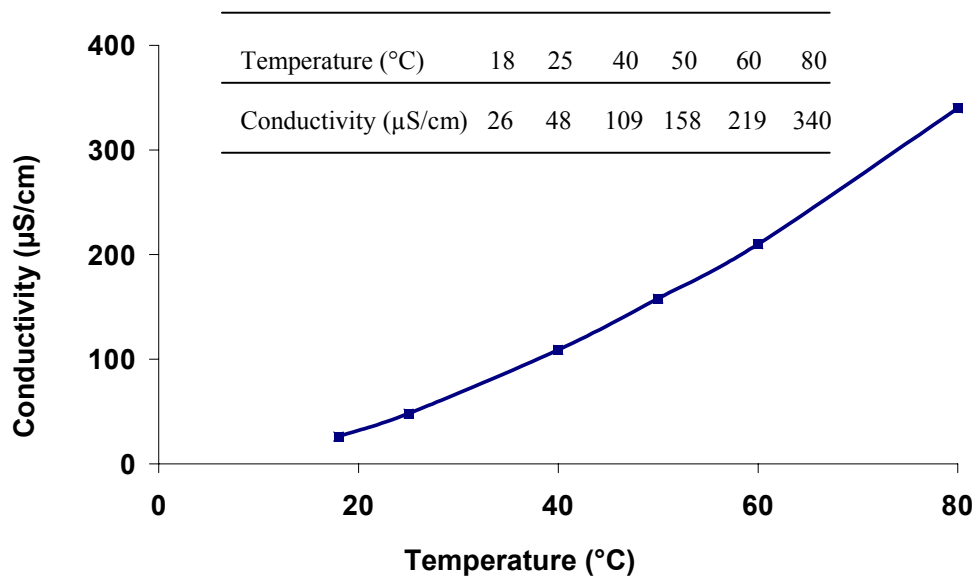


Figure 9.2 Conductivity (σ) of (-)-MBEA-TFSI as a function of temperature.

9.3.1.4 Differential Scanning Calorimetry (DSC)

The DSC profile for (-)-MBEA-TFSI between -80°C and 200°C under nitrogen is shown in Figure 9.3. A surprisingly low melting temperature of $< -40^{\circ}\text{C}$ was observed. Therefore, when the ionic liquid was kept in a freezer at -18°C for a few days, a very viscous liquid (but not solid) state was observed. Such a sub-ambient melting point is a useful characteristic for its potential use as a chiral ionic solvent.

It has been reported that low melting point for ionic liquids can be achieved by a highly dissymmetric structure for the constituent cation.³⁶ The melting point of the new chiral ionic liquid MBEA-TFSI is much lower than that reported for other chiral ionic liquids (m.p. 5° - 16°C)³⁷ and for other TFSI-based ionic liquids such as P₁₄ – P₁₁ (m.p. -10° to 130°C), EMI-TFSI (m.p. -5°C).^{8, 38} However, very low melting points ($< -45^{\circ}\text{C}$) for many pyrrolidinium salts (P₁₂, P₁₃, P₁₄) with the dicyanamide (DCA) anion have been recently reported.³⁹

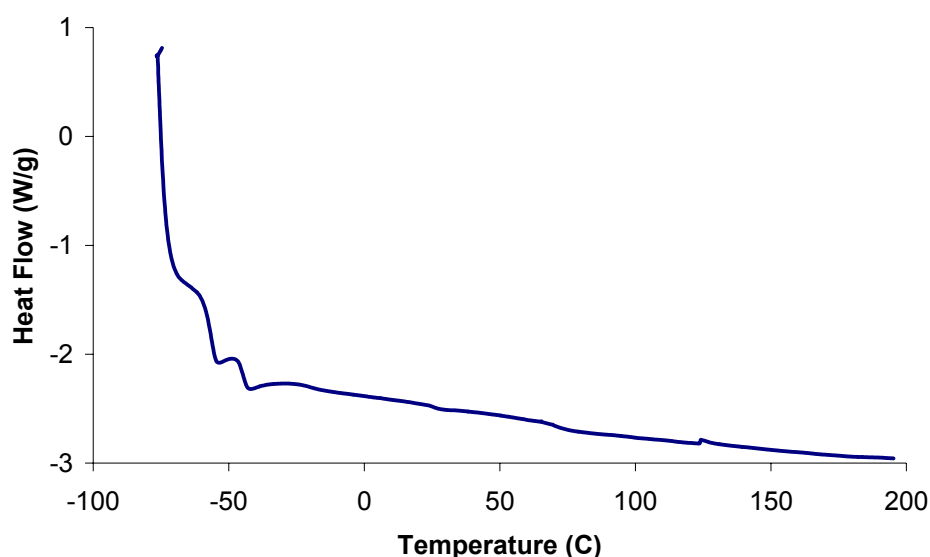


Figure 9.3 DSC of (-)-MBEA-TFSI under nitrogen atmosphere.

9.3.1.5 Thermal Stability

Thermogravimetric analyses (TGAs) of (-)-MBEA-TFSI in air and under nitrogen between 25°C and 450°C were similar, as shown in Figure 9.4. The chiral ionic liquid shows very good thermal stability up to $\geq 250^\circ\text{C}$. The TGA thermograms indicate that two decomposition steps take place during heating. The thermal decomposition temperature (defined as 5% weight loss) is at 270°C. The first step involving a *ca.* 30% weight loss is believed to be associated with the decomposition of the cation, as the ionic liquid contains *ca.* 35% cation and 65% anion by weight. Subsequent decomposition of the TFSI⁻ anion is believed to give rise to the second, larger weight loss observed at $> 300^\circ\text{C}$.

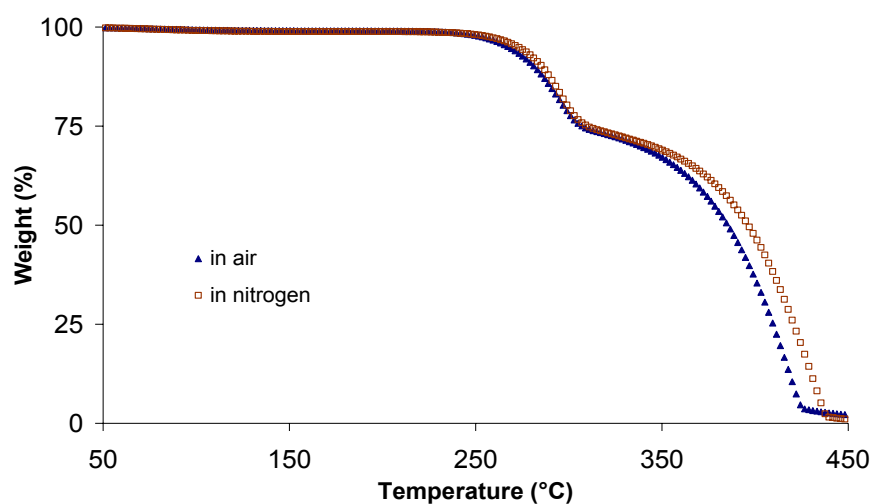
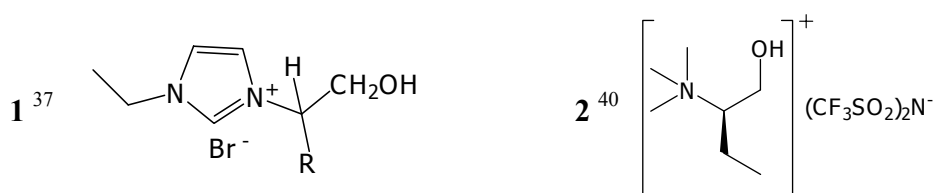


Figure 9.4 Thermogravimetry in nitrogen and in air of (-)-MBEA-TFSI.

The new chiral ionic liquid has very good thermal stability compared with previously reported chiral ionic liquids. For example, **1** decomposed at 180°C, while **2** decomposed at 150°C. In addition, MBEA-TFSI is not significantly hygroscopic, as only 1% moisture (1% weight loss at 110°C) was observed for an atmosphere equilibrated sample.



9.3.1.6 Specific Rotations

The specific rotations $[\alpha]_D$ of the chiral ionic liquids (+)- and (-)-MBEA-TFSI in methanol solvent at 24°C were 7.8 and -7.9, respectively, confirming their optical activity. Their molecular rotations $\{(\text{Mol. Wt.} \times [\alpha]_D) / 100 = -34 \text{ and } +34, \text{ respectively}\}$ were very similar to that of the (-)- and (+)-1-phenylethylamine precursors (-36 and +36), indicating quantitative retention of optical activity in the chiral amine moiety during the synthesis.

9.3.1.7 Chiroptical Properties

MBEA-TFSI is a colourless liquid. Thus, it has no absorption spectrum in the visible region. The absorption spectra of (+)- and (-)-MBEA-TFSI in acetonitrile and methanol in the ultraviolet region (230-300 nm) are presented in Figure 9.5, exhibiting a strong band at 257 nm. Vibrational bands at $\lambda_{\text{max}} = 251, 257, 258, \text{ and } 266 \text{ nm}$ were observed superimposed on this electronic absorption band, a feature also exhibited by the (+)-1-phenylethylamine precursor.

The optical activity of the new chiral ionic liquids was confirmed from circular dichroism (CD) spectra of solutions of (+)- and (-)-MBEA-TFSI in acetonitrile and methanol (Figure 9.5). The CD spectra again exhibited vibrational features. For example, (+)-MBEA-TFSI exhibit CD bands at 240, 246, 252, 258 and 266 nm, corresponding to its absorption spectrum. A mirror imaged CD spectrum was observed for (-)-MBEA-TFSI, confirming that it is the enantiomer of (+)-MBEA-TFSI. The circular dichroic absorptivity recorded for (-)-MBEA-TFSI ($\Delta\epsilon_{\text{l-r}} = 0.182 \text{ M}^{-1}\text{cm}^{-1}$) is similar to that measured for the precursor chiral amine (*R*)-(-)-1-phenylethylamine.

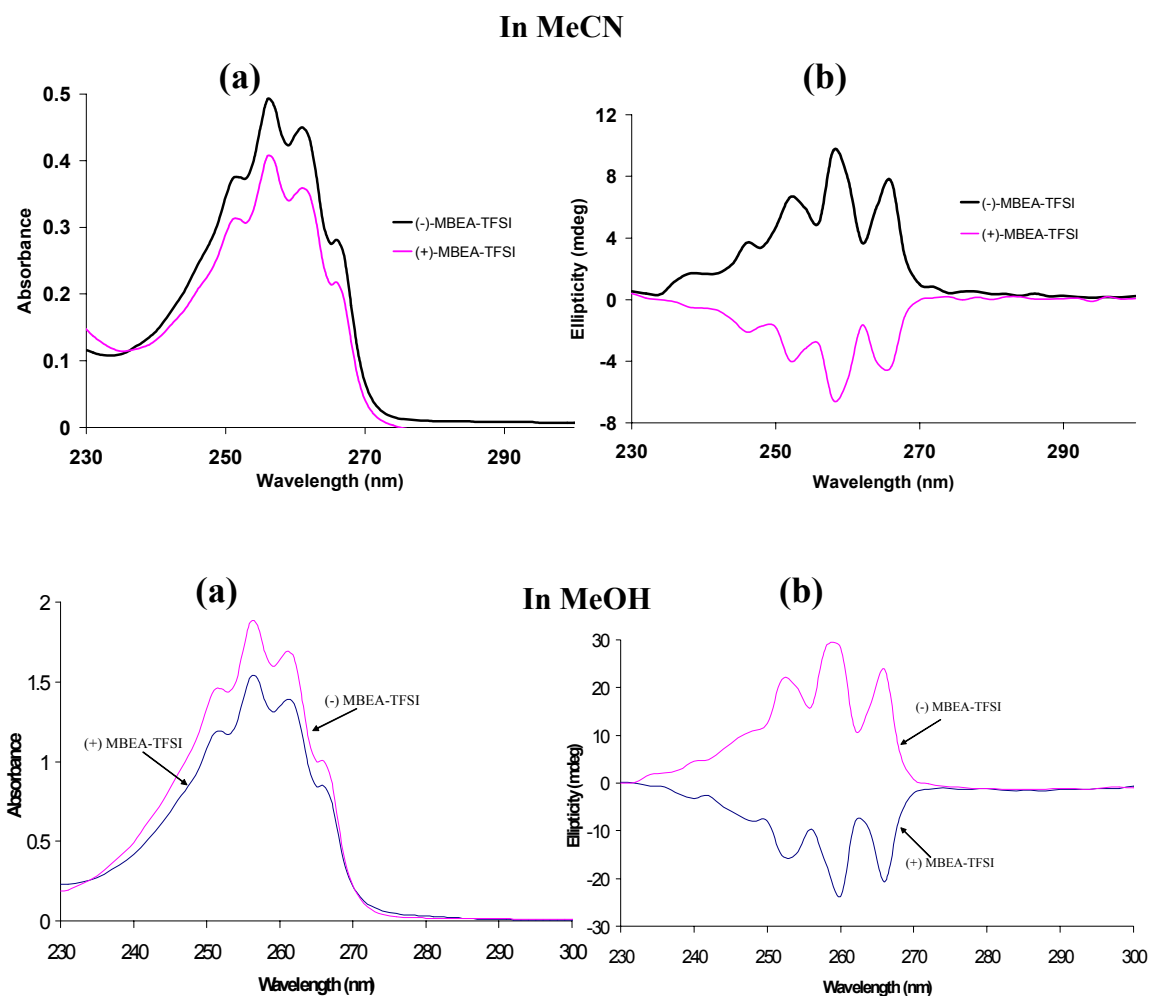


Figure 9.5 UV-visible (a) and CD (b) spectra of (-)- and (+)-MBEA-TFSI in MeCN (*ca.* 0.05% v/v) and in MeOH (*ca.* 0.15% v/v).

9.3.1.8 Electrochemical Window

The potential window of the new chiral ionic liquid was determined by recording a cyclic voltammogram using a GC-disc electrode, Pt-mesh and Ag/AgCl_(EMI-TFSI) as working, auxiliary, and references electrodes, respectively. The potential was scanned between -3.0 and +3.0 V, beginning with an initial potential of 0.0 V. The resultant CV in Figure 9.6 shows that the electrochemical window over which (\pm)-MBEA-TFSI is stable is in the range *ca.* - 2.0 V to + 2.0 V at 20°C under N₂. This broad electrochemical window,

compared with the relatively small range available in aqueous electrolytes makes this new chiral ionic liquid suitable for examining redox processes that occur at more extreme potentials.

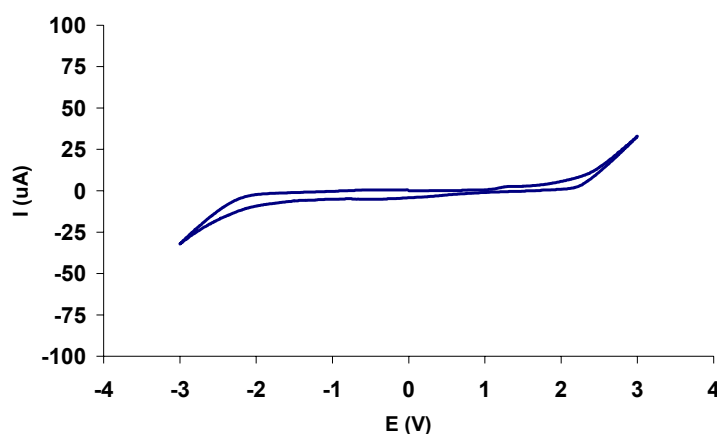


Figure 9.6 Electrochemical window of (\pm)-MBEA-TFSI (vs. $\text{Ag}/\text{AgCl}_{(\text{EMI-TFSI})}$): Cyclic voltammogram for neat (\pm)-MBEA-TFSI, with a glassy carbon electrode (0.07 cm^2 surface area) at 20°C under N_2 purging. Scan rate = 50 mV/s .

9.3.1.9 Miscibility and Solubility

The miscibility of (\pm)-MBEA-TFSI with other liquids was tested at about 10% (v/v) by mixing 2 drops of ionic liquid with 0.5 mL of various solvents at room temperature (23°C). The ionic liquid was immiscible with liquids of very low or high dielectric constant (ϵ) {e.g. n-hexane ($\epsilon = 1.88$) and water ($\epsilon = 80.1$)}, but miscible with many liquids of medium and moderately high dielectric constant {e.g. chloroform ($\epsilon = 4.81$), diethylether ($\epsilon = 4.33$), ethylacetate ($\epsilon = 6.02$), acetone ($\epsilon = 20.70$), methanol ($\epsilon = 32.70$), and acetonitrile ($\epsilon = 37.50$)}. This immiscibility with water and solvents of low polarity opens interesting perspectives for synthesis and electrochemical applications.

9.3.1.9 Redox Couple of Ferrocene in Neat (\pm)-MBEA-TFSI

Many researchers have measured the ferrocene/ferricinium ion (Fc/Fc^+) redox couple in their electrochemical systems in order to compare electrochemical potential data with others. In the present study, cyclic voltammograms for (\pm)-MBEA-TFSI containing 5 mM ferrocene on a glassy carbon disc electrode (Figure 9.7) displayed a pair of Fc/Fc^+ redox waves at $E_{\text{ox}} = 0.5 \text{ V}$ and $E_{\text{red}} = 0.2 \text{ V}$ at a scan rate of 100 mV/s, and $E_{1/2} = (E_{\text{ox}} + E_{\text{red}})/2 = 0.35 \text{ V vs. Ag}/\text{AgCl}_{(\text{EMI-TFSI})}$. However, the peak separation between E_{ox} and E_{red} was wider at higher scan rate. This might be due to IR drop caused by the relatively low conductivity of this ionic liquid.

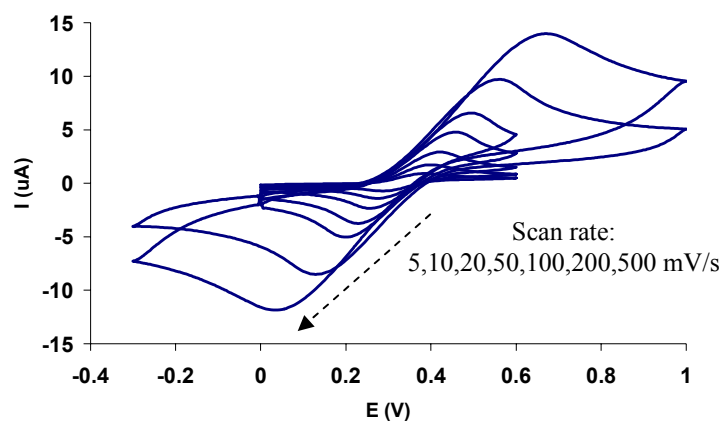


Figure 9.7 CVs of 5 mM ferrocene in (\pm)-MBEA-TFSI using a bare glassy carbon disk (0.07 cm^2) electrode, and scan rates of 5, 10, 20, 50, 100, 200, 500 mV/s.

9.3.2 Cyclic Voltammetry of PAn.(+)-HCSA Films in Acidic and Neutral Aqueous Electrolytes and Ionic Liquids

In an attempt to use PAn.(+)-HCSA films electrodeposited from aqueous acidic solution onto electrodes as chiral electrodes for asymmetric electrosynthesis in ionic liquids, the electrochemical behaviour and stability of the PAn.(+)-HCSA films in ionic liquids were

investigated using cyclic voltammetry (CV). The potential ranges over which the chiral polyaniline films are electroactive and stable (not degraded) in ionic liquids could be obtained from these experiments. For comparison, the CVs of the films were also examined in acidic and neutral aqueous electrolytes. The latter studies are described first below.

9.3.2.1 CVs of PAn.(+)-HCSA Films in Acidic and Neutral Aqueous Electrolytes

(a) CVs in Aqueous Acid Electrolyte (1.0 M HCl)

A typical CV in aqueous 1.0 M HCl for a PAn.(+)-HCSA film after electrodeposition on a GC-disc electrode is presented in Figure 9.8. It showed two well-defined redox couples, with $E_{1/2}$ values of *ca.* 0.10 and 0.85 V. It is well known that the first redox pair is associated with the interconversion between the fully reduced (leucoemeraldine) and semiquinone (emeraldine) forms of polyaniline, while the second redox couple relates to the interconversion between the emeraldine and fully oxidized (pernigraniline) forms of the polymer.^{19, 23}

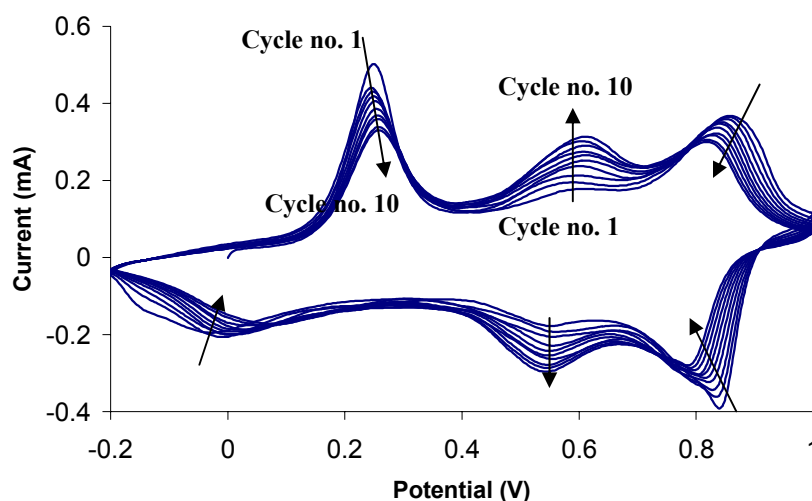
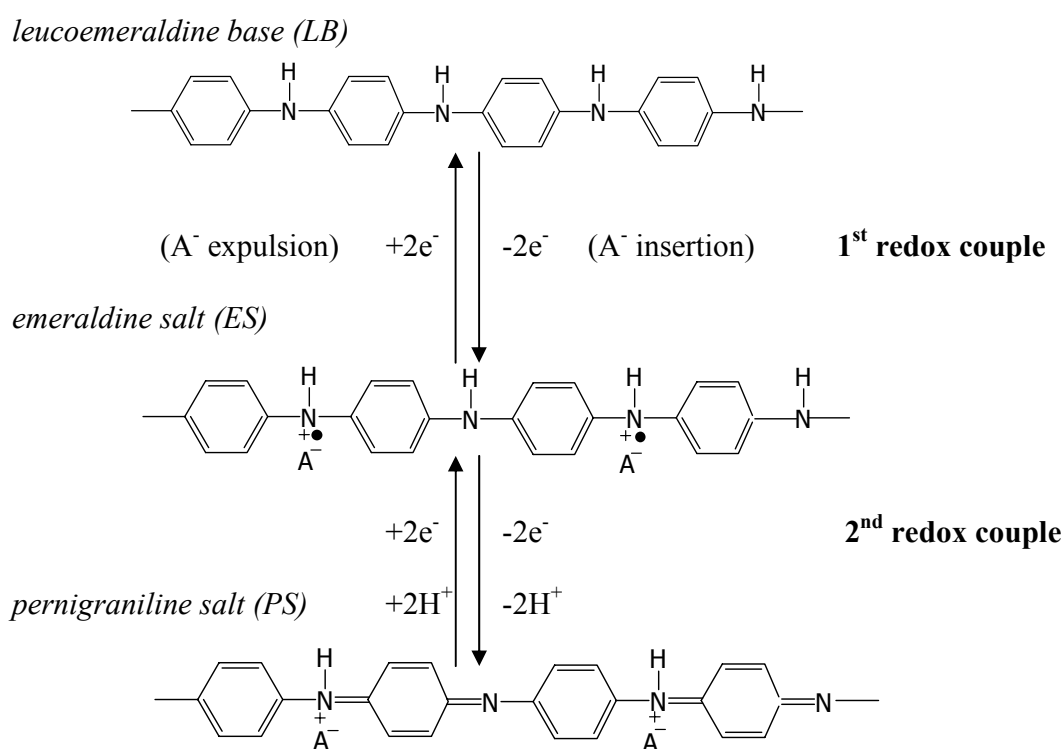


Figure 9.8 Cyclic voltammograms for a PAn.(+)-HCSA film electrodeposited on glassy carbon (surface area = 0.07 cm²), carried out in aqueous 1.0 M HCl, between -0.2 and 1.0 V (10 cycles). Scan rate = 50 mV/s.

As described in Scheme 1.5 in Chapter 1, the redox behaviour of polyaniline is pH dependent, i.e. the redox reactions depend on both the applied potential and the pH. The leucoemeraldine state of polyaniline is usually found in the leucoemeraldine base (LB) form due to the very low pK_a of leucoemeraldine salt $\{pK_a \text{ ca. } -0.5 \text{ in HCl}^{24,29}\}$. In contrast, both protonated (salt) and non-protonated (base) forms of the emeraldine and pernigraniline oxidation states can be generated in acidic ($pH \text{ ca. } \leq 2$) and more basic ($pH \text{ ca. } > 2$) solutions, respectively.^{29, 41} Thus, the main redox processes of polyaniline that usually occur in aqueous acid solution are as shown in Scheme 9.1 below.



Scheme 9.1

However, upon repeated potential scanning between -0.2 and 1.0 V (Figure 9.8), the two initial redox peaks gradually decreased in intensity and a new redox peak or “middle peak” appeared with $E_{1/2} \text{ ca. } 0.55 \text{ V}$, its intensity increasing gradually with the number of scans.

The polyaniline film was then degraded and dissolved/dispersed with successive scans. There have been several interpretations of the origin of the “middle peak” in the CVs of polyaniline. It may be due to phenazine-type structures of cross-linked products from overoxidation,⁴²⁻⁴⁵ branched structures from coupling in the *ortho*-position,^{46,47} or benzoquinone / hydroquinone type compounds generated from degradation of polyaniline chains at high positive potentials.^{19, 48} Therefore, the middle peak in the CVs of PAn.(+)-HCSA film are probably due to the redox couple of benzoquinone / hydroquinone which was the main oxidized product of polyaniline degradation in acid aqueous solutions at high positive potentials.

The effect of potential scanning on the chirality of a PAn.(+)-HCSA film electrodeposited onto an ITO-coated glass electrode was also studied. After cycling between -0.2 and 0.9 V for 15 cycles (Figure 9.9a), the UV-visible (Figure 9.9b) and CD (Figure 9.9c) spectra of the film were recorded and compared to the spectra before potential cycling. The large decrease in the intensity of the UV-visible and CD spectral bands of the PAn.(+)-HCSA film near 450 nm after potential cycling may be partly caused by dissolution of degradation products from the polyaniline film into the aqueous medium. However, the decrease in intensity of the CD band was considerably more marked than that observed for the corresponding absorption band, suggesting that some racemization of the chiral PAn.(+)-HCSA may have also occurred during the repeated potential scanning. During this redox switching, one would expect the chiral (+)-CSA⁻ doped anion in the emeraldine salt to be exchanged for the achiral Cl⁻ anion. However, this was not expected to cause significant racemization in the solid state film due to steric hindrance preventing the necessary inversion of the helical polymer chains.

In order to throw further light on this redox switching behaviour, the effect of the scan rate used during repeated potential scanning in 1.0 M HCl was also studied. The use of a very slow scan rate (5 mV/s) caused more degradation of the PAn.(+)-HCSA film, presumably due to a longer period of time that the polyaniline was exposed to high anodic potentials. Thus, for the same number of potential cycles, irreversible changes to the CV at the lowest scan rate (5 mV/s) were more pronounced than at the higher scan rates of 10 and 100 mV/s. With a scan rate of 5 mV/s, the PAn.(+)-HCSA film gradually dissolved into the aqueous electrolyte and eventually disappeared from the ITO-glass working electrode after 30 scans (not shown). This suggests degradation of the polyaniline into smaller water-soluble products. The electrode capacity of polyacetylene films has also been observed⁴⁹ to decrease at low cycling rates due to a greater degree of polymer degradation than at high cycling rates. Similarly to these cases, the oxidative degradation of polythiophene is faster at lower scan rates.⁵⁰

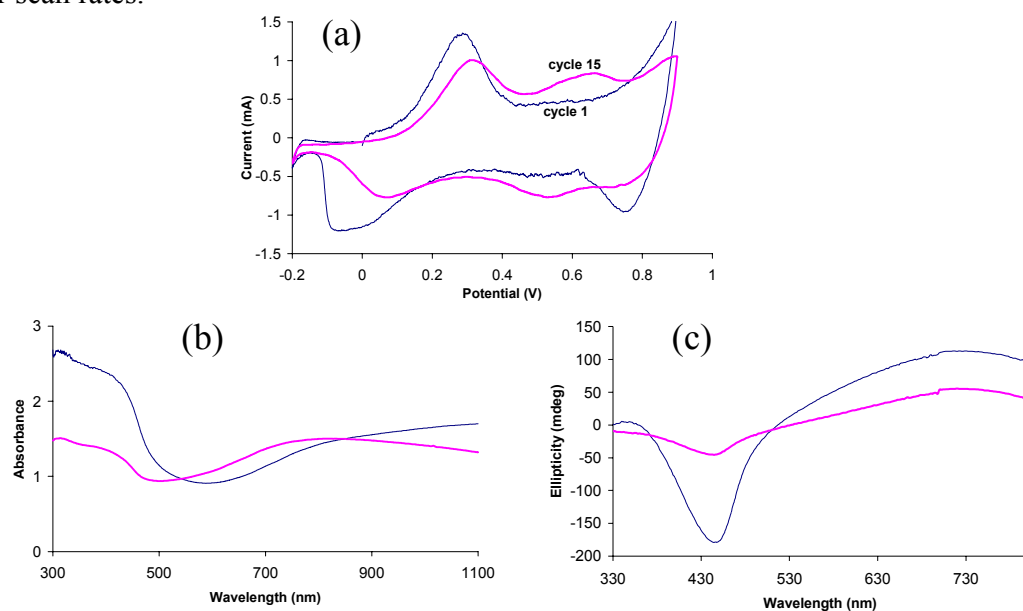


Figure 9.9 CVs (a), UV-visible spectra (b), and CD spectra (c) of a PAn.(+)-HCSA film on an ITO-glass electrode before (thin line) and after (thick line) potential cycling between -0.2 and 0.9 V for 15 cycles in aqueous 1.0 M HCl. Scan rate of 10 mV/s.

It has been previously reported that polyaniline films will be degraded when exposed to high anodic potentials sufficient to generate pernigraniline during either potentiodynamic^{15, 20, 51} or potentiostatic^{20, 22} electropolymerization, and thereafter. The degradation rate of polyaniline was strongly dependent on the applied potential, the solution pH^{22, 48} and the kind of solvent employed.²⁰ The rate of such degradation processes increases noticeably with a decrease of solution pH because the oxidation potentials of polyaniline increase by 0.12 V for each unit of decrease in pH.²² Thus, the degradation of polyaniline was observed at scanning potentials exceeding 0.5 V in pH 3 aqueous solution,⁴⁸ at 0.7 V in 1.0 M HCl⁵² and at 0.8 V in 1.0 M H₂SO₄.⁴⁸ The degradation rate was also much higher in acidic aqueous solutions than in organic solutions (1,2-dimethoxyethane and propylene carbonate).²⁰

(b) CVs in Aqueous Neutral Electrolyte (0.5 M NaNO₃)

The related cyclic voltammogram of an electrodeposited PAn.(+)-HCSA film recorded in 0.5 M NaNO₃ under potential scanning in the range of -0.2 to +0.9 V (scan rate of 50 mV/s) is presented in Figure 9.10a. In this neutral electrolyte, two anodic peaks were recorded only during the first and second scans, while the corresponding cathodic peaks were not clearly observed in the reverse cathodic scans. A broad, single anodic peak in the region 0.25-0.45 V was observed in subsequent scans. The current response decreased with successive scans until almost zero after 10 scans.

However, electroactivity of the film was restored when the film was immersed in aqueous acidic solution (1.0 M HCl), since a typical CV of polyaniline with well-resolved redox couples was seen, as shown in Figure 9.10b. It is well known that the electroactivity of

polyaniline is pH-dependent in aqueous medium. The redox activity of polyaniline ceases in aqueous media of $\text{pH} > 3-4$.^{16, 53} Thus, in the present study, the redox activity of the PAn.(+)-HCSA emeraldine salt film was observed during the initial potential sweeps in neutral aqueous NaNO_3 electrolyte. However, repetitive potential cycling of the film in the neutral medium led to a rapid decrease of current responses, due to de-doping of the emeraldine salt to give emeraldine base, an insulator. This is supported by the UV-visible and CD spectral changes observed when a PAn.(+)-HCSA emeraldine salt film ($\lambda_{\text{max}} = 350, 430, 800 \text{ nm}$) converted to emeraldine base ($\lambda_{\text{max}} = 340, 620 \text{ nm}$) when the film was immersed in water or a neutral electrolyte. For example, in Figure 9.11a the UV-visible spectrum was seen to change to that of emeraldine base over 20 min. Similar changes occurred in the corresponding CD spectrum of the polyaniline film (Figure 9.11b), giving a CD spectrum characteristic of optically active emeraldine base. A colour change from green to blue due to such de-doping during immersion of emeraldine salts in water^{22, 29} or in low acidic aqueous solution ($\text{pH} > 3-4$)⁵⁴ has been previously reported.

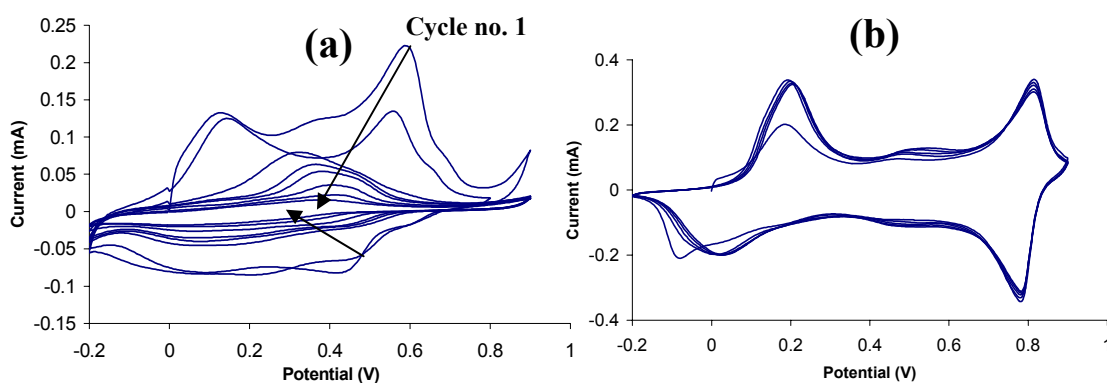


Figure 9.10 Cyclic voltammograms for a PAn.(+)-HCSA film electrodeposited onto glassy carbon (surface area = 0.07 cm^2), carried out in (a) 0.5 M NaNO_3 , between -0.2 and 0.9 V for 30 cycles (cycles 1-10 were shown); and then recorded in (b) 1.0 M HCl , between -0.2 and 0.9 V for 5 cycles. Scan rate = 50 mV/s .

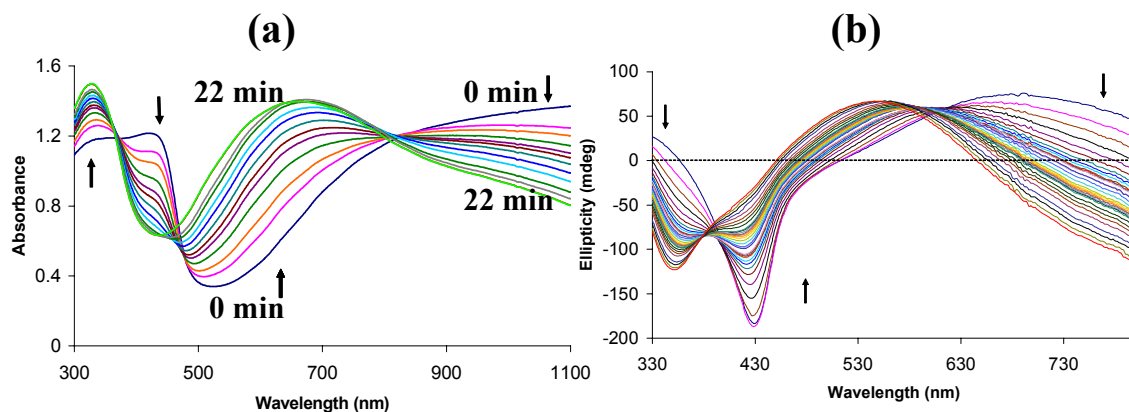


Figure 9.11 (a) UV-visible spectra of a PAN.(+)-HCSA film in water recorded at 2 min intervals; (b) CD spectra of a PAN.(+)-HCSA film in water measured after 1 min and then every 3 min.

9.3.2.2 CVs of PAN.(+)-HCSA Films in Ionic Liquids

(a) CVs in EMI-TFSI

Figure 9.12 shows the cyclic voltammograms of a PAN.(+)-HCSA modified glassy carbon electrode recorded in EMI-TFSI as electrolyte. Only one redox couple was observed when the potential was scanned between - 0.2 and 1.0 V vs. Ag/AgCl_(EMI-TFSI). An oxidation wave appeared at *ca.* 0.6 V, and a corresponding reduction in the cathodic sweep at *ca.* 0.15 V. Subsequent studies indicated that this redox couple can be attributed to the leucoemeraldine ↔ emeraldine redox transition. The redox activity of the polyaniline film underwent changes with successive scans (Figure 9.12a), and became constant after *ca.* 20 cycles (Figure 9.12b). The redox couple now exhibited oxidation and reduction waves *ca.* 0.15 and - 0.09 V, respectively. These redox changes in the early stages of potential cycling (cycles 1-50) may be attributed to electrochemically induced ion exchange between the (+)-CSA⁻ anion in the as-grown PAN.(+)-HCSA film and the ion TFSI⁻ from the EMI-TFSI ionic liquid. The initial oxidation wave (leucoemeraldine ↔ emeraldine transition)

observed at *ca.* 0.6 V gradually moved to less positive potentials with subsequent scans, suggesting that the electrolyte ion is initially more difficult to incorporate.

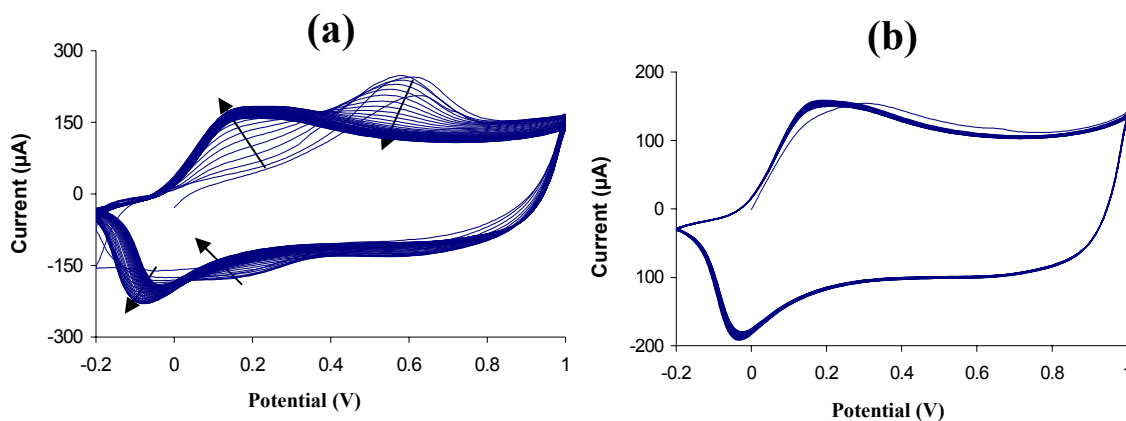


Figure 9.12 Cyclic voltammograms (50 mV/s) for a PAn.(+)-HCSA film deposited on glassy carbon (surface area = 0.07 cm²), carried out in neat EMI-TFSI: (a) cycles 1-50, (b) cycles 51-100.

Upon further potential scanning (cycles 110-310), however, a small decrease in the current response was observed for the redox couples (Figure 9.13a). The stability of PAn.(+)-HCSA films in EMI-TFSI electrolyte was also investigated by extending the potential range from -0.2 to increasingly positive potentials of 1.1 and 1.2 V in Figures 9.13b and 9.13c. Significantly, two well-defined redox couples, attributable to the conversions of leucoemeraldine \leftrightarrow emeraldine and emeraldine \leftrightarrow pernigraniline were observed (with oxidation peaks at *ca.* 0.2 and 1.05 V and reduction peaks at *ca.* 0.75 and 0.08 V), when the CV were recorded over the range of -0.2 to 1.2 V (Figure 9.13c). That is, the CV was similar to that observed in aqueous acids. In this scan range, the CV stabilized within twenty cycles.

A significant effect of the potential range on the stability of the CV response of PAn.(+)-HCSA films in EMI-TFSI was also seen. The decrease in current response noted above after prolonged scanning occurred more rapidly when the films were cycled to more positive potentials (e.g. 1.1 or 1.2 V - see Figures 9.13a-c). In these cases, the films were degraded and dissolved/dispersed in the ionic liquid medium. Degradation of polyaniline in ionic liquids will be discussed in more detail later (Section 9.3.5).

When the potential was scanned to more negative potentials -1.5 V and -2.0 V, the current response again gradually decreased with repeated cycling, and an electroinactive film was observed after *ca.* 30 cycles and 10 cycles, respectively (see Figures 9.14a and 9.14b). However, the electroactivity of this film was recovered when it was thoroughly washed with MeOH to remove EMI-TFSI and its CV then recorded in aqueous 1.0 M HCl (insets in Figure 9.14). The electroactivity lost upon extended cycling to low potentials in EMI-TFSI probably arises from de-doping, since the electroactivity of the polyaniline film was maintained when the CV of PAn.(+)-HCSA was recorded in EMI-TFSI containing 0.5 M (+)-HCSA (not shown). (A temperature of 50°C was necessary for the latter measurement in order to dissolve the camphorsulfonic acid in the ionic liquid.)

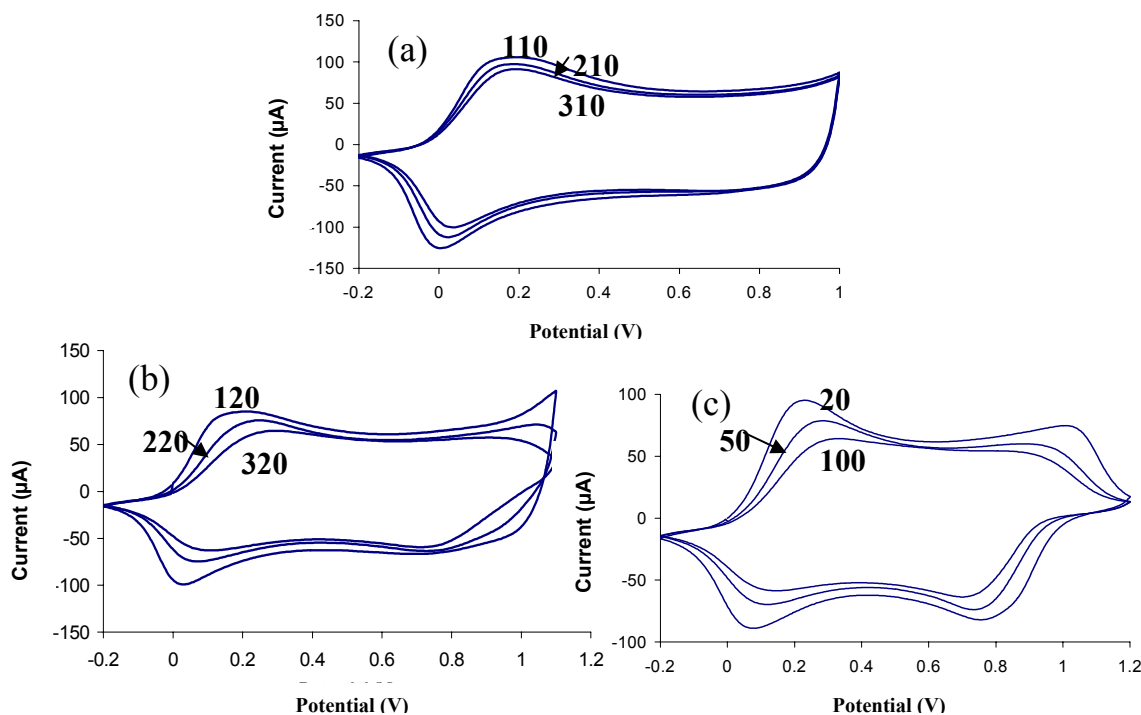


Figure 9.13 Cyclic voltammograms of PAN.(+)-HCSA films deposited on glassy carbon (surface area = 0.07 cm^2) recorded in neat EMI-TFSI (scan rate of 50 mV/s); (a) between -0.2 and 1.0 V , (b) between -0.2 and 1.1 V , (c) between -0.2 and 1.2 V .

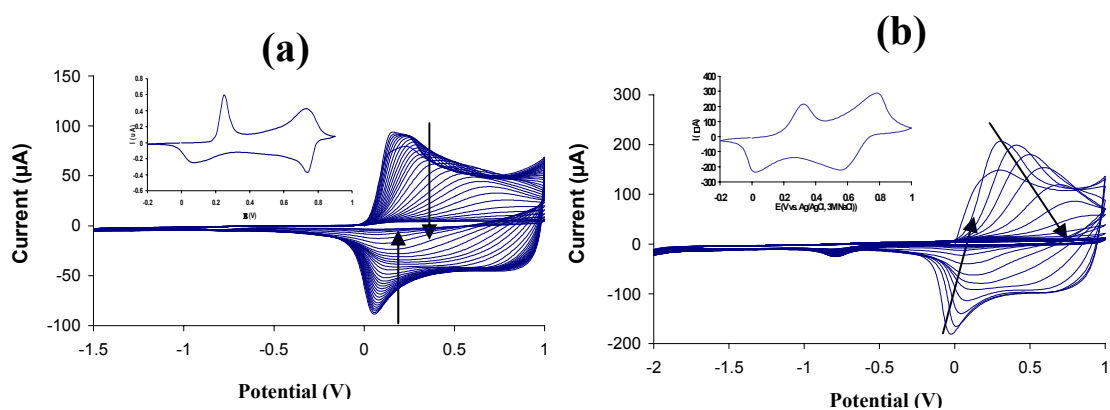


Figure 9.14 Cyclic voltammograms of PAN.(+)-HCSA films deposited on glassy carbon (surface area = 0.07 cm^2) recorded in neat EMI-TFSI (scan rate of 50 mV/s): (a) between -1.5 and 1.0 V for 40 cycles, (b) between -2.0 and 1.0 V for 50 cycles. The films had previously been cycled between -0.2 and 1.0 V in the EMI-TFSI medium for 30 cycles prior to these measurements. *Insets*: CV of the films in 1.0 M HCl after investigating in the ionic liquid.

(b) CVs in (-)-, (+)-, and (±)-MBEA-TFSI

Cyclic voltammograms were then recorded for PAn.(+)-HCSA films in the chiral ionic liquid (-)-MBEA-TFSI, containing the same TFSI anion as the above EMI-TFSI electrolyte. As for the CV recorded in EMI-TFSI, only a single oxidation wave was initially observed (at *ca.* 0.7 V), but now two distinct reduction waves (at *ca.* 0.73 and 0.2 V) were seen in the cathodic sweep (Figure 9.15a). The CV changed over 30 cycles to give a constant CV exhibiting what appeared to be two redox couples with oxidation peaks at *ca.* 0.3 and >1.1 V and corresponding reduction peaks at 0.8 and -0.1 V, respectively, and then remained constant (Figures 9.15 a-c). The two redox couples may be attributed to the conversions of leucoemeraldine ↔ emeraldine and emeraldine ↔ pernigraniline. The changes seen in Figures 9.15a-9.15b are believed to be associated with exchanging the initial (+)-CSA⁻ anions in the polyaniline films with TFSI⁻ ions.

When the potential range for the CVs was extended to more positive potentials (e.g. to 1.4 V in Figure 9.16), two redox couples were clearly observed. The initial scan (not shown) was similar to that in Figure 9.15a, but now revealed the second oxidation (emeraldine → pernigraniline) at *ca.* 1.25 V. However, oxidative degradation of the polyaniline film apparently occurs at high potentials in MBEA-TFSI, since the current responses decreased with successive scans (Figure 9.16). The film was degraded and then dissolved/dispersed in the ionic liquid.

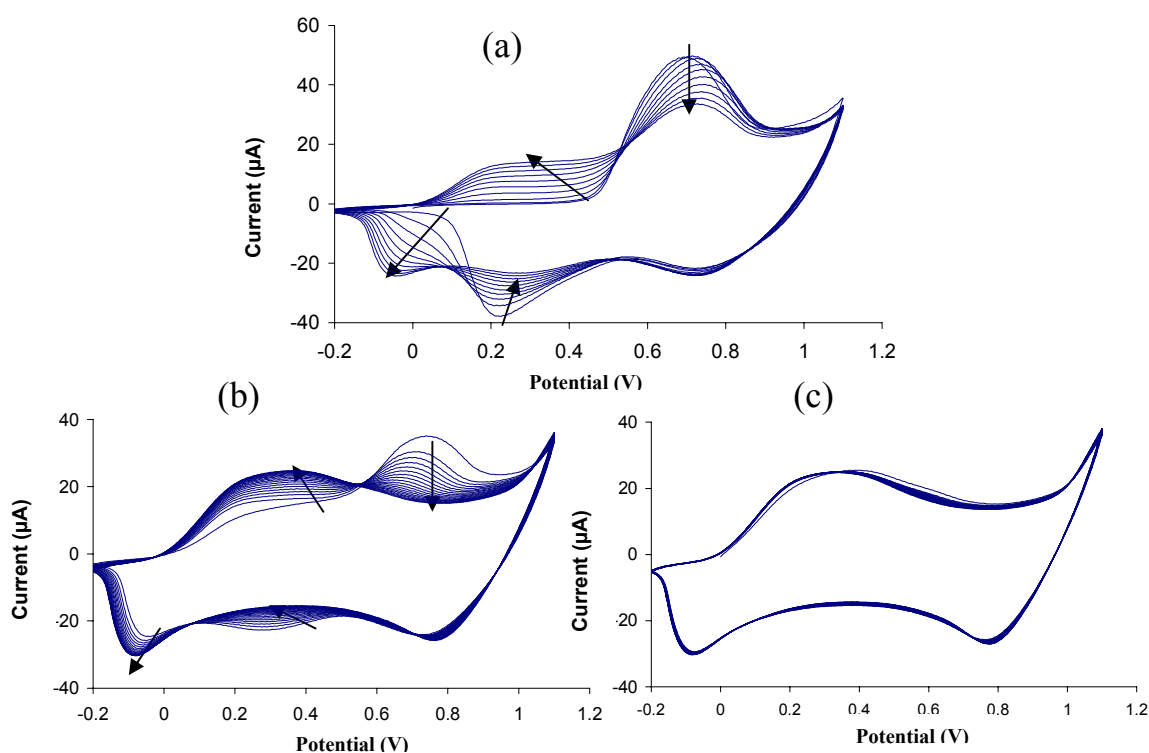


Figure 9.15 Cyclic voltammograms of a PAN.(+)-HCSA film deposited on glassy carbon (surface area = 0.07 cm^2) recorded in (-)-MBEA-TFSI between -0.2 and 1.1 V (scan rate of 25 mV/s): (a) cycles 1-10, (b) cycles 11-30, and (c) cycles 31-50.

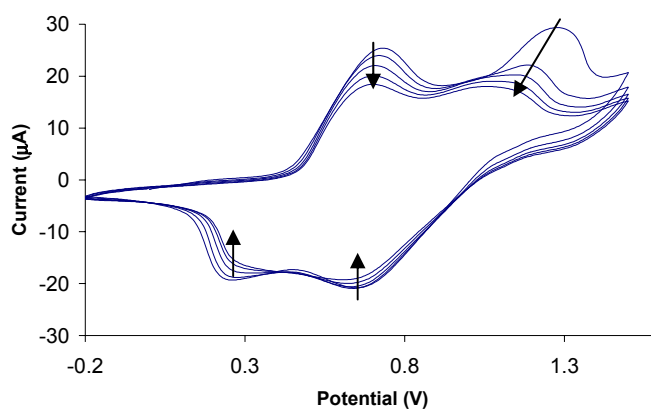


Figure 9.16 CVs of a PAN.(+)-HCSA film deposited on glassy carbon recorded in (-)-MBEA-TFSI between -0.2 and 1.5 V (scan rate 25 mV/s).

Unlike the observation above in EMI-TFSI, the electroactivity of the polyaniline film was still maintained when the potential range was extended to very low negative potentials (Figure 9.17a). An electroactive film was still observed with lower potential limits as negative as -2.0 V (Figure 9.17 b). Similar results were also obtained in analogous studies using (+)- and (±)-MBEA-TFSI as electrolyte (not shown). This suggests that the charge transfer process takes place very well during the redox process of polyaniline in each of these MBEA-TFSI electrolytes.

The retention of electroactivity for polyaniline films even at -2.0 V in MBEA-TFSI is significant, as it opens the possibility of using optically active PAn.(+)-HCSA as chiral electrodes in electrochemical asymmetric reductions requiring very negative potential (e.g. the reduction of prochiral ketones to chiral alcohols).

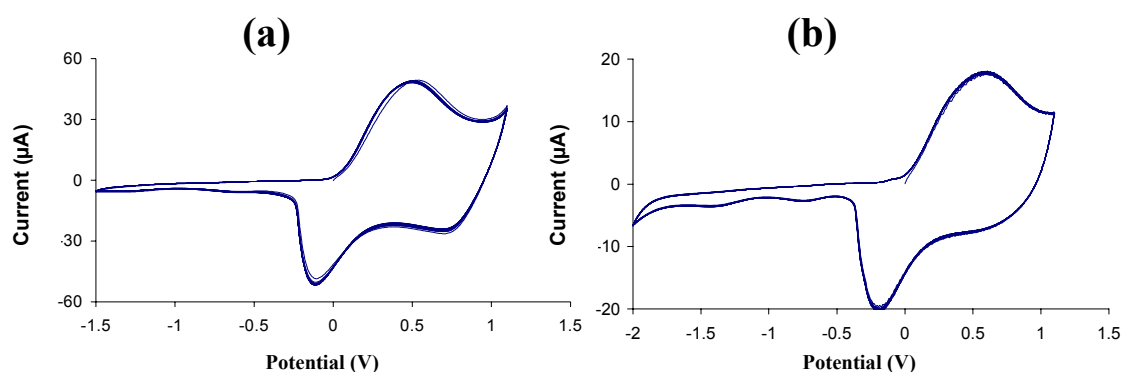


Figure 9.17 CVs of PAn.(+)-HCSA films deposited on glassy carbon recorded in (-)-MBEA-TFSI: (a) between -1.5 and 1.1 V (scan rate of 50 mV/s, cycles 91-110), and (b) between -2.0 and 1.1 V (cycles 41-60).

(c) CVs in BMI-PF₆

As with the above ionic liquid electrolyte, only a single redox couple corresponding to the conversion between leucoemeraldine and emeraldine oxidation states was observed when the CV of PAn.(+)-HCSA was recorded between -0.2 and 1.1 V in BMI-PF₆ (Figure 9.18a). The potential for this redox process shifted to lower potentials over 30 cycles, similar to the behaviour observed in EMI-TFSI and MBEA-TFSI. Again, anion exchange processes may be responsible for these changes.

Surprisingly, in contrast to EMI-TFSI and MBEA-TFSI, electroactivity of the polyaniline film was maintained for more than hundred cycles (with only small changes in CVs) when the PAn.(+)-HCSA film was cycled in BMI-PF₆ to potentials as positive as +2.0 V (Figure 9.18b). After this treatment and thoroughly washing with methanol and drying, a typical CV for polyaniline was observed when the film was re-immersed in aqueous 1.0 M HCl. To confirm the stability of PAn.(+)-HCSA films in BMI-PF₆ at high positive potentials, a constant potential of +2.0 V was applied for 30 min. Again, a normal CV for polyaniline was observed when the film was washed with methanol and the potential scanned in 1.0 M HCl (not shown).

The fact that PAn.(+)-HCSA is stable at potentials as high as 2.0 V in the BMI-PF₆ electrolyte is very significant, as it opens the possibility of exploring electrochemical asymmetric oxidation of substrates (such as the oxidation prochiral organic sulfides to chiral sulfoxides) at such potentials.

On the other hand, a PAn.(+)-HCSA film lost its electroactivity rapidly during potential cycling between -1.5 and +1.0 V in BMI-PF₆ (Figure 9.18c). However, the electroactivity could be recovered in aqueous acid. This reversible loss of electroactivity probably arises from uncompensated charge transfer processes and/or de-doping, as observed above in EMI-TFSI electrolyte.

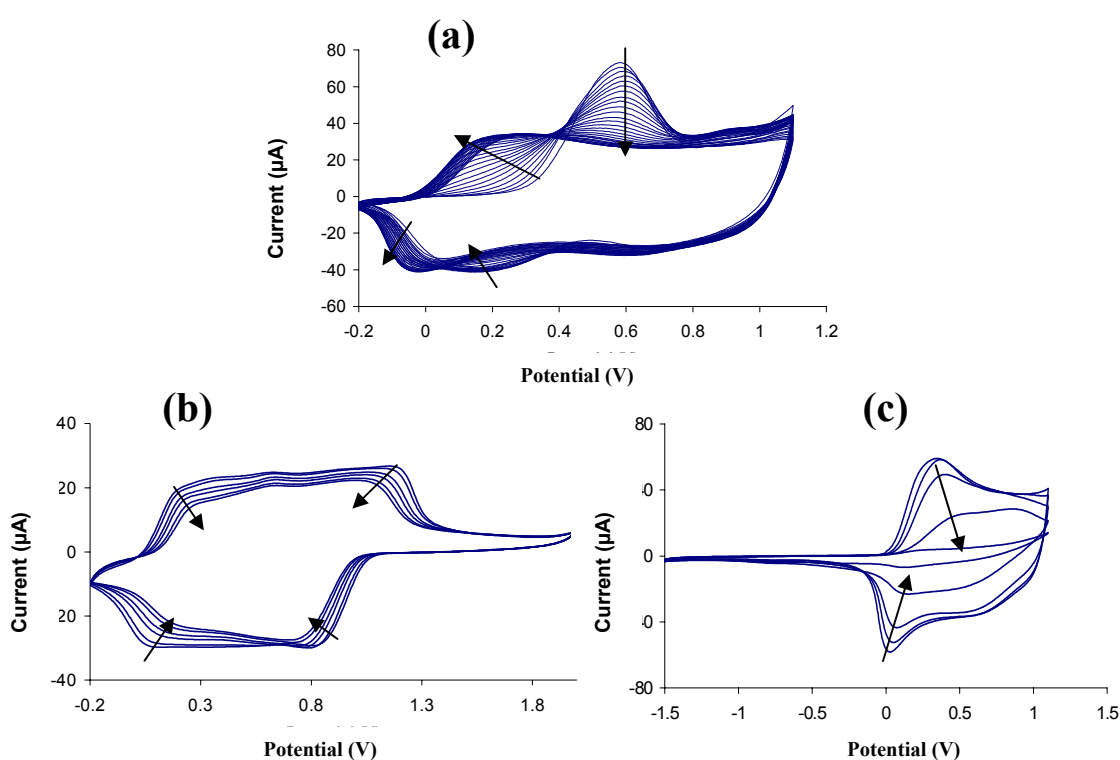


Figure 9.18 CVs of PAn.(+)-HCSA films deposited on glassy carbon recorded in BMI-PF₆ : (a) between -0.2 and 1.1 V, cycle nos. 1-30; (b) between -0.2 and 2.0 V, cycle nos. 30, 50, 80, 100, 130, 150; and (c) between -1.5 and 1.1 V, cycle nos. 1, 5, 10, 20, 30. Scan rate = 50 mV/s. (Note: a, b and c are different films)

(e) CVs of PAn.(+)-HCSA Films in BMI-BF₄

When the CV of a PAn.(+)-HCSA film was recorded over the potential range of -0.2 to 1.1 V in BMI-BF₄, only one pair of redox peaks was again initially observed (assignable to the conversion between leucoemeraldine and emeraldine oxidation states). Changes in the CV features were also observed over 20 cycles (Figure 9.19a), as seen above in the other ionic liquid electrolytes.

When the positive potential in the scans was extended to +2.0 V (Figure 9.19b), two redox couples associated with the leucoemeraldine ↔ emeraldine and emeraldine ↔ pernigraniline redox couples were observed. A gradual decrease in current response was seen. However, the film did not degrade or dissolve/disperse in the ionic liquid under the condition employed.

The electrochemical stability of PAn.(+)-HCSA in BMI-BF₄ was further investigated by holding a film at +2.0 V for 20 min. Electroactivity with a typical CV for polyaniline was observed after thoroughly washing with methanol and potential cycling in aqueous 1.0 M HCl (not shown). These results suggest that PAn.(+)-HCSA is very stable in BMI-BF₄ at high positive potentials, since no oxidative degradation of the polyaniline was detected.

However, when the CVs were carried out in the range of -2.0 to 0.8 V in BMI-BF₄, the electroactivity of the polymer was shut down (Figure 9.19c). The electroactivity could be restored in acidic solution. Losing of the polyaniline electroactivity during potential scanning to very negative potentials (-2.0 V) in BMI-BF₄ may arise from de-doping and/or uncompensated charge transfer processes.

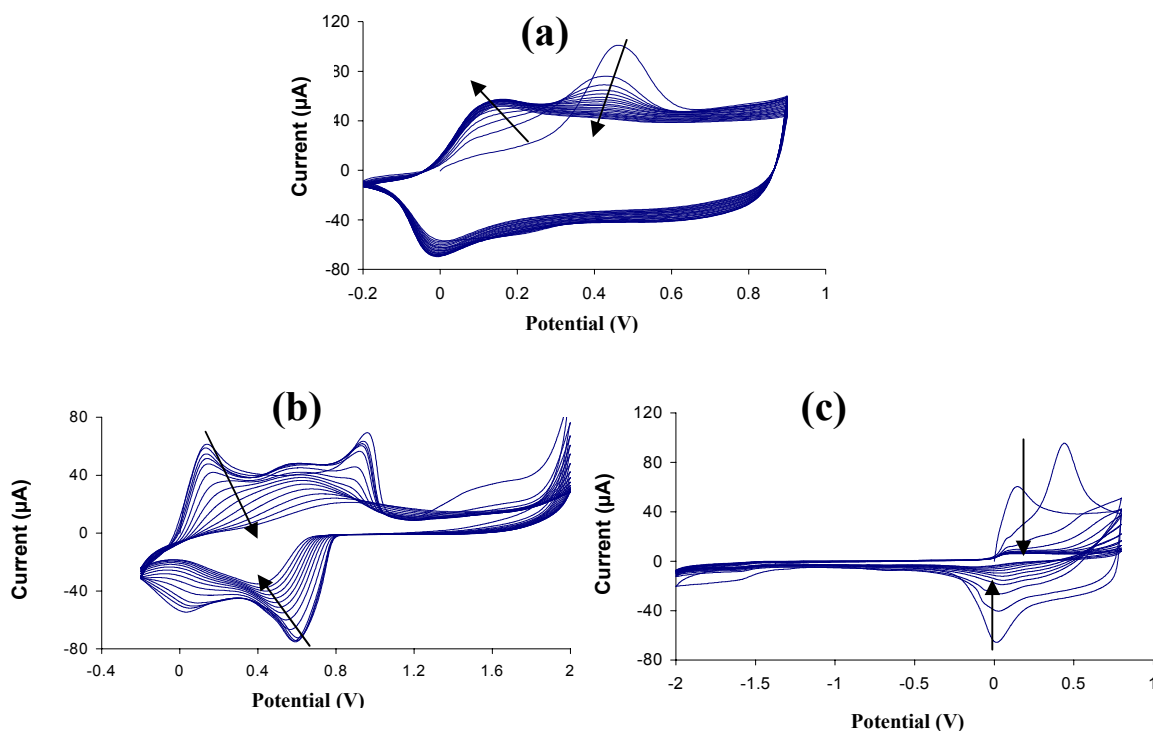


Figure 9.19 CVs of PAN.(+)-HCSA films deposited on glassy carbon recorded in BMI-BF₄: (a) between -0.2 and 1.1 V, cycle nos. 1-30; (b) between -0.2 and 1.7 V, cycle nos. 30, 50, 80, 100, 130, 150; and (c) between -1.5 and 1.1 V, cycle nos. 1, 5, 10, 20, 30. Scan rate = 50 mV/s. (Note: a, b and c is different films)

9.3.3 *In situ* Spectroelectrochemical Studies of PAN.(+)-HCSA Films in Various Electrolytes

As a critical step in using PAN.(+)-HCSA modified electrodes as chiral electrodes for electrochemical asymmetric synthesis in ionic liquids, the chiroptical properties of the chiral polyaniline films were investigated by *in situ* electrochemical UV-visible and circular dichroism. For comparison, the experiments were also carried out in acidic and neutral aqueous electrolytes.

9.3.3.1 *In situ* UV-visible and CD Spectroelectrochemical Studies of PAn.(+)-HCSA Films in Aqueous Electrolytes

(a) In situ Spectroelectrochemistry in 0.5 M (+)-HCSA

Oxidation

In situ UV-visible absorption spectra of a PAn.(+)-HCSA film as the potential was stepped from 0.1 to 0.7 V in aqueous 0.5 M (+)-HCSA are presented in Figure 9.20a. At 0.1 V, the spectrum showed absorbance peaks at *ca.* 350 and 420 nm together with a shoulder at *ca.* 900 nm and a strong free carrier tail into the near infra-red. These bands are assigned to π - π^* , polaron- π^* , and π -polaron transitions, respectively. The highest intensity band was at *ca.* 420 nm. This spectrum at 0.1 V is consistent with the polyaniline film consisting of a mixture of leucoemeraldine base and emeraldine salt states. Increasing the applied potential stepwise from 0.1 to 0.7 V, resulted in a blue shift in the spectral bands, together with decreasing absorbance in the 350-450 nm region and markedly increased intensity in the 650-1100 nm region characteristic of conversion to the emeraldine salt form.

The spectra shown in Figure 9.20a developed in each case within 1 min of applying the particular potential, and did not undergo any further changes with time. However, when the potential was increased to 0.8 V, a new spectrum was generated showing a broad λ_{max} at *ca.* 750 nm and another band at 350 nm (Figure 9.21a). This is consistent with oxidation to pernigraniline salt. This latter spectrum decreased in intensity with time, and the film was observed to fall off the ITO-glass working electrode. These observations are consistent with electrochemical oxidative degradation of the polyaniline film. Thus, once oxidation to pernigraniline salt occurred at a potential of 0.8 V, degradation of the polymer takes place in the acidic aqueous electrolyte. Similar results were previously observed for polyaniline

doped with inorganic acids.^{19, 20, 22, 55} Pernigraniline, particularly the salt form generated in acid solution, is known to be unstable, undergoing hydrolysis to produce *p*-benzoquinone as the main product.^{19, 56}

The above conclusions were supported by the corresponding CD spectra shown in Figures 9.20b and 9.21b. The CD spectrum of the polyaniline film held at 0.1 V showed a strong CD band at *ca.* 355 nm and a shoulder band at *ca.* 440 nm, but no signals above 500 nm. This is consistent with it being largely in the leucoemeraldine base form which has a single peak at *ca.* 340 nm. Upon raising the potential progressively from 0.2 V to 0.7 V, the 355 nm CD band was replaced by a strong CD band at *ca.* 465 nm and a broad CD signal (of opposite sign) at higher wavelength, characteristic of PAn.(+)-HCSA emeraldine salt generated by oxidation at these higher potentials.

A further increase in potential to 0.8 V caused a major change in the CD spectrum to that shown in Figure 9.21b, consistent with oxidation to pernigraniline salt. However, these CD signals decreased to zero over a further 15 min, as expected from the oxidative degradation of pernigraniline salt in acid solution.

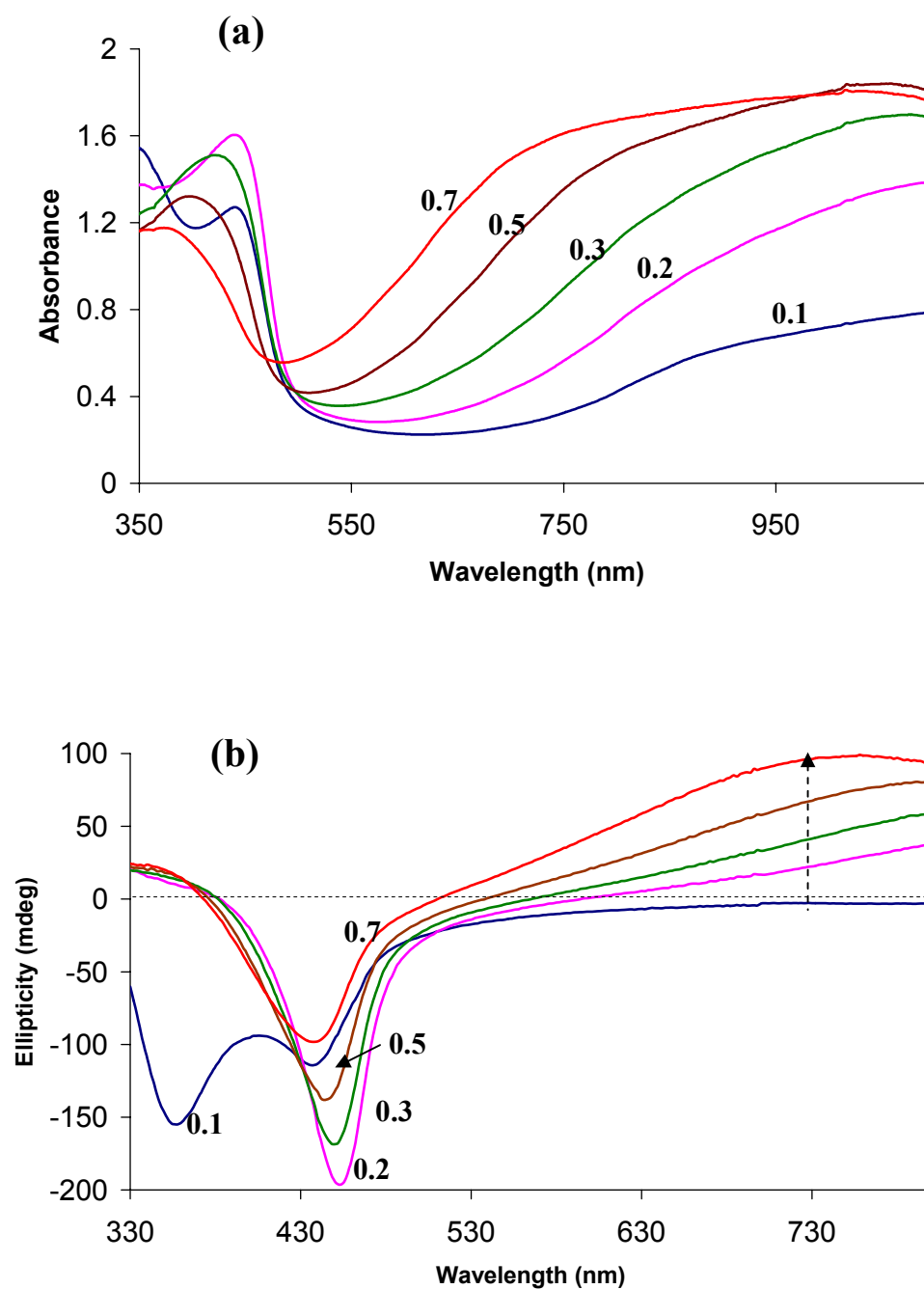


Figure 9.20 *In situ* UV-visible (a) and CD (b) spectra of PAN.(+)-HCSA films after held at various positive potentials (from 0.1 V to 0.7 V) for 1 min in 0.5 M (+)-HCSA. (a and b are different films).

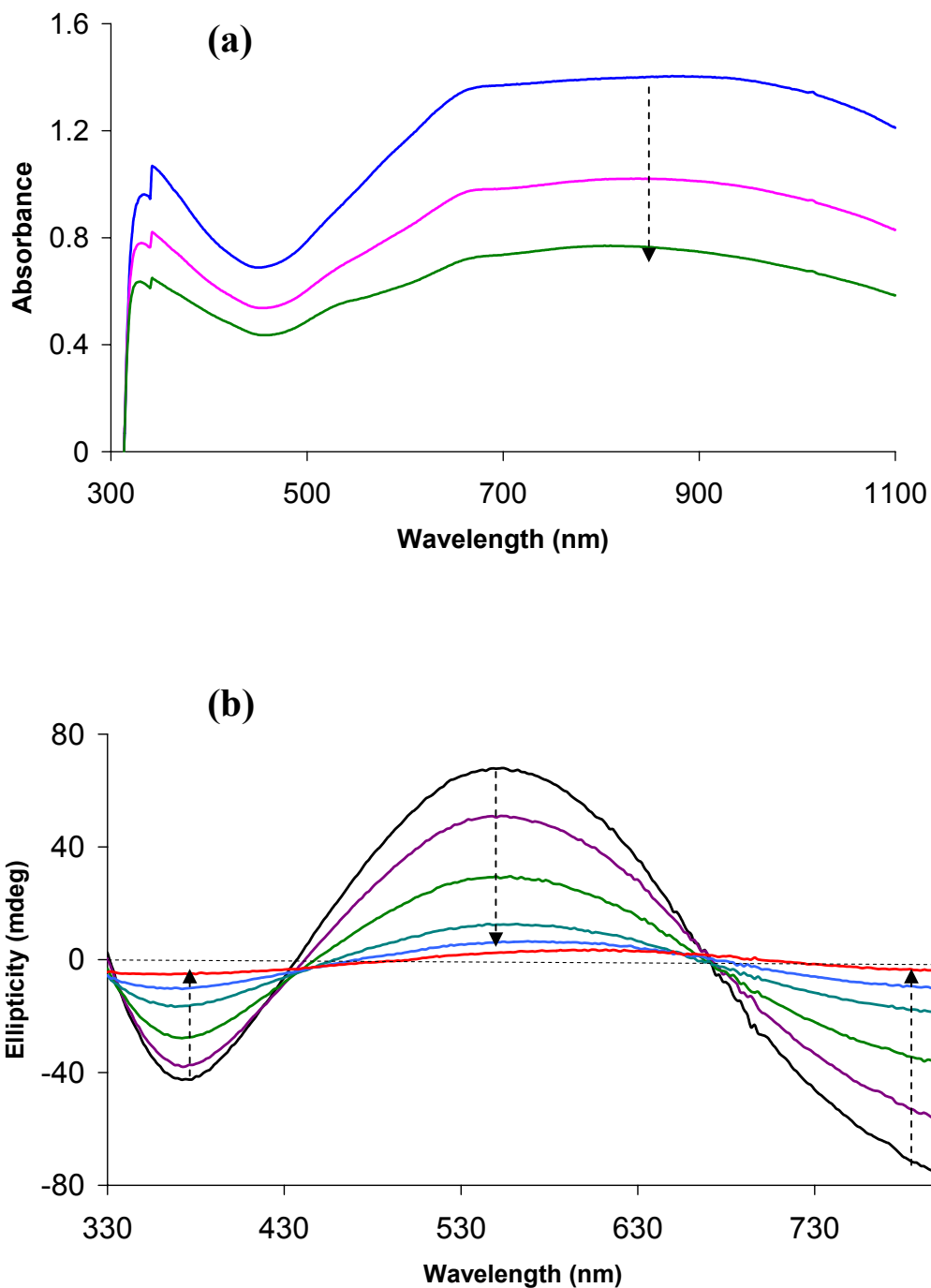


Figure 9.21 *In situ* UV-visible (a) and CD (b) spectra of PAN.(+)-HCSA films after held at 0.8 V for 1 min and then at 3 min intervals in 0.5 M (+)-HCSA. (a and b are different films).

Reduction

In situ UV-visible studies (Figure 9.22a) showed that reduction of a PAn.(+)-HCSA film to leucoemeraldine base proceeded to completion after applying a potential of -0.5 V for 10 min in aqueous 0.1 M (+)-HCSA. The absorption band generated was at *ca.* 350 nm, characteristic of leucoemeraldine base. The characteristic CD spectrum of leucoemeraldine base was also observed (Figure 9.22b), with bisignate CD bands at *ca.* 330 and 390 associated with the 350 nm absorption band. The UV-visible and CD spectra of this electrochemically produced leucoemeraldine base film are similar to those produced via chemical (hydrazine) reduction.²⁸

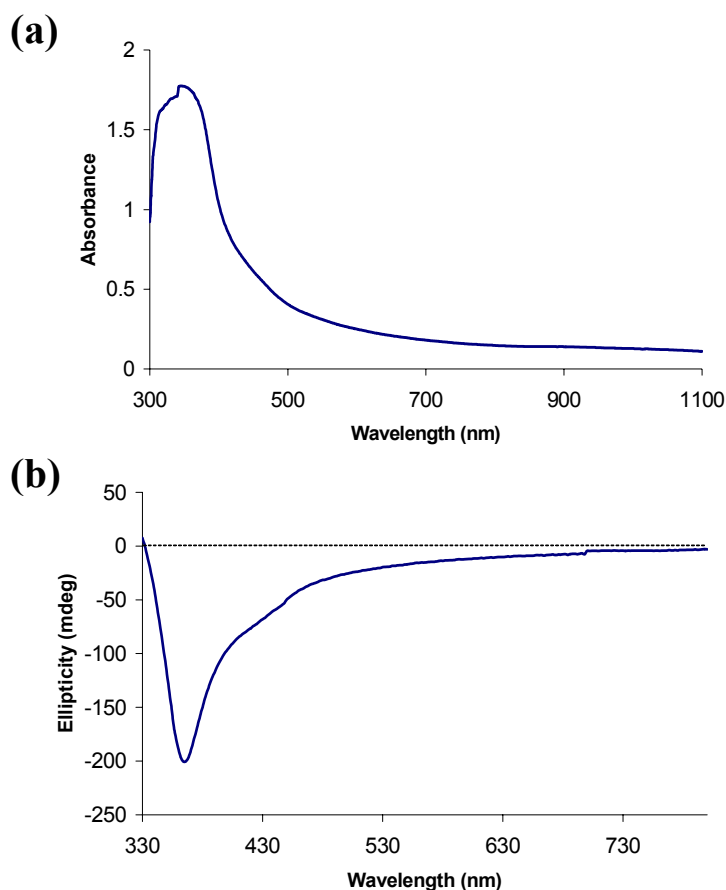


Figure 9.22 *In situ* UV-visible spectra (a) and CD spectra (b) of a PAn.(+)-HCSA film after held at -0.5 V for 10 min in 0.1 M (+)-HCSA.

(b) In situ Spectroelectrochemistry in 0.5 M NaNO₃

Oxidation

The *in situ* UV-visible spectrum for a PAn.(+)-HCSA film recorded while holding at 0.3 V for 7 min in 0.5 M NaNO₃ was characteristic of the emeraldine salt form of polyaniline, exhibiting λ_{max} at 340, 430 and 800 nm (Figure 9.23a). Little change in the emeraldine salt spectrum occurred over the 7 min, confirming its stability at this potential. When the potential was held at 0.5 V, the shoulder at 430 nm disappeared and the absorbance in the 700-1100 nm region gradually decreased in intensity; while a new band appeared at *ca.* 570 nm (Figure 9.23b) characteristic of pernigraniline base. Three isosbestic points were observed at 380, 420 and 650 nm for 27 min until the spectrum ceased changing, indicating a clean oxidation. This result is consistent with spontaneous deprotonation of polyaniline occurring during the oxidation of emeraldine salt to pernigraniline base previously reported.⁵⁷

However, the presence of significant residual absorbance at high wavelengths after 27 min at 0.5 V indicated that the oxidation, although extensive, had not proceeded to completion at this potential. Applying a potential of 0.8 V to the film drove the oxidation to pernigraniline base to completion, as shown by the UV-visible spectrum in Figure 9.23c.

The pernigraniline base film produced in neutral aqueous NaNO₃ is clearly more resistant to degradation than the pernigraniline salt produced above in 0.5 M camphorsulfonic acid. It is also interesting that the pernigraniline state can be largely generated at 0.5 V in neutral aqueous electrolyte, whereas a potential of 0.8 V was necessary in aqueous acid. As mentioned earlier, the oxidation potential of polyaniline decreases with increasing pH.²²

This presumably is the cause of the easier oxidation at higher pH (in neutral or basic solution) than at lower pH (in acid solution).

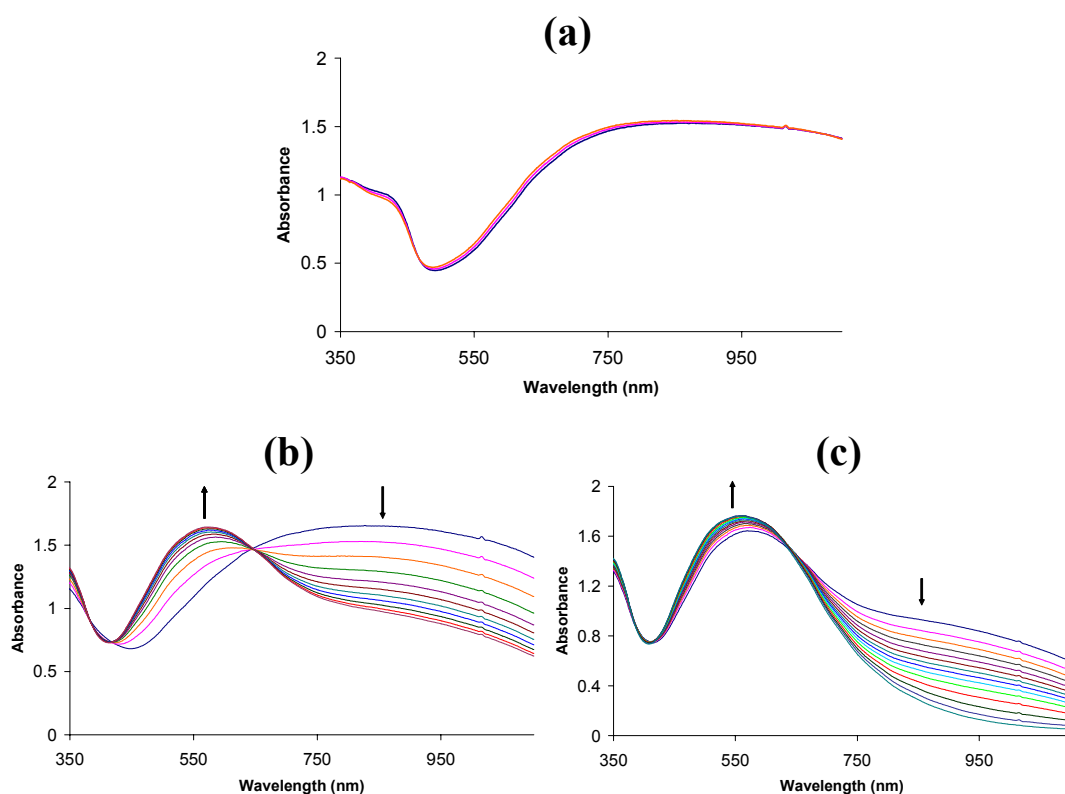


Figure 9.23 *In situ* UV-visible spectra of a PAN.(+)-HCSA film after held for 1 min at (a) 0.3 V, (b) 0.5 V and (c) 0.8 V in 0.5 M NaNO₃, and then at 2 min intervals.

The corresponding CD spectra of the PAN.(+)-HCSA film recorded after applying potentials of 0.3, 0.5 and 0.8 V in 0.5 M NaNO₃ are presented in Figure 9.24. The CD spectrum measured after 1-10 min at 0.8 V is consistent with oxidation to pernigraniline base. Bisignate CD bands at *ca.* 465 and 660 nm (crossing the zero line at *ca.* 530 nm) are associated with the absorption band at 550 nm, while the negative CD band at *ca.* 360 nm is believed to be the high wavelength component of a bisignate CD bands associated with the

340 nm absorption band of pernigraniline base. Further increases in the intensity of the CD bands for the oxidized polyaniline occurred over a further 10 min at 0.8 V (not shown), at which stage the spectrum stabilized.

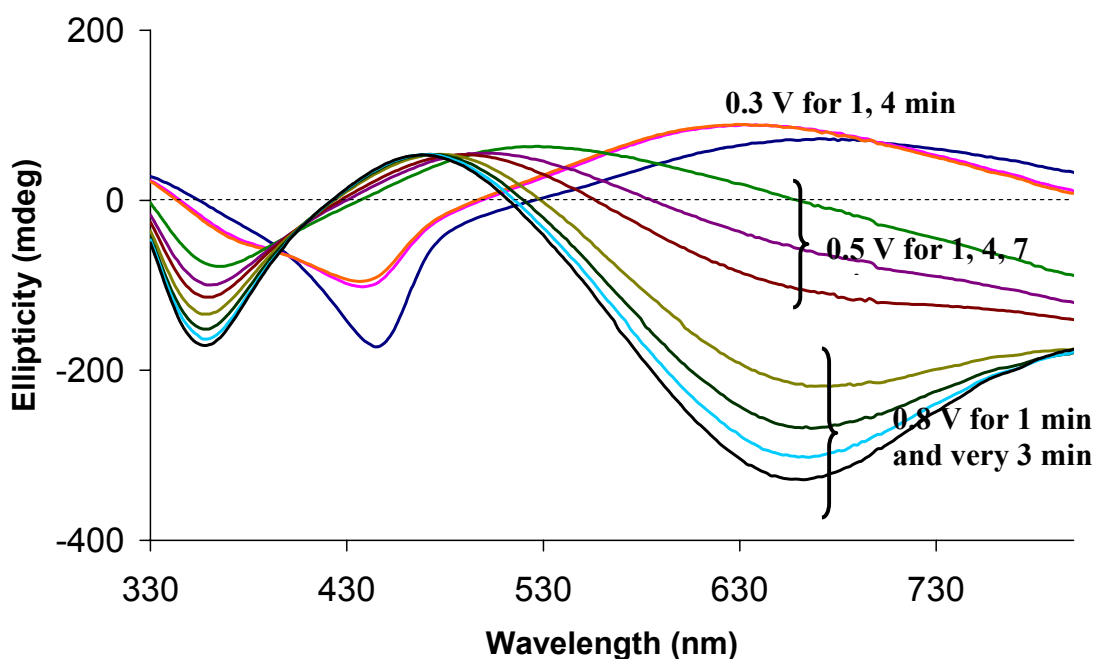


Figure 9.24 *In situ* CD spectra of a PAn.(+)-HCSA film after held for 1 min at: 0.3 V, 0.5 V and 0.8 V in 0.5 M NaNO₃ and then at 3 min intervals.

Reduction

The UV-visible spectrum of leucoemeraldine base (λ_{max} at *ca.* 340 nm) was generated after applying a potential of -0.5 V to a PAn.(+)-HCSA film in 0.5 M NaNO₃ for 30 min (Figure 9.25a), confirming electrochemical reduction. The characteristic CD spectrum of leucoemeraldine base was also generated at -0.5 V, with bisignate CD bands at *ca.* 330 and 390 associated with the 340 nm absorption band. The UV-visible and CD spectra of this electrochemically produced leucoemeraldine base film are similar to those produced via

electroreduction in 0.1 M (+)-HCSA (see Figure 9.22) and chemical (hydrazine) reduction.²⁸

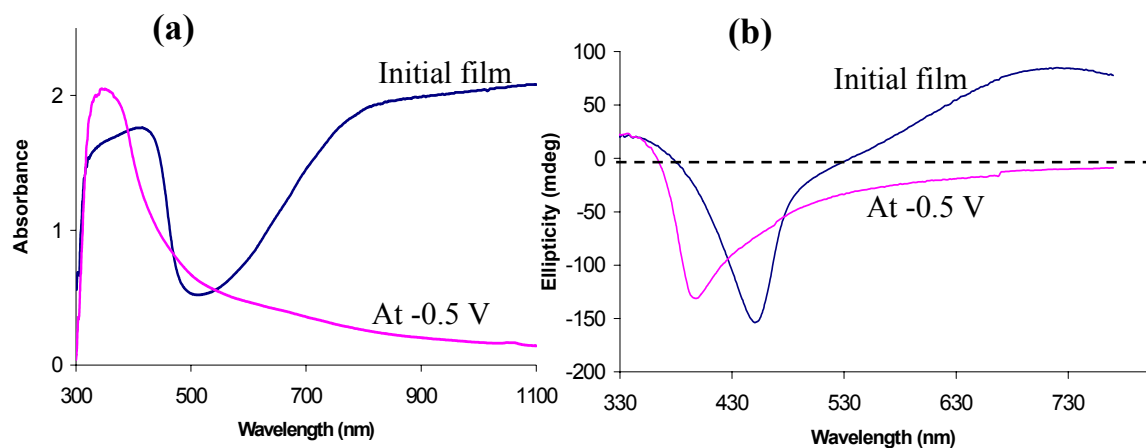


Figure 9.25 *In situ* UV-visible spectra (a) and CD spectra (b) of a PAn.(+)-HCSA film after held at -0.5 V for 30 min in 0.5 M NaNO₃.

The results described above indicate that the optical activity of chiral polyaniline can be maintained in the oxidized and reduced forms produced via electrochemical treatment in aqueous acidic and neutral solutions. However, in the presence of acid, the pernigraniline salt formed at potentials of > 0.8 V undergoes oxidative degradation with loss of optical activity, and the films eventually fall off the ITO-glass electrode.

9.3.3.2 *In situ* UV-visible and CD Spectroelectrochemical Studies of PAn.(+)-HCSA Films in Ionic Liquids

(a) *In situ* Spectroelectrochemistry in EMI-TFSI

Oxidation

The UV-visible spectrum of a PAn.(+)-HCSA film held at 0.3 V in EMI-TFSI (λ_{max} at 420 and >800 nm, Figure 9.26a) confirmed that it remained as an emeraldine salt at this

potential. When the potential was progressively stepped up from 0.5 to 1.0 V, spectral changes involving a decrease in absorbance at shorter wavelengths and an increase at longer wavelengths were observed. These could be explained by increasing the degree of doping.

Increasing the potential to 1.1 V or 1.2 V caused a marked change in the UV-visible spectrum. The free carrier tail in the near-infrared decreased markedly in intensity and a new, distinct peak characteristic of pernigraniline salt appeared at *ca.* 685 nm (Figure 9.26a). The protonated form of pernigraniline state can be generated in this condition since emeraldine salt film was used. This spectrum did not change significantly after holding the film at 1.3-1.5 V (not shown). However, a deep blue-green colour of dissolved/dispersed materials was observed near the surface of the ITO-coated glass electrode. Upon removal of the PAn-modified ITO-glass electrode from the electrolyte, only a very thin film remained on the surface. This indicates that oxidative degradation of the polyaniline may have commenced at *ca.* 1.1-1.2 V, leading to chain breaking and dispersion in the ionic liquid. Due to the high viscosity of EMI-TFSI, the degraded and dissolved/dispersion products remained in the vicinity of the ITO-coated glass electrode and did not gravitate to the bottom of the spectroelectrochemical cell during the spectral measurements. Therefore, only small changes in the UV-visible spectra were observed between 1.2 and 1.5 V.

The results from *in situ* CD spectro-electrochemical studies strongly support the above conclusions. Figure 9.26b shows that the CD signals of the emeraldine salt form at 0.5 V changed to that of pernigraniline salt when the potential applied was increased to 1.0 V.

The intensity of the CD signals rapidly decreased during polarization at 1.2 V, supporting oxidative degradation of the polyaniline at this potential.

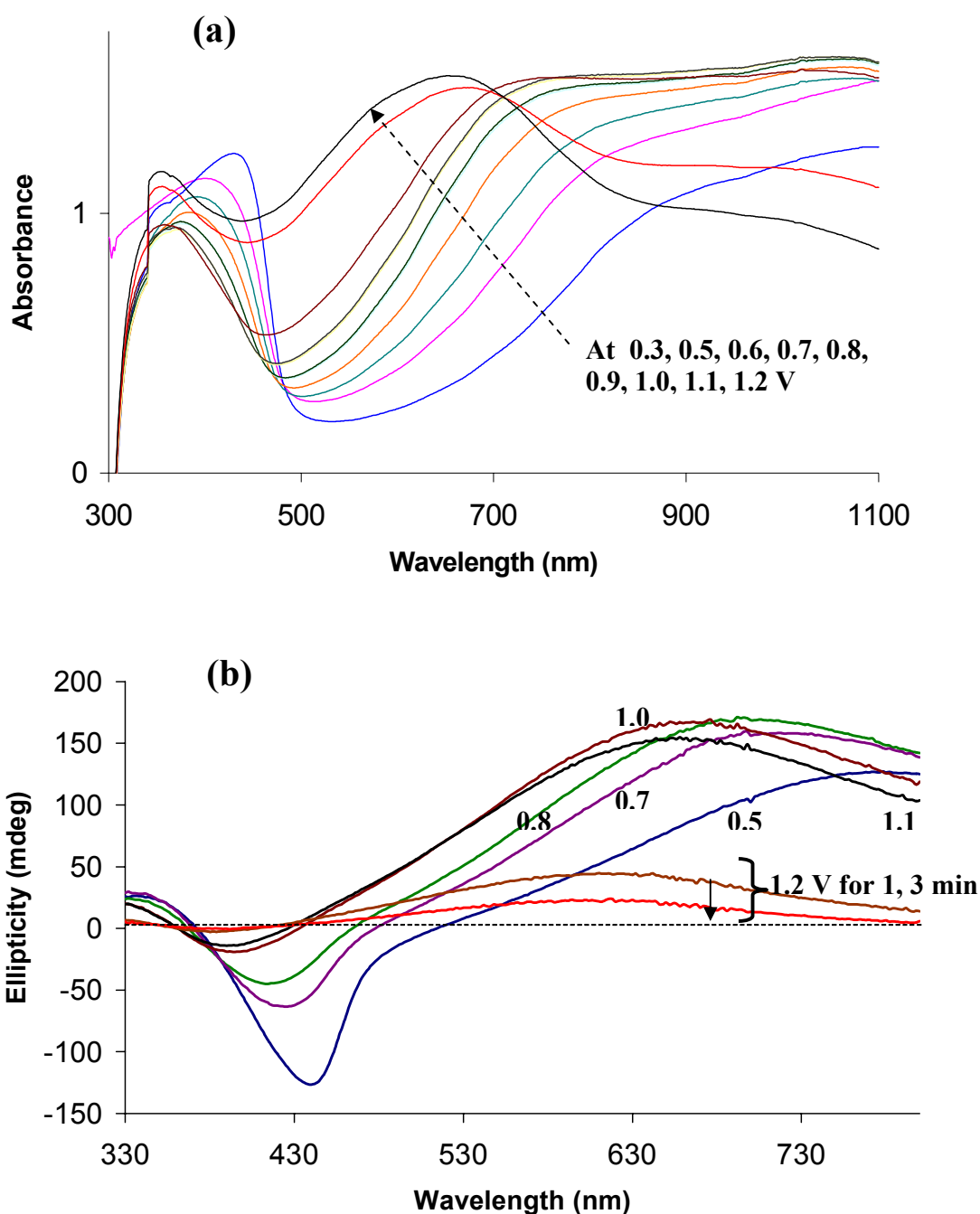


Figure 9.26 *In situ* UV-visible spectra (a) and CD spectra (b) of PAN.(+)-HCSA films after held at various positive potentials for 3 min in EMI-TFSI. (a and b are different films).

Reduction

Holding a PAn.(+)-HCSA film at -0.5 V in EMI-TFSI caused the expected reduction to leucoemeraldine base, as shown by the disappearance of the initial emeraldine salt absorption bands and the appearance of a single peak at 340 nm (Figure 9.27a). However, surprisingly the optical activity of the polymer film disappeared rapidly during this electrochemical reduction at ≤ -0.5 V, as shown in Figure 27b.

After removing these electrochemically reduced leucoemeraldine base films from the spectroelectrochemical cell and leaving in the air for a few days, their colour changed from pale yellow to blue. Aerial oxidation to emeraldine base was confirmed by their UV-visible spectra, showing characteristic bands at 340 nm and 620 nm (Figure 9.28a). Visible region optical activity was not recovered even after re-doping to the PAn.(+)-HCSA emeraldine salt with 1.0 M (+)-HCSA (Figure 9.28b). This indicated that racemization is irreversible. However, the film still showed electroactivity in acidic aqueous electrolyte with a normal shape of CVs for polyaniline (Figure 9.28c). Racemization of the reduced leucoemeraldine film was not expected, since it has previously been shown that the reduction of an optically active PAn.(+)-HCSA film by electrochemical reduction in aqueous electrolytes (Section 9.3.3.1) or by chemical reduction with hydrazine²⁸ gives optically active leucoemeraldine base. The reasons for the racemization observed here during electroreduction in EMI-TFSI electrolyte will be discussed later (Section 9.3.5).

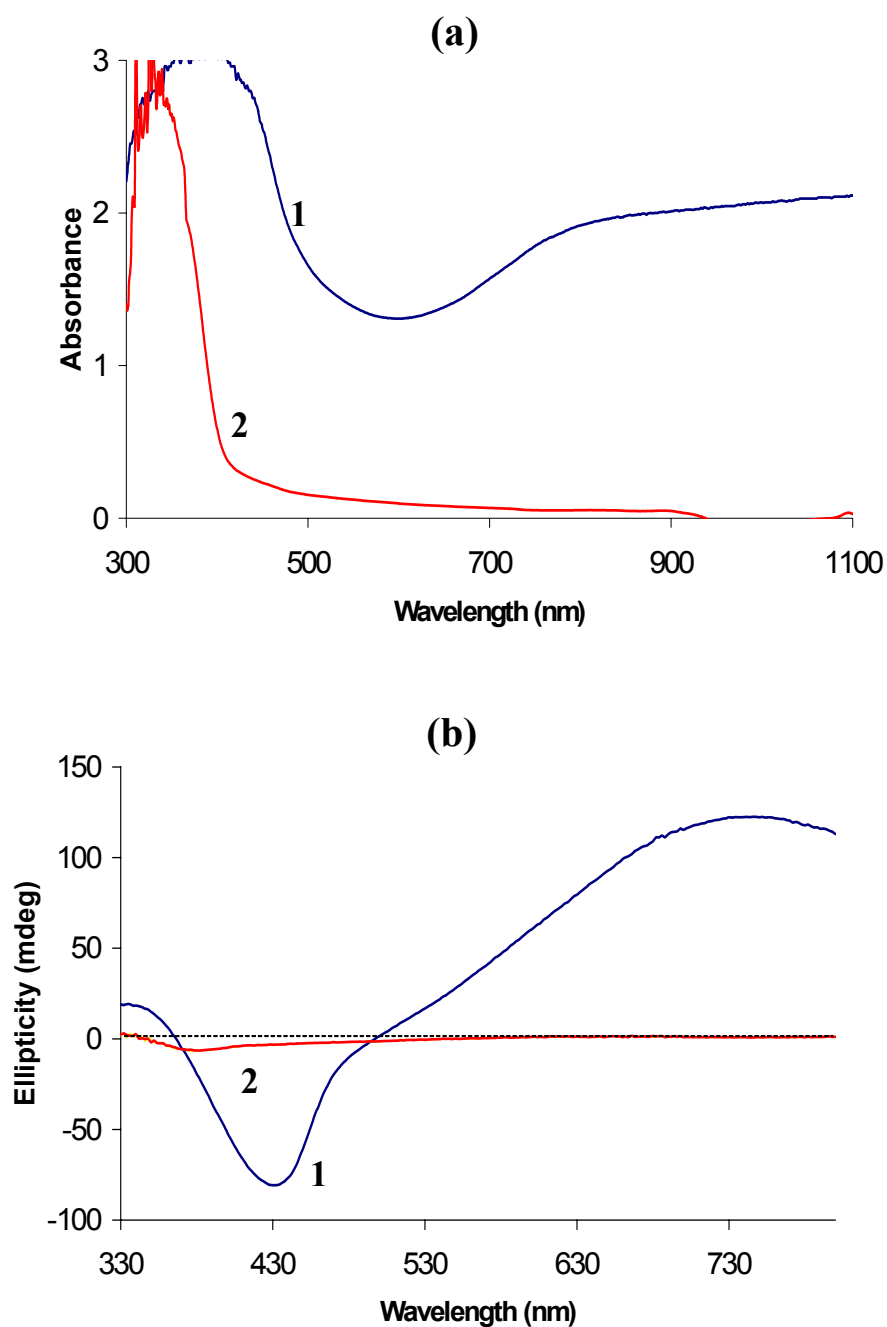


Figure 9.27 *In situ* UV-visible spectra (a) and CD spectra (b) of a PAn.(+)-HCSA film: (1) before and (2) after held at -0.5 V for 7 min in EMI-TFSI.

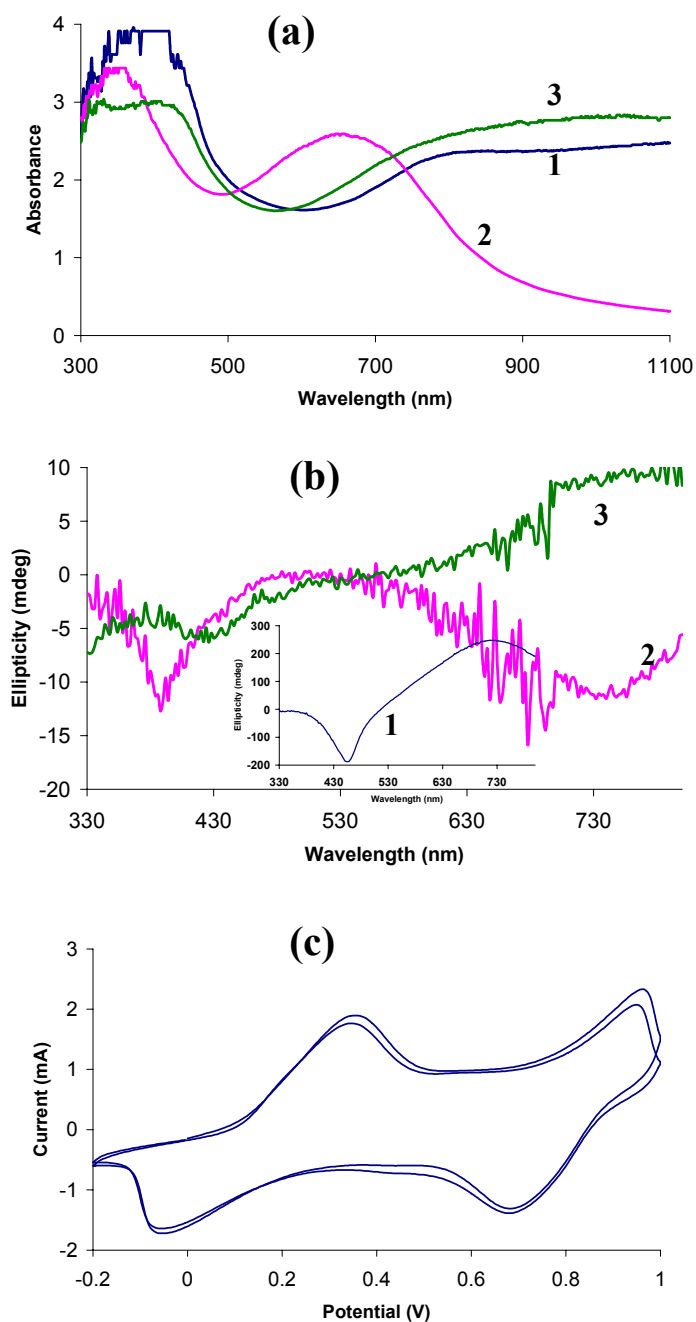


Figure 9.28 (a) UV-visible and (b) circular dichroism spectra of a PAN.(+)-HCSA film: (1) initial film, (2) after held at -1.5 V for 3 hrs in EMI-TFSI, and (3) after re-doping with 1.0 M (+)-HCSA for 2 hrs; and (c) cyclic voltammograms of the film (3) in 1.0 M HCl at a scan rate of 50 mV/s.

*(b) In Situ Spectroelectrochemistry in BMI-PF₆ and BMI-BF₄**Reduction*

The electrochemical reduction of optically active PAn.(+)-HCSA films in the ionic liquids BMI-PF₆ and BMI-BF₄ gave similar results to those observed above in EMI-TFSI. Although UV-visible spectra confirmed the formation of leucoemeraldine base (λ_{max} ca. 360 nm) at applied potentials between -0.8 and -2.0 V (see Figures 9.29a and 9.30a), the corresponding CD spectra (Figures 9.29b and 9.30b) showed that the fully reduced polyaniline films were optically inactive. That is, racemization had occurred during reduction. The cause of this racemization will be discussed in section 9.3.5.

Similar to the evidence observed in EMI-TFSI, after removing these electrochemically reduced leucoemeraldine base films from the spectroelectrochemical cell and leaving in the air for a few days, their colour changed from pale yellow to blue. Aerial oxidation to emeraldine base was confirmed by their UV-visible spectra, showing characteristic bands at 340 nm and 620 nm. However, these emeraldine base films were shown from their lack of CD bands to be optically inactive (not shown).

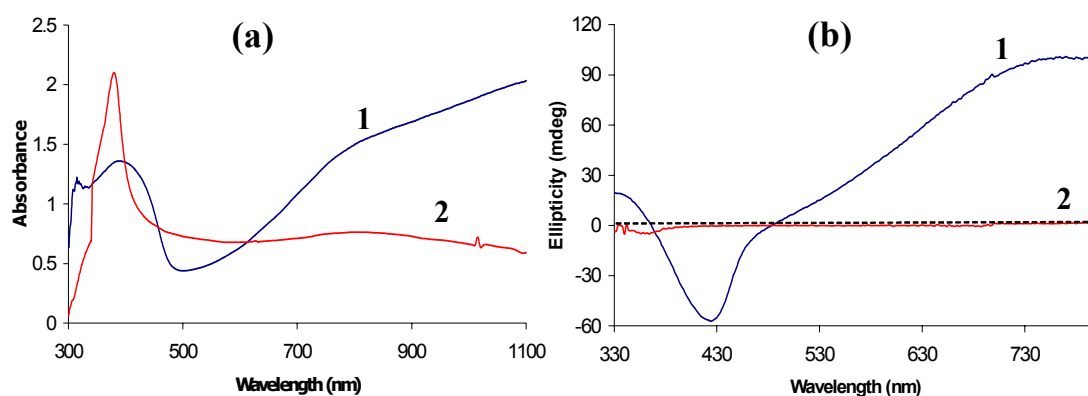


Figure 9.29 *In situ* UV-visible spectra (a) and CD spectra (b) of a PAn.(+)-HCSA film: before (1) and after (2) held at -2.0 V for 4 min in BMI-PF₆.

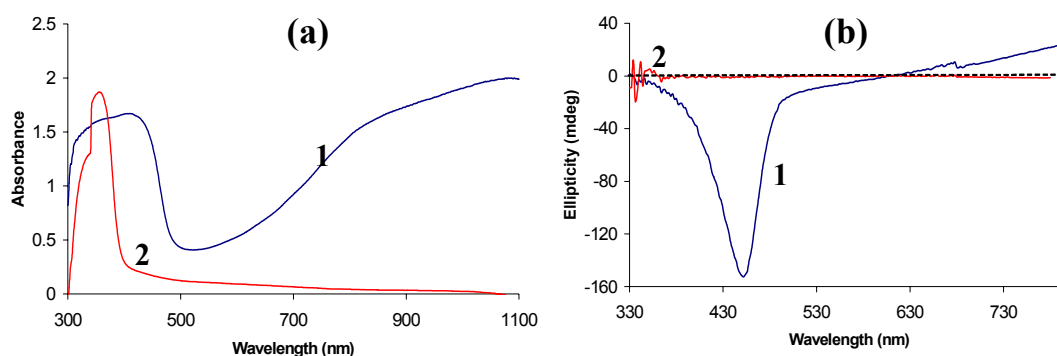


Figure 9.30 *In situ* UV-visible spectra (a) and CD spectra (b) of a PAN.(+)-HCSA film: before (1) and after (2) held at -0.8 V for 10 min in BMI-BF₄.

Oxidation

Similarly to the behaviour observed in EMI-TFSI electrolyte, increasing the potential applied to PAN.(+)-HCSA films in BMI-PF₆ and BMI-BF₄ from $+0.3$ V to $+1.2$ V caused an increase in absorption between 700 and 1100 nm (Figures 9.31a and 9.32a). This is consistent with increased doping of the emeraldine salt films with increasing potential. Further increasing the applied potential to $+2.0$ V caused a further change in the UV-visible spectrum to give a λ_{max} at *ca.* 670 nm, consistent with oxidation to the fully oxidized pernigraniline salt form.

Very significantly, in contrast to the behaviour in EMI-TFSI electrolyte, these electrochemically formed pernigraniline salts formed in BMI-PF₆ and BMI-BF₄ did not undergo oxidative degradation when held at positive potentials as high as $+2.0$ V. No dissolution/dispersion of the polymers from the ITO-coated glass electrode was observed. Furthermore, the films remained optically active, as shown by their CD spectra in Figures 9.31b and 9.32b, respectively. This is an important observation, since it opens the possibility of using such films as chiral electrodes in electrochemical asymmetric syntheses

where high positive potentials would be required (e.g. the oxidation of prochiral alkyl sulfides to chiral alkoxides).

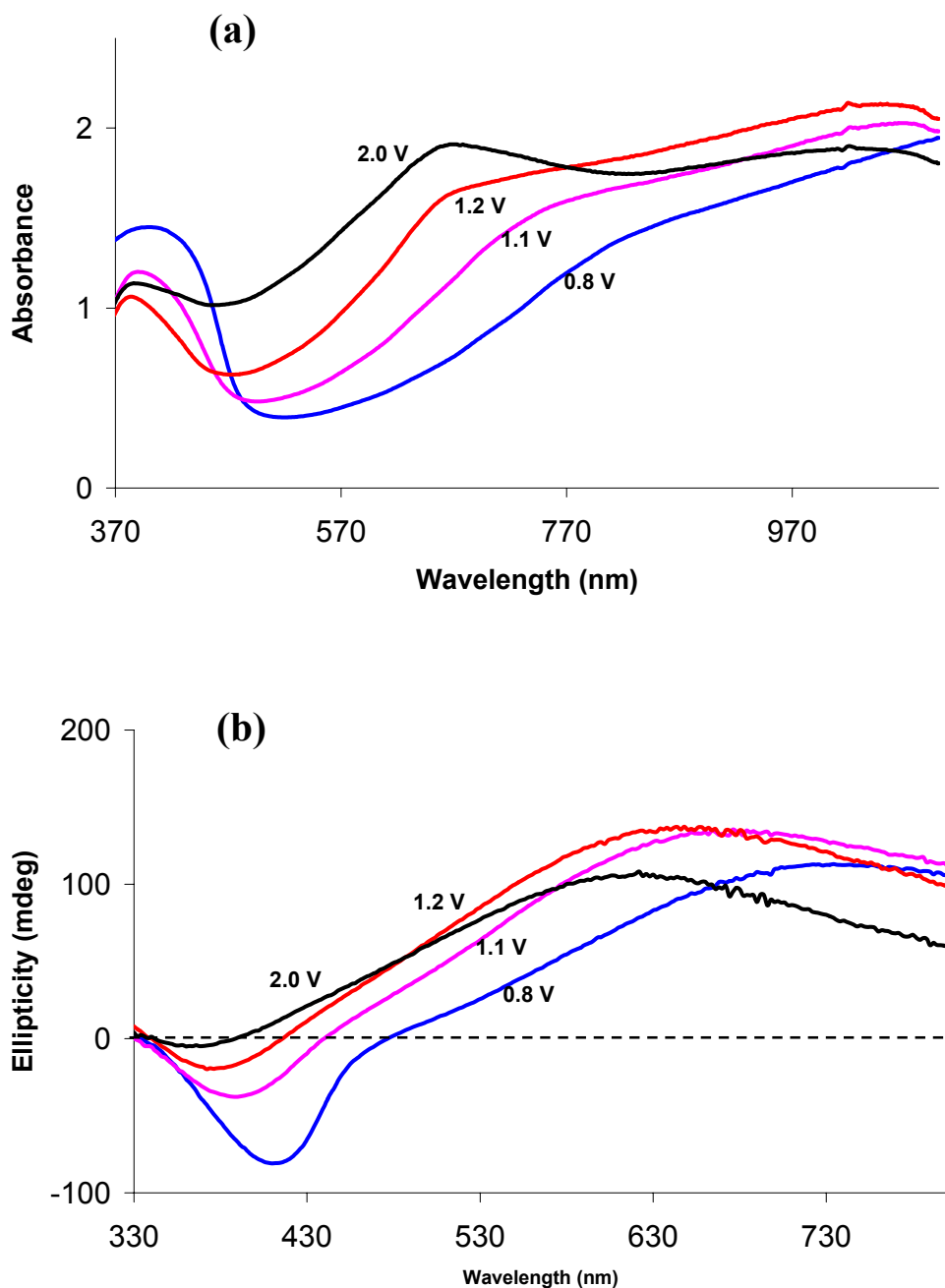


Figure 9.31 *In situ* UV-visible spectra (a) and CD spectra (b) of a PAn.(+)-HCSA film after held at various positive potentials for 5 min in BMI-PF₆.

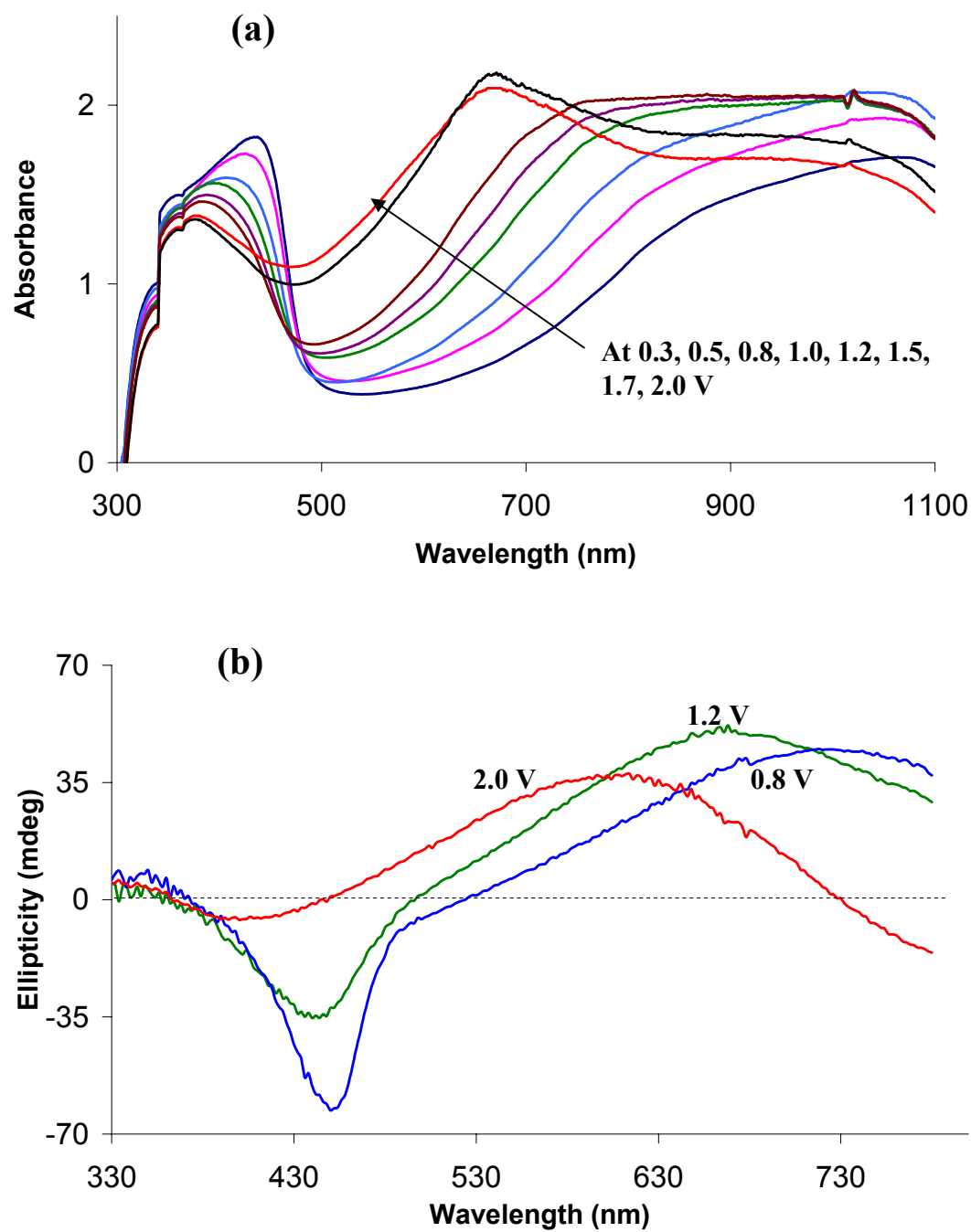


Figure 9.32 *In situ* UV-visible spectra (a) and CD spectra (b) of a PAn.(+)-HCSA film after held at various positive potentials for 5 min in BMI-BF₄.

After being left in air for one day, the above pernigraniline salt films changed colour to green, indicating conversion to emeraldine salts. This was confirmed by changes in their UV-visible and CD spectra, as shown for example in Figure 9.33.

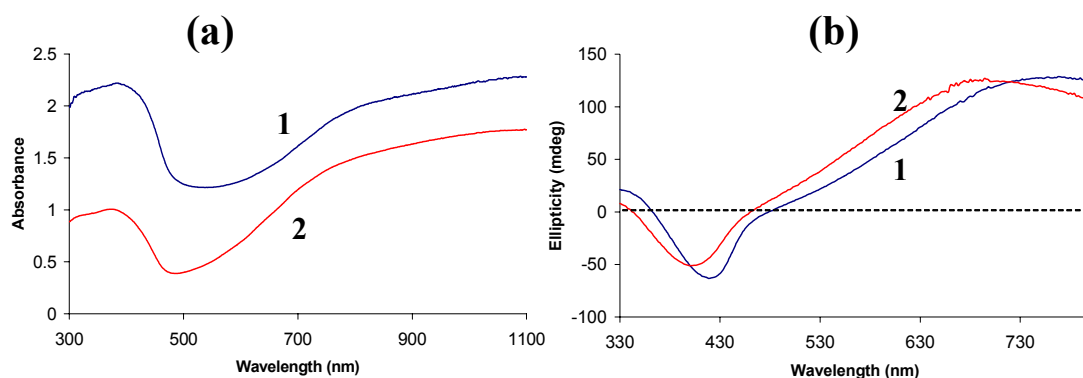


Figure 9.33 UV-visible spectra (a) and CD spectra (b) of a PAN.(+)-HCSA film: before (1) and after (2) held at various positive potentials in BMI-PF₆ (as shown in Figure 9.32) and left in air for 1 day.

(c) In situ Spectroelectrochemistry in (-), (+), and (±)-MBEA-TFSI

In an attempt to see if an optically active leucoemeraldine base could be generated by electroreduction in an ionic liquid, reduction of a PAN.(+)-HCSA film was explored in the novel chiral ionic (-)-MBEA-TFSI. It was hypothesized that even if rearrangement of the polyaniline helical chains could occur in this ionic liquid, the (-)-MBEA cation may induce a one-handed helical chirality on the leucoemeraldine base product.

Oxidation

In situ UV-visible spectra of a PAN.(+)-HCSA film when held at 0.7, 1.0, 1.1, and 1.2 V in (-)-MBEA-TFAI are presented in Figure 9.34a. The spectral changes can again be

attributed to the conversion of emeraldine salt to the pernigraniline salt form at potentials ≥ 1.0 V. When the pernigraniline salt was generated at *ca.* 1.1-1.2 V, oxidative degradation of the polyaniline film commenced, as observed in the ionic liquid EMI-TFSI above. Optical activity of the film was completely lost at 1.2 V, as clearly seen in Figure 9.34b. Similar results were observed in (+)-MBEA-TFSI and (\pm)-MBEA-TFSI.

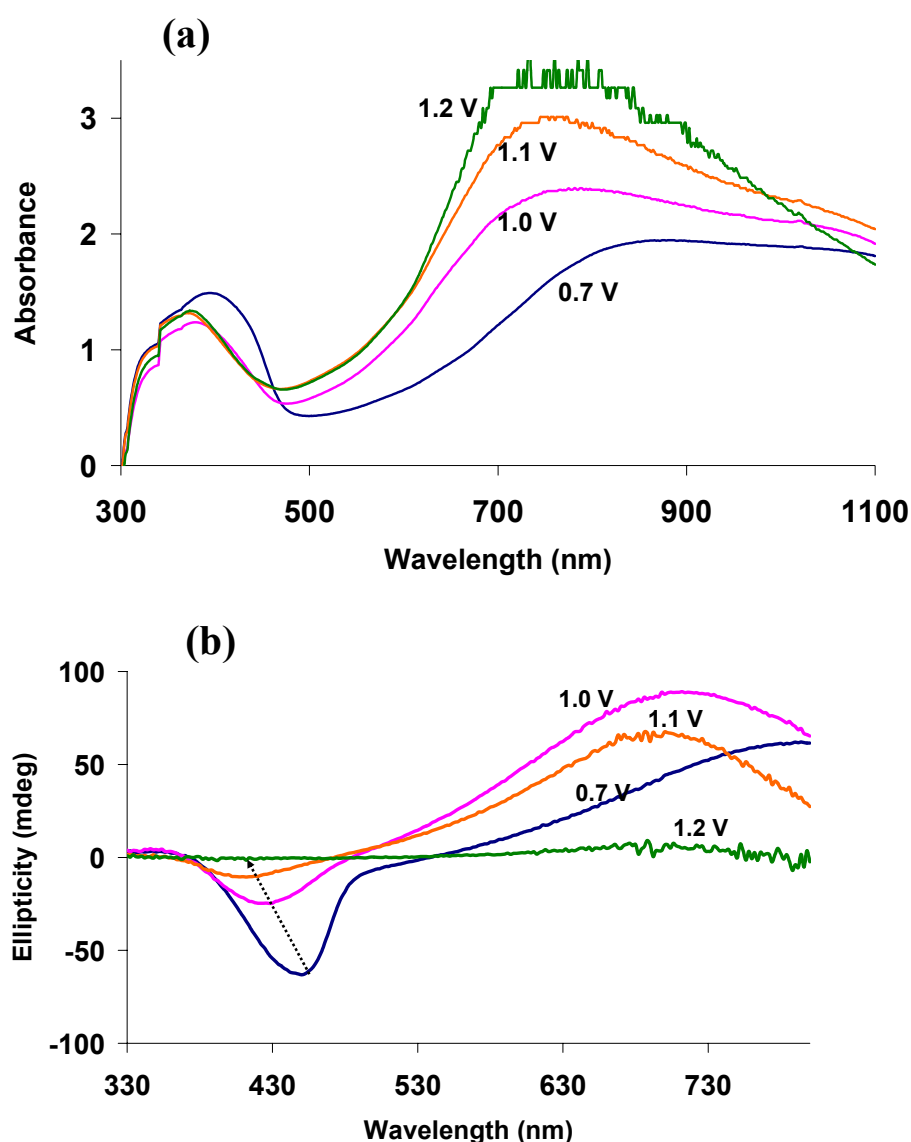


Figure 9.34 *In situ* UV-visible spectra (a) and CD spectra (b) of a PAn.(+)-HCSA film after held at various positive potentials for 5 min in (-)-MBEA-TFSI.

Reduction

Reduction of a PAn.(+)-HCSA film to leucoemeraldine base proceeded readily at -2.0 V in (-)MBEA-TFSI, as shown by the development of a spectrum typical of this reduced species (Figure 9.35a1). Very significantly, racemization of the polyaniline did not occur when the PAn.(+)-HCSA film was held at -2.0 V for 30 min. Bisignate CD bands were observed at *ca.* 330 and 390 nm characteristic of optically active leucoemeraldine base (Figure 9.35b1). Therefore, in contrast to the behaviour found for EMI-TFSI and the other ionic liquids studied above, the optical activity of chiral polyaniline films is preserved during electrochemical reduction in (-)MBEA-TFSI.

It was originally thought that optical activity in the leucoemeraldine base product may have arisen from the chiral influence of the (-)MBEA cation. However, reduction in the enantiomeric ionic liquid (+)MBEA-TFSI gave a leucoemeraldine base film with the same sign for its CD signals (Figure 9.35b2). A strongly optically active leucoemeraldine base was also produced in racemic (\pm)MBEA-TFSI (Figure 9.35b3). This latter observation shows that the chirality in the MBEA cation is not the factor responsible for producing optically active leucoemeraldine base in MBEA-TFSI ionic liquids. The observed results may alternatively be explained by good solubility of HCSA in MBEA-TFSI at room temperature (0.7 M at 20°C), which is higher than in EMI-TFSI or in BMI-BF₄ (*ca.* 0.01-0.05 M at 20°C). Then, CSA⁻ anion expulsion becomes dominant in the charge-transfer mechanism during polyaniline reduction in MBEA-TFSI. After being left in air for a few min, the above leucoemeraldine base film changed colour to green, indicating aerial oxidation. This was confirmed by the generation of the UV-visible spectrum of emeraldine salt. Optically active emeraldine salt films were observed by their CD spectra (not shown).

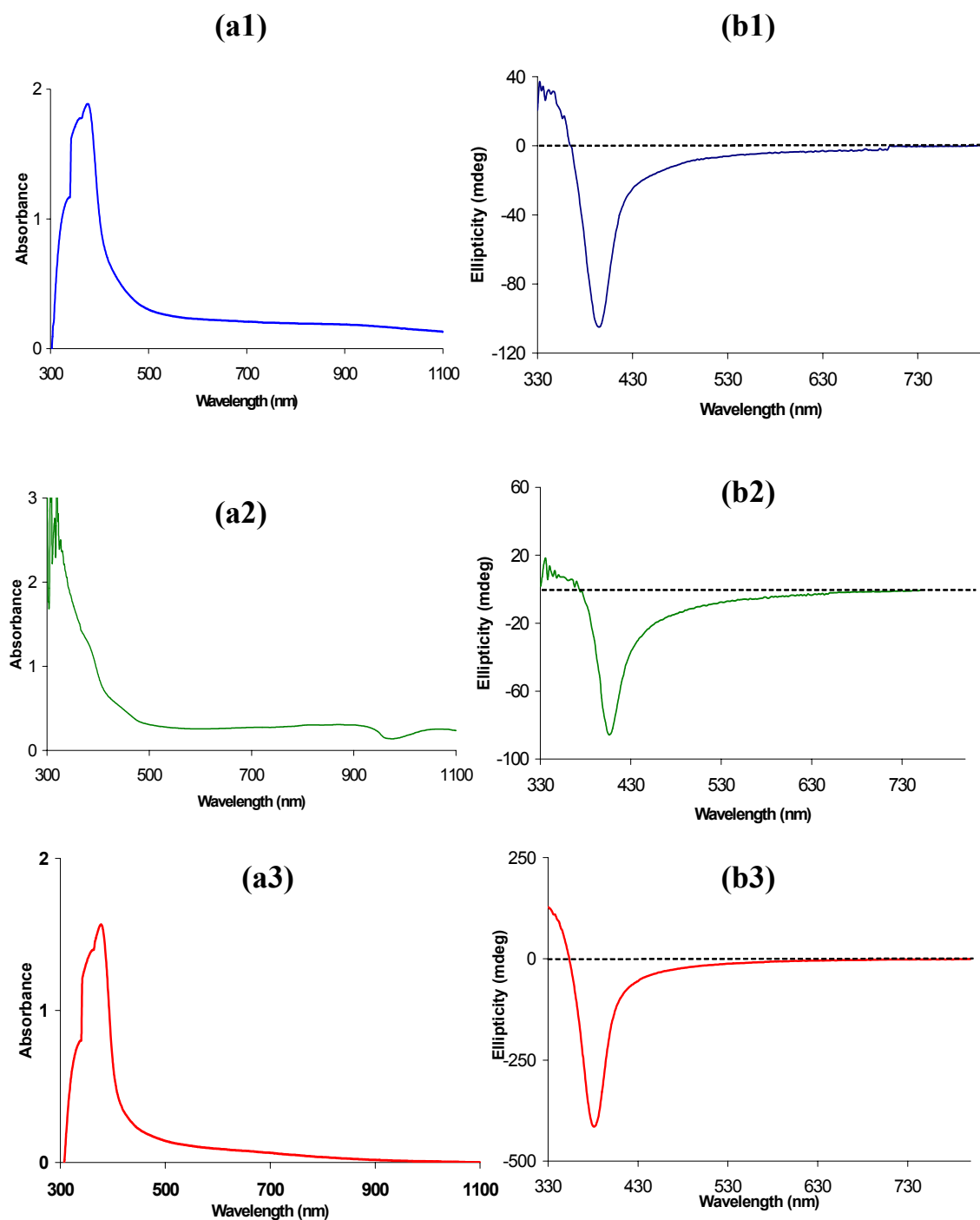


Figure 9.35 *In situ* UV-visible spectra (a1-a3) and CD spectra (b1-b3) of PAn.(+)-HCSA films after held at -2.0 V for 30 min in (-)-MBEA-TFSI (1), (+)-MBEA-TFSI (2), and (±)-MBEA-TFSI (3).

9.3.4 Raman Spectroscopy

To further investigate the chemical modifications of the polyaniline backbone that occurred after the above treatments at extremely high positive or negative potentials in ionic liquids, Raman spectra were recorded for some of the above polyaniline films following the measurement of their UV-visible and CD spectra.

9.3.4.1 Raman Spectra of PAn.(+)-HCSA Films after Holding at High Positive Potentials in Ionic Liquids

Figure 9.36 shows the Raman spectra of PAn.(+)-HCSA films after holding at +2.0 V in (a) BMI-BF₄, (b) BMI-PF₆, and (c) at +1.2 V in EMI-TFSI and left in ambient conditions for different periods of time. Raman spectra characteristic of predominantly emeraldine salt (e.g. the appearance of semiquinone radical unit at *ca.* 1330-1350 cm⁻¹) were observed in all cases. There was no evidence of chemical modification in the PAn.(+)-HCSA films after holding at +2.0 V in BMI-BF₄ and +1.2 V in EMI-TFSI, respectively; while analogous treatment at +2.0 V in BMI-PF₆ caused some different features that may be related to chemical structure changes, such as the appearance of relatively strong bands at *ca.* 579 and 1649 cm⁻¹ and a shoulder at *ca.* 1384 cm⁻¹. This confirms the previous conclusions in Section 9.3.3 from UV-visible and circular dichroism spectroscopy. All of the results indicate that the pernigraniline salt films known from our *in situ* spectroelectrochemical studies to be formed at high positive potentials (1.2-2.0 V) convert into the emeraldine salt form upon standing in ambient conditions.

The appearance of Raman bands at *ca.* 575, 1380, and 1640 cm⁻¹ has been recently attributed to an unusual cross-linking structure of polyaniline by Torresi *et al.*⁵⁸⁻⁶⁰ Such

cross-linking formation has been reported by many research groups. Two main causes to generate cross-linked polyaniline have been proposed, namely oxidation at high anodic potentials^{43-45,61} and heat treatment.⁶²⁻⁶⁷ The cross-linking structure generated by both treatments is proposed to be the same. Moreover, cross-linking may be generated during or after these treatments.

It was noted in Section 9.3.3.2 that a PAn.(+)-HCSA film degraded and dissolved/dispersed in EMI-TFSI when held at +1.2 V, but that a thin polymer film still remained on the electrode. The Raman spectrum of this thin film in Figure 9.36c suggests that the anodic degradation of polyaniline in EMI-TFSI might be chain scission, since no chemical modification of the polymer backbone was observed. This mechanism has been proposed for the degradation of polyaniline in non-aqueous electrolytes.⁶⁸

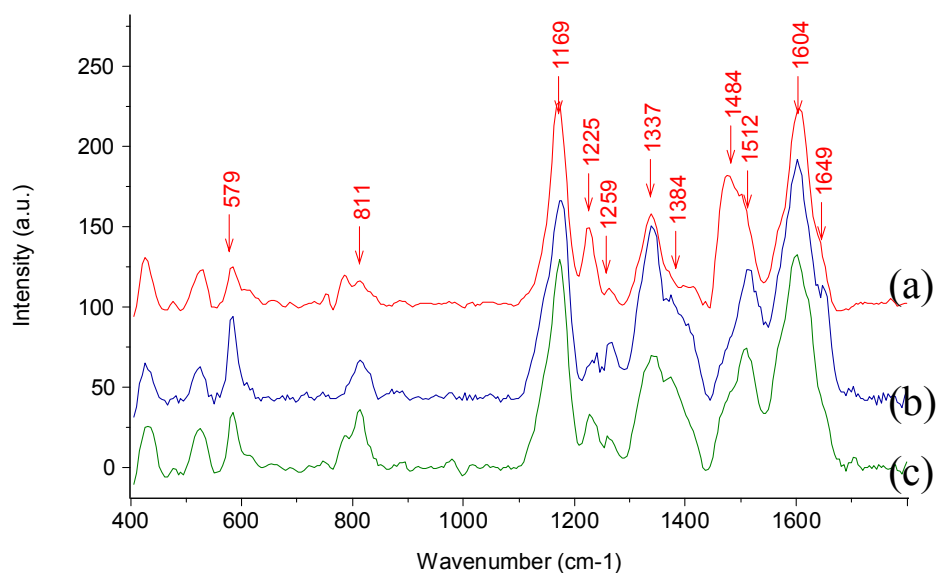


Figure 9.36 Raman spectra recorded (with 632.8 nm excitation line) for PAn.(+)-HCSA films electrodeposited on ITO-coated glass electrode after holding at: (a) + 2.0 V in BMI-BF₄, (b) + 2.0 V in BMI-PF₆, and (c) + 1.2 V in EMI-TFSI.

9.3.4.2 Raman Spectra of PAn.(+)-HCSA Films after Holding at Low Negative Potentials in Ionic Liquids

When PAn.(+)-HCSA films were held at - 2.0 V in (+)-MBEA-TFSI, BMI-BF₄ and BMI-PF₆ and at -1.0 V in EMI-TFSI, fully reduced leucoemeraldine base was generated as seen from the *in-situ* UV-visible/CD spectroelectrochemical experiments in Section 9.3.3. The very pale yellow leucoemeraldine base product turned to green quite quickly after removal from (+)-MBEA-TFSI. The UV-visible spectrum confirmed that this green species was an emeraldine salt, re-generated by aerial oxidation (see Section 9.3.3.2 (c)). However, the reduced leucoemeraldine base films obtained via electro-reduction in BMI-BF₄, BMI-PF₆ and EMI-TFSI electrolytes changed from pale yellow to blue. This suggested aerial re-oxidation to emeraldine base, which was confirmed from UV-visible spectra (see Section 9.3.3.2 (b)).

The Raman spectra of these reduced and then aerial oxidized films, presented in Figure 9.37, are in good agreement with the previous results (see Section 9.3.3.2). Raman bands characteristic of radical cations were observed at *ca.* 1300-1350 cm⁻¹ only in Figure 9.37a, confirming that the film was in the emeraldine salt form. Interestingly, a new band appeared at *ca.* 1380 cm⁻¹ which has been assigned to delocalised polarons⁶⁹ similar to those seen in the Raman spectrum of PAn.(+)-HCSA treated with *m*-cresol.^{58, 70}

The Raman spectra in Figure 9.37b-d show bands consistent with the emeraldine base form, with no characteristic bands of radical cations in the 1300-1350 region. No evidence of chemical modification during the reduction/ re-oxidation was observed.

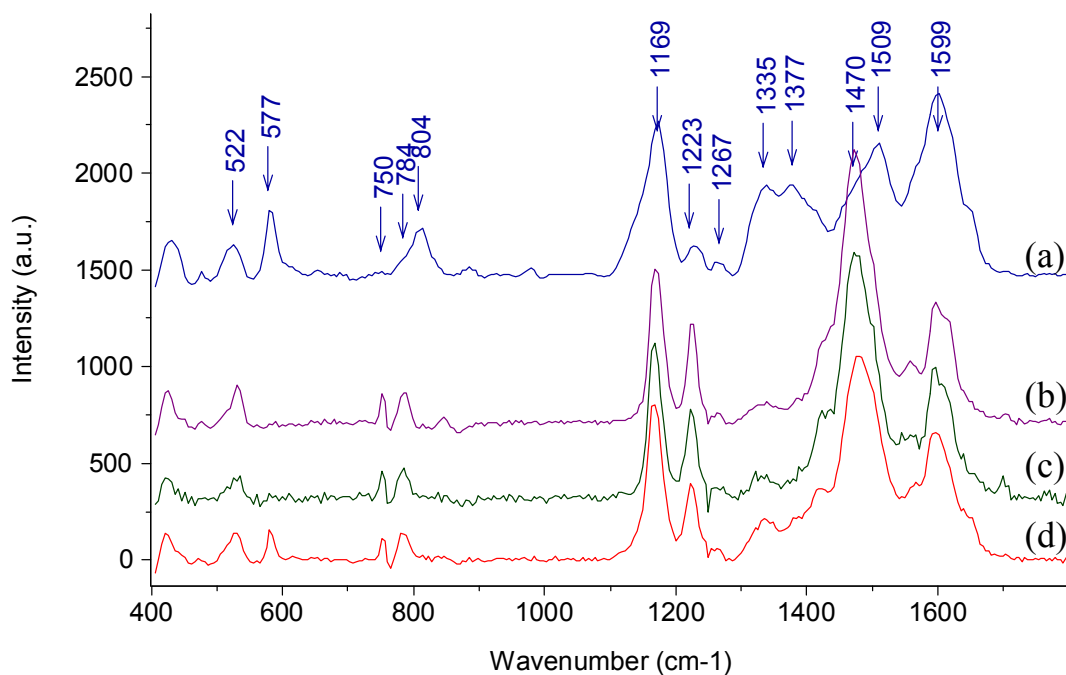


Figure 9.37 Raman spectra (recorded with 632.8 nm excitation) for PAN.(+)-HCSA films on ITO-coated glass electrode after holding at: (a) - 2.0 V in (+)-MBEA-TFSI, (b) - 2.0 V in BMI-BF₄, (c) - 2.0 V in BMI-PF₆, and (d) - 1.0 V in EMI-TFSI, and then exposed to air for 3-7 days .

9.3.5 Explanations for Electrochemical Instability and Racemization of Chiral PAN.(+)-HCSA Films in Ionic Liquids

From the above studies, three main deteriorations of chiral polyaniline PAN.(+)-HCSA films could occur during electrochemical treatments: (i) reversible loss of electroactivity, (ii) irreversible loss of electroactivity, and (iii) irreversible loss of optical activity. The causes for these are discussed below:

(i) Reversible Loss of Electroactivity of PAN.(+)-HCSA

According to the mechanism previously shown in Scheme 9.1, mobility of the dopant anion is very important for charge compensation in the first redox couple^{24, 48, 71} of polyaniline, and protons are involved in the second redox couple.^{48, 55} The former process was supported

by *in situ* electrogravimetric microbalance studies,⁴⁸ while the involvement of protons was related to shifts in the polyaniline redox potentials depending on the pH of the solution.²² At higher proton concentrations (lower pH), the emeraldine form is more difficult to oxidize to pernigraniline due to the oxidation potential moving to more positive potential.

The main reason for the *reversible* loss of the electroactivity of PAn.(+)-HCSA emeraldine salt films in 0.5 M NaNO₃ (Figure 9.10) is believed to be de-protonation / de-doping due to insufficient protons being available at neutral pH. The electroactivity, therefore, can be restored in acid solution. It has been reported that de-protonation/de-doping of emeraldine salts commences in basic, neutral, and low acidic aqueous solution (pH > 3-4).^{22, 29, 54} Generally, the definitions of acid and base used in discussions of the electrochemical behaviour of polyaniline are proton donor and proton acceptor.

When polyaniline films prepared from aqueous solution are investigated in ionic liquids used as both solvent and supporting electrolyte, the redox mechanism is probably more complicated than that which occurs in aqueous media. De-protonation/de-doping, solvent adsorption/desorption (or swelling/de-swelling), participation of the cation in charge compensation processes, and the solubility of the dopant anion as grown in ionic liquids might be significant factors effecting the electroactivity of PAn.(+)-HCSA films in ionic liquids in potential ranges where there is no anodic degradation.

Successive potential scanning within the electroactive window of polyaniline in the ionic liquids studied here results in the gradual loss of the polymer electroactivity. Partial de-protonation/de-doping of the polyaniline films is probably the main reason for this. Moreover, when the potential cycling was extended to more negative potentials, the

electroactivity of the polymer films was completely lost within a few cycles (e.g. Figures 9.14, 9.18c, and 9.19c). The exception was for cycling in MBEA-TFSI electrolyte. Potential cycling between - 2.0 V and + 1.0 V in MBEA-TFSI for a hundred cycles showed no deterioration of the electroactivity of the polymer film (Figure 9.17).

The identification of de-protonation/de-doping of PAn.(+)-HCSA as the major reason for the reversible loss of polyaniline electroactivity in most ionic liquids studied to date is supported by the fact that the electroactivity of the films can be restored in aqueous acid. However, there may be other minor factors such as charge compensation processes. The most interesting case is the cyclic voltammetry of PAn.(+)-HCSA films in MBEA-TFSI. No de-protonation/de-doping occurred during potential cycling. To evaluate the acidity of this new ionic liquid, the UV-visible spectrum of alizarin red S (alizarin sodium sulfate, an acid-base indicator) in the ionic liquid was investigated. The spectrum in MBEA-TFSI was similar to that in neutral water and different from that in acidic/basic aqueous solutions (data not shown). Therefore, generation of leucoemeraldine salt (LS) rather than leucoemeraldine base (LB) during reduction in MBEA-TFSI is not a possibility.

Another property of ionic liquids which probably affects this process is protophilicity. The ionic liquid MBEA-TFSI may be a protophobic solvent. If so, the proton from the initial PAn.(+)-HCSA emeraldine salt film will be retained around the reaction layers and can protonate the polymer during potential cycling. In contrast, the other ionic liquids studied here may be more protophilic.⁷² There is evidence that may support this idea. After the reduction of a PAn.(+)-HCSA film in MBEA-TFSI, the colourless leucoemeraldine base film re-oxidized to a green film of emeraldine salt after left in air for a time, whereas the

corresponding reduced films in the other ionic liquids underwent aerial re-oxidation to blue emeraldine base (see above). The results suggest that in the former case there are sufficient protons available to protonate the polymer during re-oxidation by air.

One of the most interesting properties of MBEA-TFSI which is different from the other ionic liquids used is the solubility of HCSA. The solubility of HCSA in MBEA-TFSI (0.7 M at 20°C) is much higher than in the other ionic liquids employed (*ca.* 0.01-0.05 M at 20°C). Therefore, in MBEA-TFSI the dopant anion CSA⁻ initially incorporated in the polymer backbone can be easily expelled into the solvent during reduction. Thus, the insertion/expulsion of the anion (TFSI⁻ and CSA⁻) from the polymer system can be a main process in charge compensation during successive scanning. In contrast, in the other ionic liquids insertion of the cation from the ionic liquid electrolyte into the film occurs to balance the negative charge of the CSA⁻ anion held within the polyaniline film. The strong interaction between incorporated cation and initial dopant anion bound to the polymer may stop movement of these ions during redox reactions, resulting in an electroinactive film.

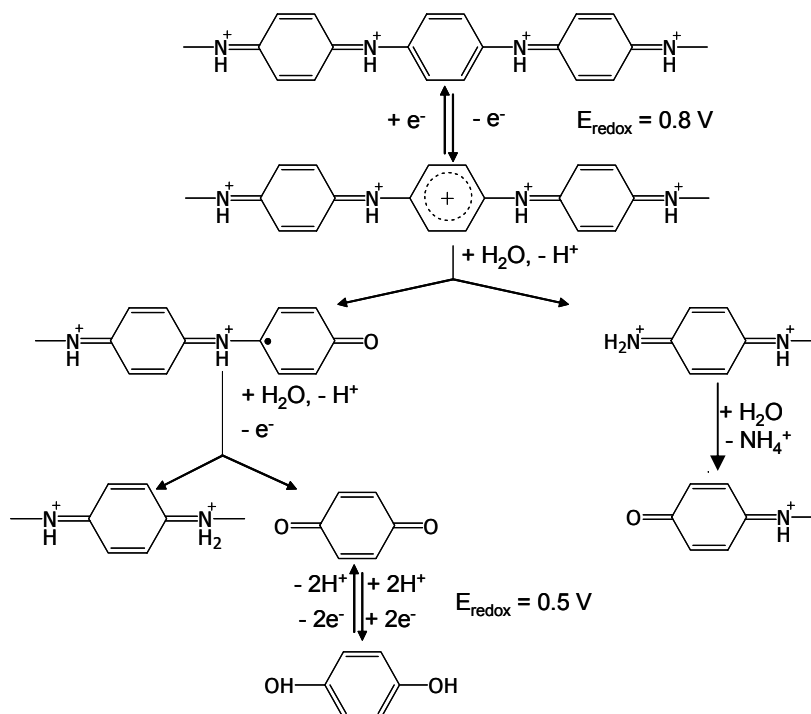
It is interesting to note that Lu and Mattes²⁵ have recently reported that the solubility of anionic dopants in non-aqueous electrolytes has a significant impact on the electrochemistry and actuation of polyaniline. Vanela and Torresi⁷³ have also reported that both the cation and anion of the electrolyte and solvent participate in the redox mechanism of polyaniline (grown from aqueous medium but investigated in the non-aqueous media, acetonitrile and propylenecarbonate). Swelling was also more pronounced in high dielectric constant solvents, which also allowed more cation movement together with the solvent.

However, the major species participating in charge compensation is cation and solvent molecules.

(ii) Irreversible Loss of Electroactivity

(a) In Aqueous Electrolytes

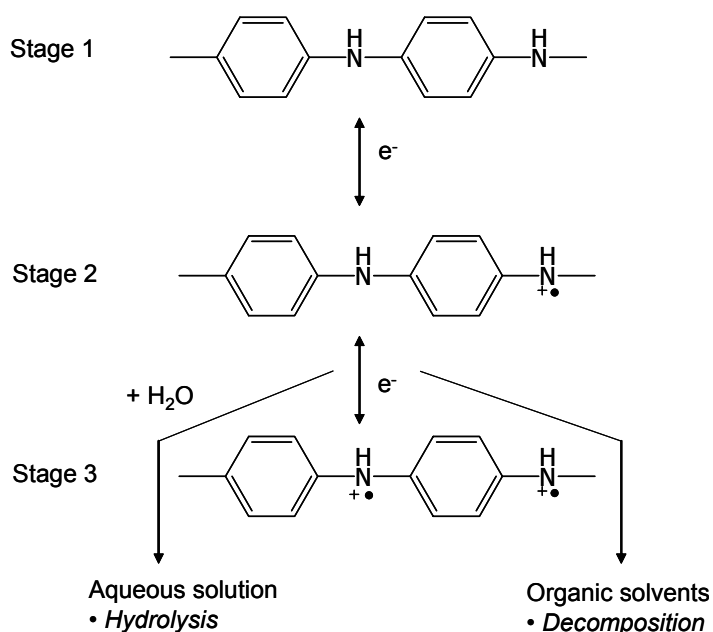
Oxidative degradation of PAn.(+)-HCSA films occurred at + 0.8 V in aqueous acid (0.5 M HCSA) (Figure 9.21). This is believed to be due to hydrolysis of pernigraniline salt, producing *p*-benzoquinone as the main product. The benzoquinone/hydroquinone redox couple was also observed as the “middle peak” at *ca.* 0.55 V in the cyclic voltammograms of PAn.(+)-HCSA in aqueous 1.0 M HCl (Figures 9.8 and 9.9a). The results are in good agreement with those previously reported for emeraldine salt oxidation by many researchers,^{19, 48} and with the mechanism proposed by Hand and Nelson (Scheme 9.2).^{74, 75}



Scheme 9.2

(b) In Ionic Liquids

The stability of PAn.(+)-HCSA films at high positive potentials was strongly dependent on the nature of ionic liquids employed. Anodic degradation of the PAn.(+)-HCSA films occurred at *ca.* 1.1-1.2 V in EMI-TFSI and MBEA-TFSI electrolytes (Figures 9.26 and 9.34). Degraded polymer dissolved/dispersed in the ionic liquids and no strong evidence of chemical modification was observed in the Raman spectra of the treated films (Figure 9.36). Thus, the chain scission mechanism proposed for the oxidative degradation of polyaniline in organic solvents by Kabumoto and Shinozaki (Scheme 9.3)²⁰ is also a possible explanation for the behaviour observed in EMI-TFSI and MBEA-TFSI.



Scheme 9.3

Another possible process for degradation of the PAn.(+)-HCSA films in these two ionic liquids could originate from trace water in the system. Trace water in organic solvents²⁴ or

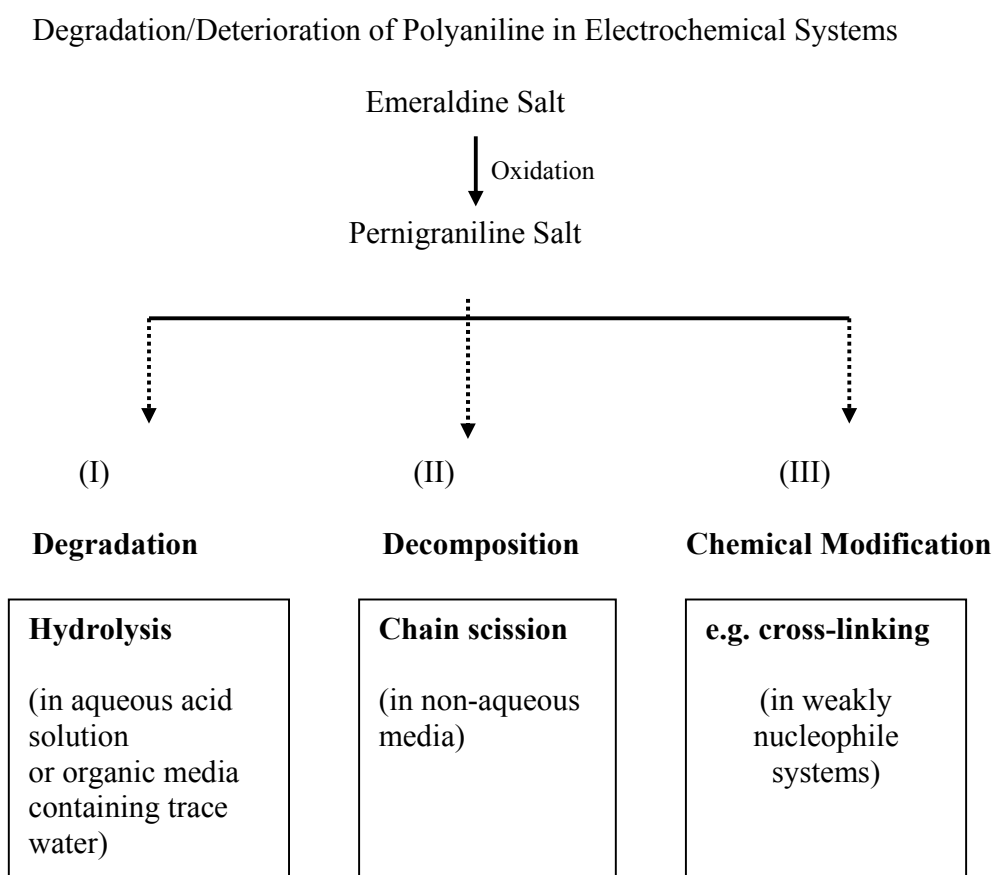
trapped within the polyaniline film²⁴ or hydrated in the supporting electrolyte⁷⁶ has been reported to cause degradation of polyaniline. However, water trapped in the polyaniline film is unlikely in the present case because oxidative degradation of the polyaniline film did not occur in the ionic liquids BMI-BF₄ and BMI-PF₆.

Hydrolysis of oxidized pernigraniline salt can take place in non-aqueous media containing trace water via a mechanism similar to that found in aqueous solution. The species involved in anodic degradation of polyaniline by this mechanism may be nucleophilic species such as H₂O, OH⁻, and/or the anion of the supporting electrolyte, or nucleophilic solvents.⁷⁷ The anion of the ionic liquids employed, particularly TFSI, might be involved in the nucleophilic attack process causing degradation of polyaniline in EMI-TFSI and MBEA-TFSI. It has been reported that the anion in the electrochemical system can effect the degradation behaviour of polyaniline.^{56, 78}

In contrast, PAn.(+)-HCSA films were very stable towards anodic degradation in the ionic liquids BMI-PF₆ and BMI-BF₄, as shown by UV-visible and CD spectra of the pernigraniline salt form recorded while holding at +2.0 V in these electrolytes (Figure 9.31 and 9.32). However, unusual chemical bonds such as cross-linking probably occurred *during* or *after* oxidation of the polymer at high anodic potential, as evidenced by the appearance of weak intensity *ex-situ* Raman bands at *ca.* 575, 1380 and 1640 cm⁻¹ for the film treated at +2.0 V in BMI-PF₆ (Figure 9.36). These bands have been previously attributed to cross-linking or phenazine-like structures.⁵⁸⁻⁶⁰ Cross-linked polyaniline was previously found when the polyaniline was treated at high anodic potential^{43-45, 61} or high temperature.⁶²⁻⁶⁷ In addition, cross-linking may be the major process involved in the

conversion of the unstable pernigraniline salt to the stable emeraldine salt form,⁴¹ that occurred during standing under ambient condition (Figure 9.33).

The degradation/deterioration of polyaniline films in electrochemical systems can be therefore summarized as presented in Scheme 9.4.



Scheme 9.4

(iii) Loss of Optical Activity

The optical activity of PAn.(+)-HCSA films can be preserved during oxidation/reduction processes in aqueous solution caused by chemical²⁸ or electrochemical means (Figures

9.20, 9.21, 9.22, 9.24 and 9.25). Movement of the polymer chains required for racemization is presumably not allowed in the solid state at room temperature.

However, unexpected results were obtained when PAn.(+)-HCSA films were reduced in ionic liquids. Complete loss of visible region optical activity was observed during the reductions in all of ionic liquids used (Figures 9.27, 9.29 and 9.30) except for (+)-, (-)-, or (\pm)-MBEA-TFSI (Figure 9.35). Cyclic voltammetric results suggest that the charge compensation process in the first redox couple of polyaniline at room temperature in MBEA-TFSI may be different from that occurring in the other ionic liquids, i.e. anion rather than cation expulsion/insertion (see Section 9.3.2.2 above).

To test this hypothesis, a PAn.(+)-HCSA film was reduced at -2.0 V in EMI-TFSI containing 0.5 M (+)-HCSA at 55°C. This high temperature permits the solubilization of relatively high concentrations of (+)-HCSA in EMI-TFSI, in contrast to the poor solubility at room temperature. The film turned to the colourless leucoemeraldine form during reduction and subsequently changed back to green after removal from the electrolyte and left in air for a time. This may be caused by aerial re-oxidation and re-doping by HCSA trapped within the film. Significantly, the film did not racemise during this reduction/re-oxidation cycle, since optically active emeraldine salt was observed (Figure 9.38). This supports the belief that at high temperature the increased solubility of HCSA in EMI-TFSI causes a change in the charge compensation mechanism from cation movement at room temperature to anion movement at high temperature.

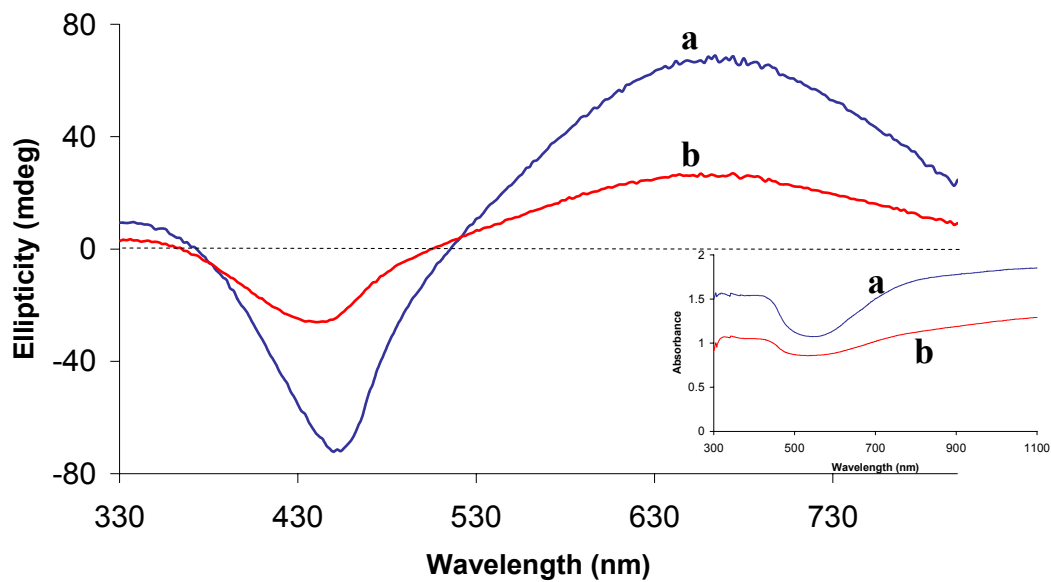
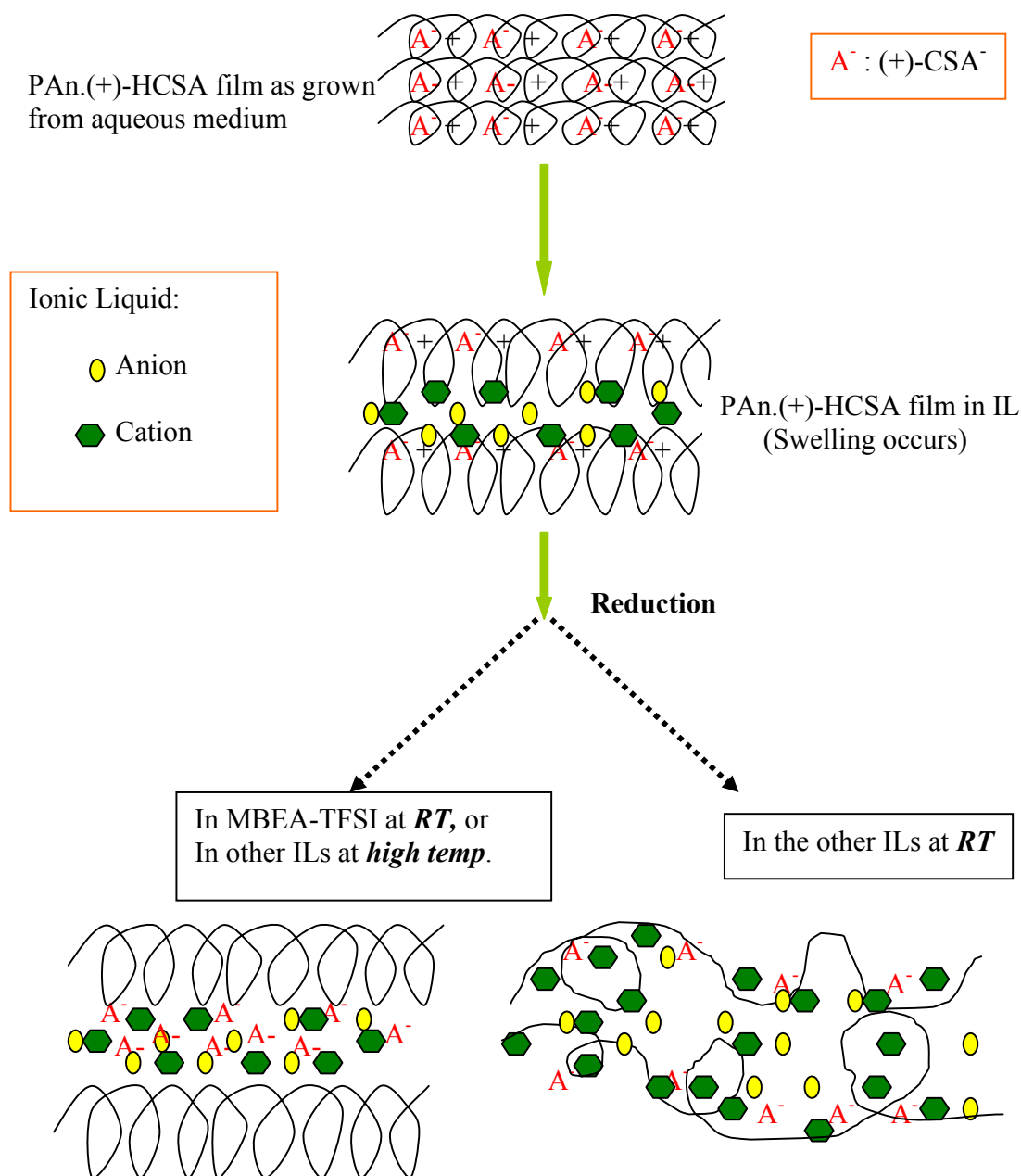


Figure 9.38 CD spectra of a PAn.(+)-HCSA film: (a) before and (b) after held at -2.0 V for 30 min in 0.5 M (+)-HCSA/EMI-TFSI at 55°C and left in air for a time. Inset: UV-visible spectra of the film.

In summary, the racemization of PAn.(+)-HCSA films during electrochemical reduction in ionic liquid electrolytes can be presented as shown in Scheme 9.5.



Scheme 9.5

Mechanism of Racemization of PAn.(+)-HCSA Films during Reduction in Ionic Liquids

9.4 Conclusions

The electrochemical stability and chiroptical properties of electrodeposited PAn.(+)-HCSA films in ionic liquid electrolytes are strongly dependent on the applied potential and on the nature of the ionic liquid used. Reversible loss of the electroactivity of the polyaniline films occurs when the polymer films are potential cycled in the ionic liquids EMI-TFSI, BMI-PF₆ and BMI-BF₄. Although electrochemical degradation of the polyaniline films occurs in EMI-TFSI and MBEA-TFSI electrolytes when they are polarized at high positive potentials (> +1.1 V), significantly, in BMI-PF₆ and BMI-BF₄ electrolytes the optical activity and electrochemical stability of the polyaniline films are retained at potentials as extreme as +2.0 V. However, cross-linking involving a phenazine-type structure occurs when the PAn.(+)-HCSA films are exposed to high positive potentials in BMI-PF₆.

Surprisingly, loss of optical activity (racemization) of the PAn.(+)-HCSA films occurs when electrochemical reduction is carried out in all of the ionic liquids examined except (+)-, (-)-, or (±)-MBEA-TFSI. In the latter ionic liquid electrolyte, strong CD signals are observed for the leucoemeraldine base film formed. Incorporation of the cation from the ionic liquids during the reduction (rather than expulsion of the (+)-CSA⁻ anion) and resultant swelling of the polyaniline films may be the reason for the racemization in the ether ionic liquids.

The nature of the ions that comprise these ionic liquids is seen to have a marked effect on the stability of chiral polyaniline films. The results open the way to the further exploration of electrochemical asymmetric synthesis using chiral polyaniline-modified electrodes and appropriate ionic liquids. BMI-PF₆ and BMI-BF₄ appear to have useful potential as

electrolytes in electrochemical asymmetric oxidations at high positive potentials, whereas MBEA-TFSIs would appear useful for electrochemical asymmetric reductions at very negative potentials.

9.5 References

1. M.R. Majidi, L.A.P. Kane-Maguire, and G.G. Wallace, *Polymer*. **35** (1994): 3113.
2. M.R. Majidi, L.A.P. Kane-Maguire, and G.G. Wallace, *Polymer*. **37** (1996): 359.
3. M.R. Majidi, L.A.P. Kane-Maguire, and G.G. Wallace, *Aust. J. Chem.* **51** (1998): 23.
4. M.R. Majidi, L.A.P. Kane-Maguire, and G.G. Wallace, *Polymer*. **36** (1995): 3597.
5. E.E. Havinga, M.M. Bouman, E.W. Meijer, A. Pomp, and M.M.J. Simenon, *Synth. Met.* **66** (1994): 93.
6. L.A.P. Kane-Maguire, M.R. Majidi, and G.G. Wallace, *Polymeric Materials Encyclopedia*. **2** (1996): 1195.
7. T. Welton, *Chem. Rev.* **99** (1999): 2071.
8. P. Bonhote, A.-P. Dias, N. Papageorgiou, K. Kalyanasundaram, and M. Gratzel, *Inorg. Chem.* **35** (1996): 1168.
9. J.S. Wilkes, *Green Chemistry*. **4** (2002): 73.
10. V.R. Kock, L.A. Dominey, and C. Nanjundiah, *J. Electrochem. Soc.* **143** (1996): 798803.
11. S.A. Forsyth, J.M. Pringle, and D.R. MacFarlane, *Aust. J. Chem.* **57** (2004): 113.
12. D.R. MacFarlane and M. Forsyth, *Adv. Mater.* **13** (2001): 957.
13. R. Vijayaraghavan and D.R. MacFarlane, *Aust. J. Chem.* **57** (2004): 129.
14. M.C. Bowyer, C.M. Gordon, S.K. Leitch, A. McCluskey, and C. Ritchie, *Aust. J. Chem.* **57** (2004): 135.
15. A.A. Syed and M.K. Dinesan, *Talanta*. **38** (1991): 815.
16. E.M. Genies, A. Boyle, M. Lapkowski, and C. Tsintavis, *Synth. Met.* **36** (1990): 139.
17. L.V. Lukachova, E.A. Shkerin, E.A. Puganova, E.E. Karyakina, and A.A. Karyakin, *J. Electroanal. Chem.* **544** (2003): 59.
18. A. Watanabe, K. Mori, M. Mikuni, and Y. Nakamura, *Macromolecules*. **22** (1989): 3323.
19. Y.-B. Shim, M.-S. Won, and S.-M. Park, *J. Electrochem. Soc.* **137** (1990): 538.
20. A. Kabumoto, K. Shinozaki, K. Watanabe, and N. Nishikawa, *Synth. Met.* **26** (1988): 349.
21. A. Malinauskas and R. Holze, *J. Electroanal. Chem.* **461** (1999): 184.
22. C.D. Batich, H.A. Laitineen, and H.C. Zhou, *J. Electrochem. Soc.* **137** (1990): 883.
23. B. Garcia, F. Fusalba, and D. Belanger, *Can. J. Chem.* **75** (1997): 1536.
24. J. Desilvestra, W. Scheifele, and O. Haas, *J. Electrochem. Soc.* **139** (1992): 2727.
25. W. Lu and B.R. Mattes, *J. Electrochem. Soc.* **150** (2003): E416.
26. W. Lu, A.G. Fadev, B. Qi, and B.R. Mattes, *Synth. Met.* **135-136** (2003): 139.
27. P.C. Innis, J. Mazurkiewicz, T. Nguyen, G.G. Wallace, and D.R. MacFarlane, *Current Applied Physics*. **4** (2004): 389.
28. L.A.P. Kane-Maguire, I.D. Norris, and G.G. Wallace, *Synth. Met.* **101** (1999): 817.
29. W.S. Huang and A.G. MacDiarmid, *Polymer*. **34** (1993): 1833.
30. E.V. Strounina, *Synthesis and Characterisation of Chiral Substituted Polyanilines*, in *Chemistry Department*. 2001, University of Wollongong.
31. E.S. Matveeva, C.F. Gimenez, and M.J.G. Tejera, *Synth. Met.* **123** (2001): 117.
32. R. Mazeikiene and A. Malinauskas, *Synth. Met.* **123** (2001): 349.
33. P. Wasserscheid and T. Welton, *Ionic Liquids in Synthesis*. (2003) Morlenbach, Germany: Wiley-VCH Verlag GmbH&Co.
34. J.S. Wilkes, *J. Molecular Catalysis A : Chemical*. **214** (2004): 11.
35. J. Fuller, A.C. Breda, and R.T. Carlin, *J. Electroanal. Chem.* **459** (1998): 29.
36. Y. Ishida, H. Miyauchi, and K. Saigo, *Chem. Commun.*, (2002): 2240.

37. W. Bao, Z. Wang, and Y. Li, *J. Org. Chem.* **68** (2003): 591.
38. D.R. MacFarlane, P. Meakin, J. Sun, N. Amini, and M. Forsyth, *J. Phys. Chem. B.* **103** (1999).
39. D.R. MacFarlane, J. Golding, S.A. Forsyth, M. Forsyth, and G.B. Deacon, *Chem. Commun.*, (2001): 1430.
40. P. Wasserscheid, A. Bosmann, and C. Bolm, *Chem. Commun.*, (2002): 200.
41. J. Stejskal, P. Kratochvil, and A.D. Jenkins, *Collect. Czech. Chem. Commun.* **60** (1995): 1747.
42. W.A. Gazotti, R. Faez, and M.A. Paoli, *J. Electroanal. Chem.* **415** (1996): 107.
43. M. Lapkowski, *Synth. Met.* **35** (1990): 169.
44. A. Kitani, M. Kaya, J. Yano, K. Yoshikawa, and K. Sasaki, *Synth. Met.* **18** (1987): 341.
45. E.M. Genies, M. Lapkowski, and J.F. Penneau, *J. Electroanal. Chem.* **249** (1988): 97.
46. E.M. Genies and C. Tsintavis, *J. Electroanal. Chem.* **195** (1985): 109.
47. E.M. Genies and M. Lapkowski, *J. Electroanal. Chem.* **236** (1987): 189.
48. D. Orata and D.A. Buttry, *J. Am. Chem. Soc.* **109** (1987): 3574.
49. G. Wieners, M. Monkenbusch, and G. Wegner, *Ber. Bun-senges. Phys. Chem.* **88** (1984): 935.
50. I. Harada and Y. Furukawa, *Vib. Spectra. Struct.* **19** (1991): 439.
51. S.-A. Chen and G.-W. Hwang, *Macromolecules.* **29** (1996): 3950.
52. T. Kobayashi, H. Yoneyama, and H. Tamura, *J. Electroanal. Chem.* **177** (1984): 293.
53. W.S. Huang, B.D. Humphrey, and A.G. MacDiarmid, *J. Chem. Soc., Faraday Trans. I.* **82** (1986): 2385.
54. J. Stejskal and P. Kratochvil, *Synth. Met.* **61** (1993): 225.
55. W.W. Focke, G.E. Wnek, and Y. Wei, *J. Phys. Chem.* **91** (1987): 5813.
56. A.M. Fenelon and C.B. Breslin, *Synth. Met.* **144** (2004): 125.
57. M. Lapkowski, K. Berrada, S. Quillard, G. Louarn, S. Lefrant, and A. Pron, *Macromolecules.* **28** (1995): 1233.
58. J.E.P. Silva, D.L.A. Faria, S.I.C. Torresi, and M.L.A. Temperini, *Macromolecules.* **33** (2000): 3077.
59. G.M. Nascimento, J.E.P. Silva, S.I.C. Torresi, and M.L.A. Temperini, *Macromolecules.* **35** (2002): 121.
60. E. Cintra and S.I.C. Torresi, *J. Electroanal. Chem.* **2002** (2002): 33.
61. C.Q. Cui, X.H. Su, and J.Y. Lee, *Polym. Degrad. Stab.* **41** (1993): 69.
62. L. Ding, X. Wang, and R.V. Gregory, *Synth. Met.* **104** (1999): 73.
63. R. Mathew, D. Yang, B.R. Mattes, and M.P. Espe, *Macromolecules.* **35** (2002): 7575.
64. H.H. Tan, K.G. Neoh, F.T. Liu, N. Kocherginsky, and E.T. Kang, *J. Appl. Polym. Sci.* **80** (2001): 1.
65. D. Rodrigue, P. Snauwaert, X. Demaret, J. Riga, and J.J. Verbist, *Synth. Met.* **41** (1991): 769.
66. J.A. Conklin, S.-C. Huang, S.-M. Huang, T. Wen, and R.B. Kaner, *Macromolecules.* **28** (1995): 6522.
67. X.-H. Wang, Y.-H. Geng, X.-B. Wang, X.-B. Jing, and F.-S. Wang, *Synth. Met.* **69** (1995): 265.
68. R.J. Holness, G. Williams, D.A. Worsley, and H.N. McMurray, *J. Electrochem. Soc.* **152** (2005): B73.
69. C. Engert, S. Umopathy, W. Kiefer, and H. Hamaguchi, *Chem. Phys.* **218** (1994): 87.
70. J.E.P. Silva, S.I.C. Torresi, D.L.A. Faria, and M.L.A. Temperini, *Synth. Met.* **101** (1999): 834.
71. R.M. Torresi and S.I. Torresi, *Synth. Met.* **61** (1993): 291.
72. M.C. Miras, C. Barbero, R. Kotz, and O. Haas, *J. Electrochem. Soc.* **138** (1991): 335.
73. H. Varela and R.M. Torresi, *J. Electrochem. Soc.* **147** (2000): 665.
74. R.L. Hand and R.F. Nelson, *J. Am. Chem. Soc.* **96:3** (1974): 850.
75. R.L. Hand and R.F. Nelson, *J. Electrochem. Soc.* **125** (1978): 1059.
76. N. Pekmez and A. Yildiz, *J. Electroanal. Chem.* **386** (1995): 121.
77. A.A. Pud, *Synth. Met.* **66** (1994): 1.
78. A.Q. Zhang, C.Q. Cui, and Y.J. Lee, *Synth. Met.* **72** (1995): 217.

Chapter 10

Electroorganic Reactions in Ionic Liquids

10.1 Introduction

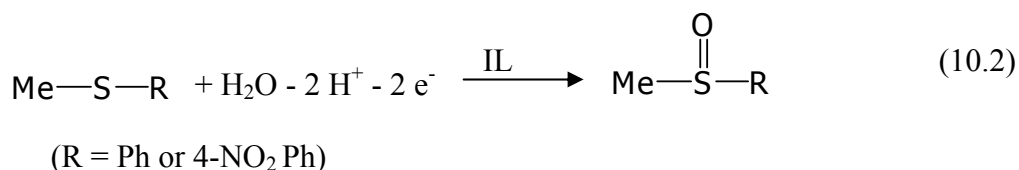
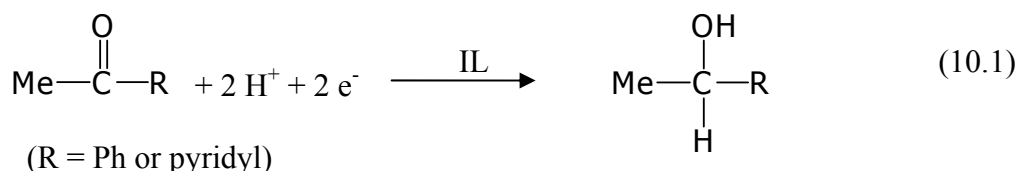
Asymmetric electrosynthesis is a subject of considerable significance because pharmaceutical drugs are increasingly required in enantiomerically pure form.¹ In this approach, enantioselectivity requires a chiral environment in the immediate location of the electrochemical reaction. As summarized in Chapter 1, electrochemical asymmetric induction can be partially achieved by using chiral solvents,² chiral supporting electrolytes or chiral additives such as alkaloids^{3,4} and chiral electrodes.⁵⁻⁹

Electrochemical reactions of organic compounds are typically performed in highly volatile and/or hazardous organic solvents, which have been blamed for increasing air pollution. Recently, however, ionic liquids (ILs) have emerged as new, recyclable “green solvents” for chemical reactions and separation processes because of their beneficial properties: (i) high ionic conductivity, (ii) large electrochemical potential window, (iii) excellent thermal stability, (iv) negligible volatility, and (v) non-flammability.¹⁰⁻¹³ Ionic liquids, therefore appear to have great potential for many applications including as solvents for chemical synthesis and catalysis,^{12,14-22} for solvent extraction,²³ and as electrolytes for electrochemical synthesis^{13,16,24-30} and electrochemical devices.³¹⁻³⁴ A large number of ionic liquids have now been synthesized^{10, 17, 35, 36} and many are commercially available.

There has been considerable recent interest in the potential of chiral conducting polymers as chiral electrodes in asymmetric synthesis.^{5, 37} Chiral polyanilines may have

a great potential in this area because of their high electrical conductivity and high optical activity. In Chapter 9, the electrochemical behaviour and chiroptical properties of chiral PAn.(+)-HCSA modified electrodes in ionic liquids was examined. These studies established the electrochemical potential range over which the polyaniline films are stable and how the chirality may be preserved in a range of ionic liquids. In addition, the new chiral ionic liquids (+)- and (-)- α -methylbenzylethylamine bis(trifluoromethanesulfonyl)imide (MBEA-TFSI) have been recently synthesized in our laboratories. The properties of these new ionic liquids were studied in Chapter 9 and suggest that they also have potential as chiral electrolytes for electrochemical asymmetric synthesis.

Based on these underpinning studies, the present Chapter explores the use of chiral polyaniline electrodes and ionic liquid electrolytes as novel systems for achieving asymmetric electrosynthesis. The particular reactions chosen for study are: (i) the reduction of prochiral carbonyl compounds such as acetophenone and acetylpyridine to the corresponding chiral alcohols (Equation 10.1), and (ii) the oxidation of prochiral organic sulfides such as methyl-*p*-tolyl sulfide (MPTS) and methyl 4-nitrophenyl sulfide (MNPS) to the corresponding chiral sulfoxides (Equation 10.2).



Although the redox processes 10.1 and 10.2 are well established in conventional solvents, these reactions have not been reported in ionic liquids to date. In the present study, due to the use of chiral polyaniline modified electrodes and ionic liquid electrolytes, it was hypothesized that optically active products may be expected from the electrochemical reductions and oxidations in Equations 10.1 and 10.2. Therefore, as a necessary preliminary to the electrochemical asymmetric studies in this Chapter, cyclic voltammetry was employed to establish the electrochemical behaviour of the prochiral organic substrates in the ionic liquids.

10.2 Experimental

10.2.1 Materials

All chemicals used were purchased in the purest form available. Methyl-*p*-tolyl sulfide (MPTS), methyl-4-nitrophenyl sulfide (MNPS) and 2-acetylpyridine were obtained from Aldrich. 4-acetylpyridine and (*R*)-(+)-1-(4-pyridyl)ethanol were purchased from Fluka, while acetophenone was obtained from Merck.

The ionic liquids EMI-TFSI, BMI-PF₆, and (+)-, (-)- and (±)-MBEA-TFSI were available in our laboratories. BMI-BF₄ was purchased from Solvent Innovation and used without further purification. General information and the chemical structures of these ionic liquids are described in Chapter 2.

TLC aluminium sheets coated with silica gel 60 F₂₅₄ and silica gel 60 (0.040-0.063 mm) were purchased from Merck. Poly(vinylidene)difluoride (PVDF) membrane (0.22 μm pore size) was obtained from Millipore.

10.2.2 Preparation of Chiral PAn.(+)-HCSA Modified Electrodes

The PAn.(+)-HCSA films were potentiostatically deposited at 0.8 V on glassy carbon electrodes, or at 0.9 V on ITO-Pt coated glass electrodes, from aqueous 0.2 M aniline/1.0 M (+)-HCSA as described in Chapter 2. The PAn.(+)-HCSA modified electrodes were then washed with methanol and dried in a vacuum desiccator.

10.2.3 Electrochemical Behaviour of Prochiral Organic Substrates in Ionic Liquids

The electrochemical behaviour of the organic carbonyl and sulfide substrates in ionic liquids were studied using cyclic voltammetry. Either a glassy carbon (surface area = 0.07 cm²) or PAn.(+)-HCSA modified glassy carbon was used as the working electrode. Platinum mesh and Ag/AgCl_(EMI-TFSI) or silver wire were used as auxiliary and reference electrodes, respectively. The cyclic voltammograms were recorded at room temperature while purging the solution with nitrogen gas. Specific details of each experiment are given in the Results and Discussion section.

10.2.4 Electrolyses

Electrolyses were carried out in a one-compartment cell (see Figure 2.2 in Chapter 2) or a divided cell (Figure 10.1) with three electrodes. A glassy carbon plate or a PAn.(+)-HCSA modified electrode was used as working electrode. Pt or stainless mesh or reticulated vitreous carbon (RVC) were employed as auxiliary electrode, while silver wire or Ag/AgCl_(EMI-TFSI) were used as the reference electrode. A PVDF membrane was used to separate the catholyte and anolyte in the divided cell. The electrolytic reductions or oxidations of the prochiral organic substrates were carried out by the controlled potential method using a BAS CV-27 potentiostat and a MacLab/2e with Chart software and monitoring the current and charge passed. All electrolyses were performed at room

temperature while magnetically stirring and flushing with nitrogen. Details of the electrolytic conditions for each experiment are given in the Results and Discussion.

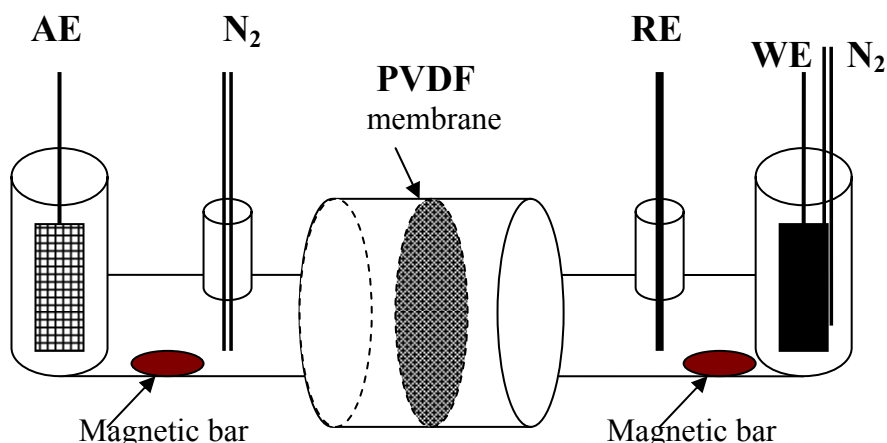


Figure 10.1 A divided electrochemical cell for electrochemical synthesis.

10.2.5 Analysis Techniques

The electrolysed solutions were preliminarily analyzed by thin layer chromatography using aluminium sheet coated with silica gel 60. The electrolytic products were isolated by solvent extraction or column chromatography packing with silica gel 60 and analyzed by mass spectrometry. Optical rotations in organic solvents were measured with a Jasco DIP-370 Digital polarimeter. Specific details of the particular procedures employed are described in the Results and Discussion.

10.3 Results and Discussion

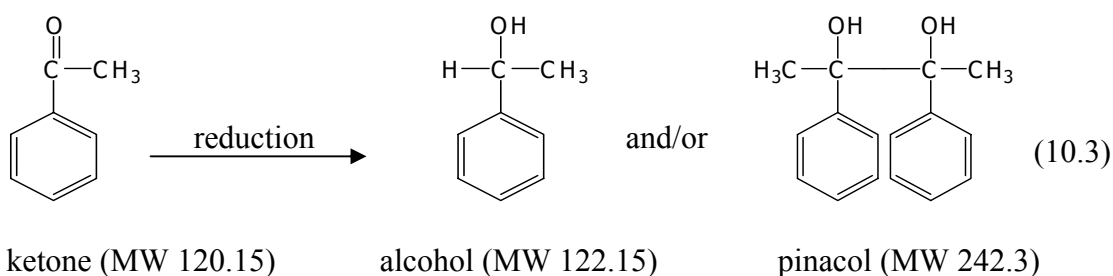
In preliminary studies, cyclic voltammetry was used to examine the electrochemical behaviour (reversibility and redox potentials) of the prochiral organic compounds acetophenone, acetylpyridine, methyl-*p*-tolyl sulfide (MPTS) and methyl 4-nitrophenyl sulfide (MNPS) in ionic liquid electrolytes using bare or PAn.(+)-HCSA modified electrodes. The electrochemical oxidation/reduction of these organic compounds has

been previously studied only in conventional organic solvents such as methanol and acetonitrile.^{3-8, 38-40} The CV studies below provided information on the potential that should be applied for electrolysis (oxidation or reduction) of each organic substrate.

10.3.1 Electrochemical Reduction of Acetophenone in EMI-TFSI

(a) CVs of Acetophenone in EMI-TFSI

The prochiral ketone, acetophenone, can be reduced to the corresponding alcohol 1-phenylethanol (or α -methyl benzyl alcohol) and/or pinacol, as shown in Equation 10.3. Chemical asymmetric reduction of acetophenone in methanol/THF using NaBH_4 supported on chiral polymeric supports has been previously reported⁴¹ to give a chemical yield of 70% and an enantiomeric excess (*ee*) of 56% for the alcohol product.



In the present study, electrochemical reduction of acetophenone in the ionic liquid EMI-TFSI as electrolyte was explored using cyclic voltammetry, by cycling the potential between -2.2 and +1.0 V (*vs.* $\text{Ag}/\text{AgCl}_{(\text{EMI-TFSI})}$) on either a glassy carbon (GC) electrode or a chiral PAn.(+)-HCSA modified electrode in a one-compartment cell. Figure 10.2a shows the influence of the concentration of acetophenone on the cyclic voltammograms using a bare GC electrode. The reduction of acetophenone was observed to occur at *ca.* -1.8 V in each case. Thus, the reduction potential was independent of concentration. Higher cathodic current responses were observed using higher concentrations of acetophenone. No oxidation peak was observed between 0.0

and + 2.0 V (not shown), indicating an irreversible reduction. The use of a PAn.(+)-HCSA modified working electrode revealed an irreversible cathodic peak current (Figure 10.2b), corresponding to the reduction of acetophenone at the same potential as observed with the bare GC-disc electrode. Anodic and cathodic peaks in the range of -0.2 to 1.0 V associated with the electroactivity of the polyaniline component of the electrode were also observed.

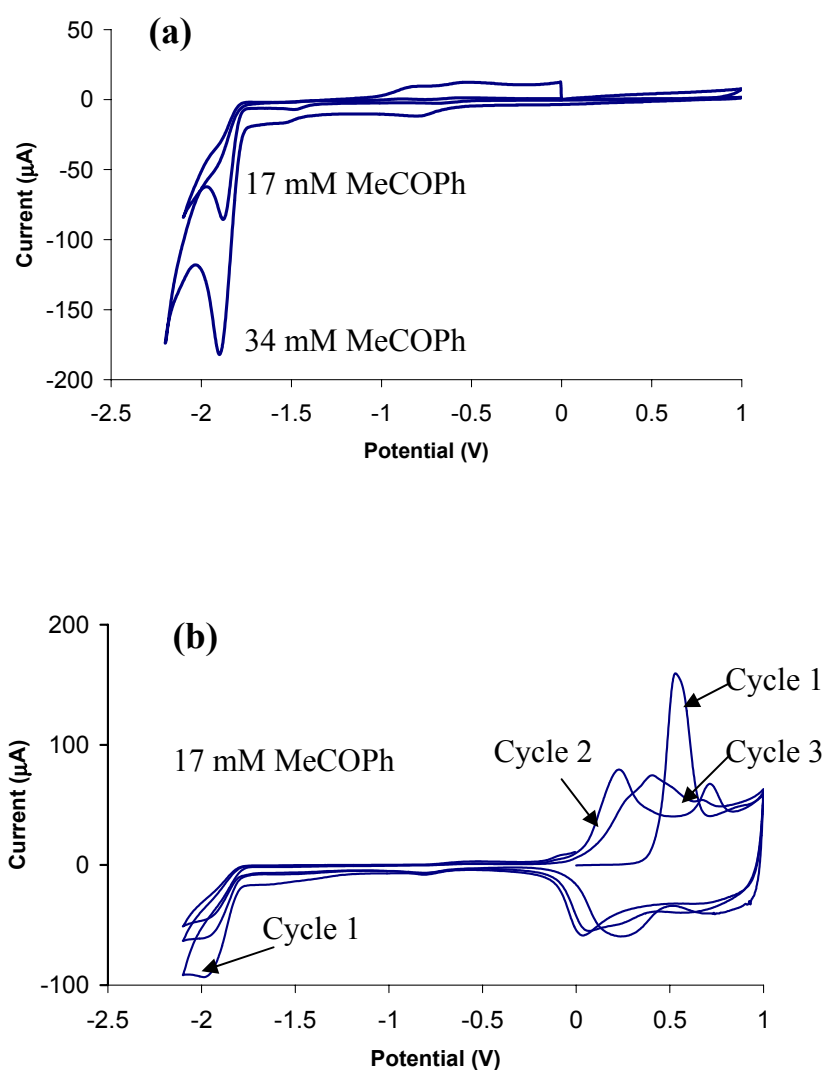


Figure 10.1 Cyclic voltammograms for acetophenone in EMI-TFSI electrolyte on: (a) a glassy carbon disc (surface area = 0.07 cm²), and (b) a PAn.(+)-HCSA modified (60 mC/cm² of deposition charge) glassy carbon electrode. Scan rate = 50 mV/s.

(b) Electrolysis of Acetophenone in EMI-TFSI

Electrolysis of acetophenone (0.10 M) in EMI-TFSI (60 μ L in 5 mL of ionic liquid) was performed in a one-compartment/three-electrode cell using a bare glassy carbon sheet (surface area in the solution 2 cm²) as the working electrode, a stainless steel mesh as the auxiliary electrode and Ag/AgCl_(EMI-TFSI) as the reference electrode. A constant potential of -1.9 V was applied. The electrolysis was continued for 11 hrs and 26 C of charge passed. (This is *ca.* 40% of the charge that would be required for complete reduction of the acetophenone). The electrolysis solution was then extracted five times with 10 mL of diethyl ether. After evaporation of the diethyl ether on a warm water bath, the crude product was analyzed using chemical ionization (CI) mass spectrometry.

The CI mass spectrum in Figure 10.3 showed strong peaks at *m/z* 121 and 122, corresponding to unreacted acetophenone and the expected reduction product (1-phenylethanol), respectively. In contrast, Schwientek *et al.*⁵ reported that no alcohol product was obtained when using a bare Pt electrode for reduction of acetophenone in DMF containing LiBr as supporting electrolyte and phenol as hydrogen donor. The main product formed was pinacol, with a low current yield.

Our successful electrochemical reduction of acetophenone to the corresponding alcohol in EMI-TFSI as solvent/electrolyte is therefore significant. However, unfortunately in Chapter 9 the chiral PAn.(+)-HCSA modified electrode was found to racemize in EMI-TFSI when a negative potential of -0.5 V was applied for 7 min. Therefore, the system would be unsuitable for electrochemical asymmetric synthesis.

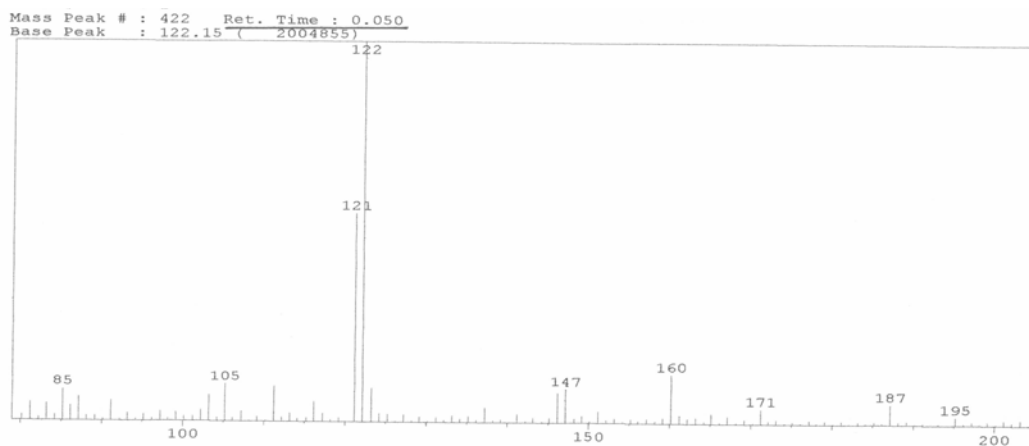
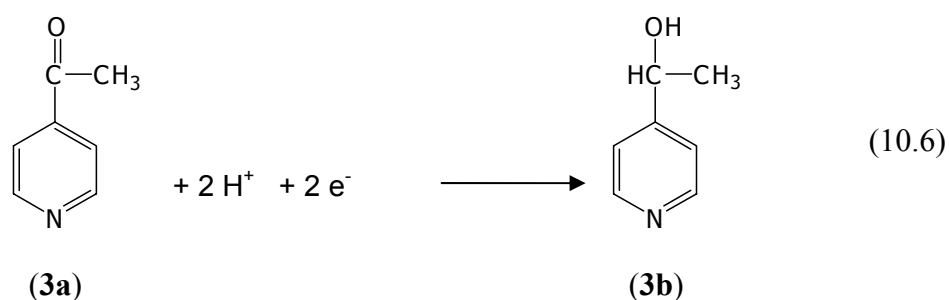
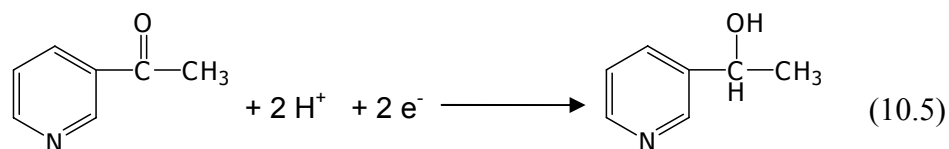
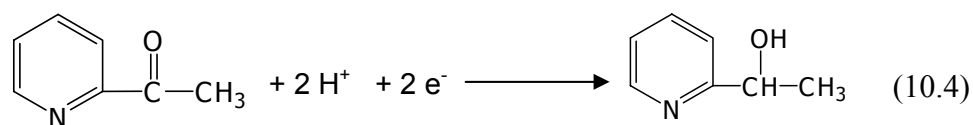


Figure 10.2 CI Mass spectrum for crude extract of electroreduction of acetophenone in EMI-TFSI.

10.3.2 Electrochemical Studies of Acetylpyridine in Ionic Liquids

Kopilov *et al.*³ have reported the electrochemical asymmetric reduction of the prochiral acetylpyridines (**1a**, **2a**, and **3a**) to the corresponding pyridylethanol (**1b**, **2b**, and **3b**), as shown in Equations 10.4, 10.5 and 10.6, by using a mercury electrode in the presence of chiral alkaloids. The optical yields depended on the nature of the chiral alkaloids used and on the conditions employed (e.g. potential, electrolyte, pH, and temperature). The optical yields were relatively high (47% and 41% *ee*) for the reductions of 2- and 4-acetylpyridine (**1a** and **3a**), respectively, but the 3-acetylpyridine (**2a**) substrate gave no asymmetric reduction.

The present work explored the electrochemical behaviour of 2- and 4-acetylpyridine (**1a** and **3a**) in EMI-TFSI and MBEA-TFSI electrolytes using cyclic voltammetry. Experiments were performed in a one-compartment or a divided cell with three-electrodes, using glassy carbon or chiral polyaniline-modified glassy carbon as working electrode.



10.3.2.1 Electrochemical Reduction of 2-Acetylpyridine in EMI-TFSI

(a) Cyclic Voltammetry of 2-Acetylpyridine in EMI-TFSI

The cyclic voltammetry was carried out in a one compartment/three-electrode cell using stainless steel mesh and Ag/AgCl_(EMI-TFSI) as auxiliary and reference electrodes, respectively. Figure 10.4 compares the cyclic voltammograms obtained for 2-acetylpyridine in EMI-TFSI on (a) a bare glassy carbon and (b) a PAn.(+)-HCSA modified electrode. Higher cathodic current response was recorded for higher concentrations of 2-acetylpyridine without a significant difference in the reduction potential (*ca.* -1.7 V) on bare GC-disc (Figure 10.4a). No anodic peak was observed in the range of cycling, -2.0 to +1.0 V. This indicates that reduction of 2-acetylpyridine in EMI-TFSI is irreversible. The corresponding cyclic voltammograms for 36 mM 2-acetylpyridine on a PAn.(+)-HCSA modified glassy carbon electrode (Figure 10.4b)

revealed two redox couples for polyaniline in the potential range of -0.2 to +1.0 V, while a poorly-defined reduction peak for 2-acetylpyridine was observed at *ca.* -1.7 V.

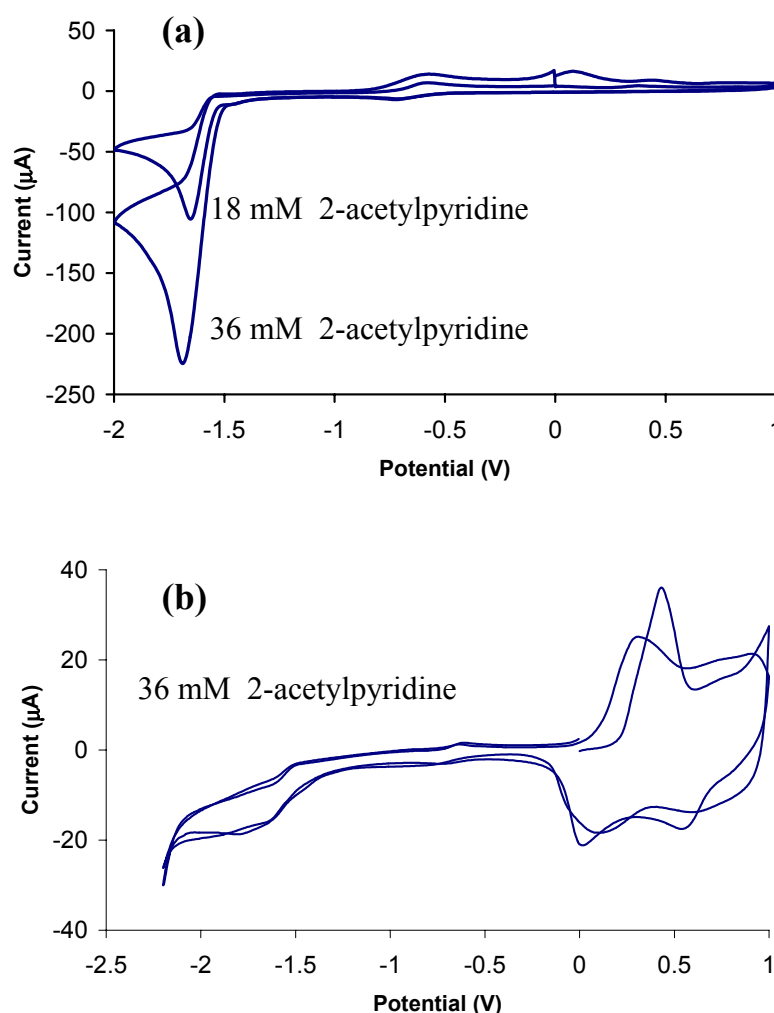


Figure 10.4 Cyclic voltammograms for 2-acetylpyridine in EMI-TFSI electrolyte on: (a) a glassy carbon electrode (surface area = 0.07 cm^2), and (b) a PAN.(+)-HCSA modified (50 mC/cm^2 of deposition charge) glassy carbon electrode.

(b) Electrolysis of 2-Acetylpyridine in EMI-TFSI

A solution of 60 μL 2-acetylpyridine in 5 mL EMI-TFSI (= 0.1 M) was employed. The electroreduction was carried out with a constant potential of -1.8 V in a one-compartment/ three-electrode cell using a bare glassy carbon plate (surface area in the solution = 2 cm^2) as the working electrode, a cylinder of stainless steel mesh as

auxiliary electrode and Ag/AgCl_(EMI-TFSI) as reference electrode, respectively. Electrolysis was performed for 6 hrs and 47 C of charge passed (this is *ca.* 46% of the charge that would be required for complete reduction of the acetylpyridine).

The electrolysis solution was then extracted ten times with 10 mL of chloroform. It should be noted that after adding the first 10 mL of chloroform, the volume of the EMI-TFSI layer almost doubled. This indicated that the EMI-TFSI partially dissolved in chloroform. After partial evaporation of the extracts, the crude products in chloroform were analyzed by mass spectrometry. The CI mass spectrum (Figure 10.5) showed that unreacted 2-acetylpyridine and the corresponding alcohol product were present (peaks at *m/z* 124 and 122, respectively).

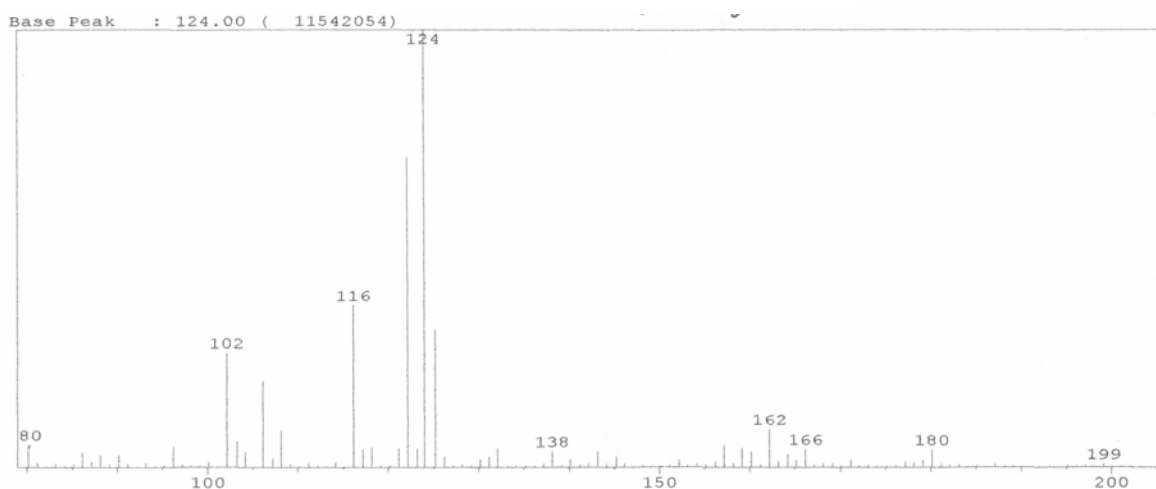


Figure 10.5 CI Mass spectrum for chloroform extract from electroreduction of 2-acetylpyridine in EMI-TFSI at -1.8 V.

Although the electroreduction of 2-acetylpyridine to the alcohol could therefore be successfully achieved in the EMI-TFSI solvent/electrolyte, unfortunately the system could not be used for asymmetric electrosynthesis since in Chapter 9 it was found that a chiral PAN.(+)-HCSA film racemized when reduced in EMI-TFSI.

10.3.2.2 Electrochemical Reduction of 4-Acetylpyridine in (-)-MBEA-TFSI

Cyclic voltammetry and electrolysis of 4-acetylpyridine were then carried out in the chiral ionic liquid (-)-MBEA-TFSI in the hope of achieving asymmetric reduction, due to the chiral electrolyte/solvent used. A divided cell with three electrodes was employed. Bare glassy carbon, Pt mesh and silver wire were used as working, auxiliary and quasi-reference electrodes, respectively. To avoid degradation of MBEA-TFSI at the auxiliary electrode, tetrabutylammonium chloride (Bu_4NCl) electrolyte salt, which can be oxidized to chlorine gas at the auxiliary electrode and eliminated from the solution, was added to the anolyte. The catholyte (5 mL of (-)-MBEA-TFSI containing 50 mM of 4-acetylpyridine) and the anolyte (5 mL of (-)-MBEA-TFSI containing 0.1 M of Bu_4NCl) were separated by a PVDF membrane. Nitrogen gas was bubbled through both compartments.

(a) Cyclic Voltammetry of 4-Acetylpyridine in (-)-MBEA-TFSI

The cyclic voltammogram for 50 mM 4-acetylpyridine in (-)-MBEA-TFSI on a bare GC-disc electrode (0.07 cm^2 surface area) is illustrated in Figure 10.6. A cathodic current peak was observed at *ca.* -1.4 V attributed to reduction of 4-acetylpyridine to 4-pyridylethanol.

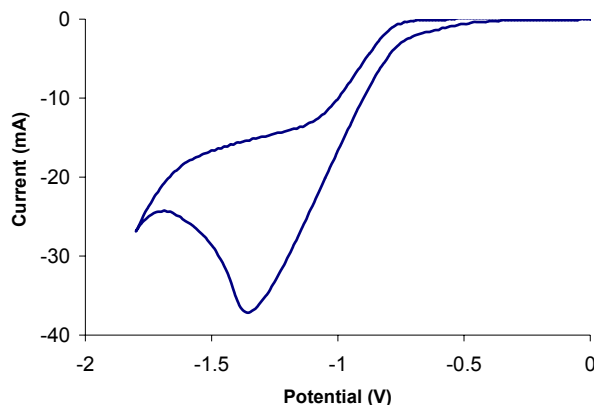


Figure 10.6 Cyclic voltammogram of 50 mM 4-acetylpyridine in (-)-MBEA-TFSI using a bare GC-disc (0.07 cm^2) electrode. Scan rate: 50 mV/s.

(b) Electrolysis of 4-Acetylpyridine in (-)-MBEA-TFSI

Electrolysis of 4-acetylpyridine in (-)-MBEA-TFSI was carried out on a glassy carbon plate (1 cm² surface area) using an applied potential of -1.6 V. It was continued for 86 hrs to complete the reduction with 52 C of charge passed. The low rate of reaction may be due to the relatively low conductivity of the MBEA-TFSI (see Section 9.3.1 in Chapter 9). After the electrolysis, the reaction mixture (catholyte) was analyzed by mass spectrometry. The ES mass spectrum (Figure 10.7) showed that 4-pyridylethanol product and unreacted 4-acetylpyridine were present (peaks at *m/z* 124 and 122, respectively).

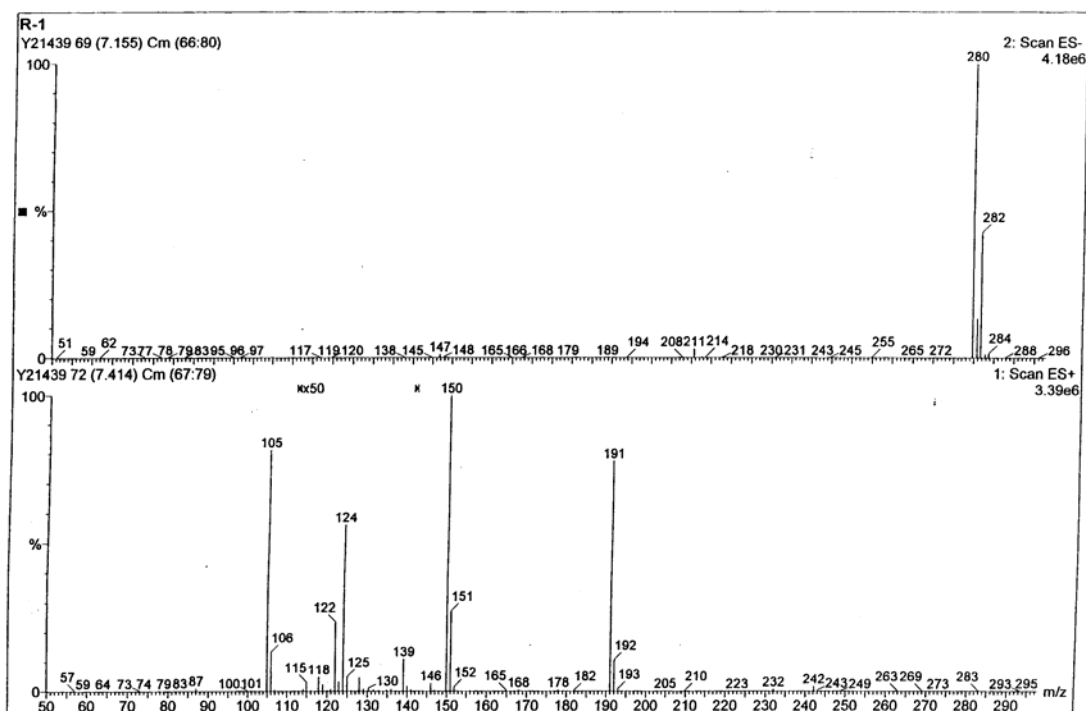


Figure 10.7 ES Mass spectrum for the reaction mixture (catholyte) from electroreduction of 4-acetylpyridine in (-)-MBEA-TFSI at -1.6 V.

However, the product was not able to be separated from the MBEA-TFSI by solvent extraction as they have nearly the same solubility properties (e.g. soluble in acetone,

chloroform, diethylether and insoluble in n-hexane) or by column chromatography using silica gel 60 (0.040 - 0.063 mm) as a stationary phase and chloroform/acetonitrile (70:20) as a mobile phase. Therefore, the optical rotation of the product could not be obtained due to interference from the optically active ionic liquid.

10.3.2.3 Electrochemical Reduction of 4-Acetylpyridine in (±)-MBEA-TFSI

In order to determine whether optically active alcohol product could be obtained from the above electro-reduction of 4-acetylpyridine in racemic (±)-MBEA-TFSI with a chiral electrode, a chiral PAn.(+)-HCSA modified electrode was used.

(a) Cyclic Voltammetry of 4-Acetylpyridine in (±)-MBEA-TFSI

Cyclic voltammetry was carried out in a one compartment/three-electrode cell. Figures 10.8a and 10.8b compare the cyclic voltammograms of 4-acetylpyridine in (±)-MBEA-TFSI on (a) glassy carbon and (b) a PAn.(+)-HCSA modified glassy carbon electrode, over the potential range -2.0 to 0.0 V. A cathodic wave was recognized at *ca.* -1.3 V in Figure 10.8a for the reduction on glassy carbon. A decrease in the peak current and a less negative potential for the cathodic peak were observed in the second cycle.

The corresponding CV of 4-acetylpyridine on a PAn.(+)-HCSA modified glassy carbon electrode similarly showed a cathodic peak at *ca.* -1.3 V in the first scan (Figure 10.8b). The cathodic peak also observed at *ca.* -0.2 V corresponds to reduction of emeraldine to leucoemeraldine at the PAn.(+)-HCSA modified electrode. This latter peak disappeared in the second scan. This is due to the fact that the potential range of -2.0 to 0.0 V is not sufficient to oxidize leucoemeraldine to emeraldine. The potential required to convert leucoemeraldine to emeraldine in MBEA-TFSI was shown in Chapter 9 (see Figure 9.15) to be *ca.* 0.2 V.

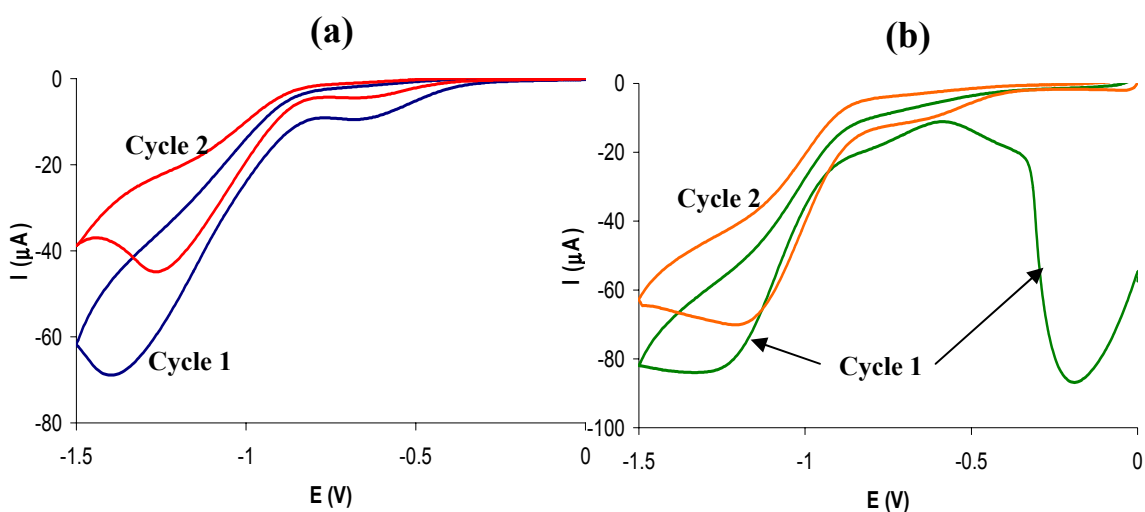


Figure 10.8 Cyclic voltammograms of 18 mM 4-acetylpyridine in (\pm)-MBEA-TFSI on (a) a GC-disc (0.07 cm^2), and (b) a PAN.(+)-HCSA modified (70 mC/cm^2 deposition charge) GC-disc. Scan rate: 50 mV/s .

(b) Electrolysis of 4-Acetylpyridine in (\pm)-MBEA-TFSI

Electrolysis was carried out in a divided cell with three electrodes. A PAN.(+)-HCSA modified ITO-Pt coated electrodes, Pt mesh and silver wire were used as working, auxiliary and quasi-reference electrode, respectively. Catholyte (5 mL of (\pm)-MBEA-TFSI containing 50 mM of 4-acetylpyridine) and anolyte (5 mL of (\pm)-MBEA-TFSI containing 0.1 M of Bu_4NCl) were separated by a PVDF membrane.

To ensure that reduction of 4-acetylpyridine occurred in the divided cell, a cyclic voltammogram was recorded. A cathodic current peak at *ca.* -1.6 V attributed to reduction of 4-acetylpyridine was observed (Figure 10.9). This is the same potential as when the CV was carried out in a one-compartment cell (see Figure 10.8a).

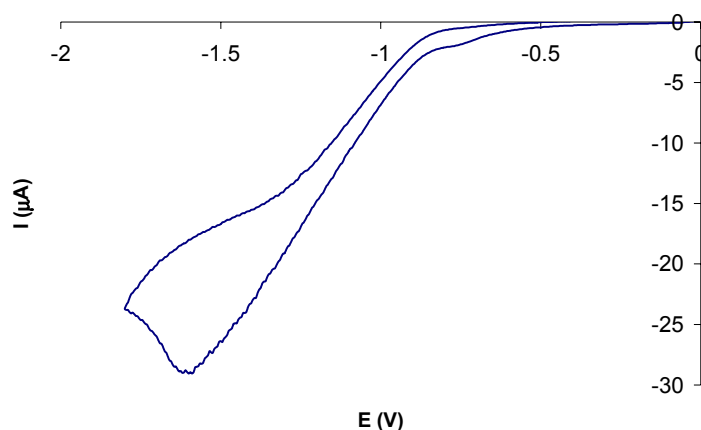


Figure 10.9 Cyclic voltammogram of 50 mM 4-acetylpyridine in (±)-MBEA-TFSI on a GC-disc (0.07 cm^2) in the catholyte compartment of a divided cell. Pt mesh and silver wire as auxiliary and quasi-reference electrodes, respectively. Scan rate: 50 mV/s.

Electrolysis was then performed by applying a constant potential at -1.7 V. During electrolysis, the PAn.(+)-HCSA film on the ITO-Pt coated electrode was colourless because the polyaniline was in the leucoemeraldine form at this potential. After 85 hrs, only 33 C of charge was passed (*ca.* 63% of the charge that would be required for complete reduction). This may be due to the relatively low conductivity of this ionic liquid and the non-conductive leucoemeraldine film. The polymer film turned to green after taken from the solution and left in air for a day. This indicates oxidation by oxygen in the air to the emeraldine salt. Significantly, the chiral polyaniline film exhibited good stability in (±)-MBEA-TFSI. Its CD spectrum showed the film to be still optically active but slightly different from the initial spectrum (Figure 10.10). This CD spectral change probably arises from a conformational change during reduction at extreme negative potential (-1.7 V) for a long period (85 hrs) in the ionic liquid MBEA-TFSI.

Unfortunately, analysis of the reaction mixture by TLC chromatography and ES mass spectrometry indicated that 4-acetylpyridine was not reduced to the corresponding alcohol, the corresponding achiral pinacol being instead formed.

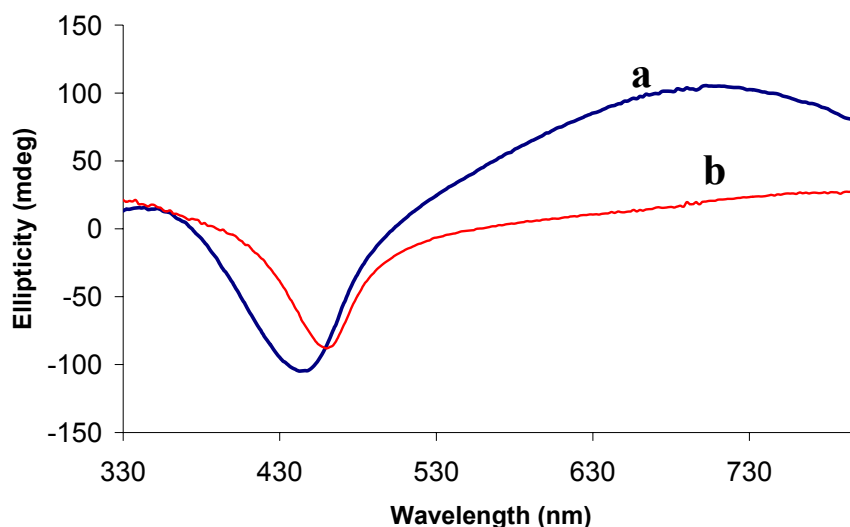
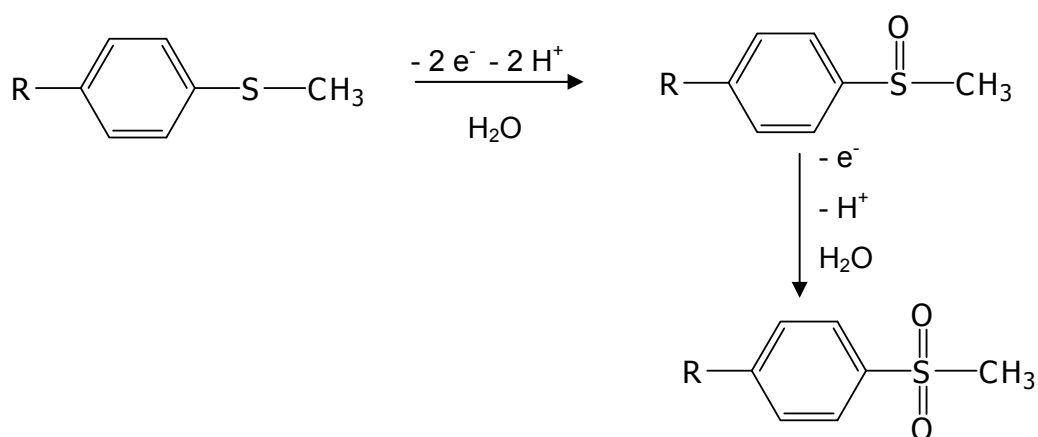


Figure 10.10 CD spectra of a PAn.(+)-HCSA modified ITO-Pt coated glass electrode (a) before and (b) after held at -1.7 V for 85 hrs in (\pm)-MBEA-TFSI containing 50 mM 4-acetylpyridine and left in air for a day.

10.3.3 Electrochemical Oxidation of Organosulfides in Ionic Liquids

Asymmetric electro-oxidation of prochiral organosulfides on chiral modified electrodes has been previously studied in acetonitrile solvent containing supporting electrolytes and 1-7% water.^{7,8,40} Weakly optically active sulfoxides (% *ee* less than 2%) were obtained. The conversions of methyl 4-nitrophenyl sulfide (MNPS) and methyl-*p*-tolyl sulfide (MPTS) in the presence of water to sulfoxides and then to sulfones are shown in Scheme 10.1 (R = Me and NO₂, respectively).

In the present study, the corresponding electrochemical behaviour of MNPS and MPTS in the ionic liquids EMI-TFSI and BMI-BF₄ are explored.



Scheme 10.1

10.3.3.1 Electrochemical Oxidation of MNPS in EMI-TFSI

(a) Cyclic Voltammetry of MNPS in EMI-TFSI

Cyclic voltammograms of 20 mM MNPS in EMI-TFSI on a bare glassy carbon electrode and on a PAn.(+)-HCSA modified glassy carbon electrode are shown in Figures 10.11 and 10.12, respectively. The potentials were scanned over the range -0.2 to +2.4 V (vs. Ag/AgCl_(EMI-TFSI)). Figure 10.11 reveals two anodic peaks at *ca.* 1.6 and 2.2 V which correspond to the successive conversion of MNPS to its sulfoxide and sulfone, respectively.

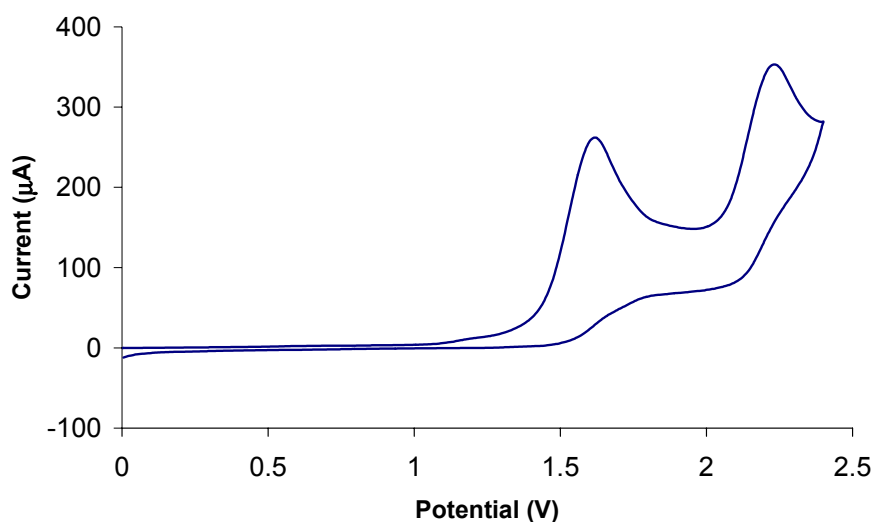


Figure 10.11 Cyclic voltammogram for 20 mM MNPS in EMI-TFSI using a bare glassy carbon disc (0.07 cm² surface area) working electrode. Scan rate: 50 mV/s.

Oxidation peaks were observed at nearly the same potentials using a PAn.(+)-HCSA modified glassy carbon working electrode (Figure 10.12a). In addition, two anodic peaks without well-defined cathodic peaks were seen in the potential range -0.2 to 1.2 V of the first cycle, associated with oxidation of the polyaniline film. These peaks disappeared in the second cycle. This is probably due to oxidative degradation of polyaniline in EMI-TFSI at high potentials (≥ 1.2 V, see Chapter 9). Therefore, potential scanning over the range 0.0 to 2.0 V (Figure 10.12b) also caused degradation of the polyaniline film. Therefore, asymmetric oxidation of MNPS to the corresponding chiral sulfoxide in EMI-TFSI using a chiral polyaniline electrode was not feasible.

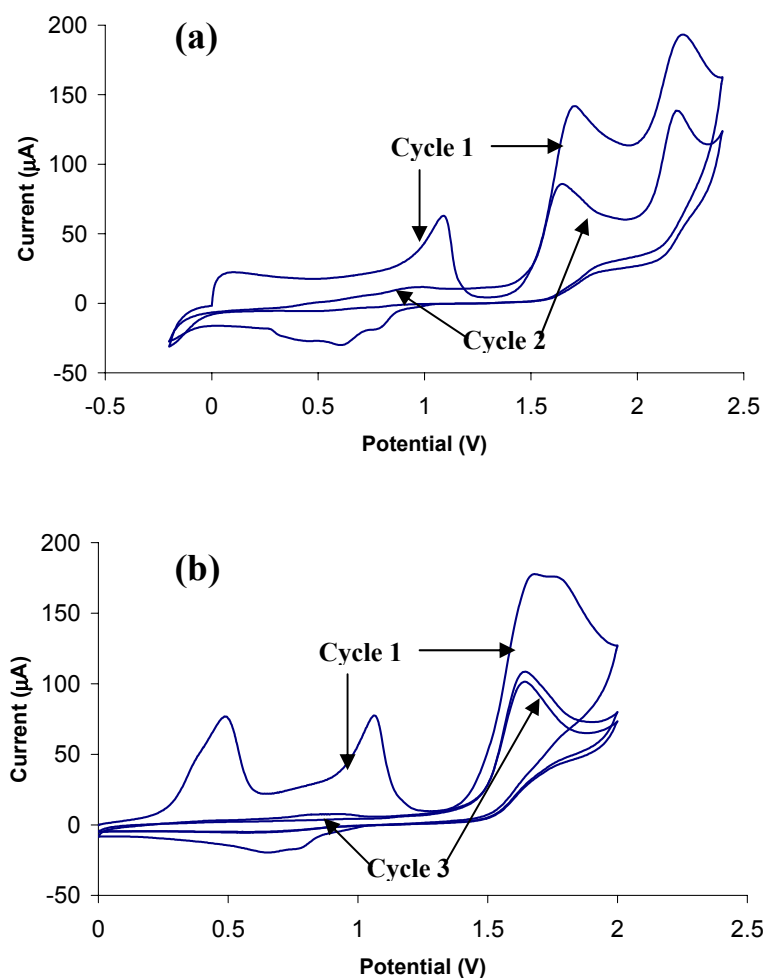


Figure 10.12 Cyclic voltammograms for 20 mM MNPS in EMI-TFSI using a PAn.(+)-HCSA modified GC-disc (0.07 cm^2 surface area) electrode. Scan rate: 50 mV/s.

(b) Electrolysis of MNPS in EMI-TFSI

A solution of methyl 4-nitrophenyl sulfide (51 mg) in 5 mL EMI-TFSI ($[MNPS] = 60$ mM) was prepared. Its electrochemical oxidation was carried out in a one-compartment/three-electrode cell using a bare glassy carbon (GC)-disc (surface area = 0.07 cm^2) as the working electrode, a Pt mesh as the auxiliary electrode and $\text{Ag}/\text{AgCl}_{(\text{EMI-TFSI})}$ as the reference electrode. A constant potential of 1.8 V was applied and the electrolysis continued until 13 C of charge were passed (*ca.* 23% of the charge required for complete reduction). The electrolysis solution was then extracted eight times with 10 mL of diethyl ether. After evaporation on a warm water bath, the product was dissolved in dichloromethane and analyzed by mass spectrometry.

The CI mass spectrum (Figure 10.13) showed that unreacted organosulfide (MNPS) and the corresponding sulfoxide product were present (peaks at m/z 170 and 186, respectively).

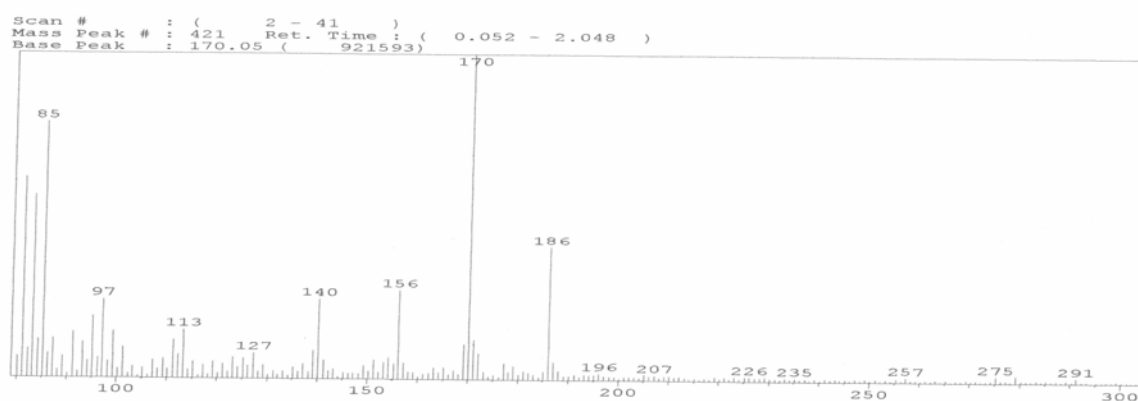


Figure 10.13 CI Mass spectrum for crude extract from electrochemical oxidation of MNPS in EMI-TFSI at 1.8 V.

10.3.3.2 Electrochemical Studies of MNPS and MPTS in BMI-BF₄*(a) Cyclic Voltammetry of MNPS and MPTS in BMI-BF₄*

Cyclic voltammograms were obtained in a solution containing 25 mM MNPS in BMI-BF₄ and using a bare glassy carbon electrode (Figure 10.14a). Anodic peaks at 1.7 and 2.3 V corresponding to the successive oxidations of MNPS to the sulfoxide and sulfone were observed. After addition of MPTS (17 mM) to the same solution, the CV showed four anodic peaks at 1.3, 1.7, 2.0 and 2.3 V. Therefore, the new peaks at 1.3 and 2.0 V were attributed to oxidation of MPTS to the sulfoxide and sulfone, respectively.

When a PAn.(+)-HCSA modified glassy carbon electrode was used as working electrode for potential cycling over the range -0.2 to 2.0 V* in the same solution as Figure 10.14b, two anodic peaks for MPTS at 1.2 and 1.9 V as well as the first anodic peak for MNPS at 1.5 V were clearly seen in the second scan (Figure 10.14c). Current response attributed to the electroactivity of the polyaniline film was also observed in the region 0 to 1.1 V.

(b) Electrooxidation of MPTS in BMI-BF₄

Electrolysis was carried out in a divided cell with three electrodes. A glassy carbon plate (1 cm²), Pt mesh and silver wire were used as working, auxiliary and quasi reference electrodes, respectively. Anolyte (5 mL of BMI-BF₄ containing 60 mM of MPTS) and catholyte (5 mL of BMI-BF₄ containing 0.1 M of water) were separated by a PVDF membrane. Water, which can be reduced to hydrogen gas at the auxiliary electrode, was added to the catholyte to avoid degradation/decomposition of the BMI-BF₄. Without water addition, the catholyte turned yellow after electrolysis for 30 min, indicating the degradation of BMI-BF₄.

* Footnote: Scanning to potential > 2.0 V was not carried out in this case, as our earlier studies had shown that this may cause oxidative degradation of PAn.(+)-HCSA films in BMI-BF₄.

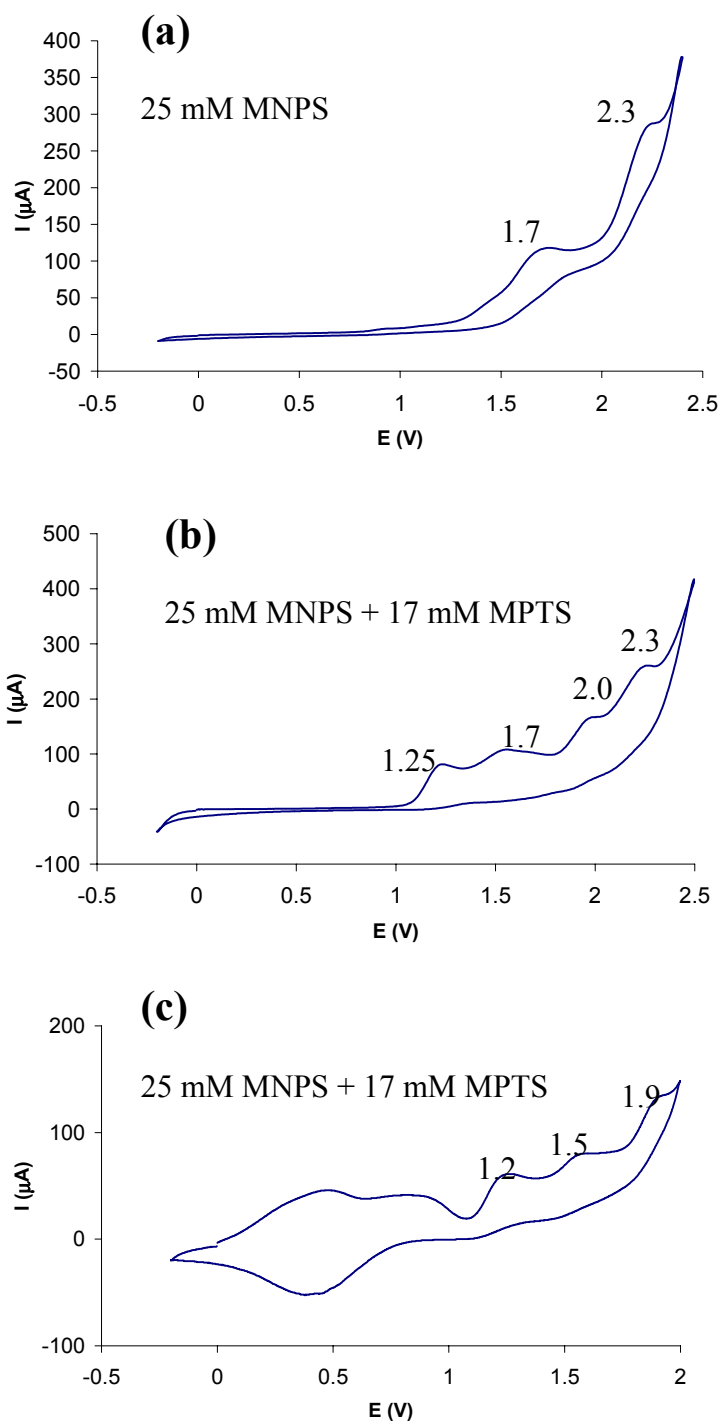


Figure 10.14 Cyclic voltammograms recorded for MNPS and MPTS in BMI- BF_4 using: (a,b) a GC-disc electrode, and (c) a PAN.(+)-HCSA modified GC-disc (0.07 cm^2 surface area) electrode. Scan rate: 50 mV/s.

To ensure that oxidation of MPTS occurred in the divided cell, the cyclic voltammogram was recorded. Figure 10.15 revealed anodic current peaks at *ca.* 1.6 and

2.5 V attributed to oxidation of MPTS to the corresponding sulfoxide and sulfone products, respectively. Both peaks were observed at more positive potentials than those previously observed using a one-compartment cell (Figure 10.14b).

Therefore, electrolytic oxidation of MPTS to the corresponding sulfoxide using a divided cell was performed at a constant potential of 1.75 V. The electrolysis was continued for 27 hrs with 28 C of charge passed. The electrolysis solution was then extracted eight times with 10 mL of diethyl ether. After evaporation, the product was dissolved in dichloromethane and analyzed by TLC chromatography and mass spectrometry.

The GC mass spectrum (Figure 10.16) showed that unreacted organosulfide (MPTS) and the corresponding sulfoxide product were present (peaks at m/z 139 and 154, respectively). This indicated that the oxidation of methyl-*p*-tolyl-sulfide was not complete at this stage.

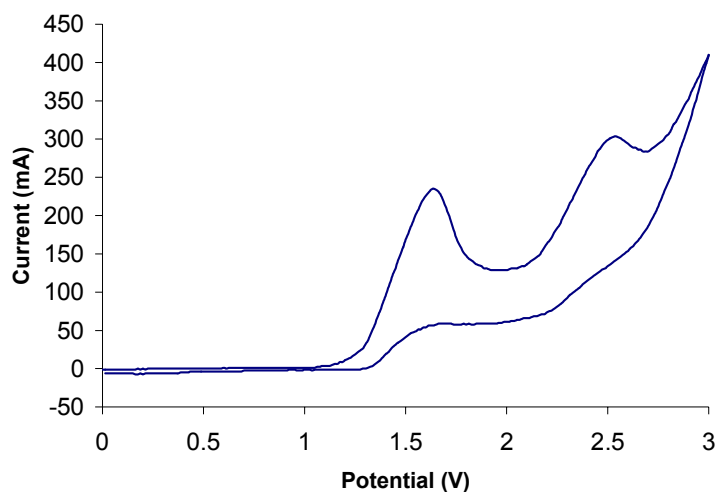


Figure 10.15 Cyclic voltammogram for 60 mM MPTS in BMI-BF₄ using a GC-disc (0.07 cm² surface area) electrode, with nitrogen gas bubbling. Scan rate: 50 mV/s.

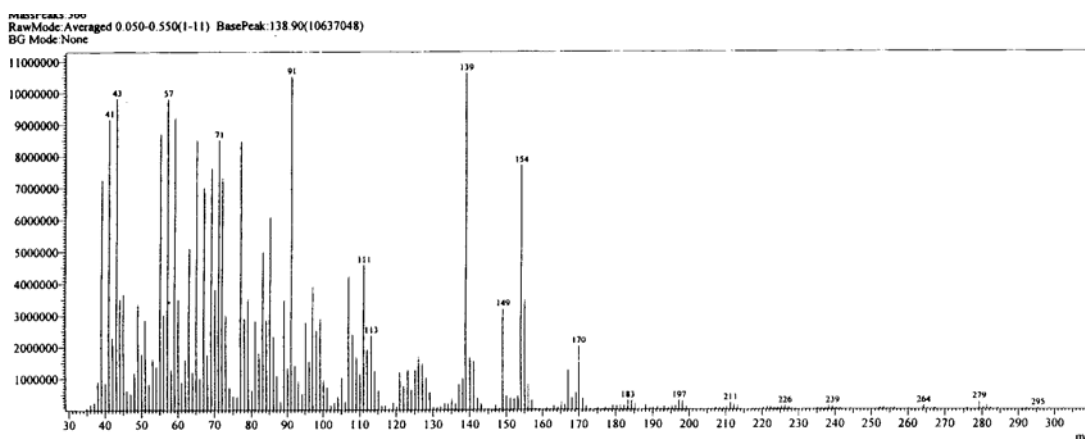


Figure 10.16 GC Mass spectrum for crude extract from electrochemical oxidation of methyl-*p*-tolyl-sulfide in BMI-BF₄ at 1.75 V.

Chiral polyaniline PAn.(+)-HCSA was found in Chapter 9 to be very stable in BMI-BF₄ even after holding at +2.0 V for 30 min. The ability to produce an optically active sulfoxide product from the electro-oxidation of methyl-*p*-tolyl-sulfide in BMI-BF₄ using a chiral PAn.(+)-HCSA as the electrode was therefore investigated. The preliminary result obtained by cyclic voltammetry (Figure 10.14) also showed that the oxidation of methyl-*p*-tolyl-sulfide in BMI-BF₄ took place on a PAn.(+)-HCSA modified electrode. Therefore, electrolysis of methyl-*p*-tolyl-sulfide in BMI-BF₄ using PAn.(+)-HCSA modified electrode was carried out using the same conditions as employed above with a bare glassy carbon electrode. Unexpected evidence was found after the electrolysis was performed for 15 min. The polyaniline film commenced to degrade and then dissolved/dispersed in the ionic liquid. This may be due to some species generated during the oxidation of the organosulfide becoming involved in oxidative degradation of the polyaniline.

10.4 Conclusions

Cyclic voltammetry studies confirm the reductions of acetophenone and 2-acetylpyridine in the ionic liquid EMI-TFSI using both a glassy carbon and a PAn.(+)-

HCSA modified glassy carbon working electrode. The corresponding alcohol products are obtained when electrolyses of acetophenone and 2-acetylpyridine in EMI-TFSI are carried out on a glassy carbon electrode at -1.9 and -1.8 V, respectively. However, using a chiral PAn.(+)-HCSA modified electrode for asymmetric reduction of these substrates could not be carried out in EMI-TFSI, since the chiral polyaniline film racemizes when reduced in EMI-TFSI.

Similar electrochemical reduction of 4-acetylpyridine occurs on glassy carbon and PAn.(+)-HCSA modified glassy carbon electrodes in the chiral ionic liquid (-)-MBEA-TFSI and racemic (\pm)-MBEA-TFSI, as evidenced by a cathodic peak in cyclic voltammetry. Electrolysis of the 4-acetylpyridine substrate in the chiral (-)-MBEA-TFSI electrolyte at a glassy carbon electrode can be successfully carried out at a -1.6 V, yielding 4-pyridylethanol product. However, the alcohol product cannot be completely separated from the chiral ionic liquid because of its similar solubility properties to the (-)-MBEA-TFSI electrolyte. Therefore, the optical rotation of the product could not be measured, and the degree of chiral discrimination in the electroreduction is unknown.

PAn.(+)-HCSA does not racemize after holding at -1.7 V for 85 hrs during electrolysis of 4-acetylpyridine in (\pm)-MBEA-TFSI. However, no alcohol product is detected, the corresponding achiral pinacol being instead formed.

Cyclic voltammetry studies confirm the oxidations of methyl-4-nitrophenyl sulfide and methyl-*p*-tolyl sulfide on glassy carbon and PAn.(+)-HCSA modified glassy carbon electrodes in the ionic liquid electrolytes EMI-TFSI and BMI-BF₄. The electrolysis of methyl-4-nitrophenyl sulfide and methyl-*p*-tolyl sulfide could be successfully carried out on a glassy carbon electrode at +1.8 V and +1.75 V in EMI-TFSI and BMI-BF₄,

respectively, and the corresponding sulfoxide products identified. However, attempted asymmetric electrolysis of the organosulfides on PAN.(+)-HCSA modified electrode are not feasible due to oxidative degradation of the polyaniline film. Since this degradation of the polyaniline electrode does not occur in the ionic liquid alone, it may be promoted by species generated during the oxidation of the sulfide substrate.

10.5 References

1. A.M. Rouhi, *C&EN*, (2004): 47.
2. D. Seebach and H.A. Oei, *Angew. Chem.* **87** (1975): 629.
3. J. Kopilov, E. Kariv, and L.L. Miller, *J. Am. Chem. Soc.*, (1977): 3450.
4. W.J.M. Tilborg and C.J. Smit, *Journal of the Royal Netherlands Chemical Society.* **97/3** (1978): 89.
5. M. Schwientek, S. Pleus, and C.H. Hamann, *J. Electroanal. Chem.* **461** (1999): 94.
6. S. Abe, T. Nonaka, and T. Fuchigami, *Journal of the American Chemical Society.* **105** (1983): 3630.
7. T. Komori and T. Nonaka, *J. Am. Chem. Soc.* **105** (1983): 5690.
8. T. Komori and T. Nonaka, *J. Am. Chem. Soc.* **106** (1984): 2656.
9. J.-C. Moutet, C. Duboc-Toia, S. Menage, and S. Tingry, *Adv. Mater.* **10** (1998): 665.
10. S.A. Forsyth, J.M. Pringle, and D.R. MacFarlane, *Aust. J. Chem.* **57** (2004): 113.
11. J.D. Holbrey and K.R. Seddon, *Clean Products and Processes 1 Springer-Verlag*, (1999): 223.
12. T. Welton, *Chem. Rev.* **99** (1999): 2071.
13. F. Endres, *Chemphyschem.* **3** (2002): 144.
14. T. Biedron and P. Kubisa, *J. Polym. Sci., Part A.* **40** (2002): 2799.
15. H. Zhang, K. Hong, and J.W. Mays, *Macromolecules.* **35** (2002): 5738.
16. E. Naudin, H.A. Ho, S. Branchaud, L. Breau, and D. Belanger, *J. Phys. Chem. B.* **106** (2002): 10585.
17. P. Lucas, N.E. Mehdi, H.A. Ho, D. Belanger, and L. Breau, *Synthesis*, (2000): 1253.
18. D. Behar, C. Gonzalez, and P. Neta, *J. Phys. Chem. A.* **105** (2001): 7607.
19. A. Nelson, *Angew. Chem. Int. Ed.* **38** (1999): 1583.
20. J.S. Wilkes, *J. Molecular Catalysis A : Chemical.* **214** (2004): 11.
21. C.R. Oh, D.J. Choo, W.H. Shim, D.H. Lee, E.J. Roh, S. Lee, and C.E. Song, *Chem. Commun.*, (2003): 1100.
22. S. Lee, Y.J. Zhang, J.Y. Piao, H. Yoon, C.E. Song, J.H. Choi, and J. Hong, *Chem. Commun.*, (2003): 2624.
23. J.G. Huddeleston, H.D. Willauer, R.P. Swatloski, A.E. Visser, and R.D. Rogers, *Chem. Commun.*, (1998): 1765.
24. M.C. Bowyer, C.M. Gordon, S.K. Leitch, A. McCluskey, and C. Ritchie, *Aust. J. Chem.* **57** (2004): 135.
25. P.G. Pickup and R.A. Osteryoung, *J. Am. Chem. Soc.* **106** (1984): 2294.
26. R. Vijayaraghavan and D.R. MacFarlane, *Aust. J. Chem.* **57** (2004): 129.
27. J. Tang and R.A. Osteryoung, *Synth. Met.*, (1991).
28. J.M. Pringle, J. Efthinmiadis, P.C. Howlett, J. Efthinmiadis, D.R. MacFarlane, A.B. Chaplin, S.B. Hall, D.L. Officer, G.G. Wallace, and M. Forsyth, *Polymer.* **45** (2004): 1447.
29. K. Matiasovsky, Z. Lubyova, and V. Danek, *Electrodepos. Surface Treat.* **1** (1972/73): 43.
30. C.A. Zell, F. Endres, and W. Freyland, *Phys. Chem. Chem. Phys.* **1** (1999): 697.
31. W. Lu, A.G. Fadev, B. Qi, E. Smela, B.R. Mattes, J. Ding, G.M. Spinks, J. Mazurkiewicz, D. Zhou, G.G. Wallace, D.R. MacFarlane, S.A. Forsyth, and M. Forsyth, *Science.* **297** (2002): 983.
32. W. Lu, A.G. Fadev, B. Qi, and B.R. Mattes, *Synth. Met.* **135-136** (2003): 139.
33. D. Zhou, G.M. Spinks, G.G. Wallace, C. Tiyapiboonchiya, D.R. MacFarlane, M. Forsyth, and J. Sun, *Electrochimica. Acta.* **48** (2003): 2355.

-
34. J. Ding, D. Zhou, G.M. Spinks, G.G. Wallace, S.A. Forsyth, M. Forsyth, and D.R. MacFarlane, *Chem. Mater.* **15** (2003): 2392.
 35. S.A. Forsyth, S.R. Batten, Q. Dai, and D.R. MacFarlane, *Aust. J. Chem.* **57** (2004): 121.
 36. M. Yoshizawa, A. Narita, and H. Ohno, *Aust. J. Chem.* **57** (2004): 139.
 37. A.L.P. Kane-Maguire. *The Synthesis and Applications of Chiral polyanilines*. in "Abstracts, 2nd Workshop on Multifunctional and Smart Polymer Systems". 1997. Wellington, N. Z.
 38. B.E. Firth, L.L. Miller, J. Lennox, and R.W. Murray, *J. Am. Chem. Soc.*, (1976): 8271.
 39. B.F. Watkins, J.R. Behling, E. Kariv, and L.L. Miller, *J. Am. Chem. Soc.*, (1975): 3549.
 40. B.E. Firth and L.L. Miller, *J. Am. Chem. Soc.*, (1976): 8272.
 41. K. Adjidjonou and C. Caze, *European Polymer Journal.* **30** (1994): 395.